GEOLOGICAL SURVEY OF CANADA
COMMISSION GÉOLOGIQUE DU CANADA

PAPER 76-1C

REPORT OF ACTIVITIES
PART C

Energy, Mines and Resources Canada
Énergie, Mines et Ressources Canada

1976

Technical editing and compilation
R. G. Blackadar
P. J. Griffin
H. Dumych
E. J. W. Irish

Production editing and layout
Leona R. Mahoney
Michael J. Kiel
Richard Fix

Typed and checked by
Debby Busby
Janet Gilliland
Sharon Parnham
W. E. Anderson

GEOLOGICAL SURVEY
PAPER 76-1C

REPORT OF ACTIVITIES
PART C

1976

Available by mail from

Printing and Publishing
Supply and Services Canada
Ottawa, Canada K1A 0S9
or through your bookseller.

Catalogue No. M44-76/1C Price: Canada: $5.00
ISBN 0-660-00560-3 Other countries: $6.00

Price subject to change without notice.

TABLE OF CONTENTS

Page

MARINE GEOSCIENCE

MINERAL DEPOSITS

MINERALOGY

PALEONTOLOGY

Page

PETROLEUM GEOLOGY

QUATERNARY GEOLOGY: ENVIRONMENTAL AND ENGINEERING GEOLOGY STUDIES

QUATERNARY GEOLOGY: INVENTORY MAPPING AND STRATIGRAPHIC STUDIES

QUATERNARY GEOLOGY: PALEOECOLOGY AND GEOCHRONOLOGY

INTRODUCTION

The principal missions of the Geological Survey of Canada are:

1. *Evaluation of energy and mineral resources available in Canada required for the formulation of national energy and mineral resources policy. This includes resource adequacy for domestic needs, surplus available for export, alternative sources in Canada for commodities that are currently largely imported, and resource conservation, etc.*

2. *Provision of geoscientific information and technology to facilitate the discovery of needed resources, as a means of promoting regional development to lessen regional disparities, and as an aid in establishing Canadian sovereignty in adjacent offshore areas.*

3. *Determination of the capability of the landmass to withstand various types of use particularly in response to resource development, urban growth and for disposal of waste.*

4. *Provision of advice and information to other government departments and agencies, and adding to the knowledge base used for research, education and for cultural purposes.*

Thus the Survey's program is concerned essentially with describing and explaining the geology of Canada, of developing better ways of identifying and evaluating its resources, and of assessing the suitability of our land for use by man. The program is also concerned with communicating the results of the Survey's work effectively.

To meet the various missions many individual projects are undertaken. Many of these are concerned with bettering our understanding of the geological framework of Canada and thus are directed to the study, mapping, description and interpretation of the geology of Canada and its adjacent offshore regions. Considerable effort is also devoted to identifying potential mineral and energy resources and to assessing the capability of terrain for various uses by man. Studies of mineral deposits, the development of geochemical and airborne radiometric techniques, investigations of the sensitivity of various terrains to man's use and the development of high resolution seismic profile techniques to determine the properties of sea bottom sediments are examples.

Studies in marine geology are carried out to provide information on the nature of past and present geological processes and the nature of onshore and offshore sedimentary basins. Twelve papers are concerned with these subjects and reflect the application of various disciplines such as biology, geophysics and chemistry to these studies. Reports 4, 6, and 10 are concerned with present day organisms in the waters off the shores of eastern Canada, Reports 1, 7, 8, 9 and 13 are devoted to coastal processes and Report 2 to applications of seismic techniques to bedrock studies in a part of the continental shelf. Reports 5, 16, 17 and 43 are also concerned with geophysical applications in offshore areas, in this case in the Arctic. Marine studies are also carried out as a natural extension of the terrain analyses being done in the Arctic and on the West Coast. Such work is designed to provide information on stratigraphy and environmental history and to develop regional understanding about pertinent physical processes and engineering attributes that affect the stability and character of coastlines. Such information is needed for planning and assessing offshore hydrocarbon developments, ecological studies and assessments of possible mineral resources, especially sources for building aggregates. Reports 27, 29 and 57 present the results of work which, although primarily done as terrain studies, shows the interplay of geophysics in such studies; in the same way Reports 11 and 15 depend on the application of geochemistry to the solution of marine studies.

A considerable part of the Survey's current effort is being given to the Uranium Reconnaissance Program including studies in radioactivity and geochemistry. Studies in the former are designed to stimulate and facilitate exploration for uranium by providing basic information on the distribution of uranium, to establish standards and calibrations for air, ground and borehole measurements of uranium by radiation methods and to develop the methodology for converting reconnaissance data into resource potential estimates. The geochemical aspect of the program is designed to gather nationally consistent, systematic data from a variety of sampling media. The work also includes research on geochemical processes, development of new methods of mineral exploration and resource appraisal and work on analytical techniques and geochemical instrumentation. Report 51 presents results of a radiometric survey in Prince Edward Island and Reports 44 to 50 the results of a variety of geochemical studies. The importance of understanding various types of occurrence in order to interpret Canadian occurrences is shown in Report 48 in which uranium studies in the Cordilleran area of the United States were examined in order to better assess the likelihood of occurrence of similar deposits in British Columbia.

The "Report of Activities" is published three times each year – early January, early June and mid-November. Part C is designed to present first results of some of the projects carried out during the preceding field season as well as results of on-going research. Material for this report was received and edited between September 1st and 17th; production editing, typing and preparation of camera ready copy were carried out between September 1st and October 5th and the manuscript sent to the printer October 6th for a mid-November release.

Individual reports are grouped together by general subject heading in the "Contents" but to permit the close scheduling required to proceed from raw manuscript to published text in about two months, it was necessary to edit and type material in the order in which it was received. Although this precludes grouping reports together in the text the user should find little difficulty in using this publication as the "Contents" gives ready access to other reports in the same field.

October 5, 1976

R. G. Blackadar
Chief Scientific Editor

REPRINTS

A limited number of reprints of the papers that appear in this volume are available by direct request to the individual authors. The addresses of the Geological Survey of Canada offices follow:

601 Booth Street,
OTTAWA, Ontario
K1A 0E8

Institute of Sedimentary and Petroleum Geology,
3303-33rd St. N.W.,
CALGARY, Alberta
T2L 2A7

British Columbia Office,
100 West Pender Street,
VANCOUVER, B.C.
V6B 1R8

Atlantic Geoscience Centre,
Bedford Institute of Oceanography,
P.O. Box 1006,
DARTMOUTH, N.S.
B2Y 4A2

When no location accompanies an author's name in the title of a paper, the Ottawa address should be used.

Project 750048

Charles T. Schafer and D. Scott[1]
Atlantic Geoscience Centre, Dartmouth

Temporal Changes in Major Foraminiferal Assemblages

Recent foraminiferal assemblages are being investigated in the Miramichi estuary, New Brunswick to aid in the interpretation of circulation patterns and sedimentary processes. Only two assemblages were recognized by Bartlett (1966) and Tapley (1969). They identified an upper river assemblage and an open bay assemblage (Fig. 1.1). They did not observe more than 7 per cent (total population) of *Ammotium cassis* at any of their stations.

Grab samples were first collected in the inner bay as part of this project in September 1975. A Q-mode cluster analysis technique (Bonham-Carter, 1967) was used initially to identify the major foraminiferal biotopes in the estuary at this time. The species used in the analysis are forms that were identified in at least 10 per cent of the total samples examined. The total percentage values (i.e., living plus empty tests) of the selected species were coded into a two-state form (Bonham-Carter, 1967, Table 2) which defined abundant (>50%), common (>5-50%), rare (>1-5%), and absent levels of occurrence. The use of total population counts, and of a minimum sample frequency limit, was elected based on the recommendations of Albani and Johnson (1975) who concluded that any statistical analysis of marginal marine foraminiferal populations where biotopes are to be determined should be based on the total population present at each station and that widespread species (as opposed to locally-distributed forms) appear to be more significant in defining biotopes. A relatively wide range of percentage values have been included in the "common" and "abundant" categories defined here in order to de-emphasize the typically overdispersed distribution patterns of species in northern temperate marginal marine environments (Schafer, 1971, 1975).

The percentage data were compared between samples using the Jaccard coefficient of association (Sj):

$$Sj = \frac{C}{N_1 + N_2 - C}$$

where C represents species present in two samples being compared, N_1 equals the total species present in the first sample and N_2 equals the total species present in the second sample (*see* Cheetham and Hazel, 1969). This coefficient essentially compares the number of positive matches between two samples to the sum of positive matches plus mismatches. It ignores negative matches and thus prevents a high degree of similarity from occurring between samples that have a large number of absent species in common. Values of association range from 0 (complete dissimilarity) to 1 (complete similarity). The clustering method used here is the unweighted pair-group method (Sokal and Sneath, 1963). This method first links ungrouped samples in pairs and then into progressively larger groups by an iterative process. In the unweighted mode equal importance is assigned to each sample so that larger groups have more weight than smaller ones. The cluster analysis results are presented graphically in the form of a two-dimensional hierarchy dendrogram in which the degree of association is represented along one axis and samples are listed along the other axis (Fig. 1.2). These results have been plotted geographically to define the basic configuration and extent of biotopes within the study area.

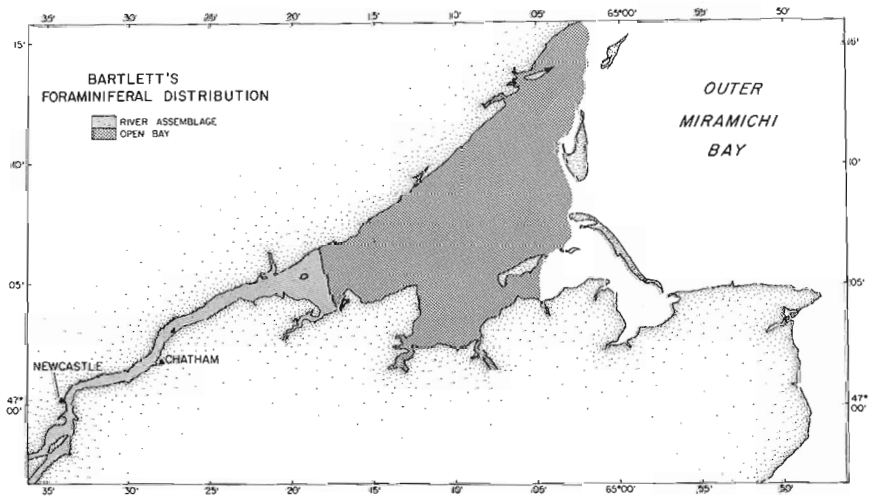

Figure 1.1.

Map of the Miramichi estuary showing the distribution pattern of major foraminiferal assemblages identified by Bartlett (1966).

[1]Department of Geology, Dalhousie University, Halifax.

From: Report of Activities, Part C;
Geol. Surv. Can., Paper 76-1C (1976)

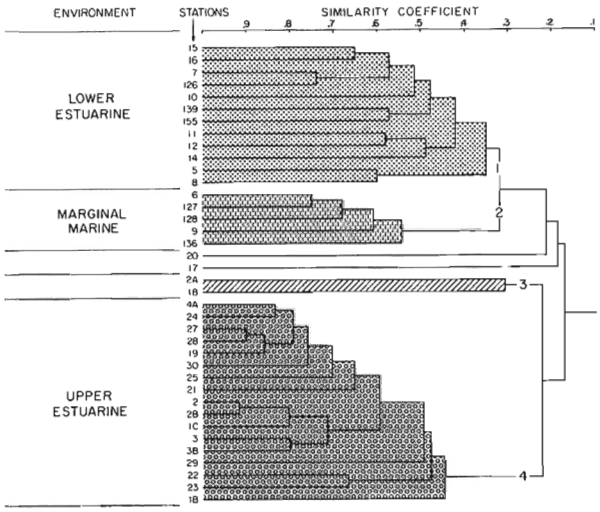

Figure 1. 2. Dendrogram showing similarity of grab samples and the three main clusters used to identify major biotopes in the inner bay.

Results

Cluster analysis of 38 samples and 25 species reveal 3 major biotopes within the estuary at the 0. 3 level of association (Fig. 1. 3). Near the mouth of Miramichi Bay a marginal marine environment supports a biotope dominated by *Cribroelphidium excavatum clavatum* and *Protelphidium orbiculare*. A second biotope is associated with an upper estuarine environment that begins near Sheldrake Island and extends upstream to about Newcastle, New Brunswick. *Miliammina fusca, Ammotium salsum, Trochammina macrescens* and the thecamoebinid *Pontigulasia compressa* are abundant here. An extensive lower estuarine environment is developed in western and norther Miramichi Bay. Its associated biotope includes a relatively large number of species that occur in the adjacent biotopes described above. The biotope is distinguished primarily by the comparatively high percentages of *Ammotium cassis* and *Eggerella advena.*

Some of the samples contain a number of species that are indigenous to the upper estuarine biotope. The samples have nevertheless been distinguished from other groups by the clustering technique at the 0. 3 level because of the additional "common" presence of *A. cassis,* a form which is typically associated with the transitional and marginal marine biotopes. Samples 20 and 17 (Fig. 1. 2) shows a linkage pattern on the cluster diagram which has been described as "straggly" by Albani and Johnson (1975). They note that this patter is related to a "mixing biotope" in Broken Bay, New South Wales in which the internal similarity structure of the associated samples is not well defined. In this case, samples 20 and 17 are considered as part of the transitional biotope on the basis of their relatively high proportion of *Cribroelphidium excavatum excavatum* and *Eggerella advena* specimens.

In terms of the observed "common" and "abundant" species, the lower estuarine group of samples can be distinguished from the marginal marine group by the presence of *Ammotium cassis, Bucella frigida, Crithionina pisum, Trochammina inflata macrescens,* and the thecamoebinid *Difflugia capreolata* in the former. The upper estuarine samples can be distinguished from those collected in the lower estuarine environment by the presence of *Ammonium salsum, Centropyxis excentricus, Pontigulasia compressa,* and by the absence of *Cribroelphidium excavatum selseyensis.* The latter calcareous species is common only in the lower estuarine and marginal marine biotopes.

The comparison of these data with those of Bartlett (1966) and Tapley (1969) suggests that a change in circulation and/or a decrease in flushing rate has occurred in the inner bay since 1964. Four short cores collected in the lower estuarine environment confirm this hypothesis. The core locations are within an area shown by Bartlett and Tapley to be occupied by an open bay fauna, but which is now occupied by the lower estuarine assemblage. This assemblage extends from the top of the core down to about 20 cm. At this level there is an abrupt change to an open bay fauna suggesting that about 20 cm of sediment has been

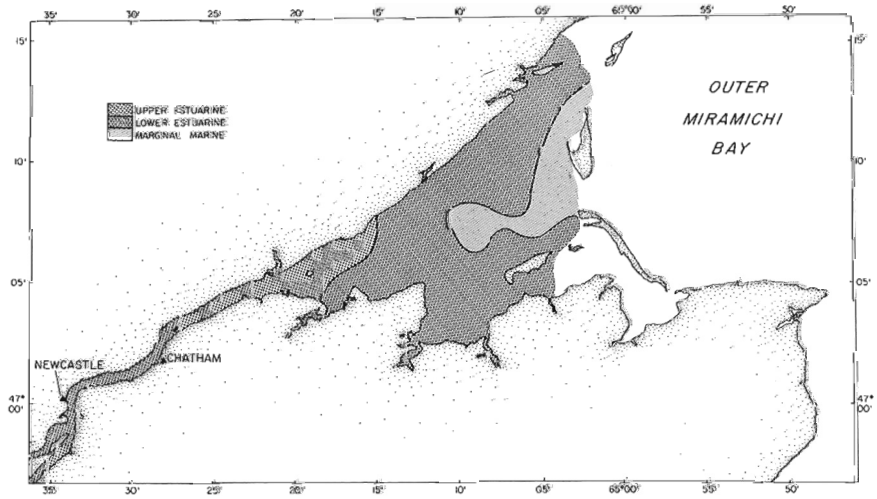

Figure 1. 3.

Distribution of major foraminiferal assemblages in the estuary in September 1975.

deposited since 1964. The change in circulation and/or sedimentation pattern appears to be related to the shifting and infilling of inlets between the several barrier islands that define the eastern margin of the inner bay.

The Miramichi estuary was selected as a common site for a multidisciplinary environmental geology investigation because of planned dredging operations that will enlarge the channel leading to the ports of Newcastle and Chatham. The aims of this project include the identification of factors and processes that are related to the over-all ecology of the estuary and can thus be used to measure the impact of the dredging operations. It is also anticipated that the identification of major sedimentary processes in the inner bay will permit a more accurate estimate of channel maintenance costs.

References

Albani, A. D. and Johnson, K. R.
1975: Resolution of foraminiferal biotopes in Broken Bay, N. S. W. Geol. Soc. Aust., J., v. 22, p. 435-446.

Bartlett, G. A.
1966: Distribution and abundance of Foraminifera and thecamoebina in Miramichi River and Bay: unpublished manuscript, Bedford Inst. Oceanogr., Rep. 66-2, 104 p.

Bonham-Carter, G. S.
1967: Fortran IV program for Q-Mode cluster analysis of non-quantitative data using IBM 7090/7094 computers; Kans. Univ., Computer Contrib. 17, 13 p.

Cheetham, A. H. and Hazel, J. E.
1969: Binary (Presence-Absence) Similarity Coefficients. J. Paleontol., v. 43, p. 1130.

Schafer, C. T.
1971: Sampling and spatial distribution of benthonic foraminiferal. Limnol. Oceanogr., v. 16, p. 944-951.

1975: Total foraminiferal distribution patterns in the Restigouche estuary. (Abstract) Benthonics '75 Symposium, Dalhousie Univ., Halifax, Canada.

Sokal, R. R. and Sneath, P. H.
1963: Principles of Numerical Taxonomy. Freeman, San Francisco, 359 p.

Tapley, S.
1969: Foraminiferal analysis of the Miramichi estuary. Marit. Sediments, 5, p. 30-39.

2. APPLICATION OF THE HUNTEC DEEP TOW HIGH-RESOLUTION SEISMIC SYSTEM TO SURFICIAL AND BEDROCK STUDIES – GRAND BANKS OF NEWFOUNDLAND

Project 730072

Lewis H. King and Gordon B. Fader
Atlantic Geoscience Centre, Dartmouth

Introduction

As part of the field studies for this project, Hudson cruise 75-009 was conducted east of the Avalon Peninsula to Flemish Cap between 46°N and 48°N from April 25 to May 29, 1975. A total of 9280 km of gravity and magnetic profiles, 4900 km of 40-in^3 (655-cm^3) air gun seismic reflection profiles, 3550 km of Huntic deep tow high-resolution seismic reflection profiles (DTS), and 1570 km of side-scan records was collected during the cruise. Also, 28 stations were occupied to obtain bedrock samples using the Bedford Institute of Oceanography electric rock core drill.

The cruise was mainly in support of the study of the surficial and bedrock geology of the Grand Banks and adjacent areas, but some emphasis was placed on further development of an integrated survey concept whereby side-scan, air gun, and DTS records can be obtained simultaneously and subsequently used as control in the identification and procurement of significant surficial bedrock samples. Two examples from the cruise are used in this report to illustrate the manner

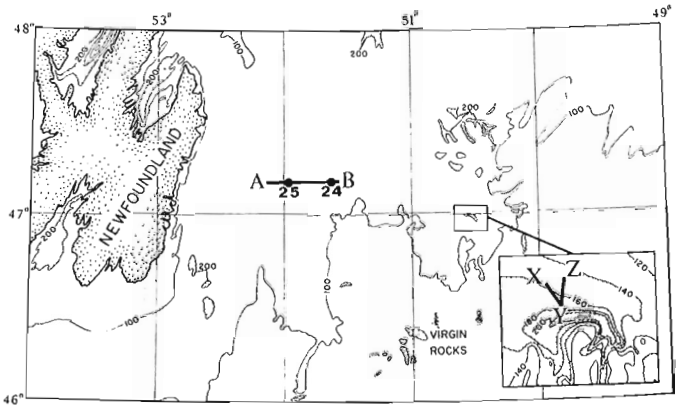

Figure 2.1. Location of profiles and sample sites described in text.

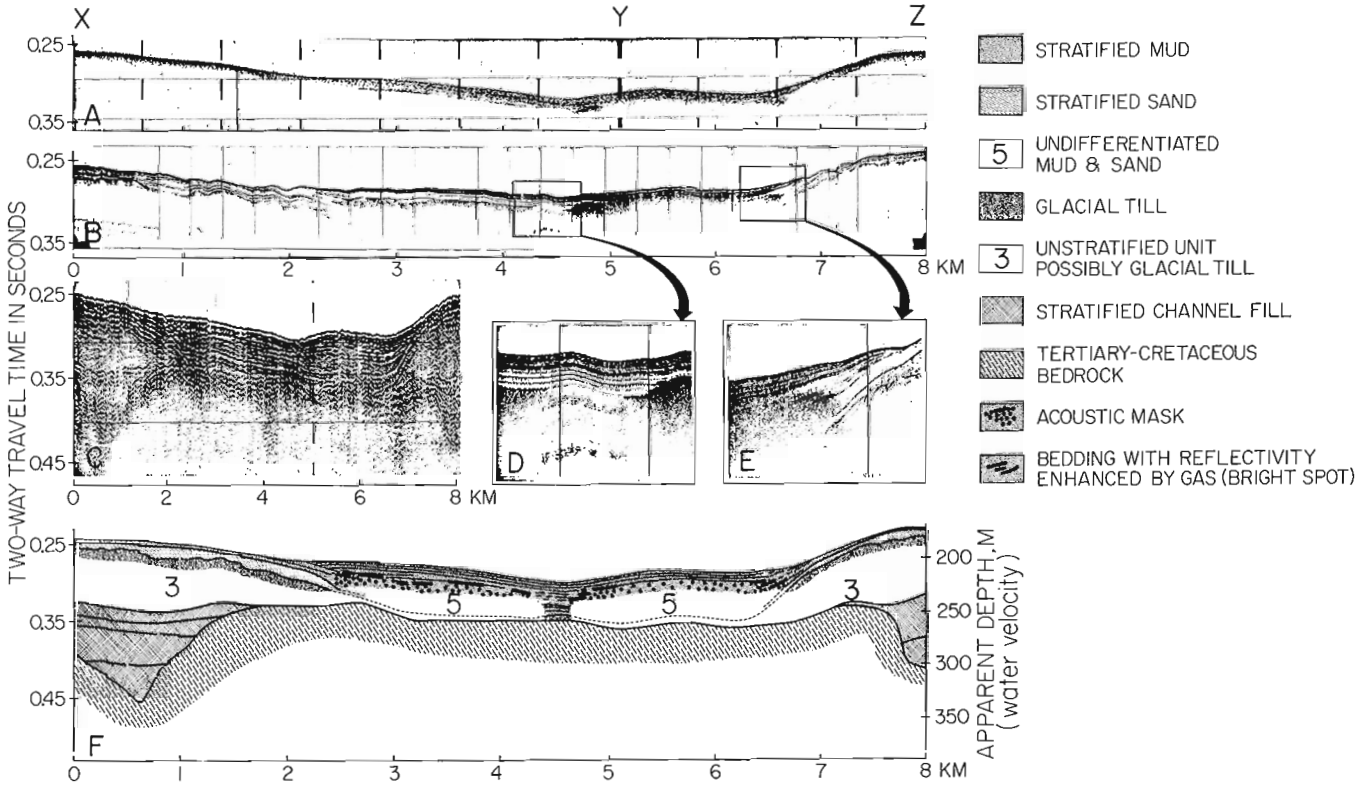

Figure 2.2. Seismic data along Profile XYZ (Fig. 2.1). (A) echogram; (B) Huntec deep tow high-resolution seismic reflection profile, DTS; (C) air gun seismic profile; (D) and (E) enlarged areas of DTS profile (B); (F) composite stratigraphic interpretation using (B) and (C) above. *See* text for interpretation.

From: Report of Activities, Part C;
Geol. Surv. Can., Paper 76-1C (1976)

in which these data can be integrated for a more complete interpretation of the near-surface geology and utilized to locate bedrock accessible to the 6-m long core barrel of the electric rock core drill. The site locations chosen for illustrative purposes are shown in Figure 2. 1.

The DTS is a new high-resolution seismic system based on the design of transient acoustic generators (Hutchins, 1974) and developed co-operatively by government and industry. The prototype system built by Huntec ('70) Ltd., was initially evaluated by the Bedford Institute of Oceanography during the Fall of 1974 (McKeown, 1975; Hutchins *et al.*, 1976). In 1975 a modified version of the original prototype DTS was operated from the CSS *Hudson* on most of the Atlantic Geoscience Centre (AGC) cruises and approximately 6500 line-km of profiles were collected. AGC and Huntec are currently processing the taped seismic data in a co-operative attempt to quantify parameters that will adequately describe the sediments.

Profile XYZ

Figure 2. 2 shows a composite interpretation (F) using an echogram (A), and DTS (B) and air gun (C) seismic records along track XYZ. The echogram (A) depicts a soft mud seabed at the base of the depression grading to a more reflective sandy bottom on the flanks of the depression. The DTS record (B) shows a greater amount of acoustic penetration than the echogram; it penetrated 30 to 40 m through the mud and sand units to an irregular undulating seismic event interpreted as a surface of glacial till. The high resolution capability of the system is well illustrated by the fine bedding of the mud and sand units (*see* also (D) and (E)). Seismic records obtained with the DTS do not have the "bubble pulse" common to seismic sources such as air guns; thus, it is possible to resolve reflection events to a precision of about 0. 3 m. In the central area of the depression, penetration is inhibited by diffused gas (acoustic mask) in the mud and sand, but full penetration to bedrock was possible between the 4. 4- to 5. 1-km marks because there was no diffused gas (acoustic window). Adjacent profiles showed the acoustic mask close to the seabed and analysis of a vibracore sample from the gas-bearing layer indicated the occurrence of methane. Also, gas bubbles leaking from the seabed were detected in the water column with the ship's echo-sounder.

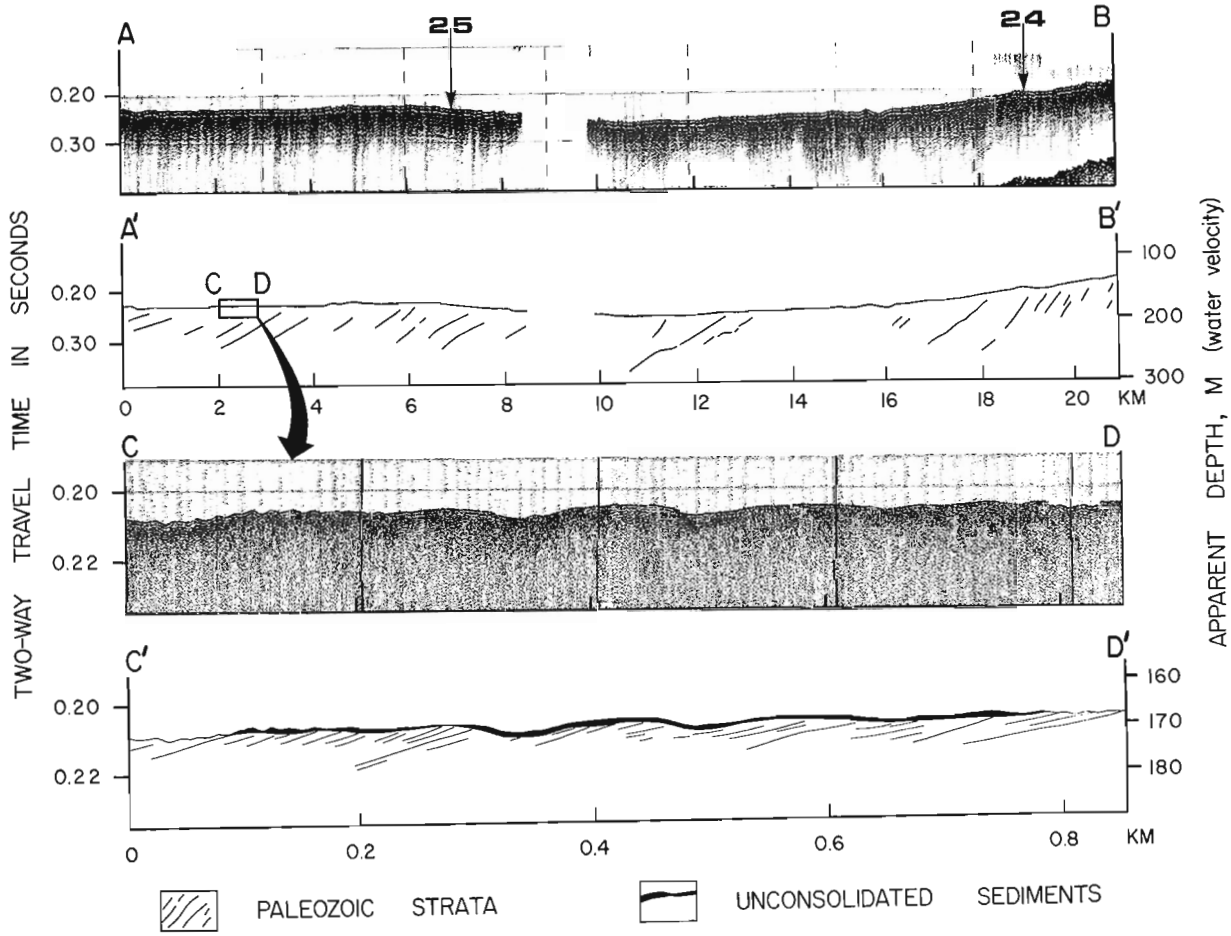

Figure 2. 3. Seismic data along Profile AB (Fig. 2. 1). (AB) air gun seismic reflection profile; (A'B') line interpretation of seismic reflection profile; (CD) Huntec deep tow high-resolution seismic profile, DTS; (C'D') line interpretation of DTS profile. CD on Profile A'B' represents area shown by DTS Profile CD. Some of the detail on the DTS profile has been lost through reduction and reproduction.

Artificial undulations of the seabed and subsurface reflectors were present on the early records (for example (B)) because of a long-period oscillation of the towed system, but this imperfection has now been removed from the system. The true morphology of the seabed is shown on the echogram (A).

The air gun section (C) resolves some of the major seismic events shown by the DTS and in addition shows a channelled bedrock surface with some stratified deposits infilling the channels. An interpretation of the records from both the DTS and air gun systems is shown as a composite stratigraphic section (F).

Sections (D) and (E) are enlarged areas of the DTS record (B); they illustrate the very fine stratigraphic detail resolved by the Huntec system although some detail is lost in reproducing the illustrations. The sections also show enhanced reflectors on the flanks and above the acoustic mask where gas has presumably migrated along some of the more porous beds creating "bright spots".

Profile AB

Figure 2. 3, Profile AB, is an air gun record across a sedimentary sequence east of the Avalon Peninsula (Fig. 2. 1), and A'B' is an interpreted line drawing from the same record. Once a sequence is defined on the basis of seismic profiles it should be sampled. In the past, normal procedure would have been to choose the best sample site from the air gun record. However, an accurate thickness of overlying unconsolidated sediment could not be measured from the record because the contact was masked by a 12-m thick bubble pulse. With the high resolution Huntec data, it is much simpler to choose drill sites within the range of the 6-m core barrel of the drill, and the number of unsuccessful attempts to obtain samples is greatly reduced. Section CD, Figure 2. 3, is a short section of DTS record along Profile AB and C'D' is an interpreted line drawing. The Huntec data show that the bedrock surface is very close to the seabed and in a few instances actually forms the seabed. Normally, the bedrock surface is deeper and the choice of suitable sites along a section such as CD would be more limited. The diagram also shows detailed information on the bedding within the bedrock and an unconformity at its surface helps define the contact between the unconsolidated sediment and Paleozoic strata.

Drill sites were chosen on the basis of the DTS data at Stations 24 and 25 along Profile AB and cores of bedrock with respective lengths of 110 and 480 cm were obtained.

Sample 24 is a well indurated, light grey to grey, fine grained, micaceous sandstone, characterized by disrupted bedding caused by burrowing. Sample 25 is a well indurated, grey to dark grey, siliceous shale composed dominantly of silt with a clay matrix. The shale is essentially massive with weak laminations caused by subtle variations in grain size. Burrows and dispersed fossils give the rock a mottled appearance. In some cases the fossils, often brachiopods, are concentrated in distinct bands. E. W. Bamber (pers. comm., 1976) reported an assemblage of chonetid brachiopods with a range of Silurian to Jurassic age. M. S. Barss (pers. comm., 1975) found corroded spores but these likewise proved undiagnostic for age determination. W. A. M. Jenkins (pers. comm., 1976) examined the chitinozoa and acritarch assemblages and found a Late Ordovician (Late Caradoc to Ashgill) age for Sample 24 and Silurian age (possibly early) for Sample 25. He found the microfossils essentially unmetamorphosed and considered the section promising for further detailed study. The authors think that the section can be expanded considerably through further sampling and that a good composite section can be obtained using present sampling techniques.

References

Hutchins, R. W.
1974: Computer simulation of a transiently excited underwater sound projector; Proc. of IEEE Ocean '74, v. 2, p. 115-119.

Hutchins, R. W., McKeown, D. L., and King, L. H.
A deep tow high resolution seismic system for continental shelf mapping; Geoscience Canada. (in press)

McKeown, D. L.
1975: Evaluation of the Huntec ('70) hydrosonde deep tow seismic system; Bedford Institute of Oceanography Report Series, BI-R-74-4, 115 p.

3. A METHOD FOR THE COMPILATION OF HIGH QUALITY CALCULATED FIRST VERTICAL DERIVATIVE AEROMAGNETIC MAPS

Project 680121

P.H. McGrath, L.J. Kornik, S.D. Dods
Resource Geophysics and Geochemistry Division

Introduction

The Geological Survey of Canada has been involved in high resolution aeromagnetic surveying since 1968. A Beechcraft B80 Queenair aircraft was acquired as a survey platform and a digital-recording, high resolution survey system was installed. A single-cell self-orienting rubidium-vapour magnetometer was mounted in a ten-foot tail boom on the aircraft. Also, a nine-term compensator built by Canadian Aviation Electronics was installed in order to limit aircraft manoeuvre noise in the data. Several experimental field surveys have been carried out (Hood and Sawatzky, 1971; Sawatzky and Hood, 1972; and Sawatzky *et al.*, 1973 and 1974). More recently the airborne system has been modified to include a second magnetometer (Sawatzky and Hood, 1975) so that both high resolution total field and vertical gradient data are obtained. To date 184 high resolution aeromagnetic maps have been published for New Brunswick, Quebec, and Ontario.

High Resolution Aeromagnetic Data

High resolution total field aeromagnetic maps are similar in many respects to the standard low sensitivity (± 10 gammas) maps published by the Geological Survey of Canada (Ready and Hood, 1975) and (Fig. 3, Hood, 1976). The high resolution data are compiled by computer with more stringent controls than was previously practical with manual compilation techniques. This permits contouring data with a much smaller contour interval with the result that more meaningful geological information becomes apparent in low magnetic gradient map regions (*see* Fig. 2, Holroyd, 1974) than can be seen on standard sensitivity maps. In addition, because of the lower noise level in high resolution data it is possible to produce superior quality high frequency enhanced maps, e.g. vertical derivative, than can be obtained using standard sensitivity aeromagnetic data. The vertical derivation process, when applied to a total field aeromagnetic map, yields a derived map on which magnetic anomalies caused by near surface geology are emphasized whereas anomalies resulting from deeper magnetic sources are suppressed. Hence, the smaller scale magnetic anomaly map patterns become more obvious because they are removed from the masking effect of the longer wavelength anomalies, consequently making high resolution data a more useful tool to support detailed as opposed to regional geological mapping programs than are standard sensitivity magnetic maps.

Figure 3.1 (map 20161 G) is one of 60 high resolution total field aeromagnetic maps published for the province of New Brunswick. It was produced using the Aeromagnetic Data Automatic Mapping (ADAM) system developed by Holroyd (1974), and plotted on a Calcomp drum plotter using the General Purpose Contouring Program supplied by California Computer Products of Anaheim, California. The contour interval is 5 gammas. The survey lines were flown in a north-south direction at an altitude of 460 m above sea level using a line spacing of 460 m. The sampling interval was 0.5 seconds which, depending upon ambient wind direction and velocity, corresponds to a sampling distance in a range between 30 and 45 m. Double control lines used for levelling the survey data were flown in an east-west direction approximately every 8 km.

The area represented by Figure 3.1 is primarily composed of complexly folded and faulted Ordovician sedimentary and metasedimentary rocks with some basaltic lavas and interlayered cherts (Fig. 3.2). The basement rocks are overlain by flat lying Pennsylvanian sandstone, siltstone and conglomerate in the southeastern corner of the region. The dominant structural trend over the map region and surrounding area is northeast. The prominent magnetic anomalies in the southwestern part of Figure 3.1 are probably caused by the basaltic lava-chert sequence, most likely by magnetite-bearing cherts (Dawson, 1956). The large magnetic anomaly covering most of the northeast quadrant of Figure 3.1 would appear to be caused by an intra-basement feature such as a weakly magnetic intrusion. Dawson (1956) has suggested on the basis of geological evidence that a granitic intrusion may underlie this region. The magnetic trend extending in a southwesterly direction from the centre of the eastern edge of Figure 3.1 is part of a lineament associated with the southwestern extension of the Caraquet dyke (Burke, *et al.*, 1973) of Triassic age. The approximate position of the dyke is shown in Figure 3.2.

Figure 3.3 is a vertical derivative map of the total field magnetic data illustrated in Figure 3.1. A two-dimensional digital operator similar to that published by McGrath (1975) was used except that the cutoff frequency employed in the design of the operator was 0.25 cycles per sampling interval with a roll-off length of 0.1 cycles per sampling interval. The filter operator was convolved with the total field aeromagnetic data which had previously been gridded by the ADAM system with a 62.5 m cell size. The contour interval is 0.025 gammas per metre, the areas of positive gradient being contoured using contours with the longer dash.

Two problems occur in Figure 3.3 which tend to degrade the visual impact of the geologically important information, and which are not apparent in Figure 3.1. First, a marked east-west hash is seen on contours in the lower gradient areas such as the north-central region of Figure 3.3. This noise occurs as a result of the one-dimensional cubic spline used in the gridding

From: Report of Activities, Part C;
Geol. Surv. Can., Paper 76-1C (1976).

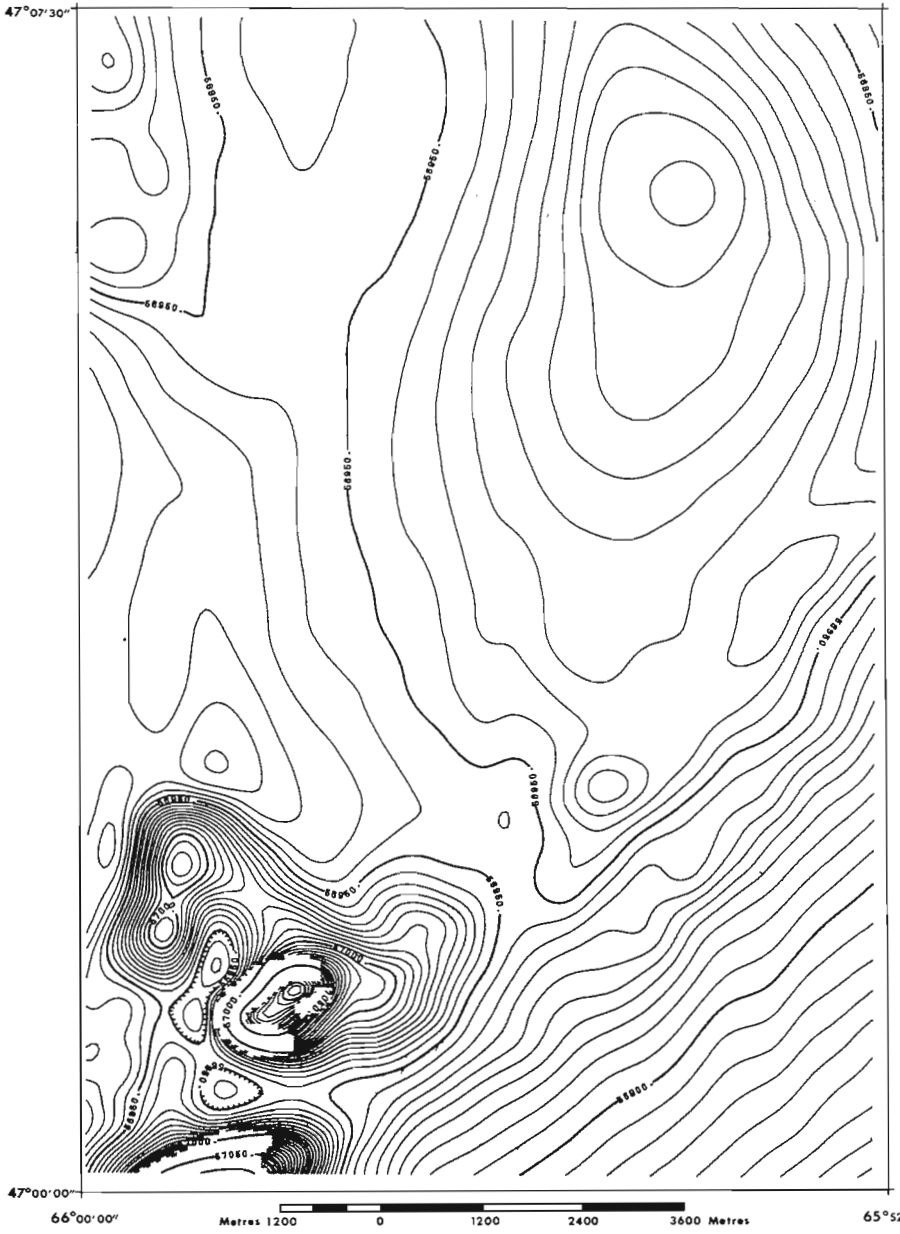

Figure 3.1. High resolution total field aeromagnetic map.

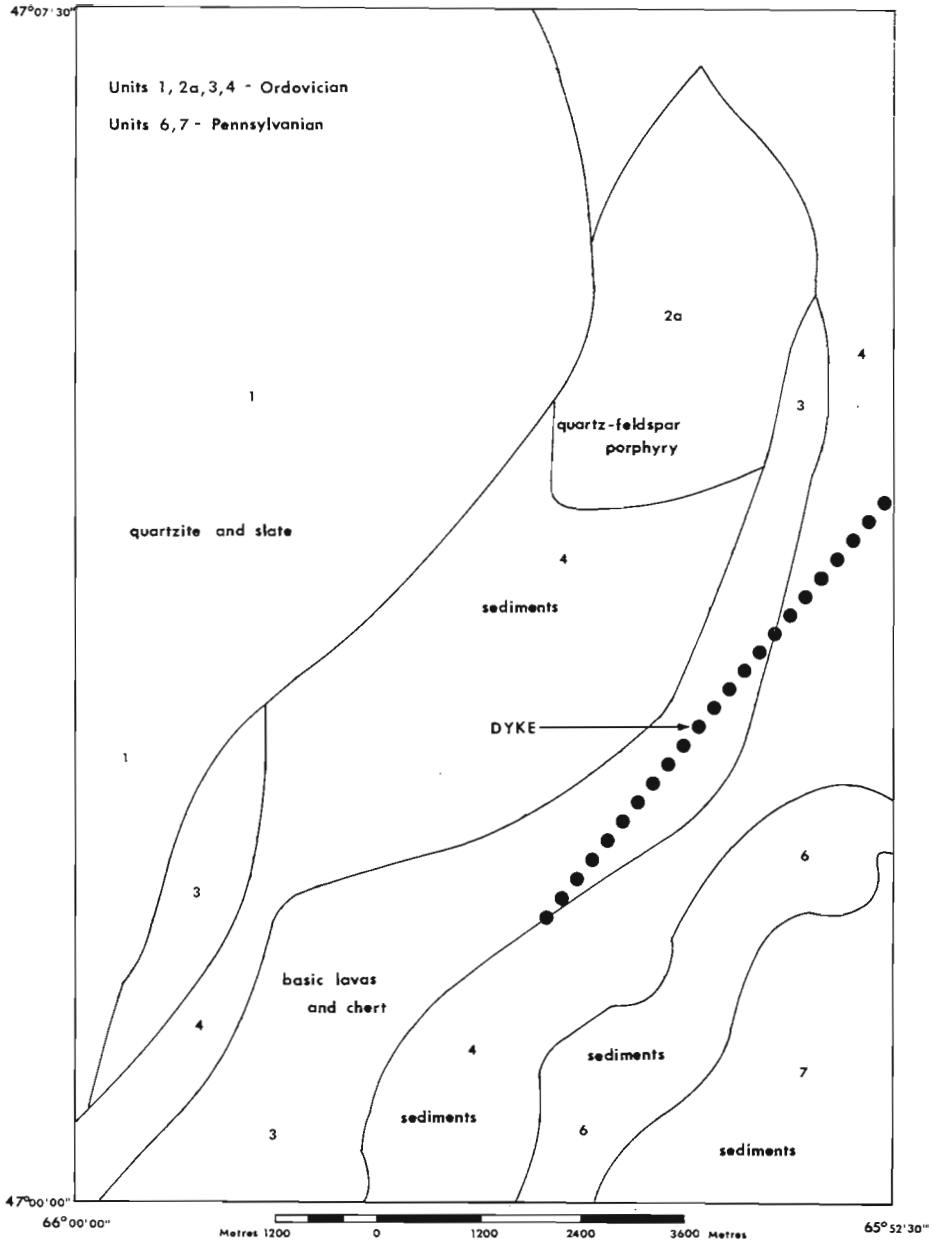

Figure 3.2. Portion of map 102A (*after* Dawson 1956).

process by the ADAM system in which the aeromagnetic survey line data are interpolated onto a rectilinear grid for the purposes of contouring. This problem is probably not unique to the ADAM system but related to any gridding scheme which utilizes a double application of a one-dimensional interpolation operator. A second problem in Figure 3.3. is the appearance of many elongated anomalies which tend to parallel the north-south flight line direction. These anomalies are caused by the presence of residual levelling errors in the original total field aeromagnetic data (Fig. 3.1) which are themselves the result of an imperfect levelling procedure. The success or failure of the present levelling method (Holroyd, 1974) revolves around obtaining accurate intersections between the survey line data (north-south) and the control line data (east-west). Most often, problems occur where the flight lines intersect at different altitudes in areas of high magnetic gradient. Analysis of this problem seems to indicate that a different approach is necessary in order to reduce the residual levelling errors to a point where they are no longer a disturbing influence on high frequency enhanced maps. It may be noted that the residual levelling errors tend to be long wavelength features in the direction of the survey lines, whereas perpendicular to these same lines they possess a much shorter wavelength. In the present case, they tend to have a fundamental wavelength of double the control line spacing (16 km) in the direction of the survey lines and of double the survey line spacing (920 m) perpendicular to the survey lines. Using digital filter operators, a method of preconditioning the total field aeromagnetic data has been developed which exploits the characteristic shape of the residual levelling errors in order to reduce their magnitude.

Derivation of First Vertical Derivative Magnetic Maps

After completion of the flight path recovery and levelling of the survey lines by the ADAM system using the double control lines, the flight line data are interpolated to a regular interval (40 m) along each of the survey lines to overcome sampling variations due to changes in the speed of the survey aircraft. Then a least squares, best fit quadratic line is removed from each survey line in order to reduce the effects of trends in the aeromagnetic data. The root mean square value of the residual survey line data is calculated for every line. Any residuals which exceed three times the root mean square value of a given survey line are replaced with a zero value. On the average 3 to 10 per cent of the residuals are screened out in this manner. The purpose of the screening is to reduce the magnitude of the low frequency components of large amplitude but small areal extent local anomalies being passed by the one-dimensional low pass filter operator which is applied to the data subsequent to the screening routine. After screening, the survey data is extended at each end of the flight line using a prediction error operator based on the maximum entropy method, developed by Burg (1968). The computer program for the prediction was obtained from a thesis by Phillips (1975). Ten aeromagnetic values on each end of the survey line, which are never altered by the screening routine, are used to calculate two sets of predictor operator weights, one set for each end of the survey line. Employing these weights the survey line data is extended by convolution a total of 168 magnetic values, 84 points at each end of the survey line. The total length of the extensions is equal to the length of the filter operator which is applied to the data in the following operation. In this manner the original survey line length is maintained during the filtering process.

The next step involves the convolution of the extended survey line data with a 169 point one-dimensional low pass filter operator in order to remove local magnetic anomalies from the data. The operator weights were obtained from an inverse Fourier transform of an ideal filter response curve which consisted of a cosine bell roll-off between zero and 0.015 cycles per sampling interval, and equal to zero at higher spatial frequencies. The output from the convolution procedure is combined with the quadratic line which was previously removed from each of the survey lines, and the resultant data are gridded using the ADAM system. Figure 3.4 is a contoured version of a portion of these data and represents the longer wavelength information contained in the total field aeromagnetic data illustrated in Figure 3.1. The contour interval is five gammas. Note the presence of the residual levelling errors in Figure 3.4 which are indicated by herringbone on the contours. Note also in the same figure in the southwest corner that some low frequency components of the prominent local magnetic anomalies seen in Figure 3.1 in this region have been passed by the filter operator. There seems to be no way of completely preventing this leakage, in fact much larger amplitude anomalies occur in this region when an equivalent high pass operator was tested. In the latter case the output from the high pass operator is subtracted from the original aeromagnetic survey line data. However, because no screening is possible in this case, much larger low frequency components appear in the resultant regional plus residual levelling error data.

Figure 3.5 is a residual total field magnetic map which represents the remainder of the total field shown in Figure 3.1 after the removal of the regional plus levelling error data (Fig. 3.4). Note the apparent absence of any significant levelling errors in Figure 3.5.

Figure 3.6 is a regional magnetic map from which most of the residual levelling errors have been removed. It was derived from the data illustrated in Figure 3.4 by convolving the data along each east-west grid line with a one-dimensional low pass operator. This was accomplished by first removing a linear trend from each grid line, by extending the grid line as was done previously with the survey line data, by convolving the extended line with a 169-point one-dimensional low pass operator, and then adding the original linear trend to the output of the filter operator. The filter operator was designed with a cut-off of 0.015 cycles per sampling interval and a cosine bell roll-off of 0.015 cycles per sampling interval. Since the residual levelling errors tend to have a higher frequency in the east-west

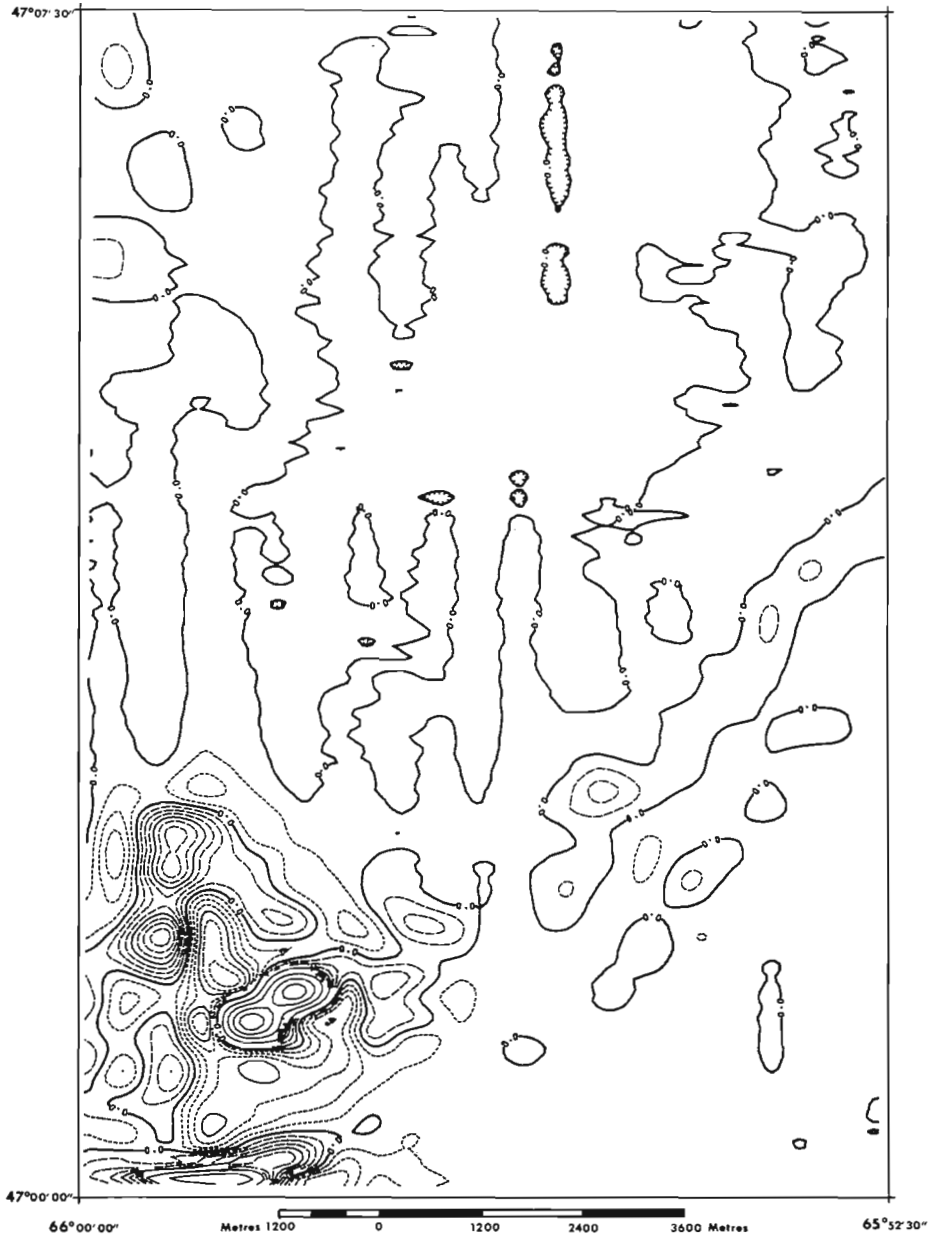

Figure 3. 3. First vertical derivative map of Figure 3. 1.

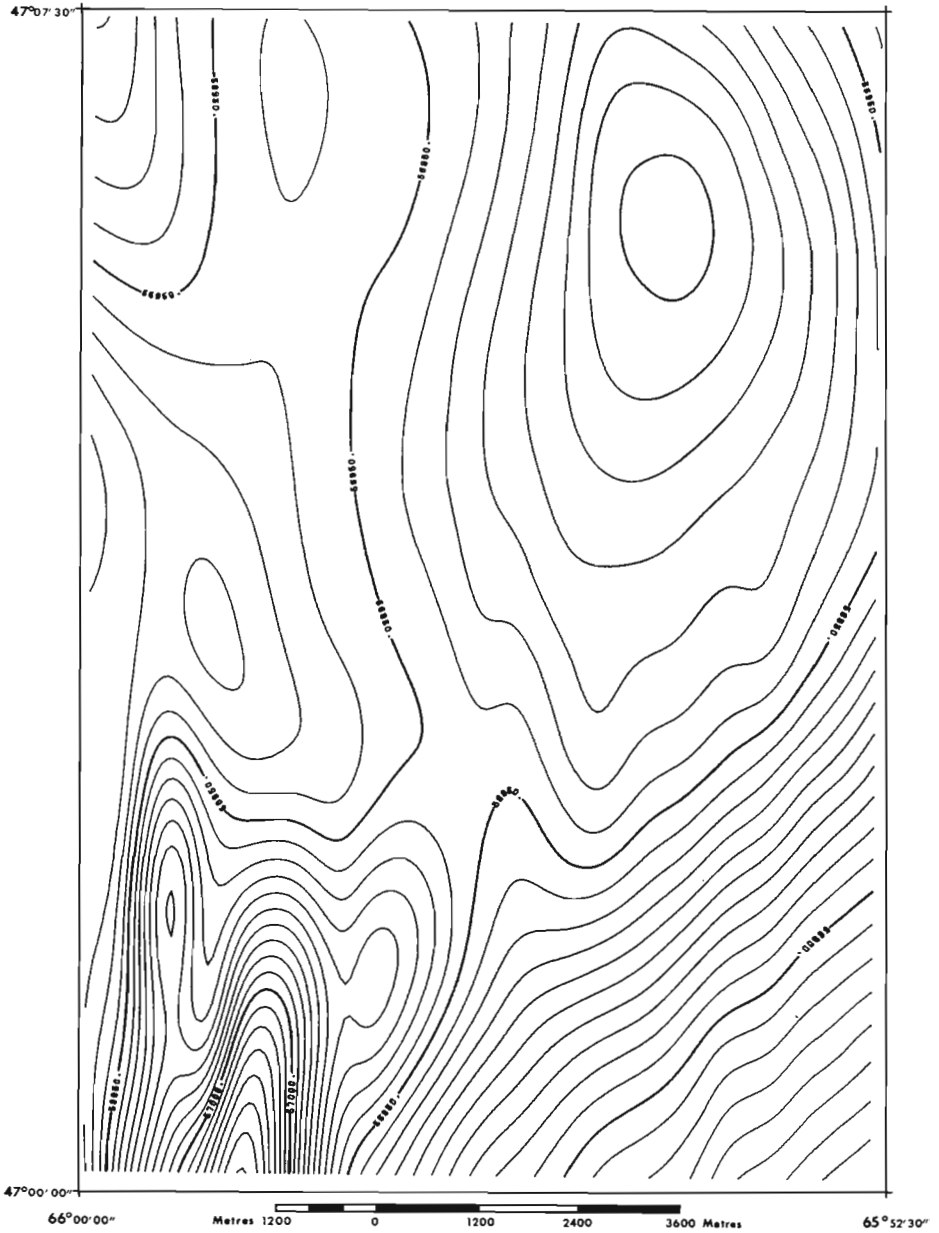

Figure 3. 4. Regional magnetic field removed from Figure 3. 1.

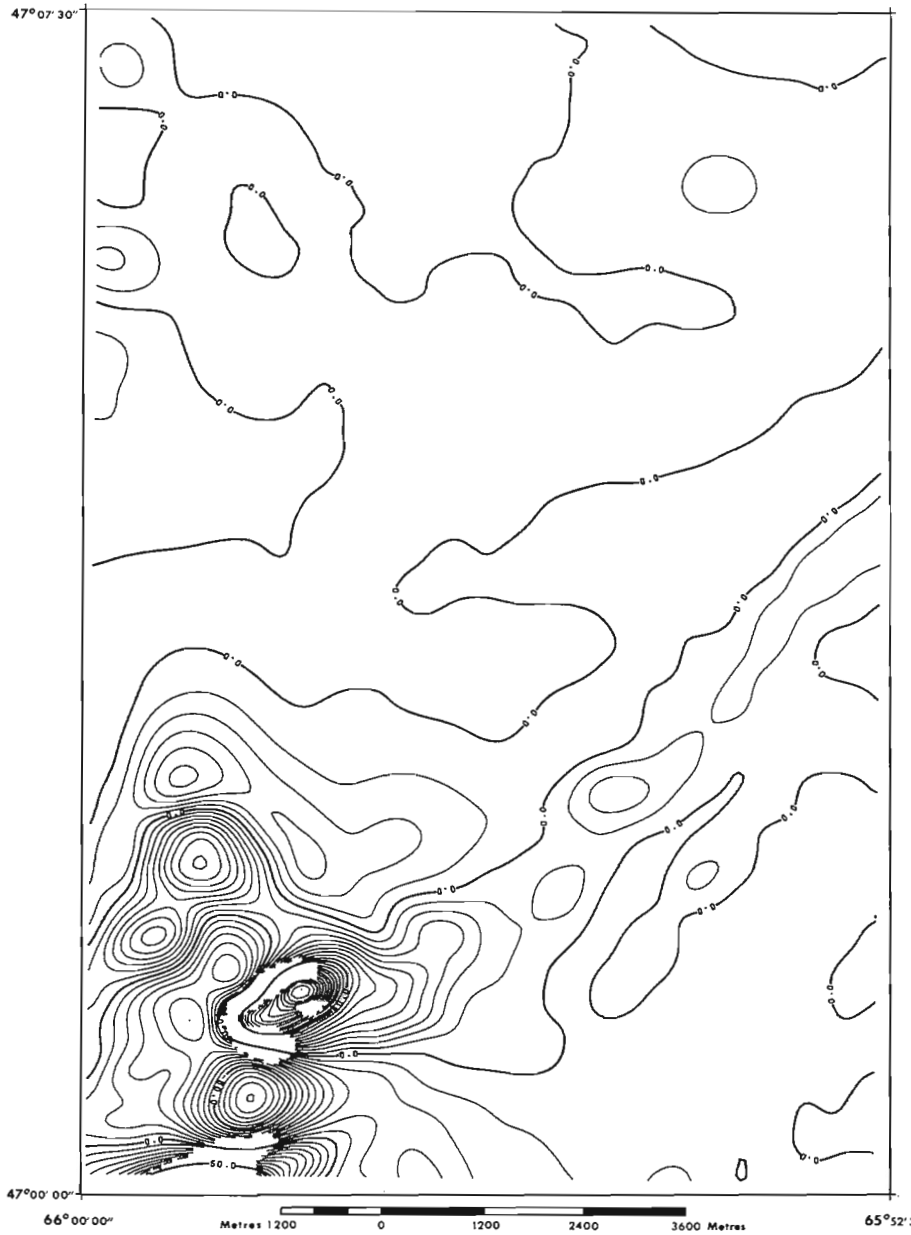

Figure 3.5. Residual magnetic field removed from Figure 3.1.

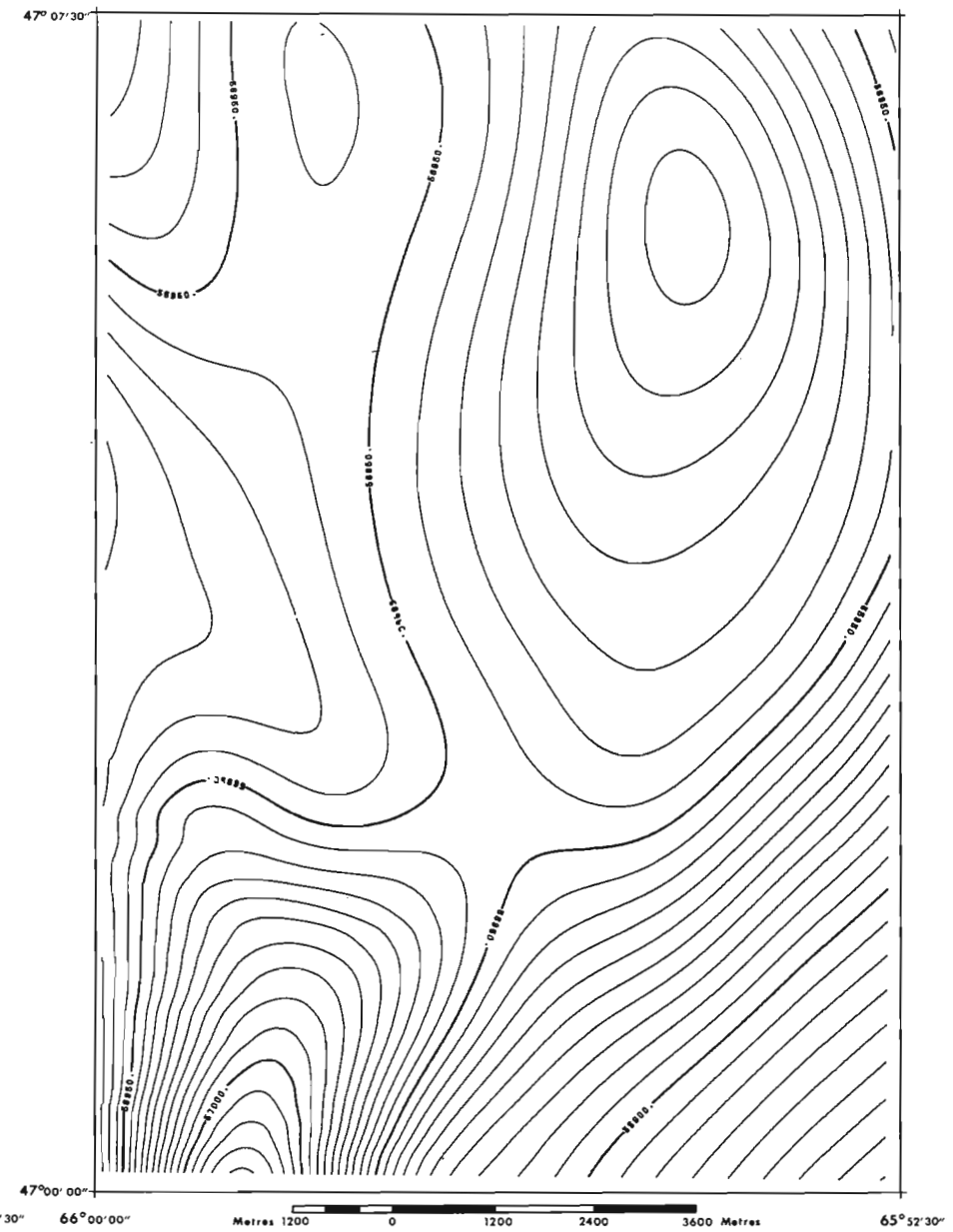

Figure 3.6. Filtered version of Figure 3.3.

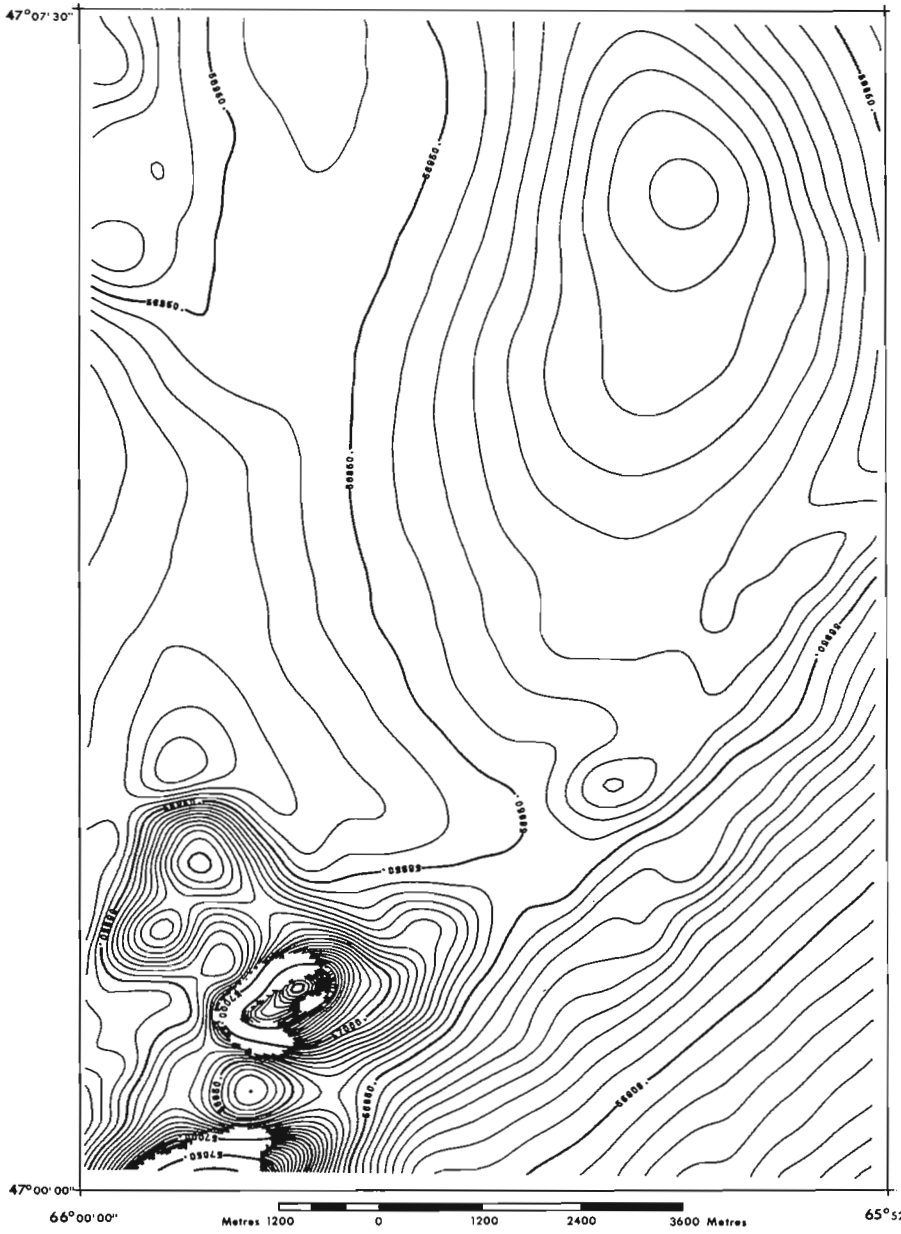

Figure 3.7. Combined data of Figures 3.4 and 3.5.

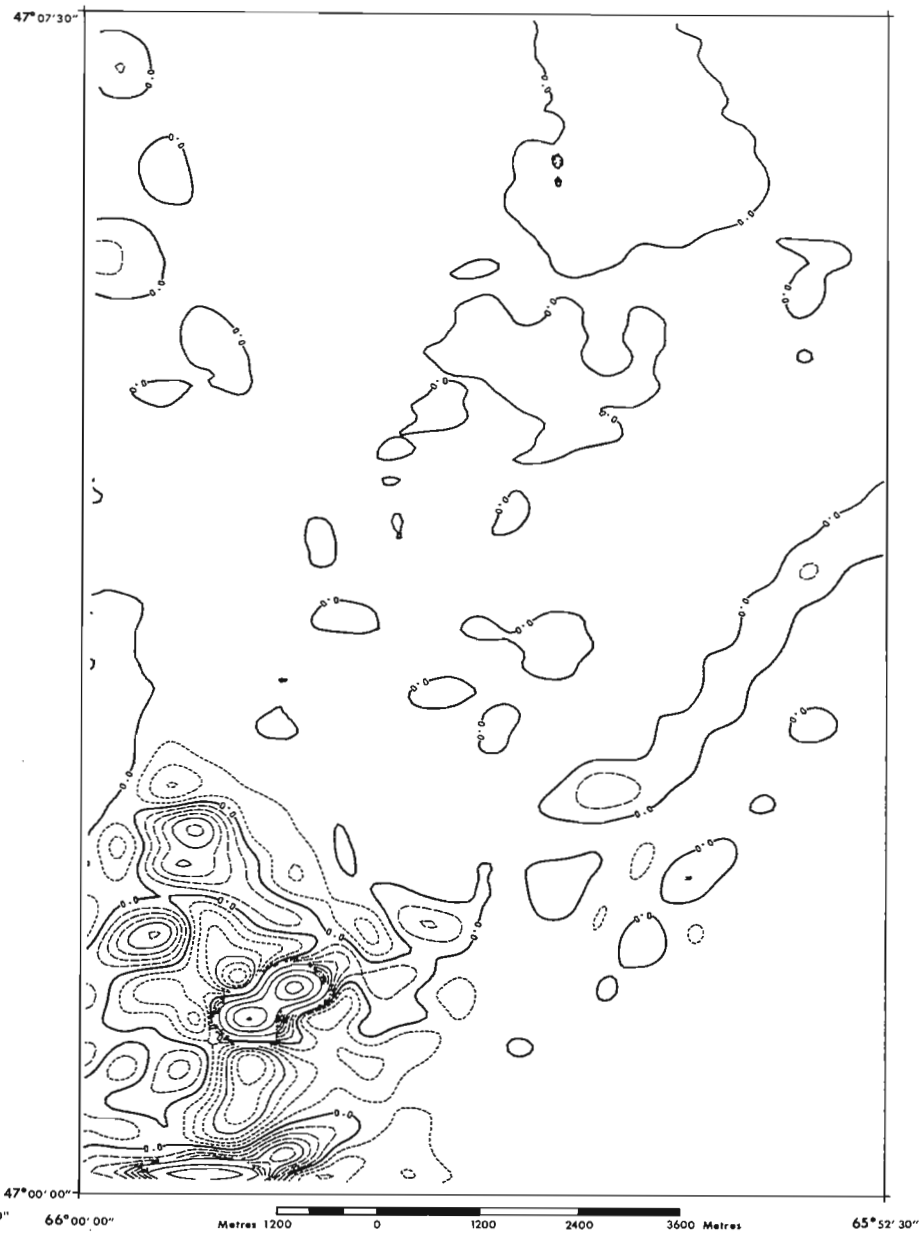

Figure 3.8. First vertical derivative map of Figure 3.6.

Figure 3.9. Summary of operations on aeromagnetic data.

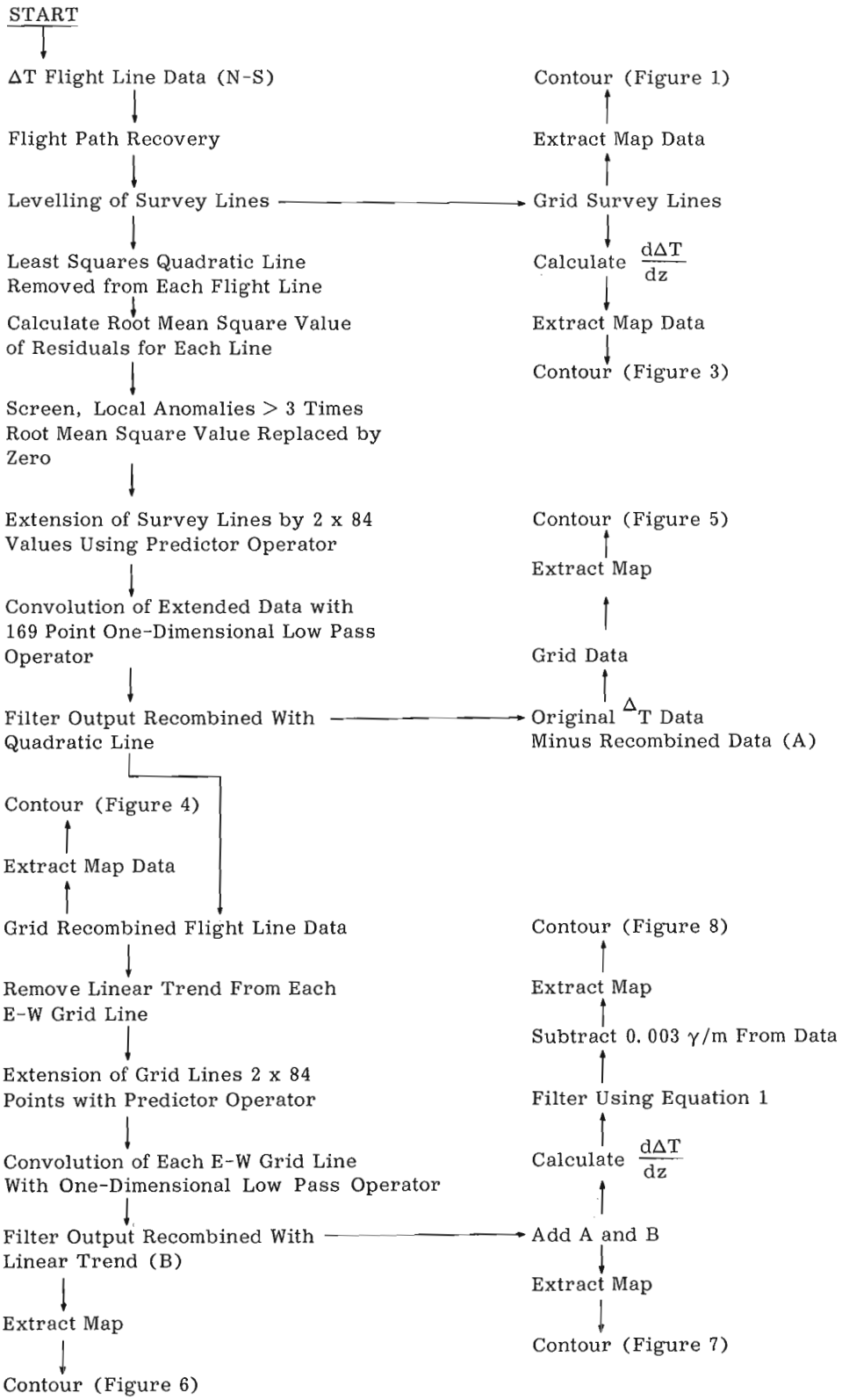

direction and a lower frequency in the north-south direction, they are removed more effectively by using a one-dimensional low pass operator applied to the east-west grid lines as opposed to using a two-dimensional low pass operator. Also the computation time required for processing the map using a one-dimensional 169-point operator is much less than would be required to process the same map using an $(169)^2$ point two-dimensional operator. However, the application of a one-dimensional filter in this manner to map data results in the introduction of noise of a wavelength similar to the grid line spacing. This noise is removed using the following two-dimensional 17-point smoothing operator,

$$F_o(x,y) = \frac{1}{259}\left[55\,F_i(x,y) + 42\,S_1 + 29S_{\sqrt{2}} - 10S_{\sqrt{5}}\right] \quad \ldots (1)$$

where $F_o(x,y)$ = the filtered magnetic value for $F_i(x,y)$,

$F_i(x,y)$ = the gridded map data,

S_r = the sum of the map data falling on circles of radius r centred at $F_i(x,y)$, where r is in sampling units.

Finally, the residual total field data (Fig. 3.5) and the filtered regional magnetic data (Fig. 3.6) are combined to yield a new total field aeromagnetic map (Fig. 3.7) similar to that illustrated in Fig. 3.1. In Figure 3.6 the residual levelling errors are much less than are found in the data used to construct Figure 3.1. This can be shown by calculating a vertical derivative map (Fig. 3.8) of Figure 3.7 and by comparing it with Figure 3.3. The contour interval for Figure 3.8 is 0.025 gammas per metre. Before contouring, 0.003 gammas per metre was subtracted from the data in order to shift the zero contour away from system noise which may become apparent in low gradient areas. Also, the vertical derivative data was filtered using equation 1 in order to reduce the east-west trending noise caused by the cubic spline interpolation when the data was gridded by the ADAM system.

Figure 3.8 represents probably as good an improvement in resolution as is both practical and necessary for high resolution total field aeromagnetic survey data obtained at a flight altitude of approximately 300 m above ground level. Marginal improvements in resolution are obtained using for example, higher order vertical derivatives or downward continuation (Kornik *et al.*, 1975), however, in these cases noise is also enhanced which decreases the coherency of the data as well as increasing the difficulties in contouring the data into map form. Hence Figure 3.7 contains the smallest scale geological information that can be derived from the high resolution aeromagnetic data shown in Figure 3.8.

In comparing Figures 3.1, 3.5 and 3.8 it is obvious that different scales of geological information are expressed on each of these maps. The large areal extent magnetic anomaly located in the northeast quadrant of Figure 3.1 does not appear in Figures 3.5 and 3.8. Notice, however, in Figures 3.5 and 3.8 that there are two northeast linear trends in the southeastern region of the figures which suggests the presence of two dykes rather than a single dyke as is apparent in Figure 3.7. Notice also in comparing Figures 3.5 and 3.8 that the magnetic anomalies in Figure 3.8 have a smaller areal extent, which is probably more representative of the true extent of the causative bodies. This is specially evident in areas of high amplitude local anomalies, and greatly improves the resolution in this type of area.

Summary and Conclusions

A procedure for producing good quality, first vertical derivative maps has been presented. Using digital filters the residual levelling errors contained in high resolution aeromagnetic maps have been reduced to a degree where they are no longer an adverse influence to high frequency enhancement. A summary of the sequence of operations is illustrated in Figure 3.9.

It has been shown also that no one particular type of magnetic map can be considered as most useful in support of a geological mapping program. It has been our experience that a set of three maps is most helpful for this purpose. These three types of maps are, the total field map (Fig. 3.7), the residual total field map (Fig. 3.5), and finally the first vertical derivative map (Fig. 3.8).

References

Burg, J.P.
1968: A new analysis technique for time series data; paper presented at NATO Advanced Study Institute on Signal Processing, Enschede, Netherlands.

Burke, K.B.S., Hamilton, J.B., and Gupta, V.
1973: The Caraquet dyke: Its tectonic significance; Can. J. Earth Sci., v. 10, no. 12, p. 1760-1768.

Dawson, K.R.
1956: Sevogle; Geol. Surv. Can., Map 1092A.

Holroyd, M.T.
1974: The aeromagnetic data automatic mapping (ADAM) system; *in* Geol. Surv. of Can., Paper 74-60, p. 71-76.

Hood, P.J. and Sawatzky, P.
1971: High resolution aeromagnetic survey of the St. Mary's river graben, Nova Scotia; *in* Report of Activities, Part A, Geol. Surv. Can., Paper 71-1A, p. 51-52.

Hood, P.J.
1976: Mineral exploration trends and developments in 1975; Can. Min. J. v. 97, no. 2, p. 163-197.

Kornik, L.J., McGrath, P.H., Holroyd, M.T., and Hood, P.J.
1975: Evaluation of high resolution aeromagnetic survey data over a test range in the Timmins area, Ontario; *in* Report of Activities, Part B, Geol. Surv. Can., Paper 75-1B, p. 23-38.

McGrath, P.H.
1975: A two-dimensional first vertical derivative operator; *in* Report of Activities, Part A, Geol. Surv. Can., Paper 75-1A, p. 107-108.

Phillips, J.D.
1975: Statistical analysis of magnetic profiles and geomagnetic reversal sequences; Ph.D. thesis, Stanford Univ., California, 134 p.

Ready, E. and Hood, P.J.
1975: Contract aeromagnetic surveys; *in* Report of Activities, Part A, Geol. Surv. Can., Paper 75-1A, p. 129-132.

Sawatzky, P. and Hood, P.J.
1972: High resolution aeromagnetic surveys: 1971; *in* Report of Activities, Part A, Geol. Surv. Can., Paper 72-1A, p. 58-60.

Sawatzky, P., Olson, D.G., and Hood, P.J.
1973: Experimental high-resolution aeromagnetic surveys: 1972; *in* Report of Activities, Part A, Geol. Surv. Can., Paper 73-1A, p. 95-97.

Sawatzky, P., Olson, D.G., Dicaire, A., and Hood, P.J.
1974: Experimental high resolution aeromagnetic surveys: 1973; *in* Report of Activities, Part A, Geol. Surv. Can., Paper 74-1A, p. 95-98.

Sawatzky, P. and Hood, P.J.
1975: Fabrication of an inboard digital-recording vertical gradiometer system for aeromagnetic surveying, a progress report; *in* Report of Activities, Part A, Geol. Surv. of Can., Paper 75-1A, p. 139-140.

4. DISTRIBUTION OF FORAMINIFERA IN CHALEUR BAY, NEW BRUNSWICK-QUEBEC

Project 730092

Charles T. Schafer
Atlantic Geoscience Centre, Dartmouth

Sediment Dynamics

Sediment textures and deposition patterns in Chaleur Bay are being analyzed as part of the long term foraminiferal ecology study in this estuarine-marginal marine environment.

Surface sediment textures range from gravelly sand to silty clays (textural description after Shepard, 1954). The silty clay facies is present in the central bay area east of Bonaventure below an average depth of 70 m (Fig. 4.1). This facies widens eastward and terminates near the mouth of the Bay. A clayey silt facies occurs immediately west of the silty clay and again in the western part of Chaleur Bay between Dalhousie, New Brunswick and New Richmond, Quebec. East of Bonaventure this facies is confined between the 60 to 72 m isobaths. West of New Richmond the clayey-silts are dominant at much shallower depths, usually between 8 and 32 m. The two "patches" of clayey silt are separated by a slightly coarser sand-silt-clay facies that has been deposited along the central axis of the Bay, and which is rather extensively distributed between Belledune and Bonaventure at water depths of 32 to 60 m. The deep water silty clay and the sand-silt-clay facies are comparable to the "sandy pelite" and the "very sandy pelite" described by Loring and Nota (1973). There appear to be only three bottom areas of the Bay that are characterized by sand facies. One of these is located near Bonaventure at a water depth of 16 to 40 m, the second occupies a relatively shallow environment (8-24 m) near Petit Rocher, New Brunswick and a third lies northwest of Miscou Island at a depth of about 32 m. Sandy silt facies are present along the coastline west of Belledune and north of Petit Rocher as well as at the mouth of the Cascapedia River near New Richmond. Much of the remainder of the Bay is covered by deposits of gravelly sand. These relatively coarse sediments extend offshore into the deeper parts of the Bay between Bathurst and Bonaventure. There is also an isolated occurrence of this material south of Port Daniel on the crest of the mid-bay topographic high at a water depth of 72 m.

The nature of sedimentary processes operating in the Bay was investigated by comparing the percentage values of 23 size fraction weights between -4ϕ and $+9\phi$ for all samples. This approach differs from the Shepard (1954) classification technique (i.e., Fig. 4.1) because it uses the entire grain size analysis to relate samples collected at different locations (*see* Klovan, 1966).

A cluster analysis technique (Parks, 1970) was used to compare samples. In this version of the method, factor score measurements are first calculated for each sample using Harman's short regression and square root method (Harman, 1960). A Q-mode (sample by sample) similarity matrix is then computed in which each sample is compared with every other sample (1, 2.... n). The similarity coefficient used here is the simple distance function (D) where

$$D_{1,2} = [\Sigma_{i=1}^{m} (X_{i_1} - X_{i_2})^2/M]^{\frac{1}{2}}$$

M is the total number of size fraction weights expressed in per cent and D varies from 0 (highest similarity) to 1 (highest dissimilarity). Samples were clustered using an unweighted pair-group method (Sokal and Sneath, 1963) and, in this instance, 5 distinct sediment types were defined at the D = 0.1 level (Fig. 4.2). Type 1 is represented by 56 samples and, east of Bonaventure, is confined to water depths greater than 60 m. The type 1 sediment contains relatively large amounts of material in the coarse to fine silt range. On the average, coarse sand and pebbles comprise less than 1 per cent of the total sample weight. Type 1 sediment also occurs in relatively shallow water west of Belledune. The western facies differs from that noted in the eastern part of the Bay in terms of a slight decrease in the abundance of pebble-size particles and by the complete absence of particles larger than -4ϕ. In addition, the proportion of particles in the coarse to fine silt sizes in the western facies is slightly higher (about 5%) while clay-sized material ($>8\phi$) is reduced by about 5 to 15 per cent compared to that noted in the eastern facies.

Type 2 sediment is represented by 96 samples and is characterized by a sediment size histogram that is bimodal. Abundance peaks occur in the 0 to 1.5ϕ and in the 3.5 to 6ϕ size range. There is a general decrease in the relative abundance of particles in the 1 and 2.5ϕ (0.2-0.5 mm), the 6 to 9ϕ (0.015-0.002 mm) size range and of particles larger than 1.5ϕ (2.8 mm). Particles finer than 9ϕ (medium clay-sized and finer particles) represent about 15 per cent of the total sample weight compared to 28 per cent in type 1 sediments. In the central part of the Bay the type 2 sediment is usually confined to water depths of 32 to 60 m. It occurs at considerably shallower depths (i.e., 2-24 m) in western Chaleur Bay.

Sediment type 3 is represented by 79 samples most of which were collected in relatively shallow water. The grain size distribution of particles is also polymodal with modes in the pebble, medium sand to coarse silt, and clay sizes. The sediment is deficient in 0.7 to 1.4 mm (0.5 to 0.5ϕ) and 0.03 to 0.002 mm (5.0 to 9.0ϕ) diameter particles. Type 3 sediments are usually confined to water depths less than 60 m but were also observed at about 70 m off Miscou Island at the eastern end of the Bay.

Type 4 was found in 14 samples that are also characterized by a polymodal particle size distribution. Sediment particles are relatively abundant in the pebble

From: Report of Activities, Part C;
Geol. Surv. Can., Paper 76-1C (1976)

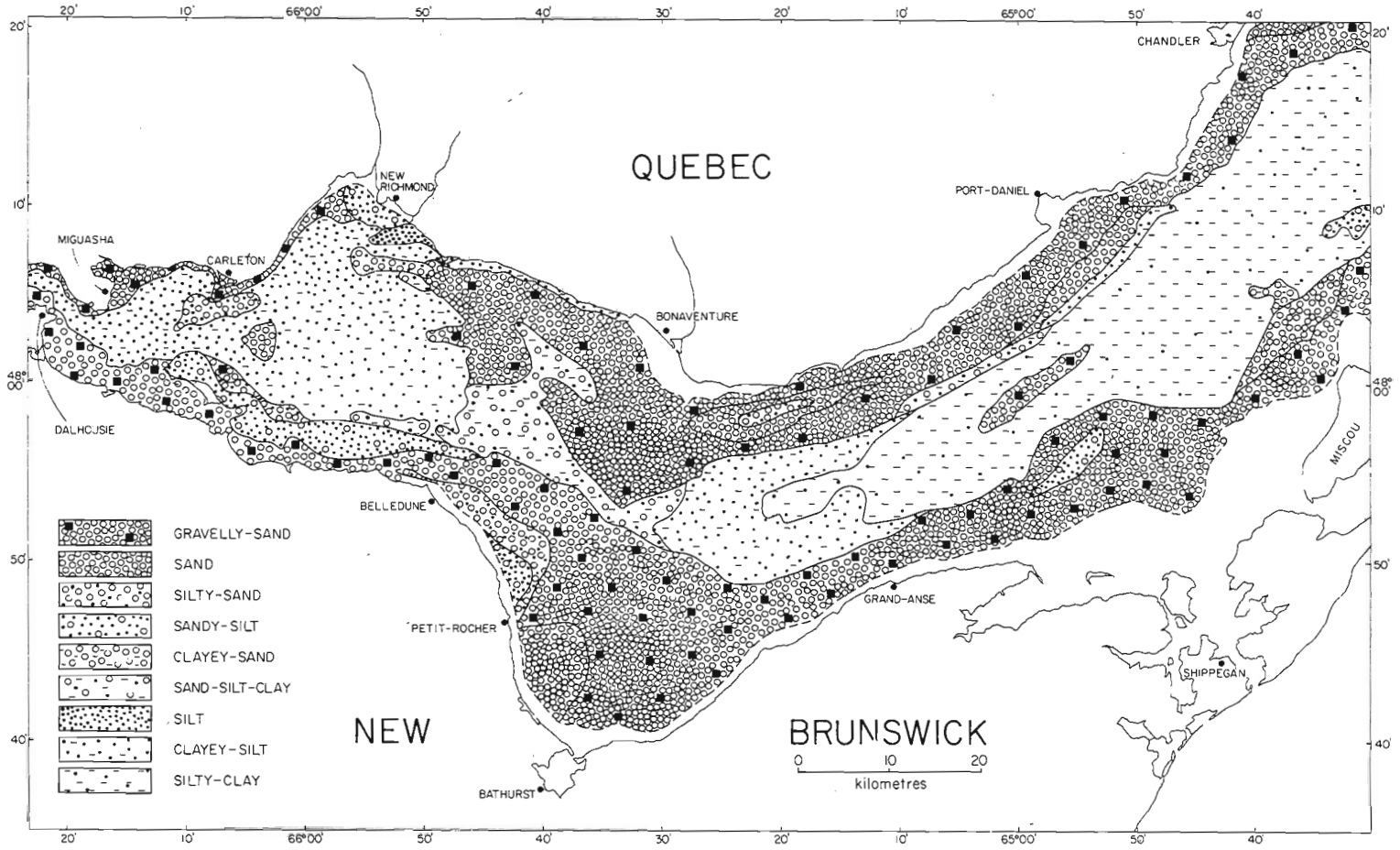

Figure 4.1. Textural characteristics and regional distribution of modern marine sediments in Chaleur Bay.

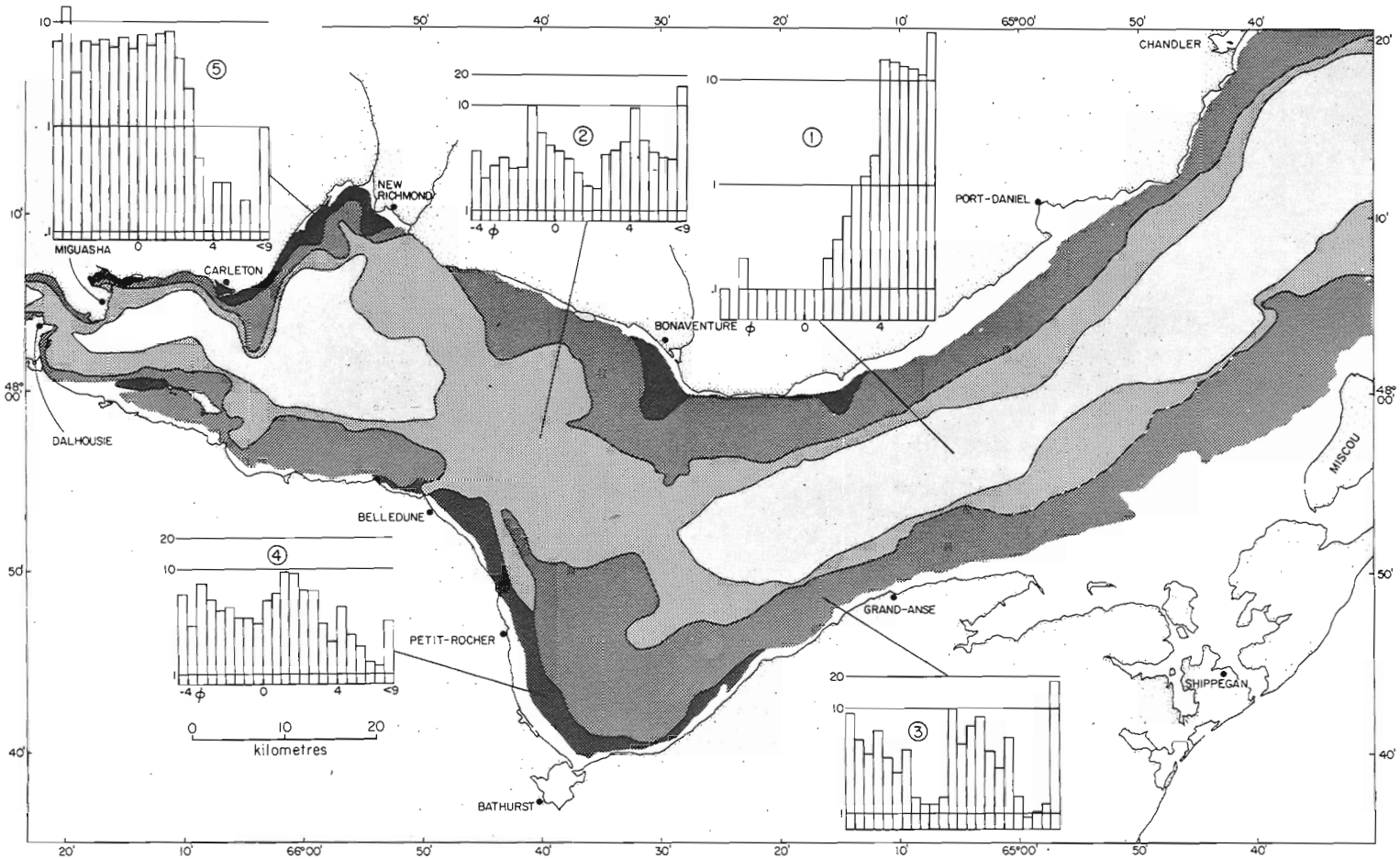

Figure 4. 2. Classification of sediment types in Chaleur Bay using cluster analysis. The class intervals in each histogram of a particular sediment type are averaged over all samples within each cluster group. The phi size classes represented are:

> -4.0	0.0 to -0.5	3.0 to 3.5
-3.5 to -4.0	0.0 to 0.5	3.5 to 4.0
-3.0 to -3.5	0.5 to 1.0	4.0 to 5.0
-2.5 to -3.0	1.0 to 1.5	5.0 to 6.0
-2.0 to -2.5	1.5 to 2.0	6.0 to 7.0
-1.5 to -2.0	2.0 to 2.5	7.0 to 8.0
-1.0 to -1.5	2.5 to 3.0	8.0 to 9.0
-0.5 to -1.0		< 9.0

and medium sand size ranges. There is a significant decrease in 0. 015 to 0. 002 mm diameter particles. Type 4 sediment is associated with shallow nearshore environments that are usually less than 16 m deep.

There are only two samples comprising type 5 sediments. Their size distribution reflects a relatively high abundance of particles larger than medium sand that have been deposited in water depths less than 8 m.

The general pattern of sedimentation in Chaleur Bay reflects the Holocene rise in sea level with increased deposition of relatively fine sediments in the deeper and/or protected parts of the Bay. These fines are well represented in the western part of the Bay, where they presumably overlie relatively coarse sediments, and have begun to infill the ancient Restigouche river channel. The coarser sand-silt-clay and gravelly sand sediments (Types 2 and 3 in Fig. 4. 2) lying in the Bay between Bathurst and Bonaventure may represent reworked relect deposits that have been modified to their present texture by wave turbulence. Eroded material derived from these sediments is probably redeposited at either of the type 1 sediment locations depending on tidal current conditions.

The type 2 sediment is deficient in particles in the 0. 2 to 0. 5 mm range. According to Reddy (1968) waves having a period of 5 seconds and a height of about 2. 1 m are common in the area of the Bay underlain by this sediment and, depending on wind direction, may have periods reaching 9 seconds. According to the equations of Komar and Miller (1975) the orbital velocities of a 5 second wave would be able to erode quartz particles of 0. 4 mm diameter to a water depth of 16 m and particles of 0. 005 mm diameter to a water depth of 25 m. Larger waves in the 7 to 8 second range and with heights of about 4. 9 m, which also occur in the Bay (Reddy, 1968), would erode the same diameter particles in water depths of 44 and 68 m, respectively. The latter depth exceeds the maximum water depth in which the type 2 sediments occur and could thus account for its observed distribution.

Type 3 sediments are deficient in relatively coarse diameter particles in the 0. 7 to 1. 4 mm range. Particles of about 1. 0 mm diameter can be eroded in water depths of 37 m by the 8 second wave described earlier and type 3 sediment extends to about this depth (40 m) near Bathurst. The shift in modes in the type 3 sediment towards coarser size ranges is probably due to increased wave energy at comparatively shallower depths.

There are other indications that the gravelly-sand (type 3) sediments have been reworked by waves and that they comprise material derived from underlying sediments. For example, they extend bayward into water depths of up to 40 m near Bathurst while sediments to the east and west of this area are relatively fine at comparable depths. The gravelly sands also tend to be very poorly sorted (classification after Folk and Ward, 1957), the sorting coefficients being usually greater than 4ϕ. This feature may be related to both the inherent textural characteristics of the modern sediments and to mixing of modern and older sediments during sampling operations. Grab samples from this area often include modern coarse sediments and an older glaciomarine material characterized by its relatively high content of clay-sized particles compared to deeper off-shore deposits of modern sediment (i. e., type 2 sediment). Observations by divers at a depth of 13 m in central Nepisiquit Bay also indicate that the bottom in this area is composed of two differing sediment types including a "clean fine gravel and sand layer overlying fairly firm brown mud" (Eaton, 1975). Echograms recorded in this area of the Bay show a strong shallow undulating subbottom reflector which often penetrates a thin veneer of overlying sediment. This reflector apparently represents the glaciomarine material that was probably partially eroded during a lower stand of sea level 6000 to 8000 years ago.

It is evident from the grain size data that, except for the clayey-silt and silty-clay facies, sediments in most parts of the Bay are being reworked to some degree by wave turbulence. This reworking is most evident in the central part of the Bay because of rapid shoaling, and because this part of the Bay is well exposed to swell from the Gulf of St. Lawrence. Observations of total suspended particulate matter concentrations in western Chaleur Bay (Cranston *et al.*, 1974) suggest that, during calm weather, suspended particulate matter discharged by the Restigouche River is initially deposited in areas and at depths from which it can be resuspended. Near Dalhousie the mean suspended particulate matter concentration during the spring season is 12. 5 mg/1, while between Dalhousie and Belledune, the mean suspended particulate matter drops to 5. 8. East of Belledune the mean suspended particulate matter concentration in surface water is only 3. 9 representing a 60 per cent decrease in concentration. Much of this material should reach the bottom in the central and eastern parts of the Bay but it is only evident in large quantities in the area delimited by the type 1 sediment. It is conspicuously absent in sediment types 4 and 5 which have been reworked in a comparatively high energy environment in which particles finer than medium sand usually represent less than 10 per cent of the total sample weight. Reddy (1968) notes that near Belledune rip currents are an important mechanism for transporting fine material from these comparatively shallow water environments into the main current circulation offshore.

References

Cranston, R. E., Fitzgerald, R. A., and Winters, G. V.
1974: Geochemical data: Baie des Chaleur; Bedford Inst. Oceanogr., Rep. BI-D-74-6, 22 p.

Eaton, P. B.
1975: A survey of the environmental implications of dredging and disposal of dredged material from Bathurst Harbour (Unpublished Report); Environment Canada, Ecological Effects Section, Atlantic Region, 12 p.

Folk, R. L. and Ward, W. C.
1957: Brazos River Bar: A study on the significance of grand size parameters; J. Sediment. Petrol., v. 27, p. 3-27.

Harman, H. H.
1960: Modern factor analysis; Univ. of Chicago Press, Chicago, 469 p.

Klovan, J. E.
1966: The use of factor analysis in determining depositional environments from grain size distributions; J. Sediment. Petrol., v. 36, p. 115.

Komar, P. D. and Miller, M. C.
1975: On the comparison between threshold of sediment motion under waves and unidirectional currents with a discussion of the practical evaluation of the threshold. J. Sediment. Petrol., v. 45, p. 362-368.

Loring, D. H. and Nota, D. G.
1973: Morphology and sediments of the Gulf of St. Lawrence; Fish. Res. Board Canada, Bull. 182, 147 p.

Parks, J. M.
1970: Fortran IV program for Q-mode cluster analysis on distance function with printed dendrogram; Kans. Geol. Surv., Computer Contr. 46, 32 p.

Reddy, M. P.
1968: Wave conditions and littoral drift near Belledune Point, Chaleur Bay. Bedford Inst. Oceanogr., Rep. 68-2, 6 p.

Shepard, F. P.
1954: Nomenclature based on sand-silt-clay ratios; J. Sediment. Petrol., v. 24, p. 151-158.

Sokal, R. R. and Sneath, P. H.
1963: Principles of numerical taxonomy; W. H. Freeman and Co., San Francisco, 359 p.

5. SEISMIC INSTRUMENT TESTS IN KUGMALLIT BAY, DISTRICT OF MACKENZIE

Project 750029

A. Overton, R. A. Burns, R. M. Gagne, and R. L. Good
Resource Geophysics and Geochemistry Division

Instrumentation has been acquired for the purpose of developing seismic techniques in difficult areas and also to improve seismic recording techniques in general. The principles underlying the development are described in another report by Overton (report 16; this pub.). The instrumentation provides the capability for magnetic recording of digital data, and stacking of repetitive observations for enhancement of signal to noise ratio. A preliminary test of the equipment was conducted during the spring of 1976 in Kugmallit Bay west of Tuktoyaktuk, District of Mackenzie. Simultaneous tests were conducted on electronic circuitry developed in the laboratory for radio transmission of the shot pulse waveform by frequency modulated carrier. This technique allows the recording of the shot pulse at the recording site simultaneously on the seismogram and its magnetic tape, thus simplifying deconvolution techniques between the source wavelet and the seismically transmitted signal. The frequency modulator and demodulator units were each constructed using the NE 565 integrated circuit in a phase locked loop as described by Jordan, (1974). A 700-m-long array of 24 equispaced 4.5 hz seismometers was set up on the shore-fast ice on the east bank of Kugmallit Bay. Shot points were spaced 7.5 km, 15 km, and 25 km north-northwest of the seismometer array. The territorial land use requirement limited the individual charge sizes to a maximum of 10 kg in shotholes drilled in the sea floor. Using the stacking capability of the instrument, aggregate charge sizes equivalent to 20, 30, 90, 100, and 200 kg of dynamite were simulated. The experiment served mainly to reveal some problems with ice noise, noise due to instrumental interreaction and some shortcomings of the stacking system. The latter two problems are being corrected in the laboratory prior to another test. The problem of ice noise required that the amplifier gain be set 54 to 60 db below its maximum capability. Thus 5 kg charges at 7.5 km were barely perceptible, while simulation of larger charges by stacking was hampered by the instrument problems and the large attenuation required by ice noise conditions. The tests should be continued after the instrument problems have been corrected. Since shorefast ice is notoriously noisy, the test location should allow the seismometer array to be placed on land with the shot points remaining in water. Further tests will probably take place in the spring of 1977.

References

Jordan, B. D.
1974: Simple f.m. modulator/demodulator for a magnetic tape recorder: Wireless World, v. 80, p. 29-30, March.

From: Report of Activities, Part C;
Geol. Surv. Can., Paper 76-1C (1976)

6. *IN SITU* ENVIRONMENTAL RESPONSES OF BENTHONIC FORAMINIFERA

Project 750042

Charles T. Schafer
Atlantic Geoscience Centre, Dartmouth

Transport and Recolonization of Foraminifera

Studies of nearshore foraminiferal distribution and their ecological significance have been based almost entirely on quasisynoptic data gathered over periods of days to years. Their suitability for analysis using numerical techniques such as cluster analysis is therefore dependent on an understanding of population stability in time and space. For example, in a cluster analysis of benthonic foraminifera in Broken Bay, New South Wales, (Albani and Johnson, 1975), the authors concluded that the more reliable descriptors of sub-environments are the relatively rare but widespread species compared to locally abundant forms. They recommended that any statistical analysis of foraminiferal populations in which biotopes are to be determined in nearshore marine environments should be based on total rather than living populations. This strategy tends to average out the short term temporal and spatial variations in species abundance that have been recognized elsewhere.

Research on spatial distribution patterns has been summarized by Murray (1973) who noted that little is known about the means of dispersal of foraminifera. Wave turbulence, ice, surface tension of seawater, rafting on submarine vegetation, and the inherent locomotive capabilities of species are among some of the mechanism that have been documented (Richter, 1965; Schafer and Prakash, 1968). Empty tests of foraminifera have also been reported from plankton tow samples (Murray, 1965). The equivalent diameters (i.e., the diameter of quartz grain having the same settling velocity) of certain common nearshore morphological types of foraminifera range between 0.10 and 0.14 mm (Haake, 1962; Grabert, 1971). They would thus be within the size range of most easily eroded particles (Shepard, 1963, p. 128), and therefore subject to continuous redistribution in nearshore environments.

This report describes the results of a quantitative *in situ* study of local spatial and temporal variability of a nearshore population of foraminifera that were eroded by wave-induced turbulence and redeposited on sterile sand substrates placed at a water depth of 13 m. Species occurrence and abundance are considered in terms of probable differences in their mobility and transportability with reference to observed physical pertubations. The results give some indication of typical spatial variability of the major species, recolonization rates, and of temporal changes in species abundance.

Environmental Setting

The experiment was conducted at a water depth of about 13 m in St. Georges Bay (Fig. 6.1). Seven stations were sampled in order to determine bathymetric distributions of major benthonic species in the area. The site is essentially a flat shelf covered by medium to fine sand. Typical bottom water temperature and salinity values in this area during the latter half of July 1975 were 13.5°C and 29.2 ‰ respectively. The bathymetric distribution of major species of benthonic foraminifera normal to the coastline is shown in Figure 6.2. Near station 6 the population is predominantly calcareous and includes species such as *Eliphidium icertum/clavatum* gp., *Protelphidium orbiculare* and *Ammonia beccarii*. The compound diversity (Margalef, 1968) of the total population is highest at station 5 (0.88) and averages about 0.72 at stations 6 and 7. Because of the dominance of *A. becarrii* and *Saccammina atlantica*, the mean diversity of stations 1 through 4 is slightly lower (0.64). The distribution of this assemblage is apparently temperature controlled

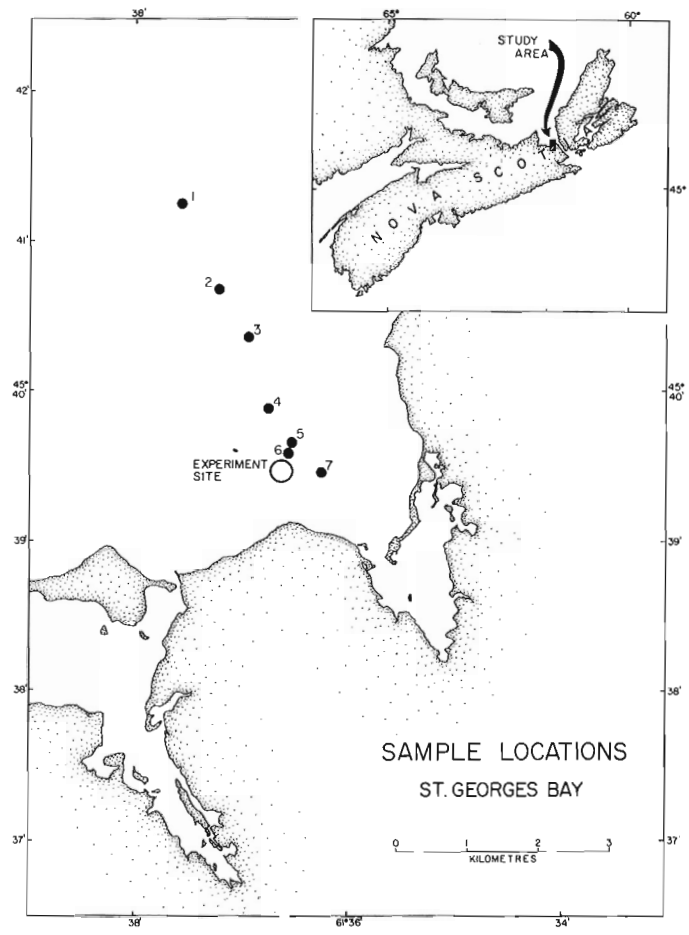

Figure 6.1. Locations of grab sample stations and the experimental site in St. Georges Bay, Nova Scotia.

From: Report of Activities, Part C;
Geol. Surv. Can., Paper 76-1C (1976)

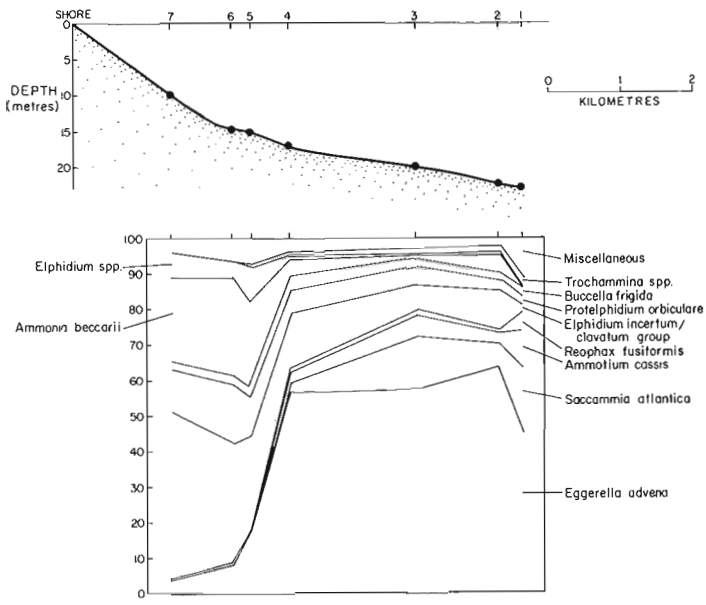

Figure 6.2. Distribution profile of diagnostic foraminifera species observed in grab samples.

and, in the case of *A. becarii*, is associated with summer bottom water temperatures that are usually 19°C or higher. Between 11 and 13 m the bottom water temperature in July drops to about 14°C. This rapid decrease is associated with an increase in the relative abundance of arenaceous species such as *Eggerella advena*, *Saccammina atlantica* and *Ammotium cassis*. The site of the experiment lies near the bayward limit of the dominantly calcareous assemblage.

Methods

A series of 0.5- by 0.5-m frames constructed from 2.5- by 2.5-cm angular aluminum were placed in a linear array at the experimental site at a distance of 0.2 m from each other. Clean quartz sand having a mean diameter of about 1.2 mm was poured onto the area bounded by each frame to a depth of about 3 cm. Two of the frames (subsample sets B and D) were underlain with aluminum foil to asses vertical mixing effects between the underlying sand substrate and the overlying layer of sterile sand. Each frame was subsampled once using five 6.6 cm ID short plastic cores (Fig. 6.3; Table 6.1). A time-lapse underwater television system (Schafer *et al.*, 1975) was used to record biological activity and major sedimentologic events. The material in each core was extruded in the laboratory using a plunger which was pressed into the bottom of each core thus forcing the sediment above the upper end of the tube. The material was sampled to a depth of about 1.5 cm below the upper surface of the sterile sand, transferred to a glass container, and fixed with buffered formalin (final pH 8.3). Samples were subsequently stained with Sudan Black according to the method of Walker *et al.* (1974), transferred to graduated cylinders to determine their total volume, sieved through a 62μ sieve, dried, floated in a bromoform-acetone solution (Gibson and Walker, 1967), dried again and counted. When possible at least 300 specimens were counted.

Living and total populations were compared between subsamples initially using an index of similarity (S) introduced by Berger and Soutar (1970) in which

$$S = \sum_{i=1}^{n} II_i Q_i / \sum_{i=1}^{n} (II_i/2 + Q_i/2)^2$$

II_i and Q_i are the proportions of the ith species in the two subsamples being compared. In this instance the four subsamples having the highest total population density were selected for each frame and compared to determine within-frame spatial variations. Temporal differences were analyzed by averaging specimen counts from the four subsamples and then comparing the composite samples between frames and between the seven control grab samples.

Water temperature and salinity were measured with an Autolab model 602 salinometer and wind velocities were recorded using a Meteorology Research Inc. model 1072 weather station.

Observations

Mean wind conditions are summarized in Table 6.2. During the period of the experiment winds originated primarily from the south and west with mean velocities ranging between 13 and 43 km h^{-1}. The relatively high mean velocities recorded before frame E was sampled (July 28) were due to a hurricane which passed through the area at this time. The highest peak and mean velocities both before and during the hurricane were due to winds blowing from the south.

In typical peak velocity situations waves having a period of 1.5 s and a height of 0.3 m would be developed by winds blowing from the southwest. However, during the hurricane, a 3.5-s wave with a height of about 0.9 m would be expected from 81 km h^{-1}

TABLE 6.1.

Summary of sampling intervals used in the experiment.

Frame	Substrate		Total Time of Substrate Exposure (hours)
	Placed	Sampled	
A	July 19-0900	July 21-1000	49
B	July 19-0900	July 23-0930	96
C	July 19-0900	July 25-1030	145
D	July 19-0900	July 27-1210	197
E	July 21-1100	July 29-1515	196

TABLE 6.2

Mean and peak velocity wind conditions in km h^{-1} for a 24-hour period prior to sampling each frame.

Frame	Wind blowing from							Peak velocity
	N	NE	SE	S	SW	W	NW	
A			11.1	29.9	25.9			S 37.0
B				12.0	16.6	9.2	11.1	SW 24.0
C	5.5	3.7		29.6	14.8	18.5	5.5	S 42.5
D					24.0	24.0		W 29.6
E			31.4	42.5	31.4			S 81.4

Figure 6.3. SCUBA diver sampling frame C substrate after about six days of exposure. The portable television system is visible in the upper left-hand corner of the photograph. The camera was focused on frame D throughout the experiment.

winds blowing from the south. The mean equivalent diameter of the species of foraminifera observed in the experiment area is about 0.13 mm. Using the equations of Komar and Miller (1975), it is evident that resuspension and transport of specimens is possible to a water depth of 0.7 m in the case of typical-force southwest winds, and to a depth of 6.5 m in the case of the hurricane generated south winds.

On July 22nd divers reported a marked decrease in bottom water temperature (20.8° to 13.2°C) and visibility compared to conditions on July 21st. By July 23rd visibility had improved and bottom water temperature had increased. This trend continued through July 27th. The hurricane noted earlier passed through the area between 1000 h and 1600 h on July 28th. On July 29th frame E was sampled and divers reported moderate visibility and relatively cold bottom water temperatures compared to July 27th conditions suggesting an onshore movement of the bottom water. They also noted a substantial deposit (i.e. several millimetres) of new material on the sterile sand substrate of frame D which had been renewed after it was sampled on July 27th. Temperature and salinity profiles taken at the experimental site on July 27th and 30th showed that the water temperature had decreased about 4°C at the surface and about 7°C at the bottom because of mixing with deeper offshore water. Salinity decreased uniformly throughout the water column from 29.2 ‰ on July 28th to 29.0 ‰ on July 30th.

Many periods of high turbidity were recorded using an underwater time-lapse television system (Schafer *et. al.*, 1975) that was positioned adjacent to frame D. The duration of these relatively turbid periods ranged from hours to days and could be correlated with winds blowing from the southwest at average velocities of about 37 km h^{-1} or from the south at 41 km h^{-1}. Large numbers of tracks made by various benthic invertebrates such as brittle stars, lobsters and crabs were also observed on the frame E substrate on July 21st, about two days after the sterile sand had been placed in the frame. The television recording also showed the development of a relatively pronounced deposit of allochthonous material during the early morning of July 25th, several hours before frame C was sampled.

Living Foraminifera

Living specimens occupied the frame A substrate after two days in numbers that are equivalent to those observed at frame C (Fig. 6.4). This suggests that the re-establishment of the major species occurs within two days and that population density becomes constant under normal conditions. The relatively depressed species counts recorded at frame B may be indicative of the importance of vertical mixing processes. Under normal circumstances this frame might be expected to reflect population densities that are equal or higher than those observed at frame A because it has been exposed to relatively turbulent conditions over a longer period. It differs from frames A and C in terms of a layer of aluminum foil which underlies the sterile sand and thus prevents vertical mixing of this material with underlying substrate. Frame D was also underlain with foil and it also shows a relatively minor increase in the total number of living specimens which again may be related to the absence of vertical sediment mixing. Inspection of unextruded cores collected at frame E suggests that the degree of mixing is probably not uniform over the entire frame. The hurricane which passed through this area caused a significant increase in the deposition of living specimens in this area.

A relatively clumped or contagious distribution pattern in terms of standard deviation (SD) values is suggested for populations that have settled on frame B and D (Table 6.3). This distribution pattern correlates with relatively low peak wind velocities (Table 6.2) and suggests that the observed pattern could be related to other factors such as the relative mobility rates of species. In this regard, it is interesting to note that $\bar{S}_S$ (the mean similarity of subsamples collected near the edge of the frame) is greater than $\bar{S}_C$ (the mean similarity of comparisons between the centre subsample and side subsamples) in all cases. This conditon could arise because certain forms might be less mobile than others so that a greater number of specimens and/or species could reoccupy the central area before it was sampled. At frame B the centre subsample (D) is at least similar to side subsample (C). (D) is distinctive compared to (C) in terms of its high percentages of *A. beccarii* (55% vs. 0%) and *M. fusca* (11% vs. 0%) and by the absence of *E. advena* and *Hemisphaerammina* sp. In frame D the centre subsample (D) contained double the number of *A. beccarii*, one half as many *E. advena* compared to side subsample (C) and was further characterized by the presence of *E. margaritaceum* and

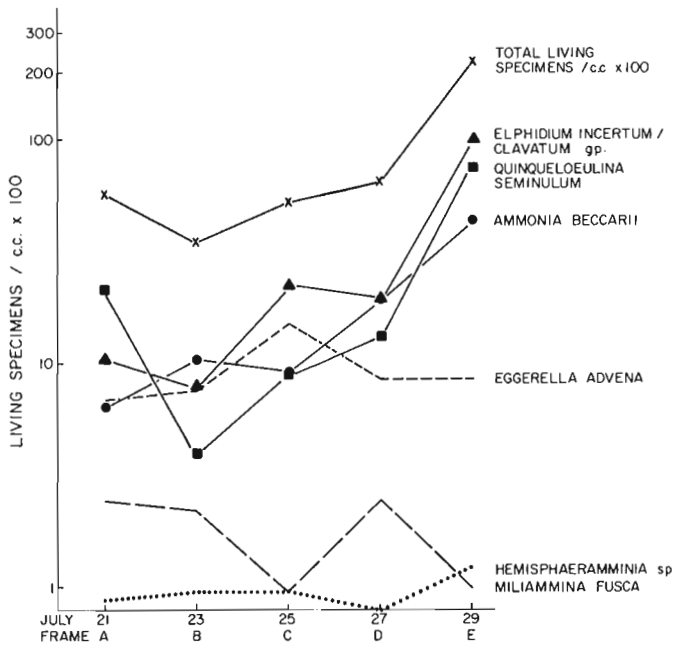

Figure 6.4. Temporal variation of the mean number of living specimens in four subsamples for six diagnostic species.

TABLE 6.3

Similarity matrix of living foraminifera counts in subsamples and between averaged samples.

Frame	Subsample comparison – Living									
	A/B	A/C	A/D	B/C	B/D	C/D	$\bar{S}$	$\bar{S}_c$	$\bar{S}_s$	SD
A	.98	.95	.93	.93	.91	.98	.967	.940	.953	.03
B	.97	.73	.87	.62	.93	.31	.738	.703	.733	.25
C	.98	.95	.92	.95	.91	.98	.984	.936	.960	.03
D	.91	.72	.91	.92	.80	.56	.803	.756	.850	.41
E	1.00	.99	.97	1.00	.97	.97	.983	.970	.996	.02

	Similarity between frames and grab samples						
	A	B	C	D	E	L5-6	L3-4
B	0.85						
C	0.87	0.93					
D	0.93	0.96	0.96				
E	0.93	0.87	0.97	0.96			
L5-6	0.51	0.74	0.70	0.65	0.56		
L3-4	0.41	0.62	0.47	0.40	0.15	0.74	
L7	0.58	0.89	0.71	0.84	0.66	0.64	0.32

$\bar{S}$ - is the mean similarity of all subsample comparisons;

$\bar{S}_c$ - is the mean similarity of comparisons between subsample (D), collected in the center of the frame and other subsamples collected near the edge of the frame;

$\bar{S}_s$ - is the mean similarity of subsamples collected near the edge of the frame;

SD - is the standard deviation of similarity values for all subsample comparisons in each frame.

Composite grab samples L3-4, L5-6, and L7 show the similarity of assemblages collected on frames to indigenous faunas seaward, at and shoreward of the experimental site.

M. fusca. Conversely, subsample (C) is characterized by 60% *Q. seminulum*, a species which is not present in the centre of subsample (D). These localized comparisons suggest that the mobility, or transportability of nearshore species such as *A. beccarii* and *M. fusca* is relatively high so that relatively underdispersed distribution patterns, developed through combinations of physical transport and/or inherent mobility, may be expected in this environment. It is evident from the frame E $\bar{S}$ value (Table 6.3) that physical transport processes have tended to generate a homogeneous population characterized by both allochthonous and indigenous species. Rotaliform species such as *E. incertum/clavatum* gp. and *A. beccarii*, and *Q. seminulum* show significant increases in abundance indicates of seaward transport. Species such as *E. advena* and *Hemisphaerammina* sp., on the other hand, show little variability in terms of their abundance. This conditions is probably related to relative transportability in the case of *Hemisphaerammina* sp. compared to other species because it is more abundant in shallow water and would be expected to be transported seaward at the same time as other calcareous forms. *E. advena*, on the other hand, is a deep water form and also may not be as easily eroded.

References

Albani, A.D. and Johnson, K.R.
1975: Resolution of foraminiferal biotopes in Broken Bay, N.S.W.; Gel. Soc. Aust.; J. v. 22, p. 435-446.

Berger, W.H. and Soutar, A.
1970: Preservation of plankton shells in an anaerobic basin off California; Geol. Soc. Am. Bull.; v. 81, p. 275-282.

Gibson, T. G. and Walker, W. W.
1967: Flotation methods for obtaining foraminifera from sediment samples. J. Paleontol.; v. 41, p. 1294-1297.

Grabert, B.
1971: Sur Eignung von Foraminiferen als Indikatoren für Sandwanderung. Sonderdr. Deutsch. Hydr. Z.; v. 24, p. 1-14.

Haake, W. H.
1962: Untersuchungen an der Foraminiferen-fauna in Wattgebiet zwischen Langeogg und dem Festland Meynian; v. 12, p. 25-64.

Komar, P. D. and Miller, M. C.
1975: On the comparison between threshold of sediment motion under waves and unidirectional currents with a discussion of the practical evaluation of the threshold. J. Sed. Petrol.; v. 45, p. 362-368.

Margalef, R.
1968: Perspectives in Ecological Theory; Univ. Chicago Press, Chicago, Ill., 111 p.

Murray, J. W.
1965: Significance of benthic foraminiferids in plankton samples. J. Paleontol.; v. 39, p. 156-157.

1973: Distribution and Ecology of Living Benthic Foraminiferids; Crane, Russak & Co., New York, 274 p.

Ritchter, G.
1965: Zur Okologie der Foraminifern III – Verdriftung und Transport in der Gezeitenzone. Natur. Mus., Frankf., v. 95, p. 51-62.

Schafer, C. T. and Prakash, A.
1968: Current transport and deposition of foraminiferal tests, planktonic organisms and lithogenic particles in Bedford Basin, Nova Scotia. Marit. Sediments, v. 4, p. 100-103.

Schafer, C. T., Godden, C. A., and Payzant, P.
1975: A portable underwater Videorecorder. Proceedings, Offshore Technology Conf., Houston, Texas, p. 725-729.

Shepard, F. P.
1963: Submarine Geology; Harper and Row, 557 p.

Walker, D. A., Linton, A. E., and Schafer, C. T.
1974: Sudan Black B: A superior stain to Rose Bengal for distinguishing living from non-living foraminifera. J. Foraminiferal. Res., v. 4, p. 205-215.

7. CHANNEL AND SHOAL MORPHOLOGY IN THE ENTRANCE TO THE MIRAMICHI ESTUARY, NEW BRUNSWICK

Project 750047

G. E. Reinson
Atlantic Geoscience Centre, Dartmouth

Introduction

As part of a study of the sediment dynamics and coastal morphology of the Miramichi barrier island-inlet system, this paper presents preliminary interpretations on the evolution of channel and shoal morphology in the main entrance to the Miramichi estuary, New Brunswick (Fig. 7.1). The reader is referred to another paper in this volume (Reinson, 1976), for the location and regional setting of the area illustrated in Figure 7.1.

According to Hayes (1975), the major processes which govern sand deposition at the mouths of microtidal estuaries (tidal range 0-2 m) are waves and winds, whereas in mesotidal estuaries (tidal range 2-4 m), sediments deposited by tidal currents begin to predominate. Characteristic sand deposits associated with microtidal estuaries are extensive barrier islands with washover fans, aligned beaches, recurved and cuspate spits, and small flood-tidal deltas. In mesotidal estuaries, tidal deltas and inlets are the most conspicuous morphological features, and associated barrier island features are secondary (Hayes, 1975).

Miramichi Inlet Morphology

The Miramichi estuary is in the microtidal zone of the eastern New Brunswick coast, an area characterized by barrier islands and spits (Owens, 1974a, b). Although the estuary is microtidal the morphology of the shoals near the main inlet suggests that abundant sediment deposition by tidal currents, as well as by wave- and wind-generated processes has occurred (Fig. 7.1). The 5-m isobath delineates a number of channel-shoal relationships, some of which are very similar to the models developed by Hayes and co-workers (Hayes, 1975; Coastal Research Group, 1969) for estuaries along the New England coastline. These features include a flood-tidal delta (Horse Shoe Shoal),

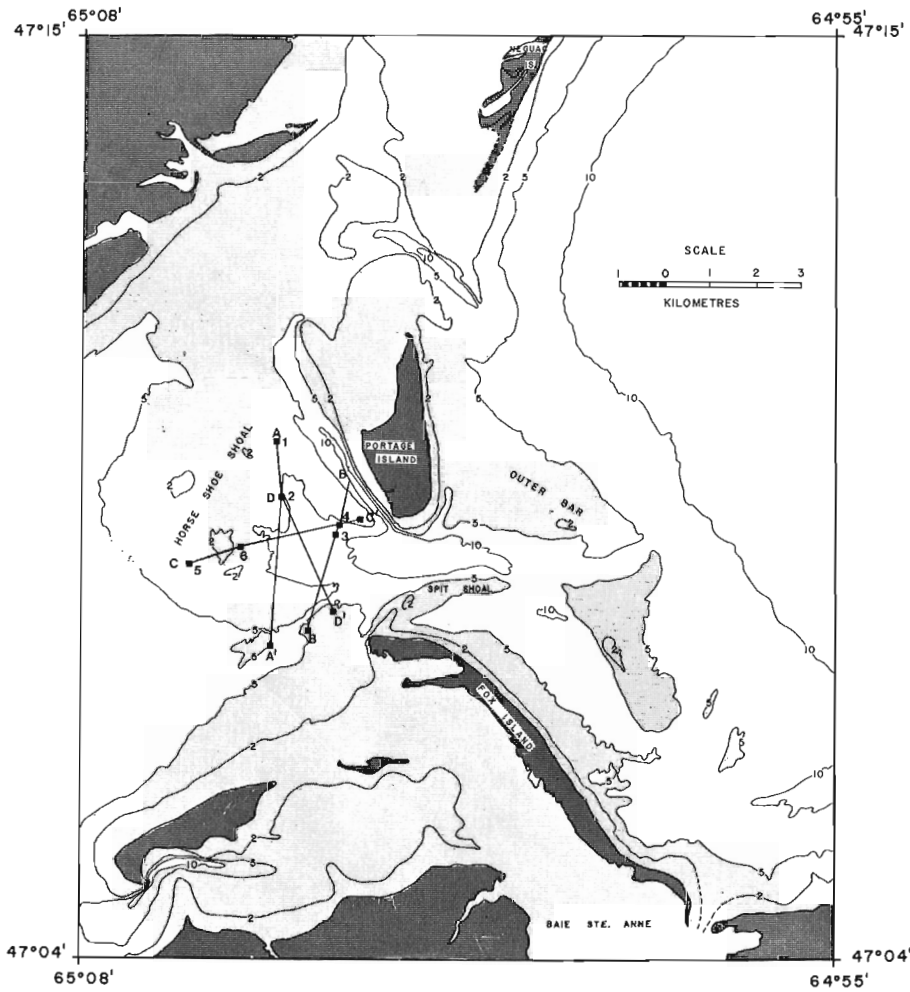

Figure 7.1.

Shoal and channel bathymetry at the entrance to the Miramichi estuary (contours are in metres, light stipple outlines the areas shoaler than 5 metres). The locations of the echo-sounding profiles depicted in Figure 7.2 are also shown.

From: Report of Activities, Part C;
Geol. Surv. Can., Paper 76-1C (1976).

and ebb-tidal deltaic forms. However, in contrast to the New England estuarine sand accumulations, no shoal-portion of either the flood-tidal delta or the ebb-tidal deltaic features, at the main inlet to the Miramichi, are anywhere close to being exposed at low water.

Because of this completely subtidal occurrence, the morphology of the shoals cannot be investigated using aerial photography. Underwater photography and diver observations have been unsuccessful so far, because of the extremely poor visibility encountered at depth. Echo-sounding (Fig. 7.2) has proven to be fruitful, in conjunction with the overall bathymetric pattern, for interpreting the channel-shoal morphology of Horse Shoe Shoal (Figs. 7.1 and 7.2).

The orientation of sand waves on Horse Shoe Shoal indicates that the dominant flood and ebb currents follow mutually evasive paths. This channel segregation is

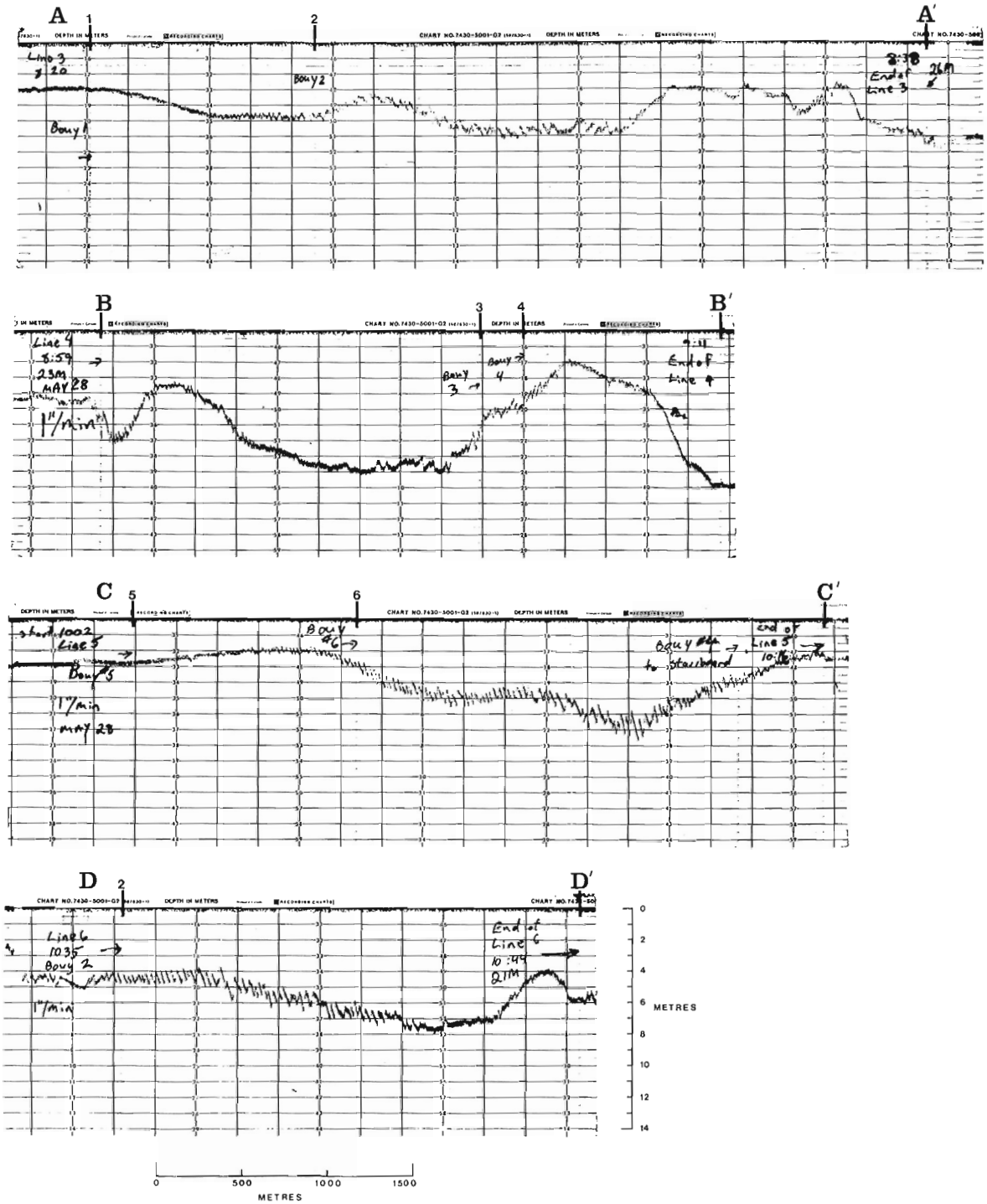

Figure 7.2. Echo-sounding profiles from Horse Shoe Shoal, May 28, 1976 (*see* Fig. 7.1 for location of profile lines). Note the presence of numerous sand waves indicated by every profile.

responsible for the "horseshoe-like" shape of the shoal (Fig. 7.3). Features such as a flood ramp covered with flood-oriented sand waves, ebb-spits, and flood channels (Fig. 7.3), are characteristic of the flood-tidal deltaic model developed by Hayes (1975).

The morphological features of the ebb-tidal delta are shown in Figure 7.3, using some of the terminology of Hayes (1975). The ebb-tidal delta does not strictly fit Hayes' model, and from a genetic viewpoint has not been formed predominantly by ebb-tidal currents. There is a strong north to south littoral-drift component in this region, in response to wind-generated waves from the northeast quadrant (Owens, 1974a). This is probably the cause of the southward elongation of the Outer Bar (Fig. 7.1). As far as can be determined from historical bathymetric charts, the channel through the Outer Bar formed sometime between 1921 and 1954. This may indicate that ebb-tidal currents have a greater influence on channel-shoal morphology (outside of the entrance) at the present time, than they did in the past, when longshore currents may have dominated. This change may be due to a decrease in the amount of sediment supplied by southward longshore currents in recent years.

Along the south shore of Miramichi Outer Bay (Reinson, 1976, Fig. 9.1) and immediately adjacent to Fox Island (Fig. 7.1), a reversal of drift occurs because the waves from the northeast generate westerly and northwesterly longshore currents (Owens, 1975). This reversal contributes to the growth of the ebb spit south

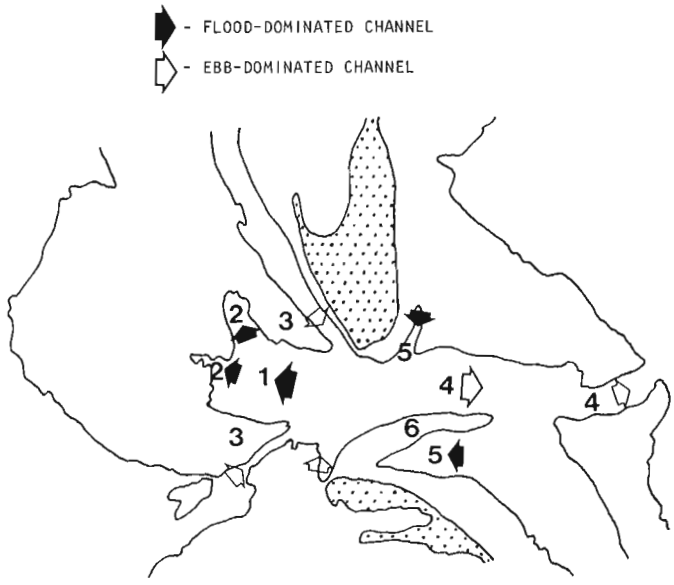

FLOOD-TIDAL DELTA	EBB-TIDAL DELTA
1 - Flood Ramp	4 - Main Ebb Channel
2 - Flood Channels	5 - Marginal Flood Channels
3 - Ebb Spits	6 - Ebb Spit (Channel Marginal Bar)

Figure 7.3. Interpretation of the channel-shoal pattern (as delineated by the 5-m isobath) in the main entrance to the Miramichi estuary.

of the main ebb channel, and to the maintenance of the marginal flood channel between Fox Island and the ebb spit (Fig. 7.3).

Further work is planned to expand on the preliminary ideas presented here. Such work will include; detailed analyses of sand-wave orientations using existing CHS echo-sounding rolls, analysis of current-velocity data obtained from the main channels, additional echo-sounding, side-scan sonar, and comparative studies of historical bathymetric charts.

References

Coastal Research Group,
1969: Coastal environments: northeast Massachusetts and New Hampshire; Contrib. no. 1-CRG, Univ. Mass., Dep. Geol. Pub. Ser., 462 p.

Hayes, M.O.,
1975: Morphology of sand accumulation in estuaries: an introduction to the symposium; *in* Proceedings of the Second International Estuarine Research Conference, *ed.* L.E. Cronin; Academic Press, New York, p. 3-22.

Owens, E.H.,
1974a: A framework for the definition of coastal environments in the southern Gulf of St. Lawrence; Geol. Surv. Can., Paper 74-30, p. 47-76.

1974b: Coastline changes in the southern Gulf of St. Lawrence; *in* Report of Activities, Part A, Geol. Surv. Can., Paper 74-1A, p. 123-124.

1975: Barrier beaches and sediment transport in the southern Gulf of St. Lawrence; *in* Proc. of the 14th Coastal Engineering Conference, Copenhagen, Denmark, June 1974; ASCE, New York, p. 1177-1193.

Reinson, G.E.,
1976: Surficial sediment distribution in the Miramichi estuary, New Brunswick; *in* Report of Activities, Part C, Geol. Surv. Can., Paper 76-1C, rep. 9.

8. THE EFFECTS OF STORMS ON NEARSHORE MORPHOLOGY, NEGUAC ISLAND, NEW BRUNSWICK

Project 750047

H. D. Munroe
Atlantic Geoscience Centre, Dartmouth

Neguac Island, located in the Miramichi estuary, New Brunswick, is one of the most dynamic segments of the southern Gulf of St. Lawrence barrier island system (Owens, 1974). This report deals with field observations of changes in the beach and littoral zone of Neguac, in response to two storms during June and July, 1976 (Fig. 8.1). Net longshore transport is to the south due to the northeast winds, which because of the available fetch, generate the largest most damaging waves.

Maximum relief on the island is 3 m, with vegetation consisting chiefly of marram grass (*Ammophilia brevigulata*). Storm channels and washovers are common because of the low relief and sparse vegetation and are reactivated during a "Noreaster", especially if the storm occurs during spring tides. Under normal weather conditions the longshore currents are relatively weak, with a mean velocity of less than 20 cm/s. Local breezes greatly influence these currents which commonly change direction from north to south daily. The net longshore transport under these conditions is very low.

Two sections of beach profile lines – station one (0.5 km long) and station two (1.0 km long) were tied into a permanent bench mark in order to monitor beach and littoral zone changes (Fig. 8.1). Within each section individual profile lines, spaced 50 m apart, were periodically surveyed from the back beach to a point seaward of the inner bar.

At station two an inner bar was attached to the beach at its updrift end. Here the bar was very low and wide but along the southerly part, which paralleled the beach, sections of the bar were exposed at low tide. A similar feature existed at station one, but was more advanced in that it had been cut by several rip current channels and several segments were close to becoming welded onto shore. This feature, no longer part of the inner bar system, was moving onto shore in a ridge and runnel-like fashion (Fig. 8.2). An outer bar existed at both sites.

On June 11, 1976 a northeast wind prevailed for 36 hours. During this storm, waves would break at the outer bar, reform, and break on the inner bar and finally reform and break on the beach face. By this time most of the wave energy had been dissipated. This disturbance happened during spring tides which, when coupled with the storm surge, resulted in extensive erosion and the reactivation of a huge washover, trending northeast in the area of station two. During these high energy storm conditions the morphology of the inner bar changed very little, because most of the wave energy was expended on the outer bar.

On July 13th another disturbance of lesser magnitude hit the area. In the course of this storm it was possible to measure nearshore currents and collect wave data, unlike the June 11th event when conditions were too violent to measure process variables. The maximum water level during this storm was somewhat less than in June, but conditions were such that the washover was again flooded.

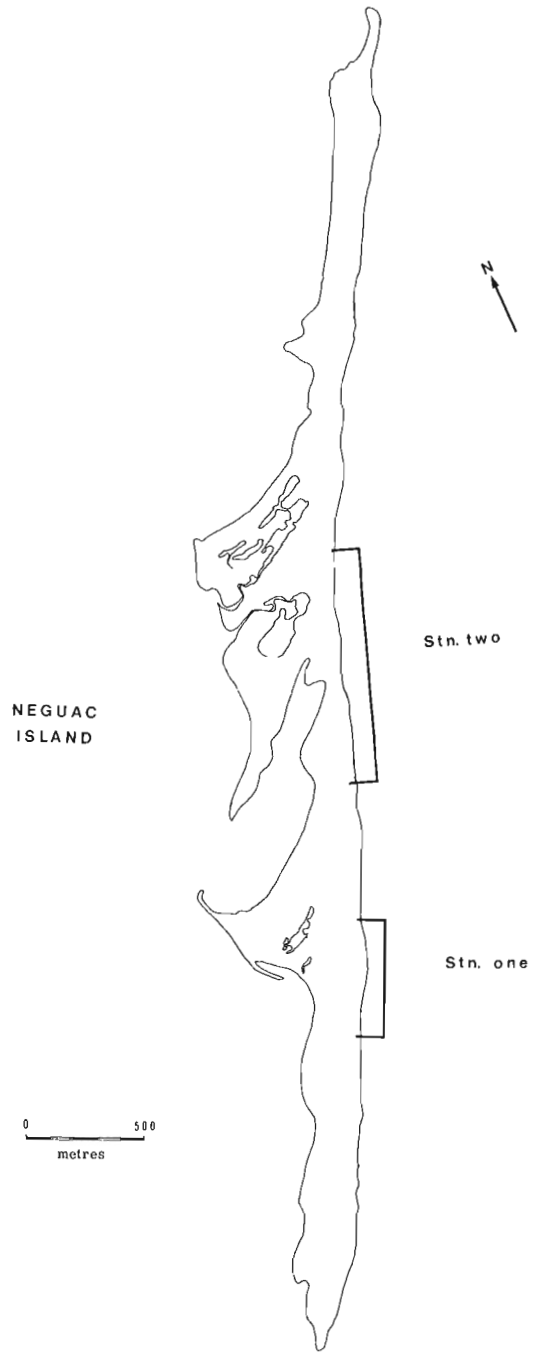

Figure 8.1. Location of stations one and two on Neguac Island.

From: Report of Activities, Part C;
Geol. Surv. Can., Paper 76-1C (1976)

Figure 8. 2. Station one: Bar, at a later stage of development, is moving onshore.

Figure 8. 3. Station two: Arrow shows where the attached low portion of the bar was cut by rip currents.

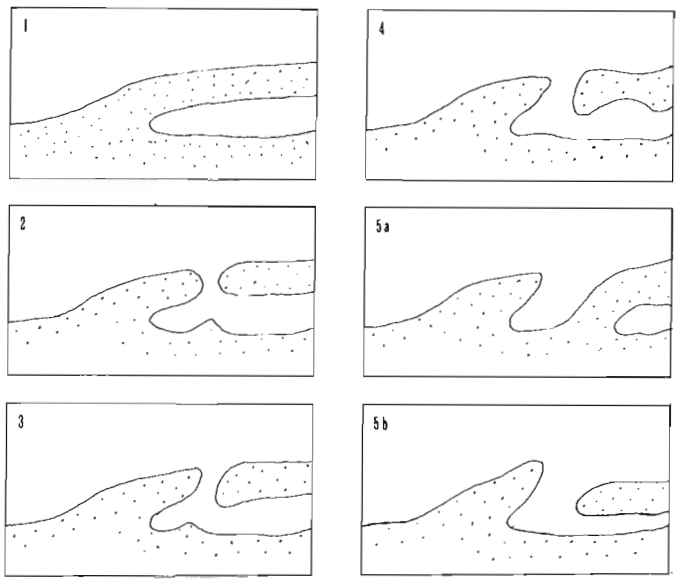

1 – Initial bar, low and wide in the updrift attached portion.

2 – Rip current channel develops in the area of the attachment and small protuberance forms as the result of these currents.

3 – Rip current channel is slightly skewed downdrift.

4 – Remaining segments of the bar are greatly modified by wave action.

4-5a – Updrift end of bar may become welded onto the beach face.

4-5b – Segments of bar may move onshore in a ridge and runnel-like fashion.

Figure 8.4. Stages in bar development (Net longshore transport is from left to right in all diagrams).

The inner bar crest at station one was planed off by wave action and most of the sediment was deposited in the landward trough. The inner bar at station two received most of the wave energy, which resulted in a super elevation of the water surface between the bar crest and the beach face. Peak longshore current velocities measured in the trough at this time ranged from 147 to 167 cm/s. As the water depth continued to increase with the flooding tide, rip current channels were cut into the bar where it was joined onto the beach face (Fig. 8.3). As conditions slowly returned to normal, a slight protuberance developed behind the rip current channel and at the same time rates of erosion were increased by the currents moving out of the channel (Fig. 8.4-3). On the downdrift side of the rip current channel the bar became welded to the beach face (Fig. 8.4-5a). This resulted in either overlapping bars or portions of the bar moving onto shore in a ridge and runnel-like fashion (Fig. 8.4-5b).

In order to properly assess the stability of the Miramichi barrier island system (Neguac, Portage and Fox islands) a comprehensive monitoring program of coastal processes should be carried out in the more active areas of Fox and Portage islands. The field program should be broken up into spring, summer, and autumn portions, so that any seasonal changes in the littoral zone could be recorded. In the spring and autumn portions the higher frequency of northeast storms would provide investigators with a better knowledge of shore-line changes under high energy conditions. Some effort should also be made to evaluate the effect of tidal currents in dispersing sediment transported alongshore.

Reference

Owens, E.H.
1974: Coastline changes in southern Gulf of St. Lawrence; *in* Report of Activities, Part A, Geol. Surv. Can., Paper 74-1A, p. 123-124.

9. SURFICIAL SEDIMENT DISTRIBUTION IN THE MIRAMICHI ESTUARY, NEW BRUNSWICK

Project 750048

G. E. Reinson
Atlantic Geoscience Centre, Dartmouth

Introduction

This paper presents preliminary results of a surficial sediment survey of the Miramichi estuary, eastern New Brunswick (Fig. 9.1). It is part of an on-going multidisciplinary study of the Miramichi estuarine system.

The Miramichi estuary is a typical funnel-shaped estuary, and is the "bar-built" estuary type of Pritchard's classification (1967). Pritchard considers the bar-built type to be a composite system, consisting of an outer embayment enclosed by a coastal barrier, and an inner major drowned river valley. He also considers that estuaries of this type are usually shallow and affected considerably by winds. The Miramichi fits this description almost perfectly.

A shipping channel, which has been maintained by periodic dredging operations, extends through the estuary to Newcastle (Fig. 9.1). Although the last maintenance dredging to occur inside the barrier islands was in 1940, the effects of this dredging can be seen clearly in the bathymetric chart compiled from field-survey data of 1974-75 (Fig. 9.1).

Sedimentary Environments

Five major sedimentary environments can be recognized in the Miramichi estuarine system: river channel, inner bay, tidal-delta complex, coastal barrier and outer bay.

The river has downcut into bedrock forming a confined channel, the lower reaches of which have been submerged by rise in sea level following glacial retreat. Water depth in the river is variable; maximum depths occur near the shore on the outside of meander bends, and minimum depths occur on the inside of meander bends near the opposite shore (Fig. 9.1). Point bar deposits are the cause of this cross channel shallowing. Flat lying Paleozoic sandstones form a low cliffed shoreline along most of the river channel except on the inner side of meander bends where Pleistocene(?) to Holocene alluvial deposits occur.

The inner bay environment is relatively unrestricted geomorphologically compared to the river channel, and has a rather constant water depth and smooth submarine topography. It is a shallow basinal area which formed as a result of the drowning of the alluvial valley and

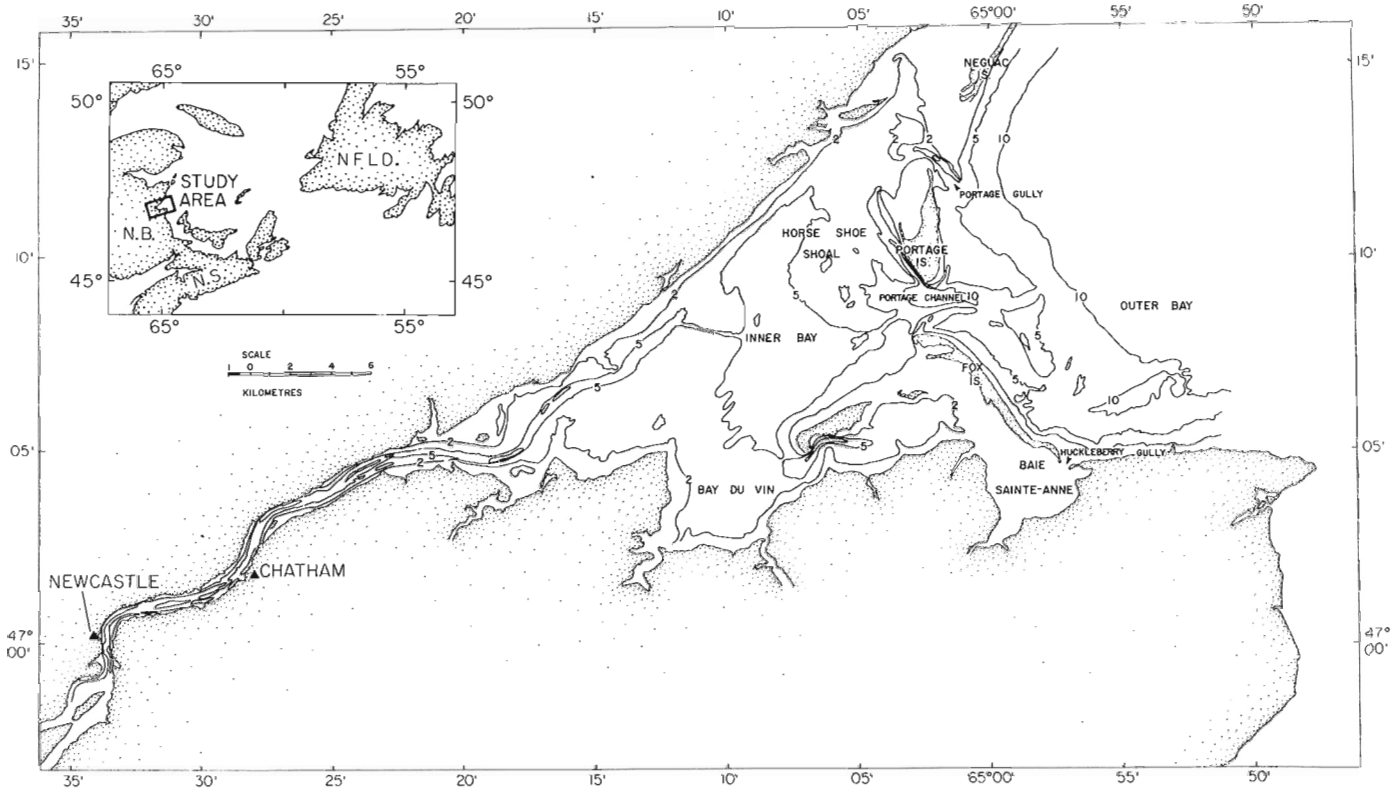

Figure 9.1. Bathymetry of the Miramichi estuary depicting the 2-, 5- and 10-metre isobaths (datum mean low water). Modified from a detailed bathymetric map (compiled from 1974 and 1975 Can. Hydrographic Service field surveys) supplied by Miramichi Channel Study.

From: Report of Activities, Part C;
Geol. Surv. Can., Paper 76-1C (1976).

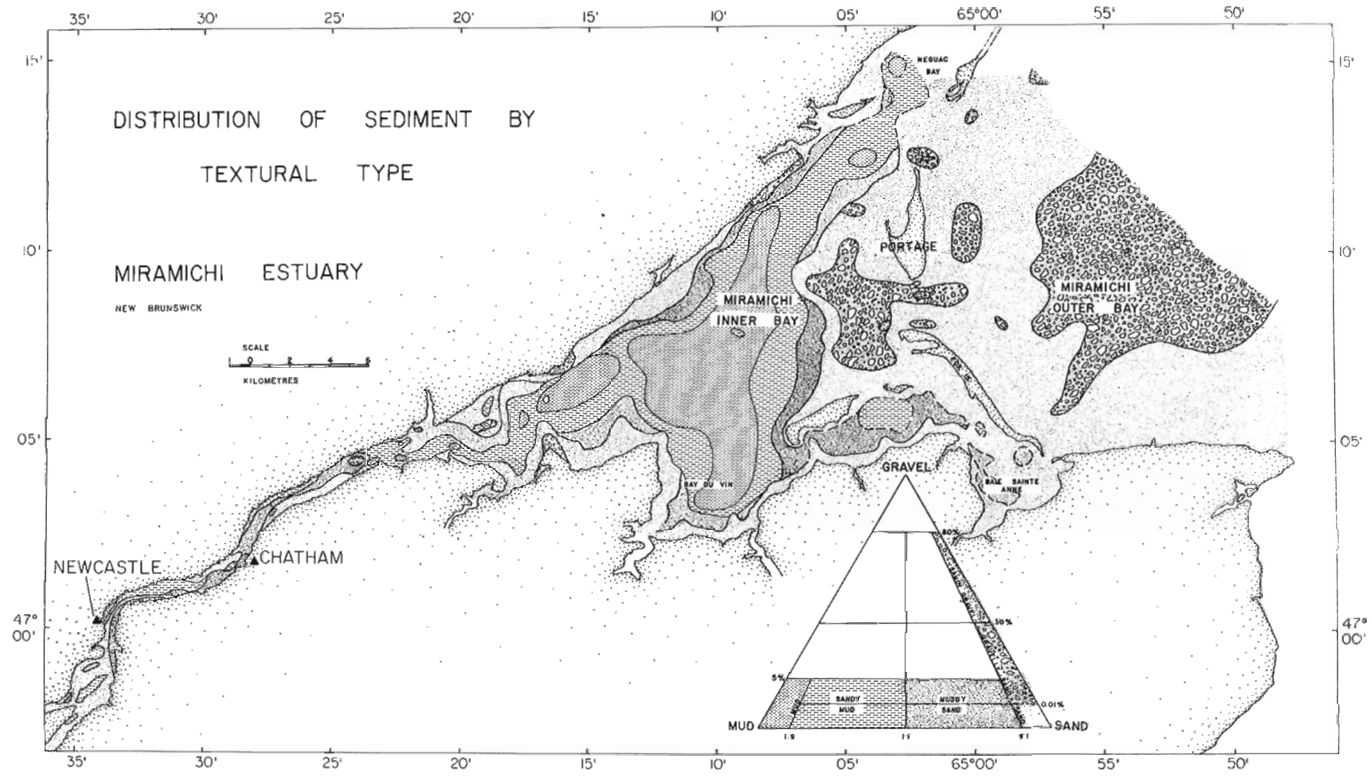

Figure 9.2. Distribution of surficial sediment by textural type (classification scheme after Folk, 1968).

plain adjacent to the river mouth. Very low cliffs of flat lying Paleozoic sandstone rim the north and south shores. These outcrops often occur as sandstone pavement extending well into the nearshore zone below low-water mark. Pleistocene(?) and Holocene alluvial deposits form the shoreline near tributary river mouths, and deposits of peat occur in a few areas (in particular at Cheval Point).

The tidal-delta complex is the term used for the shallow, sand-dominated area, which is present on both sides of the coastal barrier. The 5-m isobath roughly delineates this environment and the subenvironments within it (Fig. 9.1). Three subenvironments make up the tidal-delta complex; the tidal inlets (from north to south, Portage Gully, Portage Channel, and Huckleberry Gully), coalescing flood-tidal deltas, and ebb-tidal deltas. The terms "flood-tidal delta" and "ebb-tidal delta", as used here, are defined respectively as, "sediment accumulation formed inside an inlet by flood-tidal currents", and "sediment accumulation seaward of a tidal inlet, deposited by ebb-tidal currents" (Coastal Research Group, 1969, p. 456). The relatively continuous, shallow north-south trending belt of sand banks and shoals which extends well into the estuary at Baie Ste. Anne and Horse Shoe Shoal, and to a lesser extent in the Neguac Bay regions, comprises coalescing flood-tidal deltas. The extent of the flood-tidal delta complex as compared to the small shoal areas (ebb-tidal deltas) seaward of Portage Gully and Portage Channel (Fig. 9.1), indicate that the predominant, or net, movement of marine detritus is landward, or into the estuary.

The term "coastal barrier" as used here, is defined by Bird (1964) as "a strip of depositional land extending above high-tide level, and standing offshore or across the mouths of inlets or embayments". The coastal barrier at Miramichi is broken by the three inlets which divide it into four segments known, from north to south, as Neguac Island, Portage Island, Fox Island, and Preston Beach. These coastal-barrier segments consist essentially of two major zones: 1) the contemporary foredune and beach environments, which forms the present shoreline, and is activley changing in response to waves, winds and tidal currents (Owens, 1974), and 2) the ancient vegetated barrier tract which is a succession of parallel beach ridges with intervening swales consisting of marsh, swamp and small lagoons. The ancient barrier is being modified to some degree at present, but its overall morphology is generally the result of progradational accretion during the Holocene.

The outer bay environment is a typical shallow, arcuate, open marine bay. The bottom slopes gently in a seaward direction thus wind-generated swell and tidal currents are rarely dissipated before they reach well into the inshore areas.

Distribution of Surficial Sediment

Sediment types and their distribution are depicted in Figure 9.2 and the distribution of sand plus gravel (weight per cent of material coarser than 0.0625 mm) in Figure 9.3. The textural classification used for construction of Figure 9.2 is that of Folk (1968). There are six major sediment types depicted on the

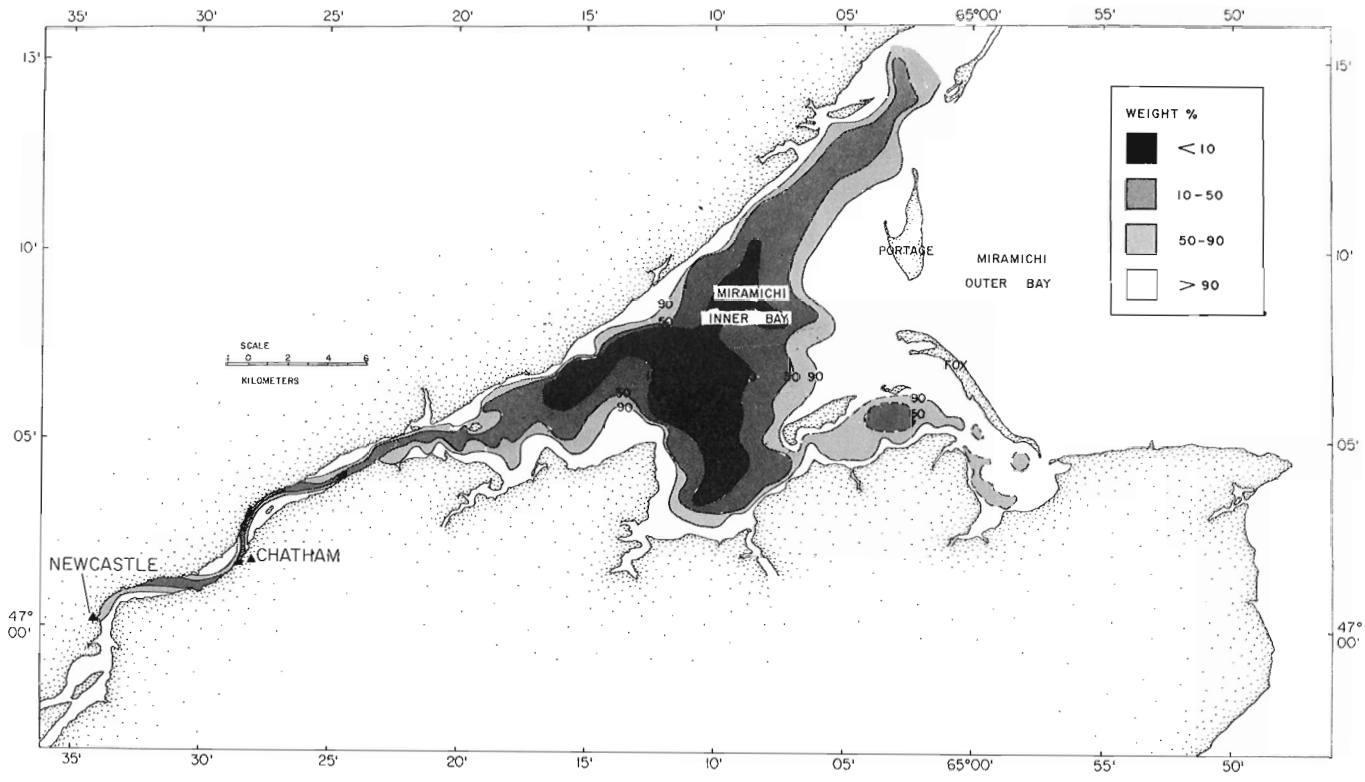

Figure 9.3. Distribution of sand (material coarser than 0.0625 mm) in the surficial sediments of the Miramichi estuary.

map; sandy gravel, gravelly sand, sand, muddy sand, sandy mud, and mud. These six types are derived from grouping of classes (on the triangular diagram) such that their distribution illustrates most meaningfully the varying depositional regimes existing in the estuary. For example, the gravelly sand boundary is extended below the 5 per cent cutoff to include the slightly gravelly sand category because the two classes, when considered together, are more meaningful in illustrating that sands containing gravel occur more often in the high energy zones such as Portage Channel and the outer bay region.

The variations in distribution of textural types correspond closely with the various depositional environments (Fig. 9.2). In the outer bay gravelly sand and sand are the predominant sediment types. The gravelly sand facies is situated seaward of the sand facies suggesting that onshore transport of sediment is occurring. The predominance of flood-tidal deltaic sand deposits over their ebb-tidal counterparts, combined with the presence of gravelly sand, as channel-lag deposits in the regions of the tidal inlets, indicates that net transport of marine sand is directed into the estuary.

The sediments in the river channel are characterized by extreme textural variability, ranging from mud to sandy gravel. The upper reaches of the channel are dominated by moderately- to poorly-sorted, medium- to coarse-grained sands of fluvial origin. Further downstream, similar sands occur as broad, shoaler areas on the inside of meander bends. In fact, sand dominates areally in the river, and mud deposits occur only along the thalweg of the channel, and in local off-channel deep areas.

The inner bay environment is characterized by muddy sediments with a paucity of sand. This area is the main depositional sink for fine grained fluvial detritus coming downstream, and it is thought that very little coarse grained fluvial detritus is carried as far down as the inner bay region. Similarly, very little coarse grained marine detritus is transported farther into the estuary than the inner bay region. The sandy mud and muddy sand facies between the flood-tidal delta and the inner bay basin represent mixed deposits of fine grained fluvial material and marine sand.

It can be inferred, from the dispersal pattern displayed by the mud facies in the inner bay (Fig. 9.2), that current velocities are consistently lower (over a given time interval) in this region than in other regions of the estuary. This interpretation is substantiated by the recent work of R.R. Johnson, National Research Council, who constructed a two-dimensional numerical model of velocity distribution in Miramichi Bay.

The hydrodynamic circulation in the estuary is related not only to tidal forces and river discharge, but also to bottom topography, lateral physical dimensions of the estuary, and to the wind. The splayed pattern of the mud deposits in the inner bay (Figs. 9.2 and 9.3), reflects all of these controls. The seaward moving water, as it leaves the river portion of the estuary, tends to flow through the submarine shipping channel adjacent to the northern shore (Fig. 9.1), and continues in this direction well into the northern part of the inner bay where water depths are greatest. The incoming sea water flows westward over Horse Shoe Shoal, deflecting outflowing water toward the northeast, as

it moves into the inner bay. The intrusion of marine sand farther into the southern half of the estuary, and the tongue of mud farther seaward in the northern half of the estuary, seem to substantiate this interpretation. A tongue of marine sand extends into the inner bay along the shipping channel reflecting the region through which the maximum volume of sea water intrudes (Fig. 9.3). Apparently some "ponding-up" of water occurs in the Bay du Vin region, (as evidenced by the presence of bottom mud there), due to the interaction of the circulation forces described above. In addition, wind may play a dominant role in the "ponding" of water in the Bay du Vin region; this situation is indicated in the numerical model constructed by R.R. Johnson, (pers. comm.), especially when prevailing winds are from the northeast.

To summarize, the preliminary interpretation of surficial sediment distribution in the Miramichi suggests that dominant sediment-transporting energies are directed inland in the tidal delta region, seaward at the river channel, and laterally in the inner bay region (where currents are lowest in terms of overall transporting energy, and where the effects of winds on circulation are highest).

The above discussion suggests that there are two main sources of estuary sediments, marine and fluvial. In fact, there is a third source, shoreline erosion of sandstone bedrock. It is as yet unknown how important shoreline erosion is in supplying sediment to the estuary, but in the inner bay region, a significant part of the nearshore sand which extends as a belt along the north and south shores (Fig. 9.3), is supplied directly from erosion of adjacent shoreline outcrops. At numerous shoreline localities friable sandstone debris and bedding-plane outcrops can be seen to extend a considerable distance below low-water mark. The low-cliffed shore at these same localities appears to have receded considerably in recent years. It is hoped that shoreline recession can be investigated further to ascertain the amount of material which is being supplied to the nearshore zone through such erosion.

References

Bird, E.C.F.
1964: Coastal Landforms; Canberra, Australian National University Press.

Coastal Research Group
1969: Coastal Environments of Northeastern Massachusetts and New Hampshire; Contrib. no. 1 - CRG, Univ. Mass., Dep. Geol. Pub. Ser., 462 p.

Folk, R.L.
1968: Petrology of Sedimentary Rocks; Austin, Hemphills Pub. Co.

Owens, E.H.
1974: Coastline changes in the southern Gulf of St. Lawrence; *in* Report of Activities, Part A, Geol. Surv. Can., Paper 74-1A, p. 123-124.

Pritchard, D.W.
1967: What is an estuary: physical viewpoint; *in* G.H. Lauff (Editor), Estuaries; AAAS Pub. 83, p. 3-5.

10. MOLLUSC DISTRIBUTIONS, MIRAMICHI ESTUARY, NEW BRUNSWICK

Project 750048

F.J.E. Wagner
Atlantic Geoscience Centre, Dartmouth

A determination of the distribution of molluscan species forms one phase of the multidisciplinary study to outline the environmental conditions existing in the lower Miramichi River and estuary area where a major dredging program is proposed. Molluscs were collected from 10 stations in February 1976. In May and June four of these stations were revisited and an additional 15 stations were sampled. All of the February samples have been examined together with 15 samples collected in May and June. Computer analysis has been performed on the data collected to date.

Eighteen species have been identified from the February samples and 16 species from samples collected in May and June. Twelve species were common to both suites of samples. The two sets of data were combined and analyzed by the method described by Bonham-Carter (1967) to ascertain the coefficient of association. The dendrogram, produced by the unweighted pair-group method indicates six major groupings at the 0.3 level of similarity. No seasonal differences were apparent for stations sampled both in February and in May and June.

The areal distribution of the biotopes suggests that species distribution is linked to salinity. Three biotopes were identified between the Chatham-Newcastle area and the mouth of the river. Index species for these biotopes are *Macoma balthica* (Linné), *Mytilus edulis* (Linné) and *Mya arenaria* (Linné). *M. balthica* is characteristic of the area of lowest salinity. A single-station biotope is delineated in Bay du Vin in the southern part of the estuary. Diagnostic species are *Ensis directus* (Conrad) and *Crepidula fornicata* (Say). Index species for the biotope representative of marginal marine conditions just inside the barrier islands are *Nassarius trivittatus* (Say) and *Retusa canaliculata* (Say). The sixth biotope, encompassing the less saline major part of the estuary, has *Mulinia lateralia* (Say) as its diagnostic species.

Some cores have been obtained and more will be taken in the estuary. A comparison of the areal distribution of molluscan species in the cores with the present biotope data should indicate what, if any, environmental changes have occurred during, at least, historic times, and may allow a prediction of changes that could result from the planned dredging.

Reference

Bonham-Carter, G.F.
1967: Fortran IV program for Q-mode data cluster analysis of non-quantitative data using IBM 7090/7094 computers; State Geol. Surv., Univ. Kansas, Computer Contrib. 17, 13 p.

From: Report of Activities, Part C;
Geol. Surv. Can., Paper 76-1C (1976).

11. SEASONAL VARIATIONS IN THE OCEANOGRAPHY AND SEDIMENT GEOCHEMISTRY IN THE MIRAMICHI ESTUARY, NEW BRUNSWICK: A PRELIMINARY REPORT

Project 750048

Joan D. Willey
Atlantic Geoscience Centre, Dartmouth

Introduction

The Miramichi estuary in New Brunswick is a shallow, funnel shaped estuary with five sedimentary environments: river channel, inner bay, tidal delta complex, coastal barrier, and outer bay. The geomorphology and physical sedimentology of this area are discussed by Reinson (this pub., rep. 9). This study is confined to the river, inner bay and tidal delta complex; no samples from the barrier islands or outer bay were included. There is considerable variation in texture in the areas studied. Muds occur in the river channel, where the greatest depths occur, and in the inner bay basins. Sands occur upriver, in the river shallows along point bars, and in the shoals in the inner bay and tidal delta complex.

Considerable seasonal variation has been found in the oceanographic parameters. In September 1975, the influence of salt water extended well up the river channel, and the water column was well mixed. No current measurements were made at that time, however strong currents were evident and caused large wire angles (with subsequent grab sampler malfunction). Currents at certain phases of the tide were strong enough to hinder diver operations. In February 1976, the salt water influence again extended far upriver; in this season however the water column was very well stratified. This stratification probably resulted from the sheltering effect of the ice cover at this time; no wind mixing could occur. Current measurements in February showed that current velocities generally did not exceed one knot and that bottom currents were usually much less. In May (1976), a different kind of system was found. This sampling period corresponded to shortly after the time of maximum spring freshwater runoff. Because of the large amount of freshwater contributed by the river, the influence of salt water was restricted to just past the opening of the estuary. The water column at this time was well mixed by both strong tidal currents and by wind-generated currents. Current velocities were measured to be up to three knots at the surface, and one knot at the bottom.

The different oceanographic conditions in the three seasons affect the suspended load. In September 1975, the average concentration (based on 12-18 samples taken throughout the estuary) of suspended particulate material (that which was retained on a 0.4 micrometre pore size filter) was 7.5 mg/litre at the surface, and 12.9 mg/litre near the bottom. In February, these concentrations, based on 12 samples taken throughout the estuary, were 1.2 mg/litre at the surface and 4.0 mg/litre near the bottom. In May, on the basis of 37 samples taken primarily from the river area, the surface concentration of suspended particulate material was 6.4 mg/litre, and near the bottom it was 12.9 mg/litre. This shows that the suspended loads in September were very similar in amount to those found the following May. In February 1976, reduced quantities were found. The low concentration in February are probably caused by the reduced mixing which results from the sheltering effect of the ice cover, and also by a reduced input of suspended particulate material from the large pulp and paper mill which was not operating during the February sampling. This mill however is located 10 km upstream of the nearest station in February.

Methods of Sampling and Analysis

Six locations throughout the river and inner bay of the Miramichi estuary system have been chosen for sediment resampling on a seasonal basis. The grabs that had a clearly defined surface layer were subsampled at time of collection by taking off the surface centimetre, and then sampling the subsurface material. This was done because seasonal variations may have a greater effect on the uppermost layer of sediment. Difficulties arise in attempts to resample exact locations; sediment types change quickly over small distances, and the accuracy of navigation even near shore is limited. It is not uncommon to obtain a sediment sample of one type, and then several months later, when trying to resample, to obtain a completely different texture; this probably indicates that the two samples were taken from different locations rather than indicating a major change in sediment type during the sampling interval. This problem can be overcome to some extent by fractionating each sample into the coarse and the fine fraction, and then analyzing each fraction separately. In this way muds or mud fractions can be compared for a given locality on a seasonal basis, and the same can be done with sands.

Some of the major chemistry controlling parameters – organic carbon, total Si and Al, calcium carbonate and total Fe – have been investigated on a seasonal basis because these might indicate any major sediment changes. Total Co was included as a parameter because it can be used as a mineralogical indicator; total Cu because it is generally associated with the organic fraction and so might give more information about this important parameter. Total Hg is included because it is environmentally interesting. For Fe, Mn and Zn, in addition to analyzing total metal content (Buckley and Cranston, 1971), the concentration of metal removable by weak acid leaching (which removes metal bound in calcium carbonate and those which are loosely bound or absorbed; Chester and Hughes, 1967), the concentration removable by hydrogen peroxide leaching

From: Report of Activities, Part C;
Geol. Surv. Can., Paper 76-1C (1976).

(which removes some fraction of the metals bound in the organic material; Presley *et al.*, 1972) and the concentration of metals removable by hydroxylamine hydrochloride leaching (which gives an indication of the importance of oxide coatings; Chester and Hughes, 1967) have also been determined.

Results and Discussions

Results are shown in Tables 11.1A and 11.1B. No changes were found in total Si, total Al, $CaCo_3$, Co or Cu; this indicates no major seasonal variations in the aluminosilicate mineralogy or carbonate content. The organic carbon content also did not vary seasonally in the muds (surface or subsurface). In the sands, a much higher organic carbon content was found in May compared with September or February. This increase corresponds to an increased amount of lignin (wood particles) at this time, and these occur primarily in the sand size fraction. Whether this increased wood input is a seasonal variation, or a random fluctuation resulting from human activities is not yet determined. The Hg content was found to be much greater in February than in the other seasons. The difference was most pronounced in the surface muds, but was also discernible in the surface sand and subsurface mud fractions.

Some seasonal variations were observed for the various fractions of Fe. Total Fe and easily reducible (oxide layers) Fe were found to be greatest in February in the fine fraction; total Fe was least in May in this fraction. These effects extended with reduced importance into the subsurface layer. There was no variation in the peroxide leachable Fe or in the weak acid leachable Fe in the fines. In the sands, the total Fe was much less than in the fine fraction, and this decreased in concentration from September through May. There was no seasonal variation in the other fractions of Fe in the sands.

In the fine fraction, the only seasonal variation that is significant for Mn is in the reducible fraction; this is 30 per cent of the total in February, and is insignificant during the other two seasons. In the sand fraction, total Mn is least in February and the reducible fraction is not significant at any season.

In the surface muds, and to a lesser extend in the subsurface muds, the reducible fraction of Zn was found to be significant only in February, when it was 20 per cent of the total Zn. In these fractions, total Zn was least in May. In the sand fraction, total Zn was least in February, and this is reflected in decreases in the other fractions at that time. The reducible fraction was a very small fraction of the total Zn in the sands at all seasons.

Table 11.1A

	Organic C %		$CaCO_3$, %		Si_T, %		Al_T, %		Co_T, ppm		Cu_T, ppm		Hg_T, ppm	
	$\bar{x}$	σ	$\bar{x}$	σ	$\bar{x}$	σ	$\bar{x}$	σ	$\bar{x}$	σ	$\bar{x}$	σ	$\bar{x}$	σ
September, 1975	2.5	0.6	0.19	0.07	29.7	2.0	6.15	0.75	13	2	29	10	0.22	0.14
February, 1976	3.0	0.4	0.26	0.12	28.0	1.2	5.40	0.53	20	4	27	5	0.62	0.45
May, 1976	3.5	1.7	0.42	0.53	26.0	2.0	7.64	1.54	23	7	31	20	0.19	0.08

	Fe_T, %		Fe_w, ppm		Fe_p, ppm		Fe_H, ppm		Mn_T, ppm		Mn_w, ppm	
	$\bar{x}$	σ	$\bar{x}$	σ	$\bar{x}$	σ	$\bar{x}$	σ	$\bar{x}$	σ	$\bar{x}$	σ
September, 1975	3.62	0.8	2010	680	2040	620	1840	490	483	48	60	35
February, 1976	4.83	0.3	1470	530	1680	690	4760	2500	413	145	179	160
May, 1976	1.71	0.3	2140	760	1840	110	1350	450	292	105	158	92

	Mn_p, ppm		Mn_H, ppm		Zn_T, ppm		Zn_w, ppm		Zn_p, ppm		Zn_H, ppm	
	$\bar{x}$	σ	$\bar{x}$	σ	$\bar{x}$	σ	$\bar{x}$	σ	$\bar{x}$	σ	$\bar{x}$	σ
September, 1975	81	16	23	7	270	77	74	23	132	72	6	7
February, 1976	204	129	114	93	213	83	28	7	93	89	42	5
May, 1976	97	58	0	0	-	-	42	21	76	54	2	4

Sediment geochemical parameters for the surface fines (<63 μm) fraction for the three seasonal samplings. $\bar{x}$ = average, σ = standard deviation, Me_T = total metal concentration, Me_w = weak acid leachable metal concentration, Me_p = hydrogen peroxide leachable metal concentration, Me_H = hydroxylamine hydrochloride leachable metal concentration. Number of samples varied from 4 to 7. (-) indicates no analytical result.

The results indicate that the reducible fraction (the oxide layers) of Fe, Mn and Zn is only significant in February, and then only in the fine fraction. This change is accompanied by higher levels of total Fe and Hg in the fine fraction in February. This is followed in May by the lowest concentrations of total Fe, Mn and Zn in the fines, and the lowest total Fe and Zn in the sands. One possible mechanism for this variation is related to the movements of the suspended particulate material.

Suspended particulate material has been found by several investigators (for example, Spencer and Sachs, 1970; Piper, 1971) to be enriched with Fe, Mn and Zn compared with bottom sediments. Cranston and Buckley (1972) reported that suspended material is also enriched with Hg. Kranck (1974) reported that an increased amount of suspended material was found in the Miramichi estuary where mixing of different salinity water occurred (for samples collected in the autumn), which indicates that at that time some flocculation and scavenging may have been occurring. Rust and Waslenchuk (1974) found that in sediments from the Ottawa River, Fe, Mn and Hg concentrations in surface coatings are interrelated, with higher concentrations in finer particulate sizes, and they find greater concentrations of Fe in the sediments during times of quiescent waters, which could indicate settling of suspended particulate material during times of low water movements.

These findings indicate that in the Miramichi estuary, suspended particulate material may be settling out onto the surface of the bottom sediments in February when currents are at a minimum because of the ice cover. The presence in the sediment of this deposited particulate material is indicated by the increased concentrations of Fe, Mn, Zn and Hg because these are all enriched in suspended material relative to bottom sediments. Oxide coatings should also be more important in suspended particulate material because it is exposed to well oxygenated water, and it has scavenged metals from the surrounding water. The high concentrations of metals in February are subsequently removed by flushing out of the fine grained sedimented particulate material during the high current velocities that occur during spring runoff, and this removal of fine material causes the low concentrations of metals that are found in May. This theory is substantiated by the greatly reduced amounts of suspended particulate material in the water column in February compared with the other two samplings; additional sampling during the coming year should show if this kind of process recurs.

This kind of sedimentation pattern has several environmental implications. Kranck (1974) reported that the pulp and paper industry contributes a significant amount of suspended particulate material to the Miramichi estuary; this material enters the environment as a warm surface layer. The settling out of suspended particulate material from this surface layer provides a mechanism

Table 11.1B

	Organic C %		Wood, %		$CaCO_3$, %		Si_T, %		Al_T, %		Co_T, ppm		Cu_T, ppm	
	$\bar{x}$	σ	$\bar{x}$	σ	$\bar{x}$	σ	$\bar{x}$	σ	$\bar{x}$	σ	$\bar{x}$	σ	$\bar{x}$	σ
September, 1975	1.9	1.6	2.6	2.8	0.16	0.10	31.2	2.9	4.90	0.38	14	2	16	6
February, 1976	1.1	0.8	3.2	2.3	0.37	0.26	31.5	1.6	3.56	0.22	11	5	10	2
May, 1976	3.4	3.5	9.8	7.9	0.24	0.18	20.4	4.8	4.46	0.55	13	2	9	2

	Hg_T, ppm		Fe_T, %		Fe_w, %		Fe_p, ppm		Fe_H, ppm		Mn_T, ppm		Mn_w, ppm	
	$\bar{x}$	σ	$\bar{x}$	σ	$\bar{x}$	σ	$\bar{x}$	σ	$\bar{x}$	σ	$\bar{x}$	σ	$\bar{x}$	σ
September, 1975	0.17	0.15	2.63	1.20	1350	850	1470	910	1740	1320	310	160	56	43
February, 1976	0.33	0.29	1.54	0.14	670	220	980	560	1200	970	124	62	63	66
May, 1976	0.09	0.05	0.65	0.12	830	520	990	1060	870	1420	203	130	109	69

	Mn_p, ppm		Mn_H, ppm		Zn_T, ppm		Zn_w, ppm		Zn_p, ppm		Zn_H, ppm	
	$\bar{x}$	σ	$\bar{x}$	σ	$\bar{x}$	σ	$\bar{x}$	σ	$\bar{x}$	σ	$\bar{x}$	σ
September, 1975	112	59	26	37	139	35	89	58	53	32	9	12
February, 1976	96	148	12	21	53	23	12	6	22	23	10	11
May, 1976	76	69	1	2	-	-	23	15	46	46	2	4

Sediment geochemical parameters for the surface coarse (>63 μm) fraction for the three seasonal samplings. All symbols are defined in Table 11.1A.

for transporting contaminants from the surface waters into the bottom sediments. This settling process would also act to increase the residence time of any particulate contaminants introduced into the estuary in the winter.

Additional analyses of the suspended particulate material, and continuing sampling of both the sediments and the suspended material should assist in further interpreting these preliminary ideas.

References

Buckley, D.E. and Cranston, R.E.
1971: Atomic absorption analyses of 18 elements from a single decomposition of aluminosilicate: Chem. Geol., v. 7, p. 273-284.

Chester, R. and Hughes, M.J.
1967: A chemical technique for the separation of ferro-manganese minerals, carbonate minerals and adsorbed trace metals from pelagic sediments: Chem. Geol., v. 2, p. 249-262.

Cranston, R.E. and Buckley, D.E.
1972: Mercury pathways in a river and estuary: Environ. Sci. Tech., v. 6, no. 3, p. 274-278.

Kranck, K.
1974: The role of flocculation in the transport of particulate pollutants in the marine environment: *in* Proceedings of the International Conference on Transport of Persistent Chemicals in Aquatic Ecosystems, Ottawa, Canada, May 1-3, 1974, p. 1-41-1-46.

Piper, D.Z.
1971: The distribution of Co, Cr, Cu, Fe, Mn, Ni and Zn in Framvaren, a Norwegian anoxic Fjord: Geoch. Cosmochim. Acta, v. 35, p. 531-550.

Presley, B.J., Kolodny, Y., Nissenbaum, A., and Kaplan, I.R.
1972: Early diagenesis in a reducing fjord, Saanich Inlet, British Columbia-11. Trace element distribution in interstitial water and sediment: Geoch. Cosmochim. Acta, v. 36, p. 1073-1090.

Reinson, G.E.
1976: Surficial sediment distribution in the Miramichi estuary, New Brunswick; *in* Report of Activities, Part C; Geol. Surv. Can., Paper 76-1C, rep. 9.

Rust, B.R. and Waslenchuk, D.G.
1974: The distribution and transport of bed sediments and persistent pollutants in the Ottawa River, Canada: *in* Proceedings of the International Conference on Transport of Persistent Chemicals in Aquatic Ecosystems, Ottawa, Canada, May 1-3, 1974, p. 1-25-1-40.

Spencer, D.W. and Sachs, P.L.
1970: Some aspects of the distribution, chemistry, and mineralogy of suspended matter in the Gulf of Maine: Marine Geol., v. 9, p. 117-136.

12. AN INTERACTIVE GRAPHIC SYSTEM FOR INTERPRETATION OF DIPOLE E.M. SOUNDING DATA

Project 730004

A.K. Sinha
Resource Geophysics and Geochemistry Division

Introduction

In geophysical exploration, the physical parameters of the earth are deduced on the basis of recording and interpreting the interaction of one or more potential fields with the earth's crust, or more specifically, with the top layers of the earth's crust. Interpretation of field data may be approached from two angles; direct and indirect. In the indirect method, the observed data is graphically compared with a set of previously compiled and plotted 'standard curves' drawn for an assumed model for various combinations of parameter values until a satisfactory match is obtained between the field curve and one of the standard curves. However, a perfect match is rarely obtained between the field and the standard curves, thus necessitating the use of interpolation for the interpretation. Hence a prerequisite for this type of interpretation is ready availability of a large number of standard curves. In the direct method, on the other hand, the parameters of the ground are obtained without using any master curves by manipulating the field data suitably after choosing a proper model.

For the interpretation of D.C. sounding data, both direct and indirect methods have been available for some time (Zohdy, 1975; Kunetz, 1966). However, the progress in the interpretation of electromagnetic sounding data has been slow. The reason for this is the solution of the e.m. wave equation for the layered media is much more complex analytically than the corresponding D.C. case. Furthermore, since there are many extra parameters to consider in e.m. sounding, specially dipole-dipole sounding, even the indirect methods of interpretation have progressed to the extent that only one and two layer cases may be considered.

The formal solutions for the forward problem of generating the e.m. response of multilayer earth sections excited by dipolar sources have been developed (Wait, 1962). Complete solutions as well as appropriate computer programs for obtaining the dipolar response of multilayer earth sections have been developed and published (Sinha and Collett, 1973). Even with that it would be impractical to compile a set of master curves similar to those in D.C. resistivity prospecting since the number of possible parameters is very large and consequently, the number of master charts would be enormous.

Interactive Graphic System

To get around this problem, an interactive graphic system to interpret electromagnetic sounding data may be used. Basically, this means that instead of plotting theoretical master curves for comparison with the field curve (say, a frequency sounding curve), the field and theoretically computed curves are displayed on an interactive terminal screen. Looking at the field and the theoretical curve obtained from an approximate model, one may decide to change the theoretical model parameters in such a way that the two match. The experience of a trained geophysicist however will be required to decide which of the model parameters should change for a better match. All the necessary commands are sent via the attached teletype machine, thus accomplishing a good man-machine interaction. Since the program to generate the theoretical response of an n-layer earth excited by dipolar sources is available in five coil configurations (Sinha and Collett, 1973), all that is needed is to build a suitable interface between the graphic terminal and the computer for the man-machine interaction. In our case, the Princeton 801 Graphic Terminal available at the Geological Survey of Canada, Department of Energy, Mines and Resources was used which is compatible with the CDC-6400 computer. A contract was awarded to Ottawa University to design the software for the interfacing and this was completed in 1975. The salient features of the system are described in the next section.

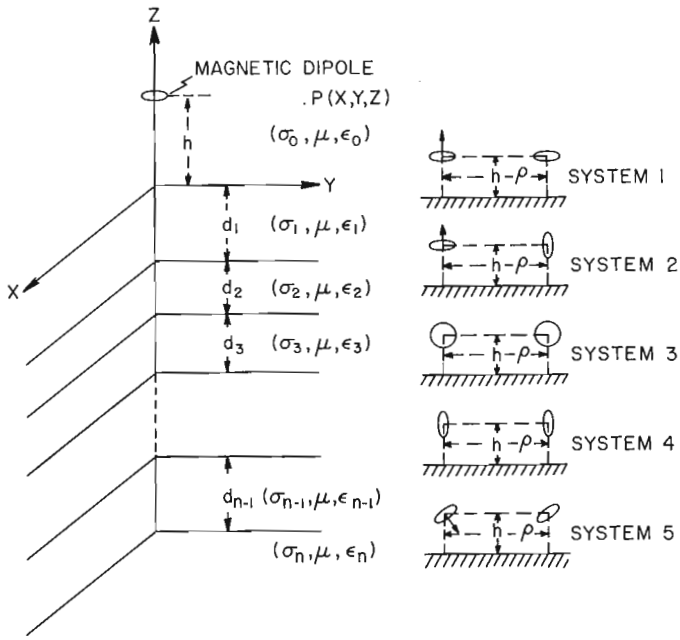

Figure 12.1. Magnetic dipole source over an an n-layer earth and the five coil configurations.

From: Report of Activities, Part C;
Geol. Surv. Can., Paper 76-1C (1976).

Operation of the System

There are three versions of the interactive package called GRAPOL. In version 1, the parameters on both X and Y axes are plotted on linear scale, version 2 plots them on semi-log scale (X-axis linear) and in version 3 double-log plotting is used. The user may indicate his preference for any of them while attaching the relevant files to the computer. The input is provided in several steps as the system asks for it.

Step 1: System Code (Syscod) This defines the coil system under consideration. This is entered as a single digit which varies from 1 to 5 (Fig. 12.1).

Step 2: Height of the coil system over the ground.

Step 3: Coil separation RH.

Step 4: Number of points to be computed for the theoretical curves.

Step 5: Field data points digitized to read (frequency)$^{\frac{1}{2}}$ versus real and imaginary parts of the mutual coupling ratio (Z/Z_o) in parts per million.

Looking at the field curves (real and imaginary), the geophysicist at the control makes a rough guess about the parameters and inputs those values to the system. The theoretical input is provided in several steps.

Step 1: Number of layers (NUM).

Step 2: Conductivity of the top layer (SIGMA 1).

Step 3: Conductivity ratios for the layers (K_n).

Step 4: Thicknesses of the layers (d_n).

Once these inputs are provided, the system computes the real and imaginary parts of (Z/Z_o) versus B for the model and plots them on the screen. B is given by

$$B = RH \left(\frac{\omega \mu \sigma_1}{2}\right)^{\frac{1}{2}} \quad \ldots\ldots\ldots\ldots\ldots\ldots (1)$$

where

ω = 2π x frequency in hertz

μ = permeability = $4\pi \times 10^{-7}$ H/m

σ_1 = conductivity in Siemens/m of the top layer.

This may be repeated as many times as needed until a good match is obtained. All the computed values during the trial are retained in memory and may be brought back on the screen if desired. In addition sixteen precalculated 'standard curves' with different combinations of thicknesses and conductivities are kept permanently stored in the system for recall any time. The real and imaginary curves are indicated by letters R_n and I_n, n indicating the sequence number.

There are various operation codes (OPCODES) for carrying out different operations. They are:

(i) Plotting theoretical real and imaginary plots and specifying the curve number n.

(ii) Erasing either one or both real and imaginary curves selectively by curve number n.

(iii) Displaying input parameters that the operator has specified earlier and specifying the set number n.

(iv) Displaying the computed numerical values for any set of input data by specifying the set number n.

(v) Displaying the scales used along X and Y axes.

(vi) Erasing all lines in the display and start a new page with new co-ordinate axes.

(vii) Shifting any theoretical curve along X-axis by specified amounts. The total shift of one line from the original position may always be obtained. This operation is necessary for getting the σ_1 value.

The interactive graphic system was used on some synthetic dipole-dipole sounding data and it was seen that in general 4 or 5 trials brought the interpretation quite close to the originally assumed parameters. However, as in many geophysical problems, the basic ambiguity of the field allows many possible models to have the same response. The cost of computing the real and imaginary parts of (Z/Z_o) at one point varied according to the number of layers chosen. Since dipole electromagnetic methods can scarcely distinguish more than three layers, only two and three layer models were selected. The computing time for each point varied from 0.2 to 0.4 seconds on the computer.

Concluding Remarks

The technique of interactive interpretation of e.m. dipole sounding data is superior to methods used previously and permits a geophysicist sitting at the terminal to control the direction in which the interpretation should proceed. It should be noted, however, that for large scale surveys, the cost of interpretation may become quite high.

In order to ensure good penetration of the ground, the highest frequency of the transmitter current in normal electromagnetic mapping work rarely exceed 40-50 Khz. Since displacement currents are negligible in that range for most earth materials, they have been ignored in all the media.

Acknowledgments

I am thankful to Prof. J. Raymond and Prof. D. Banerji of the University of Ottawa for their help in designing the software for the interactive interpretation of e.m. sounding data.

References

Kunetz, G.
1966: Principles of direct current resistivity prospecting; Geoexploration Monographs, Ser. 1, No. 1, Stuttgart.

Sinha, A.K. and Collett, L.S.
1973: Electromagnetic fields of oscillating magnetic dipoles placed over a multilayer conducting earth; Geol. Surv. Can., Paper 73-25, 48 p.

Wait, J.R.
1962: Electromagnetic waves in stratified media; Pergamon Press, New York.

Zohdy, A.A.R.
1975: Automatic interpretation of Schlumberger sounding curves using modified Dar Zarrouk parameters; U.S. Geol. Surv., Bull. 1313-E, Washington.

13. SUSPENDED SEDIMENT ANALYSIS OF SEAWATER USING LANDSAT IMAGERY, MINAS BASIN, NOVA SCOTIA

Project 740012

C. L. Amos
Atlantic Geoscience Centre, Dartmouth

Introduction

Satellite imagery and digital data, recorded by LANDSAT 1 and LANDSAT 2, were analyzed in order to determine the variation in suspended sediment concentration (S. S. C.) within the tidal waters of the Minas Basin-Cobequid Bay region, Nova Scotia (Fig. 13. 1). The satellite information will be used in conjunction with an extensive field program which involves the study of the budget of sediments within the Minas Basin. The lack of monitoring equipment for direct field study and the complexity of sediment-transport theory makes satellite imagery a very attractive tool for tracing suspended sediment. By interfacing the field data collected on S. S. C. (over 200 hours monitoring in the field) with the LANDSAT imagery, it is hoped that the sediment budget will be defined more accurately in terms of the transport paths of the suspended sediment, the relative concentrations of suspended sediment at any one time across the study area, and the factors which control the S. S. C. within the water column.

The Study Area

The Minas Basin-Cobequid Bay system is a semi-enclosed body of water at the head of the Bay of Fundy. The system is 77 km long and up to 31 km wide (Pelletier and McMullen, 1972). It contains a body of water approximately 15. 3 km^3 of which 3. 81 x $10^9 m^3$ is the intertidal volume of water flooding the system during spring tides (spring tidal range = 18 m, Canadian Hydrographic Service, 1966). The perimeter is

Figure 13. 1. A black and white LANDSAT image of the study area in M. S. S. band 4. Note the areas of relatively high and low sediment concentrations.

From: Report of Activities, Part C;
Geol. Surv. Can., Paper 76-1C (1976).

bordered by cliffs, composed of soft glacial outwash sand, friable Triassic sandstone and indurated Paleozoic rocks. These cliffs are regressing 0.5 metres/year and supply the major part of the sediment to the system. Very little sediment is supplied by fresh water discharge (average concentration = 3 ppm, Atlantic Tidal Power Programming Board, written comm., 1969) or from the open sea (Vilks and Amos, 1975). The depositional sites of the derived sediments are within Cobequid Bay, parts of the intertidal zone and the heads of the estuaries leading from the system. It has recently been discovered that there is an ebb delta at the seaward end of the mouth of Minas Basin. In contrast to the majority of inlets which have an influx of sediment, this was formed by the transport of sediment seaward from the system. The existence of this delta substantiates calculations made on the residual transport of sediment through Minas Channel (Amos, *et al.*, 1976). These calculations suggest a net outflux of sediment of $16.8 \times 10^3 m^3$/tide.

The suspended sediments of the study area are evenly distributed and appear texturally and mineralogically homogeneous throughout the water column. The S.S.C. varies from approximately 1 ppm in the central part of the system to approximately 30 ppm at the margins. During periods of high wave activity the marginal concentrations can be as high as 90 ppm. Initial microscopic and granulometrix examination of the suspended sediments indicate that they are bimodal. One mode is in the sand and the second in the silty clay range.

Table 13.1

Station No.	Suspended Sed. Conc. ppm*	Chlorophyll "a" µg/ℓ**	Transformed Radiance Value
1	25.92	-	.447
2	26.08	.12	.465
3	24.68	.11	.475
4	19.76	.10	.465
5	15.48	-	.500
6	36.40	.11	.445
7	39.40	.11	.425
8	34.28	-	.425
9	79.48	.07	.405
10	92.92	.06	.375
11	-	.06	.462

*Taken 23/8/75 **Taken 5/8/75

The S.S.C. at any one point within the study area is dependent on at least five variables. These are:

1. Wave activity; during periods of high wave activity, the S.S.C. has been observed to increase three-fold.
2. Mean water depth; the highest concentrations of sediment are generally found in the shallower water.
3. The stage of the tide; the highest concentrations are observed at low water.
4. The range of the tide; the highest S.S.C. would be expected during the spring tides due to the greater tidal currents.
5. The season; the S.S.C. is high during the autumn and spring due to the higher sediment supply from a terrestrial source; during the summer the S.S.C. is intermediate, and during the winter it is lowest, due to wave damping by floating ice and freezing of the sediment otherwise available for suspension (Knight and Dalrymple, in press).

Satellite Imagery

Satellite imagery was used in two ways during the course of this study:

1. As a qualitative guide to the transport of suspended sediment and as a means of defining areas of relatively high and low S.S.C.
2. As a means of determining the absolute concentration of suspended sediments within the water column synoptically, across the entire system.

In the first application false colour images (scale 1:1 000 000) were examined, together with images of M.S.S. band 4 (500nm-600nm; blue/green) and band 5 (600nm-700nm; red). Figure 13.1 is an image of the study area in M.S.S. band 4. In the figure the highest chromatic densities of the seawater (highest S.S.C.) occurs near the shore. The sediment in the water behaves as a passive tracer, illuminating the complicated tidal circulation patterns occurring in the system. The images represent one instant of time only, therefore a statement on the S.S.C. and associated transport paths can only be made for that time interval and suite of environmental conditions. In order to generate a representative model, a number of images of the area, constituting a wide variation in the relative combinations of the five variables considered affecting sediment concentration, will be generated. For example, the satellite passes overhead at the exact same time every 18th day (1430 G.M.T.). Since tidal range and tidal flow follow a 12 hr 25 min frequency, the satellite will pass overhead at different stages and ranges of the tides. In Figures 13.2A and 13.2B the magnitude of the range in the tide has been plotted against stage of the tide for the overpass of LANDSAT 1 and LANDSAT 2 during the summers of 1975 and 1976 respectively.

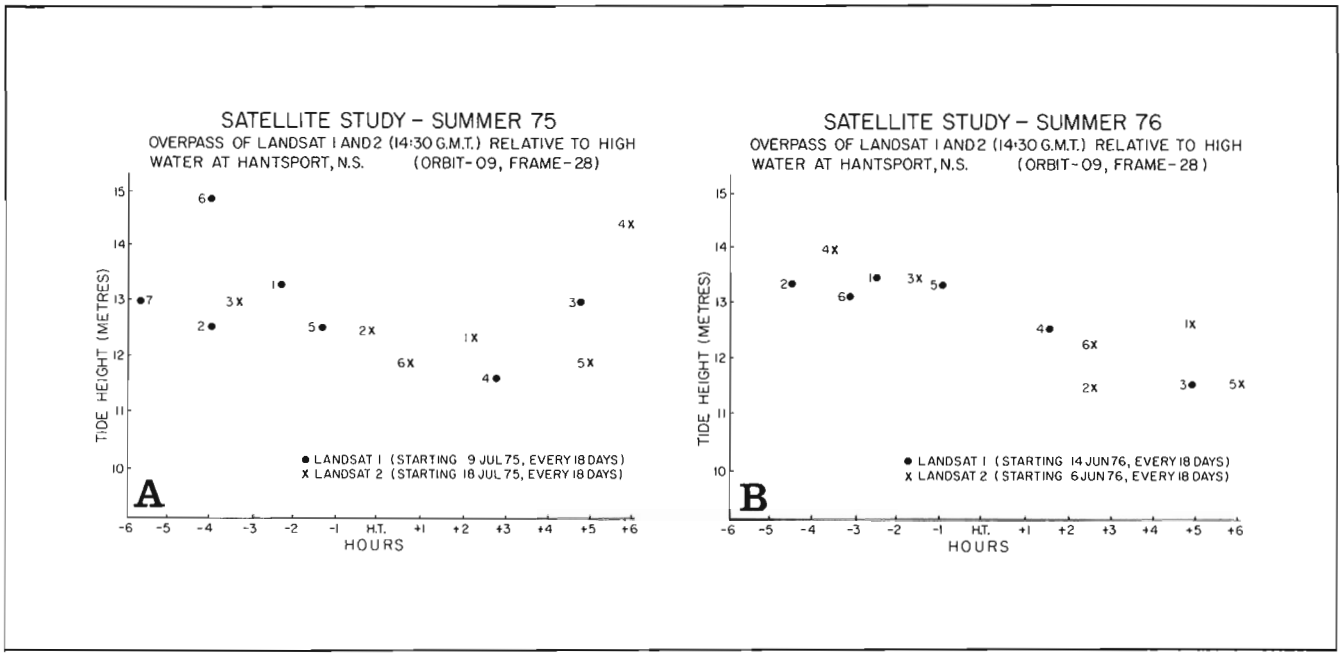

A — Summer 1975 B — Summer 1976

Figure 13.2. A scatter diagram of the tide height against stage of the tide for each overpass of LANDSAT 1 and 2 for the study area (orbit-09, frame-28).

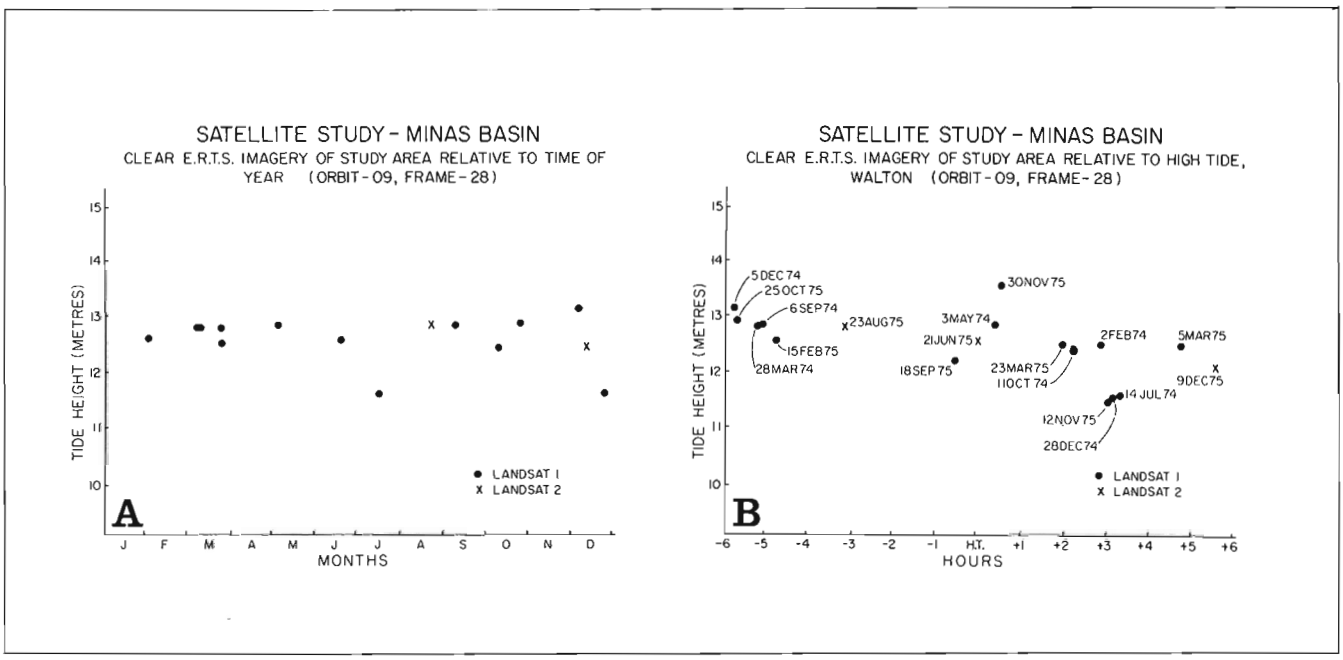

Figure 13.3A — A scatter diagram of the tide height against season for each of the clear overpasses of LANDSAT 1 and 2 for the study area (orbit-09, frame-28).

B — A scatter diagram of the tide height against stage of the tide for each of the clear overpasses LANDSAT 1 and 2 for the study area (orbit-09, frame-28).

In Figures 13.3A and 13.3B the tide height has been plotted against season and stage of the tide respectively for the clear imagery of the study area. An examination of this LANDSAT imagery indicates that a representative suite of the variables plotted are covered by the clear imagery.

The derivation of the absolute concentration of suspended sediment, using LANDSAT imagery, was attempted by ground truthing during times of clear satellite overpasses. This involved sampling of surface waters at specified sites representative of the range in S.S.C. found in the study area. During the summer of 1975, five attempts were made in the Avon Estuary (Minas Basin), only one of which coincided with acceptable atmospheric conditions. Samples were collected, using a series of speed boats, across a S.S.C. gradient at sampling intervals of 1 km (*see* Fig. 13.4). The results of S.S.C. and chlorophyll analysis of these samples are plotted in Table 13.1.

The digital chromatic intensities in M.S.S. band 4 radiated from the ground truth sites, were normalized by using the following transformation:

$$x = \frac{Hi}{\Sigma Hi}$$ Where Hi is the water radiance in band i

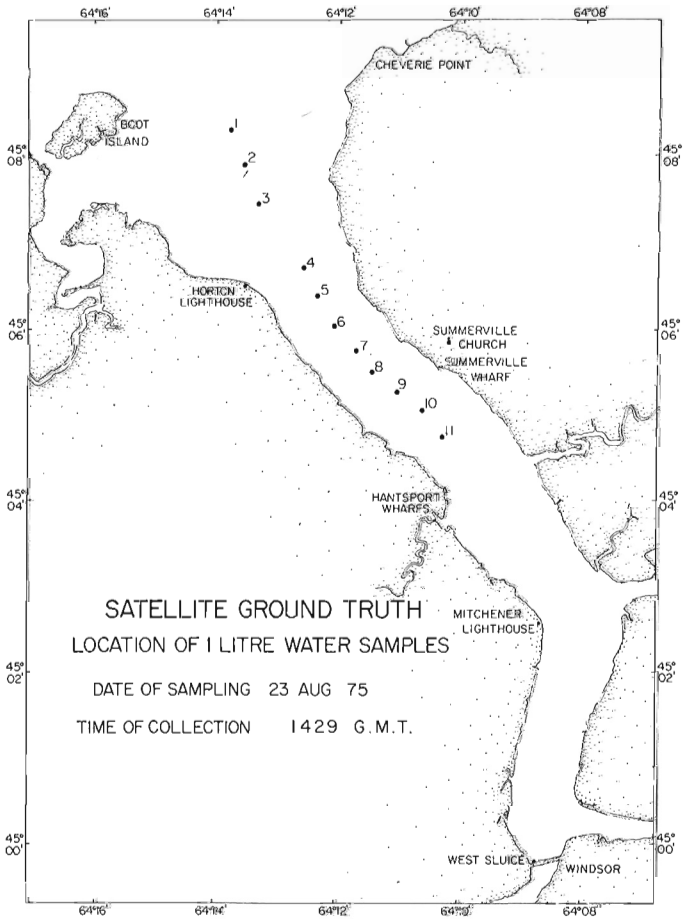

Figure 13.4. A location map of the surface water samples, taken in the Avon estuary as part of the ground truthing program for LANDSAT imagery; 23 August 1975.

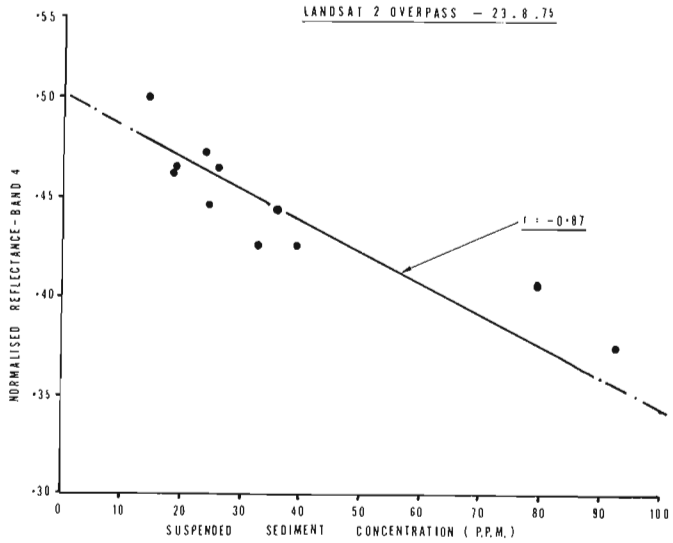

Figure 13.5. A plot of the linear regression analysis of suspended sediment concentration on the transformed reflectance value in M.S.S. band 4 for the overpass of 23 August 1975, LANDSAT 2 (orbit-09, frame-28).

(Alföldi and Munday, in prep; Munday, 1974a; Munday, 1974b). A linear regression of S.S.C. on the transformed radiance value was performed in the S.S.C. range 10-90 ppm. The result of this is plotted in Figure 13.5, which shows an inverse relationship of the two variables with a correlation (r) of -0.87. This relationship is significant at the 99.9 per cent confidence level.

During the summer of 1976, a similar survey to that described above was conducted at sites with S.S.C. values within the 0-10 ppm range. A further regression analysis will be performed to derive a correlation of S.S.C. to the transformed radiance values. Once these relationships have been generated, quantitative determinations of the S.S.C. can be made directly for each clear overpass of the area.

Facilities are available at Canada Centre for Remote Sensing to analyze digitized radiance signals, transmitted from the satellite, by means of a General Electric, Image 100 (Alföldi and Munday, in prep). A colour video screen will be used to study the images created from the data (stored on 9-track tape at 1500 bpi). In this manner, enhancement techniques (*see* Fig. 13.6A) can be adopted to define subtle changes in chromatic intensity (chromatic intensity $\propto \frac{1}{\text{chromatic density}}$) representing corresponding changes in S.S.C. These subtle differences will be enhanced further by slicing the chromatic intensities into a series of classes which can then be plotted as shown in Figure 13.6B. Each class has a narrow range of S.S.C. It is hoped to analyze at least 15 tapes of the area, in this fashion, all with acceptable atmospheric conditions. Twenty sites will be chosen and examined on each of the 15 clear images generated (representative of the entire study area) and the S.S.C. will be calculated based on the

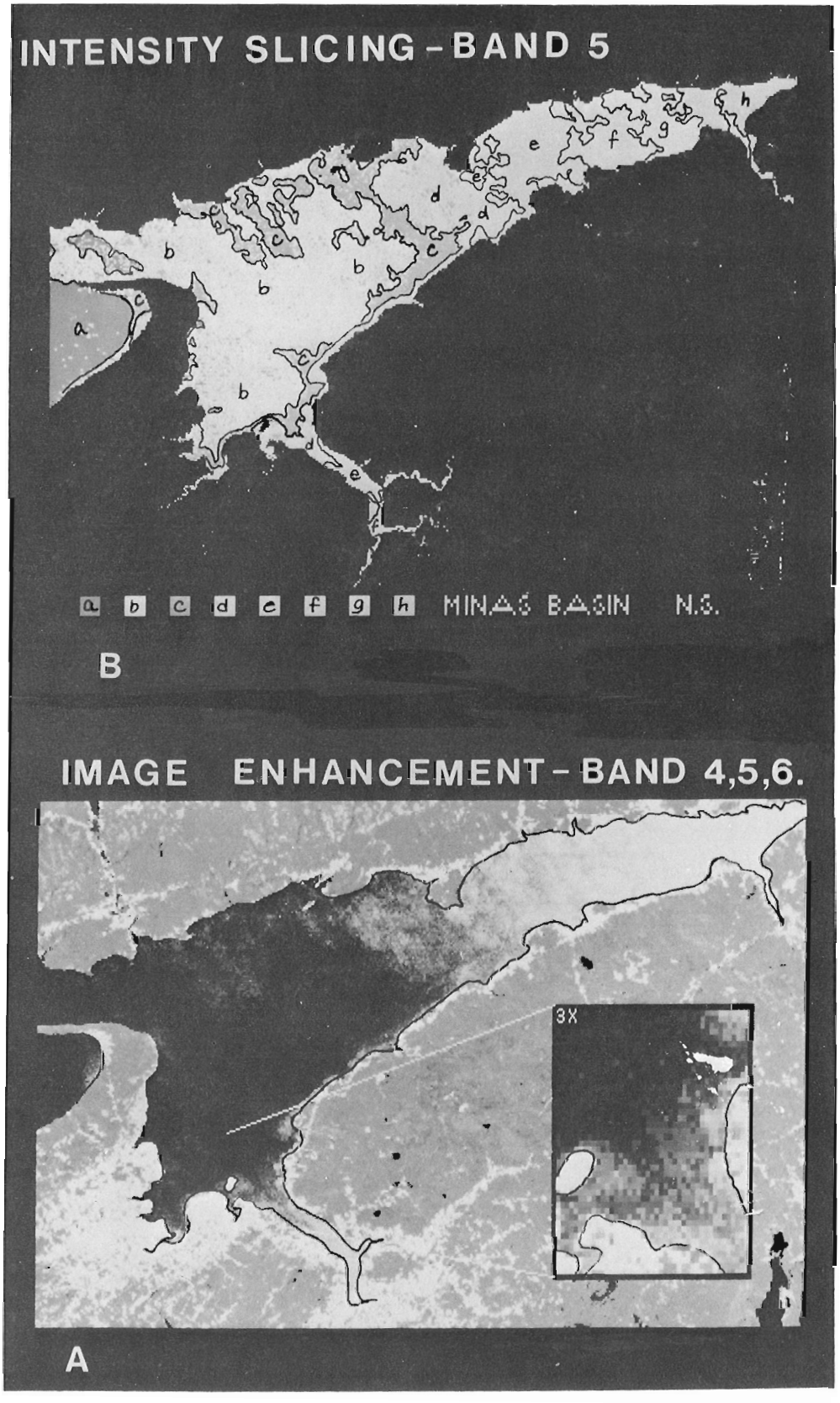

Figure 13.6

A — A black and white copy of a false colour enhanced image of Minas Basin. The inset indicates the ground-truth area enlarged three times.

B — A black and white copy of a false colour image of an 8 class intensity slice of M.S.S. band 5. The lowest S.S.C. (highest intensity) is indicated by symbol: a, the highest S.S.C. (lowest intensity) is indicated by symbol: h.

regression analysis. A stepwise multiple regression analysis of S.S.C., at the 20 sites on the five variables considered to be affecting the sediment concentration, will then be performed. This analysis will indicate the relative and absolute significance of each of the independent variables on the S.S.C., and the percentage of the S.S.C. variation accounted for by the combined effects of the five variables.

Finally, from the above manipulation of the satellite imagery a history of the S.S.C. development, transport paths and controlling factors can be derived which will then be incorporated into the sediment budget model currently under study.

References

Alföldi, T.T. and Munday, J.C.
Water quality analysis by digital chromaticity mapping of Landsat data. in prep.

Amos, C.L., Long, B.F., and Schafer, C.T.
1976: Cruise report No. 76-014(2). C.S.S. DAWSON; Bedford Institute of Oceanography Report Series, May 21-28, 1976.

Canadian Hydrographic Service
1966: Bay of Fundy, data report on tidal and current survey, 1965; Bedford Institute of Oceanography Data Series 66-2-D, Aug. 1966.

Knight, J.R. and Dalrymple, R.W.
Winter conditions in a Macrotidal environment, Cobequid Bay, Nova Scotia; Rev. Geogr., Montreal, v. 30, p. 65-86. in press.

Munday, J.C.
1974a: Lake Ontario water mass delineation from ERTS-1; Proc. 9th Int. Symp. on Remote Sensing, v. 2, April, 1974, p. 1355-1368.

1974b: Water quality of lakes of southern Ontario from ERTS-1; 2nd Canadian Symp. on Remote Sensing, v. 1, April-May, 1974, p. 78-82.

Pelletier, B.R. and McMullen, R.M.
1972: Sedimentation patterns in the Bay of Fundy and Minas Basin; *in* Tidal Power, Ed. Gray, T.J., Gashus, O.K., Plenum Publ. Co., p. 153-187.

Vilks, G. and Amos, C.L.
1975: Cruise report No. 75-028(2). C.S.S. DAWSON; Bedford Institute of Oceanography, Report Series, 1975.

14. GEOLOGY OF THE CONTINENTAL SHELF OFF SOUTHEASTERN LABRADOR

Projects 750001, 730081, and 750061

R. T. Haworth, A. C. Grant, and R. A. Folinsbee
Atlantic Geoscience Centre, Dartmouth

Introduction

In continuation of the hydrographic-geophysical multiparameter surveys off the east coast of Canada, a co-operative project of the Atlantic Geoscience Centre and the Canadian Hydrographic Service (Department of the Environment), the M/V Martin Karlsen completed reconnaissance coverage of the entire Labrador Sea and began detailed coverage of the Labrador Shelf in 1975. The area of detailed coverage lies to the north of the area of a geoscience survey northeast of Newfoundland (Fig. 14.1; Haworth *et al.*, 1976). The seismic reflection, magnetic gravity and bathymetry data collected from M/V Martin Karlsen are sufficient to extend the southern geological framework across a large portion of the Labrador inner shelf and the adjacent troughs and banks (Fig. 14.2).

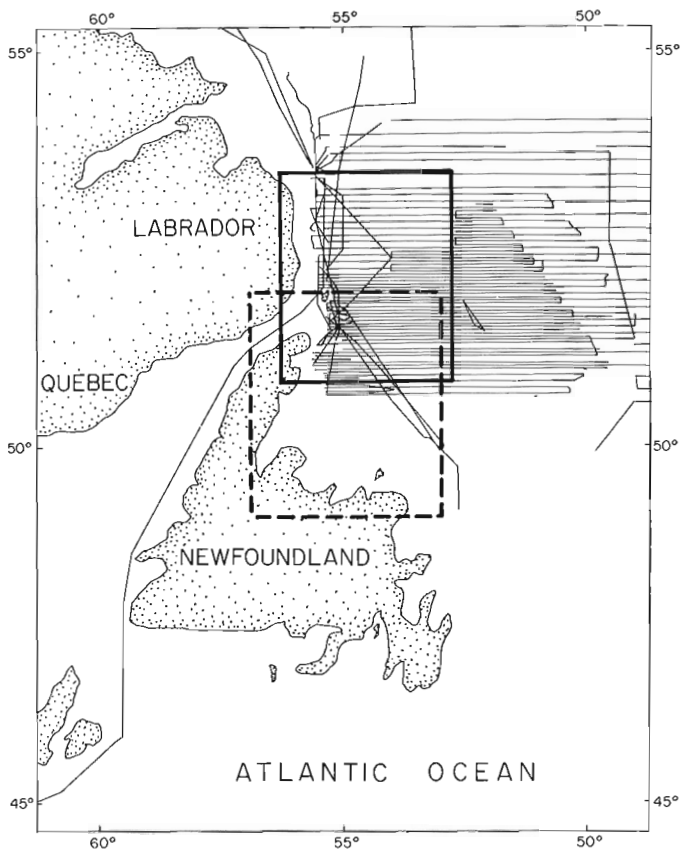

Figure 14.1. Location of study area (solid outline) with respect to the survey lines of M/V Martin Karlsen cruise 75-018 and the study area of Haworth *et al.* (1976).

Data Collection

Navigation for the survey was provided by the Loran-C chain of Angissoq (southern Greenland) and Cape Race (southeast Newfoundland) with the support of a Decca 12f system near the Loran-C baseline. Continuous comparison with satellite navigation fixes allowed correction for variations in Loran-C ranges due to changes in clock rate and overland phase delay. The navigation system operated well and it is estimated that the maximum positional error is of the order of 200 m (Warren, 1976). Some errors in positioning of the data collected by Haworth *et al.* (1976) were discovered during its integration with the Martin Karlsen data. These errors have been corrected in this presentation.

Bathymetric data were collected using a 12 kHz wide-beam echo sounder from which bottom returns were processed with a Raytheon signal correlator. A representative sample of these data was used in the hand plotting of the hydrographic field sheets. A contour map of much of the area, prepared by Warren (1976), was supplemented in the preparation of Figure 14.3 by information on the Labrador Inner Shelf collected during U.S. hydrographic surveys (*see* Canadian Hydrographic Service charts 4731, 4701 and 4702), on Hamilton Bank from van der Linden *et al.* (1976), and south of Belle Isle from Haworth *et al.* (1976).

Seismic reflection information was collected on lines at an average spacing of 37 km using Bolt airguns with chamber sizes of 164, 656, 1966 and 4916 10^{-6} m^3 (10, 40, 120 and 300 in^3), the largest gun being used only over the shelf edge, outside this study area. Intersecting seismic lines collected by Grant (1972) and van der Linden (1973) have been used in the interpretation and correlation of the Martin Karlsen data.

The gravity field was measured on all tracks with a Graf-Askania Gss-2 surface ship gravimeter whose output was recorded automatically at intervals of one minute. Gravity values were calculated with reference to IGSN '71 datum (Morelli *et al.*, 1973). These were then reduced to Bouguer anomalies using the Geodetic Reference System (1967) and an infinite slab correction for water depth assuming a crustal density of 2.67 g/cm^3. Anomalies are therefore approximately 7 mgal higher than values calculated with reference to the Canadian gravity mapping datum and the International Gravity Formula of 1930 (as used for example by Weaver (1968), Haworth *et al.* (1976) and Thomas (1976)). Bouguer anomalies along selected tracks and the areas of positive anomaly on Labrador (Thomas, 1976) and Newfoundland (Weaver, 1968) as adjusted to the new datum are shown in Figure 14.4.

From: Report of Activities, Part C;
Geol. Surv. Can., Paper 76-1C (1976).

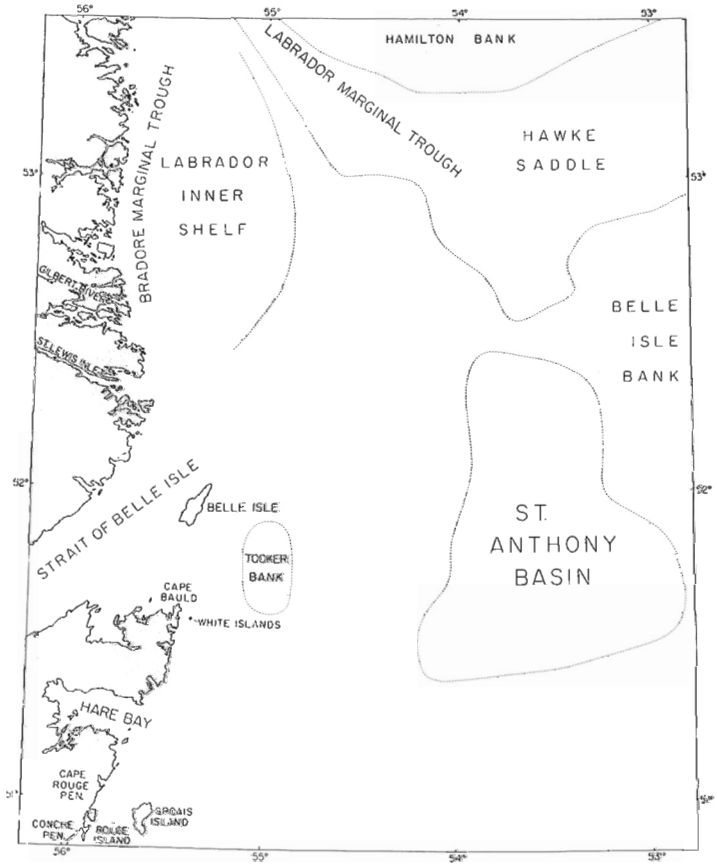

Figure 14.2. Index map of study area showing locations referred to in text.

Magnetic field data were collected on all tracks using a Barringer proton precession magnetometer. Although data were collected at 6 second intervals, only one minute values were used in the preparation of the profiles of anomalies (with respect to IGRF) selected for inclusion in Figure 14.5. On Labrador between 52°15'N and 53°N the dark shading in Figure 14.5 indicates the area with total magnetic field values greater than 55500 nT (Geological Survey of Canada Aeromagnetic Map 7377G, Battle Harbour). The boundary of that area corresponds approximately to the zero IGRF anomaly contour in the vicinity of 52°30'N, and its trend approximates the anomaly trends.

Geological Interpretation

The primary control over the interpretation is provided by the cores collected during the cruise HUDSON 75-009 (Haworth *et al.*, 1976) at the southern edge and south of the Martin Karlsen survey. Subsequent to their onboard examination, the cores have undergone petrographic, lithostratigraphic and palynological analysis. These analyses have in general confirmed the shipboard interpretation (Haworth *et al.*, 1976) and the units thereby defined have been extended northward across the Martin Karlsen survey area using a combination of the geophysical parameters and seabed morphology. All of the diagrams accompanying this report are compatible in scale and method of presentation with those of Haworth *et al.* (1976) except that all the dips indicated are only as resolved along track by seismic reflection, with the strike direction indicated perpendicular to the ships track. The previous report interpreted true strike direction from the more closely spaced seismic lines in the south, but because this is not possible with as much confidence in the north, a consistent policy of showing only apparent dips and strikes has been adopted. A similar policy has also been used for indicating the apparent dip of cuestas (*see* Fig. 14.6). However, the density and number of intersections of bathymetry lines inshore makes it possible to indicate true strike direction in some places. A double triangle is used in that case.

The geological units indicated in Figure 14.6 are discussed in the following sections as units of pre-Middle Paleozoic Western and Eastern Autochthonous sequences and their common subsequent intrusive and cover rocks.

Western Autochthonous Rocks

"Helikian and/or older" – The onshore Precambrian geology of Labrador has been compiled from Eade (1962) and Bostock *et al.* (1976) although some of Eade's mapping units have been disputed in the recent mapping of a portion of the Labrador coast (Wardle, 1976). The Gilbert River fault, however, is a major boundary between the units defined by both Eade (1962) and Wardle (1976). An abrupt change from positive magnetic and Bouguer gravity anomalies north of the fault to negative anomalies to the south (Figs. 14.4 and 14.5) emphasizes the crustal importance of the fault. North of Gilbert River and close to the coast the bedrock topography has a northeasterly trend, imparted by a series of northeast trending minor faults (Wardle, 1976). A gabbro dyke (Fig. 14.6) has intruded along one of these faults. Offshore extension of faults with this northeasterly trend, and also with the general southeasterly trend of the Gilbert River fault, the bedrock boundaries and the aeromagnetic anomalies, are probably all reflected in the offsets of the Bradore Marginal Trough. The southeast-trending offsets have a slightly greater morphological expression, but since neither set of faults appears to have any expression east of the marginal trough and the morphologies on either side of the trough are different, it is assumed that the Bradore Marginal Trough marks the eastern outcrop limit of the Helikian and older rocks, as proposed by Grant (1972).

"Upper Hadrynian – Cambrian" – The formations within this unit are exposed on the shores of the Gulf of St. Lawrence, as outliers in southeast Labrador, and along the coast of Belle Isle. The cuestas that are characteristic of this unit within the Gulf of St. Lawrence (Haworth and Sanford, 1976) are clearly seen north of Belle Isle within zones that strike northeastward, parallel to the cuestas. These zones within the unit presumably reflect the different lithologies between and within the component formations. Morphological boundaries on the profile running east from Labrador

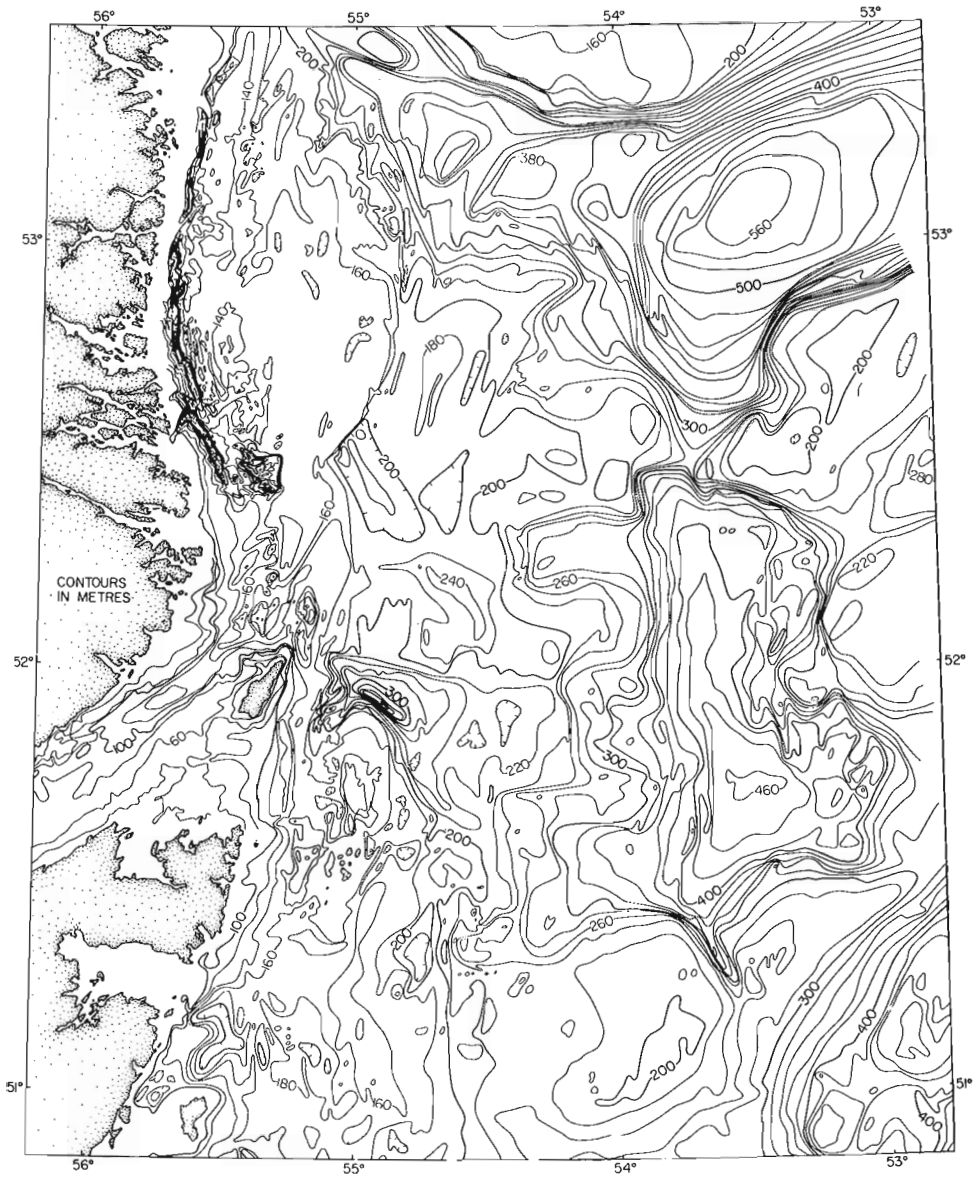

Figure 14. 3

Bathymetry of the continental shelf off southeastern Labrador. Scale 1: 2 000 000.

between Belle Isle and Cape Bauld coincide with the southerly projection along trend of the faults observed on Belle Isle (Williams and Stevens, 1969; Bostock *et al.*, 1976). North of Belle Isle, a magnetic high trending northeastward from the contact between the Helikian gneiss and the Bateau Formation can be traced for 20 km before gradually dying out. This may be an expression of the mafic volcanics within the Lighthouse Cove Formation or one of the feeder dykes (Williams and Stevens, 1969). It is doubtful that the magnetic high correlates with a magnetic rock in the basement gneiss since magnetic highs originating within the gneiss appear uncorrelated between adjacent survey lines. The western boundary of the sedimentary unit is defined morphologically and by the decrease in wavelength of magnetic anomalies as the Helikian basement emerges from beneath the Hadrynian-Cambrian cover. If this boundary is a fault, the change in magnetic character does not indicate a major vertical displacement.

The cuestas characteristic of the south are also seen within the area of the Labrador Inner Shelf east of the Bradore Marginal Trough. This is particularly apparent close to the trough between 52°35'N and 52°50'N where a series of distinct ridges is distinguishable on the bathymetry map (Fig. 14. 3). Seismic penetration within this area is extremely limited and the present number of line crossings does not permit identification of true dip directions, but all apparent dips are compatible with a regional dip to the east and southeast. The eastern edge of the Labrador Inner Shelf is inferred to be the limit of the Hadrynian-Cambrian unit on the basis of changes in morphological, seismic and magnetic character. However, in the eastern part of the shelf, a series of morphological units between which there are

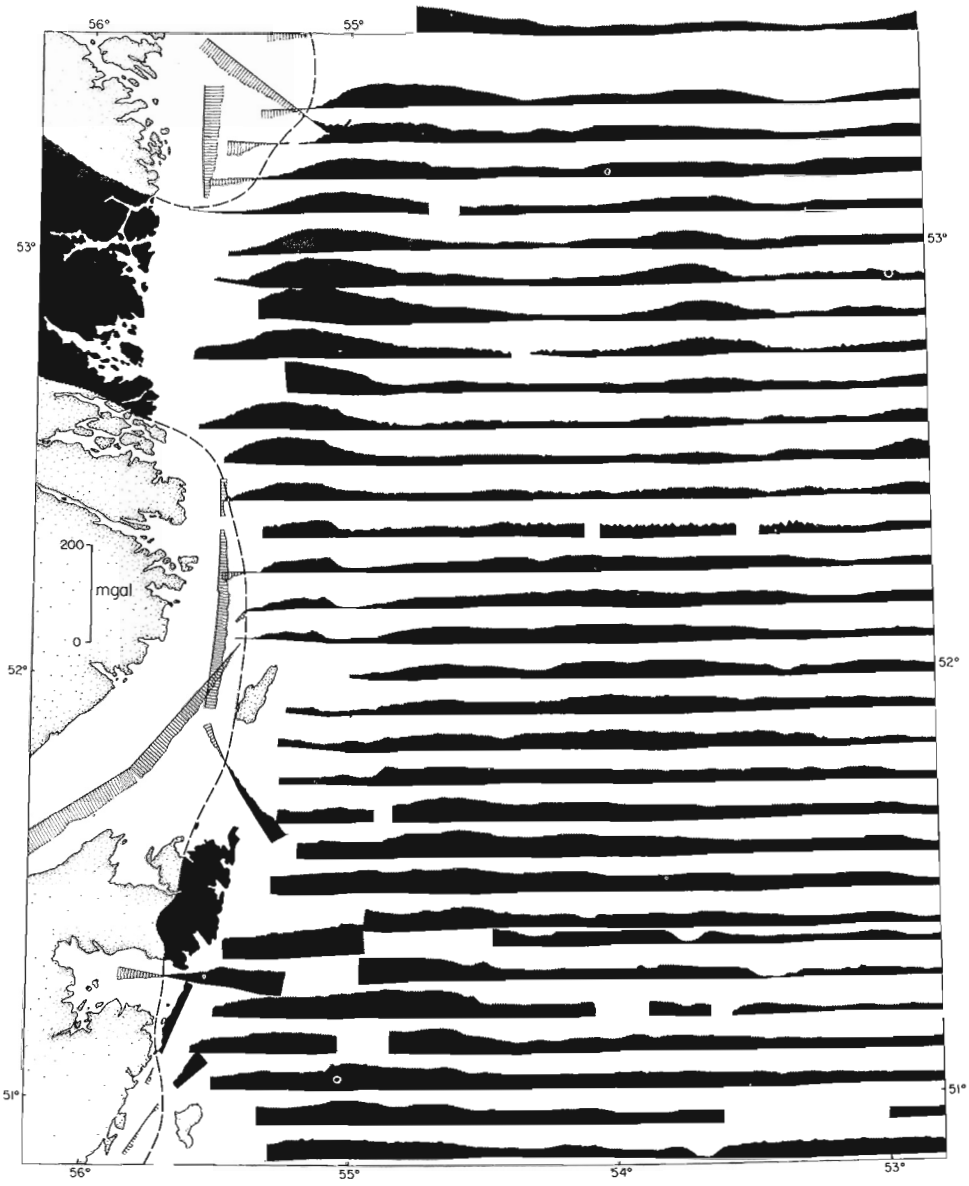

Figure 14.4

Bouguer gravity anomaly profiles of the continental shelf off southeastern Labrador. Darker shading indicates positive anomalies. Scale 1: 2 000 000.

subtle variations in surface texture trend northeastward generally parallel to that inferred further west.

The general east to southeast dip of the unit is interrupted where the Bradore Marginal Trough swings eastward into an area of complex topography centred at 52°30'N, 55°30'W. This complex area has a distinct southern morphological boundary that is also the southern termination of a broad zone of high magnetic anomalies that lies east of the Bradore Marginal Trough. The boundary probably marks the extension of the Gilbert River fault, but is slightly offset from it, possibly by an extension of northeast-trending fault that cuts the marginal trough east of Gilbert River. Immediately north of the Gilbert River extension, the cuestas indicate a northeasterly dip away from the fault, but south of it the southeasterly dip of this unit as seen in the Gulf of St. Lawrence is maintained.

The morphological similarity of the surface of the Labrador Inner Shelf to that of the northern Gulf of St. Lawrence and Strait of Belle Isle, and its apparent similarity in structural setting provide the main reasons for assigning the bedrock of this area to the Upper Hadrynian-Cambrian unit. However, its lateral extent may mean that on the Labrador Shelf the unit also includes younger Paleozoic strata.

"Upper Cambrian-Middle Ordovician" — The boundary of this unit with the Upper Hadrynian-Cambrian unit has been defined on purely morphological grounds as extending around the northern tip of Newfoundland from its observed contact in the Gulf of St. Lawrence (Bostock *et al.*, 1976). No formations within this unit are observed on Belle Isle or White islands (Williams and Stevens, 1969).

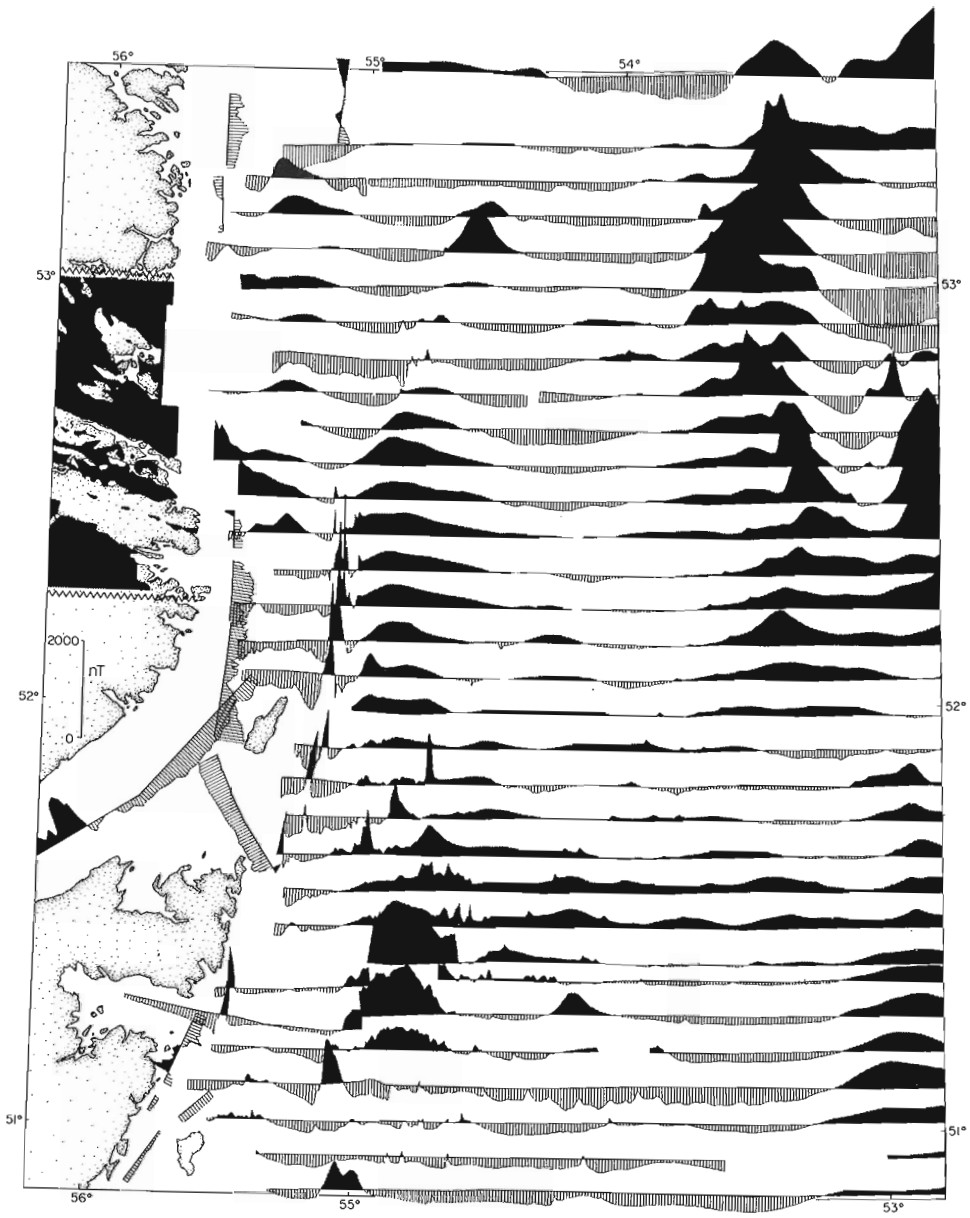

Figure 14.5

Magnetic anomaly profiles of the continental shelf off southeastern Labrador. Darker shading indicates positive anomalies. "Positive anomaly" onshore does not have regional gradient removed.
Scale 1: 2 000 000.

Eastern Autochthonous Rocks

"Hadrynian and Cambrian (Fleur de Lys equivalent)" – This unit is interpreted to be an extension of the Fleur de Lys Supergroup as identified on Groais and Bell islands (Kennedy *et al.*, 1973). Probable zones of chlorite schist have been outlined separately within the unit because of their distinctive magnetic character. On Groais Island the chlorite schists are seen exposed in the anticlinal axes of upright folds overturned to the west (Kennedy *et al.*, 1973). The trends of the fold axes on land are west of north, but their magnetic expression offshore (Geological Survey of Canada Aeromagnetic Map 7357G, Port Saunders) indicates that the axes veer towards the northeast. This northeast trend of the chlorite schists is continued off Hare Bay as indicated by the linear magnetic high from within whose bounds a chlorite schist core was recovered at drill hole 15 (Haworth *et al.*, 1976). A sinistral offset of the unit is therefore indicated at approximately 51°10'N although the apparent offset may have been caused by normal faulting. The linear magnetic high off Hare Bay is not continuous with either of the highs east of Belle Isle, except that they all fall within the same anomaly zone. Individual magnetic "ridges" might therefore be interpreted as indicating anticlines within which chlorite schist is exposed or close to the seafloor similar to the structures interpreted on Groais Island (Kennedy *et al.*, 1973). The other rocks on Groais Island are psammitic schists whose magnetic and morphologic character is similar to that of the Hadrynian-Cambrian unit of the Gulf of St. Lawrence. Core hole 17 recovered foliated metamorphosed sandstone and quartz

GEOLOGY OF THE CONTINENTAL SHELF OFF SOUTHEASTERN LABRADOR

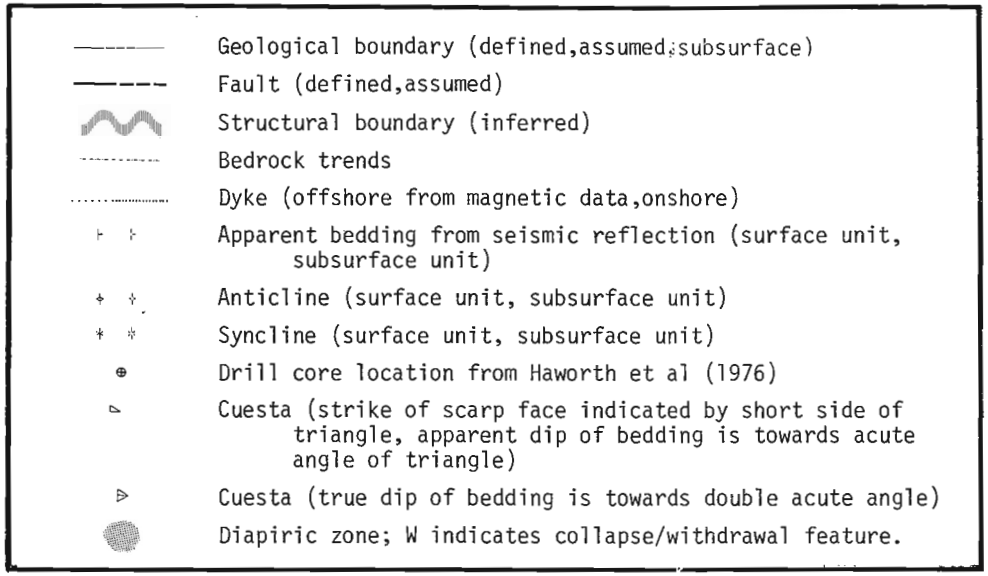

CRETACEOUS (?) AND TERTIARY

KT Siltstone, mudstone, sandstone

MISSISSIPPIAN AND PENNSYLVANIAN

MP Grey, red and brown sandstone, conglomerate and shale (mainly Barachois Group)

MISSISSIPPIAN

Mc Red and grey conglomerate, sandstone, siltstone, shale, limestone and evaporites (mainly Codroy and Windsor Groups)

MA Grey, green and red conglomerate, sandstone, siltstone, shale (mainly Anguille, Crouse Harbour and Cape Rouge Formations)

DEVONIAN?

Dg Granitic rocks

WESTERN AUTOCHTHONOUS ROCKS

UPPER CAMBRIAN TO MIDDLE ORDOVICIAN

€O Limestone, dolomite, and in upper part, shale and slate (includes Doucers, St. George, Table Head and Goose Tickle Formations.

UPPER HADRYNIAN AND CAMBRIAN

HC Quartzite, slate, limestone, dolomite,locally minor basalt (includes Bateau, Lighthouse Cove Bradore, Forteau and Hawke Bay Formations); HC ? possibly also includes younger units on Labrador Inner Shelf.

HELIKIAN AND OLDER

H Grenvillian rocks. Gneiss, schist, granitic and gabbroic rocks; (Hpg , paragneiss; Hg , granite, granodiorite; Hgb , gabbro; all as defined by Eade, 1962).

HARE BAY ALLOCHTHON

HADRYNIAN (?) TO MIDDLE ORODOVICIAN

HO Quartzose greywacke and slate; basalt, tuff, schist and amphibolite, structurally beneath peridotite sheets (HOP); Lower Ordovician basalt, tuff and black slate; Middle Ordovician melange locally at base of and within the allochthon (includes strata of Hare Bay Allochthon).

EASTERN AUTOCHTHONOUS ROCKS

ORDOVICIAN OR SILURIAN

OS Felsic and mafic volcanics, minor sedimentary rocks (includes Cape St. John Group)

HADRYNIAN AND CAMBRIAN mainly

HCF Psammitic and pelitic schists, Locally basic schist and amphibolite derived from basalt (includes undifferentiated plutonic rocks); HCV , mainly chlorite schist derived from basaltic rocks and may include meta-gabbro and meta-peridotite (includes Fleur de Lys Supergroup)

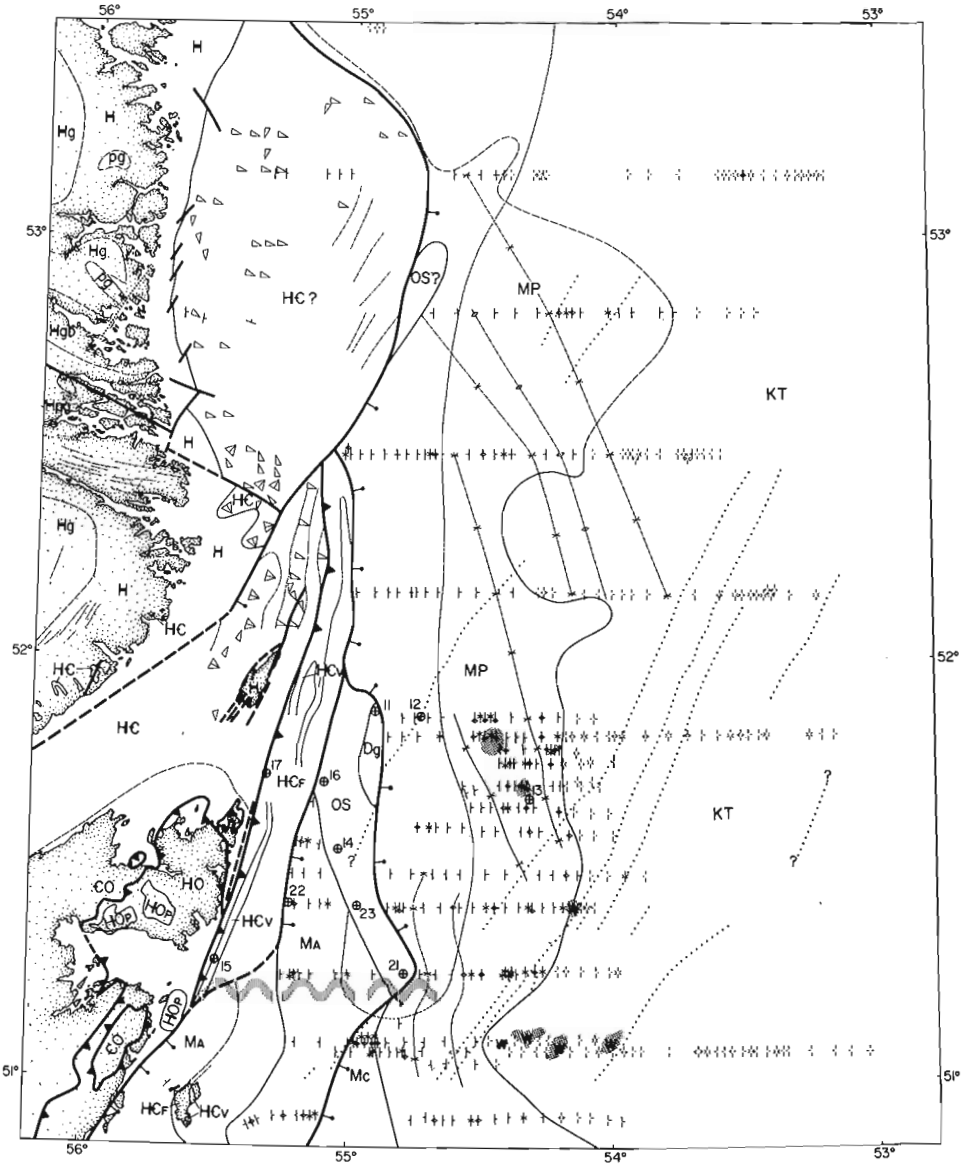

Figure 14.6

Geology of the continental shelf off southeastern Labrador. Key to map is on opposite page. Scale 1: 2 000 000.

conglomerate of the Fleur de Lys type. However, Bateau Formation is exposed on Belle Isle and White islands. The western boundary of the Fleur de Lys unit must therefore lie east of the Bateau exposures, and west of core hole 17 and the magnetic chlorite schists. This boundary has been extended northward on morphological and magnetic evidence. The eastern contact is well defined by the contrast between the seismically opaque Fleur de Lys unit and the easily penetrated Mississippian and Mississippian-Pennsylvanian units. No evidence of the Fleur de Lys unit is seen after it meets the boundary of the western Hadrynian-Cambrian unit at the edge of the Labrador Inner Shelf. That shelf edge is therefore presumed to be the location of a fault, probably a normal fault.

"Ordovician-Silurian (Cape St. John equivalent)" – A north-trending magnetic high with a width of 30 to 40 km lies east of the Fleur de Lys unit. In the central and northern parts of the map-area (for example 52°15'N, 54°50'W) the magnetic high is smooth and broad suggesting that the causative body is subsurface. In the south, however (for example 51°45'N, 55°W) short wavelength magnetic variations within the overall high indicate that the body is exposed at the seafloor. Four drill cores (cores 14, 16, 21 and 23, Haworth *et al.*, 1976) towards the western edge of this unit yielded igneous rocks that are possibly correlated with the Cape St. John Group lying at the eastern edge of the Fleur de Lys Supergroup on Burlington Peninsula. This unit may also be exposed at the eastern edge of the Labrador Inner Shelf where short wavelength magnetic variations are observed. However, this northern extension of the unit is not assured because of some changes in its magnetic character. It is possible that the unit cored in the south terminates against the faulted edge of the Labrador Inner Shelf, similar to the termination of the Fleur de Lys equivalent, and that the magnetic high seen on the

northern lines represents a different unit. The trend of this magnetic high coincides with a ridge that separates two deep areas in the Labrador Marginal Trough (Fig. 14.3). However, on the basis of seismic reflection information the bedrock in that location is the non-magnetic Mississippian-Pennsylvanian unit.

Post-Middle-Paleozoic Rocks

"Devonian(?) Granite" – Core hole 11 recovered pink granite from a distinct morphological unit of limited extent at the northeastern edge of the Tooker Bank. The extent of this unit has been better defined than by Haworth *et al.*, (1976) with the more detailed coverage of the Martin Karlsen survey. In particular, a distinct magnetic low seen on the numerous unpublished profiles over Tooker Bank are interpreted to define the outcrop of the granite. The age of the granite is unknown, and its petrological analysis indicates that the quantity of core is insufficient and unsuitable for accurate geochronological dating.

"Early Mississippian (Anguille equivalent)" – West of Groais Island a unit showing good seismic penetration is interpreted to be the offshore extension of the Crouse Harbour and Cape Rouge formations (early Mississippian equivalents of the Anguille Formation) which outcrop on Cape Rouge and Conche peninsulas, Rouge Island and Groais Island (Baird, 1966). A similar seismic unit east of the Fleur de Lys equivalent unit yielded a sandstone core (core hole 22) whose correlation with the Cape Rouge Formation was supported by petrographic examination (L.F. Jansa, pers. comm.). The western boundary of the eastern limb of this unit is poorly defined due to the inability of the seismic reflection profiling system to resolve steep dips and distinguish them from seismically opaque units. However, its eastern boundary with the Codroy equivalent unit is reasonably clear, as is its boundary with the Cape St. John equivalent. The nature of these contacts is not obvious and those indicated as faults are so designated purely in continuation of faults inferred elsewhere.

"Mississippian (Codroy equivalent)" – In the survey to the south (Haworth *et al.*, 1976), this unit exhibited little seismic penetration and was only distinguishable from adjacent opaque units by its non-magnetic character. The Codroy (Windsor) equivalent designation, assigned on the basis of macroscopic examination of cores obtained within the unit, was confirmed by palynology (M.S. Barss, pers. comm.) and petrography (L.F. Jansa, pers. comm.). However, no seismically opaque non-magnetic unit is distinguishable as outcropping north of approximately 51°N. The Codroy equivalent unit is therefore assumed to underlie the Mississippian-Pennsylvanian unit to the north and east, thereby providing a source for its salt tectonism, but it is interpreted as not being exposed on the seafloor north of 51°10'N.

This mapping differs from that of Haworth *et al.*, (1976) which was based on onboard examination of core 12 and the assumption that the seismic character of the unit might change along strike. However, this northward extension of the geophysical survey shows that core 12 (which is petrographically compatible with the Mississippian-Pennsylvanian unit) was recovered from gently eastward dipping strata which continues northward along the western edge of a unit within which there is good seismic penetration and whose fold axes can be directly correlated with those of the Mississippian-Pennsylvanian unit.

"Mississippian-Pennsylvanian" – This is a gently folded unit within which there is good seismic reflection. Its western boundary with older, seismically opaque units is therefore clearly defined. The density of lines between 51°30'N and 52°N is sufficient to permit definite correlation of structures, particularly in establishing the major fold axes of the region (Fig. 14.6). The general trend of these fold axes is west of north, and the apparently broader folding north of 52°N makes it possible to correlate structures with the same trend between the more widely spaced seismic lines. Confidence in the correlations was increased by using the seismic lines of Grant (1972) which, although originally subject to poor navigation, were repositioned by comparison of water depths with those in Figure 14.3. The correlations between structures north of 52°30'N indicate an even more westerly trend than established at 52°N, parallel to the continental margin. In the south it is difficult to correlate the details between adjacent lines. This may be partly the result of increased salt tectonism in the south because salt withdrawal features similar to those at 51°05'N, 54°20'W (Haworth *et al.*, 1976) were not found north of 52°, although some anticlinal features could perhaps be interpreted as the result of salt tectonism.

"Cretaceous-Tertiary (Coastal Plain unit)" – The Coastal Plain sequence covers more than half of the area underlain by the Mississippian-Pennsylvanian unit. On Hamilton Bank and Belle Isle Bank the unit is so thick that detail within the Mississippian-Pennsylvanian unit is lost in the first multiple of the seismic record. South of 52°30'N, the erosional edge of the coastal plain lies at a depth of about 200 m, but in Hawke Saddle its edge was crossed at depths of 460 m and 380 m before regaining its 200 m elevation in the Labrador Marginal Trough. This may be indicative of the glacial overdeepening proposed for the Labrador Marginal Trough (Grant, 1972). The seismic profiles indicate a complicated sequence of deposition and erosion within the unit, but this is not discussed in this report.

"Dykes" – The series of northeast-trending linear magnetic features interpreted as dykes by Haworth *et al.* (1976), were more clearly delineated during the Martin Karlsen survey, and additional ones were found. One of the newly discovered dykes, which apparently outcrops on the seafloor as a 50 m high, 300 m wide ridge at approximately 52°15'N, 54°20'W, produces a negative magnetic anomaly whereas all the others are positive. These dykes appear to post-date the latest deformation of the Paleozoic units and may cut

strata as young as Cretaceous-Tertiary. They have the same trend as the older gabbro dykes on the Labrador coast just northwest of the map-area (Eade, 1962) which have a K Ar age of 544 ±22 Ma (Analysis GSC 67-141 in Wanless *et al.*, 1970), and also as an undated gabbro dyke intersecting the Labrador coast just south of 53°N (Wardle, 1976).

Structure

The boundaries of the western autochthonous Hadrynian-Cambrian unit underlying the Labrador Inner Shelf have been interpreted as a set of faults whose interrelationship is complicated. The extension of the Gilbert River fault, the southern boundary of the unit, is offset by the southernmost of the northeast-trending faults cutting the Hadrynian-Helikian boundary along the Bradore Marginal Trough, and is truncated at the faulted eastern edge of the Labrador Inner Shelf. The Fleur de Lys unit (possibly contemporaneous with the Hadrynian-Cambrian inner shelf unit) is also truncated by that fault. It is obviously important to verify the ages of the units affected by these intersecting faults in order to establish the chronology of the tectonic development of the continental shelf northeast of Newfoundland.

In addition to the boundaries between the geological units discussed in the previous sections, a structural boundary is tentatively inferred to cross the map-area at approximately 51°10'N on the basis of the coincidence between several otherwise unrelated events occurring at that latitude. The most obvious indications of it are the appearance of the highest structural slices of the allochthon onshore (Williams, 1975), the onset of the linear magnetic high off southern Hare Bay (perhaps faulted westward from the trend established north of Groais Island), and the southern termination of the magnetic high interpreted as reflecting Cape St. John Group equivalents in the subsurface. In addition, some difficulty is encountered in correlation structures in the Carboniferous units in the vicinity of this latitude, although it has been noted earlier that this may be related to salt tectonics rather than the proposed structural boundary. The regional gravity field of the continental shelf northeast of Newfoundland indicates two prominent gravity highs, one trending northeastward out of Notre Dame Bay and one trending northward east of the coast between Hare Bay and Cape Bauld (Haworth *et al.*, 1976). The decay of the Notre Dame Bay trend and the onset of the Hare Bay trend occurs between 50°30'N and 51°N, possibly indicating the location of a crustal boundary whose surface and near-surface effects are those described above. The significance (or even existence) of this proposed boundary will only be ascertained through interpretation of the basement tectonics of the continental shelf northeast of Newfoundland. Additional seismic refraction information is needed to support such an interpretation which is proceeding at present primarily on the basis of the gravity and magnetic data.

References

Baird, D.M.
1966: Carboniferous rocks of the Conche-Groais Island area, Newfoundland; Can. J. Earth Sci., v. 3, p. 247-257.

Bostock, H.H., Cumming, L.M., Williams, H., and Smyth, W.R.
1976: Strait of Belle Isle region, Newfoundland; Geol. Surv. Can., Open File 347.

Eade, K.E.
1962: Geology, Battle Harbour-Cartwright, Coast of Labrador, Newfoundland; Geol. Surv. Can., Map 22-1962.

Geodetic Reference System 1967.
1967: International Assoc. Geodesy, Special Publication No. 3, Paris.

Grant, A.C.
1972: The continental margin off Labrador and eastern Newfoundland – morphology and geology; Can. J. Earth Sci., v. 9, p. 1394-1430.

Haworth, R.T. and Sanford, B.V.
1976: Paleozoic geology of northeast Gulf of St. Lawrence; *in* Report of Activities, Part A; Geol. Surv. Can., Paper 76-1A, p. 1-6.

Haworth, R.T., Poole, W.H., Grant, A.C., and Sanford, B.V.
1976: Marine geoscience survey northeast of Newfoundland: *in* Report of Activities, Part A; Geol. Surv. Can., Paper 76-1A, p. 7-15.

Kennedy, M.J., Williams, H., and Smyth, W.R.
1973: Geology of the Grey Islands, Newfoundland – Northernmost extension of the Fleur de Lys Supergroup; Proc. Geol. Ass. Can., v. 25, p. 79-90.

Morelli, C., Gantar, C, Honkasalo, T., McConnell, R.K., Szabo, B., Tanner, J.G., Uotila, U., and Whalen, C.T.
1973: The International Gravity Standardization Net 1971 (IGSN 71); Intl. Assoc. Geodesy, Spec. Publ. No. 4, Paris.

Thomas, M.D.
1976: The correlation of gravity and geology in southeastern Quebec and southern Labrador; Earth Physics Branch, Gravity Map Series Nos. 64-67, 96-98.

van der Linden, W.J.M.
1973: Cruise report No. 73-027 CSS DAWSON; Bedford Institute of Oceanography unpublished report.

van der Linden, W.J.M., Fillon, R.H., and Monahan, D.
1976: Hamilton Bank, Labrador Margin; Origin and evolution of a glaciated shelf; Marine Science, Paper 14, Geol. Surv. Can., Paper 75-40.

Wanless, R.K., Stevens, R.D., Lachance, G.R., and Delabio, R.N.
1970: Age determinations and geological studies, K-Ar isotopic ages, Report 9; Geol. Surv. Can., Paper 69-2A.

Wardle, R.J.
1976: The Alexis Bay-Snug Harbour region of southern Labrador; Min. Dev. Div. Dept. Mines and Energy, Prov. of Nfld., Rept. 76-1, p. 80-87.

Warren, J.S.
1976: The morphology of two transverse channels on the northeast Newfoundland shelf; B.Sc. Honours thesis, Geology Dept. Dalhousie University, also Maritime Sediments (in press).

Weaver, D.F.
1968: Preliminary results of the gravity survey of the Island of Newfoundland; Dominion Observatory Gravity Map Series, nos. 53-57.

Williams, H.
1975: Structural succession, nomenclature, and interpretation of transported rocks in western Newfoundland; Can. J. Earth Sci., v. 12, p. 1874-1894.

Williams, H. and Stevens, R.K.
1969: Geology of Belle Isle – northern extremity of the deformed Appalachian miogeosynclinal belt; Can. J. Earth Sci., v. 6, p. 1145-1157.

15. REACTIONS WHICH REMOVE TRACE METALS FROM SEAWATER: PRELIMINARY OBSERVATIONS

Project 740083

Joan D. Willey
Atlantic Geoscience Centre, Dartmouth

Preliminary experiments have been performed to determine the extent of removal of trace metals from seawater by different types of sediments. These kinds of reactions are environmentally important because they limit concentrations of trace metals that can occur in seawater, and they provide a mechanism for producing sediments enriched with trace metals. Initial experiments were performed using sediments from Placentia Bay, in southeastern Newfoundland, because of the extensive background information (Stehman, 1976; Willey, 1976a). On the basis of factor analysis (Willey, 1976a), three chemically distinct sediment types (muds, sands and tills) were defined. Samples from each were chosen for experiments. The three trace metals which showed the most diverse associations (Pb, Zn and Co) were also chosen for experiments; this approach should give some indication of the extremes of variation that occur in the natural environment.

The experimental design was simple. A suspension of each type of sediment (0.1, 1 or 10% solid in solution) was made in seawater to which one trace metal had been added (to contain either 1.00 or 0.50 ppm metal). The concentration of trace metal and pH were then monitored with time. The pH must remain within the natural seawater range for the experiment to simulate environmental conditions. Careful use of blanks is necessary to check for losses of metal not due to sediment uptake, or additions of metal by contamination. Replicate experiments must also be run to define limits of experimental variation.

The experiments showed removal of trace metals by each sediment type, with removal by muds being the most rapid and most extensive and removal by sands the least. Pb was removed completely and rapidly, Co was removed slowly, and Zn was removed at an intermediate rate. The reactions were rapid, with extensive reaction occurring within the first day.

The rate of reaction observed suggests an ion exchange, surface adsorption or organic chelation mechanism. Another possibility is a precipitation reaction with dissolved silica released from the sediments; similar precipitation reactions have been observed to occur with Mg (Mackenzie and Garrels, 1965; Wollast *et al.*, 1968; and Harder, 1972) and with Al (Harder, 1965 and 1974; Hem *et al.*, 1973; and Willey, 1975). This possibility was investigated by mixing seawater containing silica with seawater containing a trace metal, and monitoring both silica and trace metal concentrations, and pH with time. A decrease in silica and trace metal concentrations should indicate coprecipitation. This kind of coprecipitation was observed to occur with silica and Zn, (Willey, 1976b), but not with silica and Pb or Co. However, removal of a large amount of zinc by sediments had occurred before enough silica was released to initiate coprecipitation, so this reaction mechanism probably was not significant in the initial experiments. This kind of reaction may prove to be an important mechanism for removing Zn from contaminated waters or from interstitial water, and it provides a mechanism for formation of authigenic zinc sillicate.

Future experiments will attempt to define better the roles of organic material, clays and other minerals in trace metal uptake reactions by sediments from several geographic areas. The effects of varying salinity and temperature (like that which would occur during an estuarine tidal cycle) will also be investigated. The effect of the form of occurrence of the introduced trace metal (inorganically bound, or organically chelated) will be studied.

References

Harder, H.
1965: Experimente zur "Ausfällung" der Kiesesäure; Geochim. Cosmochim. Acta, v. 29, p. 429-442.

1972: The role of magnesium in the formation of smectite minerals; Chem. Geol., v. 10, p. 31-39.

1974: Illite mineral synthesis at surface temperature; Chem. Geol., v. 14, p. 241-253.

Hem, J.D., Robertson, C.E., Lind, C.J., and Polzer, W.L.
1973: Chemical interactions of aluminium with aqueous silica at 25°C; U.S. Geol. Surv., Water-Supply Paper, 1827-E, 57 p.

Mackenzie, F.T. and Garrels, R.M.
1965: Silicates: Reactivity with seawater; Science, v. 150, p. 57-58.

Stehman, C.F.
1976: Pleistocene and recent sediments of northern Placentia Bay, Newfoundland; Can. J. Earth Sci., v. 13, in press.

Willey, J.D.
1975: Reactions which remove dissolved alumina from seawater; Mar. Chem., v. 3, p. 227-240.

1976a: Geochemistry and environmental implications of the surficial sediments in northern Placentia Bay, Newfoundland; Can. J. Earth Sci., v. 13, in press.

1976b: Coprecipitation of zinc with silica in seawater and in distilled water; Submitted to Marine Chemistry.

Wollast, R., Mackenzie, F.T., and Bricker, O.P.
1968: Experimental precipitation and genesis of sepiolite at earth surface conditions; Am. Mineral., v. 53, p. 1645-1662.

From: Report of Activities, Part C;
Geol. Surv. Can., Paper 76-1C (1976).

16. SEISMIC TECHNIQUES FOR RECONNAISSANCE STUDIES IN DIFFICULT ICE-COVERED OFFSHORE AREAS

Project 750029

A. Overton
Resource Geophysics and Geochemistry Division

The need for seismic techniques for reconnaissance studies in difficult ice-covered offshore areas such as the Arctic coastal plain and continental margin has been described by Overton (1976). Seismic exploration in these areas has been hampered by moving ice floes which create hazards to equipment and navigational problems. Established practices among the Arctic Islands utilizing the seismic refraction technique have required long and cumbersome seismometer arrays, large distances between the shotpoint and seismometers, and very large dynamite charges for the study of the entire geological section down to the Mohorovicic discontinuity, including sedimentary and crustal layers. These practices and their associated heavy, bulky equipment have been impediments to studies on the Arctic Coastal Plain. On the other hand, seismic exploration techniques used by industry have used the reflection method with smaller seismometer arrays, smaller distances and much smaller dynamite charges. This has been going on in the face of environmental-biological studies by governments concerned with the effects of exploration and associated activities on terrain and wildlife. It is not surprising then to see limits on dynamite charges reduced to a maximum of 10 kg, in some marine environments, compatible with industrial requirements rather than the unlimited charge sizes of up to 1000 kg used for previous refraction profiles. Indeed, some industrial seismic prospecting has been done with low powered mechanical vibrators using a swept frequency source signal, cross correlation of the source signal with the seismically transmitted signal for pulse compression, and stacking of repetitive observations; this technique is called "Vibroseis". The problems encountered in difficult ice-covered areas appear to be amenable to solution by keeping the equipment as lightweight and portable as possible and to minimize the logistic problems further by working with the small maximum charge size enforced by regulations. In this way, helicopter support could be used most efficiently to do the job quickly, which would also minimize the navigation problems posed by moving ice floes. The navigation problems will be dealt with in due time; the seismic aspects of the problem are of primary importance.

As experience has developed using more sophisticated seismic refraction techniques, it appears that a great degree of sophistication does not necessarily yield a correspondingly better knowledge of the geological section. In fact, in terms of reconnaissance studies of geological sections by seismic refraction methods, the very simple techniques used between 1960 and 1965 in the Arctic (Hobson and Overton, 1967) appear to be adequate and, except for the large amounts of dynamite used, seem to afford the logistic simplicity required for reconnaissance studies in the more difficult areas.

The concept of the technique to be developed combines the advantages of numerous available techniques:

1. The portability and logistic simplicity of the small scale seismic arrays used by reflection and early refraction methods.
2. The relatively high energy density of dynamite, within the limits posed by biological and environmental factors.
3. The effectiveness of the "Vibroseis" technique using cross correlation of shaped input and output signals, data stacking for signal to noise enhancement, but using dynamite as the source generator rather than mechanical vibrators.
4. Source wave shaping using delayed sequential detonation techniques, shot patterns, charge size, depths of shots in water; it should be noted that water reverberation, commonly regarded as a problem, may be used to advantage as an expanded energy source similar to the swept frequency source of the "Vibroseis" method.
5. Combination of methods to define by both reflected and refracted events the time-distance relationships within 100 km. Particular emphasis should be placed on the enhancement of secondary seismic events. This would require that each observation be recorded for at least 25 seconds to allow for the possibility of recording reflected events from the deepest discontinuity of interest beneath the crustal section.

The concept of the controlled frequency source of the "Vibroseis" should be retained, but the weight, costs and bulk of the "Vibroseis" source machinery can be replaced with high energy density of dynamite. Frequency content and shape of the source signal can be controlled by varying the charge sizes, patterns, depths in water, and detonation times using sequential firing techniques to optimize energy transmission. In order to effect a deconvolution and pulse compression process the source signal must be recorded from a suitable shotpoint seismometer so that the signal is available for cross correlation with the seismically transmitted wavetrain. Stacking, or summation, of a number of repeated observations is desirable to accentuate the signal to noise ratio. Patterns of seismometer arrays on ice should be tried to reduce ice noise. Vertical hydrophone arrays suspended in water may be quieter than arrays set up on ice. It is expected that a great deal of data manipulation using computer techniques for filtering, deconvolution,

From: Report of Activities, Part C;
Geol. Surv. Can., Paper 76-1C (1976).

stacking, and Fourier analysis will be required. Digital recording on magnetic tapes is therefore necessary. Some preliminary tests were conducted during the spring of 1976. These are described in another report 5 in this publication.

References

Hobson, G.D. and Overton, A.
1967: A seismic section of the Sverdrup Basin, Canadian Arctic Islands. In Seismic refraction prospecting (A.W. Musgrave, Ed.). Soc. Explor. Geophys., Sec. 7, p. 550-562.

Overton, A.
1976: Ice reconnaissance on the Beaufort Sea; *in* Report of Activities, Part A, Geol. Surv. Can., Paper 76-1A, p. 419.

17. AN APPLICATION OF HYDRAULIC JET DRILLING TECHNIQUES TO MAPPING OF SUB-SEABOTTOM PERMAFROST

Project 740102

A.S. Judge[1], H.A. MacAulay[2], and J.A. Hunter[2]

During April 1976, five experimental holes were drilled into the seabottom of the Beaufort Sea Shelf near the Mackenzie Delta. Thermistor cables were installed in all holes and temperatures were read at periodic intervals during the weeks following installation. Accurate measurements of sub-seabottom temperatures indicated permafrost was present.

Location of Drillholes

Land-fast ice can be found extending as much as 20 miles offshore in the Mackenzie Delta area. In March and April the ice is often greater than 2 m thick and offers an excellent platform for a light-weight drilling operation.

The locations for the five holes were selected on the basis of existing sub-seabottom permafrost anomalies (*see* Fig. 17.1). Two holes were drilled in Shallow Bay; T-1 and T-2 were placed over locations of holes previously drilled by Northern Engineering where indications of ice-bonded permafrost had been found at shallow depths. Holes T-3, T-4 and T-5 were located on an east-west line approximately 32 km north of Hooper Island perpendicular to a seismic boundary delineated by Hunter *et al.* (1976). West of 134°W; the seismic results indicated the absence of ice-bonded permafrost.

Drilling Procedure

Hydraulic water-jet drilling techniques have been used extensively for water-well drilling in overburden in non-permafrost areas and to some extent in permafrost (Cederstrom and Tibbits, 1961). A simplified version of the technique was applied to thermistor cable installation in permafrost by Judge *et al.* (1975). From this experiment a more elaborate technique was designed

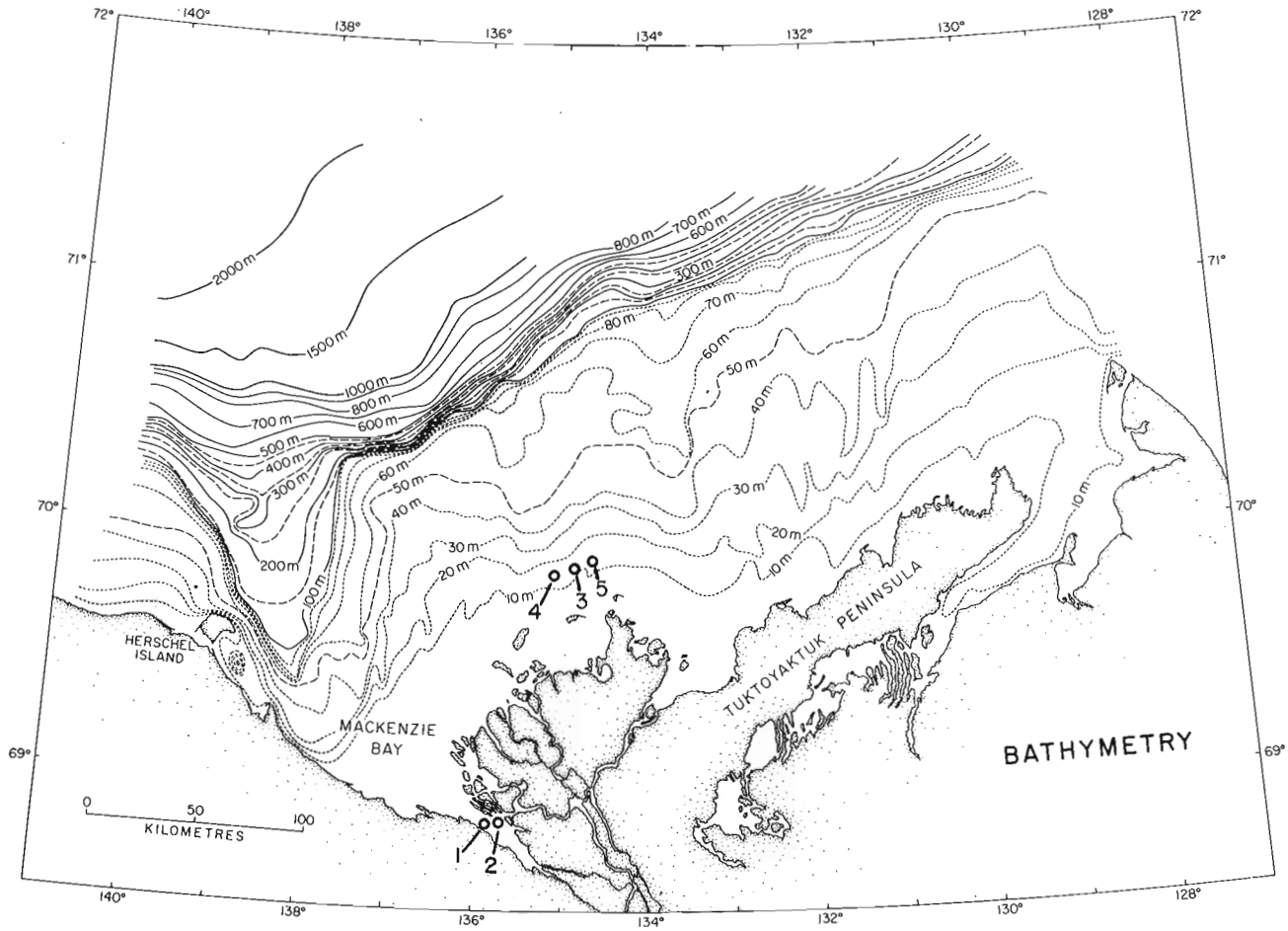

Figure 17.1. Location of drillholes.

[1]Earth Physics Branch

[2]Resource Geophysics and Geochemistry Division

From: Report of Activities, Part C;
Geol. Surv. Can., Paper 76-1C (1976).

to drill into seabottom materials from an ice platform. The procedure is shown in Figure 17.2. Jetting is done through a 2.5-cm steel water pipe (3-m sections). The first section contains a bit (cutting teeth fashioned from a 2.5-cm coupling) and 1 m of flighted section.

A water pump system delivering 235 psi (1.74 MPa) shutoff pressure was used. Pressure losses at the bit as a result of frictional losses in the pipe and the hydraulic head are estimated to be 1 psi per foot (.023 MPa/m) depth below sea-surface. Additional frictional losses in connector hoses, couplings and swivel-head could not be accurately estimated but probably result in the loss of a further 5-10 psi (.04 to .08 MPa).

Immediately after disconnecting at the swivel to add sections, washed samples were obtained from return flow up the pipe.

It was found that changes in drilling rates could be correlated with change in type of material washed as well as the degree of ice-bonding. In unfrozen recent muds drilling rates as high as 6 m/min were achieved; however, when drilling in ice-bonded sand, the rate dropped as low as 0.03 m/min.

Holes T-3, T-4, T-5 were drilled to refusal. In all cases temperature cables were installed by lowering through the drill pipe. After cable installation the drill pipe was disconnected at the coupling close to the sea floor, raised up several feet and was allowed to freeze into the surface ice; hence, ice movement could occur without damage to the installation. Most installations were visited and temperatures were read at least three times during the survey period.

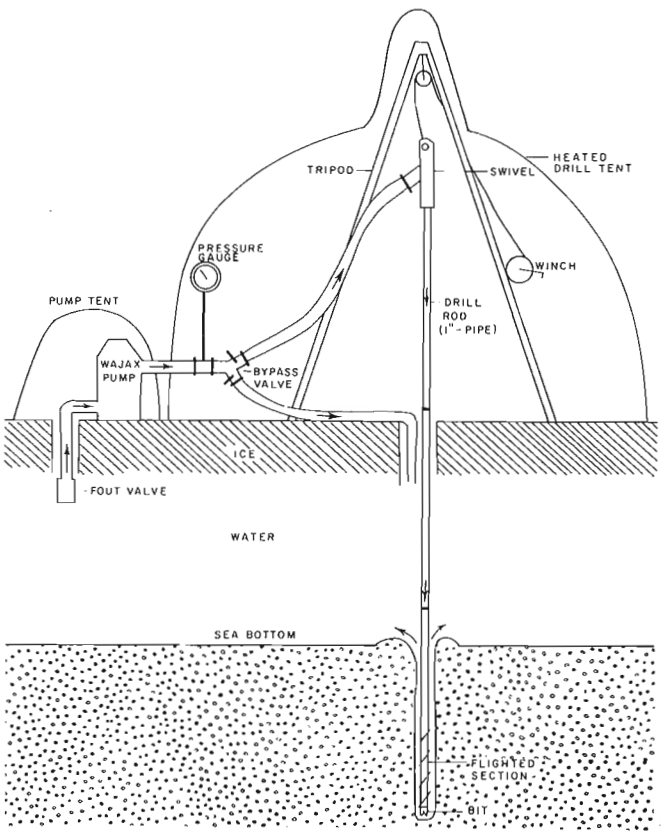

Figure 17.2. Diagrammatic representation of drilling technique.

Results

Shallow Bay (Fig. 17.3a, 17.3b)

Two thermistor cables were installed in the Shallow Bay holes to depths of 30 and 50 m and the cables were periodically monitored for more than 500 hours after drill completion. A resulting ratio of settling to monitoring time of 58 on the last log should be sufficient to determine an equilibrium temperature if not to achieve equilibrium conditions.

Both temperature curves shown in Figure 17.3a and 17.3b exhibit the same characteristics of high positive temperatures (maximum of +2.6°C) 6 m below the sediment surface, negative temperature gradients (60 to 260 mKm^{-1}) and negative bottom hole temperatures (minimum of -1.4°C). Although no sensors were placed above 5.5 m in T-2 the springtime near-surface sediment temperatures are probably close to 0°C which is similar to T-1.

Since the sensors used had a calibration accuracy of only ±0.1°C there is some uncertainty in the depth of the 0°C isotherm. In T-1 the isotherm lies at 15 ± 2 m below the sediment surface compared with a frozen ground depth determined from drilling of 14 ± 1 m, and in T-2 at 24 ± 2 m compared with 25 ± 1 m. The close correspondence between permafrost depth and the depth of ice-bonding suggests a lithology of fairly pure sand containing fresh water (0 to < 5000 ppm dissolved salts).

The observed temperature profiles can be explained in two fundamentally different ways. One involves essentially an equilibrium or near-equilibrium situation in which the two holes were drilled through topographic lows which locally retain water beneath the ice in winter but are surrounded by a sea bottom to which ice freezes in the winter. In this case permafrost at very shallow depths, and perhaps ice-bonded, would be widespread with talik zones developed in the topographic lows and on a surrounding shallow thaw zone corresponding to a sub-sea summer "active-layer". A second explanation involves non-equilibrium conditions in which the mean temperature at the sediment surface has increased from below freezing to above freezing temperatures and the permafrost is accordingly degrading from the top. This might be explained by a myriad of surface phenomena such as rising sea level, depression of the surface by sediment loading, shifting river channels, etc. The current depths to the top of permafrost suggest an increase which commenced 500 to 1000 years ago, present bottom-hole temperatures suggest that the previous sediment surface temperatures were at least -3°C, and that permafrost thickness may be in excess of 100 m.

To distinguish between these two explanations for the curves requires further geophysical work and drilling in Shallow Bay.

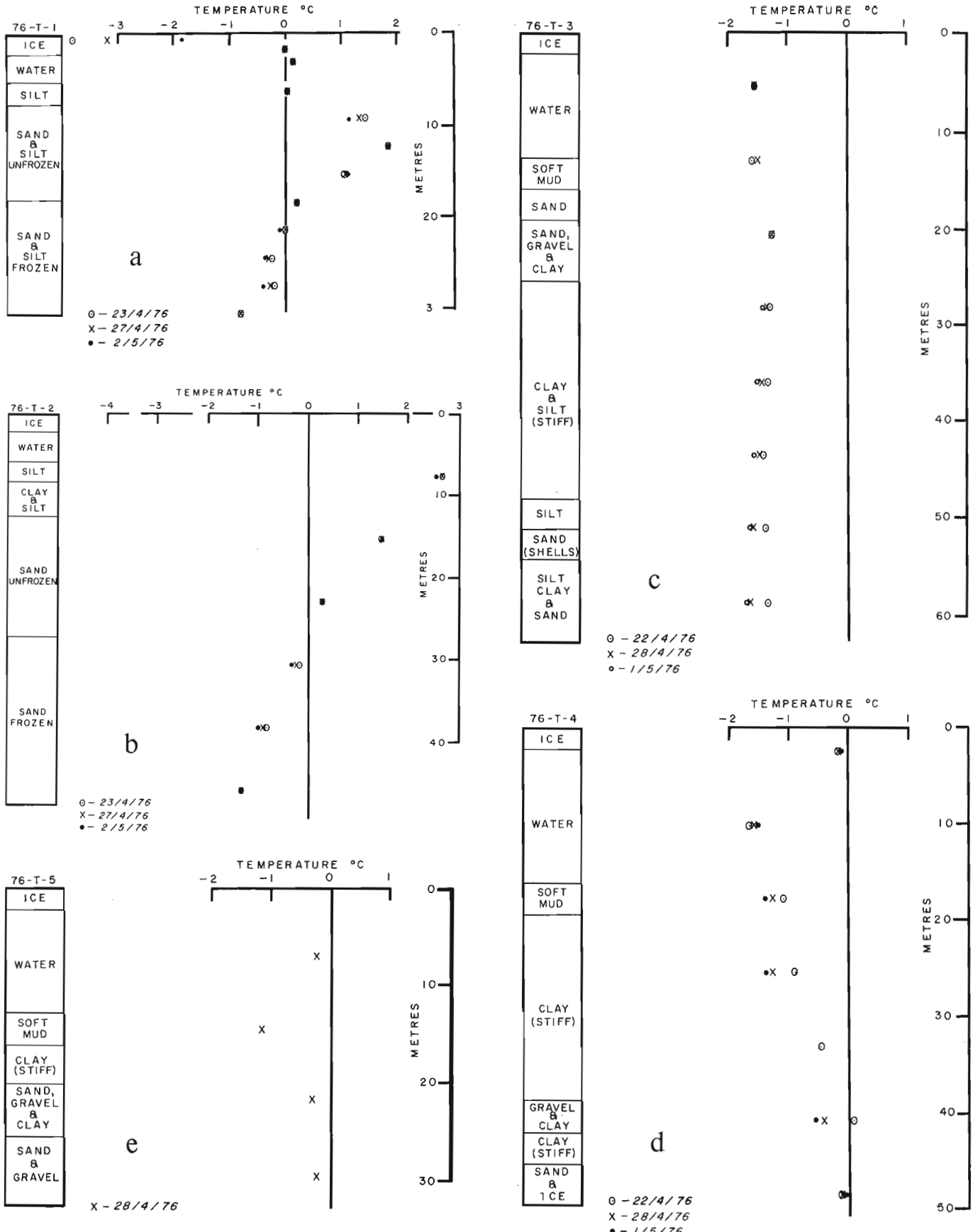

Figure 17. 3a-e. Temperature curves for various locations.

Beaufort Sea (Fig. 17.3c, 17.3d, 17.3e)

Three further thermistor cables were installed to depths of 30 to 59 m beneath water depths of 13 to 16 m on an east-west line approximately 32 km north of Hooper Island. The cables were monitored for periods of up to 340 hours after completion and since drilling time was somewhat less than in Shallow Bay reasonable ratios of settling to drilling time of 60 to 70 result for two of the holes. At hole T-5 the ice surface shifted between logs breaking the cable at the sea bottom, so that a single log at a time ratio of 77 is the only sub-bottom information obtained.

The appearance of the temperature logs at two of the sites differ dramatically from one another. Although in all three cases the temperatures at the sea bottom are similar at about -1.5°C, T-4 shown in Figure 17.3d exhibits a positive temperature gradient of 57 mKm^{-1} at a depth 10 m below the sediment surface and the temperature rises to 0°C at a depth of 35 m, whereas T-3, shown in Figure 17.3c exhibits a negative temperature gradient of 15 mKm^{-1} at a depth of 6 m below the sediment surface and the temperature falls to -1.9°C at a depth of 44 m. The limited data on T-5, shown in Figure 17.3e, is inconclusive; however negative temperatures were encountered 17 m beneath the sediment surface.

Unlike the Shallow Bay holes no particularly hard boundaries which could be attributed to a frozen to unfrozen interface were encountered during drilling, although ice was encountered in the sand near the base of T-4. Because this sand is at temperatures between -0.3°C and 0°C it must contain fresh water. The presence of ice-bonding or lensing in other horizons in holes T-3 to T-5 is unproven.

The temperature profiles exhibited by T-3 and T-4, sites separated by only 7.6 km, seem to reflect two very different situations. Whereas T-4, the westernmost site, seems to reflect a situation in which permafrost has grown to be observed depth and at present is in equilibrium with the earth's heat flux and the sea bottom temperature, T-3 reflects a non-equilibrium situation in which, similarly to Shallow Bay, the sediment surface temperature has increased from below -3°C to the present seabottom temperature, and permafrost thickness degraded from greater than 110 m. Two sets of results provide insufficient evidence on which to develop regional models; however, T-3 and T-4 are on the east and west sides of a major north-south seismic boundary described by Hunter *et al.* (1976). It is tempting to relate this boundary to the sea level and glacial history of the area. As suggested in Hunter *et al.* (1976) this complex history resulted largely in thin permafrost close to thermal equilibrium beneath sea bottom to the west of 135°W in contrast with the thick, relic, degrading permafrost found to the east. Since the thin permafrost to the west is mainly in clays, ice-bonding is unlikely to be present and any ice-lensing present may not appear on conventional seismic records. Wherever sands are present at shallow depth intermittent reflections might appear. The thick but warm permafrost to the east incorporates both sands and clays; presumably each sand horizon is ice-bonded if it contains freshwater, will act as a seismic reflactor whereas the clays containing ice-lenses only may not, this results in a very complex seismic pattern of refraction, reflection and diffraction below the first refracting horizon.

Obviously an explanation for the regional distribution of permafrost in the Beaufort Sea based on two sub-surface temperature profiles is open to question but the combination of seismic and thermal profiles provide strong supporting evidence. Further thermal profiling and additional geophysical profiling using electrical and more sophisticated seismic systems are required. Part of the thermal profiling should include instrumentation of both offshore island sites and Dome's drillship sites.

Conclusions

Combined thermal and seismic profiling of the offshore areas of northern Canada can provide valuable evidence for present permafrost distribution and character as well as provide some understanding of permafrost genesis and geological history. The jet-drilling technique is a simple and cheap method of drilling holes for thermal profiling to depths of at least 50 m beneath water depth of up to 20 m from a platform of winter ice.

Acknowledgments

The authors thank V. Allen for assistance in drilling, Polar Continental Shelf Project for providing logistics support and C.P. Lewis for donation of a 30 m thermistor cable.

References

Cederstrom, D.J. and Tibbits, G.C.
1961: Jet Drilling in the Fairbanks Area, Alaska, U.S. Geol. Surv., Water Supply Paper 1539-B.

Hunter, J.A.M., Judge, A.S., MacAulay, H.A., Good, R.L., Gagne, R.M., and Burns, R.A.
1976: The Occurrence of Permafrost and Frozen Sub-Seabottom Materials in the Southern Beaufort Sea; Beaufort Sea Project Tech. Rep. no. 22.

Judge, A.S., Hunter, J.A., Good, R.L., Cowan, J., and Robb, G.
1975: Thermistor Cable Installation in Permafrost Materials with a Water-Jet Drilling Method; *in* Report of Activities, Part A, Geol. Surv. Can., Paper 76-1A, p. 479-480.

18. VLF NAVIGATION IN THE NORTH STAR AIRCRAFT OF THE NATIONAL AERONAUTICAL ESTABLISHMENT

Project 650007

Margaret E. Bower
Resource Geophysics and Geochemistry Division

Introduction

On May 8, 1976, the National Aeronautical Establishment's venerable North Star made its last research flight and was retired from active duty. During its 14 years and 4612 flying hours as an aeromagnetic research platform experiments in various other fields were also conducted, and one of the most important of these concerned Very Low Frequency (VLF) navigation.

There were several reasons for embarking on navigation research, the most pressing one being that most of the North Star's flying was at low altitude over the ocean or in the Arctic, where, lacking a very expensive inertial system, there are no other good, long range navigation aids. Tasks such as geophysical surveying, military reconnaissance, search and rescue, submarine tracking, could all benefit from any improvement. Two types of VLF equipment have been used in the North Star, namely the Omega system and the Global Company's GNS-200 and GNS-500 receivers which utilize the U. S. Navy Communications transmitters. The stations currently available to both systems are shown in Table 18.1, along with their frequency and radiated power. The Omega and Comm stations are all in the frequency range of 10-24 Khz, but there is one crucial difference – radiated power. The experience at NAE had been that the Omega stations at this time are just too weak to be used in the areas where they are needed the most. Therefore this report will describe only the work done with the VLF Comm stations and the Global systems.

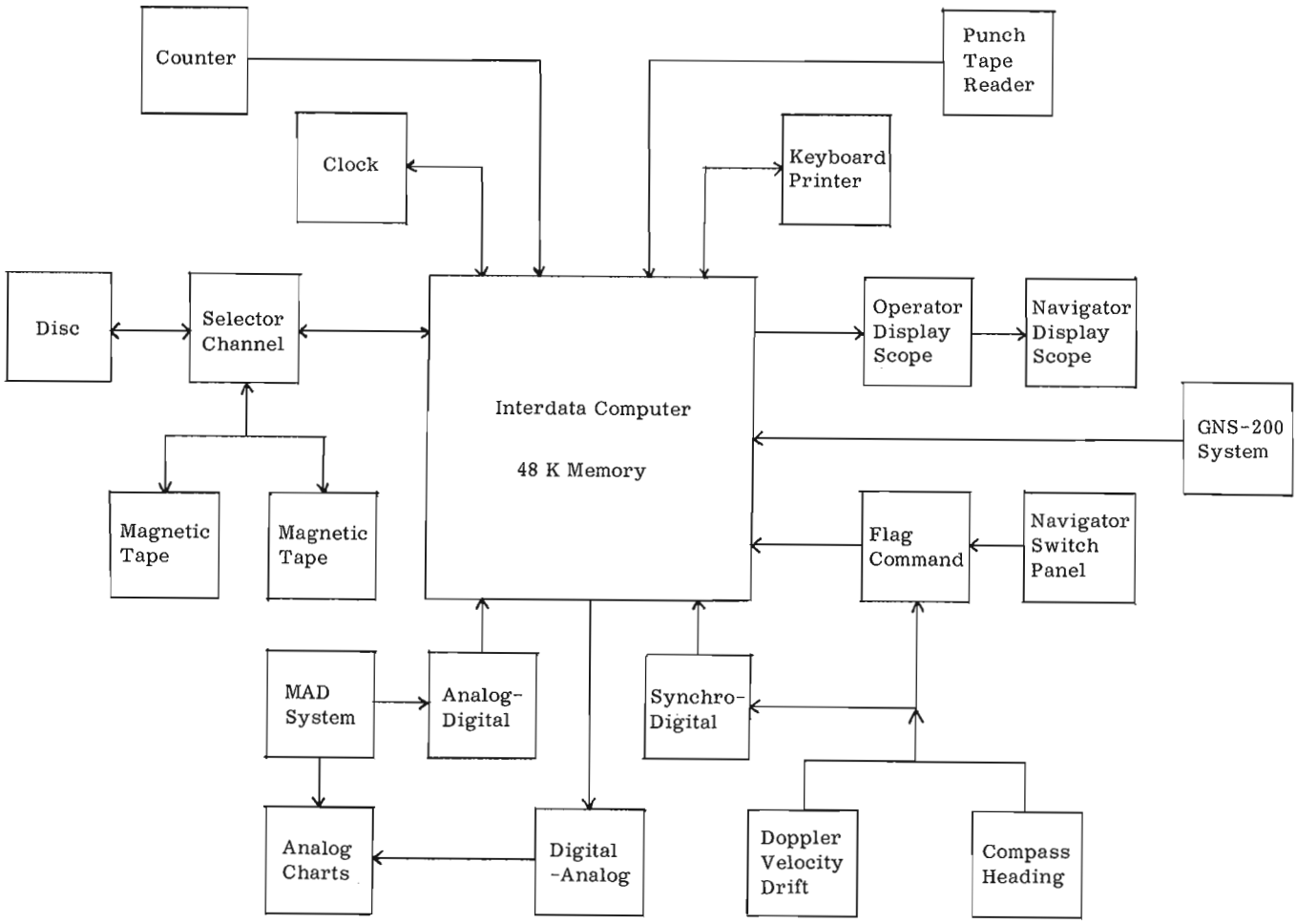

Figure 18.1. North Star Computer System.

From: Report of Activities, Part C;
Geol. Surv. Can., Paper 76-1C (1976).

Table 18.1

Omega and Communications Stations

Station	Location	Frequency KHZ	Radiated Power KW *
JXN	Norway	16.4	150 - 890
GBR	Great Britain	16.0	250 - 300
NAA	Maine	17.8	890 - 1000
NBA	Panama	24.0	150 - 1000
NLK	Washington State	18.6	250 - 1000
NSS	Annapolis	21.4	500 - 1000
NDT	Japan	17.4	125 - 500
NWC	Australia	22.3	1000 - 1260
NPM	Hawaii	23.4	140 - 1000
A	Norway	12.3	All Omega
B	Liberia		stations
C	Hawaii	12.2	1 - 10 kw
D	North Dakota	12.85	
E	La Reunion	13.1 + 10.2, 11.3, 13.6	
F	Argentina		
G	Trinidad	12.0	
H	Japan		

* First number is nominal power according to published figures; second number is authorized maximum power.

Evaluation of the VLF equipment was done at two levels:

(1) as a "black box" just as it came from the supplier, and as it would be used in a non-research aircraft. Of concern here was both the accuracy of the system compared to other navigation aids and visual checks, and the reactions of pilots and navigators. Results of this aspect, and description of the basis of VLF navigation have been reported by Hardwick (1973).

(2) by bringing the basic VLF signals into the onboard computer and running a totally independent navigation program. Both the raw signals and computed positions were recorded on magnetic tape; later the data could be analyzed both for performance on that flight and for a better understanding of the nature and peculiarities of VLF wave propagation.

North Star Data Acquisition and Navigation System

The heart of the system is an Interdata 4 computer with 48K bytes of memory and custom ROM for an extended command set. Interfaced to the computer (Fig. 18.1) are typewriter, punch tape reader, memory disc, two magnetic tape units, two display storage scopes, digital clock, counter for magnetic field, 8-channel digital to analog converter, 16-channel analog to digital converter, 4-channel synchro to digital converter, GNS-200, and flag-command interface. The computer has a high speed interrupt system, that is the operator can communicate with the computer through the keyboard to modify memory or request information without interfering with the running program.

Table 18.2

VLF Navigation Results

Trip No.	Elapsed Time (hr:min.)	Distance (naut. miles)	Error (naut. miles)	Comments
1	4:00	694	0.27	
2	4:51	878	0.91	
3	5.34	1159	3.93	Computer down 3 minutes
4	5:26	908	3.1	
5	5:46	827	1.71	
6	2:09	328	0.63	
7	2:20	443	1.43	
8	2:10	443	1.02	
9	2:42	456	2.71	
10	1:54	322	2.50	(1)
11	4:55	733 MAD circles	1.23	(1)
12	5:19	694	3.31	(1) Precipitation static
13	7:00	1179	1.33	(1)
14	2:40	450	1.62	(2)
15	4:04	747	2.88	(2)
16	7:02	1127 MAD circles	1.12	(2) Computer down twice
17	2:01	381	0.30	(2)
18	5:29	1007	2.43	(2)

(1) These trips affected by false signal on Great Britain channel.
(2) These trips contain zig-zag survey patterns with numerous turns and circles.

The navigation function is an integral part of the program and operates concurrently with several other tasks. The time cycle of the tasks vary from 200 milliseconds for the MAD magnetic data to 10 seconds for the navigation cycle. At the beginning of each 10-second period the computer reads the VLF interface, obtaining a phase difference between each of the seven stations and the rubidium clock, in units of 0.1 microsecond; to provide a reading less susceptible to noise, each reading is taken 64 times. A lengthy computation routine is then entered to calculate the distance and direction of change of aircraft position relative to each of the stations. Each of these results is weighted according to previous information on the stability of the signal, stations not being received are eliminated from the calculation, and a new VLF position arrived at. At the same time the aircraft doppler, drift and heading are read every 0.5 second to produce an independent doppler latitude-longitude position. These are put through a simple filter which combines the short term smoothness of the doppler with the long term accuracy of the VLF. The resulting 'master' latitude-longitude of the aircraft is displayed to the navigator and operator; the VLF and doppler positions can also be displayed if requested. The 10-second update value is used to obtain heading and ground speed, and the distance and bearing to a waypoint are calculated. Each waypoint table consists of 15 positions and a 'here now' slot in which the aircraft's current position can be saved if there is a requirement to return to the same place. The waypoint table must be put into the computer before flight, but 5 sets of waypoints (80) positions can be pre-loaded and moved into the active program at any time. By means of some switch buttons the navigator can roll the waypoint table backward or forward, initialize the computer position over a known point or put his display scope on 'hold'. The operator can also do this through the keyboard. All the VLF readings, positions and

doppler information go to the magnetic tape where they are interspersed with time, magnetometer and MAD data.

The above description is a much-simplified description of the functioning of the navigation system. The program must also be aware of and contend with station outages and returns, spurious signals producing abnormal position changes, calibration of the GNS-200 by the navigator, biasing of the VLF readings (the actual magnitude of the numbers has no meaning) failure of doppler or compass or any other of the peripherals. It should also be noted that navigation is not the primary function of the program, and on occasion it has been necessary to stop the computer because of a problem in the magnetics work. However, the navigation program will normally recover its position after a halt of two or three minutes.

Some 1976 Results

In the spring of 1976 the North Star flew two geophysical surveys, one north to Resolute Bay and one over the ocean as far south as the Republic of Guyana. These provided an excellent opportunity to evaluate the VLF on long flights, and for the southern trip to use a borrowed GNS-500 in parallel with the normal system. The operating procedure was as follows. The positions of radio beacons enroute, (VOR or NDB) were loaded into the computer's waypoint tables. As the aircraft flew over the beacon at the start of the trip the navigator initialized the computer to that position by means of his panel buttons. At the end of the trip the aircraft again flew over a beacon, and the precise on-top time was recorded. The computer's position could then be compared with the actual position of the beacon. The results of a number of these trips are given in Table 18.2. Distances are in nautical miles as this is still the standard unit in aviation.

The number in the ERROR column is the difference between the 'master' latitude-longitude and the published beacon position at the end of the trip. It should be noted that the published positions of most of the beacons are given to the nearest minute of latitude and longitude. Therefore if the positions at both ends of the line were in error by 0.5 minutes in both directions, there could be a maximum discrepancy in 1.4 nautical miles in the length of the line and a computer error of this magnitude may not be significant.

One problem that has occurred on several occasions is an erratic signal from one station, usually Great Britain. On trips 13 to 16 it was discovered later that the Great Britain signal, although appearing stable and normal at first glance, was actually incrementing in the wrong direction. The cause of this is not known, but back-plotting indicates that a transmitter on the same frequency somewhere in North Africa could have given these results. However, it could also have been a malfunction in the receiver, although no problem could be found later. When events such as this occur the procedure is to 'refly' the trip on the ground. A few modifications to the program allow it to use the VLF data from the magnetic tape instead of from the receiver. A station can be eliminated from the solution or a station's weight changed to give a more accurate track recovery.

Future Possibilities

Work is progressing on the Convair 580 which will replace the North Star, and it is planned to continue and expand the research in navigation. An Interdata 7-32 computer will be used along with an elaborate display system.

One new problem to be tackled will be the determination of absolute position from VLF. In all previous systems it was necessary to know where one was to start with, and a prolonged outage of any kind over the ocean makes this difficult. The possibility of 'air start' without reference to a known point on the ground would be a great improvement to any system. Current work on this problem is reported by Hardwick and Barszczewski (1975).

It is hoped that the Omega system will eventually be upgraded to the point where it is usable in the remote areas of Canada and the Arctic. A navigation system combining VLF, Omega and perhaps satellites could be a powerful and truly worldwide system.

References

Hardwick, C.D. and Brownley, T.R.
1973: An Evaluation of Aircraft Navigation using VLF Communications Stations, Can., Nat. Res. Counc. LTR-FR-38.

Hardwick, C.D. and Barszczewski, A.
1975: Determination of Absolute Position by Demodulating the VLF Communications Signals. Second Canadian Symposium on Navigation, C.A.S.I.

Hardwick, C.D.
1973: Aircraft Navigation using VLF Transmission. 27th Annual Frequency Control Symposium, Cherry Hill, N.J.

Skerk, Capt. W.D.
Evaluation of the GNS-500, Can., Nat. Res. Counc., LTR. (in prep.)

Project 630049

T.J. Katsube, M. Wadleigh[1], and R. Erickson[1]

Introduction

It is necessary for geotechnical engineering purposes to find out whether the ice content and temperature of permafrost can be detected by electrical exploration methods (Katsube, 1976). Laboratory work on the electrical properties of permafrost samples carried out by Olhoeft (1975a, b) and King (1975) show interesting characteristics of permafrost, but do not fulfill the requirements. A set of permafrost samples from the Tuktoyaktuk area in the MacKenzie Delta, Northwest Territories, has been used for laboratory electrical measurements over the frequency range from 1.0 to 10^6 Hz, at different temperatures. This paper comprises frequency spectrum data at -5°C and -10°C, and discussions of the ice content and temperature effect on the electrical properties of these permafrost samples.

Electrical Theory

In the past work on permafrost by Olhoeft (1975a), a combination of the DC resistivity and Debye Relaxation Equation has been used as the theoretical basis. This basis is considered, but as a result of work by Katsube (1975a, b, in prep.) a different theoretical approach using complex combinations of the Warburg Admittance concept is used.

Based on the work by Polubarinova-Kochina (1962) and Katsube (in prep.) the electrical model shown in Figure 19.1a is considered for the permafrost samples. The model in Figure 19.1b is also being considered, but for simplicity the former is used in this case.

The Warburg Admittances are expressed as follows (Bauerle, 1969):

$$\sigma_{w1} = a_1\omega^{1/\alpha_1} + j\, b_1\omega^{1/\alpha_1} \quad \ldots\ldots\ldots\ldots (1)$$

$$\sigma_{w2} = a_2\omega^{1/\alpha_2} + j\, b_2\omega^{1/\alpha_2} \quad \ldots\ldots\ldots\ldots (2)$$

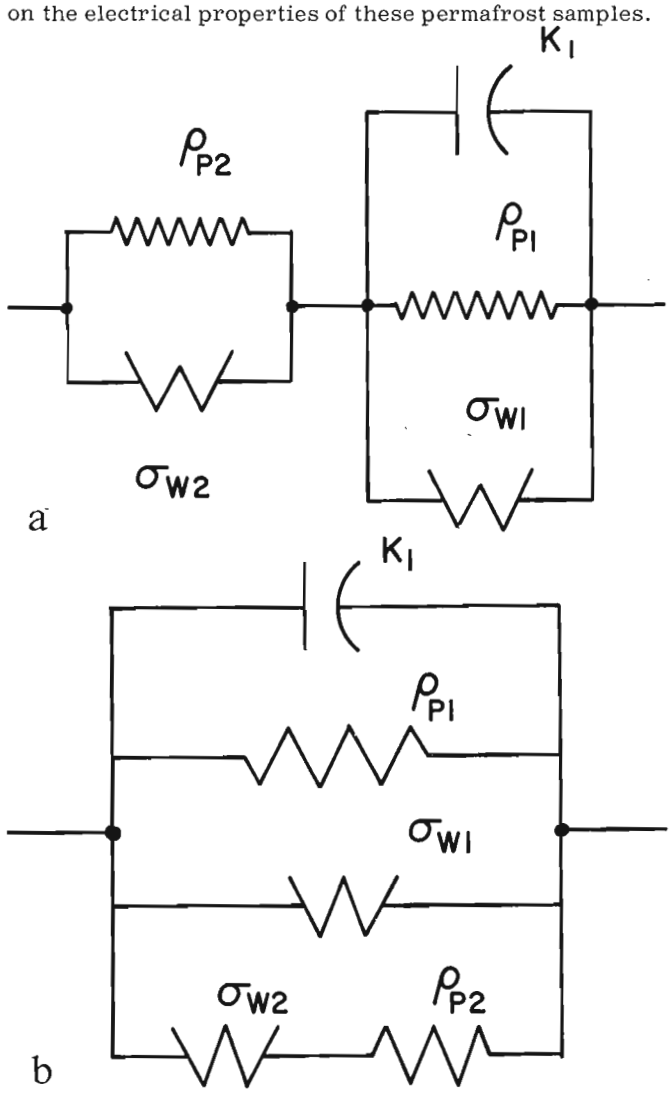

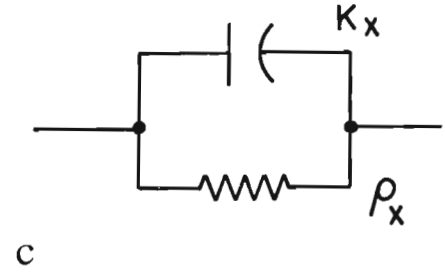

a, b : The models with all coefficients included.

c : Simplified model with only bulk parameters. The parameters are:

K_1 : dielectric constant of the sample,

ρ_{P1} : resistivity of free water in the pores,

σ_{w1} : Warburg Admittance of the bond layer that is formed by the water molecules around the mineral grains,

ρ_{P2}, σ_{w2} : resistivity and Warburg Admittance of another electrical mechanism which is often observed but whose physical significance has yet to be defined.

Figure 19.1. Electrical model for permafrost samples.

[1]Carleton University, Ottawa, Ontario

From: Report of Activities, Part C;
Geol. Surv. Can., Paper 76-1C (1976).

Table 19.1

Coefficients of the Permafrost Samples

SAMPLE	°C TEMP	% wt	ρ_{p_1} Ωm	a_1/b_1	b_1	ρ_{p_2} Ωm	a_2/b_2	b_2
14-R	-5.8	12	1.88E2	.4787	2.58E-8	1.00E2	.3750	-
	-9.5	12	4.05E2	.5308	7.92E-8	3.75E2	.4800	-
16-C	-5.27	13	3.52E2	.4886	2.90E-8	1.01E2	.1980	-
	-10.3	13	1.54E3	.6493	5.09E-7	9.80E2	.2959	8.49E-7
1-A	-5.4	20	6.50E1	.4923	1.37E-7	2.50E1	.2800	-
	-10.0	20	2.95E2	.5932	2.50E-7	3.35E2	.3283	-
13-14	-11.0	21	7.95E2	.3899	4.37E-9	5.60E2	.2321	3.27E-8
13	-10.0	23	1.19E3	.4201	1.13E-9	8.60E2	-.1279	8.26E-9
14-4	-10.0	54	3.20E3	.1718	2.72E-10	3.30E3	.2348	6.23E-8
14-7	-11.0	59	4.25E3	.3058	6.14E-10	1.26E4	.1904	6.20E-8
14-6	-9.6	60	2.55E3	.1764	2.75E-9	4.05E3	.2962	8.93E-8
14-1 (b)	-10.3	66	3.14E3	.2547	1.26E-10	2.18E3	.2408	3.43E-8
13-1	-10.0	66	9.0E3	.2444	1.75E-10	2.60E4	.3269	5.87E-8
17A	-5.5	76	3.35E3	.2388	1.32E-10	3.70E3	.3513	1.59E-7
	-9.8	76	1.38E4	.3260	5.36E-11	4.68E4	.1121	1.46E-7
14-1 (a)	-10.0	83	3.5E3	-.2286	2.39E-10	3.30E3	-.1936	1.14E-7
20C-1CE	-5.0	100	3.4E4	.2647	2.39E-11	5.25E4	-.7048	5.03E-8
	-9.5	100	3.80E4	.2631	2.29E-12	4.10E4	-.4146	8.42E-9
20C-1	-5.7	100	1.62E4	.0617	2.07E-11	3.60E4	.0666	4.63E-9
	-9.5	100	3.04E4	.0657	1.29E-11	7.70E4	-.6711	6.69E-8
20C-3	-5.7	100	1.70E4	.1176	1.95E-11	3.28E4	.0914	4.28E-9
	-10.0	100	3.60E4	.1750	1.08E-11	9.30E4	-.5054	1.01E-7

where a_1, a_2, b_1, b_2, α_1, α_2 are constants, and ω is the angular frequency. The complex resistivity for the equivalent circuit in Figure 19.1a is,

$$\rho^* = \rho_R - j\rho_I = \frac{1}{(1/\rho_{P1} + a_1\omega^{1/\alpha_1}) + j\,(\omega K_1\varepsilon_o + b_1\omega^{1/\alpha_1})} + \frac{1}{(1/\rho_{P2} + a_2\omega^{1/\alpha_2}) + jb_2\omega^{1/\alpha_2}} \quad \ldots . (3)$$

where ρ_R and ρ_I are the real and imaginary resistivities. If it is assumed that the right hand part of the circuit in Figure 19.1a has a shorter time constant than the left hand part, the curve for Equation 3 will appear as in Figure 19.2. The electrical properties are conventionally expressed in a general form using dielectric constant and resistivity and are represented here by K_x and ρ_x which are not coefficients but represent the bulk effect of all the coefficients and electrical mechanisms shown

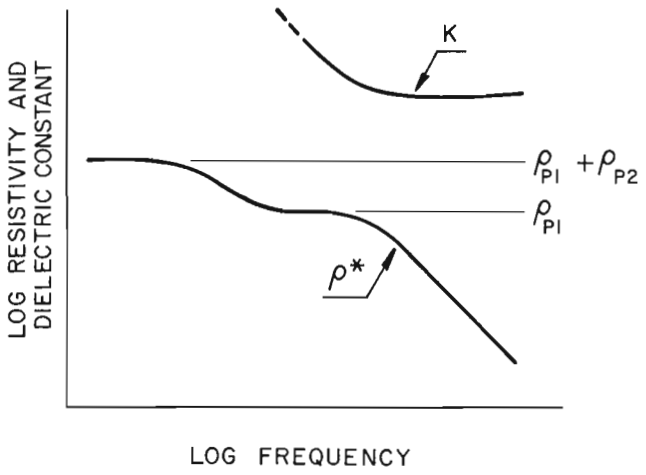

Figure 19.2. Theoretical model curves for complex resistivity (ρ^*) and dielectric constant (K').

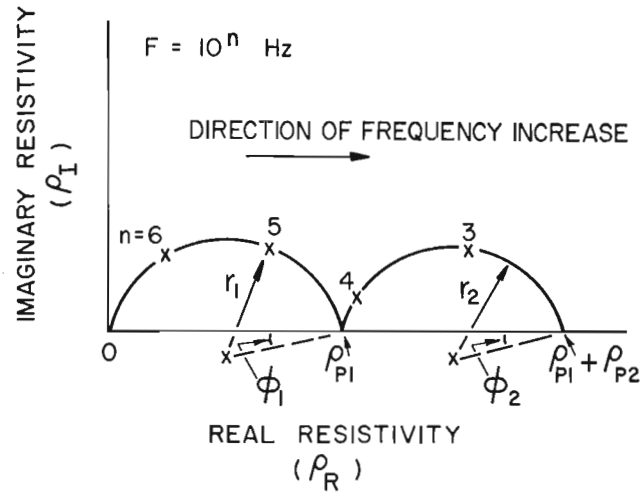

Figure 19.3. Cole-Cole plot of the theoretical model arcs in the complex resistivity plane.

in Figure 19.1a. The complex resistivity in this case is expressed by:

$$\rho^* = \frac{1}{1/\rho_x + j\omega K_x \varepsilon_o} \quad \ldots\ldots\ldots\ldots (4)$$

If only the right hand part of the equivalent circuit in Figure 19.1a is considered, the bulk dielectric constant can be expressed by:

$$K_x = K_1 + \frac{b_1}{\varepsilon_o}\ \omega^P \quad \ldots\ldots\ldots\ldots (5)$$

where $P = 1/\alpha_1 - 1$ and is shown in the upper part of Figure 19.2. If ρ_I is plotted against ρ_R, the Cole-Cole plots in Figure 19.3 are obtained. The arcs can be expressed by the following equations:

$$[\rho_R - \rho_{P1}/2]^2 + [\rho_I - (a_1/b_1)(\rho_{p1}/2)]^2 = [r_1\rho_{p1}/2]^2 \quad .. (6)$$

$$[\rho_R - \rho_{p2}/2]^2 + [\rho_I - (a_2/b_2)(\rho_{p2}/2)]^2 = [r_2\rho_{p2}/2]^2 \quad .. (7)$$

where $$r_1 = \rho_{P1}\sqrt{1 + (\frac{a_1}{b_1})^2} \quad \ldots\ldots\ldots (8)$$

$$r_2 = \rho_{P2}\sqrt{1 + (\frac{a_2}{b_2})^2} \quad \ldots\ldots\ldots (9)$$

The dissipation factor D is defined as the following:

$$D = \frac{\rho_R}{\rho_I} \quad \ldots\ldots\ldots\ldots\ldots (10)$$

The distribution angles ϕ_1 and ϕ_2 can be expressed by:

$$\phi_1 = \tan^{-1}(\frac{a_1}{b_1})$$
$$\phi_2 = \tan^{-1}(\frac{a_2}{b_2}) \quad \ldots\ldots\ldots (11)$$

Samples and Experimental Procedures

The permafrost specimens were cut from core samples drilled at "Involuted Hill" near Tuktoyaktuk (Annon, 1976). Most of the samples are clay permafrost samples, with some containing organic material. The diameters of the cores ranged from 4 to 5 cm. Disk specimens with thicknesses ranging from 1.0 to 2.5 cm were cut from these cores. The ice content (ϕ) of these specimens varied from 12 to 100 per cent Table 19.1.

The ice content is measured by melting the permafrost samples at room temperature, and then drying them in the oven for over 10 hours at 150°C. The ice content ϕ is determined by

$$\phi = \frac{g_W - g_D}{g_w} \times 100 \quad \ldots\ldots\ldots (12)$$

and is expressed in per cent, where g_W and g_D are the weights of the specimens in wet and dry conditions.

The specimens are placed in a sample holder that holds six specimens at a time (Fig. 19.4). The stray capacitance and leakage resistance between each set of electrodes is in the order of 12 picofarads and 2×10^7 ohms, respectively. Corrections are made for these effects. Each set of electrodes is connected one at a time to the measuring system.

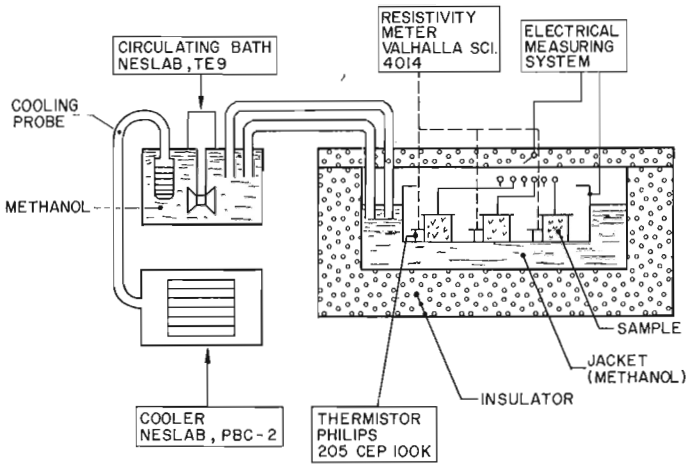

Figure 19.4. Block diagram of the electrical measuring and cooling system.

A jacket containing methanol surrounds the sample holder. The jacket is connected to a cooling bath that controls the temperature and the circulation of the liquid through the system. The lowest temperature reached in the sample holder is -16°C. Thin glass thermistors are placed in a position where their tips touch the specimens. The temperature of the specimens is monitored by a digital resistivity meter.

The specimens are measured over the frequency range from 1.0 to 10^6 Hz by the Automatic Electrical Rock Property Measuring system that is described by Gauvreau and Katsube (1975). Since graphite has a larger surface capacitance than iron or stainless steel ($10 - 100\mu F/cm^2$) when in contact with water, graphite discs are inserted between the electrodes and specimen. The contact surfaces of the specimens are slightly heated and melted by the palms of one's hands before making contact with the graphite discs. Good electrode contacts are insured by this method.

Four-electrode systems were considered for elimination of electrode effects, but due to the high resistance that can be expected at the contacts of the potential electrodes, only the two electrode system is used. However, the electrode effects are not expected to be significant unless the resistivity of the samples is very low.

Results

The 15 permafrost samples were measured over the frequency range from 1.0 to 10^6 Hz. Typical results for an ice rich sample (Sample 20C-1, ϕ = 100%) and a sample with little ice (Sample 1A, ϕ = 20%) are shown in Figures 19.5 to 19.8. The entire curve for ρ^*, and the high frequency part of the curve for K'_x in Figure 19.5 resemble the theoretical curves in Figure 19.2. It is interesting to see how the right hand arc in Figure 19.6 grows with decrease in temperature.

The higher frequency portion of the curve for K'_x in Figure 19.7 resembles that of Figure 19.2. The curve for ρ^* in Figure 19.7 shows little resemblance

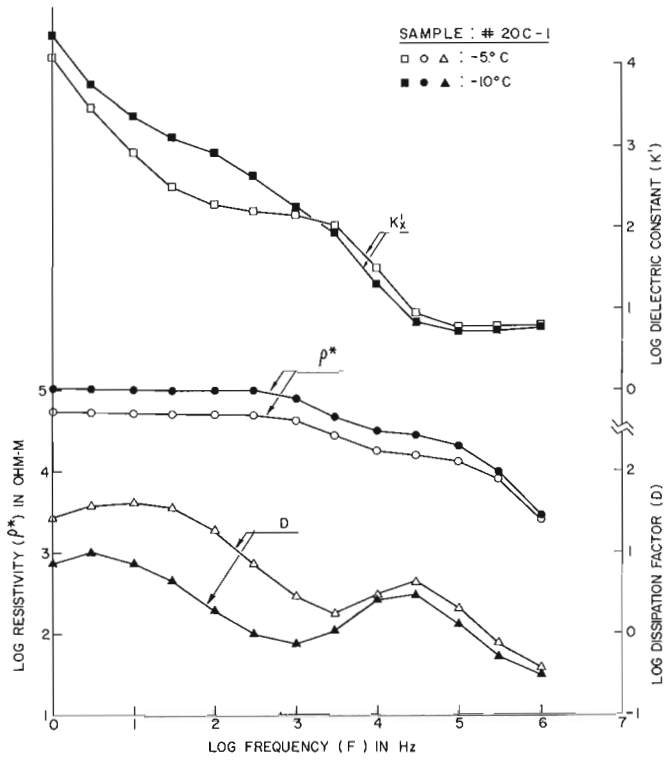

Figure 19.5. Frequency spectra of complex resistivity (ρ^*), dielectric constant (K'_x) and dissipation factor (D) for an ice rich permafrost sample (Sample 20C-1).

to that in Figure 19.2, perhaps because the ρ_{p2} value for sample 1A is small. Katsube (1974) showed that when the electrode materials are varied with the rock specimen being the same, only the right hand portion of the Cole-Cole plot changes with the main arc on the left hand side being unaffected. Based on this fact, and on the work of Katsube (1975a), the dispersion of ρ^* at the lower frequencies in Figure 19.7, and the dispersion of ρ_I at the right hand side in Figure 19.8 are considered to be the result of electrode effects. The right hand arc in Figure 19.8 grows with decrease in temperature, but it is not as evident as it is in Figure 19.6.

Various coefficients (ρ_{p1}, a_1/b_1, b_1, ρ_{p2}, and a_2/b_2) shown in Figure 19.1 and in Equation 3 are determined from the electrical measurements. The values for these coefficients are listed in Table 19.1. A correlation can be seen between ρ_{p1}, ρ_{p2} and ϕ as shown in Figures 19.9 and 19.10 respectively. Curve fitting by the least square method produces the following results:

$$\log \rho_{p1} = A_1\phi + C_1$$

$$\log \rho_{p2} = A_2\phi + C_2$$

$$A_1 = 0.021$$

$$C_1 = 2.5$$

$$A_2 = 0.033$$

$$C_2 = 1.67$$

It can be seen that ρ_{p2} is more strongly dependent on ϕ than ρ_{p1}. Correlations between a_1/b_1, a_2/b_2, b_1 and ϕ can also be seen as demonstrated in Figures 19.11 to 19.13 respectively. Temperature effects are not evident in Figures 19.9 to 19.13.

Discussion

The general trends in this work, for dielectric constant (K') and dissipation factor or loss tangent (D) are similar to those of Olhoeft (1975a). There are, however, minor differences at the lower and higher ends of the frequency spectrum. The resistivity (ρ^*) values for the samples with low ice content are generally in the same order as the sandstone and slate samples that were measured by King (1975).

There are a number of parameters that seem to show a correlation with the ice content. For example the increase in ρ_{p1} and ρ_{p2} with ϕ is quite evident. Based on the model in Figure 19.1, this implies that the free water available for ionic conduction decreases with increase in ice content, which seems to be an acceptable explanation. The values of b_1 vs ϕ show a very strong negative correlation with ϕ (Fig. 19.13). From the definitions (Equations 1 and 2), a decrease in b_1 implies a decrease in capacitance. This relationship can be broken into three parts:

ϕ = 0 - 30% : rapid decrease of b_1 with ϕ,

ϕ = 30 - 90% : moderate decrease of b1 with ϕ,

ϕ = 90 - 100% : rapid decrease of b_1 with ϕ.

These trends suggest the following situation. In the ϕ = 0 - 30% region, the mineral grains are perhaps all in contact with each other, and the capacitance of the bond layer in the clay decreases with increasing ice content. In the ϕ = 30 - 90% region, the mineral grains are presumably separated by an ice matrix, and thus the effect of the bond layer of the ice increases with increasing ice content. The ϕ = 90 - 100% region, perhaps, exhibits pure ice characteristics. The capacitance of the bond layers in ice appears to be lower than that of the clay. The values of a_1/b_1 decreases with increasing ice content (Fig. 19.11). This implies

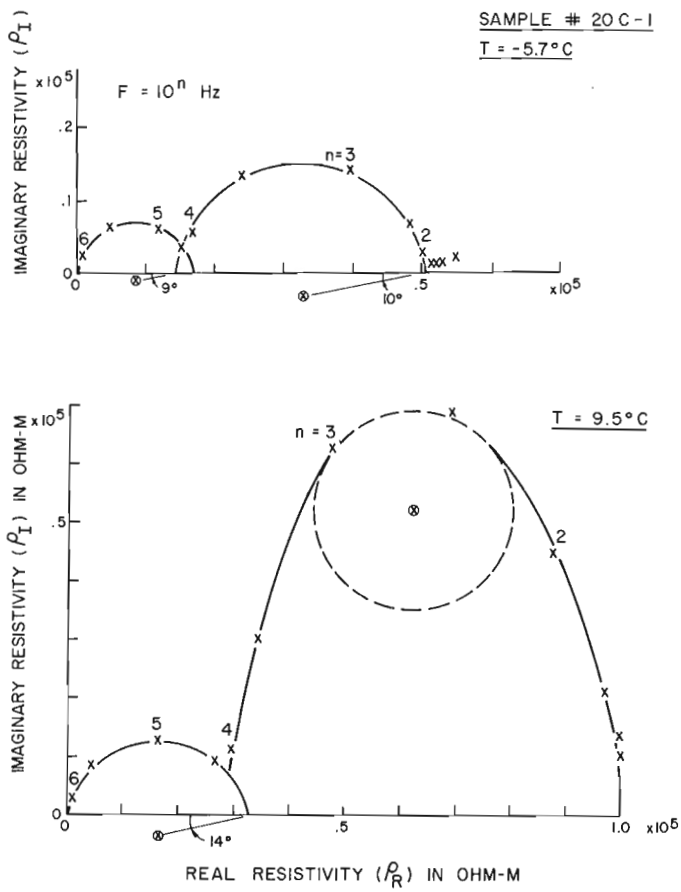

Figure 19.6. Cole-Cole plot for an ice rich permafrost sample (Sample 20C-1).

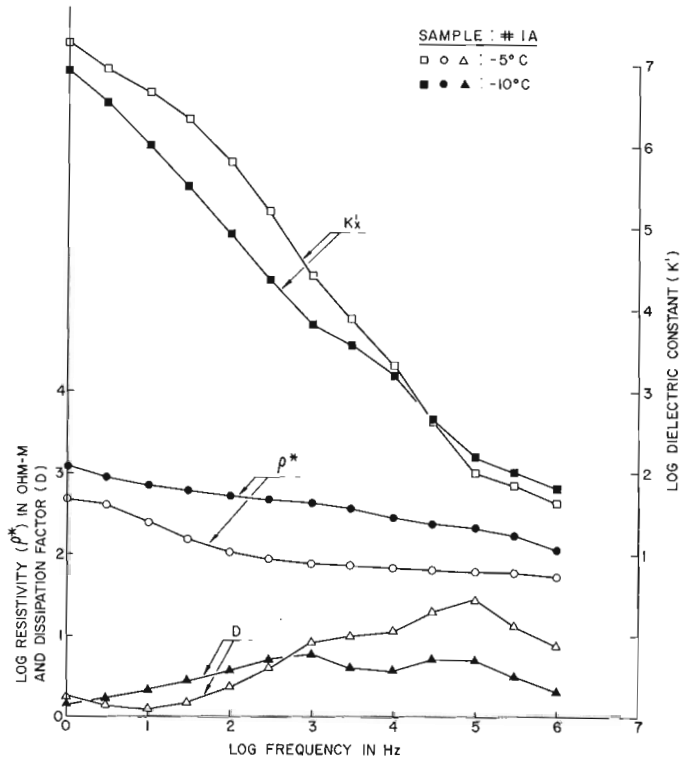

Figure 19.7. Frequency spectra of complex resistivity (ρ^*), dielectric constant (K') and dissipation factor (D) for a clay rich permafrost sample (Sample 1A).

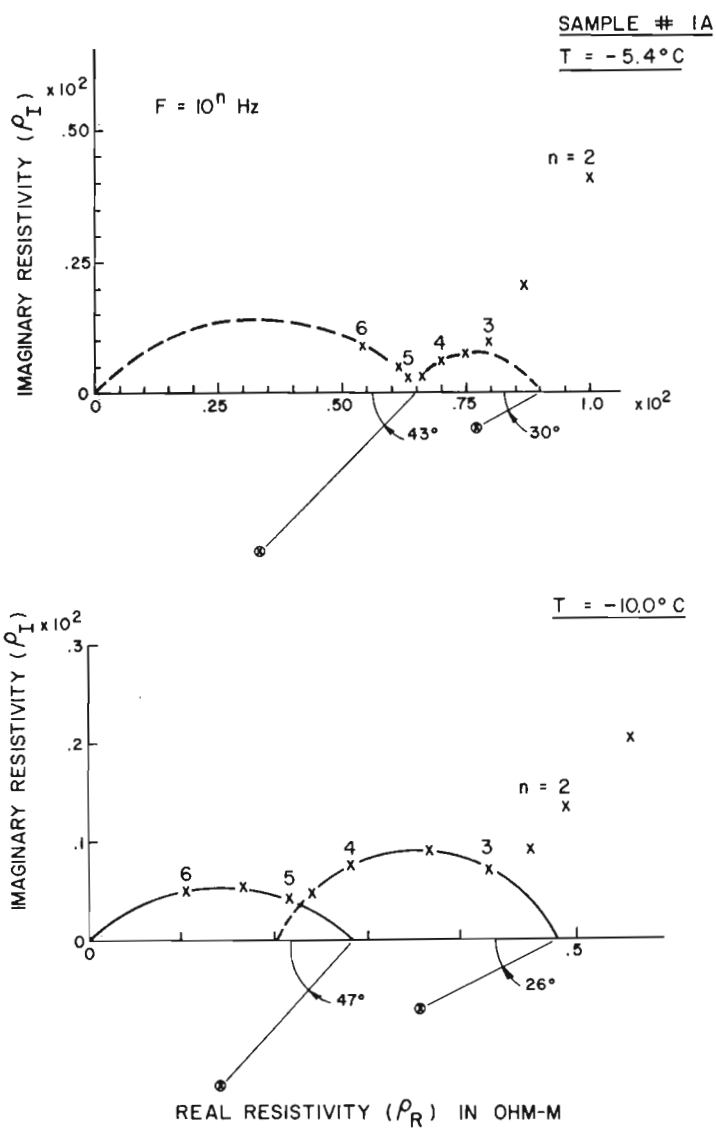

Figure 19.8. Cole-Cole plot for a clay rich permafrost sample (Sample 1A).

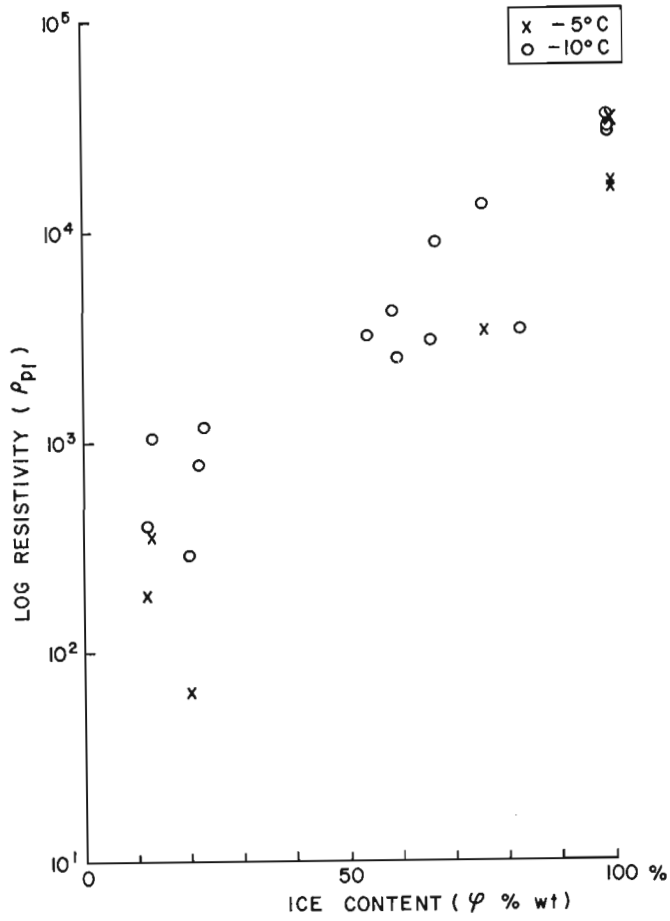

Figure 19.9. ρ_{p1} vs. ice content (ϕ).

that the bond layers in the ice and clay become relatively less conductive as the ice content increases. Interesting trends are seen in the ρ_{p2} and a_2/b_2 vs ϕ diagrams (Figs. 19.10 and 19.12). However, little is known about the electrical mechanism that governs these parameters.

The temperature effect in these measurements is not evident. This is, perhaps, because measurements are made at only -5 and -10°C. It is necessary to carry out measurements over a wider range of temperatures before drawing any conclusions on this subject. The fact that a growth of the second arc with decreasing temperature can be seen in Figure 19.6 and Figure 19.8 implies that there is a possibility that one of the coefficients of the electrical model (Fig. 19.1) may be used for temperature detection.

Conclusion

There are a number of parameters or coefficients that have the potential to detect or monitor the ice content in permafrost. The parameters ρ_{p1} and ρ_{p2} are most promising. However, further work on the temperature effect is necessary before any conclusions can be reached on this subject.

It seems that further work may produce a parameter or coefficient that can be used for detection or monitoring of the temperature in permafrost. The trend of b_1 vs ϕ shows a possibility of providing some information on the distribution of ice.

Acknowledgments

Thanks are expressed to L.S. Collett for his encouragement of this work, to W.J. Scott for supplying the permafrost samples, and to G.R. Olhoeft for his advice and designs for the low temperature measuring system used in this work.

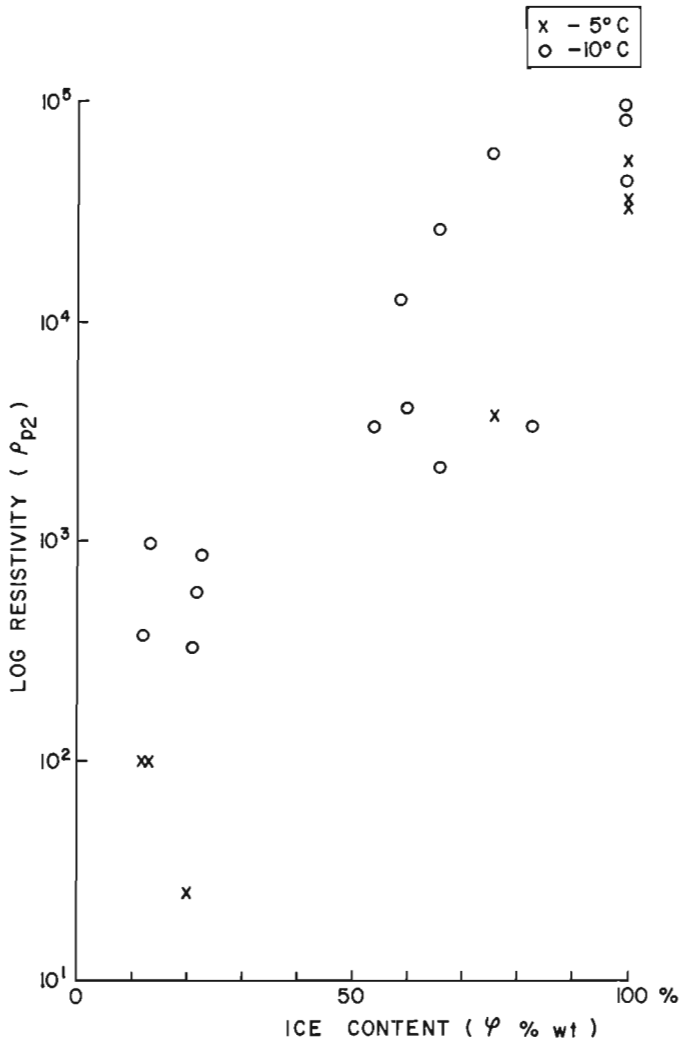

Figure 19.10. ρ_{p2} vs. ice content (ϕ).

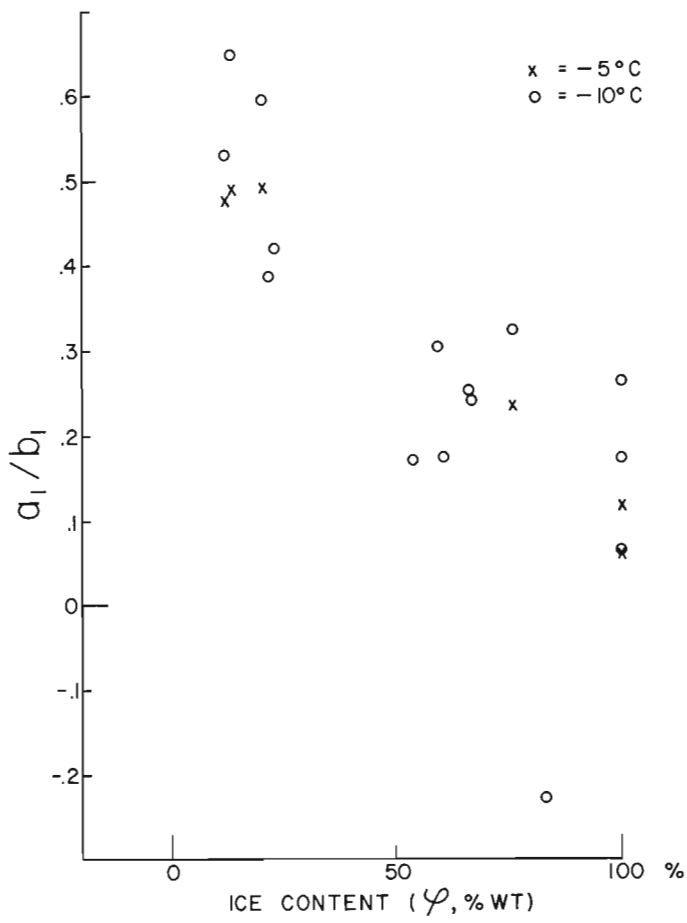

Figure 19.11. a_1/b_1 vs. ice content (ϕ).

References

Annan, A.P.
1976: Density of ice samples from "Involuted Hill" test site, District of Mackenzie; *in* Report of Activities, Part C; Geol. Surv. Can., Paper 76-1C, Rep. 20.

Bauerle, J.E.
1969: Study of solid electrolyte polarization by a complex admittance method; J. Phys. Chem. Solids, v. 30, p. 2657-2670.

Gauvreau, C. and Katsube, T.J.
1975: Automation in electrical rock property measurements; *in* Report of Activities, Part A; Geol. Surv. Can., Paper 75-1A, p. 83-86.

Katsube, T.J.
1974: Electrical characteristics and electrical mechanism of some ultramafic rocks; Presented at the Second Workshop on Electromagnetic Induction in the Earth. Ottawa Ont. Aug. 22-28.

1975a: The electrical polarization mechanism model for moist rocks; *in* Report of Activities, Part C; Geol. Surv. Can., Paper 75-1C, p. 353-360.

1975b: The critical frequency and its effect on EM propagation; *in* Report of Activities, Part A; Geol. Surv. Can., Paper 75-1A, p. 101-105.

1976: New requirements for electrical exploration methods and for laboratory R and D; *in* Report of Activities, Part A; Geol. Surv. Can., Paper 76-1B, p. 229-232.

Electrical properties of soils in relation to soil moisture detection. in prep.

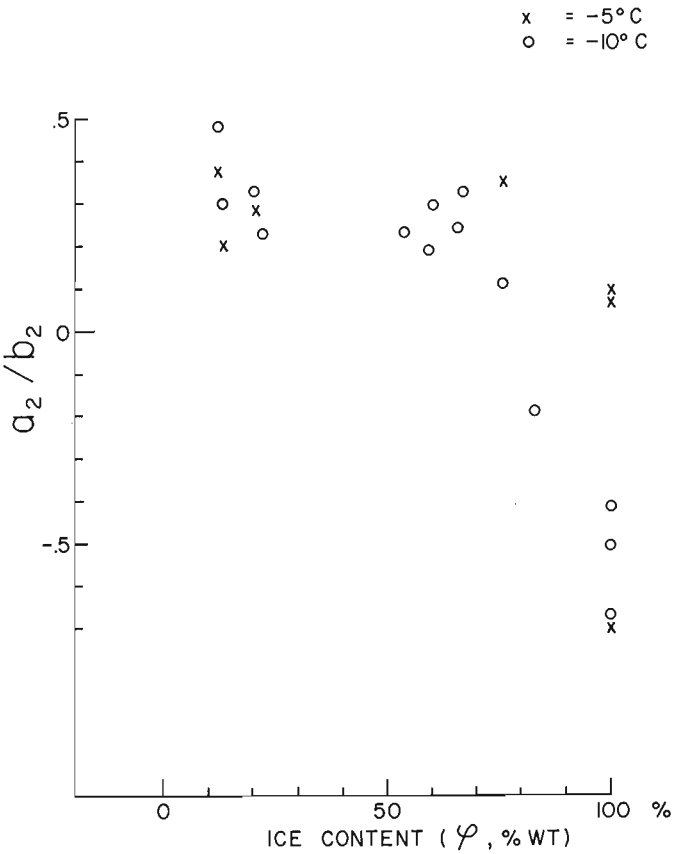

Figure 19.12. a_2/b_2 vs. ice content (ϕ).

King, M.S.
1975: Acoustic velocities and electrical properties of frozen sandstones and shales; Presented at Waterloo '76, May 15-17, Waterloo, Ontario.

Olhoeft, G.R.
1975a: The electrical properties of permafrost; Ph.D. thesis, University of Toronto.

1975b: Electrical properties of natural clay permafrost; Presented at Waterloo '76, May 15-17.

Polubarinova-Kochina, P. Ya.
1962: Theory of ground water movement. Princeton University Press, Princeton, New Jersey.

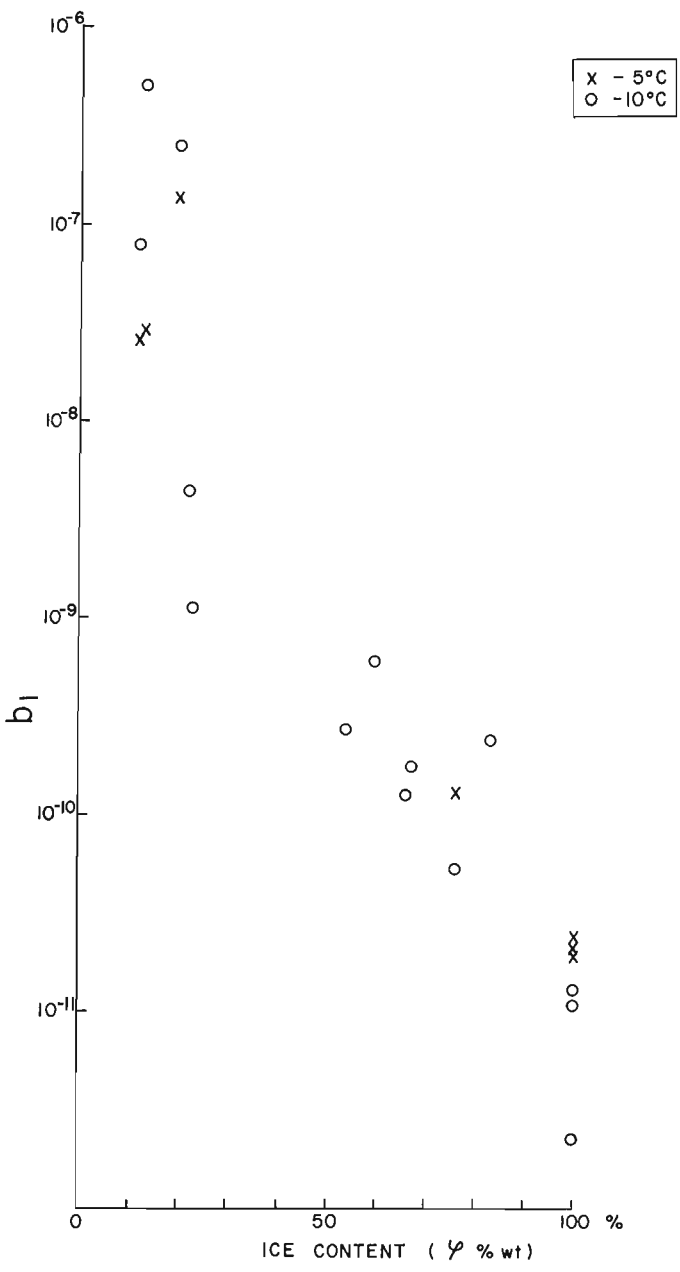

Figure 19.13. b_1 vs ice content (ϕ).

20. DENSITY OF ICE SAMPLES FROM "INVOLUTED HILL" TEST SITE, DISTRICT OF MACKENZIE

Project 750037

A. P. Annan
Resource Geophysics and Geochemistry Division

Introduction

The ice density of massive ice structures in permafrost is a useful parameter in attempting to determine the genesis of the ice (MacKay, 1971) and to interpret gravity survey data over such areas (Rampton and Walcott, 1974). The Geological Survey of Canada test site at "Involuted Hill" near Tuktoyaktuk, is an ice cored hill (MacKay, 1963; Rampton and Walcott, 1974) typical of many such hills in the area. Interpretation of recent radar soundings at the test site (Annan *et al.*, 1975a, b; Annan and Davis, 1976) has indicated anomalously high propagation velocities for radar signals in the ice rich hill. A large air content in the ice core of the hill was suggested as a possible explanation of the high velocity. Using an empirical relationship between ice density and the dielectric constant of ice (Robin *et al.*, 1969) the radar results were used to estimate a mean ice density and air content. To explain the radar results densities of the order of 0.7 Mgm/m^3 and air contents in the order of 20 to 25 per cent by volume were required. Visual examination of air bubbles in ice samples from core drilling suggested that the ice did contain considerable amounts of air. In order to assess the validity of the air bubble hypothesis, the densities of a number of ice samples collected during core drilling and preserved in cold storage were determined.

Ice Samples

The ice samples for the experiment were selected from a large number of frozen soil and ice specimens collected during a drilling program in the 1975 spring field season. The location of drillholes is shown on the aerial photograph of "Involuted Hill" (Fig. 20.1). The section of the hill most densely drilled is between 0 and 6 W on the baseline of the grid shown in Figure 20.1; the geologic cross-section in this area as inferred from the drilling is shown in Figure 20.2. The samples were stored in insulated containers, shipped to the Geological Survey of Canada in Ottawa and are currently stored in a freezer at -20°C. None of the samples melted during this process. The ambient air temperature at the time of drilling was -15° to -40°C. Extreme precautions were taken to assure that the samples did not melt during shipment.

The ice samples selected for density determinations were chosen to be representative of the large amount of available core. The samples spanned the range from clear ice with very few bubbles to opaque ice with very large numbers of small bubbles. Samples were also selected which contained trace and large amounts of soil and organic material. About half the selected samples were taken from one drillhole, IR, which was drilled to a depth of 13 m. This was the deepest hole drilled in 1975 and nearly all of the hole was through ice. The remaining samples were taken from 2- to 10-m holes, SEC 6, SEC 15 and SEC 16, which encountered massive ice. The logs of these holes are shown in Figure 20.3.

Density Determination Technique

The density measurements were carried out in a manner which caused little if any disturbance to the samples. This required making all measurements in a cold room held at -8°C in order to avoid melting the samples. As the first step, the samples were weighed on a balance which provided weight determinations accurate to 0.1 gm. The second step of determining the volume of the irregularly shaped samples was slightly more difficult.

The simplest way to determine volume of irregularly shaped objects is to measure the weight of the object while it is immersed in a liquid of known density and find the change from the weight in air. For rocks this process is straight forward since water can be used as the liquid. To measure the volume of the ice sample without destroying it required a material which would be liquid to -10° to -20°C, would not dissolve the samples, and would not coat or contaminate the samples for future experimental work. In addition, the density of the liquid had to be less than 0.7 Mgm/m^3 in order that ice would not float if the ice densities were indeed as low as this. After much discussion, the optimum liquid for the purpose was found to be n-Hexane (C_6H_{14}). This liquid has an extremely low freezing point and does not dissolve ice. In addition it is highly volatile with a 4 x 10^{-4} per cent residue after evaporation which leaves the specimen uncontaminated after the experiment. The density of n-Hexane was 0.67Mgm/m^3.

Discussion of Experimental Results

The results of the experimental work are tabulated in Table 20.1. Each sample is accompanied by a brief description, its weight (w), volume (v), density (ρ), estimated volume fraction air content (η), and inferred dielectric constant (K). The density is obviously computed via the expression:

$$\rho = \frac{w}{v} \qquad \ldots\ldots\ (1)$$

The error in determining w was about 1 per cent or less while in v it was about 2 per cent. The limiting factor was the accuracy of the scale used for the weight

From: Report of Activities, Part C;
Geol. Surv. Can., Paper 76-1C (1976)

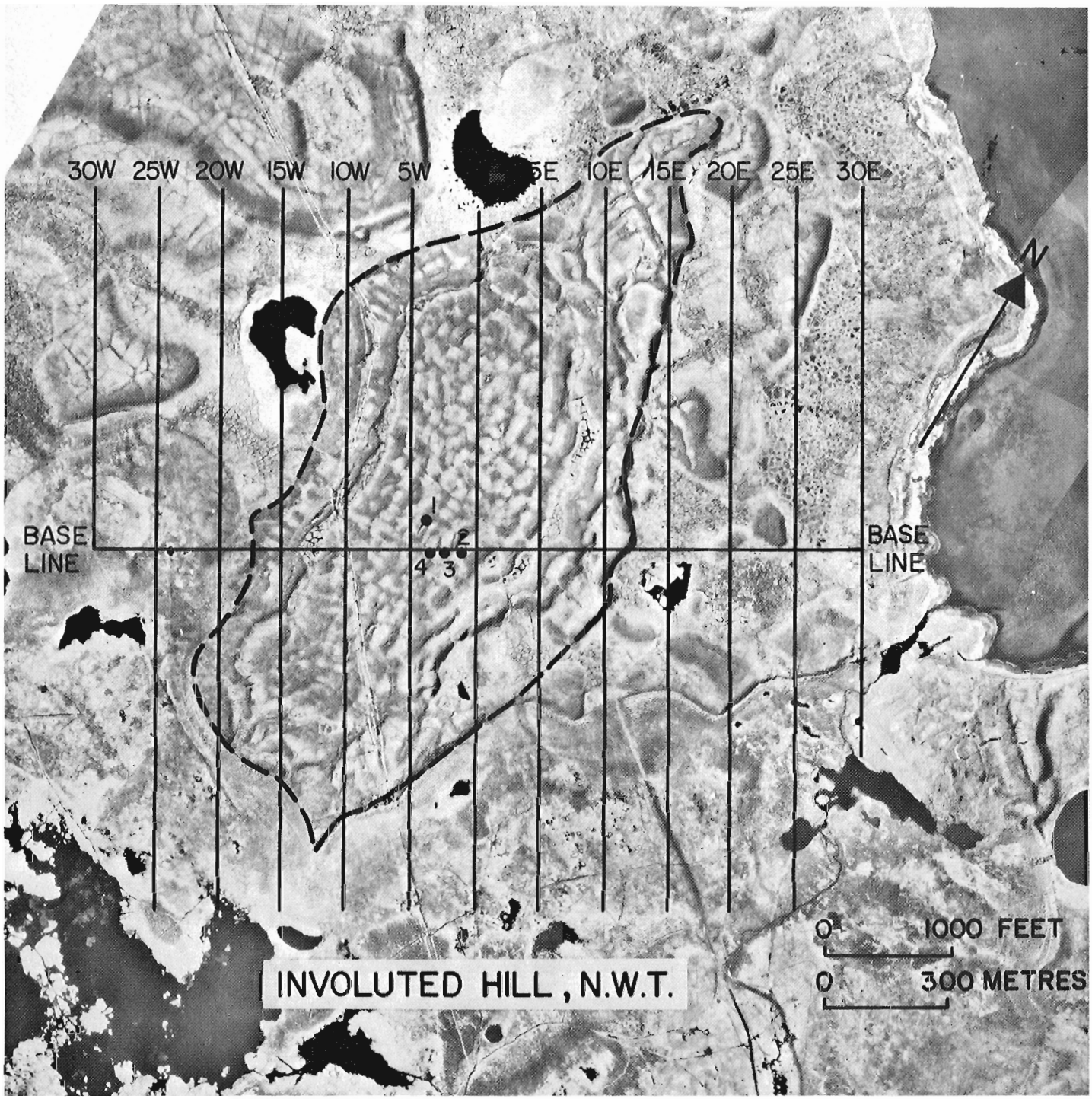

Figure 20. 1. Aerial photograph of "Involuted Hill" test site. The dashed line indicates the edge of the hill. The geophysical survey grid is indicated by blackllines. Line numbers are indicated by distance in units of hundreds of feet from line o. Drillholes are indicated by • . The numbers and holes correspond as follows: 1 – ER, 2 – SEC 6, 3 – SEC 15, 4 – SEC 16.

TABLE 20.1

Summary of weight (w), volume (v), density (ρ), air fraction, (η), and inferred dielectric constant (K) for ice samples analyzed.

SAMPLE NUMBER	SAMPLE DESCRIPTION HOLE NO.		VISUAL	W (gm)	V ml	ρ Mgm/m^3	η	K
1		–	Ice cube, no obvious bubbles	25.2	29.9	0.84	0.09	2.98
2	IR	5.6 – 12.8	Fairly clear ice, few bubbles	15.2	17.2	0.88	0.04	3.07
3	IR	5.6 – 12.8	Numerous 1 mm bubbles	13.8	16.3	0.85	0.08	3.01
4	IR	5.6 – 12.8	Numerous 1 mm bubbles	12.7	15.4	0.82	0.11	2.94
5	IR	5.6 – 12.8	Numerous 1 mm bubbles	18.6	22.2	0.84	0.09	2.98
6	IR	5.6 – 12.8	Some soil but few bubbles	14.1	16.9	0.83	0.10	2.96
7	IR	5.6 – 12.8	Numerous 1 mm bubbles	14.9	18.4	0.81	0.12	2.91
8	IR	5.6 – 12.8	Numerous 1 mm bubbles	22.1	25.7	0.86	0.07	3.03
9	IR	5.6 – 12.8	Large bubbles (>1 mm)	13.6	16.7	0.81	0.12	2.91
10	IR	5.6 – 12.8	Clear sample few bubbles	13.8	15.7	0.88	0.04	3.07
11	IR	0 – 5.6	Fine bubbles and soil flecks	20.1	23.7	0.85	0.08	3.01
12	IR	0 – 5.6	Fine bubbles perpendicular to bedding	18.5	22.1	0.84	0.09	2.98
13	IR	0 – 5.6	Fine bubbles perpendicular to bedding	18.6	21.3	0.87	0.05	3.05
14	IR	0 – 5.6	Fine bubbles perpendicular to bedding	18.5	21.3	0.86	0.05	3.05
15	SEC 6		Sample opaque, long strings of fine bubbles perpendicular to bedding	103	120	0.86	0.07	3.03
16	SEC 6		Sample opaque, long strings of fine bubbles perpendicular to bedding	61.1	75	0.81	0.12	2.91
17	SEC 15		Very dirty sample, numerous cracks, bubbles perpendicular to bedding of soil particles	71.3	80	0.89	0.03	3.10
18	SEC 16	8.7 – 10.0	Bubbles of various sizes	15.6	18.5	0.84	0.09	2.98
19	SEC 16	8.7 – 10.0	Bubbles of various sizes	22.3	26.9	0.83	0.10	2.96
20	SEC 16	8.7 – 10.0	Bubbles of various sizes	17.5	20.0	0.88	0.04	3.07
21	SEC 16	8.7 – 10.0	Bubbles of various sizes	16.7	19.9	0.84	0.09	2.98
22	IR	0 – 5.6	Bubbles of various sizes	13.5	15.8	0.85	0.08	3.01
			– Average values –			0.85	0.08	3.01

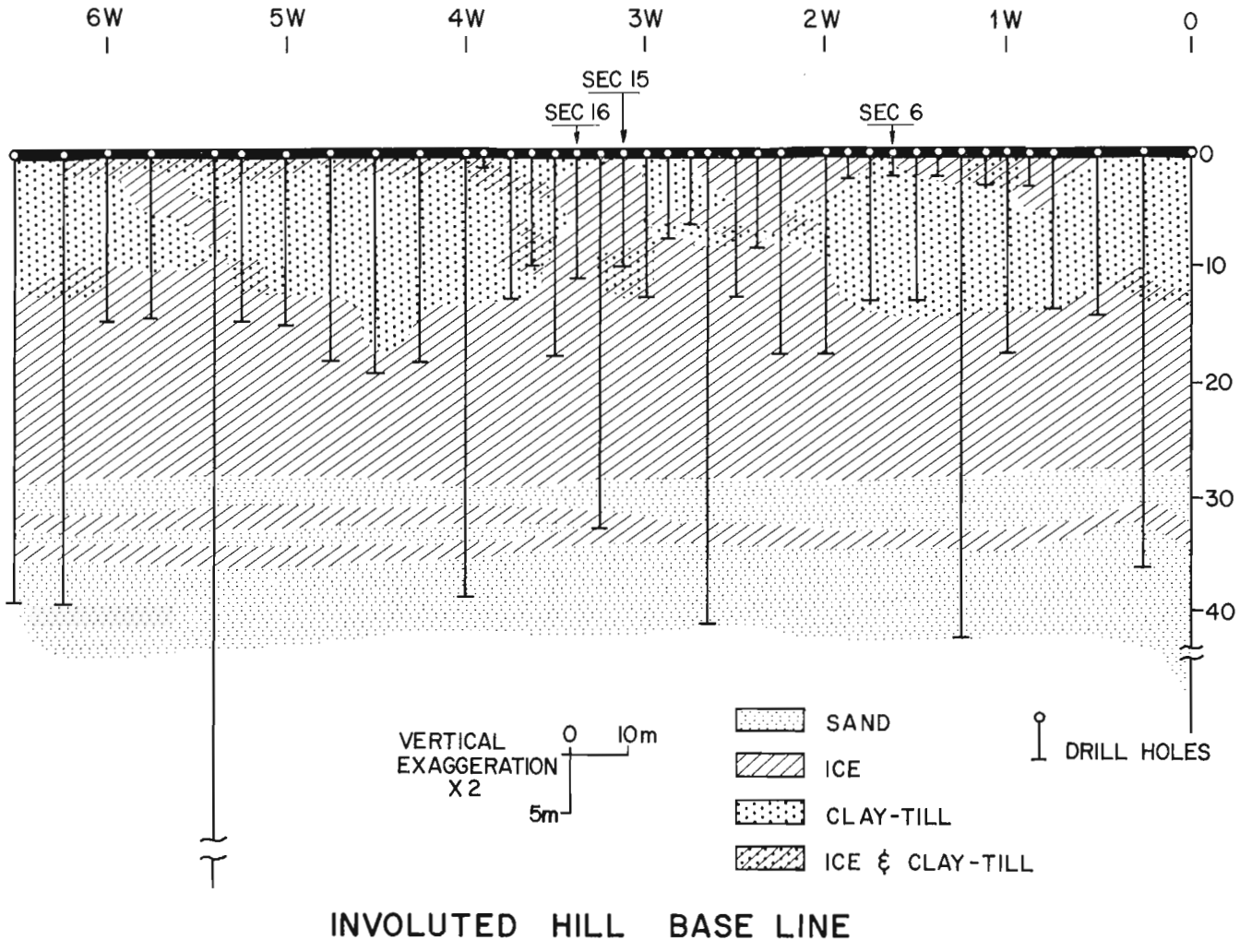

Figure 20. 2. Geological cross section of the "Involuted Hill" between 0 and 6 W on the base line as inferred from the drilling results. Position numbers are given in units of hundreds of feet.

measurements both in air and in fluid. The maximum experimental error in the density estimates is less than 3 per cent. The volume fraction of air is determined from

$$\eta = \frac{.92 - \rho}{0.92} \qquad \ldots\ldots\ (2)$$

where 0. 92 Mgm/m^3 is the density of pure ice. This expression assumes that the sample contains only air and ice. As a result, air content estimates for samples with large soil contamination may be inaccurate. The dielectric constant is inferred from ρ using the linear relationship

$$K = 1 + 2.36\rho \qquad \ldots\ldots\ (3)$$

discussed by Robin *et al.* (1969). As with the air content estimation, the dielectric constant estimation may be contaminated by a large soil content in some of the samples.

The data in Table 20. 1 indicate that the density of the ice samples is significantly lower than that of pure ice. The densities, however, are not as low as predicted by the radar results. The average density for the measured samples was 0. 85 Mgm/m^3 which corresponds to an 8 per cent air content and an average inferred dielectric constant of 3. 01.

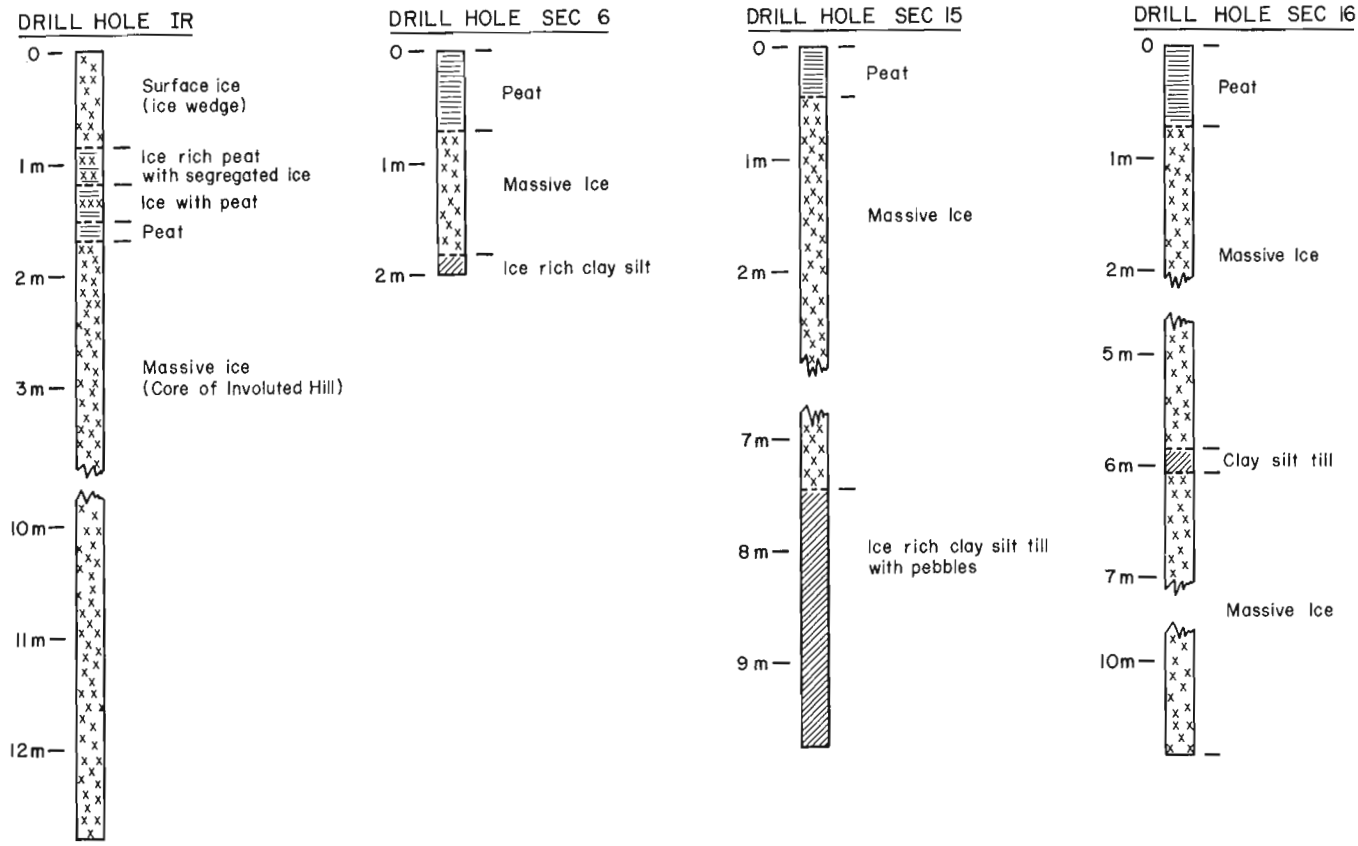

Figure 20.3. Drill logs for holes IR, SEC 6, SEC 15 and SEC 16.

Conclusions

The density of ice in massive ice structures in permafrost areas can be significantly lower than that of pure ice. The density decrease is due to air bubbles trapped in the ice at the time of freezing. The low density of ice in such structures must be considered in the interpretation of gravity and radar surveys. A more extensive study of ice densities in these bodies may provide a better understanding of air entrapment during freezing and aid inferences about the genesis of the structures. The density measurements do not confirm the low density inferred from the high electromagnetic wave velocity. Either an alternate interpretation of the radar data must be made or the empirical relationship 3 is not valid for the ice.

Acknowledgments

The cold room measurements were made with the assistance of R. Sloka, Geological Survey of Canada. The drill data used to infer the structure of the Hill were provided by V. Rampton (5 holes in 1973), and J. Veillette, M. Nixon, D. Butterfield and R. Sloka of Geological Survey of Canada (14 holes in 1975). In addition, 21 holes were drilled in 1974 and logged by J. Dugal and K. Drubinski of Geological Survey of Canada. Part of the support of these operations was provided by the Polar Continental Shelf Project.

References

Annan, A.P. and Davis, J.L.
1976: Impulse radar sounding in permafrost; Radio Science, v. 11, p. 383-394.

Annan, A.P., Davis, J.L., and Scott, W.J.
1975a: Impulse radar profiling in permafrost; *in* Report of Activities, Part C, Geol. Surv. Can., Paper 75-1C, p. 343-351.

1975b: Impulse radar wide angle reflection and refraction sounding in permafrost; *in* Report of Activities, Part C, Geol. Surv. Can., Paper 75-1C, p. 335-341.

MacKay, J.R.
1963: The Mackenzie Delta Area, N.W.T., Geol. Surv. Can., Misc. Rep. 23, First Puplished as Geographical Branch, Memoir 8, 202 p.

1971: The origin of massive icy beds in permafrost, Western Arctic Coast, Canada; Can. J. Earth Sci., v. 8, p. 397-422.

Rampton, V.N. and Walcott, R.I.
1974: Gravity profiles across ice-cored topography: Can. J. Earth Sci., v. 11, p. 110-122.

Robin, G. de Q., Evans, S., and Bailey, J.T.
1969: Interpretation of radioecho sounding in polar ice sheets: Proc. Roy. Soc. London, v. A265, p. 437-505.

21. STUDIES OF BASIC COPPER AND ZINC CARBONATES: THREE-POWDER X-RAY DATA FOR ZINCIAN MALACHITE, ROSASITE, AND COBALT ANALOGUES

Project 700041

J. L. Jambor[1]

Regional and Economic Geology Division

Introduction

Part 1 of this study dealt with hydrozincite (Jambor, 1964), and at that time data had been accumulated for anticipated papers which were to deal with aurichalcite and rosasite. With the subsequent passing of more than a decade, it became apparent that work on these carbonates would not be continued. Consequently, aurichalcite $(Zn, Cu)_5(CO_3)_2(OH)_6$ was dispensed with in a brief note (Jambor and McGregor, 1974) which showed the effect of Cu-Zn variations on the refractive indices and powder X-ray diffraction patterns. The struggle to obtain single-crystal data for the enigmatic mineral rosasite, $(Cu, Zn)_2(CO_3)(OH)_2$, has continued intermittently but has not met with significant success. However, the impetus to publish powder X-ray data available for zincian malachite and rosasite was derived in part from the recent discoveries of what are apparently the Ni and Co analogues of these minerals (Pryce and Just, 1974; Deliens, 1975; Deliens *et al.*, 1973).

Malachite, $Cu_2(CO_3)(OH)_2$, is the most common basic copper carbonate and is crystallographically well-defined (Wells, 1951). Rosasite is chemically a zincian malachite in that copper predominates but is partly replaced by substantial but variable zinc: $(Cu, Zn)_2(CO_3)(OH)_2$. Rosasite with Zn greater than Cu was reported by Strunz (1959) to occur at Tsumeb. Strunz named his mineral zincrosasit, but did not give supporting quantitative mineralogical data.

Rosasite has a density and refractive indices lower than those of malachite, but precise correlations of these properties and Cu:Zn variation have not been attained. Malachite has inclined extinction ($X:c \sim 23°$) whereas in rosasite it is only slightly inclined to parallel. The powder X-ray diffraction patterns of both carbonates are similar, but distinct differences are present. The principal difficulty in defining rosasite is that the mineral is invariably too fine grained for single-crystal work and apparently has not been examined by electron-diffraction methods. Inevitably, therefore, some writers have concluded that rosasite is zincian malachite (Lauro, 1938; Cocco, 1951; Bolgov and Rozybakieva, 1956; Shimazaki, 1957), others have concluded the opposite (Santoro and Sitzia, 1964; Pryce and Just, 1974), and others (e.g., Mincheva-Stefanova, 1961; Zidarov, 1962) have advocated the resurrection of names previously applied to ill-defined minerals such as "cuprozincite" (*cf.* Palache *et al.*, 1951). The present study does not unequivocally resolve these problems, but does demonstrate that zinc replacement of copper in malachite results in systematic variations in the powder X-ray patterns, and these variations lead to a possible alternative for the unit cell of rosasite.

Zincian Malachite

Powder X-ray data for malachite (Fisher, cupric carbonate-purified) and zincian malachites are given in Table 21.1. Ratios of Cu:Zn for the latter were obtained by X-ray spectroscopy of fused samples containing 1-5 mg of mineral. X-ray patterns were obtained either with 114.6 mm Debye-Scherrer camera or a Guinier focusing camera using Cu radiation. Cell dimensions were refined for Cu$K\alpha$, with the least-squares program PARAM (Stewart *et al.*, 1972). The results obtained for malachite and zincian malachite (Fig. 21.1) show that a, c, and β decrease systematically as Zn increases; this trend is accompanied by an increase in b so that the change in cell volume is relatively small up to Zn/Cu = 0.3.

In the remainder of the samples studied Zn/Cu ranged from 0.40 to 0.68. If the trends in cell dimensions that are evident for zincian malachites were continuous to members very rich in zinc, then cell parameters for these samples should have been easily determinable. It was found, however, that all lines of the powder patterns of zinc-rich members cannot be indexed with a zincian malachite unit cell. A specimen from Hayden, Arizona, with Zn/Cu = 0.40 fits this category, and as it has the best crystallinity of all zincian malachites and rosasites known to this writer, the material was examined in more detail.

Hayden Rosasite

The X-ray powder pattern of the Hayden material is similar to those given in the literature for rosasite. Rotation and precession photographs of the Hayden fibres gave diffraction effects for multiple crystals, but the results in some cases were adequate to indicate the presence of an a^*b^* net which is dimensionally similar to that of malachite, with $h00$ and $0k0 = 2n$ as in malachite. Rotation films of these same fibres showed that c is 3.2 ± 0.3Å (Jambor, 1976). Thus the cell dimensions could be presumed to be similar to those of malachite, and would not explain why all the powder diffraction lines cannot be indexed. However, electron microprobe analyses of the Hayden fibres demonstrated that they are variable in composition, with the range extending from low-zincian malachite to Zn/Cu = 0.6; powder X-ray patterns therefore must be composites, and the broadness of the layer lines on the c-axis rotation films are undoubtedly attributable to composition variation as well as multiple-crystal diffraction. The most significant aspect is that a malachite unit cell corresponding to the zinc-poor phase(s) should be extractable from the powder data, with the remnants attributable to the zinc-rich phase(s), hereafter

[1]Present address: CANMET, 555 Booth Street, Ottawa

From: Report of Activities, Part C;
Geol. Surv. Can., Paper 76-1C (1976).

referred to as rosasite. Because zincian malachite and rosasite have *hk*0 lines in common (their correspondence is incontrovertible at high *d*-values), the remnant unindexed diffraction lines should involve the *c*-axis (*l*-indices) of rosasite.

Table 21.2 contains the results obtained from Debye-Scherrer films of Hayden fibres rotated both parallel and normal to the morphological elongation and indexed with the unit cell of malachite. Although each of the malachite cell parameters yields a different Zn/Cu from Figure 21.1, all indicate that the remnant, unindexed lines should be due to the zinc-rich rosasite phase. If, for extrapolation purposes, it is assumed that the latter has Zn/Cu = 0.5-0.7, then a series of approximate cell dimensions can be obtained from Figure 21.1. However, none of these provides a cell

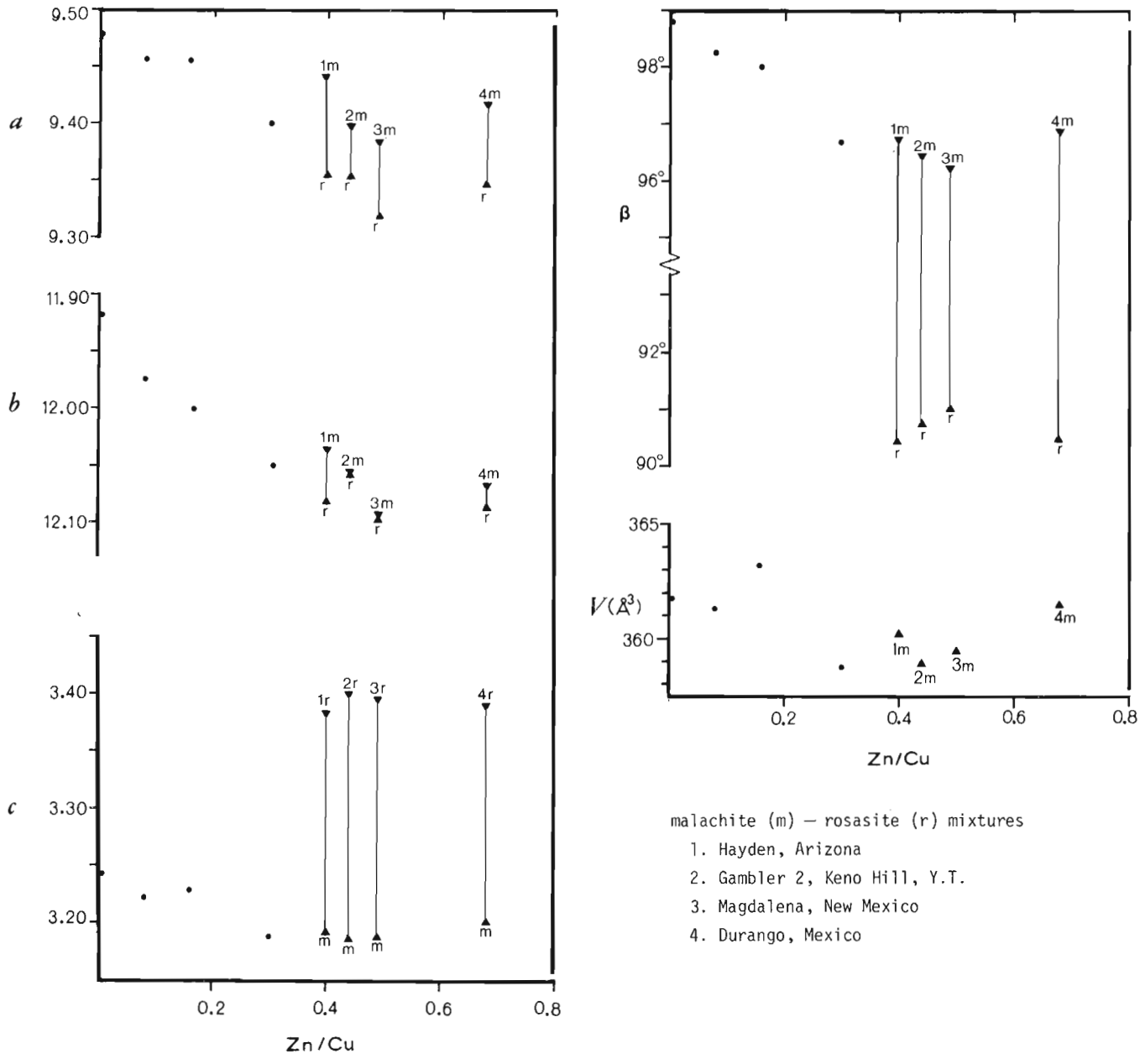

Figure 21.1. Variation in cell dimensions (in Å) with atomic Zn/Cu for zincian malachites (solid dots), and samples interpreted to be mixtures of zincian malachite and rosasite. Vertical tie lines join the coexisting pairs indexed with malachite (m) and rosasite (r) unit cells calculated from powder X-ray diffraction patterns.

Table 21.1

Powder x-ray data for malachite and zincian malachite

malachite, synthetic				Mapimi Mexico* Zn/Cu=0.08			Gambler property, Keno Hill, Yukon Zn/Cu=0.16				Magdalena, New Mexico Zn/Cu=0.30			
I_{est}	d_{meas}	d_{calc}	hkl	d_{meas}	d_{calc}	hkl	I_{est}	d_{meas}	d_{calc}	hkl	I_{est}	d_{meas}	d_{calc}	hkl
1	7.37	7.36	110	7.38	7.37	110	½	7.38	7.39	110	½	7.39	7.38	110
7	5.97	5.96	020	6.00	5.99	020	5	6.01	6.00	020	8	6.03	6.03	020
8	5.03	5.03	120	5.04	5.04	120	7	5.06	5.05	120	9	5.06	5.06	120
2	4.69	4.68	200	4.67	4.68	200	1	4.68	4.69	200	1	4.67	4.67	200
9	3.68	3.68	220	3.68	3.69	220	8	3.69	3.69 3.68	220 130	10	3.69	3.69 3.69	130 220
½	3.20	3.20	001	3.19	3.19	001	<½	3.19	3.20	001				
½	3.09	3.09	011	3.09	3.08	011								
2	3.03	3.03 3.02	230 310	3.02	3.02	310	2	3.02	3.02	310	5	3.01	3.01 3.01	040 310
3	2.980	2.980	040	2.994	2.994	040		3.00	3.00	040	<½	2.946	--	--
				2.851	2.852	140	1	2.857	2.857	140	2	2.866	2.868	140
10	2.851	2.855	$\bar{2}01$	2.832	2.832	$\bar{2}01$	10	2.823	2.825 2.823	111 021	3	2.809	2.804	021
4	2.773	2.776 2.666	$\bar{2}11$ 320	2.756	2.766 2.756	320 $\bar{2}11$	2	2.754	2.76	$\bar{2}11$	4	2.704	2.704	$\bar{2}11$
½	2.574	2.575	$\bar{2}21$	2.563	2.560	$\bar{2}21$								
5	2.516	2.514	240	2.521	2.522	240	5	2.529	2.527	240	6	2.531	2.532	240
				2.493	2.492	031								
2	2.478	2.474	201	2.475	2.479 2.476	$\bar{1}31$ 201	2	2.489	2.487	201	3	2.491	2.490 2.487	201 031
1	2.456	2.455	330	2.458	2.458	330	½	2.464	2.462	330	2	2.454	2.460 2.460	330 $\bar{1}31$
2	2.424	2.422	211	2.426	2.425	211	2	2.433	2.435	211	2	2.438	2.439	211
½	2.381	2.380	$\bar{3}11$	2.363	2.363	$\bar{3}11$								
2	2.343	2.342 2.342	400 131	2.338	2.344 2.339	131 400	½	2.339	2.343	400				
2	2.312	2.310	150	2.320	2.320	150	1	2.326	2.325	150	3	2.334	2.334 2.334	150 400
2	2.285	2.285	221	2.288	2.288	221	2	2.297	2.297	221	2	2.302	2.301	221
1	2.249	2.249	$\bar{3}21$	2.236	2.237	$\bar{3}21$	½B	2.23	2.235	$\bar{3}21$				
2	2.182	2.182 2.180	041 420	2.180	2.183	041	2	2.186	2.188 2.183	041 420	2	2.180	2.183 2.176	041 420
<½	2.155	2.156	340	2.161	2.160	340	<½	2.162	2.164	340				
3	2.126	2.124	250	2.132	2.132	250	2	2.137	2.136	250	3	2.142	2.142	250
<½	2.100	2.100	231				<½	2.107	2.112	231				
2	2.076	2.078	141				½	2.087	2.088	141	½	2.089	2.089	141
2	2.053	2.052	311				3	2.060	2.064 2.063 2.059	311 $\bar{3}31$ $\bar{2}41$	1	2.069	2.070	311
½	2.018	2.017 2.016	430 $\bar{4}11$				<½	2.019	2.022	430	1	2.036	2.041 2.036	$\bar{2}41$ $\bar{3}31$
1	1.989	1.987	060				1	2.001	2.001 2.000	$\bar{4}11$ 060	1	2.009	2.009	060
2	1.968	1.966	321				2	1.977	1.978	321	1	1.985	1.984	321
2	1.945	1.943	160				1	1.955	1.956	160	1	1.962	1.966 1.964	$\bar{4}11$ 160
	1.935	1.934	$\bar{4}21$											
2	1.912	1.912	051				2	1.916	sev. poss.		3	1.905	1.906 1.906	350 $\bar{1}51$
								1.906	1.903	350	½	1.888	1.892	$\bar{4}21$
a	9.478Å			9.455Å			9.465Å				9.399Å			
b	11.919			11.976			12.000				12.053			
c	3.241			3.224			3.230				3.189			
β	98.78°			98.25°			97.97°				96.67°			
V	361.8Å^3			361.3Å^3			363.3Å^3				358.8Å^3			

* Guinier focusing camera; others with 114.6 mm Debye-Scherrer cameras.

appropriate for the unindexed lines. In order to resolve the problem, the *c*-axis and space group of rosasite must be assumed to differ from those of malachite (Table 21.2). Although the length of the new *c*-axis (3.4Å) is within the range of broadness of the rotation-film layer lines, it is also necessary to assume that the *hk*0 net obtained on precession films is that of the Zn-poor (malachite) component of the fibre intergrowths. Of the 13 diffraction lines in Table 21.2 which showed intensity increases when fibres were rotated normal to the elongation, one (2.428Å) could not be indexed, and one (3.118Å - 300) is in violation of the space group of malachite; all others involve *l*-indices, as would be anticipated. The most characteristic lines which signify that the rosasite component is present are those at 2.952Å (rosasite 021) and 2.586Å (rosasite 031).

Powder diffraction data for samples with Zn/Cu > 0.4 are given in Table 21.3. All are interpreted to consist of mixtures of zincian malachite and rosasite; the most zinc-rich material (Durango, Zn/Cu = 0.68) seems to consist largely of rosasite with only a minor malachite component.

On crystal-structural grounds, complete solid solution between Cu^{2+} and Zn^{2+} would not be expected; more probable is that Zn preferentially enters one of the two non-equivalent copper environments in malachite and structural distortion becomes severe as Zn increases. Although the rosasite cell adopted here has not been proved to be correct, a structural change and a decrease in symmetry from that of malachite nevertheless could be expected to occur at high zinc levels. It also seems likely that the potential for disorder and non-stoichiometry of the carbonate and hydroxyl groups increase as Zn increases. Intimate intergrowths of zincian malachite and rosasite could lead to unit-cell distortion, with "anomalous" cell dimensions for one or both components being a result of this interaction.

Cobalt Analogues

Although a few powder X-ray diffraction patterns of rosasite are available in the literature, examination of the data suggested that unit-cell refinements, of the type done here, were not warranted. However,

Table 21.2

Composite debye-scherrer pattern of Hayden fibres

	malachite cell			rosasite cell			malachite cell			rosasite cell	
I_{est}	d_{meas}	d_{calc}	*hkl*	d_{calc}	*hkl*	I_{est}	d_{meas}	d_{calc}	*hkl*	d_{calc}	*hkl*
mw	7.38	7.40	110	7.40	110	m	2.462	2.466 2.463	330 $\bar{1}31$	2.466	330
s	6.00	6.02	020	6.04	020	w*	2.428	--	--	--	--
vs	5.07	5.07	120	5.08	120	w*	2.352	2.352	131	--	--
m	4.67	4.69	200	4.68	200	m	2.338	2.342 2.336	400 150	2.340 2.339	150 400
vw	4.35	4.37	210	4.36	210	w	2.325	2.324	$\bar{3}11$	--	--
vs	3.69	3.69	130	3.70	130 220	vw	2.298	2.299	410	2.296	410
f*	3.28	--	--	3.26	011	Indexed with		a= 9.44 (3)Å		9.355(6)Å	
w*	3.175	3.171	001	3.174	101†			b=12.036(15)		12.083(6)	
vw*	3.116	--	--	3.118	300†			c= 3.193(8)		3.384(3)	
f*	3.063	3.066	011	3.070	111			β=96.78 (17)		90.46 (6)	
s	3.019	3.025 3.018	310 $\bar{1}11$	3.021 3.019	040 310						
w	3.003	3.009	040	--	--						
s**	2.952	--	--	2.952	021						
mw	2.872	--	--	2.875	140						
mw	2.860	2.865	140	--	--						
s**	2.811	2.805	021	2.810	121						
m	2.776	2.774	320	2.771	320						
w**	2.733	--	--	2.731	201						
vw**	2.684	--	--	2.684	$\bar{2}11$						
vs**	2.586	--	--	2.591	031						
vs	2.533	2.532	240	2.538	240						
	2.522	2.526	$\bar{2}21$	--	--						
mw**	2.495	2.493	201	2.493	131						
w*	2.481			2.489	221						

Intensities estimated visually and are for fibres rotated about the elongation axis except as noted:

* line appears only when fibre rotated normal to elongation, or pronounced increase in intensity (**) when rotated normal to elongation.

† not permitted with malachite space group ($P2_1/a$).

vs = very strong w = weak

s = strong f = faint

m = medium 114.6 mm camera, Cu$K\alpha_1$ radiation

Table 21.3

Powder x-ray data* for zinc-rich, rosasite-type samples

Gambler 2, Keno Hill, Yukon Zn/Cu=0.44						Tsumeb, S.W. Africa Zn/Cu=0.49						Durango, Mexico Zn/Cu=0.68					
I_{est}	d_{meas}	d_{calc}	hkl	d_{calc}	hkl	I_{est}	d_{meas}	d_{calc}	hkl	d_{calc}	hkl	I_{est}	d_{meas}	d_{calc}	hkl	d_{calc}	hkl
1	7.42	7.38	110	7.39	110	1	7.38	7.39	110	7.38	110	1	7.39	7.39	110	7.39	110
6	6.06	6.03	020	6.03	020	8	6.04	6.05	020	6.05	020	6	6.05	6.04	020	6.03	020
8	5.08	5.07	120	5.07	120	9	5.07	5.08	120	5.07	120	7	5.07	5.07	120	5.07	120
1	4.68	4.67	200	4.68	200	1	4.68	4.67	200	4.66	200	1	4.68	4.67	200	4.67	200
10	3.70	3.69 3.69	220 130	3.70 3.70	220 130	10	3.70	3.70 3.70	130 220	3.70 3.69	130 220	10	3.69	3.70 3.70	220 130	3.70 3.69	220 130
<½	3.07	3.06	011	3.08	111												
3	3.02	3.02 3.01 3.01	040 310 $\bar{1}11$	3.02 3.02	310 040	4	3.02	3.03 3.01	040 310	3.02 3.01	040 310	4	3.02	3.03 3.02	$\bar{1}11$ 040	3.02 3.02	310 040
1b	2.96	--	--	2.96	021	3	2.96	--	--	2.96	021	4	2.96	--	--	2.96	021
1	2.87	2.87	140	2.87	140	1	2.876	2.878	140	2.877	140	2	2.87	2.87	140	2.87	140
2	2.822	2.822	111	2.817	121	½	2.813	2.809	021	2.810	121						
6	2.773	2.770	$\bar{2}01$	2.770 2.769	320 $\bar{2}01$	3	2.766	2.767 2.766 2.764	320 $\bar{2}01$ $\bar{1}21$	2.767 2.763	$\bar{2}01$ 320	1	2.77	2.79 2.78	$\bar{2}01$ $\bar{1}21$	2.77	320
3	2.700	2.699	$\bar{2}11$	2.699	$\bar{2}11$	½	2.691	2.697	$\bar{2}11$	2.697	$\bar{2}11$	2	2.623	2.618	121	--	--
1b	2.600	--	--	2.598	031	7	2.594	--	--	2.597	031	9	2.592	--	--	2.593	031
4	2.534	2.533	240	2.535	240	7	2.536	2.539	240	2.537	240	7	2.534	2.537	240	2.535	240
3	2.495	2.495	201	2.497 2.491	131 221	2	2.497	2.500 2.493	201 031	2.494	131	3	2.500	--	--	2.507 2.503	$\bar{2}21$ $\bar{1}31$
½	2.461	2.461 2.459	330 $\bar{1}31$	2.464	330	1	2.463	2.464 2.461	330 $\bar{1}31$	2.461	330	3	2.466	2.469 2.464	$\bar{1}31$ 330	2.463	330
1	2.447	2.443	211														
												½	2.352	2.356	131	--	--
3	2.337	2.336 2.334	150 400	2.339 2.337	400 150	4	2.338	2.343 2.334	150 400	2.342 2.337	150 400	4	2.335	2.340 2.337	150 400	2.337 2.336	150 400
1	2.310	2.312 2.305	$\bar{3}11$ 221	2.314	$\bar{3}01$**												
						½	2.287	2.291	410	2.287	410						
						<½	2.238	--		2.233	311						
½	2.190	2.195	$\bar{3}21$	2.190	141	½	2.207	--		2.201	$\bar{1}41$	<½	2.202	2.207	$\bar{3}21$	--	--
1	2.183	2.184 2.177	041 420	2.181	420	1	2.179	2.177	420	2.174	420	½	2.177	2.179	420	2.178	420
3	2.145	2.143	250	2.145	250	4	2.146	2.148	250	2.147	250	4	2.144	2.146	250	2.145	250
						<½	2.104	--	--	--	--						
<½	2.094	2.091	141	--	--												
1	2.074	2.074	311	--	--	<½	2.076	2.078	311	--	--						
½	2.038	2.040 2.033	$\bar{2}41$ $\bar{3}31$	2.040	$\bar{2}41$	2	2.019	2.020 2.017	430 060	2.017 2.016	430 060	3 ½	2.039 2.027	2.043 --	$\bar{3}31$ --	2.035 2.026	$\bar{2}41$ 241
<½	2.011	2.010	060	2.011 2.006	060 $\bar{3}31$												
3	1.989	1.989 1.988	$\bar{4}01$ 321	1.987	331												
2	1.967	1.965 1.962	160 $\bar{4}11$	1.969 1.966	051 160	2	1.969	1.971	160	1.971 1.971	160 051	5	1.967	1.973 1.968	$\bar{4}11$ 160	1.967 1.966	051 160
1	1.909	1.907 1.906	350 $\bar{1}51$	1.915 1.909	$\bar{4}11$ 350	2	1.909	1.910 1.909	350 $\bar{1}51$	1.912 1.909	$\bar{4}11$ 350	1	1.908	1.912 1.909	$\bar{1}51$ 350	1.908 1.907	350 $\bar{4}11$
1	1.891	1.889	$\bar{4}21$	1.892	411	½	1.878	--	--	1.882	411	½	1.874	--	--	1.869	500**
1	1.862	1.865 1.857	331 $\bar{3}41$	1.871	500**												
	1.848	1.846 1.846 1.845	260 440 510	1.849 1.848 1.846	510 440,260 $\bar{4}21$	2	1.850	1.851 1.848	260 440	1.850 1.845	260 440	2	1.848	1.849 1.848 1.847	260 440 510	1.848 1.847 1.847	260 440 510

	malachite cell	rosasite cell	malachite cell	rosasite cell	malachite cell	rosasite cell
a	9.395Å	9.351Å	9.382Å	9.318Å	9.414Å	9.344Å
b	12.061	12.060	12.093	12.098	12.082	12.069
c	3.188	3.403	3.188	3.396	3.201	3.392
β	96.44°	90.74°	96.23°	90.99°	96.87°	90.48°
V	358.96Å^3	383.73Å^3	359.56Å^3	382.77Å^3	361.47Å^3	382.51Å^3

* Camera diameter 114.6 mm; Cu$K\alpha_1$ radiation.
**Not permitted with malachite space group.

Table 21.4

Powder x-ray data for cobaltoan members

No.:	M1				M2				M3				M4				M7					M6			
Wt % Co:	0.25				0.90				1.79				4.22				16.05					18.46			
I_{est}	d_{meas}	d_{calc}	hkl	I_{est}	d_{meas}	d_{calc}	hkl	I_{est}	d_{meas}	d_{calc}	hkl	I_{est}	d_{meas}	d_{calc}	hkl	I_{est}	d_{meas}	d_{calc}	hkl	d_{calc}	hkl	I_{est}	d_{meas}	d_{calc}	hkl
30	7.42	7.40	110	20	7.37	7.37	110	20	7.42	7.37	110	10	7.37	7.37	110	10	7.42	7.45	110	7.40	110	10	7.42	7.39	110
80	5.98	5.98	020	80	5.98	5.98	020	80	6.01	5.99	020	80	6.00	6.00	020	80	6.04	6.04	020	6.04	020	80	6.08	6.04	020
80	5.05	5.05	120	80	5.03	5.04	120	80	5.06	5.04	120	80	5.05	5.05	120	80	5.08	5.09	120	5.07	120	80	5.08	5.07	120
30	4.72	4.71	200	20	4.70	4.68	200	20	4.71	4.68	200	10	4.72	4.67	200	5	4.78	--							
								10	4.18	--	--	5	4.01	--	--	5	4.02	--							
90	3.69	3.70	220	90	3.69	3.69	220	90	3.68	3.69	220	100	3.69	3.69	220	100	3.70	3.70	130	3.70	220	100	3.69	3.70	130
		3.67	130			3.67	130			3.67	130			3.68	130					3.70	130			3.69	220
40	3.03	3.04	230	40	3.005	2.990	040	40	3.00	2.99	040	40	3.01	3.00	040	40	3.02	3.02	040	3.02	310	40	3.02	3.02	040
		3.04	310															3.01	$\bar{1}11$	3.02	040			3.01	310
																50	2.956	--		2.955	021	40	2.958	2.960	021
								5	2.925	--		5	2.920	--											
100	2.854	2.854	$\bar{2}01$	100	2.842	2.845	$\bar{2}01$	100	2.835	2.835	$\bar{2}01$	90	2.830	2.832	$\bar{2}01$	5	2.873	2.877	140	2.872	140				
		2.849	140																						
80	2.777	2.780	320	60	2.765	2.768	$\bar{2}11$	60	2.758	2.759	$\bar{2}11$	50	2.749	2.756	$\bar{2}11$	10	2.789	2.791	111	--		5	2.762	2.764	$\bar{2}01$
		2.776	$\bar{2}11$			2.767	320											2.790	$\bar{2}01$						
																		2.786	021						
																80	2.591	2.591	121	2.592	031	70	2.599	2.596	031
60	2.519	2.524	240	50	2.516	2.520	240	50	2.518	2.522	240	50	2.524	2.525	240	50	2.535	2.533	$\bar{2}21$	2.537	240	40	2.531	2.535	240
50	2.479	2.484	$\bar{1}31$	40	2.479	2.484	$\bar{1}30$	40	2.478	2.480	$\bar{1}31$	40	2.487	2.484	201	20	2.500	--		2.503	$\bar{2}21$	20	2.494	2.494	131
		2.478	201			2.477	201			2.479	201			2.483	$\bar{1}31$					2.500	$\bar{1}31$				
50	2.431	2.427	211	30	2.428	2.425	211	30	2.426	2.427	211	30	2.429	2.433	211	5	2.454	2.458	$\bar{1}31$	--		5	2.455	2.462	330
10	2.384	2.383	$\bar{3}11$	10	2.372	2.372	$\bar{3}11$																		
30	2.345	2.344	131	10	2.342	2.345	131	20	2.341	2.346	131	30	2.332	2.337	400	40	2.338	2.342	$\bar{3}11$	2.342	400	30	2.344	2.338	150
						2.341	400			2.340	400							2.341	150	2.338	150				
																		2.337	131						
30	2.316	2.320	$\bar{2}31$	20	2.313	2.318	150	20	2.318	2.320	150														
		2.317	150			2.316	$\bar{2}31$																		
40	2.285	2.289	221	20	2.285	2.288	221	30	2.290	2.290	221	30	2.301	2.295	221										
														2.294	410										
30	2.252	2.252	$\bar{3}21$	20	2.249	2.243	$\bar{3}21$	20	2.241	2.237	$\bar{3}21$	10	2.241	2.234	$\bar{3}21$										
40	2.184	2.183	041	30	2.184	2.185	041	30	2.183	2.185	041	30	2.186	2.189	041	10	2.186	2.181	340	2.190	141	5	2.189	2.189	141
						2.180	420			2.179	420									2.183	420				
40	2.131	2.132	250	30	2.130	2.130	250	30	2.130	2.132	250	30	2.130	2.135	250	30	2.141	--		2.146	250	30	2.144	2.145	250
																				2.143	321				
40	2.073	2.076	$\bar{3}31$	40	2.065	2.069	$\bar{3}31$	40	2.058	2.064	$\bar{3}21$	30	2.063	2.063	$\bar{3}31$	5	2.060	2.060	311	--					
						2.061	$\bar{2}41$			2.058	$\bar{2}41$			2.061	311										
										2.057	311			2.059	$\bar{2}41$										
40	2.059	2.058	311													20	2.014	2.013	060	2.012	060	20	2.021	2.024	241
																								2.019	430
5	1.995	1.992	060	5	1.996	1.994	060	5	1.998	2.003	$\bar{4}11$														
										1.996	060														
30	1.970	1.972	321	30	1.969	1.969	321	40	1.973	1.971	321	20	1.974	1.975	321	20	1.969	1.969	160	1.967	160	20	1.967	1.968	051
																				1.966	051			1.968	160
30	1.942	1.939	$\bar{4}21$	30	1.928	1.929	$\bar{4}21$	30	1.920	1.924	$\bar{4}21$														
										1.916	051														
30	1.905	1.908	241	30	1.903	1.907	241	30	1.905	1.909	241	30	1.907	1.913	241	20	1.908	1.912	241	1.910	350	20	1.907	1.912	$\bar{4}11$
		1.902	350							1.900	350			1.913	$\bar{1}51$			1.907	$\bar{1}51$	1.906	$\bar{4}11$			1.912	401
														1.901	350									1.908	350
20	1.886	1.886	$\bar{3}41$	10	1.883	1.881	$\bar{3}41$	5	1.877	1.878	$\bar{3}41$					20	1.854	1.856	331	1.851	510	20	1.851	1.848	260
																		1.852	260					1.847	440
20	1.822	1.823	$\bar{4}31$	10	1.820	1.815	$\bar{4}31$	5	1.814	1.811	$\bar{4}31$														
30	1.789	1.797	520	20	1.789	1.787	520	20	1.788	1.786	520	20	1.787	1.785	520	20	1.786	--		1.789	520	20	1.784	1.784	520
																30	1.741	--		1.740	$\bar{4}31$	30	1.739	1.745	$\bar{4}31$
		1.691	061			1.688	$\bar{1}61$			1.683	170			1.686	170			1.698	$\bar{3}51$	1.699	530			1.696	170
30	1.691	1.691	$\bar{4}41$	50	1.684	1.684	$\bar{4}41$	40	1.681	1.681	$\bar{4}41$	40	1.682	1.683	360	20	1.696	1.698	170	1.696	170	10	1.690	1.694	530
		1.688	$\bar{1}61$			1.681	170			1.681	360			1.680	$\bar{4}41$			1.697	360	1.695	002			1.690	360
																		1.695	061						
30	1.671	1.673	$\bar{5}21$	20	1.661	1.663	$\bar{5}21$	5	1.660	1.659	$\bar{5}21$					20	1.659	1.657	$\bar{5}21$	1.662	351				
30	1.638	1.642	161	20	1.640	1.643	161																		
		1.634	$\bar{2}61$																						
	malachite cell				malachite cell				malachite cell				malachite cell				malachite cell				rosasite cell		rosasite cell		
a	9.532Å				9.467Å				9.456Å				9.441Å				9.538Å				9.368Å		9.338Å		
b	11.953				11.961				11.973				12.000				12.080				12.070		12.076		
c	3.235				3.235				3.229				3.233				3.167				3.389		3.396		
β	98.67°				98.50°				98.24°				98.03°				97.56°				90.23°		90.78°		

Measured data and wt % Co from Deliens *et al.* (1973).

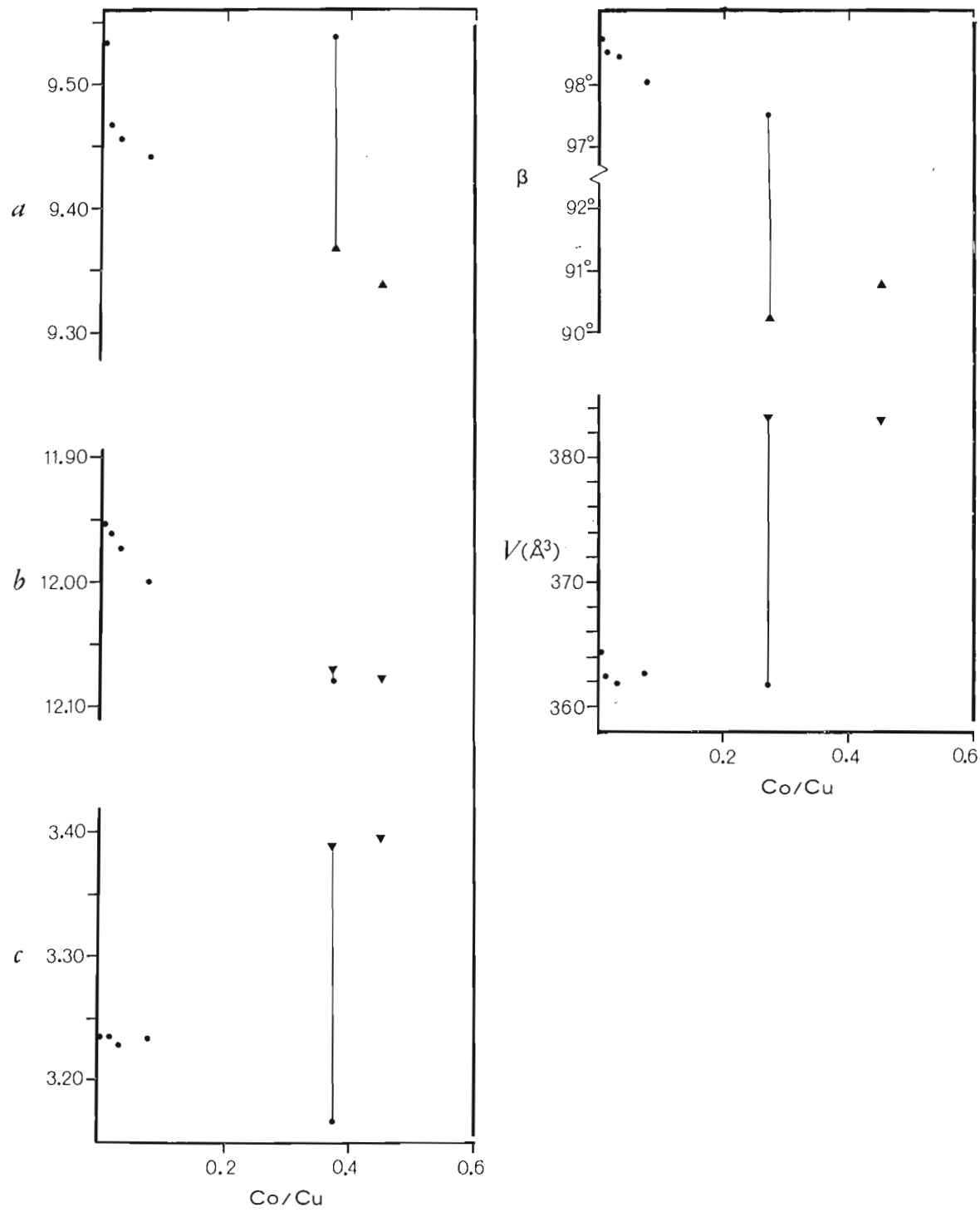

Figure 21.2. Variation in cell dimensions (in Å) with atomic Co/Cu based on weight per cent Co and powder X-ray data of Deliens *et al.* (1973); Co/Cu calculated from assumed formula $(Cu, Co)_2(CO_3)(OH)_2$, and cell dimensions calculated with malachite-type unit cells (dots) and rosasite-type cells (triangles); one sample, M7 of Deliens *et al.*, is interpreted to be a mixture of the two types.

Deliens *et al.* (1973) published good powder data for a cobaltoan series in which weight per cent Co (only) was determined by wet chemical analyses. The results for unit-cell refinements are given in Table 21.4 and Figure 21.2. As noted by Deliens *et al.*, *a* and *c* decrease and *b* increases as the malachites are progressively more cobaltoan. For the two samples with the highest Co (Sample M7 16.05 wt.%; Sample M6 18.46 wt.%), indexing of the powder data requires that the larger, rosasite-type *c*-axis be used. The present interpretation is that Sample M7 contains admixed cobaltoan malachite which, from the intensity of $\bar{2}01$, may make up about 10 per cent of the sample. Sample M6 is the most cobalt-rich and can be indexed completely with a rosasite-type cell.

Densities and Cell Volumes

Specific gravity determinations of rosasite seem to be rare; the range 4.0-4.2 quoted in Palache *et al.* (1951) is not with certainty that of rosasite, and it is probable that most published chemical analyses represent mixtures of zincian malachite and rosasite. The following specific gravity measurements of rosasite-type minerals were reported by Shimazaki (1957): rosasite, Pima County, Arizona, 3.89 ± 0.02; "paraurichalcite", Tsumeb, 3.85 ± 0.02; "paraurichalcite", Durango, Mexico, 3.88 ± 0.02; "cuprozincite", Tsumeb, 3.85 ± 0.02. Shimazaki analyzed the Durango material and obtained a Zn/Cu ratio of 0.49. These specific gravity values are significant because the enlarged *c*-axis proposed for rosasite leads to cell volumes of 380-385Å^3 whereas volumes with a malachite-type unit cell would be smaller. Specifically, at Zn/Cu = 0.5, the latter would have a cell volume of about 357Å^3, which would give D_{calc} = 4.15 g/cm^3. The rosasite-type cell volume is much larger (~ 383Å^3), thus leading to a calculated density of 3.87 g/cm^3, comparable to the measured value of 3.88 ± 0.02 g/cm^3 obtained by Shimazaki (1957).

In the cobaltoan series, measured densities were not reported by Deliens *et al.* (1973). The calculated density for Sample M6, assuming a stoichiometric formula and with the cell dimensions in Table 21.4, is approximately 3.78 g/cm^3.

Atomic weights and radii of Co^{2+} and Ni^{2+} are almost identical, and their mutual substitution in a rosasite-type unit cell should lead to similar densities for both the cobalt and nickel analogues of rosasite. The measured density of glaukosphaerite, $(Cu, Ni)_2(CO_3)(OH)_2$, which may be the nickel analogue of rosasite, is 3.78 g/cm^3 for Ni/Cu = 0.67 and increases as Ni decreases (Pryce and Just, 1974). Jambor (1976) took the above data point (3.78 and 0.67), extrapolated it to the cell volume of malachite, and obtained reasonable agreement between the measured and calculated densities for two additional specimens of glaukosphaerite with Ni/Cu = 0.34 and 0.24. From this correlation, it is apparent that, assuming stoichiometric compositions, the cell volume of glaukosphaerite must increase as Ni substitutes for Cu. In contrast, zincian and cobaltoan malachites seem to change little or decrease slightly in cell volume. Thus, there is indirect evidence of a possible crystallographic discontinuity between Ni-Co-Zn-bearing malachites and the Ni-Co-Zn-rich rosasite-type members.

Pryce and Just (1974) contended that the powder-diffraction patterns of malachite, rosasite, and glaukosphaerite are each unique and that the minerals represent three distinct monoclinic species. There seems to be little doubt that malachite and rosasite are two distinct species; whether glaukosphaerite and its cobaltoan analogue are distinct, or merely varieties of rosasite, is more difficult to resolve because all three can be indexed with a rosasite-type unit cell. The agreement among cell dimensions and densities for the Ni and Co minerals is not as close as expected and they cannot be declared as isomorphous on the basis of the present study. Infrared work by Tarte and Deliens (1974) indicates that the spectrum of the cobalt-rich member is nearly identical to that of rosasite whereas glaukosphaerite has a distinctive spectrum of its own. These results support the Pryce and Just (1974) claim of species status for glaukosphaerite.

Acknowledgments

The writer is grateful to G.R. Lachance of the Geological Survey of Canada for XRF analyses, to D.R. Owens of CANMET for microprobe analyses of Hayden rosasite, and to E. Murray of CANMET for assistance with the computer refinements of the X-ray data.

References

Bolgov, G.P. and Rozybakieva, N.A.
1956: Rosasite and its paragenesis in the oxidation zone; Sbornik Nauk. Trudov Kazakh. Gorno-Met. Inst., No. 14, p. 34-43 (Chem. Abstr., v. 53, 7868).

Cocco, G.
1951: Carbonati basici di rame e zinco; Periodico Mineral., v. 20, p. 93-115.

Deliens, M.
1975: La glaucosphaerite de Kasompi (Shaba méridional, Zaire). Bull. Soc. franc. Minéral Crist., v. 98, p. 175-178.

Deliens, M., Oosterbosch, R., and Verbeek, T.
1973: Les malachites cobaltifères du Shaba méridional (Zaire); Bull. Soc. franc. Minéral. Crist., v. 96, p. 371-377.

Jambor, J.L.
1964: Studies of basic copper and zinc carbonates: I - synthetic zinc carbonates and their relationship to hydrozincite; Can. Mineral., v. 8, p. 92-108.

1976: A possible unit cell for glaukosphaerite. Can. Mineral. v. 14, pt. 4 (in press).

Jambor, J.L. and MacGregor, I.D.
1974: Studies of basic copper and zinc carbonates: 2 - aurichalcite; *in* Report of Activities, Part B; Geol. Surv. Can., Paper 74-1B, p. 172-174.

Lauro, C.
1938: Su alcuni carbonati basici di rame e zinco naturali; Periodico Mineral., v. 9, p. 105-136.

Mincheva-Stefanova, I.
1961: Cuprozincite, rosasite and aurichalcite from the Vracha ore district; Bull. Inst. Geol. Bulgarian Acad. Sci., v. 9, p. 197-207.

Palache, C., Berman, H., and Frondel, C.
1951: The System of Mineralogy, Volume 2, 7th ed. John Wiley & Sons, New York.

Pryce, M.W. and Just, J.
1974: Glaukosphaerite, a new nickel analogue of rosasite; Mineral. Mag., v. 39, p. 737-743.

Santoro, F. and Sitzia, R.
1964: Le costanti della rosasite; Boll. Accad. Gioenia, v. 8, ser. 4, p. 207-211.

Shimazaki, Y.
1957: Mineralogy of basic carbonate minerals of copper and zinc; Ph.D. Thesis, Stanford University.

Steward, J.M., Kruger, G.J., Ammon, H.L., Dickinson, C., and Hall. S.R.
1972: The X-ray system of crystallographic program for any computer; Univ. Maryland Computer Sci. Center Tech. Rept. TR-192.

Strunz, H.
1959: Tsumeb, seine Erze und Sekundärmineralien, insbesondere der neu aufgeschlossenen zeveiten Oxydationszone; Fortsch. Mineral., v. 37, p. 87-90.

Tarte, P. and Deliens, M.
1974: Caracterisation des malachites nickelifères et cobaltifères par leur spectre infra-rouge; Bull. Soc. Roy. Sci. Liège, v. 43, p. 96-105.

Wells, A.F.
1951: Malachite: re-examination of crystal structure. Acta Crystalloyr., v. 4, p. 200-204.

Zidarov, N.
1962: Comparative characteristics of rosasite, cuprozincite, and malachite from the Madau ore field; Izv. Geol. Bulgar. Akad. Nauk, v. 11, p. 81-87.

"BITUMEN" IN POST-BURIAL DIAGENETIC CALCITE

(A)

EII. I.

Project 720060

Graham R. Davies
Institute of Sedimentary and Petroleum Geology, Calgary

Introduction

Bitumen and "pyrobitumen" inclusions are common in secondary and later diagenetic carbonate minerals and pore systems in many limestones and dolostones. Often, the type of enclosing pore system and the type of bitumen provide clues to the relative timing of emplacement (not necessarily equivalent to primary migration) of the precursor liquid hydrocarbon and to the degree of thermal maturation.

During the concluding phase of a study of diagenesis in Pennsylvanian and Lower Permian carbonate rocks exposed on Ellesmere Island, attention has been focussed on the significance of bitumen inclusions in late diagenetic (post-burial) calcite spar in some of these rocks. As the calcite spar may be placed within a diagenetic sequence developed during earlier phases of the study, some constraints may be placed on the time of emplacement of the hydrocarbon, and conversely on the precipitation of the calcite, especially when considered in conjunction with depth of burial and thermal maturation data.

Host rock

Although the general diagenetic study of the Arctic carbonate rocks includes a variety of rocks of various ages and depositional settings, the complete sequence of diagenetic events is revealed best in Middle Pennsylvanian bryozoan reefs exposed in the Blue Mountains and vicinity on northwestern Ellesmere Island (Davies, 1975, Figs. 47.1, 47.7, 47.8). These reefs are characterized by an abundance of fenestellid bryozoans that commonly are cemented by fibrous calcite of submarine origin. The reef rocks form part of the upper Paleozoic fill in the northern region of the Sverdrup depositional basin.

Diagenetic sequence

The calcite spar and associated bitumen in the bryozoan reefs represent a late phase in the diagenetic history of these rocks. To place this phase in sequence, a summary of diagenetic events is given here:

Submarine processes:

1. Cementation in primary pores by magnesian calcite.
2. Fracturing of cemented rock by settling.
3. Cementation of fracture walls and continued cementation in primary pores by magnesian calcite.
4. Precipitation of botryoidal aragonite in larger primary pores and fracture cavities.

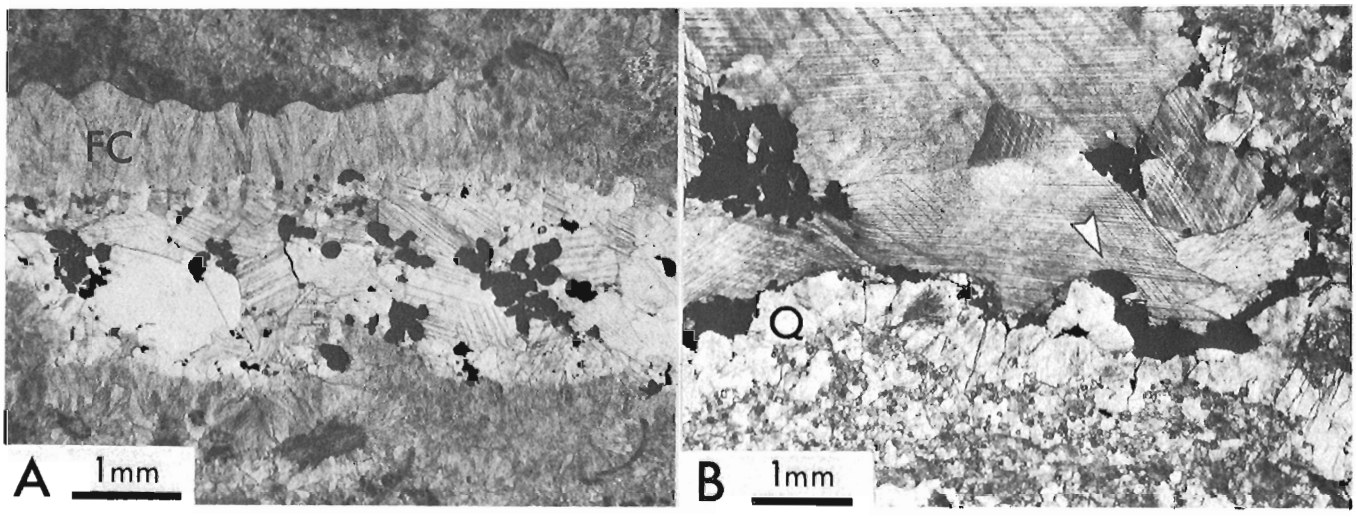

A. Bitumen inclusions (black) in former primary shelter pore line by fibrous calcite cement (FC) of submarine origin followed by a thin rim of ferroan calcite (not differentiated in this view), and filled by low-iron calcite spar. Note the globular shape of some of the bitumen, and its irregular distribution within the calcite, with most of the bitumen concentrated at the interfaces of crystals in the former cavity centre.

B. Bitumen enclosed within low-iron calcite and directly overlying (arrow) authigenic quartz (Q) in a former primary shelter pore.

Figure 22.1. Thin-section photomicrographs of bitumen inclusions in low-iron calcite in Pennsylvanian bryozoan reefs.

From: Report of Activities, Part C;
Geol. Surv. Can., Paper 76-1C (1976)

Post-burial processes

5. Infilling of megafractures by burial sediment; minor solution.
6. Neomorphism of magnesian calcite and aragonite to stable calcite.
7. Precipitation of zoned ferroan calcite in cement-lined primary pores and in one set of microfractures.
8. Precipitation of authigenic quartz and zoned ferroan dolomite in some pore spaces.
9. *Precipitation of iron-depleted calcite spar in pore spaces and in second set of microfractures, and contemporaneous introduction of liquid hydrocarbons.*
10. Etching (minor solution) of calcite and precipitation of authigenic clays in remaining open spar-lined pores.
11. Thermal alteration of liquid hydrocarbons to solid bitumen.

"Bitumen" in diagenetic calcite

The term "bitumen" is used in this paper for black, solid organic residues with conchoidal fracture that commonly have a spheroidal to globular form. Rogers *et al.* (1974) consider similar material as reservoir bitumens, and distinguish "pyrobitumen" as a variety with very low solubility (less than 2%) in carbon disulphide. Although solubility of the Arctic bitumen has not been analyzed, and only one hydrogen

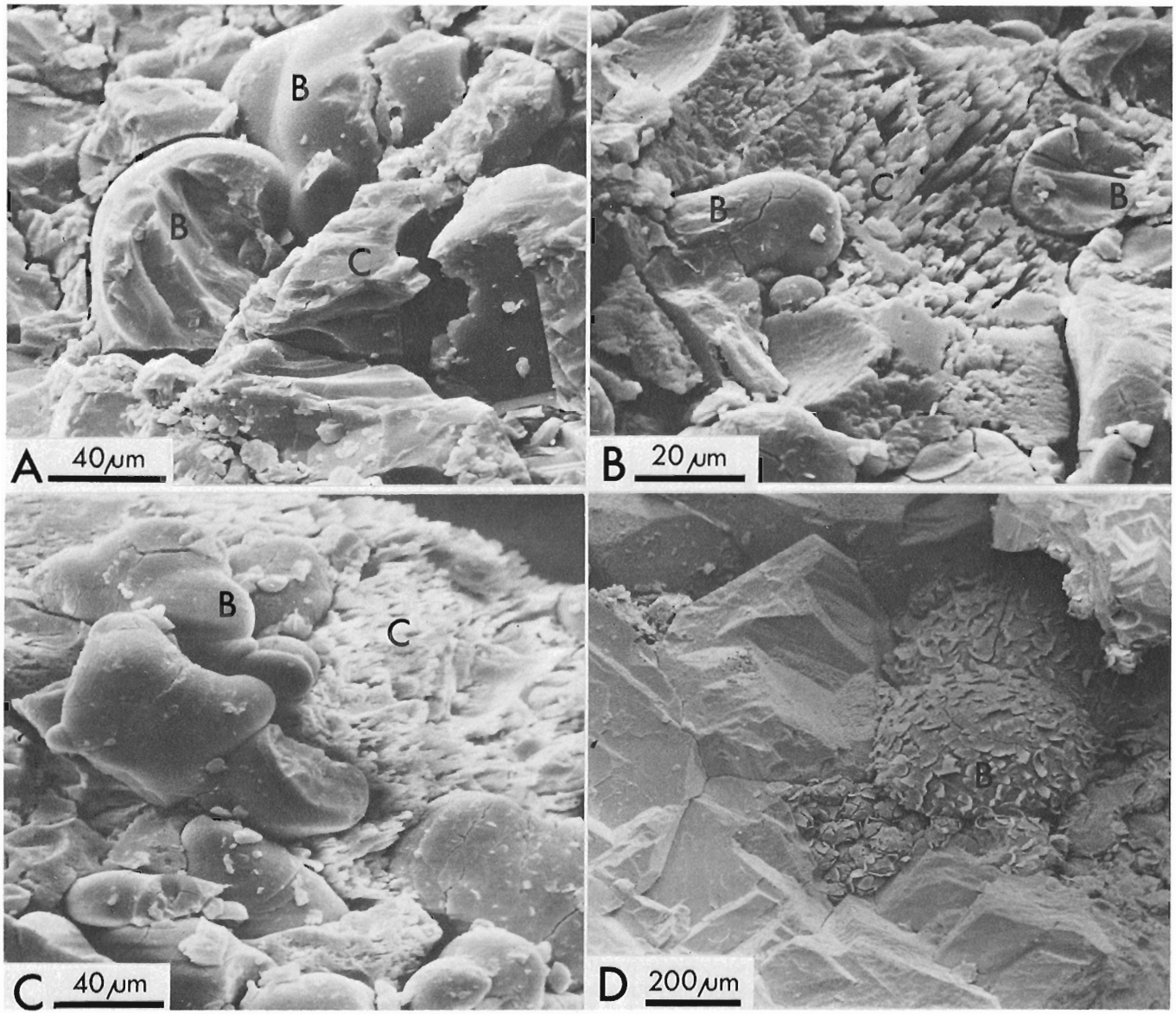

A. **Bitumen totally enclosed in calcite, revealed by artificial fracture surface.**
B and C. Bitumen partly enclosed in calcite; note globular shape of bitumen, etched surface of calcite.
D. Globular bitumen with flaky surface (possibly artifact?) lying geopetally on crystals of low-iron calcite lining internal cavity of brachiopod.

Figure 22.2. Scanning electron photomicrographs of bitumen (B) in late digenetic calcite spar (C), Pennsylvanian bryozoan reef.

to carbon atomic ratio measurement (0.35) has been made on this material, extrapolation from the data of Rogers *et al.* (1974, Table I) suggests that some if not all of the Arctic bryozoan reef bituminous material is "pyrobitumen".

Reservoir bitumens may form by three main processes: thermal alteration, gas deasphalting, and water washing and biodegradation (Rogers *et al.*, 1974, p. 1809). The products of these processes are graphitic reservoir bitumens from the first two processes, and asphaltic reservoir bitumens from the third (*ibid.*). From burial data and other diagenetic criteria for the bryozoan reefs, discussed in following sections, it is apparent that thermal alteration played a major role in the transformation of liquid hydrocarbon inclusions to solid bitumen in these rocks.

Bitumen in the bryozoan reef rocks is found most commonly in residual pore spaces within brachiopods but also in other pore systems and in some microfractures (Figs. 22.1 to 22.3). Much of the bitumen is enclosed totally or partly by crystals of calcite characterized by their relative purity and low content of iron. Some of the bitumen, however, lies on the surface of the calcite crystals and thus postdates some crystal growth. Where authigenic quartz or dolomite crystals are a component of the diagenetic cavity fill, bitumen often is found in contact with the crystal faces of the quartz or dolomite, with low-iron calcite enclosing both the authigenic crystal and the bitumen (Fig. 22.1B). The quartz-dolomite to bitumen interface usually appears to be corroded or etched. These spatial relationships suggest that liquid hydrocarbons were introduced after precipitation of dolomite and quartz, but contemporaneously with an early phase of low-iron calcite. In other types of former pore system, bitumen inclusions lie totally within low-iron calcite spar and clearly are postdated by continued crystal growth of the calcite (Figs. 22.2A to 22.2C, 22.3A). In contrast, in some brachiopod microcavities, bitumen is present as inclusions in the internal low-iron calcite fringe but also as a more abundant granular geopetal deposit in the cavity, overlying or distributed between calcite crystals projecting from the floor of the cavity (Fig. 22.2D).

Of fundamental significance to this discussion is the inference that the globular morphology of the bitumen is inherited from a liquid hydrocarbon (oil) precursor. Thus, the question of origin of the bitumen is actually one of origin of oil in these rocks, and the conditions necessary for its generation and migration. Further, the presence of globules larger than intercrystalline micropores in cavities indicates that the oil must have been introduced into the cavities in solution, in micelles, in micro-globules that later coalesced, or through microfractures that intersected the cavities.

The inference that most of the hydrocarbon in the reef rock was introduced from external sources, specifically the surrounding argillaceous rocks, is supported by the following points.

1. The low-iron calcite host of the hydrocarbon represents precipitation from many thousands of pore volumes of carbonate-saturated water (Bathurst, 1975, p. 440-441), and thus both calcite and hydrocarbon must have accumulated in the reef pores under a dynamic hydrologic system in which water was migrating through the reef and the surrounding argillaceous rocks.

2. Five samples of very dark coloured limestone from the reef analyzed for organic carbon averaged only 0.17 per cent organic carbon by weight, less than the average value for limestones of about 0.25 per cent, in itself an indicator of poor hydrocarbon source potential. Although

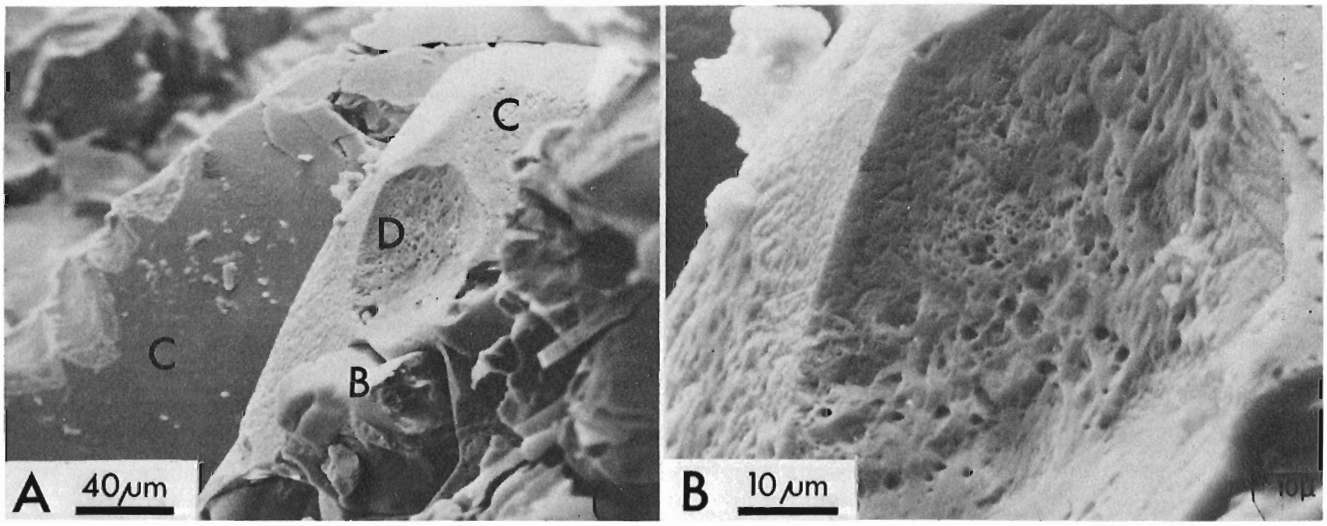

A. Bitumen (B) partly enclosed by low-iron calcite (C) lining brachiopod internal cavity, with depression (D) interpreted to be the former attachment site for a dislodged bitumen globule.

B. Detail of depression (D) in A, illustrating the etched nature of the surface.

Figure 22.3. Scanning electron photomicrographs of bitumen in calcite.

some sourcing of hydrocarbons from within the reef cannot be ruled out, these data suggest an external source for most of the reef hydrocarbons.

3. Field observation indicates that the abundance of bitumen inclusions and cavity fillings in the reef increases at the contact between the reef limestone and the overlying argillaceous rocks.

In summary, the spatial relationships between bitumen and carbonate and other diagenetic mineral phases indicate that the precursor liquid hydrocarbon was introduced after precipitation of authigenic dolomite and quartz, but perhaps early in the precipitational history of low-iron calcite spar. Both low-iron calcite and hydrocarbons were derived mainly from surrounding

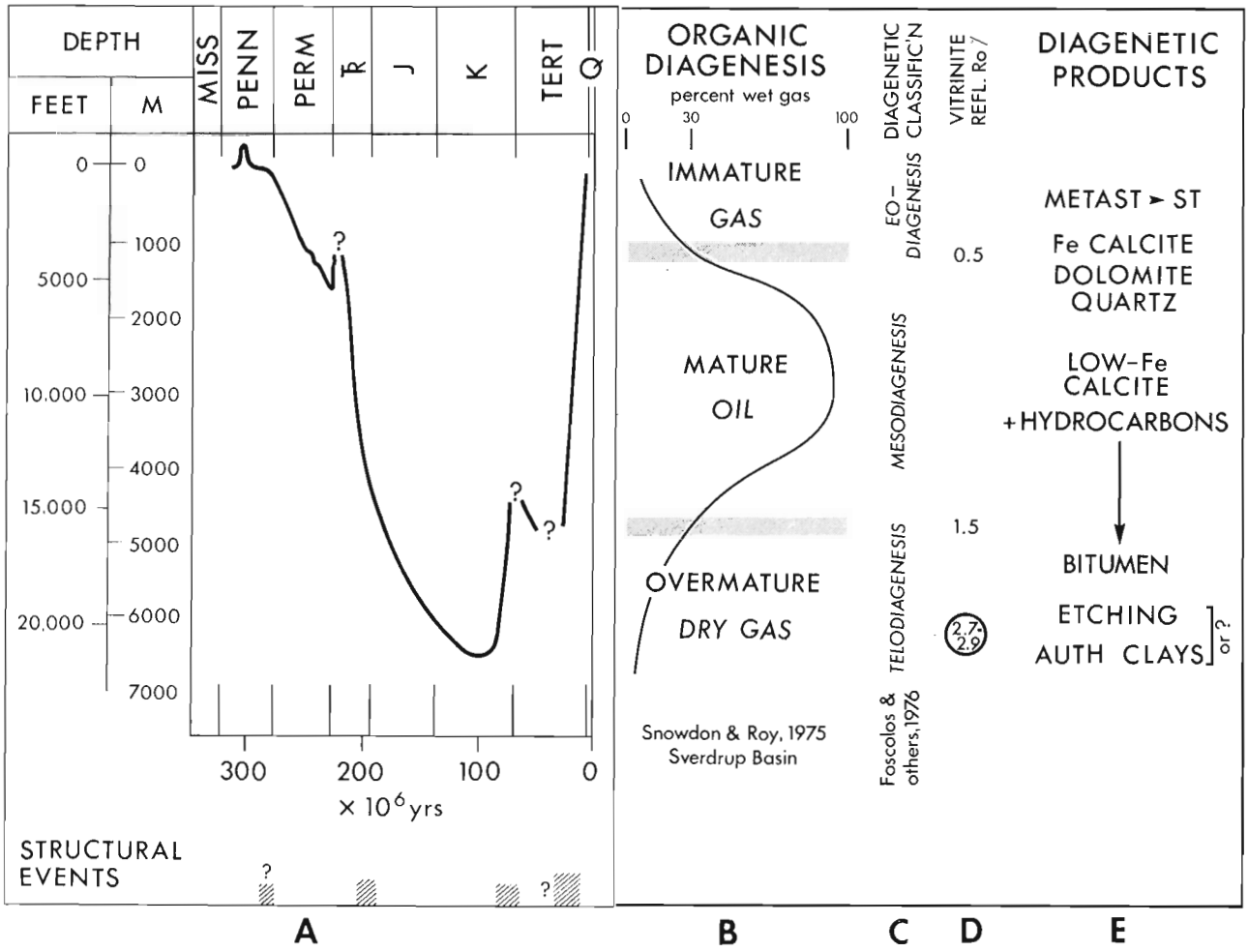

A. Plot of depth of burial against time, indicating maximum burial of 6500 m (22 000 ft) by mid-Cretaceous time.

B. Simplified curve of per cent wet gas in drill cuttings from 14 wells in the Sverdrup Basin from Snowdon and Roy (1975, Fig. 3) plotted against the same depth scale as A, with the three main divisions of organic maturation and hydrocarbon type superimposed; from these data alone, it is apparent that at maximum burial, the bryozoan reefs were in the dry gas zone.

C. Generalized division into the three major inorganic-organic diagenetic zones of Foscolos *et al.* (1976).

D. Approximate threshold values for vitrinite reflectance between diagenetic zones of B and C, with reflectance values for samples above a bryozoan reef encircled (approximate logarithmic scale).

E. Principal diagenetic products related tentatively to the foregoing burial and diagenetic stages. Etching of calcite and clay precipitation may be related more closely to the introduction of hydrocarbons, and thus belong higher in the sequence. "Metast to St" denotes neomorphism of metastable carbonate minerals to stable calcite.

Figure 22. 4. Composite illustration of burial history and diagenesis for Middle Pennsylvanian bryozoan reefs exposed on northwestern Ellesmere Island.

argillaceous rocks. Thermal cracking under deep-burial conditions later altered the oil to bitumen.

To place the occurrence and significance of the bitumen inclusions in these rocks in context, the burial history of the reefs and the probable sequence of organic diagenesis must be considered.

Burial depth and organic diagenesis

A plot of burial depth against time for the Pennsylvanian bryozoan reefs (Fig. 22. 4) reveals that they were buried to a maximum depth of about 6500 m by mid-Cretaceous time. Rates of loading were at a maximum in Triassic and Jurassic times.

To understand the consequences of this depth of maximum burial on maturation of organic matter and generation of the hydrocarbons from which bitumen is formed, it is necessary to outline the stages of diagenesis through which source rocks and organic matter should pass under conditions of progressive burial (increasing temperature and pressure). Although there is a large and growing volume of literature on this subject, it is convenient to use the classification scheme adopted by geochemists at the Institute of Sedimentary and Petroleum Geology (Foscolos *et al.*, 1976). This classification (Fig. 22. 4) and its principal characteristics are summarized as follows.

Eodiagenesis – early stage of diagenesis: the zone in which most pore water is lost from shale source rocks by compaction and in which little change occurs in mixed-layer clays; little hydrocarbon is generated, decarboxylation of fatty acids begins, and biogenic methane is the main hydrocarbon product; the proportion of wet gas in well cuttings is less than 30 per cent of total gas; vitrinite reflectance values are at or below 0. 5 per cent Ro, corresponding with coals of lignitous or sub-bituminous rank; depending on the type of kerogen (amorphous, herbaceous, woody), the H: C atomic ratio of kerogen may range from more than 1. 5 to 0. 8.

Mesodiagenesis – middle stage of diagenesis: the zone in which major changes occur in mixed layer clays, and in which oil is generated; oil generation occurs by thermal cracking, with gas-condensate forming in late mesodiagenesis (higher temperatures); wet gas in cuttings exceeds 30 per cent to more than 60 per cent; vitrinite reflectance values usually lie between 0. 5 and 1. 5 per cent Ro, corresponding with coals of bituminous type; depending on type, H: C atomic ratios of kerogen range from 1. 5 to 0. 5.

Telodiagenesis – late stage of diagenesis: the zone in which the illite content of mixed layer clays generally exceeds 75 per cent, and in which extensive thermal cracking of organic matter leads to dry gas production; vitrinite reflectance values are higher than about 1. 5 per cent Ro, corresponding with coals of semi-anthracite to anthracite type; residual organic matter tends toward graphite, with H: C atomic ratios of kerogen less than 0. 5, regardless of type.

Using this diagenetic framework, the burial history of the Pennsylvanian reefs may be re-examined. Several lines of evidence indicate that at maximum burial the reefs lay within the telodiagenetic zone characterized by overmature or metamorphosed organic matter:

a. A plot of per cent wet gas in drill cuttings against maximum depth of burial for 14 wells in the Sverdrup Basin (Snowdon and Roy, 1975, Fig. 3)

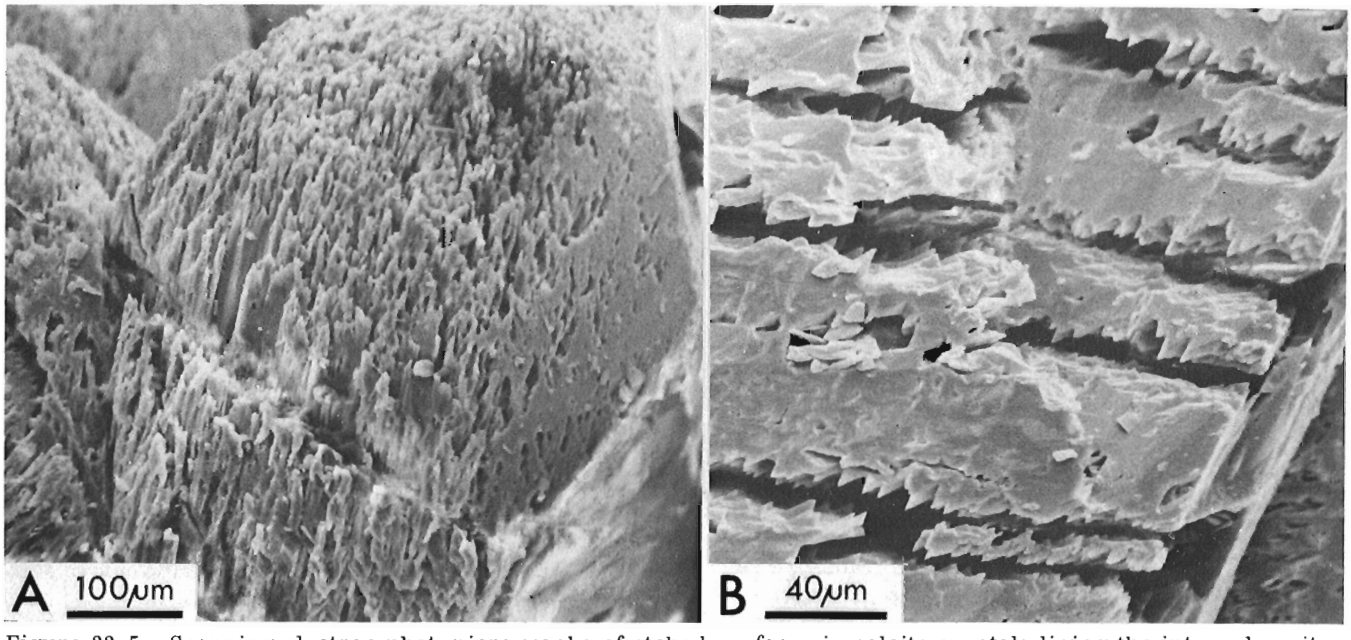

Figure 22. 5. Scanning electron photomicrographs of etched surfaces in calcite crystals lining the internal cavity of a brachiopod. Both examples are associated closely with bitumen that is concentrated in the lower part of the cavity (geopetal distribution). Note that etching in A is face-selective, and in B is closely controlled by cleavage or other parallel lattice structures.

shows that the average transition from the mature oil (mesodiagenetic) zone to the dry gas (telodiagenetic) zone in Mesozoic rocks in this basin lies in the depth range from 4300 to 4900 m (Fig. 22.4). If this average condition is projected onto the burial curve for the Pennsylvanian reefs (with some reservations), it is apparent that at maximum depth of burial (6500 m), the reefs lay within the telodiagenetic zone, and associated organic matter would be overmature or metamorphosed (dry gas).

b. More direct indications of organic thermal metamorphism for the Pennsylvanian reefs are provided by vitrinite reflectance data and other analyses. Vitrinite reflectance values from two samples immediately above a bryozoan reef in the northern Blue Mountains-Krieger Mountains area are 2.69 ± 0.12 and 2.90 ± 0.26 per cent Ro, respectively (Fig. 22.4). These values lie well within the telodiagenetic range and are correlated with coal of anthracite rank (P. Gunther, I.S.P.G., Coal Petrology Unit, Report CP76-R42, 1976). Secondly, conodonts extracted from a sample immediately above a small bryozoan reef near Stepanow Creek on Hare Fiord have a colour alteration index (Epstein *et al.*, 1975) of 6 (T.T. Uyeno, pers. comm., 1976), consistent with thermal conditions of late telodiagenesis. The same sample contains authigenic garnets, also consistent with high temperatures. X-ray diffractograms of lustrous black coatings on brachiopod valves at the same locality show a broad peak at 3.35 Å, indicative of mainly amorphous carbon with some ordered structure approaching graphite, again consistent with telodiagenesis. Finally, the hydrogen to carbon atomic ratio for one sample of bitumen from the calcite spar-lined internal cavity of a brachiopod from the same reef locality is 0.35, well beyond the threshold of about 0.5 marking the transition from mesodiagenesis into telodiagenesis.

Post-burial diagenetic processes and products are considered to result from infiltration of the cemented yet permeable reef mass by water expressed by compaction from the surrounding and overlying argillaceous carbonate sediments (Hare Fiord Formation). The earliest interstitial water probably was a slightly modified marine-like fluid, but with progressive burial the composition of the water may have been altered by the addition of water from amorphous matter and clays and perhaps other minerals (adsorbed water, in part). Water of this type may have been enriched in dissolved silica, iron and other elements, and may have carried early liquid hydrocarbons (Barefoot and Van Elsberg, 1975). These hydrochemical conditions may coincide with the beginning of the mesodiagenetic stage.

Iron-depleted calcite postdates ferroan calcite and thus, if the preceding interpretation is correct, it postdates the onset of mesodiagenesis. The presence of bitumen in the low-iron calcite may be used to support this conclusion, as the liquid oil precursor, by definition, should have formed only under the thermal maturation conditions of mesodiagenesis.

Diagenetic calcite that precipitated in pore spaces during progressive burial (diagenetic steps 7, 9), and thus at elevated temperatures, maintained the marine-like, heavy carbon isotopic signature of the source

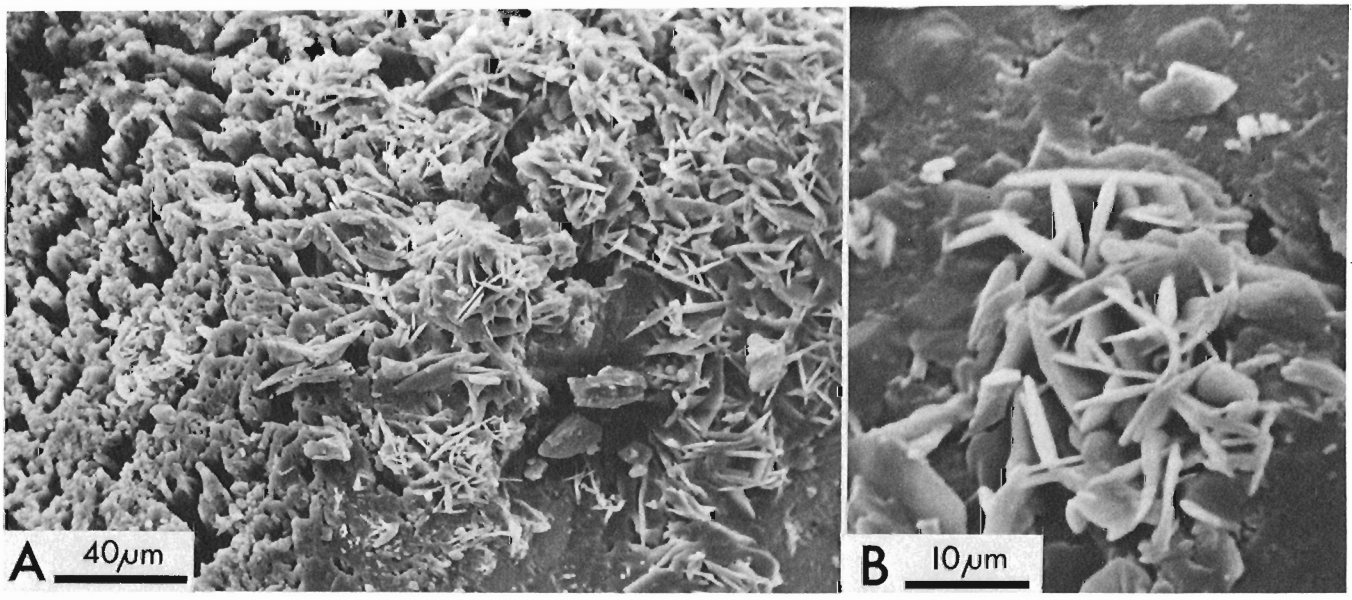

A. A general view of clay crystal aggregates on an etched calcite crystal. Note that the clays are confined mainly to the transition zone from slightly etched (lower right) to intensely etched (upper left) calcite surfaces; etching increases outward into the cavity.

B. Detail of an authigenic clay rosette or aggregate on a calcite surface. This clay mineral contains at least a trace of potassium, and thus is not kaolinite.

Figure 22.6. Scanning electron photomicrographs of authigenic clay minerals in the internal cavities of brachiopods in the Pennsylvanian bryozoan reefs.

carbonates (interpreted to include skeletal carbonates undergoing solution in the enclosing Hare Fiord Formation), but were depleted in isotopically heavy oxygen by high-temperature fractionations. The general range of isotopic ratios for ferroan calcite and low-iron calcite spar (undifferentiated) in these rocks is +4.0 to +6.5 ‰ δC^{13} and -3 to -11‰ δC^{18} (*see* Davies and Krouse, 1975, Fig. 48.5 for plot of data, and Scholle *in* Hancock and Scholle, 1975, for discussion of similar trend in postburial calcite cements).

The etching of the calcite crystals (Fig. 22.5) and apparently closely related precipitation of authigenic clay minerals (Fig. 22.6) inside brachiopod valves and in other open pore spaces is more equivocal in terms of diagenetic classification. As the examined material always included hydrocarbons in the form of bitumen in the same micro-cavities, it is possible that etching and clay precipitation occurred as a terminal phase of hydrocarbon introduction. Alternatively, the etching and the precipitation of clay may have been late deep-burial events related to migration of pore fluids enriched in CO_2 (and thus acidic) and CH_4 (methane) by thermal cracking of organic matter and hydrocarbons in the telodiagenetic (dry gas) zone. Thermal alteration of the liquid hydrocarbons to bitumen in the micro-cavities also occurred in this deep-burial zone.

Conclusions

1. Bitumen or "pyrobitumen" enclosed in and partly overlying late diagenetic calcite in Middle Pennsylvanian bryozoan reefs on Ellesmere Island is the thermal alteration byproduct of liquid hydrocarbons (oil). The oil was introduced into the reef pore system at the same time as the water from which the calcite precipitated.

2. The bitumen and the enclosing calcite postdate several types of submarine cement and ferroan calcite, quartz and dolomite of post-burial origin. The calcite in which the bitumen is enclosed is characterized by a low-iron content.

3. All post-burial diagenetic minerals and the hydrocarbons are considered to have been derived mainly if not totally from water expressed from argillaceous rocks surrounding and overlying the buried reefs; some generation of hydrocarbons within the reefs cannot be ruled out. Carbonate and silica phases probably were derived from solution of skeletal clasts and siliceous spicules in the argillaceous rocks.

4. Introduction of oil into the reef pore system was contemporaneous with thermal maturation of organic matter in the enclosing argillaceous rocks and the reef rocks under conditions of moderate burial, probably in the depth range between 1500 and 4000 m; this interval is correlated with the post-burial mesodiagenetic zone of Foscolos *et al.* (1976).

5. Oil may have migrated in solution, in micelles, as microglobules, or in liquid phase through microfractures. Within cavities, the oil formed liquid globules larger than adjacent micropores and thus were trapped.

6. Precipitation of the enclosing calcite at elevated temperatures consistent with this degree of burial is supported by the isotopic composition of the calcite.

7. Bitumen probably formed from liquid hydrocarbon inclusions by thermal cracking under deep-burial conditions between 4000 and 6500 m, corresponding with the telodiagenetic (dry gas) zone of Foscolos *et al.* (1976).

8. Calcite lining microcavities containing bitumen usually is etched selectively, with authigenic clay mineral aggregates precipitated preferentially in an interzone between less etched and more intensely etched surfaces. Etching and probably precipitation of clays may be a product of migrating acidic waters saturated in CO_2 and CH_4 (methane) coincident with the deep-burial telodiagenetic dry gas zone.

Acknowledgments

The scanning electron microscope used in this study is housed in the Department of Geology of the University of Calgary. Samples were examined under the guidance of A. E. Oldershaw of the Department of Geology.

References

Barefoot, R. R. and Van Elsberg, J. N.
1975: The role of adsorbed or structured water in the diagenesis of the Tertiary sediments in the Mackenzie Delta: a preliminary report; *in* Report of Activities, Part C; Geol. Surv. Can., Paper 75-1C, p. 303-309.

Bathurst, R. G. C.
1975: Carbonate sediments and their diagenesis (2nd ed.); Elsevier, Amsterdam.

Davies, G. R.
1975: Upper Paleozoic carbonates and evaporites in the Sverdrup Basin, Canadian Arctic Archipelago; *in* Report of Activities, Part B; Geol. Surv. Can., Paper 75-1B, p. 209-214.

Davies, G. R. and Krouse, H. R.
1975: Carbon and oxygen isotopic composition of late Paleozoic calcite cements, Canadian Arctic Archipelago – preliminary results and interpretation; *in* Report of Activities, Part B; Geol. Surv. Can., Paper 75-1B, p. 215-220.

Epstein, A. G., Epstein, J. B., and Harris, L. D.
1975: Conodont color alteration – an index to organic metamorphism; U. S. Geol. Surv., Open File Rep. 75-379.

Foscolos, A. E., Powell, T. G., and Gunther, P. R.
1976: The use of clay minerals and inorganic and organic geochemical indicators for evaluating the degree of diagenesis and oil generating potential of shales; Geochim. Cosmochim. Acta, v. 40, p. 953-966.

Hancock, J.M. and Scholle, P.A.
1975: Chalk of the North Sea *in* Petroleum and the continental shelf of Europe, A.W. Woodland, ed.; Applied Science Publishers, Ltd., v. 1, p. 413-425.

Rogers, M.A., McAlary, J.D., and Bailey, N.J.L.
1974: Significance of reservoir bitumens to thermal-maturation studies, Western Canada Basin; Am. Assoc. Pet. Geol., Bull. v. 58, p. 1806-1824.

Snowdon, L.R. and Roy, K.J.
1975: Regional organic metamorphism in the Mesozoic strata of the Sverdrup Basin; Bull. Can. Pet. Geol., v. 23, p. 131-171.

23. BERRIASIAN DINOFLAGELLATE ASSEMBLAGE, MARTIN CREEK, NORTHWESTERN DISTRICT OF MACKENZIE

Project 710019

W. W. Brideaux
Institute of Sedimentary and Petroleum Geology, Calgary

INTRODUCTION

An assemblage of dinoflagellate cysts, recovered from rocks of putative Berriasian age that are exposed along the south bank of Martin Creek, northwestern District of Mackenzie (Fig. 23.1), is described and selectively illustrated in this paper. The samples used in this investigation were collected by the author in the 1973 and 1975 field seasons. They come from the Red-weathering shale member and Upper member of the Husky Formation (Jeletzky, 1958, 1967), and from the overlying Buff sandstone unit of the Lower sandstone division (Jeletzky, 1958, 1960, 1967, 1972). The latter unit may be correlated with the lower part of the subsurface "Parsons sandstone" of Cote *et al.* (1975). A description of the lithology for the parts of the three measured sections from which samples were derived is given at the end of the report. Information on lithology, age, sampling intervals and the occurrence of dinoflagellate species is given diagrammatically in Figures 23.2a, 23.2b, 23.3 and 23.4. Some data used in this report and derived from samples taken from the upper members of the Husky Formation have been published previously by Brideaux and Fisher (1976, p. 2-5, Fig. 3). However, this paper presents the results of a more comprehensive study of the dinoflagellate assemblages, offers a comparison with Berriasian assemblages from other regions and comments on the regional setting of the assemblages.

The Berriasian age of the lithologic units is based on published information derived from macrofossil collections (Jeletzky, 1958, 1967, 1973). It is confirmed for parts of the three sections by new macrofossil collections made by D. W. Myhr and the author in the 1975 field season. These collections were examined and reported on by J. A. Jeletzky (pers. comm., 1976).

Published information on Lower Cretaceous palynology and the status of microplankton studies in the Canadian Arctic have been discussed by Brideaux and McIntyre (1976) and Brideaux (1975), respectively. Recent papers include those by Brideaux and Fisher (1976) on uppermost Jurassic and lowermost Cretaceous miospore and microplankton assemblages from the northern Canadian mainland and Canadian Arctic Archipelago; Brideaux and Myhr (1976) and Brideaux (1976) on the Lower Cretaceous rocks penetrated in the Gulf Mobil Parsons N-10 well (Lat. 60°59'42.52"N, Long. 133°31'50.33"W); and the preliminary zonation for the uppermost Jurassic and Lower Cretaceous given by Pocock (in press). Data on Berriasian dinoflagellate assemblages from other regions are included in the following papers: Williams (1975) from the Atlantic continental margin, offshore eastern Canada; Warren (1967) from the Sacramento Valley, California, USA; Habib (1972, 1974, 1975) from cored intervals of putative

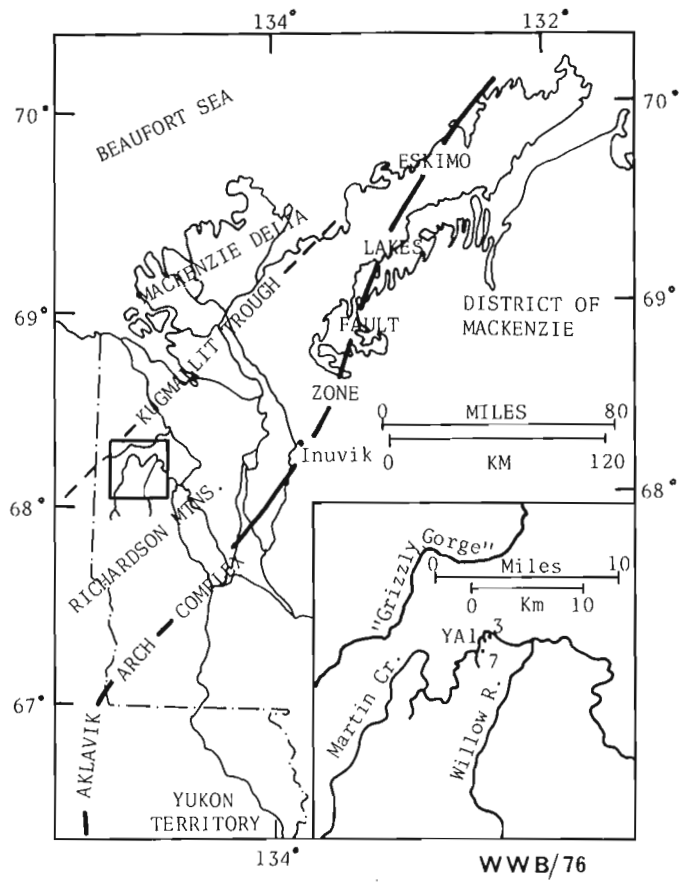

Figure 23.1. Location map showing approximate location (inset map) of Sections 75-BIA-007 (7), 75-MKA-YA-001 (YA1), 75-BIA-003 (3) and geographic and geologic features mentioned in the text.

Berriasian and Valanginian rocks taken at deep sea drilling sites in the western North Atlantic; Millioud (1967, 1969) from the Berriasian stratotype in France (Ardêche); and Habib and Warren (1973).

The author acknowledges the excellent palynological preparations made by S. Pickering and E. O'Keefe, the field assistance of S. Perry (1973) and A. Hedinger (1975), and the critical reviews of the manuscript offered by D. W. Myhr (I. S. P. G., Calgary), now with Husky Oil Limited, Calgary, and D. J. McIntyre (Union Oil Company of Canada, Calgary).

STRATIGRAPHY

Regional setting

The upper two members of the Husky Formation, a lower Red-weathering shale member and an overlying

From: Report of Activities, Part C;
Geol. Surv. Can., Paper 76-1C (1976)

Upper member, and the Buff sandstone unit of the Lower sandstone division, were deposited in the Kugmallit Trough (Yorath *et al.*, 1975) and adjacent to the southern flank of the northwest-southwest-trending Aklavik Arch Complex (Yorath and Norris, 1975) (Fig. 23.1). The presumed axis of the trough lies to the west and northwest of those sections measured along Martin Creek. To the east and southeast lies the Eskimo Lakes Fault Zone (Cote *et al.*, 1975) which transects the Aklavik Arch Complex but represents a later period of tectonic activity. The beds at the measured sections strike approximately north and dip 15° east.

Stratigraphic position, thickness and lithology

Husky Formation (upper members)

Jeletzky (1958, 1960, 1967) gives general summaries of the lithology and stratigraphic relationships of the upper members of the Husky Formation in the northeastern Richardson Mountains. The basal Cretaceous Red-weathering shale member is underlain conformably by the uppermost Jurassic Arenaceous member of the Husky Formation (Jeletzky, 1967) and, along Martin Creek, by 18.1 m (60 ft) of light grey, fine grained sandstone and siltstone which are considered correlative in part with the Arenaceous member. The contact with the overlying Upper member is presumably conformable but, along Martin Creek, is obscured by overburden or slumping. Based on observations elsewhere in the region, an estimated 5 to 10 m (16-33 ft) of section are obscured. The contact of the Upper member with the overlying Buff sandstone unit is conformable and transitional and, along Martin Creek, is placed at the base of the first massive sandstone bed in the Buff sandstone unit. The two upper members of the Husky Formation are exposed at numerous localities throughout the Martin Creek-lower Willow River region, along the eastern flank of the northern Richardson Mountains and in subsurface sections throughout the region.

The thickness of the Red-weathering shale member as measured in surface exposure by Jeletzky (1967) is at least 18 to 23 m (55-75 ft) thick and may be as much as 30.5 m (100 ft) thick. Along Martin Creek a thickness of 25 m (82 ft) was measured (Fig. 23.2b) and an estimated 5 m (16 ft) were covered by overburden or slumping. The lithology along Martin Creek comprises dark grey shale with minor amounts of interbedded siltstone, ferruginous siltstone and indurated clay-ironstone horizons scattered throughout the section.

The Upper member is from 26 to 43 m (85-140 ft) thick in surface exposures and possibly as thick as 61 m (200 ft) according to Jeletzky (1967). Along Martin Creek (Fig. 23.3), 46.5 m (153 ft) were measured and up to 3 m (10 ft) may be covered by slumping. Strata at the base of the member consist of grey shales and siltstone which, near the middle grade to mudstone, in places bioturbated, and some fine grained sandstone beds. The sandstone content increases upward from this point and the top beds of the member comprise fine grained sandstone with thin shale partings.

Lower sandstone division (Buff sandstone unit)

The contact of the Buff sandstone unit with the underlying Upper member of the Husky Formation is transitional and conformable. The upper contact with the overlying Bluish-grey shale unit (a tongue of the thicker Bluish-grey shale division of Jeletzky, 1960, 1972, 1974) is conformable and marked, along Martin Creek, by an increase in clay content of the sandstone beds. The uppermost beds of the Buff sandstone unit may be bioturbated and contain wood fragments and segments of branches.

The total thickness of the Buff sandstone unit, obtained from measurements at surface exposures in the northeastern Richardson Mountains, ranges from 60 to 100 m (200-330 ft). Myhr and Young (1975) report a measured thickness of 88 m (288.6 ft) in sections along "Grizzly Gorge", 6 km (4 miles) north of Martin Creek. The measured thickness of 98.6 m (323 ft) in sections along Martin Creek (Figs. 23.3, 23.4) is near the maximum exposed thickness for the unit Jeletzky, 1972) in this area. The thickness of the unit in the northeastern Richardson Mountains decreases westward from Martin Creek (Jeletzky, 1972). Along Martin Creek, the Buff sandstone unit comprises grey, very fine to fine grained sandstone that weathers light brown to grey-brown and is commonly iron-stained. Silty or shaly beds occur mainly in the middle and upper part of the unit. Scattered indurated ferruginous claystone horizons also are present. The more argillaceous beds yield the dinoflagellate assemblages described from the Buff sandstone unit.

Age

The Red-weathering shale member falls within the *Buchia okensis* zone, the basal Berriasian macrofossil zone in this region (Jeletzky, 1967, 1973). The underlying beds of the Arenaceous member and its lithological equivalents in this region fall within zones of the Upper Tithonian. Therefore, the contact between the two members is essentially the contact between the Jurassic and Cretaceous Systems in this region (Jeletzky, 1967, 1973; Brideaux and Fisher, 1976, p. 25-28, Fig. 12). The *Buchia okensis* zone is assigned an Early Berriasian age (Jeletzky, 1965, 1966, 1967, 1973).

The Upper member of the Husky Formation falls within the *Buchia* n. sp. aff. *volgensis* zone (Jeletzky, 1958, 1960, 1973). Macrofossil collections made by D.W. Myhr and the writer in the 1975 field season were reported on by J.A. Jeletzky (pers. comm., 1976). The assemblage includes *Buchia* n. sp. aff. *volgensis* (Lahausen, 1888), *Buchia* aff. *terebratuloides* (Lahausen, 1888) sensu lato and is suggestive of the lower part of the zone according to Jeletzky (*op. cit.*). This zone is assigned a Late Berriasian age by Jeletzky (1973).

The Buff sandstone unit, as exposed along Martin Creek, also is placed within the *Buchia* n. sp. aff. *volgensis* zone. Jeletzky (*op. cit.*) comments that the macrofossil collections made from this unit along the

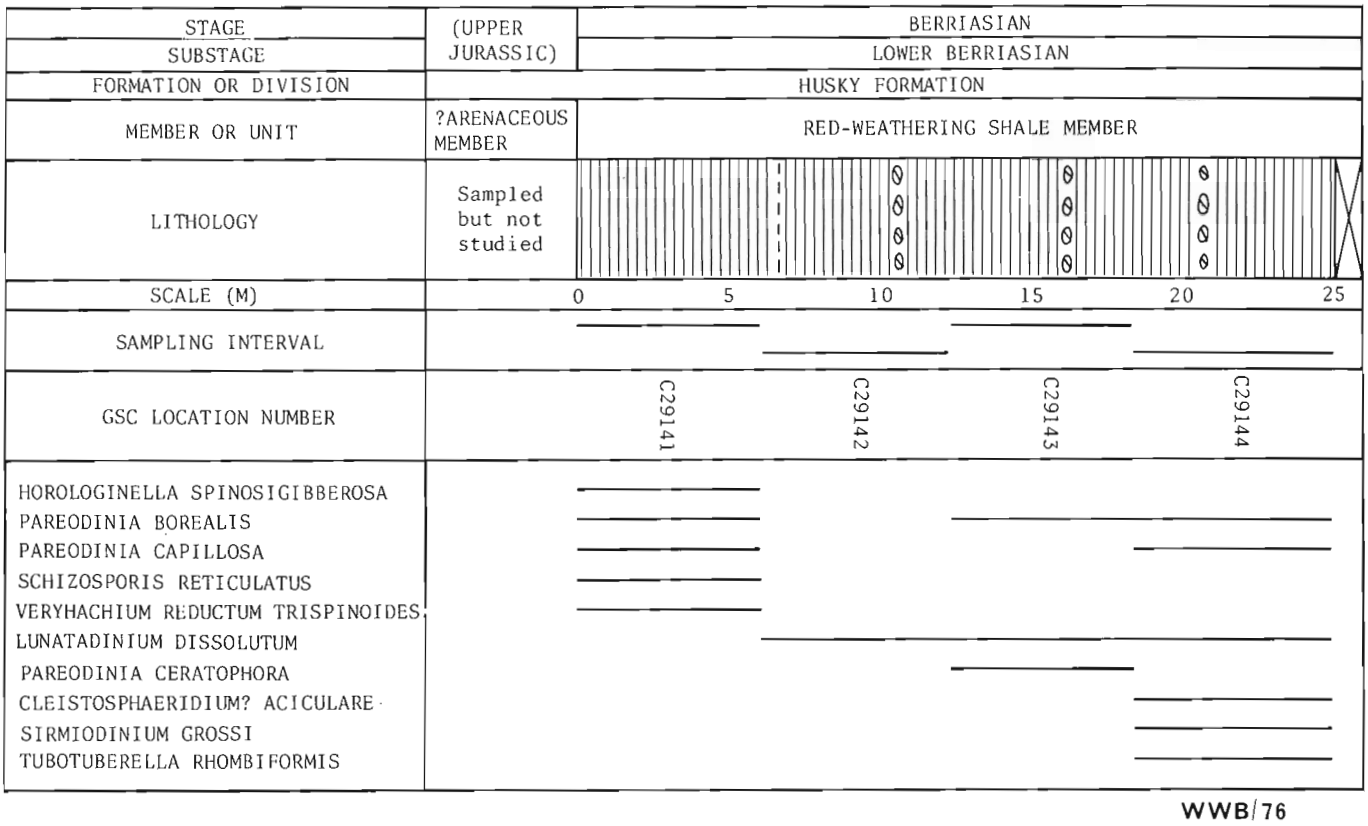

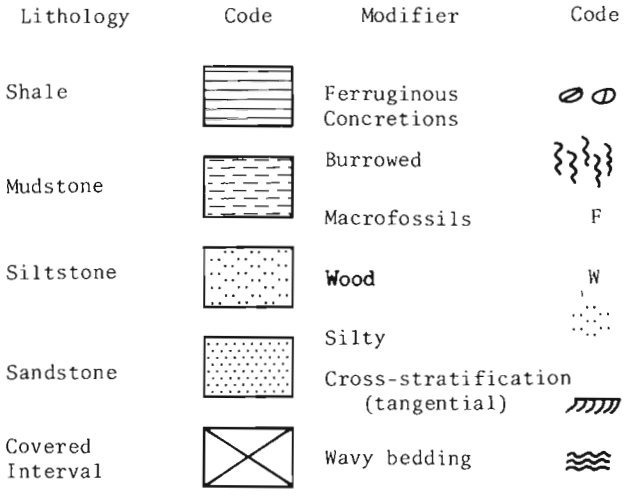

Figure 23.2a.

Generalized lithologic column, biostratigraphy and occurrence of dinoflagellate and acritarch species in Section 75-BIA-007 (upper part) along Martin Creek.

Figure 23.2b.

Lithologic legend for Figures 23.2, 23.3 and 23.4.

south bank of Martin Creek at 5.8 m (19 ft) above the base of the unit (GSC loc. C-49970) may represent the middle part of the zone. Macrofossil collections made by D.W. Myhr from the upper part of the Buff sandstone unit on the north bank of Martin Creek may represent the upper part of the zone (Jeletzky, *op. cit.*). That part of the Buff sandstone unit is the same as that exposed along the south bank of Martin Creek and sampled by the writer (Fig. 23.4).

Depositional Environment

The Red-weathering shale member is thought to have been deposited in a shallow-marine offshore environment along the eastern margin of the Kugmallit Trough (Young *et al.*, in press). The recurring ferruginous siltstone beds and indurated clay-ironstone horizons, although suggestive of a somewhat restricted environment, may also be diagenetic in origin and not environmentally controlled.

The Upper member, along Martin Creek, consists of strata typical of an environment transitional between an offshore marine environment of deposition in the lower and middle parts and a littoral environment in the upper part. The characteristics of the transition unit, as summarized by Myhr and Young (1975, p. 249), are typical of a lower shoreface environment.

The Buff sandstone unit along Martin Creek represents various aspects of a shoreface environment, principally upper shoreface in approximately the lower third of the unit, and alternating lower to upper shoreface in the remainder of the unit. The shoreface environment is succeeded by a basinal marine environment in which the Bluish-grey shale unit was deposited (D.W. Myhr, pers. comm., 1976).

Myhr and Young (1975) consider the Upper member of the Husky Formation and the Buff sandstone unit of the Lower sandstone division, in the vicinity of Martin Creek, to represent a complex of barrier-shoreline deposits. Just north of Martin Creek, along "Grizzly Gorge", Myhr and Young (1975, p. 249) suggest that these lithostratigraphic units are "... stacked shoreline (?barrier island) deposits in a nearshore setting, where cyclical conditions prevailed in one area for a considerable time..."

SPECIES LIST AND COMMENTS

(Dinoflagellates)

Apteodinium sp. DE

Pericyst ambitus ovoid, length greater than width, with short apical horn, 5 to 7μ in length; endocyst similar in shape; no pericoel development. Periphragm scabrate. Archeopyle not observed. Dimensions (4 specimens): pericyst length, 70 to 108μ; pericyst width, 68 to 77μ.

Caligodinium aceras (Manum and Cookson) Lentin and Williams, 1973. *Cleistosphaeridium? aciculare* Davey, 1969.

This species occurs also in the Bluish-grey shale unit of Valanginian age (McIntyre and Brideaux, unpublished data) and in rocks of Hauterivian age from the northern Canadian mainland (Brideaux, in press).

Cleistosphaeridium polypes subsp. *clavulum* Davey, 1969. (Pl. 23.1, fig. 9).

This species occurs also in Valanginian and Hauterivian rocks of the northern Canadian mainland (McIntyre and Brideaux, unpublished data; Brideaux, in press).

Cleistosphaeridium sp. JE. (Pl. 23.1, figs. 5, 6).

Pericyst ambitus ovoid to subcircular; endocyst of similar shape; no pericoel development. Periphragm bearing numerous processes, the processes broader basally and tapering distally, their terminations bifid to bifurcate, occasionally two long, acuminate extensions; processes discrete except along presumed paracingular parasutures where they may be joined basally; processes 10 to 25μ in length. Archeopyle apical. Dimensions (5 specimens): pericyst length, 45 to 50μ (no complete specimens); pericyst width, 40 to 55μ.

Cyclonephelium distinctum Deflandre and Cookson, 1955. *Endoscrinium campanula* (Gocht) Vozzhennikova, 1967. (Pl. 23.1, fig. 2).

Rare specimens of this species have been recorded in basal beds of the Upper member of the Husky Formation (late Berriasian age).

Gardodinium sp. cf. *G. eisenackii* Alberti, 1961 (Pl. 23.1, fig. 4).

A single specimen, recorded in basal beds of the Buff sandstone unit, is poorly preserved and therefore attributed only provisionally to the species, *eisenackii*. Well-preserved specimens of *G. eisenackii* have been observed previously in rocks of Hauterivian to Albian age on the northern Canadian mainland (Brideaux, in press).

Heslertonia sp. BE. (Pl. 23.1, fig. 12).

A single specimen with ovoid pericyst, the periphragm produced into high (25-32μ), striated parasutural crests, and overall length and width, 118μ and 125μ, respectively.

Horologinella spinosigibberosa Brideaux and Fisher, 1976.

Brideaux and Fisher (1976) recorded this species only from Upper Jurassic rocks. The report from the basal beds of the Red-weathering shale member of the Husky Formation thus is an extension of its stratigraphic record. A few specimens have been observed in younger rocks (Brideaux, in press), but these are considered to have been derived from older rocks. The confirmed range of the species in the Canadian Arctic is Upper Oxfordian (*Buchia concentrica* sensu lato zone) to Lower Berriasian (base of *Buchia okensis* zone).

Lecaniella sp. AE. (P. 23.1, fig. 11).

Only separated halves of this species were observed. The halves are ovoid to subcircular in outline and possess a reticulate ornament comprised of simple muri, 1 to 3μ wide and about 1μ high and ovoid to rounded lumina, 2 to 8μ in maximum diameter. There is no peripheral reticulum with radially directed muri as in several other species assigned to this genus. Dimensions (4 specimens): maximum diameter, 45 to 65μ.

Leptodinium sp. EE. (Pl. 23.1, fig. 1).

A single specimen was observed near the top of the *Buchia* n. sp. aff. *volgensis* zone in the upper part of the Buff sandstone unit. The species occurs with greater frequency in the overlying Bluish-grey shale

unit of Valanginian age (McIntyre and Brideaux, unpublished data). It is characterized by low parasutural crests and small, discrete, intratabular spines, 1 to 2μ high. Dimensions: pericyst length, 40μ pericyst width, 38μ.

Lunatadinium dissolutum Brideaux and McIntyre, 1973.
Oligosphaeridium sp. FE. (Pl. 23.2, fig. 7).

This species is characterized by relatively long processes which are open distally and have quadrate to subquadrate terminations which bear four to six (typically four) aculei. The archeopyle is apical, the operculum detached. The species is represented in the upper part of the *Buchia* n. sp. aff. *volgensis* zone by isolated opercula, but is most abundant in the overlying Bluish-grey shale unit (McIntyre and Brideaux, unpublished data). It is comparable with *Oligosphaeridium vasiformum* (Neale and Sarjeant) Davey and Williams, 1966, from the Middle Hauterivian of England, but lacks the densely perforate body (?preservational) of that species.

"Organism" sp. AE. (Pl. 23.1, figs. 7, 13).

Ambitus rounded to subcircular. Outer wrinkled, diaphanous layer, commonly not preserved, bearing widely spaced fine grana; outer layer in some specimens forming a short, rounded prominence at one pole. Inner body, scabrate to finely punctate, with a reticulate peripheral band or, more rarely, a thickened peripheral ridge; the reticulum with thin, simple muri and irregular lumina 1 to 2μ in maximum diameter. At one pole, an irregular thinning or opening observed on many specimens. Dimensions (22 specimens): (maximum and minimum diameters) outer layer 43 to 55μ and 39 to 53μ; inner layer, 35 to 50μ and 32 to 47μ.
Pareodinia borealis Brideaux and Fisher, 1976.
Pareodinia capillosa Brideaux and Fisher, 1976.
Pareodinia ceratophora Deflandre emend. Gocht, 1970.
Schizosporis reticulatus Cookson and Dettmann, 1959.
Sirmiodinium grossii Alberti, 1961 emend. Warren, 1973.

Tanyosphaeridium sp. DE.

Pericyst and endocyst closely appressed; ambitus elongate; periphragm surface granular and bearing up to 50 smooth processes; the processes tubiform, hollow, distally open, slightly flared, 10 to 15μ long, 1 to 2μ wide. Archeopyle apical; operculum not observed. The large number of non-bucinate processes distinguishes this species from similar forms (cf. Brideaux and McIntyre, 1976, p. 31, 32).

Tubotuberella rhombiformis Vozzhennikova, 1967.

This species occurs rarely, but consistently, throughout rocks of Berriasian and Valanginian ages along Martin Creek, in some places in association with obviously derived Jurassic dinoflagellates. This pattern of occurrence suggests that the species is indigenous and that the range of the species should be extended, in northern Canada, from Upper Volgian (Vozzhennikova, 1967) to Valanginian (McIntyre and Brideaux, unpublished data).

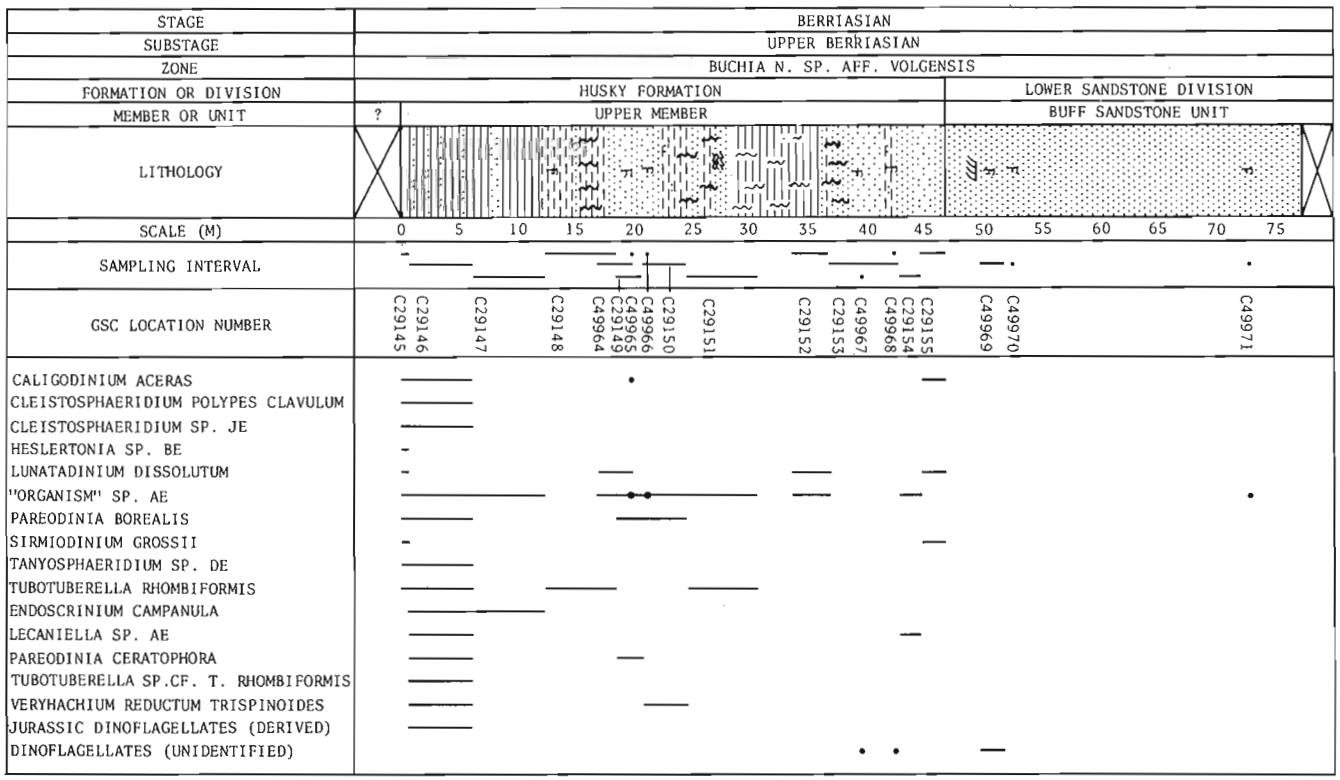

Figure 23.3. Generalized lithologic column, biostratigraphy and occurrence of dinoflagellate and acritarch species in Section 75-YA-MKA-001 (= Section 73-BIA-25) along Martin Creek.

PLATE LEGENDS

In the explanation of figures, the species name is followed by the GSC (I.S.P.G.) locality number, the height of the sample above the base of section, the section number, slide number, stage co-ordinates for Reichert Zetopan Microscope No. 56395 at the Institute of Sedimentary and Petroleum Geology, Calgary, Canada, focus level and orientation if needed, the GSC Type Number, the magnification and the size in microns. IC refers to Interference Contrast.

Slides containing figured specimens are stored in collections of the Geological Survey of Canada, 601 Booth Street, Ottawa, Canada, K1A 0E8. Other slides and samples from these surface sections are stored in the collections at the Institute of Sedimentary and Petroleum Geology, Calgary, Canada, T2L 2A7.

Plate 23.1

Figure 1. *Leptodinium* sp. EE. C-50865, 77.0 m, 75-BIA-003, P1101-12A, 16.9 x 128.2, lo-focus on paraplate 3", GSC 45921, x1250 (40μ x 38μ).

Figure 2. *Endoscrinium campanula.* C-29147, 6.1-12.2 m, 75-BIA-003, P912-42C, 46.9 x 128.1, mid focus, IC, GSC 45922, x500 (90μ).

Figure 3. *Tubotuberella* sp. cf. *T. rhombiformis.* C-50863, 19.5 m, 75-BIA-003 P1101-10C, 41.6 x 118.4, mid-focus, IC, GSC 45923, x500 (112μ).

Figure 4. *Gardodinium* sp. cf. *G. eisenackii.* C-50862, 6.0-6.3 m, 75-BIA-003 P1101-9A, 35.7 x 122.3, mid-focus IC, GSC 45924, x1000 (61μ x 41μ).

Figures 5, 6. *Cleistosphaeridium* sp. Je. C-29145, 0.0-0.6 m, 75-YA-MKA-001, P912-40C, 40.7 x 119.2, (5) hi-focus and (6) lo-focus, GSC 45925, x1000 (50μ x 42μ).

Figures 7, 10, 13. "Organism" sp. AE.

7. C-49965, 18.9-19.0 m, 75-YA-MKA-001, P1131-2A, 42.5 x 124.2, mid-focus, IC, GSC 45926, x1000 (outer layer, 43μ x 39μ; inner layer, 39μ x 36μ).

10. C-49964, 16.8-18.9 m 75-YA-MKA-001, P1131-1A, 39.4 x 120.6, mid-focus, IC, GSC 45927, x1000 (outer layer, 55μ x 50μ; inner layer, 48μ x 43μ).

13. C-49964, 16.8-18.9 m 75-YA-MKA-001, P1131-1A, 23.6 x 134.2, focus on fine grana on outer layer, IC, GSC 45928, x1000 (outer layer, 58μ x 53μ; inner layer, 50μ x 47μ).

Figure 8. *Canningia* sp. C-49964, 16.8-18.9 m, 75-YA-MKA-001, P1131-1A 47.1 x 122.4, mid-focus, IC, GSC 45929, x500 (45μ x 43μ).

Figure 9. *Cleistosphaeridium polypes* subsp. *clavulum.* C-29145, 0.0-0.6 m, 75-YA-MKA-001, P912-40A, 16.5 x 127.3, mid-focus, GSC 45931, x5000 (47μ x 50μ).

Figure 11. *Lecaniella* sp. AE. C-50862, 6.0-6.3 m, 75-BIA-003, P1101-9A, 34.0 x 119.6, mid-focus, IC, GSC 45932, x1000 (max. diam. 65μ).

Figure 12. *Heslertonia* sp. BE. C-29145, 0.0-0.6 m 75-YA-MKA-001, P912-40C, 18.9 x 131.2, hi-focus on crests, GSC 45940, x1000 (pericyst length, 75μ).

Figure 14. *Canningia* sp. C-29146, 0.6-6.1 m, 75-YA-MKA-001, P912-41D, 24.0 x 120.3, mid-focus on low rugulo-reticulate ornament, GSC 45930, x1000 (57μ x 60μ).

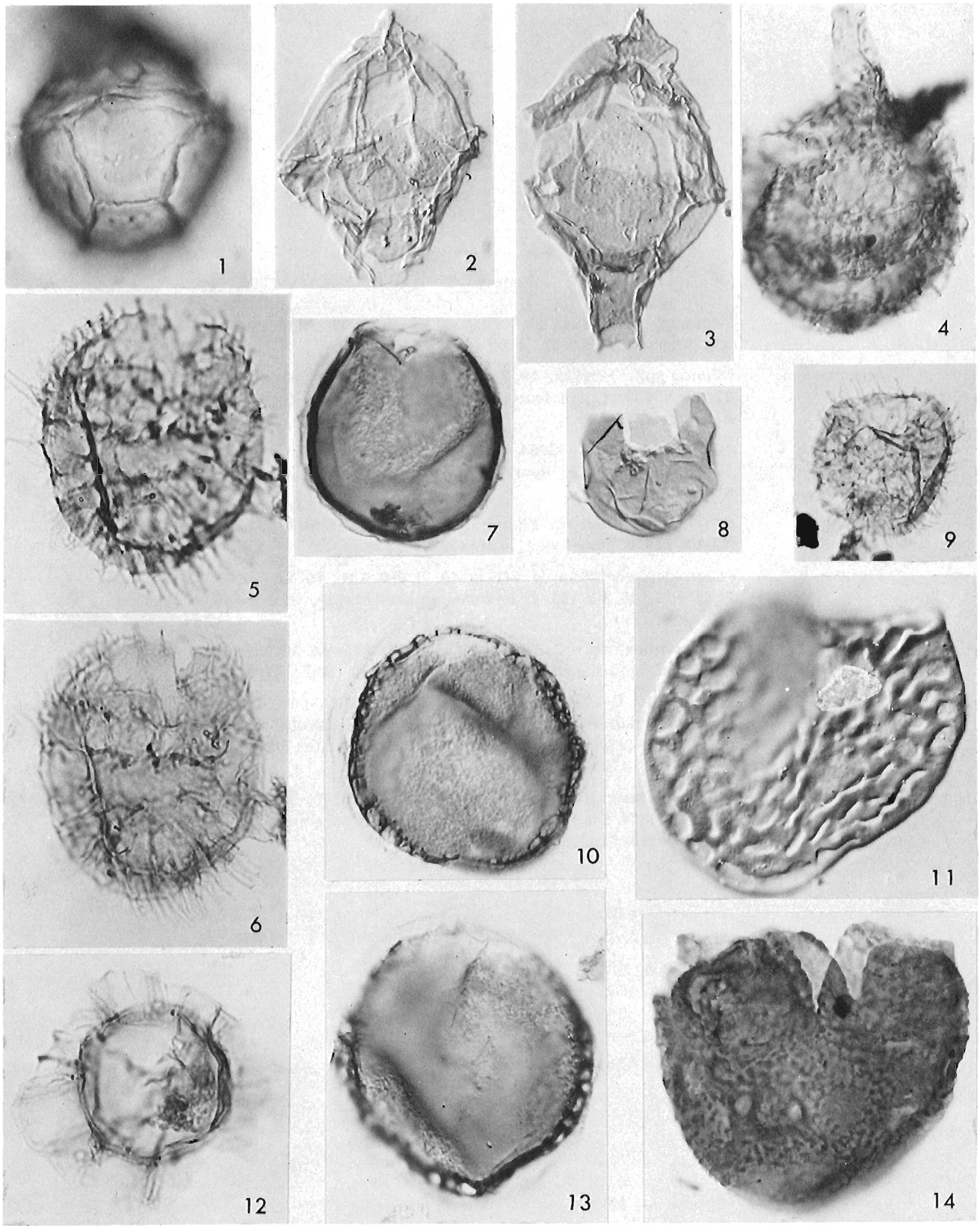
1
2
3
4
5
6
7
8
9
10
11
12
13
14

Plate 23.2

Figure 1. *Tenua* sp. C-50864, 60.1-60.5 m, 75-BIA-003, P1101-11D, 37.6 x 116.8, mid-focus, GSC 45933, x500 (65μ x 63μ).

Figures 2-4. *?Tenua* sp. C-29149, 18.3-20.7 m, 75-YA-MKA-001, P912-44A, 21.8 x 120.3, (2) hi-focus, (3) mid-focus, (4) lo-focus, IC, GSC 45934, x1000 (42μ x 55μ).

Figures 5, 6. *?Canningia* sp. C-49964, 16.8-18.9 m, 75-YA-MKA-001, P1131-1A, 34.9 x 130.3, (5) lo-focus on archeopyle (6) hi-focus, IC, GSC 45935, x500 (40μ x 44μ).

Figure 7. *Oligosphaeridium* sp. FE. C-50865, 77.0 m, 75-BIA-003, P1101-12A, 45.4 x 120.0, mid-focus, GSC 45941, x500.

Figure 8. *?Cleistosphaeridium* sp. C-29145, 0.0-0.6 m, 75-YA-MKA-001, P912-40C, 30.8 x 129.4, lo-focus on archeopyle, GSC 45936, x 1000 (43μ x 46μ).

Figure 9. *Gardoninium?* sp. C-29155, 44.5-46.6 m, 75-YA-MKA-001, 31.4 x 122.1, P912-50C, mid-focus, IC, GSC 45937, x1000 (83μ x 67μ).

Figure 10. *?Tenua* sp. C-49965, 18.9-19.0 m, 75-YA-MKA-001, 24.8 x 128.9, P1131-2C, mid-focus on archeopyle and well-developed accessory parasuture separating anterior parts of paraplates 5" and 6", IC, GSC 45938, x1000 (max. width, 57μ).

Figure 11. *?Cleistosphaeridium* sp. C-29145, 0.0-0.6 m, 75-YA-MKA-001, P912-40C, 24.4 x 121.0, lo-focus on dorsal paracingulum, GSC 45939, x1000 (46μ x 51μ).

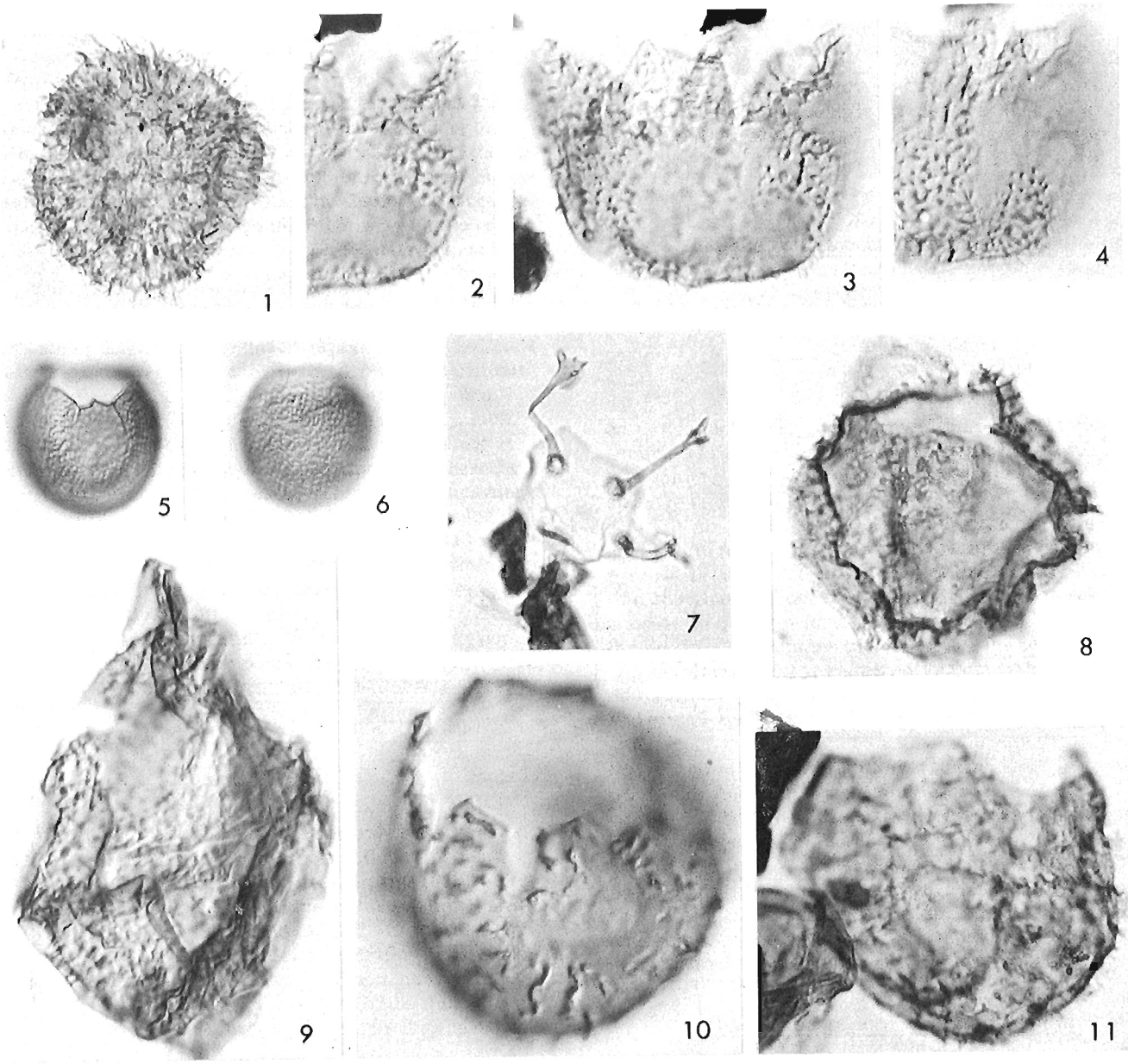
1
2
3
4
5
6
7
8
9
10
11

PALEOGEOGRAPHIC DISTRIBUTION

Seven species, reported elsewhere from basal Cretaceous rocks of putative Berriasian age, occur also in Berriasian rocks along Martin Creek. These are *Schizosporis reticulatus, Pareodinia ceretophora, Sirmiodinium grossii, Tubotuberella rhombiformis, Caligodinium aceras, Cyclonephelium distinctum* and *Endoscrinium campanula. Lunatadinium dissolutum,* widely reported in the Canadian Arctic (Brideaux and McIntyre, 1973; Brideaux, in press), has been recorded elsewhere only from the Sacramento Valley, California (Warren, 1967). Other species, including *Horologinella spinosigibberosa, Pareodinia borealis, P. capillosa, Tanyosphaeridium* sp. DE and "Organism" sp. AE, and seven other species recorded only as single occurrences, have been reported only from Arctic Canada.

A comparison with dinoflagellate assemblages of Berriasian or probable Berriasian age indicates that little similarity exists between assemblages from the Canadian Arctic and other areas. The differences can be attributed in part to the following factors: paleoenvironmental constraints discussed above which influence the composition of the Martin Creek assemblages; the uncertainty attached to the broadly dated assemblages of other areas; and the scarcity of data that are available for comparative purposes.

There is, however, enough evidence to suggest that Berriasian dinoflagellate assemblages from this representative Canadian Arctic locality belong to a Boreal assemblage having little affinity with desribed Tethyan or Pacific assemblages. Unfortunately, Vozzhennikova (1967) did not encounter Berriasian assemblages in her studies on Russian material and no published data exist for Berriasian assemblages from Alaska or for well-dated Berriasian assemblages from Australia. The rough quantitative comparison in support of the suggestion presented above is given below. The first of the figures is the number of species common to both assemblages; the second figure, after the slash, is the total number of species that occur in one or the other but not in both of the assemblages.

Eastern Canada offshore (*Phoberocysta neocomica* assemblage zone); Williams (1975): 1/35

Western North Atlantic (*Biorbifera johnewingi* zone); Habib (1975): 0/34

Southeastern France (Berriasian stratotype and other sections); Millioud (1969): 2/24

California, USA (*Buchia okensis* and *B. uncitoides* zones); Warren (1967): 4/83

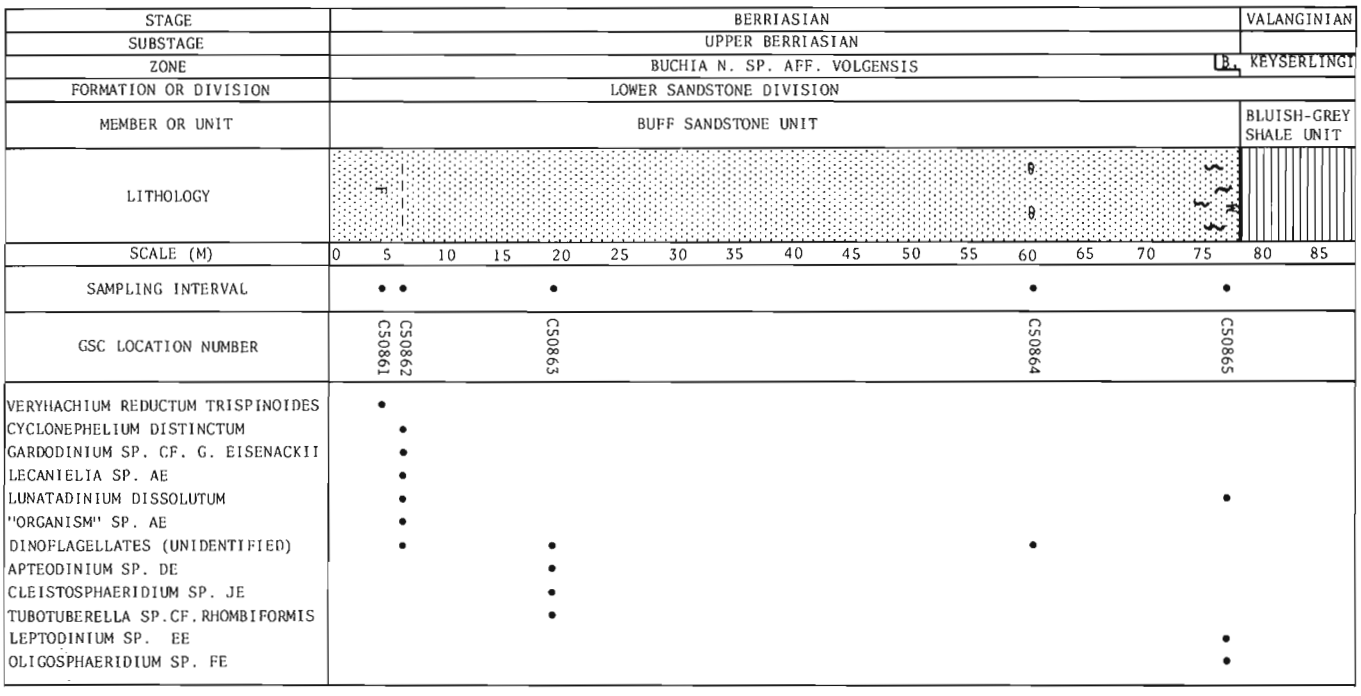

Figure 23. 4. Generalized lithologic column, biostratigraphy and occurrence of dinoflagellate and acritarch species in Section 75-BIA-003 (lower part) along Martin Creek. Upper part of the section comprises 16. 7 m of Bluish-grey shale unit and 33. 5 m of White sandstone unit

Tubotuberella sp. cf. *T. rhombiformis* Vozzhennikova, 1967. (Pl. 23.1, fig. 3).

This species occurs rarely. It does not possess parasutures and thus is similar to *Psaligonyaulax apatela* (Cookson and Eisenack) Sarjeant, 1966, but lacks the pronounced apical horn of that species and therefore, is more like *T. rhombiformis*.

Other dinoflagellates (Pl. 23.1, figs. 8, 14; Pl. 23.2, figs. 1-6, 8-11).

A number of well-preserved, single specimens were encountered in this study, commonly referable to the genera, *Canningia*, *Tenua*, or *Cleistosphaeridium*. They are figured without comment, principally in the hope that they may be observed as abundant constituents of assemblages described in later studies. Their presence in the Berriasian of northern Canada at least will be established.

(Acritarchs)

Veryhachium reductum forma *trispinoides* de Jekhowsky, 1961.

BIOSTRATIGRAPHY

Buchia okensis zone

Husky Formation: Red-weathering shale member

Rocks assigned to this zone along Martin Creek contain ten dinoflagellate species, several of which have restricted ranges. *Horologinella spinosigibberosa*, previously thought to be restricted to rocks of Late Jurassic (Late Oxfordian-Kimmeridgian-?Portlandian) age, occurs in the lower 6.1 m (20 ft) of the member, but does not range higher (cf. Brideaux and Fisher, 1976, Fig. 13). *Pareodinia capillosa* does not range above this zone. The species was reported from the overlying *Buchia* n. sp. aff. *volgensis* zone by Brideaux and Fisher (1976, Fig. 3), but re-examination of the specimens assigned to that species has established that these were misidentified. *Schizosporis reticulatus* is restricted to the lower 6.1 m (20 ft) of the member and, locally, does not range higher.

Buchia n. sp. aff. *volgensis* zone (lower part)

Husky Formation: Upper member

Nine species first appear in the basal part of the zone in the lower 6.1 m (20 ft) of the Upper member. Only one species, *Caligodinium aceras*, ranges into older rocks elsewhere in the region. Three species occur only in the basal part of the zone along Martin Creek, but are known to range higher elsewhere in the region. These are: *Cleistosphaeridium polypes* subsp. *clavulum*; *Endoscrinium campanula*; and *Tanyosphaeridium* sp. DE. The single specimen of *Heslertonia* sp. BE occurs in the basal sample from this zone.

Buchia n. sp. aff. *volgensis* zone (middle and upper parts)

Lower sandstone division: Buff sandstone unit

Nine species occur rarely within the lower part of the Buff sandstone unit (middle part of the zone), of which three make their first and only appearance: *Cyclonephelium distinctum*; *Gardodinium* sp. cf. *G. eisenackii* (a single specimen); and *Apteodinium* sp. DE. Two other species, *Leptodinium* sp. EE and *Oligosphaeridium* sp. FE occur for the first and only time in the upper part of the unit and the zone, but are present in the overlying Bluish-grey shale unit (McIntyre and Brideaux, unpublished data).

Of the fourteen species which make their appearance within the zone, and the additional seven species which range into the zone, only five are restricted to the zone: *Heslertonia* sp. BE; "Organism" sp. AE; *Lecaniella* sp. AE; *Apteodinium* sp. DE; and *Tubotuberella* sp. cf. *T. rhombiformis*. *Pareodinia borealis* does not range above the lower part of this zone along Martin Creek. Rare specimens of *P. borealis* observed in the overlying Bluish-grey shale unit (McIntyre and Brideaux, unpublished data) are considered to have been derived from older rocks.

Concluding remarks

The influence of the paleoenvironment of deposition, and of the predominance of sandstone lithofacies in the upper part of the *Buchia* n. sp. aff. *volgensis* zone, on the composition and abundance of individual dinoflagellate species which comprise the assemblages, probably is considerable. Therefore, cautious application of the biostratigraphic data derived from the study of Berriasian assemblages along Martin Creek is advisable. There is promise, however, that a subdivision of the Berriasian Stage in northern Canada can be accomplished based on dinoflagellated cyst assemblages.

PALEOECOLOGY

The following species persist through the offshore basinal-marine and lower shoreface (transitional lithofacies) environments outlined earlier: *Lunatadinium dissolutum*; *Sirmiodinium grossii*; *Caligodinium aceras*; "Organism" sp. AE; and *Lecaniella* sp. AE (rare). A number of species occur in an offshore basinal-marine environment but do not occur in the lower shoreface environment of the upper part of the Upper member. These include *Pareodinia borealis*, *P. capillosa*, *P. ceratophora*, *Tubotuberella rhombiformis*, *Endoscrinium campanula* and *Cleistosphaeridium polypes clavulum*. Three species, *Lunatadinium dissolutum*, "Organism" sp. AE and *Lecaniella* sp. AE, occur in the shallow-marine beds of the shoreface environment in which the Buff sandstone unit is thought to have been deposited. Other species recorded from Berriasian rocks along Martin Creek occur too rarely for anything to be inferred about their distribution in relation to depositional environment.

REFERENCES

Brideaux, W. W.

1975: Status of Mesozoic and Tertiary dinoflagellate studies in the Canadian Arctic; Am. Assoc. Stratigr. Palynol., Contrib., Series, No. 4, p. 15-28.

1976: Taxonomic notes and illustrations of selected dinoflagellates from the Gulf Mobil Parsons N-10 well; *in* Report of Activities, Part B, Geol. Surv. Can., Paper 76-1B, p. 251-257.

Taxonomy of Upper Jurassic-Lower Cretaceous microplankton from the Richardson Mountains, District of Mackenzie, Canada; Geol. Surv. Can., Bull. (in prep.)

Brideaux, W. W. and Fisher, M. J.

1976: Upper Jurassic-Lower Cretaceous dinoflagellate assemblages from Arctic Canada; Geol. Surv. Can., Bull. 259.

Brideaux, W. W. and McIntyre, D. J.

1973: *Lunatadinium dissolutum* gen. et sp. nov., a dinoflagellate cyst from Lower Cretaceous rocks, Yukon Territory and northern District of Mackenzie; Bull. Can. Pet. Geol., v. 21, p. 395-402.

1976: Miospores and microplankton from Aptian-Albian rocks along Horton River, District of Mackenzie, Canada; Geol. Surv. Can., Bull. 252.

Brideaux, W. W. and Mhyr, D. W

1976: Lithostratigraphy and dinoflagellate cyst succession in the Gulf Mobil Parsons N-10 well; *in* Report of Activities, Part B, Geol. Surv. Can., Paper 76-1B, p. 235-249.

Cote, R. P., Lerand, M. M., and Rector, R. I.

1975: Geology of the Lower Cretaceous Parsons Lake gas field, Mackenzie Delta, Northwest Territories *in* Canada's continental margins and offshore petroleum exploration, C. J. Yorath *et al.*, ed.; Can. Soc, Pet. Geol., Mem. 4, p. 613-632.

Habib, D.

1972: Dinoflagellate stratigraphy, Leg 11, Deep Sea Drilling Project *in* Initial reports of the deep sea drilling project, Volume XI, Washington, p. 367-425.

1974: Morphogenetic relationship between *Scriniodinium campanula* Gocht and *Scriniodinium dictyotum* Cookson and Eisenack; Geosci. Man, v. 9, p. 45-51.

1975: Neocomian dinoflagellate zonation in the western North Atlantic; Micropaleontology, v. 21, p. 373-392.

Habib, D. and Warren, J. S.

1973: Dinoflagellates near the Cretaceous Jurassic boundary; Nature, v. 241, p. 217-218.

Jeletzky, J. A.

1958: Uppermost Jurassic and Cretaceous rocks of Aklavik Range, northeastern Richardson Mountains, Northwest Territories; Geol. Surv. Can., Paper 58-2, p. 1-84.

1960: Uppermost Jurassic and Cretaceous rocks, east flank of Richardson Mountains between Stony Creek and Donna River, Northwest Territories; Geol. Surv. Can., Paper 59-14, p. 1-31.

1965: Late Upper Jurassic and early Lower Cretaceous fossil zones of the Canadian western Cordillera, British Columbia; Geol. Surv. Can., Bull. 103, p. 1-70.

1966: Upper Volgian (latest Jurassic) ammonites and buchias of Arctic Canada; Geol. Surv. Can., Bull. 128, p. 1-49.

1967: Jurassic and (?) Triassic rocks of the eastern slope of Richardson Mountains northwestern District of Mackenzie 106M and 107B (parts of); Geol. Surv. Can., Paper 66-50.

1972: Stratigraphy, facies and palaeogeography of Mesozoic and Tertiary rocks of northern Yukon and northwest Mackenzie District, N. W. T. (NTS 107B, 106M, 117A, 116-O (N1/2), 116I, 116H, 116J, 116K (E 1/2); Geol. Surv. Can., Open File 82.

1973: Biochronology of the marine boreal latest Jurassic, Berriasian and Valanginian in Canada in The Boreal Lower Cretaceous, R. Casey and P. F. Rawson, eds.; Geol. J., Spec. Issue no. 5, p. 41-80.

1974: Contribution to the Jurassic and Cretaceous geology of northern Yukon Territory and District of Mackenzie, Northwest Territories: Geol. Surv. Can., Paper 74-10.

Millioud, M. E.

1967: Palynological study of the type localities at Valangin and Hauterive; Rev. Palaeobot. Palynol., v. 5, p. 155-167.

1969: Dinoflagellates and acritarchs from some western European Lower Cretaceous type localities *in* Proc. First Intern. Conf. Planktonic Microfossils Geneva, 1967, P. Bronnimann and H. H. Renz, eds.; E. J. Brill, Leiden, v. 2, p. 420-434.

Myhr, D. W. and Young, F. G.

1975: Lower Cretaceous (Neocomian) sandstone sequence of Mackenzie Delta and Richardson Mountains area; *in* Report of Activities, Part C, Geol. Surv. Can., Paper 75-1C, p. 247-266.

Pocock, S. A. J.
A preliminary dinoflagellate zonation of the uppermost Jurassic and lower part of the Cretaceous in the Canadian Arctic and possible correlation southward into the Western Canada Basin; Geosci. Man. (in press)

Vozzhennikova, T. F.
1967: Iskopaemye peridinei yruskikh, melovykh i paleogenovykh otlozheniy SSSR; Akad Nauk SSSR, Sib. Otd., Inst. Geol. Geofiz., Tr., (Fossil peridinians of the Jurassic, Cretaceous and Paleogene deposits of the U. S. S. R.).

Warren, J. S.
1967: Dinoflagellates and acritarchs from the Upper Jurassic and Lower Cretaceous rocks on the west side of the Sacramento Valley, California; Unpubl. Ph. D. Dissert., Stanford University, Palo Alto, California.

Williams, G. L.
1975: Dinoflagellate and spore stratigraphy of the Mesozoic-Cenozoic, offshore Eastern Canada; Geol. Surv. Can., Paper 74-30, v. 2, p. 107-161.

Yorath, C. J., Myhr, D. W., and Young, F. G.
1975: The geology of the Beaufort-Mackenzie Basin; Geol. Surv. Can., Open File 251.

Yorath, C. J. and Norris, D. K.
1975: The tectonic development of the southern Beaufort Sea and its relationship to the origin of the Arctic Ocean basin in Canada's continental margins and offshore petroleum exploration, C. J. Yorath, *et al.*, eds.; Can. Soc. Pet. Geol., Mem. 4, p. 589-611.

Young, F. G., Myhr, S. W., and Yorath, C. J.
The geology of the Beaufort-Mackenzie Basin; Geol. Surv. Can., Paper 76-11. (in prep.)

APPENDIX

Description of sections

Section 75-BIA-007 (upper part)
lat. 68°12'00"N, long. 135°37'20"W

	Unit Thickness (m)	Height above base (m)
HUSKY FORMATION		
Red-weathering shale member		
Dark grey shale, in places interbedded with siltstone, weathering light grey or brownish grey; ferruginous brown-weathering siltstone bed 18.2 to 18.3 m above base of unit; ferruginous, often indurated clay-ironstone, beds at 14.4, 8.8 and 4.2 m above base of unit. Top of section and unit concealed beneath overburden and overgrown slope.	25.0	(136.1)*

(*) The unit is underlain by 18.3 m assigned to the ?Arenaceous member and further underlain by 92.8 m of Lower member, both of the Husky Formation but not described for purposes of this paper.

Section 75-YA-MKA-001
(= Sec. BIA-73-26)
lat. 68°12'20"N, long. 135°36'00"W.

Lower sandstone division		
Buff sandstone unit		
Light grey to brownish white, fine grained to very fine grained sandstone, thickly bedded, wedge-shaped t festoon cross-stratification. Cliff-forming resistant unit. Top concealed by overburden and overgrown slope. Fossiliferous beds 3.0-5.0 m (GSC loc. C-49969), 5.6 m (GSC Loc. C-49970) and 26.1 m (GSC loc. C-49971) above the base of the unit	30.6	77.1
HUSKY FORMATION		
Upper member		
Light brownish grey, fine grained sandstone, brown weathering; shale partings	0.7	46.7
Interbedded, very fine grained crossbedded sandstone weathering brownish grey; siltstone, argillaceous, well laminated, weathering brownish grey	1.8	46.0
Dark grey mudstone, silty to sandy, laminated, with minor fine grained sandstone beds (1 cm thick) grading into interlaminated brown, fine grained sandstone with shale partings	2.8	44.2
Brownish grey, very fine grained sandstone or siltstone, poorly consolidated, friable, with argillaceous partings at base of unit. Fossiliferous bed 1.0 m (GSC loc. C-49967) above base of unit	2.7	41.4

	Unit Thickness (m)	Height above base (m)
Very fine grained sandstone and mudstone, bioturbated sandstone beds with parallel or faintly cross-stratified laminae, grading into very fine grained, bioturbated sandstone; sandstone content about 70 per cent	3.6	38.7
Dark grey shale, strongly bioturbated where exposed; mostly covered, recessive unit	6.9	35.1
Light grey, fine grained sandstone with wavy rippled laminae, flaggy weathering; interbedded with medium grey mudstone, bioturbated, weathering reddish brown	4.2	28.2
Dark grey mudstone, silty; recessive unit	1.2	24.0
Interbedded dark grey siltstone and cross-laminated fine grained sandstone, grading into interbedded mudstone and fine grained sandstone, crossbedded, weathering bluish grey to greenish grey; a lens of carbonaceous shale occurs in the top 0.4 m of the unit. Fossiliferous beds 0.0 to 1.0 m (GSC loc. C-49964) (in part), 1.0 to 1.9 m (GSC loc. C-49965) and 3.2 m (GSC loc. C-49966) above base of unit	4.9	22.8
Medium grey to dark grey shale and siltstone, reddish brown to yellow weathering, and yellow-streaked near the base of the unit; some fine grained sandstone ferruginous and reddish brown weathering, grading to dark grey mudstone, bioturbated and blocky weathering. Fossiliferous beds 4.0 to 4.8 m (GSC loc. C-49963) and 8.1 to 9.2 m (GSC loc. C-49964) (in part) above base of unit	9.2	17.9
Argillaceous siltstone, dark grey, weathering reddish brown	0.4	8.7
Medium grey to dark grey shale, interbedded with medium grey siltstone, weathering reddish brown to grey; rare laminae of fossil hash	8.3	8.3
Base of section concealed, likely containing the contact with the underlying Red-weathering shale member. An estimated 5 to 10 m of section obscured by slumped material		

Section 75-BIA-005 (lower part)
(= Sec. BIA-73-27 in part)
lat. 68°12'10"N, long. 135°34'50"W.

Approximately 33.5 m of the White sandstone unit, underlain by 16.7 m of the Bluish-grey shale unit, overlie the Buff sandstone unit at this location. These units are not described in this paper.

Lower sandstone division Buff sandstone unit	Unit Thickness (m)	Height above base (m)
Yellowish grey, fine grained sandstone, weathering yellowish brown to pale reddish brown, bioturbated with flecks or lenses of carbonaceous material; laterally, beds at about 1.0 m below the top of the unit yield fossil wood fragments or parts of trunks	4.3	78.0
Light to medium grey, fine grained sandstone, weathering maroon; high-angle cross-stratification; resistant unit	13.2	73.7
Fine grained sandstone weathering yellowish brown, with carbonaceous flecks and bands; discontinuous ferruginous concretionary bed at base of the unit	0.4	60.5
Light to medium grey fine grained sandstone, maroon weathering; high-angle cross-stratification resistant, cliff-forming unit	14.4	60.1
Fine- to medium-grained sandstone, yellowish brown to reddish brown weathering, low-angle cross-stratification, thin bedded; some sandy siltstone beds; 3 cm shale bed occurs 26.2 m from the top of the unit; fossiliferous bed 41.2 m from the top of the unit	45.7	45.7
Base of section concealed beneath slumped material. An approximate overlap of 10 m exists between the basal unit of this section and the topmost unit of Section 75-YA-MKA-001		

24. NEW RECORDS AND RANGE EXTENSIONS OF SEVEN RUGOSE CORAL GENERA IN SILURIAN STRATA OF NORTHWESTERN AND ARCTIC CANADA

Project 500029

A. E. H. Pedder and R. A. McLean
Institute of Sedimentary and Petroleum Geology, Calgary

Occurrences of the rugose coral genera *Stylopleura, Niajuphyllum, Yassia, Migmatophyllum, Prohexagonaria, Stereoxylodes* (*Nanshanophyllum*), *Xystriphyllum, Mazaphyllum* and *Rhyzophylloides* in Upper Silurian rocks of either Yukon Territory or the Canadian arctic islands have been demonstrated previously (Pedder, 1971, 1976a, b). The present paper adds *Denayphyllum, Ptychophyllum, Radiastraea, Kymocystis* and *Spinolasma* to the list of the Late Silurian coral genera present in these regions. It also demonstrates a possible Wenlock (*amorphognathoides* Conodont Zone) occurrence of *Ketophyllum* in southwestern District of Mackenzie (hitherto no western or arctic Canadian occurrence of this genus was known), and extends the known geographic range of *Prohexagonaria* in North America from Nevada and Cornwallis Island to northern Yukon Territory.

Formal description of the species represented by these occurrences will be attempted as more material becomes available. At the present time several of the genera are known from only one or two specimens collected during reconnaissance geological studies.

Family STAURIIDAE Milne-Edwards and Haime, 1850

Genus *Denayphyllum* Merriam, 1974, p. 56, 57

Type species. *Denayphyllum denayense* Merriam, 1974, p. 57, pl. 7, figs. 15-18. Roberts Mountain Formation, lower beds of unit 3. Silurian coral zone C. Northwest side of Roberts Creek Mountain, Nevada. Merriam correlated his coral zone C with the Wenlock Series, but Pedder (1976b, p. 290) and Johnson and Oliver (in press) have concluded, independently, that it is probably Pridolian.

Remarks. *Denayphyllum* may be diagnosed as follows: corallum phaceloid to subcerioid, produced by non-parricidal, lateral increase. Corallite wall thin to moderately thick, not a septal sterozone. Septa well differentiated into two orders, wavy without being carinate. Dissepiments relatively large, typically in one uniform series. Tabulae complete, widely spaced and normally slightly concave.

The genera *Spongophyllum* Milne-Edwards and Haime, 1951 and *Neomphyma* Soshkina, 1937 are distinguished from *Denayphyllum* by having presepiments as well as dissepiments. *Fasciphyllum* Schlüter, 1885 and its possible senior synonym *Battersbyia* Milne-Edwards and Haime, 1951 have a peripheral septal stereozone. *Loyolophyllum* Chapman, 1914 is cerioid and locally lacks dissepiments. *Planetophyllum* Crickmay, 1960, which appears to be a direct offshoot from *Spongonaria* and is unlikely to be closely related to

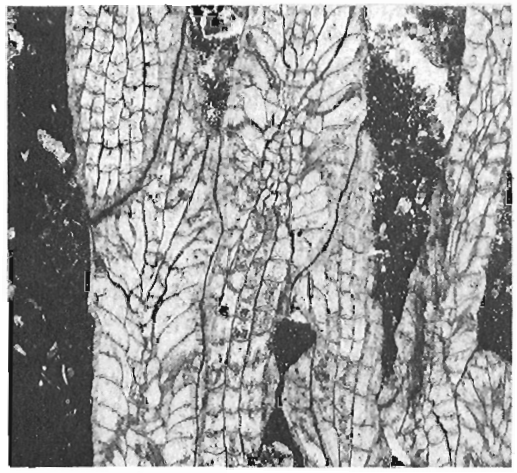

1

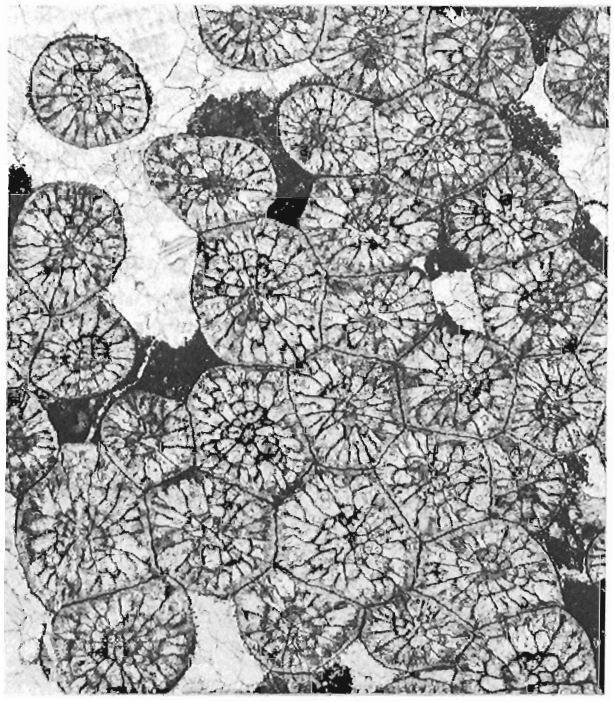

2

Figures 24.1 and 24.2

Denayphyllum sp. nov., x5. GSC 44918. Road River Formation; lower Pridolian part; 109.8-119.2 m (360-391 ft.) above base of section. Royal Creek headwaters Section 2, Yukon Territory; 64°46'30"N, 135°14'10"W; GSC locality 69307. Collected by A. C. Lenz, 1965.

From: Report of Activities, Part C;
Geol. Surv. Can., Paper 76-1C (1976).

Denayphyllum, is dendroid, has much shorter major septa, relatively longer minor septa, and a much narrower dissepimentarium.

The Royal Creek occurrence of *Denayphyllum* is the only one known outside Nevada. It is dated as Pridolian by direct association with conodonts, recognized by G. Klapper as being indicative of the *Pelekysgnathus index* fauna (Klapper and Murphy, 1974). The new specimen is probably not conspecific with *D. denayense* as it is larger (corallite diameter 3.5 mm, compared with 2.5 mm in *D. denayense*), has better developed minor septa, and generally more numerous major septa (typically 14, compares with 12 in *D. denayense*).

Family KETOPHYLLIDAE Lecompte, 1952

The genera assigned to this family are *Heterolasma* Ehlers, 1919 (=*Heterelasma* Lang, Smith and Thomas, 1940), *Ketophyllum* Wedekind, 1927 (=*Dokophyllum* Wedekind, 1927, *Cetophyllum* Lang, Smith and Thomas, 1940 and *Docophyllum* Lang, Smith and Thomas, 1940), *Lindstroemophyllum* Wang, 1947, *Mictocystis* Etheridge, 1908, and *Yassia* Jones, 1930 (=*Crinophyllum* Jones, 1932 and *Klamathastraea* Merriam, 1972).

These have broad tabularia, composed of wide, characteristically grouped tabulae, that may be depressed, flat or elevated. Their septa are amplexoid, appearing discontinuous in transverse section, and are commonly well withdrawn from the axis. A tabular fossula may be present. Dissepiments appear to be absent from *Heterolasma* and *Lindstroemophyllum*; in other genera they tend to be relatively large and elongated.

Many previous workers have placed these genera in either the Omphymatidae Wedekind, 1927, or the Chonophyllidae Holmes, 1887. However, the genus *Omphyma* Rafineque and Clifford, 1820 is unrecognizable (Lang *et al.*, 1940, p. 90, 91), and Oliver and Galle's (1971, p. 67-69) review of the Chonophyllidae suggests that *Ketophyllum* and other forms with simple amplexoid septa should not be included in the family. We are unable to accept Ivanoviskiy's (1975, p. 77) interpretation of the Ketophyllidae, since we consider *Dentilasma*, *Nipponophyllum* and *Cayugaea* to be cystiphyllids. The family Dokophyllidae Soshkina, 1962 is synonymous with Ketophyllidae.

Genus *Ketophyllum* Wedekind, 1927, p. 48, 51, 52

Type species. *Ketophyllum* (*Omphyma*) *elegantulum* Wedekind, 1927, p. 55, Pl. 10, figs. 5, 6, 8-11, Pl. 13, figs. 3, 4. Omphymenmergel, which is the Klinteberg Beds (Upper Wenlock to Lower Ludlow) of current terminology. Eksta, Djupvik, Gotland. Smith (1945, p. 26, 27) believed this species to be conspecific with *Turbinolia turbinata verrucosa* Hisinger, 1831, which is based on specimens from the same locality.

Remarks. Species of this genus are normally solitary, have patellate to subcylindrical corralites, and commonly develop tubercles or supporting talons. Internally they

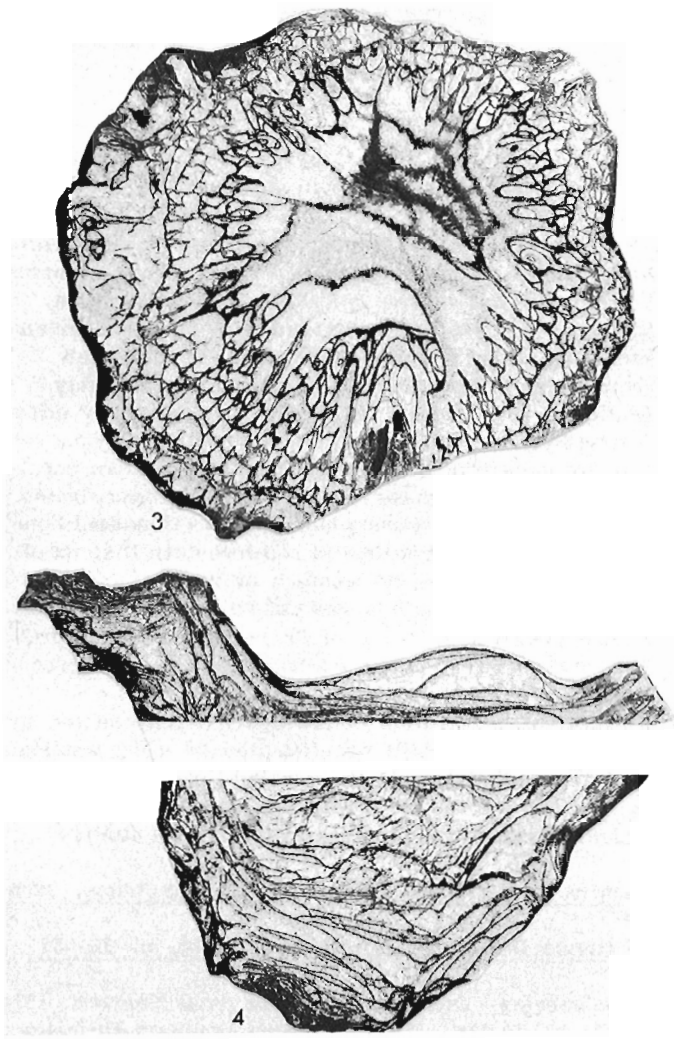

Figures 24.3 and 24.4

Ketophyllum sp. undet, x2. GSC 44919. Whittaker/Road River transition beds; possibly equivalent to the Wenlock Series. 9.7 km (6.0 miles) east of Avalanche Lake, District of Mackenzie; 62°23'N, 127°03'W. Collected by A.C. Lenz, 1975.

are characterized by well-developed amplexoid septa, large, elongate presepiments and broad, more or less flat tabulae, that may be grouped, and may also form a tabular fossula.

Dokophyllum Wedekind, 1927, which is based on *D. annulatum* Wedekind (1927, p. 49, Pl. 9, figs. 13-15, Pl. 14, fig. 1), from Wenlock strata, north of Kneippbyn, Visby, Gotland, is synonymous with *Ketophyllum* (Smith, 1945, p. 27; Hill, 1956, p. 300; Minato, 1961, p. 91).

Ketophyllum is known from the Upper Llandovery (Adavere Stage) of Estonia (Kal'o, 1970, Upper Llandovery (Rosyth Limestone) of New South Wales (McLean, 1974), Upper Llandovery and/or Wenlock (Manistique Dolomite) of Michigan (Stumm, 1965), Upper Llandovery and Wenlock (La Vieille Formation) of Gaspé Peninsula, Quebec (Lambe, 1901; Northrop, 1939),

Lower Wenlock (K Beds) of the Zeravshan-Gissar Mountains region of Tadzhikistan (Lavrusevich, 1971b), Wenlock of Britain (Butler, 1937), Wenlock and Lower Ludlow of Gotland (Wedekind, 1927), Wenlock of Vaygach Island (Strel'nikov, 1965), Wenlock (Chagyrska Suite) of Mountain Altay (Zheltonogova, 1960, 1965), Wenlock? (age in doubt) of Yunnan (Wang, 1944), Upper Wenlock and/or Lower Ludlow (Louisville Limestone) of Indiana and Kentucky (Stumm, 1965) Wenlock and/or Lower Ludlow (Tachlowitz Limestone) of Czechoslovakia (Pocta, 1902), Lower Ludlow (Gascons Formation) of Gaspé Peninsula, Quebec (Northrop, 1939), Ludlow of the Karagandin Basin, central Kazakhstan (Bul'vanker *et al.*, 1960), Pridolian (Jack Limestone), northern Queensland (Hill *et al.*, 1969; Telford, 1975) and from undifferentiated Upper Silurian of the western slope of the southern Urals (Tyazheva and Zhavoronkova, 1972). Faunal lists assembled by Bassler (1950) indicate its presence in Upper Llandovery strata of Britain and Ireland, but we have not seen specimens, or illustrations of specimens, from these strata. *Ketophyllum* may also occur in the Ludlow or Pridolian Borovushka Suite of Rudney Altay (Sytova, 1966) and the Pridolian Kunzhak Beds of the Zeravshan-Gissar Mountains region of Tadzhikistan (Lavrusevich, 1968). The new specimen, figured here, comes from beds regarded by A. C. Lenz as being transitional between the Whittaker and Road River formations, near Avalanche Lake in southwestern District of Mackenzie. It occurs 105 m (345 ft) below a Wenlock brachiopod and trilobite fauna, identified by A. C. Lenz, and with *Atrypella* sp. ex. gr. *scheii*, also identified by A. C. Lenz, and conodonts of the *amorphognathoides* Zone, identified by B. D. E. Chatterton and D. G. Perry. It is possibly equivalent to the Upper Llandovery Series, but is considered by Lenz to be more likely equivalent to the Lower Wenlock Series because of the presence of *Atrypella*.

Family CYATHOPHYLLIDAE Dana, 1846

Subfamily ARACHNOPHYLLINAE Dybowski, 1973

Genus *Prohexagonaria* Merriam, 1974, p. 50

Type species. *Entelophylloides* (*Prohexagonaria*) *occidentalis* Merriam, 1974, p. 50, 51, Pl. 9, figs. 1-4. Roberts Mountains Formation, lower beds of unit 3, Silurian coral zone C. Northwest side of Roberts Creek Mountain, Nevada. Pedder (1976b, p. 290) and Johnson and Oliver (in press) have concluded, independently, that the age of the type horizon is probably Pridolian, not Wenlock as Merriam supposed.

Remarks. A generic diagnosis and the known distribution of *Prohexagonaria* has been given by Pedder (*op. cit.*). The earlier diagnosis should now be emended to include forms with subcerioid, as well cerioid coralla. The specimen illustrated here comes from unnamed limestone at the southwest corner of the White Mountains. The associated fauna is Silurian, and since it overlies a Ludlow or Pridolian fauna (GSC loc. C-10934), consisting

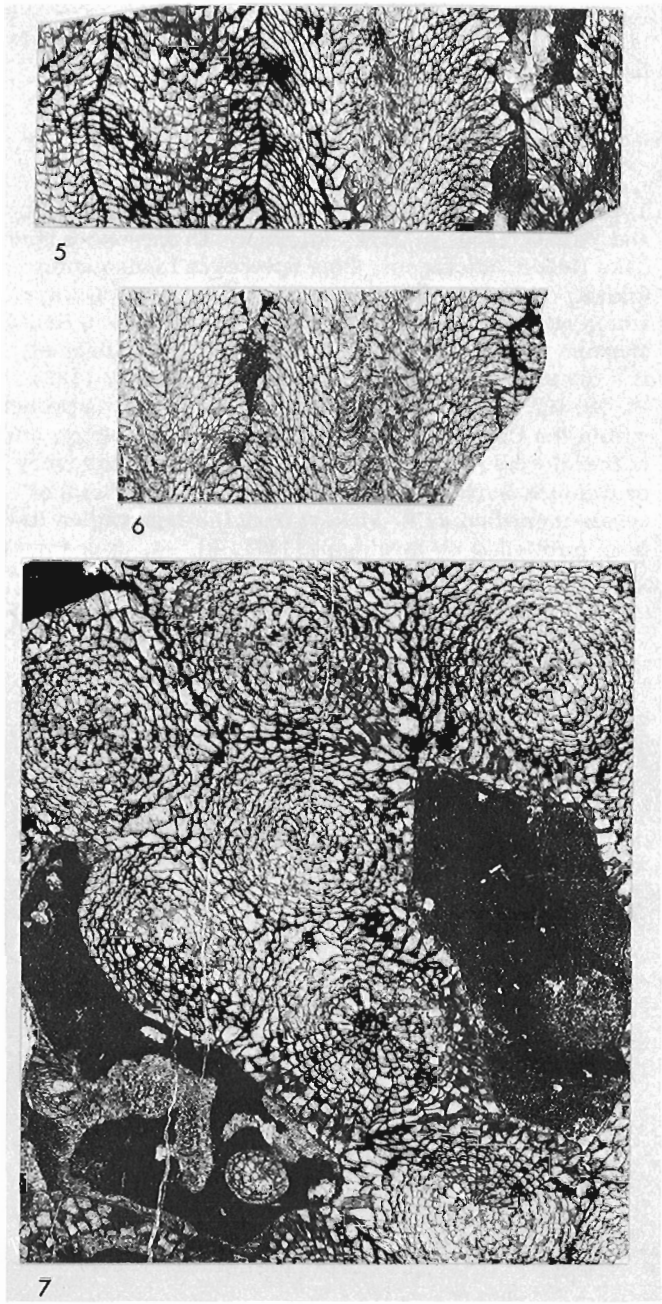

Figures 24.5 to 24.7

Prohexagonaria sp. nov., x3. GSC 44920. Unnamed limestone of probable Pridolian age. Southwest corner of the White Mountains, Yukon Territory; 67°54'N, 136°41'W; GSC locality C-10933. Collected by L. D. Dyke, 1971.

of *Amphipora* sp., *Parastriatopora* sp., and *Zelophyllum* sp., is probably Pridolian. The new specimen is similar to the specimen from Pridolian strata on Cornwallis Island, but is subcerioid and slightly larger (corallite diameter mostly 9.0-11.0 m, compared with 8.0-9.0 m in the Cornwallis Island specimen); it also has more septa (about 22 x 2, compared with 19 x 2 in the Cornwallis

Island specimen). With the limited material available it is not known whether the White Mountains and Cornwallis Island specimens represent one or two new species.

Genus *Ptychophyllum* Milne-Edwards and Haime, 1850, p. 1xix

Type species. *Ptychophyllum stokesi* Milne-Edwards and Haime, 1850, p. 1xix, Silurian. Drummond Island, Lake Huron, Michigan. This species is inadequately known. The only illustration available of the lectotype, which was chosen by Smith (1945, p. 51) and is British Museum specimen R 25162, Charles Stokes Collection, is a drawing of the calice published by Bigsby (1824, Pl. 29, fig. 1, right figure). The type stratum is probably within the Cordell Dolomite of present terminology, and is therefore equivalent to either the Upper Llandovery or Wenlock Series. Photographs of exterior views of corals identified as *P. stokesi* from the type region have been published by Rominger (1877, Pl. 44, upper tier), Smith (1945, Pl. 35, fig. 2a), Bolton (1966, Pl. 5, fig. 10) and Ehlers (1973, Pl. 6, figs. 5, 6). The only photograph of the interior of a specimen from the type area to date are of a transverse section given by Smith (1945, Pl. 35, fig. 2b). Hill (1935, Textfigs. 21C, D) published drawings of longitudinal and transverse sections of one or two corals identified as *P. stokesi*. However, the stratigraphic and geographic origin of this material was not provided.

Remarks. Species currently referred to *Ptychophyllum* have: 1) a solitary, patellate to subcylindrical corallum; 2) long, typically slender, axially rotated major septa and variably developed minor septa; 3) relatively small, globose to elongate dissepiments, that commonly fail to bridge the interseptal loculus; 4) abundant, incomplete and locally vesicular tabulae. Where axial rotation of the major septa is strong the tabularial floors are generally broadly elevated, forming an axial boss; where the rotation is weak, they are generally elevated periaxially and depressed axially.

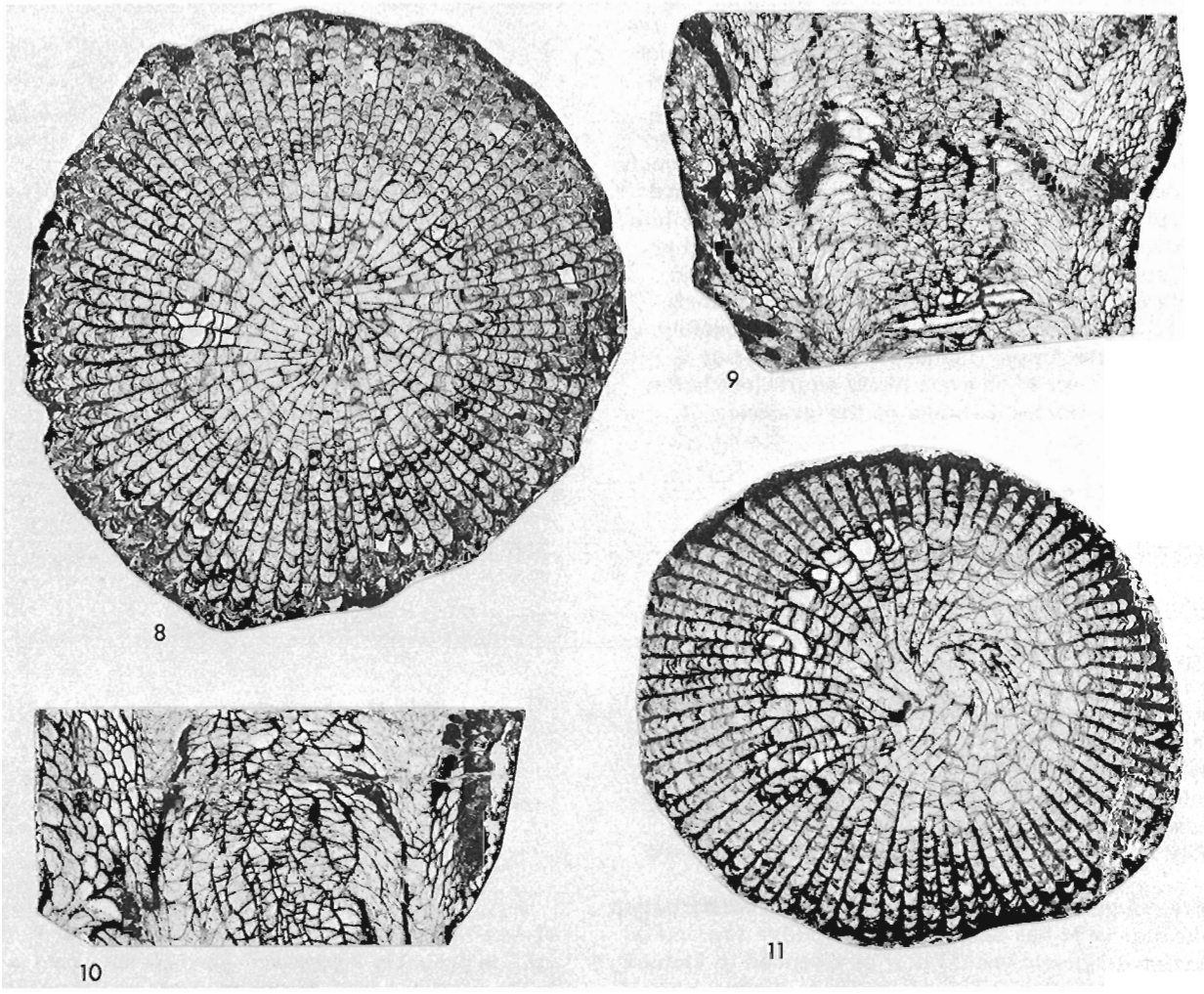

Figures 24.8 to 24.11. *Ptychophyllum* sp. nov., x3. Figures 24.8, 24.9, GSC 44921. Figures 24.10, 24.11, GSC 44922. Douro Formation, equivalent probably to lower Pridolian, possibly to Middle or Upper Ludlow Series. Grinnell Peninsula, Devon Island, District of Franklin; UTM Zone 15, 445100 m E, 8467700 m N; GSC locality C-22907. Collected by J. W. Kerr, 1972.

Sytova (*in* Sytova and Ulitina, 1966, p. 239) erected the genus *Implicophyllum* for corals differentiated from *Ptychophyllum* only in lacking lateral dissepiments. The type species is *I. vesiculosum* Sytova (*op. cit.*, p. 240, 241, Pl. 46, figs. 2a-v) from the upper part of the Ayansu "Horizon" of the Karaganda Basin, central Kazakhstan. We regard the development of lateral dissepiments to be too variable in *Ptychophyllum* to justify a separate genus for specimens lacking them.

The known distribution of *Ptychophyllum* is Upper Llandovery (Sandpile Group), Cassiar Mountains, northern British Columbia (Norford, 1962); Upper Llandovery (Offley Island Formation), northwestern Greenland (McLean, in prep.); Upper Llandovery of the Siberian Platform (Ivanovskiy, 1963, 1965); Upper Llandovery (Rosyth, Quarry Creek and other limestones), central New South Wales (McLean, 1975; Upper Llandovery and/or Wenlock of northern Michigan and southern Ontario (*see* above); Wenlock, River Kozhim, Pripolar Urals (Strel'nikov, 1972), undifferentiated Silurian (Graveyard Creek Formation), northern Queensland (Hill *et al.*, 1969); undifferentiated Upper Silurian (Hardwood Mountain and Cranbourne Limestones) of Maine and Quebec (Stumm, 1962) and possible Pridolian strata (*Nataliella poslavskajae* Zone of the Upper Aynasu "Horizon") of central Kazakhstan (*see* above).

The new material comprises two specimens from the Douro Formation of Grinnel Peninsula, Devon Island. Conodonts of the associated fauna include *Ozarkodina confluens* α and γ morphotypes of Klapper (*in* Klapper and Murphy, 1974), *O. excavata* and "*O.*" *ziegleri*, all of which were identified by T. T. Uyeno. These indicate a Middle Ludlow to early Pridolian age, but since *Radiastraea* is also present in the fauna, an early Pridolian age seems more probable. The Devon Island species of *Ptychophyllum* is probably new. It resembles *P. sibiricum* Ivanovskiy, but has finer and less numerous septa (43 x 2 where diameter of corallite is 28.0 mm in the Devon Island species; 46 x 2 where the diameter is 21.0-22.0 mm in *P. sibiricum*).

Genus *Radiastraea* Stumm, 1937, p. 439

Type species. *Radiastraea arachne* Stumm, 1937, p. 439, 440, Pl. 53, fig. 13, Pl. 55, figs. 8a, b. Basal 152 m (500 ft) of the Nevada Limestone. Lone Mountain, 28 km (18 miles) northwest of Eureka, Nevada. Additional figures of this species have been published by Merriam (1940, Pl. 13, fig. 5) and Pedder (1964, Pl. 72, figs. 1-3, Pl. 73, figs. 1-5). The type stratum is within the Bartine Member of the McColley Canyon Formation of current nomenclature, and is either late Pragian or Zlichovian (Early Devonian) in age.

Remarks. Most corals assigned to *Radiastraea* have a massive, asteroid to thamnasterioid corallum; a few are just aphroid, or pseudocerioid (term defined by Scrutton, 1968, p. 192). Major septa commonly reach the axial region where they may form an axial vortex; minor septa generally only just penetrate the tabularium. The two orders of septa are normally indistinguishable in the dissepimentarium. Septa may be smooth, but more commonly are carinate; zigzag carinae predominate over crossbar carinae. Trabeculae are vertical, or almost so, in the outer dissepimentarium, but radiate inward in the inner region of the dissepimentarium. In our Upper Silurian and Lower Devonian material they are scarce, fine and recrystallized, whereas in our Eifelian material they may be abundant, in some cases causing considerable dilation of the septa in the inner dissepimentarium, and are clearly monacanthine. Dissepiments are well inflated and show periodic variations in size, although normally they are never either horseshoe shaped or large. Typically they are horizontal at the periphery, and steeply inclined and smaller adaxially; some dissepimentarial surfaces are slightly elevated immediately exterior of the tabularium. Tabulae are almost invariably incomplete and display considerable variation in shape. Tabularial floors also vary, but commonly are flat to gently concave peripherally, outwardly inclined periaxially, and depressed, flat or elevated axially.

Radiastraea was erected principally because intersections of rotated major septa were interpreted as an axial aulos. Stumm (1949, p. 35) later corrected this misinterpretation and suppressed *Radiastraea* in favour of *Billingsastraea* Grabau, 1917. This synonymy was rejected by Pedder (1964, p. 447), and by Oliver (1974, p. 167, 168) who argued convincingly that the type species of *Billingsastraea* may well have been based on a Silurian species of *Arachnophyllum* from the Hopkinton Dolomite of southwestern Wisconsin.

Radiastraea most probably evolved from a Silurian species of *Arachnophyllum* by acquisition of lamellar septa, although, as one of us has pointed out (McLean, 1975, p. 54, 55), *Arachnophyllum* requires further study. In Early Devonian time certain species of *Radiastraea* appear to have given rise to *Phillipsastrea* by development of a more prominently everted dissepimentarium, containing some horseshoe dissepiments, and a narrower, more symmetrical zone of trabecular divergence. These changes may have occurred in more than one lineage.

Several of the less well described species of *Phillipsastrea* may be better placed in *Radiastraea*. Omitting these, the previously known distribution of *Radiastraea* may be summarized as Upper Lochkovian to Pragian (Martin's Well Limestone), northern Queensland (Hill *et al.*, 1967; Telford, 1975); Pragian (part of the Garra Formation), Wellington area of New South Wales (Strusz, 1965); upper Pragian (*Etymothyris* Zone of Gaspé Limestone), Gaspé Peninsula, Quebec (Oliver, 1964); upper Pragian or Zlichovian (Bartine Limestone) of Nevada (*see* above); Eifelian (Hume, Nahanni, Headless and other limestones), northwestern Canada (Pedder, 1964); Eifelian of Vaygach Island, northwestern Soviet Union (Spasskiy and Cherepnina, 1972); Givetian (Wolborough Quarry Limestone), southwestern Britain (Scrutton, 1967). The new material, which represents two species, is from unnamed limestone on Cornwallis Island and the Douro Formation on Grinnell Peninsula, Devon Island. Evidence for a Pridolian age determination for the

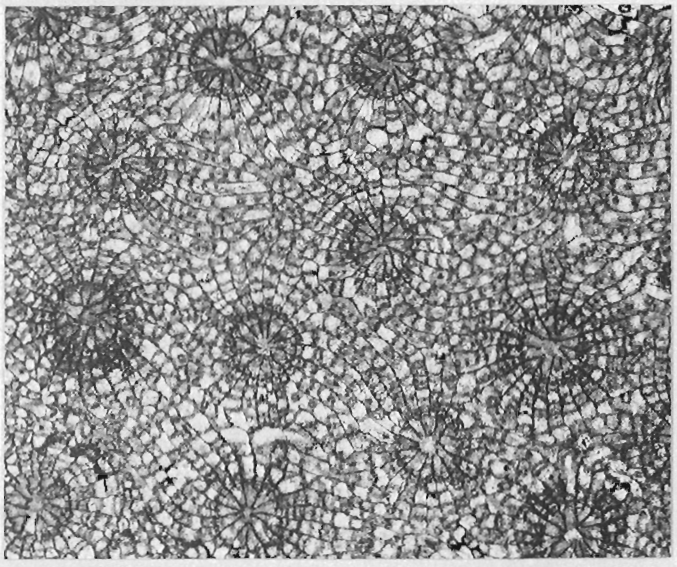

12

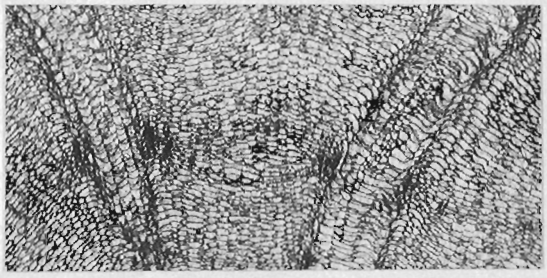

13

14

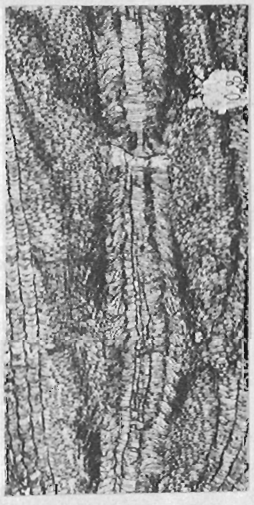

15

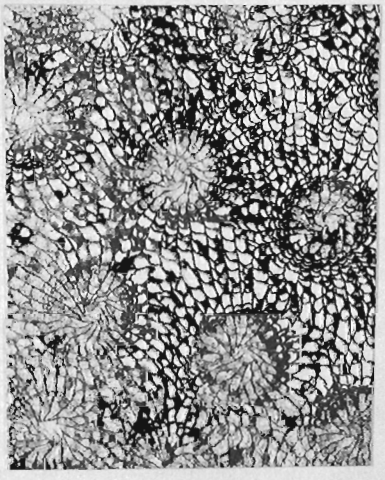

16

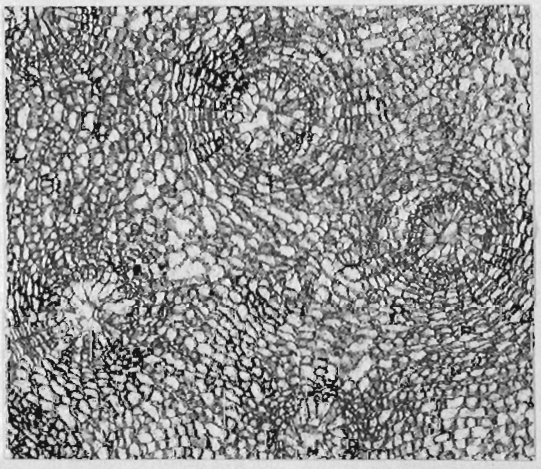

17

18

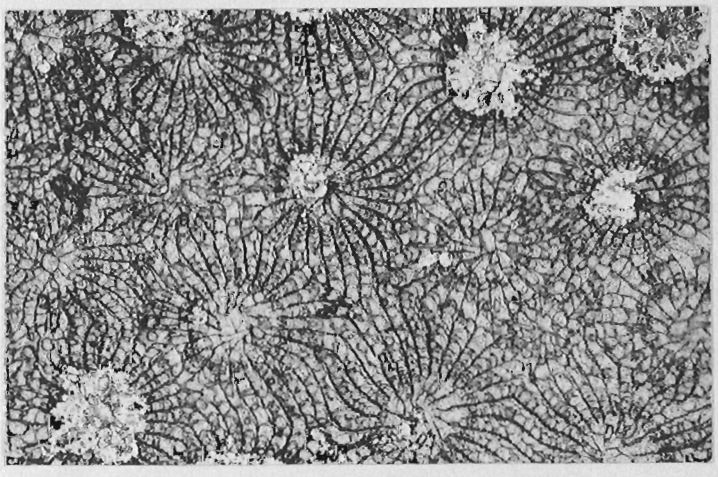

19

Cornwallis Island occurrence was given recently by Pedder (1976b, p. 290). The other occurrence is the same as that of the *Ptychophyllum* species discussed above. It may be equivalent to the Upper Ludlow Series, but the presence of *Radiastraea* itself argues for a Pridolian age.

Family CYSTIPHYLLIDAE Milne-Edwards and Haime, 1850

Subfamily CYSTIPHYLLINAE Milne-Edwards and Haime, 1850

Genus *Kymocystis* Strel'nikov, 1968, p. 15

Type species. *Kymocystis notabilis* Strel'nikov, 1968, p. 15, 16, Pl. 1, figs. 1a-2. Upper Wenlock. River Shar'yu, central part of the Chernyshev Ridge, northwestern Russia.

Remarks. Species of *Kymocystis* are solitary and have short, discrete holacanthine septal spines, based on dissepimental crests and commonly displaying weak radial alignment. Dissepiments and tabellae are generally clearly differentiated. The most diagnostic feature, differentiating the genus from *Cystiphyllum*, is the irregular undulatory surface of the dissepiments.

The distribution of *Kymocystis*, as presently known, is Upper Llandovery of the Siberian Platform (Ivanovskiy, 1963); Upper Wenlock of Chernyshev Ridge, northwestern Russia, and Pripolar Urals (Strel'nikov, 1968); Upper Ludlow or Pridolian (Douro Formation), Grinnell Peninsula, Devon Island (undescribed material) and Pridolian (unnamed limestone), near the mouth of Rookery Creek, northwestern Cornwallis Island (Figs. 20, 21). The age of the Cornwallis Island occurrence has been discussed previously (Pedder, 1976b, p. 290).

Figures 24.12 to 24.19 (opposite)

Radiastraea spp. nov., x4.
Figures 24.12, 24.14, GSC 44923. Unnamed Pridolian limestone. Marshall Peninsula, northwestern Cornwallis Island, District of Franklin; UTM Zone 14, 580100 m E, 8367600 m N; GSC locality C-3095. Collected by J.W. Kerr, 1965.
Figures 24.13, 24.17, GSC 44924. Unnamed Pridolian limestone. Near the mouth of Rookery Creek, northwestern Cornwallis Island, District of Franklin; UTM Zone 15, 420250 m E, 8365250 m N; GSC locality C-3094. Collected by J.W. Kerr, 1965.
Figure 24.15, GSC 44925. Douro Formation, equivalent probably to lower Pridolian, possibly to Middle or Upper Ludlow Series. Grinnell Peninsula, Devon Island, District of Franklin; UTM Zone 15, 445100 m E, 8467700 m N; GSC locality C-22907. Collected by J.W. Kerr, 1972.
Figure 24.16, GSC 44926. Same collection data as for specimen in Figure 24.15.
Figures 24.18, 24.19, GSC 44927. Same collection data as for specimen in Figure 24.15.

Genus *Spinolasma* Ivanovskiy, 1965, p. 124, 125

Type species. *Spinolasma crassimarginalis* Ivanovskiy, 1965, p. 125, 126, Textfig. 77, Pl. 39, figs. 3a, b. Upper Llandovery. River Gorbiyachin, Siberian Platform.

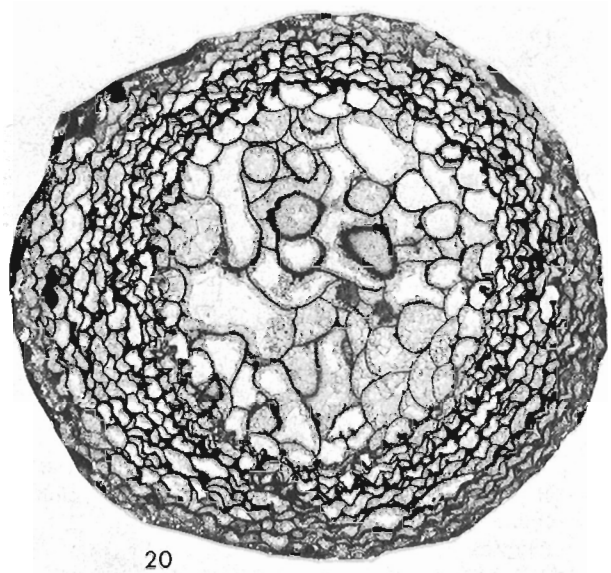

20

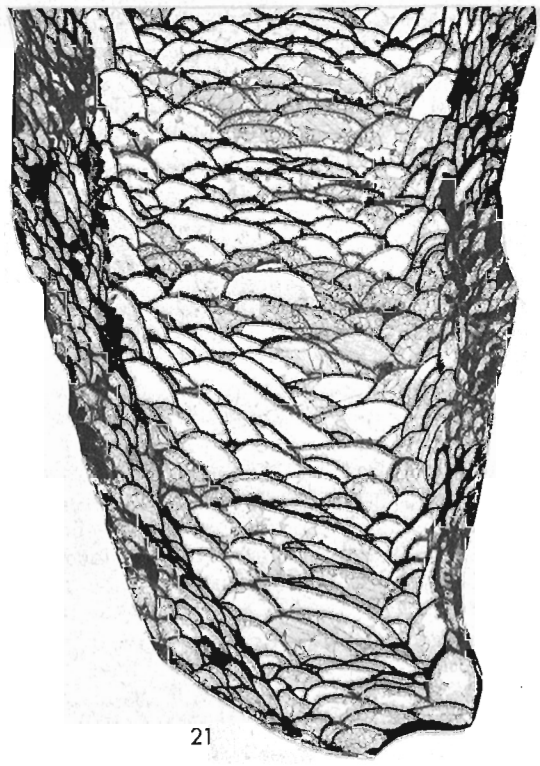

21

Figures 24.20 and 24.21

Kymocystis sp. nov., x3. GSC 44928. Unnamed Pridolian limestone. Marshall Peninsula, northwestern Cornwallis Island, District of Franklin; UTM Zone 14, 580100 m E, 8367600 m N; GSC locality C-3095, Collected by J.W. Kerr, 1965.

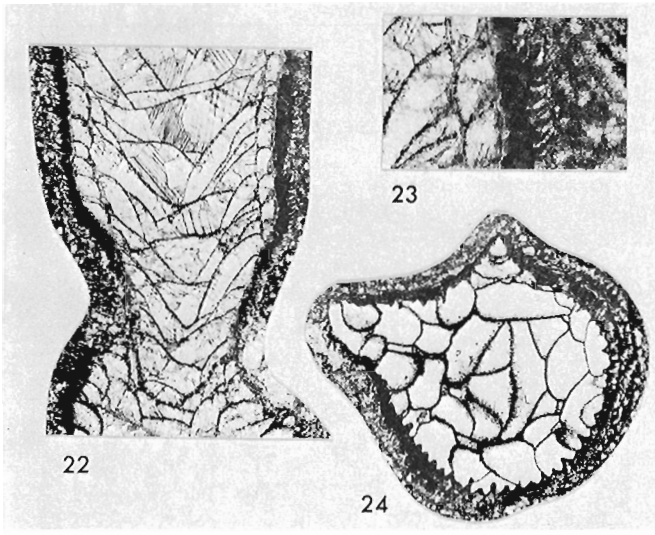

Figures 24.22 to 24.24

Spinolasma sp. cf. *S. squamosum* (Lavrusevich), Figure 24.22, 23 x 10, 24 x 4. GSC 44929. Unnamed limestone of probable Pridolian age. Southwest corner of the White Mountains, Yukon Territory, 67°54'N, 136°41'W. Collected by L.D. Dyke, 1971.

Remarks. *Spinolasma* is characterized by short, stout, septal spines, based mainly on the corallite wall and adjacent dissepiments, a narrow, clearly differentiated dissepimentarium, and a broad tabularium composed of both complete and incomplete tabulae. It differs from *Microplasma* Dybowski, 1873 in having a prominent tabularium and coarser trabeculae, and from *Dentilasma* Ivanovskiy, 1962 in having coarser and more abundant trabeculae.

The species *Holmophyllum taltiense* Nikolaeva, 1949 (=*H. heterovesiculosum* Nickolaeva, 1949) and *H. squamosum* Lavrusevich, 1960 differ from *H. holmi* Wedekind (Jell and Hill, 1970, Pl. 4, figs. 7a, b), the type species of *Holmophyllum* in having coarse, short trabeculae. In view of this, and since their horizontal skeletal elements are similar to those of *Spinolasma crassimarginalis*, McLean (1976, p. 297) suggested they be removed from *Holmophyllum* to *Spinolasma*. According to Lavrusevich (1971a, p. 40) both *S. taltiense* and *S. squamosum* have rhabdacanthine trabeculae. In the new material from Yukon Territory and possibly also in *S. crassimarginalis* the trabeculae are holacanthine, probably due to recrystallization.

Species of *Spinolasma* are known from Upper Llandovery of the Siberian Platform (*see* above), Wenlock (Chagyrska Suite), Mountain Altay (Zheltonogova, 1965), Upper Wenlock (Shikorkhonin Beds), Zeravshan-Gissar Mountains region of central Tadzhikistan (Lavrusevich, 1960, 1971b), Pridolian ("superludlovian Bobrovka Horizon"), River Tal'tiya, northern Urals (Nikolaeva, 1949; Sytova, 1971), probable Pridolian (unnamed limestone discussed above in the remarks concerning *Prohexagonaria*), White Mountains, northern Yukon Territory (Figs. 22-24), and Lochkovian (Shishkat "Horizon"), Zeravshan-Gissar Mountains region of central Tadzhikistan (Lavrusevich, 1968, 1971a).

Our new specimen closely resembles *S. squamosum* (Lavrusevich) from the Shikonkhonin Beds of Tadzhikistan and despite disparities of age may be conspecific with it. Epithecal scales are present on the Yukon specimen, but appear to be more abundant in specimens figured by Lavrusevich (1960, Textfigs. 1, 2; 1971b, Textfigs. 5a, b) from Tadzhikistan. Also, dissepiments are slightly longer in the Tadzhikistan specimens. The taxonomic significance of these differences will have to be evaluated when more material becomes availabe.

References

Bassler, R.S.
1950: Faunal lists and descriptions of Paleozoic corals; Geol. Soc. Am., Mem. 44.

Bigsby, J.
1824: Notes on the geography and geology of Lake Huron; Geol. Soc. London, Tr., ser. 2, v. 1, p. 175-208.

Bolton, T.E.
1966: Illustrations of Canadian fossils. Silurian faunas of Ontario; Geol. Surv. Can., Paper 66-5.

Bul'vanker, E.Z., Vasilyuk, N.P., Zheltonogova, V.A., Zhizhina, M.S., Nikolaeva, T.V., Spasskiy, N.Ya., and Shchukina, V.Ya.
1960: Novye predstaviteli chetyrekhluchevykh korallov SSSR, *in* Novye vidy drevnikh rasteniy i bespozvonochnykh SSSR, chast' I, B.P. Markovskiy, ed.; Gosgeoltekhizdat, Moskva, p. 220-254, 510-545.

Butler, A.J.
1937: A new species of *Omphyma* and some remarks on the *Pycnactis-Phaulactis* group of Silurian corals; Ann. Mag. Nat. Hist., ser. 10, v. 19, p. 87-96.

Ehlers, G.M.
1973: Stratigraphy of the Niagaran Series of the Northern Peninsula of Michigan; Univ. Michigan, Mus. Paleont., Papers Paleont., no. 3.

Hill, D.
1935: British terminology for rugose corals; Geol. Mag., v. 72, p. 481-519.

1956: Rugosa *in* Treatise on invertebrate paleontology, R.C. Moore, ed.; Geol. Soc. Am. and Univ. Kansas Press, Pt. F, Coelenterata, p. 233-324.

Hill, D., Playford, G., and Woods, J.T.
1967: Devonian fossils of Queensland; Queensland Palaeontogr. Soc., Brisbane.

Hill, D., Playford, G., and Woods, J.T. (cont'd.)
1969: Ordovician and Silurian fossils of Queensland; Queensland Palaeontogr. Soc., Brisbane.

Ivanovskiy, A.B.
1963: Rugozy ordovika i silura Sibiriskoy platformy; Akad. Nauk SSSR, Sib. Otdel., Izdatel'stvo Akad. Nauk SSSR, Moskva.

1965: Drevneyshie rugozy; Akad. Nauk SSSR, Sib. Otdel., Izdatel'stvo Nauka, Moskva.

1975: Rugozy; Akad. Nauk SSSR, Sib. Otdel., Inst. Geol. Geofiz., Trudy, vyp. 242.

Jell, J.S. and Hill, D.
1970: The Devonian coral fauna of the Point Hibbs Limestone, Tasmania; Roy. Soc. Tasmania, Papers Proc., v. 104, p. 1-16.

Johnson, J.G. and Oliver, W.A.
Silurian and Devonian coral zones in the Great Basin; Geol. Soc. Am., Bull. (in press)

Kal'o, D.L.
1970: Silur Estonii; Izdatel'stvo Valgus, Tallin.

Klapper, G. and Murphy, M.A.
1974: Silurian-Lower Devonian conodont sequence in the Roberts Mountains Formation of central Nevada; Univ. California Public. Geol. Sci., v. 111.

Lambe, L.M.
1901: A revision of the genera and species of Canadian Palaeozoic corals. The Madreporaria Aporosa and the Madreporaria Rugosa; Contri. Can. Palaeont., v. 4, pt. 2, p. 97-197 (1900).

Lang, W.D., Smith, S., and Thomas, H.D.
1940: Index of Palaeozoic coral genera; Brit. Mus. (Nat. Hist.), London.

Lavrusevich, A.I.
1960: *Holmophyllum* s cheshuychatoy epitekoy iz silura Zeravshano-Gissarskoy gornoy oblasti; Doklady Akad. Nauk Tadzhik. SSR, Trudy, tom 3, no. 4, p. 21-25.

1968: Rugozy postludlovskikh otlozheniy doliny r. Zeravshan (tsentral'nyy Tadzhikistan); *in* Biostratigrafiya pogranichnykh otlozheniy silura i devona, B.S. Sokolov and A.B. Ivanovskiy, eds.; Izdatel'stvo Nauka, Moskva, p. 102-130.

1971a: Cheshuychatye rugozy tsentral'nogo Tadzhikistana; *in* Rugozy i stromatoporoidei paleozoya SSSR, A.B. Ivanovskiy, ed., Trudy 2 Vsesoyuznogo simpoziuma po izucheniyu iskopaemykh korallov SSSR, vyp. 2, Izdatel'stvo Nauka, Moskva, p. 32-41, 138, 139.

Lavrusevich, A.I. (cont'd.)
1971b: Rugozy rannego silura Zeravshano-Gissarskoy gornoy oblasti; Upravleniya Geol. Soveta Ministrov Tadzhik. SSR, Trudy, Paleontol. i Stratigraf., vyp. 3, p. 38-136.

McLean, R.A.
1974: Chonophyllinid corals from the Silurian of New South Wales; Palaeontology, v. 17, pt. 3, p. 655-668.

1975: Lower Silurian rugose corals from central New South Wales; Roy. Soc. N.S.W., J. Proc., v. 108, p. 54-69.

1976: Genera and stratigraphic distribution of the Silurian and Devonian rugose coral family Cystiphyllidae Edwards and Haime; *in* Report of Activities, Part B; Geol. Surv. Can., Paper 76-1B, p. 295-301.

Merriam, C.W.
1940: Devonian stratigraphy and paleontology of the Roberts Mountains region, Nevada; Geol. Soc. Am., Spec. Papers, no. 25.

1972: Silurian rugose corals of the Klamath Mountain Region, California; U.S. Geol. Surv., Prof. Paper 738, Part IV, 50 p., 8 pl.

1974: Silurian rugose corals of the central and southwest Great Basin; U.S. Geol. Surv., Prof. Paper 777 (1973).

Milne-Edwards, H. and Haime J.
1850: A monograph of the British fossil corals. Part 1. Introduction and chapters I-VII; Palaeontogr. Soc. London.

Minato, M.
1961: Ontogenetic study of some Silurian corals of Gotland; Stockholm Contri. Geol., v. 8, no. 4, p. 37-100.

Nikolaeva, T.V.
1949: Otryad Tetracoralla (Rugosa); Atlas rukovodyashchikh form iskopaemykh faun SSSR, vyp. 2, Siluriyskaya sistema, p. 102-111 (not seen).

Norford, B.S.
1962: The Silurian fauna of the Sandpile Group of Northern British Columbia; Geol. Surv. Can., Bull. 78.

Northrop, S.A.
1939: Paleontology and stratigraphy of the Silurian rocks of the Port Daniel-Black Cape region, Gaspé; Geol. Soc. Am., Spec. Papers, no. 21.

Oliver, W.A.
1964: The Devonian colonial coral genus *Billingsastraea* and its earliest known species; U.S. Geol. Surv., Prof. Paper 483-B.

Oliver, W.A. (cont'd.)
1974: Classification and new genera of noncystimorph colonial rugose corals from the Onesquethaw State in New York and adjacent areas; U.S. Geol. Surv., J. Research, v. 2, no. 2, p. 165-174.

Oliver, W.A. and Galle, A.
1971: Rugose corals from the Upper Koněprusy Limestone (Lower Devonian) in Bohemia; Sborník Geol. Věd, Paleontol., řáda P., svazek 14, p. 35-106.

Pedder, A.E.H.
1964: Correlation of the Canadian Middle Devonian Hume and Nahanni Formations by tetracorals; Palaeontology, v. 7, pt. 3, p. 430-451.

1971: An Upper Silurian (Pridolian) coral faunule from northern Yukon Territory; Geol. Surv. Can., Bull. 197, p. 13-21.

1976a: Initial records of two unusual Late Silurian rugose coral genera from Yukon Territory; *in* Report of Activities, Part B; Geol. Surv. Can., Paper 76-1B, p. 285-286.

1976b: First records of five rugose coral genera from Upper Silurian rocks of the Canadian Arctic Islands; *in* Report of Activities, Part B; Geol. Surv. Can., Paper 76-1B, p. 287-293.

Pocta, P.
1902: Système Silurien du centre de la Bohême, v. 8, tome 2, Anthozoaires et Alcyonaires; Prague.

Rominger, C.
1877: Palaeontology Fossil corals; Geol. Surv. Michigan, v. 3, pt. 2 (1876).

Scrutton, C.T.
1967: Marisastridae (Rugosa) from south-east Devonshire, England; Palaeontology, v. 10, pt. 2, p. 266-279.

1968: Colonial Phillipsastraeidae from the Devonian of south-east Devon, England; Brit. Mus. (Nat. Hist.), Bull., Geol., v. 15, no. 5.

Smith, S.
1945: Upper Devonian corals of the Mackenzie River region, Canada; Geol. Soc. Am., Spec. Papers, no. 59.

Spasskiy, N.Ya. and Cherepnina, S.K.
1972: Novye devonskie tetracorally SSSR *in* Novye vidy drevnikh rasteniy i bespozvonochnykh SSSR, I.E. Zanina, ed.; Izdatel'stvo Nauka, Moskva, p. 82-86, 348-349.

Strel'nikov, S.I.
1965: Ordovikskie i siluriyskie rugozy ostrovov Vaygach i Dolgogo; Nauchno-Issled. Inst. Geol. Arktiki, Uchen. Zap., Paleont. i Biostratigr., vyp. 8, p. 24-57.

1968: Novye tsistifillidy (Rugosa) iz silura Pripolyarnogo Urala i gryady Chernysheva; Paleontol. Zh., 1968, no. 3, p. 12-22.

1972: Novye pozdnesiluriyskie korally Pripolyarnogo Urala *in* Novye vidy drevnikh rasteniy i bespozvonochnykh SSSR, I.E. Zanina, ed.; Izdatel'stvo Nauka, Moskva, p. 97-101, 349-350.

Strusz, D.L.
1965: Disphyllidae and Phacellophyllidae from the Devonian Garra Formation of New South Wales; Paleontology, v. 8, pt. 3, p. 518-571.

Stumm, E.C.
1937: The lower Middle Devonian tetracorals of the Nevada Limestone; J. Paleont., v. 11, no. 5, p. 423-443.

1949: Revision of the families and genera of the Devonian tetracorals; Geol. Soc. Am., Mem. 40.

1962: Silurian corals from the Moose River Synclinorium, Maine; U.S. Geol. Surv., Prof. Paper 430, p. 1-7.

1965: Silurian and Devonian corals of the Falls of the Ohio; Geol. Soc. Am., Mem. 93 (1964).

Sytova, V.A.
1966: Rugozy borovushkinskoy svity (verkhniy silur) Rudnogo Altaya; Voprosy Paleont., tom 5, p. 93-100, 138-143.

1971: Tetrakorally grebenskogo gorizonta Vaygacha *in* Stratigrafiya i fauna siluriyskikh otlozheniy Vaygacha, S.V. Cherkesova, ed.; Nauchno-Issled. Inst. Geol. Arktiki, Leningrad, p. 65-86 (1970).

Sytova, V.A. and Ulitina, L.M.
1966: Rugozy isen'skoy i biotarskoy svit *in* Materialy po geologii Tsentral'nogo Kazakhstana, tom 6, Stratigrafiya i fauna siluriyskikh i nizhnedevonskikh otlozheniy Nurinskogo sinklinoriya, A.A. Bogdanov, ed.; Izdatel'stvo Moskovskogo Univ., p. 198-253.

Telford, P.G.
1975: Lower and Middle Devonian conodonts from the Broken River Embayment, north Queensland, Australia; Paleont. Ass., London, Spec. Papers Paleont., no. 15.

Tyazheva, A.P. and Zhavoronkova, R.A.
1972: Korally i brakhiopody pogranichnykh otlozheniy silura i nizhneg devona zapadnogo sklona Yuzhnogo Urala; Izdatel'stvo Nauka, Moskva.

Wang, H.C.
1944: The Silurian rugose corals of northern and eastern Yunnan; Geol. Soc. China, Bull., v. 24, p. 21-32.

Wedekind, R.
1927: Die Zoantharia Rugosa von Gotland (Bes. Nordgotland); Sver. Geol. Unders., Avhandl., ser. Ca, no. 19.

Zheltonogova, V.A.
1960: Siluriyskaya sistema Podklass Tetracoralla (Rugosa). Tetracorally; Sib. Nauchno-Issled. Inst. Geofiz. Mineral. Syr. (SNIIGGIMS), Trudy, vyp. 20, tom 2, p. 74-88, 152-169.

1965: Znachenie rugoz dlya stratigrafii silura Gornogo Altaya i Salaira, *in* Rugozy Paleozoya SSSR, B.S. Sokolov and A.B. Ivanovskiy, ed.; Trudy 1 vsesoyuznogo simpoziuma po izucheniyu iskopaemykh korallov SSSR, vyp. 3, Izdatel'stvo Nauka, Moskva, p. 33-44.

25. A STUDY EMPLOYING OPTICAL METHODS TO EVALUATE ORGANIC METAMORPHISM AND OIL-GENERATING POTENTIAL OF SEDIMENTS IN THE MACKENZIE DELTA AREA, DISTRICT OF MACKENZIE

Project 740032

P. R. Gunther
Institute of Sedimentary and Petroleum Geology, Calgary

Introduction

In 1973, a project, involving drilling eight boreholes, was proposed to evaluate the organic maturity and related hydrocarbon potential of this particular area. An earlier paper (Gunther, in press) described the following wells: I.O.E. Ellice O-14 (lat. 69°03'56"N, long. 135°48'16"W); B.A.-Shell-I.O.E. Reindeer D-27 (lat. 69°06'05"N, long. 134°36'54"W); and Gulf-Mobil Parsons F-09 (lat. 68°54'34"N, long. 133°31'33"W). Five boreholes remained to be investigated to complete the project. The wells chosen and described in this report are: I.O.E. Atkinson H-25 (lat. 69°44'18"N, long. 131°50'21"W); I.O.E. Mayogiak J-17 (lat. 69°26'42"N, long. 132°48'12"W); Shell Kugpik O-13 (lat. 68°52'50"N, long. 135°18'15"W); I.O.E. Taglu D-43 (lat. 69°22'14"N, long. 134°57'00"W); and Imp. Adgo F-28 (lat. 69°27'17"N, long. 135°51'16"W). A location map (Fig. 25.1) shows all eight boreholes as they are positioned within the delta.

Subsequent to Gunther (in press), Vassoevich *et al.* (1974) and Correia and Peniguel (1975) convincingly showed that kerogen types were critical to a correct interpretation of hydrocarbon-generating potential. As a result, the present report consists of vitrinite reflectance information, kerogen typing and interpretation from the combined data.

In general, vitrinite reflectance values can be used to evaluate past thermal histories and, consequently, broad limits can be placed on sedimentary rocks with respect to hydrocarbon potentials (Hacquebard and Donaldson, 1970; Castaño and Sparks, 1974; Teichmüller, 1971, 1974). Kerogen typing adds a further refinement to vitrinite reflectance data. It is used to indicate the richness of organic source material and, therefore, can be used to assess the relative quantity and quality of the generated hydrocarbons. Because the wells described in this report are potential producers of liquids or gases, it is appropriate to show the general relationship between the actual hydrocarbon occurrences

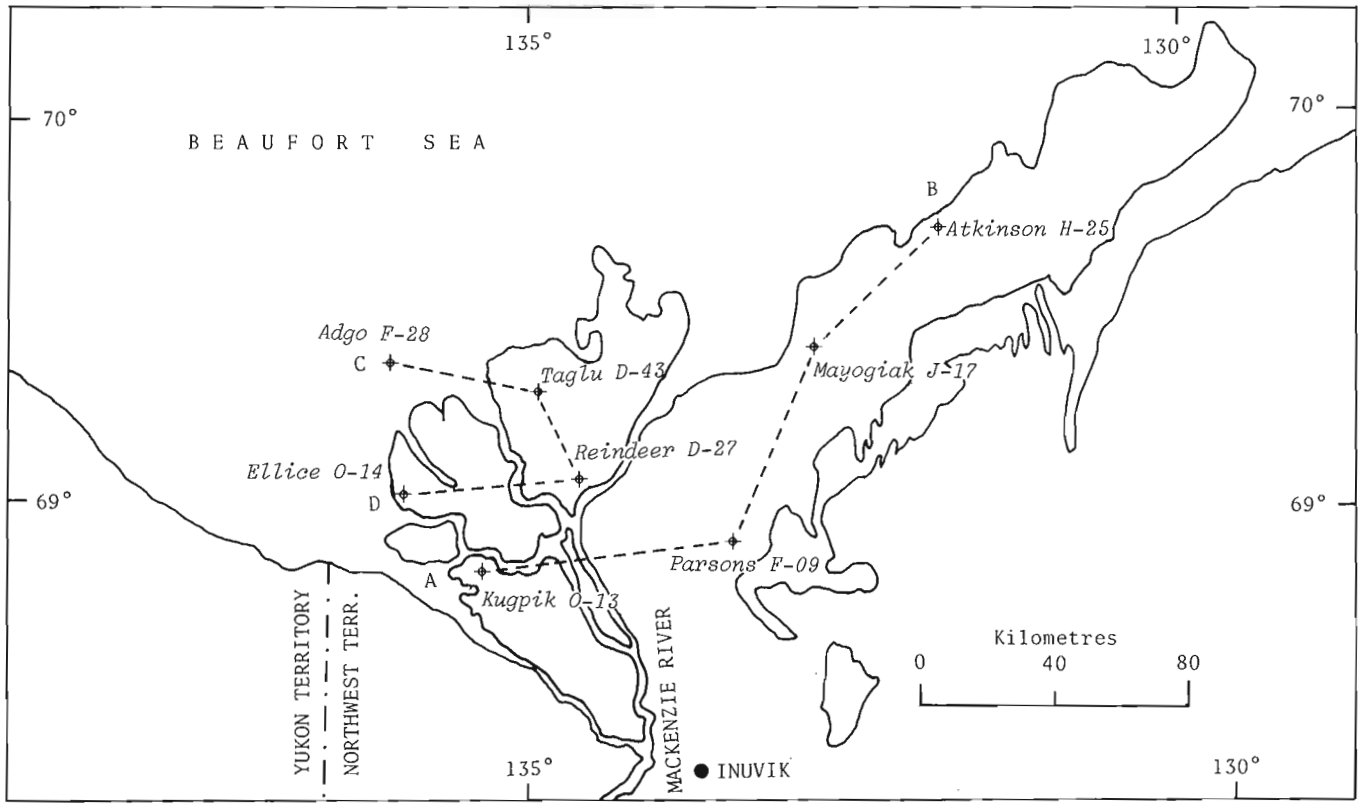

Figure 25.1. Location map of eight selected boreholes in the Mackenzie Delta area.

From: Report of Activities, Part C;
Geol. Surv. Can., Paper 76-1C (1976).

Table 25.1

Maturity richness data and assessment of I.O.E. Atkinson H-25 well.

Depth		Av. Max Ro ± 1 Std	Kerogen Type (X10%)			Kerogen Colour (Determined on	Assessment		Hydrocarbons		Comments
							Ro				
Metres	Feet	Deviation	Sap.	Herb.	W-C	Membrane Material)	Maturity	Richness	Pred.	Actual	
159	520	0.43 ± .07	2	2	6	Lt. yellow					
308	1010	0.45 ± .1	1	6	3	Lt. yellow					
454	1490	0.33 ± .06	0.5	6.5	3	Lt. yellow	<0.4				Immature
607	1990	0.29 ± .06	0.5	6.5	3	Lt. yellow			Bio.		
756	2480	0.37 ± .05	0.5	8	1.5	Lt. yellow-yellow		Fair	Gas		
896	2940	0.44 ± .05		7	3	Lt. yellow					Too Immature for all kerogens except sapropel
1055	3460	0.42 ± .03		5	5	Yellow					
1219	4000		1	4	5	Yellow	>0.4				
1366	4480		2	4	4	Dk. yellow					
1756	5760	0.40	5	3	2	Yellow		Good	Oil?	Oil	24° A.P.I. reservoir @ 118°F T.D.= 5941

and the vitrinite-kerogen information. The intention is that, in the future, better predictions will be made within the Mackenzie Delta area because of this type of documentation. D.W. Myhr kindly supplied the cross-sections.

Procedure

Unwashed cuttings were sampled every 152 m (500 ft.), where possible, and then treated with HCl and HF to remove mineral matter. Coal fragments were separated from the dispersed organic material and made into plastic pellets, while the finer material was used for smear slides. Reflected light microscopy followed the guidelines set by the 1973 A.S.T.M. Book of Standards and transmitted light work was done at x250 magnification with a blue filter in the light path (BG 38).

Where possible, fifty reflectance measurements were made on the vitrinite component of the coals and a mean and a standard deviation were calculated. In the event that less than 50 vitrinite fragments were available, only a mean was calculated and, finally, if no coal was available, the kerogen coloration was used to determine the degree of organic metamorphism. Kerogen included sapropelic, herbaceous and woody-coaly materials and subjective percentages of each of these were recorded as well as the coloration of the thin-walled spores and thin membranes.

Interpretation

With respect to liquid hydrocarbon potential

If sapropelic material predominates in a sample or range of samples, then the generation of petroleum probably can commence at a reflectance value of 0.40 per cent (G. Bayliss, Geochem. Lab., pers. comm., 1976). Vassoevich *et al.* (1974) indicate that oil can be generated at reflectance values of 0.29 per cent Ro while Teichmüller (1974, p. 380) states "the maximum formation of petroleum takes place at the same temperature-time-conditions at which the coals reach the rank stage of high volatile bituminous coals" (approximately 0.50% Ro), but both authors distinctly separate the concepts of maximum generation and maximum accumulation of hydrocarbons. Sapropel, especially the marine variety, is an excellent source of liquid hydrocarbons (Staplin, 1969; Philippi, 1974; Tissot *et al.*, 1974) and, therefore, large quantities of liquids may be generated. If herbaceous materials predominate in the sample, then generation of hydrocarbons will commence at a reflectance of 0.50 to 0.80 per cent (Correia and Peniguel, 1975; Vassoevich *et al.*, 1969, English translation, 1970). Herbaceous material is not as good a source as sapropel (Tissot *et al.*, 1974; Vassoevich *et al.*, 1974) and so smaller quantities of oil and condensate will be generated. Finally, if woody-coaly material predominates in the

Table 25. 2

Maturity richness data and assessment of I. O. E. Mayogiak J-17 well

Depth		Av. Max. Ro ± 1 Std	Kerogen Type (X10%)			Kerogen Colour (Determined on	Assessment		Hydrocarbons		Comments
Metres	Feet	Deviation	Sap.	Herb.	W-C	Membrane Material)	Ro Maturity	Richness	Pred.	Actual	
27	90	0.30 ± .05	1	3	6	Lt. yellow					
152	500	0.32 ± .05	1	3	6	Lt. yellow					
305	1000	0.33	1	1	8	Lt. yellow		Fair-Good			
457	1500	0.27 ± .02	3	3	4	Yellow	<0.4				fine kerogen
610	2000	0.28 ± .05	4	2	4	Yellow					
765	2510	0.33 ± .06	1	4	5	Yellow			Bio. Gas		
917	3010	0.40 ± .04		2	8	Yellow					coarse kerogen
1070	3510	0.42 ± .07		5	5	Yellow-brown	>0.4			Oil	32°A.P.I. reservoir @ 96°F
1219	4000		1	6	3	Lt. brown		Fair-Poor			
1381	4530			6	4	Brown					
1524	5000			6	4	Lt. brown	<0.5				
1820	5970			7	3	Lt. brown	>0.5				coarse kerogen
2472	8110	0.49	5	2	3	Dk. yellow					
2594	8510	0.56	5	3	2	Dk. yellow		Good			marine phytoplankton
2746	9010		5	3	2	Dk. yellow			Oil		
2896	9500	0.53	3	5	2	Brown				Oil	32° A.P.I. res @ 184°F
3048	10000			1	9	Black					
3200	10500			1	9	Black					over mature
3353	11000				10	Black		Poor	Gas		therefore gas prone
3505	11500				10	Black					
3627	11990				10	Black					Limestone?
											T.D 12 093

sample, then few if any liquids will be generated at any reflectance values (Tissot *et al.*, 1974). The generation of liquid hydrocarbons is considered to reach a maximum in the vitrinite reflectance range from 0. 80 to 0. 90 per cent Ro and has been termed the principal zone of oil formation by Vassoevich *et al.* (1974).

With respect to gaseous hydrocarbon potential

Gas can be generated from all types of kerogen including the woody-coaly materials, but large quantities are not generated from the latter material until reflectance values of 0. 80 per cent are reached (G. Bayliss, Geochem. Lab., pers. comm., 1976). The peak generation position probably is fairly close to 1. 8 per cent Ro, but ranges from 1. 2 to 3. 0 per cent Ro (Vassoevich *et al.*, 1974). However, it is known that gas can be produced at low temperatures by biochemical processes (Tissot *et al.*, 1974; Pusey, 1973) and, therefore, gas may be present in significant quantities from the early stages of sedimentation.

Table 25. 3

Maturity richness data and assessment of Shell Kugpik O-13 well

Depth		Av. Max. Ro ± 1 Std	Kerogen Type (X10%)			Kerogen Colour (Determined on	Assessment		Hydrocarbons		Comments
Metres	Feet	Deviations	Sap.	Herb.	W-C	Membrane Material)	Ro Maturity	Richness	Pred.	Actual	
168	550			4	6	Lt. yellow	<0.5		Bio. Gas		
311	1020	0.42 ± .03		2	8	Yellow	>0.5				
472	1550	0.57 ± .05	0.5	3	6.5	Yellow					
497	1630	0.54 ± .04	0.5	3	6.5	Yellow					
613	2010	0.55	0.5	4	5.5	Yellow-brown					
774	2540	0.61		2	8	Brown		Fair-Poor			mature, poor source therefore gas prone
927	3040	0.55 ± .09		2	8	Brown					
1064	3490	0.64		1	9	Dk. brown			Gas		
1204	3950	0.61	1	4	5	Brown					
1359	4460	0.67		5	5	Brown					
1548	5080			2	8	Brown					
1679	5510	0.66		4	6	Brown					
1838	6030		1	3	6	Brown					
1993	6540	0.56	5	2	3	Yellow					
2137	7010	0.58	6	2	2	Yellow				Oil	48° A.P.I. res @ 156°F
2289	7510	0.63 ± .05	4	3	3	Dk. yellow		Good			
2442	8010		4	4	2	Brown					
2530	8300		4	5	1	Brown			Oil		
2868	9410	0.64	2	4	4	Dk. brown					mature poorer source therefore less chance for oil
2899	9510	0.72	2	4	4	Dk. brown					
3051	10010	0.96	1	4	5	Dk. brown	0.8				
3182	10440	0.90 ± .05	1	7	2	Dk. brown					
3203	10510	1.12 ± .04	2	6	2	Dk. brown	<1.2	Fair			
3356	11010	1.41	4	4	2	Lt. brown	>1.2				
3511	11520		1	7	2	Dk. brown			Gas		over mature for oil
3661	12010	0.60	2	2	6	Dk. brown					TD=12 103'

With respect to destruction of hydrocarbons

Most workers in the field agree that peak accumulation and preservation of liquid hydrocarbons coincide with a reflectance value of from 0. 80 to 0. 90 per cent (Vassoevich *et al.*, 1974; Correia and Peniguel, 1975; Hood *et al.*, 1975). There are instances where oil-condensate mixtures have been found coincident with reflectance values of 1. 2 per cent (Vassoevich *et al.*, 1974, p. 310, scheme I) but these occurrences are rare

Table 25.4

Maturity richness data and assessment of I.O.E. Taglu D-43 well

Depth		Av. Max. Ro ± 1 Std	Kerogen Type (X10%)			Kerogen Colour (Determined on	Assessment		Hydrocarbons		Comments
Metres	Feet	Deviation	Sap.	Herb.	W-C	Membrane Material)	Ro Maturity	Richness	Pred.	Actual	
256	840	0.34	1	8	1	Lt. yellow					
311	1020	0.34 ± .03	2	6	2	Lt. yellow		Fair			
457	1500		2	5	3	Lt. yellow					
613	2010	0.32 ± .04	7	2	1	Yellow					rich, but
759	2490		3	3	4	Yellow		Good			not mature
914	3000	0.37 ± .07	7	3		Lt. yellow	<0.4				enough
1067	3500	0.33	1	7	2	Yellow					
1219	4000	0.39 ± .05	0.5	6.5	3	Yellow			Bio.		
1366	4480	0.37 ± .06		5	5	Lt. yellow		Poor	Gas		
1524	5000	0.38		4	6	Yellow					
1679	5510	0.38		2	8	Yellow					fine
1823	5980	0.40 ± .03	1	3	6	Yellow					kerogen
2006	6580		3	4	3	Dk. yellow	>0.4				
2112	6930	0.43 ± .06	1	5	4	Yellow		Fair-			Interesting
2365	7760		2	4	4	Yellow		Good	Oil		zone
2438	8000	0.46 ± .08	0.5	7.5	2	Yellow					
2594	8510	0.52 ± .08		8	2	Yellow					fine
2743	9000	0.49 ± .07		8	2	Yellow			Gas?		Kerogen
2896	9500	0.46 ± .06	1	6	3	Yellow					fine Kerogen
3048	10000	0.49		8	2	Dk. yellow	<0.5				
3200	10500		1	6	3	Dk. yellow				Oil	29° A.P.I.
3353	11000	0.50 ± .05		4	6	Lt. brown		Fair-			res @ 172°F
3505	11500	0.51 ± .05		6	4	Brown		Poor			
3661	12010	0.63 ± .08		5	5	Lt. brown			Oil		mature
3810	12500	0.64 ± .04		7	3	Dk. yellow	>0.5				but not the best
3962	13000	0.60 ± .08	1	6	3	Dk. yellow					oil source
4115	13500	0.62 ± .07	0.5	6	3.5	Dk. yellow					
4267	14000	0.72 ± .04		5	5	Lt. brown					
4420	14500			2	8	Brown					
4554	14940			6	4	Brown					
											TD=14 944'

and condensate usually is the main constituent. Even values of 1.1 per cent Ro are considered to be in the destructive phase of liquids (Robert, 1974). As the liquids are cracked, more and more gas and condensate are produced and this is why the peak accumulation range for gas is from 1.2 to 3.0 per cent Ro (Vassoevich *et al.*, 1974; Robert, 1974). Beyond the 3.0 per cent reflectance range, gas is seldom found.

Results

Tables 25.1 through 25.5 contain the reflectance and kerogen data obtained from the five boreholes being investigated for this report. The tables include an assessment of maturity (in Ro % ranges) and richness (poor, fair and good) and predicted versus actual hydrocarbons.

There seems to be a correlation between the occurrence of pooled hydrocarbons and the occurrence of high quality source material in the adjacent fine grained sediments. However, it must be emphasized that many other geological factors influence the accumulation of oil, other than the availability of rich source rocks. In cases of good correlation, the source appears to be adjacent to the reservoir.

Table 25.5

Maturity richness data and assessment of Imp. Adgo F-28 well

Depth		Av. Max. Ro ± 1 Std	Kerogen Type (X10%)			Kerogen Colour (Determined on	Assessment		Hydrocarbons		Comments
Metres	Feet	Deviation	Sap.	Herb.	W-C	Membrane Material)	Ro Maturity	Richness	Pred.	Actual	
155	510	0.35 ± .07	1	6	3	Lt. yellow		Fair	Bio.		
165	540	0.40 ± .05	1	6	3	Lt. yellow	<0.4		Gas		
1359	4460	0.40 ± .03	5	4	1	Lt. yellow	>0.4			oil	18° A.P.I. res @ 85°F
1381	4530	0.44 ± .03	4	5	1	Lt. yellow		Good	Oil?		
1430	4690	0.58 ± .04	3	4	3	Lt. yellow					
1524	5000	0.48 ± .03	1	7	2	Lt. yellow		Fair	Gas?		
1695	5560	0.46 ± .04	4	4	2	Yellow				oil	16.5°A.P.I res @ 116°F
1789	5870	0.42 ± .05	4	5	1	Yellow					fine kerogen
1884	6180	0.43	4	5	1	Yellow	<0.5	Good	Oil		fine kerogen
1996	6550	0.54 ± .03	3	3	4	Yellow					
2057	6750	0.52 ± .05	5	3	2	Lt. brown					
2152	7060	0.54 ± .03	4	3	3	Dk. yellow					
2292	7520	0.52 ± .04	1	7	2	Dk. yellow					
2435	7990	0.50 ± .03	1	5	4	Lt. brown	>0.5				
2652	8700	0.61 ± .04	1	6	3	Lt. brown			Oil-gas		mature but source poorer
2765	9070	0.62 ± .05	0.5	4.5	5	Brown					
2905	9530	0.61 ± .06		5	5	Black		Fair			
2938	9640	0.60 ± .02		3	7	Black					
3054	10020	0.50		8	2	Lt. brown					
3115	10220	0.61 ± .06	1	6	3	Brown					TD=10 528'
3200	10500	0.63 ± .06	1	5	4	Brown					

Discussion

Figures 25.2 and 25.3 are cross-sections containing the eight boreholes mentioned in the introduction (lines of section can be found on Fig. 25.1). The correlations were made in consultation with D.W. Myhr. The points of interest concerning each borehole are as follows:

I.O.E. Atkinson H-25

The Upper and Lower Cretaceous strata (Fig. 25.2) in this well are immature probably because the borehole is located on the northeastern-plunging nose of the Aklavik arch complex (Yorath and Norris, 1975). This indicates a shallow depth of burial. A source for this oil is very speculative, but the kerogen data suggest it may be local because of the good source richness of the Lower Cretaceous as indicated at 1756 m (5938 ft.) (Table 25.1).

I.O.E. Mayogiak J-17

The strata in this well vary from immature to overmature and the oil lies in the overmature zone at 2864 m (9395 ft.). This is just below (5 m; 16 ft.) the Jurassic-Devonian unconformity (Fig. 25.2) and probably indicates good reservoir conditions rather than optimum oil-generating capabilities. The kerogen colour (Table 25.2) certainly indicates an overmature status for the sub-Jurassic rocks, while Jurassic and Lower Cretaceous beds themselves could be excellent source rocks from both the standpoint of reflectance

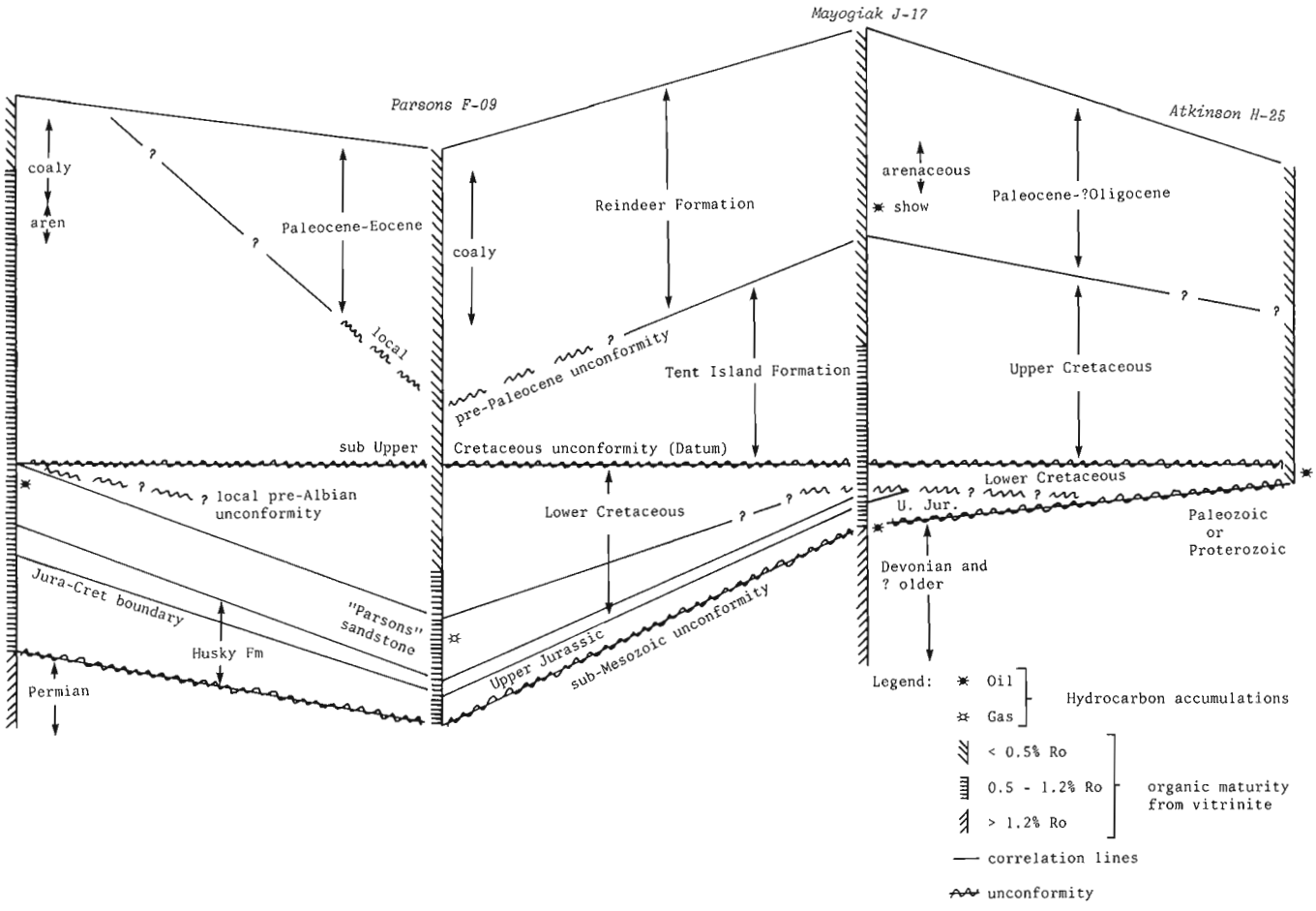

Figure 25.2. Cross-section A-B Correlations by D.W. Myhr.

(>0.50% Ro) and kerogen type (50% sapropel). There is also an oil show at 1155 m (3790 ft.), but this appears to be oil that has migrated vertically (T.G. Powell, pers. comm., 1976) or oil that has moved updip from the same source as the lower oil.

Gulf *et al.* Parsons F-09

Two earlier papers (Myhr and Gunther, 1974; Gunther, in press) adequately describe this borehole, but it is interesting to note that gas and condensate were recovered from the Lower Cretaceous strata which, as indicated from the previous two wells, contain a rich source. The vitrinite reflectance values adjacent to the reservoir range from 0.55 to 0.68 per cent Ro. Kerogen analyses were not run on this borehole. The Lower Cretaceous strata are in the mature zone, but the reported reservoir temperatures are somewhat higher than one would anticipate. Upper Cretaceous strata (Fig. 25.2) are immature which suggests the depth of burial was not as great as the other wells in the A-B cross-section. This probably was due to (?) pre-Paleocene or late Maastrichtian uplift and erosion (Fig. 25.2).

Shell Kugpik O-13

This borehole penetrated strata in the mature zone which contained good rich kerogen (Table 25.3). The oil accumulation tested at 2915 m (7202 ft.) in Lower Cretaceous sediments correlated perfectly with the predicted most favourable position for oil generation. This is strong evidence for local oil generation and accumulation. Burns *et al.* (1975) consider this oil as unaltered. The Upper Cretaceous strata in the well are nearly all within the mature zone suggesting deeper burial than the other wells of Figure 25.2. Its location, near the Richardson Mountain front, was an area of rapid subsidence during Late Cretaceous time; the sediments being deeply buried caused the advanced maturation. The well is now on a structural high, the Cache Creek uplift.

I.O.E. Ellice O-14

This well is described with respect to vitrinite reflectance and palynomorph colour by Gunther (in press), but unfortunately kerogen analysis data are not available. The reflectance values range from 0.36 to 0.87 per cent Ro. The hole is dry, but hydrocarbons

should have been generated somewhere within its depth, irrespective of the kerogen type. Migration could have occurred before the structure was formed on which the well is located.

B.A. *et al.* Reindeer D-27

Most of the Reindeer Formation (Fig. 25.3) is immature in this well and, as such, is similar to the Parsons F-09 borehole (Fig. 25.2). The well penetrates thick sequences of Tertiary and Upper Cretaceous sediments (Fig. 25.3; Young, 1975), reaching Lower Cretaceous rocks at approximately 3353 m (11 000 ft.). Vitrinite reflectance data from Gunther (in press) indicate that the mature zone commences at approximately 1524 m (5000 ft.). Gas kicks are reported at 1768 and 2072 m (5800 and 6800 ft.).

I.O.E. Taglu D-43

The maturity level of the coal-bearing unit, Reindeer Formation, is higher in this well as compared to the others in cross-section C-D (Fig. 25.3). This indicates the deepest burial for this unit and, probably the least amount of uplift. The borehole contained many coaly intervals and, therefore, the reflectance data (Table 25.4) are the best documented for this study. The transition from the immature to mature zone is at 2926 m (9600 ft.) and the hydrocarbon accumulation is at 3170 m (10 400 ft.). The kerogen is mainly herbaceous throughout the mature zone but tends to be composed of a higher percentage of darker coloured material than normally is expected. This could indicate reworking.

Imp. Adgo F-28

The mature zone is situated stratigraphically lower in this well than in Taglu D-43. The reason could be attributed to an area of weaker subsidence suggested by the stratigraphically higher coal-bearing interval, combined with a higher geothermal gradient or slightly shallower burial, but much greater erosion at the pre-Neogene unconformity (Fig. 25.3), and subsequent uplift. Two biodegraded oil accumulations (Burns *et al.*, 1975) are reported from this borehole at 1247 and 1731 m (4090 and 5680 ft.). The respective reflectance values at these levels are 0.40 and 0.46 per cent Ro.

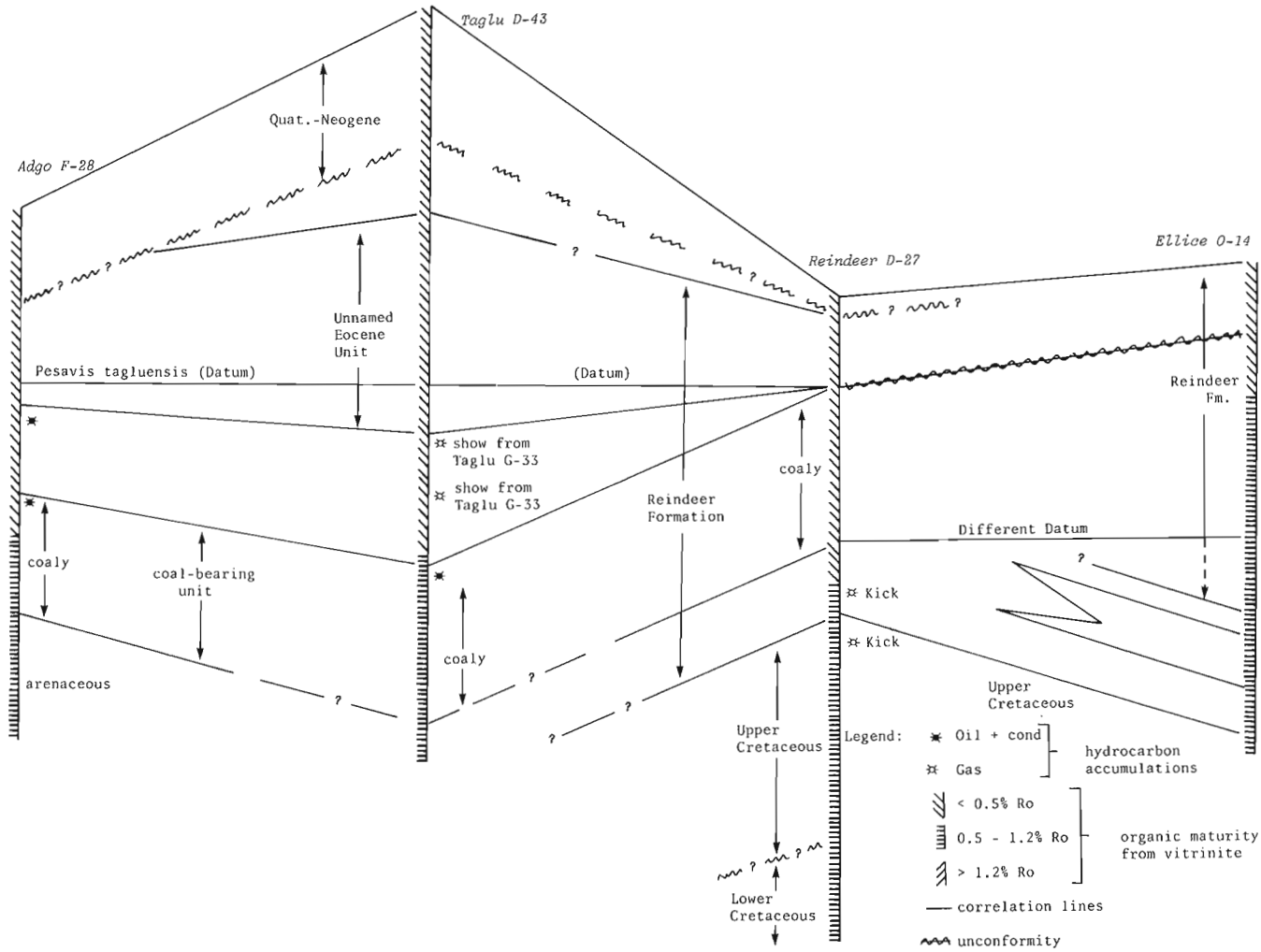

Figure 25.3. Cross-section C-D Correlations by D.W. Myhr and F.G. Young, 1973.

Because the kerogen contains a high percentage of sapropel throughout this interval (Table 25.5), immature oil would have been predicted as the product. The mature zone commences at 1980 m (6500 ft.), but the kerogen is predominantly herbaceous from that depth downward, and so is less favourable for oil generation.

General conclusions

By quickly scanning the maturity data (reflectance values) in Tables 25.1 through 25.5, it can be seen that there are different degrees of prediction reliability for each well. Atkinson H-25 and Mayogiak J-17 are rather poorly documented below 1070 m (3510 ft.), whereas the remaining wells have much more control. Further examinations of the reflectance data reveals small irregularities with depth in the values. These could be attributed to many phenomena, but the most reasonable ones are: reworked coaly material, slight oxidation, warm fluid migration or surrounding rock matrix differentially conducting heat.

Maturation occurs at different depths in each well depending on the local geology, but when rich source rock and adequate maturation combine, hydrocarbons usually are observed. In general, the Paleozoic rocks which were penetrated by the boreholes tended to be overmature at least in terms of liquid hydrocarbons. The Lower Cretaceous-Jurassic sequence (mainly marine?) seemed to be the most prospective because it was buried deep enough and contained rich kerogen (a high percentage of sapropel). The Tertiary and Upper Cretaceous sediments nearly always contained large percentages of herbaceous material (land plant derived material) which is less prospective at shallow depths of burial. When rich lenses were encountered in these sediments, they usually were not mature enough to indicate the generation of significant hydrocarbons.

References

American Society for Testing and Materials
1973: Book of ASTM standards, Part 19, Gaseous fuels, coal and coke; Philadelphia, Pennsylvania, p. 416-419.

Burns, B.J., Hogarth, J.T.C., and Milner, C.W.D.
1975: Properties of Beaufort Basin liquid hydrocarbons; Bull. Can. Pet. Geol., v. 23, no. 2, p. 295-303.

Castaño, J.R. and Sparks, D.M.
1974: Interpretation of vitrinite reflectance measurements in sedimentary rocks and determination of burial history using vitrinite reflectance and authigenic minerals *in* Carbonaceous materials as indicators of metamorphism; Geol. Soc. Am., Spec. Paper 153, p. 31-52.

Correia, M. and Peniguel, G.
1975: Etude microscopique de la matière organique – ses application à l'éxploration pétroliere; Bull. Centre Rech. Pau – SNPA, v. 9, no. 2, p. 99-127.

Gunther, P.R.
Palynomorph colour and dispersed coal particle reflectance in three Mackenzie Delta boreholes; Geosci. Man. (in press)

Hacquebard, P.A. and Donaldson, J.R.
1970: Coal metamorphism and hydrocarbon potential in the upper Paleozoic of the Atlantic Provinces, Canada; Can. J. Earth Sci., v. 7, no. 4, p. 1139-1163.

Hood, A., Gutjahr, C.C.M., and Heacock, R.L.
1975: Organic metamorphism and the generation of petroleum; Bull. Am. Assoc. Pet. Geol., v. 59, no. 6, p. 986-996.

Myhr, D.W. and Gunther, P.R.
1974: Lithostratigraphy and coal reflectance of a Lower Cretaceous deltaic succession in the Gulf-Mobil Parsons F-09 borehole, N.W.T.; *in* Report of Activities, Part B; Geol. Surv. Can., Paper 74-1B, p. 24-28.

Philippi, G.T.
1974: The influence of marine and terrestrial source material on the composition of petroleum; Geochim. Cosmochim. Acta, v. 38, p. 947-966.

Pusey, W.C.
1973: How to evaluate potential gas and oil source rocks; World Oil, v. 176, no. 5, p. 71-75.

Robert, P.
1974: Analyse microscopique des charbons et des bitumes dispersés dans les roches et mesure de leur pouvoir réflecteur *in* Advances in organic geochemistry, B. Tissot and F. Bienner, eds.; Proc. 6th Intern. Mtg. on Organic Geochemistry, 1973, p. 549-569.

Staplin, F.L.
1969: Sedimentary organic matter, organic metamorphism, and oil and gas occurrence; Bull. Can. Pet. Geol., v. 17, no. 1, p. 47-66.

Teichmüller, M.
1971: Anwerdung kohlenpetrographischer Methoder bei der Erdöl-und Erdgasprospektion; Erdöl und Kohle, v. 24, no. 2, p. 69-76.

1974: Generation of petroleum-like substances in coal seams as seen under the microscope *in* Advances in organic geochemistry, B. Tissot and F. Bienner, eds.; Proc. 6th Intern. Mtg. on Organic Geochemistry, 1973, p. 379-406.

Tissot, B., Durand, B., Espitalie, J., and Combaz, A.
1974: Influence of nature and diagenesis of organic matter in formation of petroleum; Bull. Am. Assoc. Pet. Geol., v. 58, no. 3, p. 499-506.

Vassoevich, N.B., Akramkhodzhaev, A.M., and Geodekyan, A.A.
1974: Principal zone of oil formation *in* Advances in organic geochemistry, B. Tissot and F. Bienner, eds.; Proc. 6th Intern. Mtg. on Organic Geochemistry, 1973, p. 309-314.

Vassoevich, N.B., Korchagina, Yu. I., Lopatin, N.V., and Chernyshev, V.V.
1969: Principal phase of oil formation; Moskov. Univ. Vestnik, no. 6, p. 3-27 (in Russian) *in* Int. Geol. Rev., 1970, v. 12, no. 11, p. 1276-1296 (in English).

Yorath, C.J. and Norris, D.K.
1975: The tectonic development of the southern Beaufort Sea and its relationship to the origin of the Arctic Ocean Basin *in* Canada's continental margins and offshore petroleum potential, C.J. Yorath, E.R. Parker and D.J. Glass, eds.; Can. Soc. Pet. Geol., Mem. 4, p. 589-612.

Young, F.D.
1975: Upper Cretaceous stratigraphy, Yukon Coastal Plain and northwestern Mackenzie Delta; Geol. Surv. Can., Bull. 249.

EOCENE BEDS AT LAKE HAZEN, NORTHERN ELLESMERE ISLAND

Project 630003

R. L. Christie and G. E. Rouse[1]
Institute of Sedimentary and Petroleum Geology, Calgary.

Introduction

The Tertiary rocks of the Lake Hazen region were described briefly by Christie (1976, p. 259-262) who reported that rather young ages, Oligocene-Miocene, had been assigned recently to palynological material from the Lake Hazen beds, and some conclusions based on those ages were discussed. The palynological material was re-examined by G. E. Rouse, of the University of British Columbia, at about the time the earlier report was published; the Oligocene-Miocene assignments were revised in favour of an Eocene age, and this information was added as a footnote.

The following remarks are presented to summarize the data of the earlier paper and to revise the conclusions.

Stratigraphy and Structural Setting

The Tertiary rocks of the Lake Hazen region underlie a rolling lowland about 80 by 15 km (50 by 10 miles) extending northeasterly from the northeastern shore of Lake Hazen, and scattered erosional remnants of Tertiary rocks lie in certain parts of the Hazen Plateau south and east of the lake.

The nearly flat-lying Tertiary rocks at Lake Hazen lie adjacent to moderately folded Mesozoic and upper Paleozoic rocks, which occur as a small, basin-form outlier of the Sverdrup Basin. The Tertiary beds appear to overlap the northeastern edge of the outlier. The structure of the Tertiary formation is one of open and irregular undulations except for a limited area or zone of extreme folding on the lower Gilman River[2]. These folds presumably are a consequence of movement on faults related to the Lake Hazen Fault Zone (Fig. 26. 1). Upper Paleozoic and Mesozoic beds are overthrust onto Tertiary beds at a locality on the north shore of Lake Hazen.

Sections ranging in thickness from 90 to 270 m (300-900 ft) were measured at three localities (Fig. 26. 1): (1) along the north shore of Lake Hazen; (2) in a steep-sided valley a few kilometres north of the lake; and (3) on the flanks of a 'Boulder Gravel Hill' about 16 km (10 miles) north of the lake. The three sections are presented in Figure 26. 2. Section 1 is composite, after Petryk (1969). The three sections occur at successively higher elevations and appear to represent successively younger parts of the Tertiary sequence. A total thickness of 600 m (2000 ft) of Tertiary beds probably is represented.

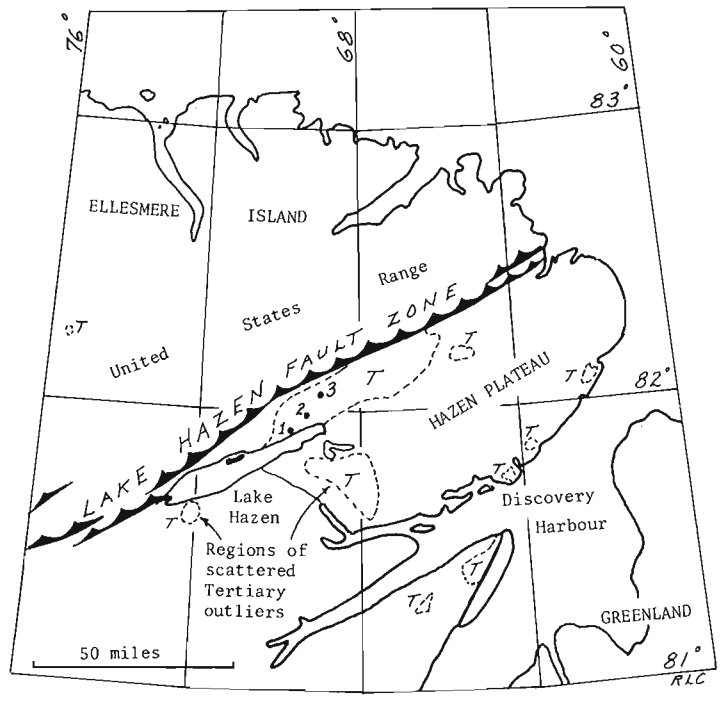

Figure 26. 1. Index map showing distribution of Tertiary rocks and location of sections.

The Tertiary beds comprise mainly weakly lithified sandstone, sandy shale, and shale with coal beds and coaly layers. Thick conglomerate beds occur at the top of the section.

The two measured stratigraphic sections and the composite section (Sec. 1) of Petryk are described below in ascending order.

The lower part of the Tertiary sequence of Lake Hazen (Sec. 1; *see* Fig. 26. 2) comprises sandstone and siltstone characterized by abundant crossbedding and channelling, and by numerous coal layers and ironstone concretionary bodies. The coal, in beds up to 3 m (10 ft) thick, is compact, bright, and moderately friable. Some coal is brownish. A subbituminous B rank (ASTM) has been determined for coal from the lowest exposed beds.

Sediments of the middle part of the Tertiary sequence (Sec. 2) are similar to those of the lower section, but have a smaller proportion of coal. Also, the rank of the coal and coaly layers appears to be lower. Stumps, twigs, and fragments of carbonized and silicified wood are characteristic of the middle section.

The upper Tertiary beds (Sec. 3) can be divided into two parts: the lower, mainly fine grained, sandstone beds with a few carbonaceous and shaly layers; and the upper, mainly coarse conglomerate. The transition from sandstone to conglomerate is abrupt, but a thin

[1]Department of Botany, University of British Columbia, Vancouver.

[2]Gilman River enters Lake Hazen from the northwest between localities 1 and 2 of Figure 26. 1.

From: Report of Activities, Part C;
Geol. Surv. Can., Paper 76-1C (1976).

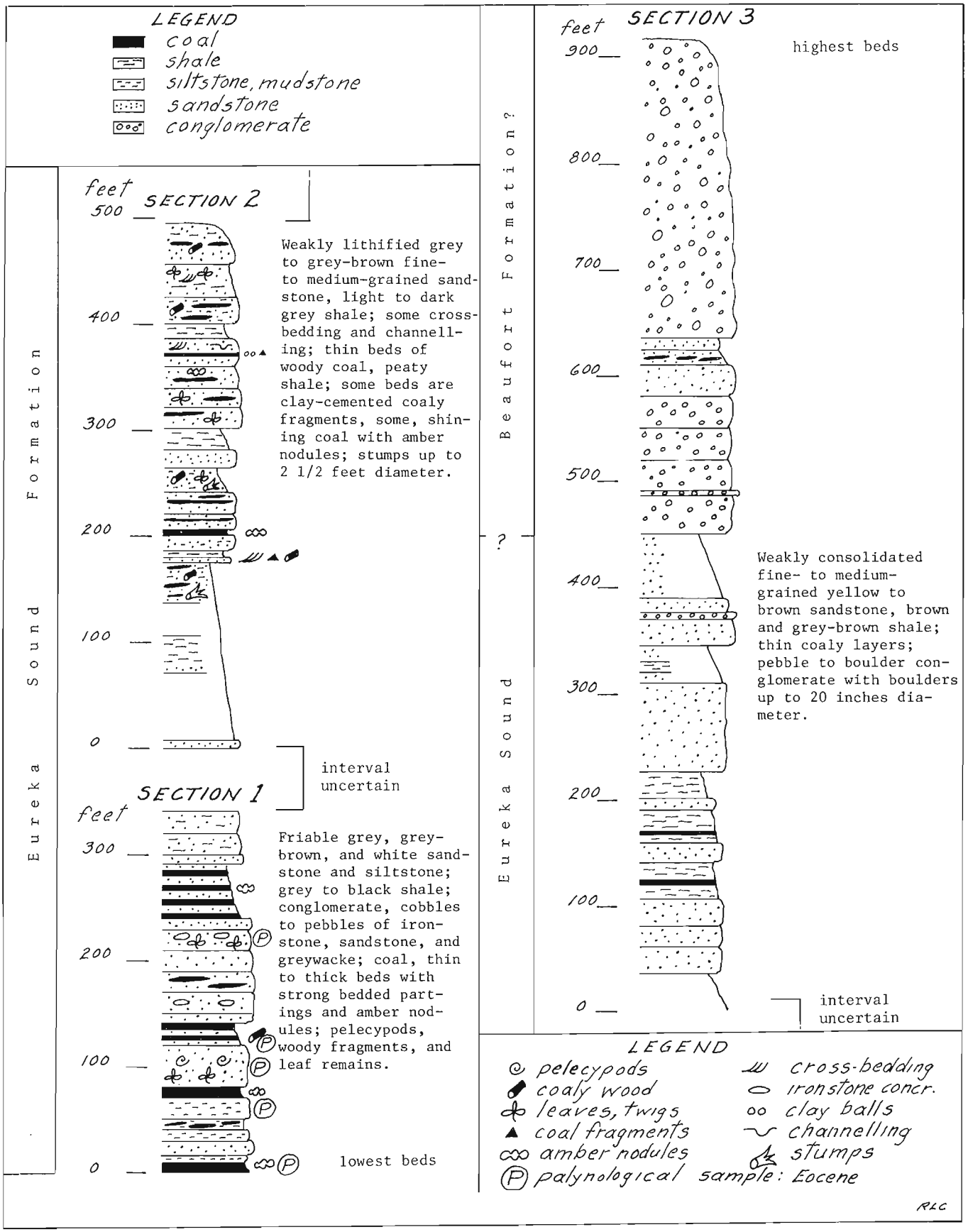

Figure 26. 2. Stratigraphic sections of Tertiary rocks at Lake Hazen, Ellesmere Island.

cobble conglomerate layer lies within the sandstone sequence and sandstone beds are several tens of metres thick about one third of the way from the base of the conglomerate. The conglomerate is brown-weathering, weakly consolidated, and contains well-rounded cobbles and boulders in a sand matrix. The largest boulders in the lowest conglomerate bed are 25 cm (10 in) in diameter, whereas, in the upper beds, they are up to 50 cm (20 in). About half of the clasts resemble sandstones that occur in the Permian Sabine Bay Formation, exposed in the mountainous region some tens of kilometres to the northwest (Nassichuk, 1967); the remainder are of dark bluish grey limestone typical of lower Paleozoic miogeosynclinal rocks that are developed extensively in the region. Diabase boulders form a conspicuous part of the conglomerates.

Age

A Miocene age was suggested by Heer (1878) for coal-bearing beds of Watercourse Valley (near Discovery Harbour) on the southeastern margin of the Hazen Plateau, and Fry (*in* Blackadar, 1954) suggested an age "not older than Miocene and possibly more recent" for a tree cone recovered from the Lake Hazen region in 1953. Palynological collections from Lake Hazen, assembled in 1957 and 1958, were assigned a Paleocene to Oligocene age by the author's colleague, D. C. McGregor, who noted also that plant remains from Watercourse Valley (collected in 1958) indicated a Paleocene or possibly an Eocene age.

Seventeen samples collected in 1965 from beds shown here as Section 1 (Fig. 26.2) yielded variable numbers of palynomorphs. These were examined by Rouse, who reports as follows. Most of the assemblages are relatively poor in species and numbers, and contain palynomorphs that typically are found in Oligocene and Miocene assemblages, or in certain Eocene palynofacies that are skewed to resemble the conifer and deciduous, broadleaf, angiosperm tree palynofloras typical of the Neogene. Included here are pollen assignable to *Pinus, Picea, Tsuga, Cedrus, Fagus, Quercus, Carya, Pterocarya, Corylus/Carpinus, Betula, Alnus* and the Ericaceae. However, several palynomorphs that are characteristic of the lower and middle Eocene segment of the Eureka Sound Formation are present also, but in very low numbers. Examples are *Pistillipollenites mcgregorii, Rhoiipites cryptocorpus* type, several other species of *Rhoiipites, Aesculiidites* sp., *Holkopollenites* sp., and *Tricolporopollenites kruschii* (sensu Elsik). These were interpreted initially, in a report to Christie, as representing a Paleogene age, correlative with part of the Eureka Sound Formation. Later, however (*see* Christie, 1976), they were considered to be Eocene palynomorphs recycled into Oligocene or Miocene assemblages – not an uncommon phenomenon in the wells of the Mackenzie Delta region. From additional study, it now seems apparent that the assemblages are indeed Eocene in age, but with most assemblages representing palynofacies skewed to appear more like those of the Oligocene or Miocene that are dominated by pollen of conifer and deciduous, broadleaf, angiosperm tree genera. This skewing of palynofacies is a common feature also of Eocene sediments of the Mackenzie Delta.

Correlation and Tectonic Events

The following correlations, based on the field relationships and the age assignments now accepted, appear to hold.

(a) The Tertiary beds at Lake Hazen, at least in the lower part, evidently are correlative with part of the Eureka Sound Formation of western Ellesmere Island; this correlation is based on lithological similarity and the Eocene age from palynological data.

The Eureka Sound Formation is mainly a lower Tertiary clastic marine and nonmarine unit of the northern Arctic Islands. Deposition of these beds evidently began within the Sverdrup Basin in latest Cretaceous time; elsewhere, the Eureka Sound Formation is entirely of Paleocene and Eocene ages. The formation was affected by several tectonic events during the Eurekan Orogeny (*see* Thorsteinsson and Tozer, 1970, p. 584-586; Balkwill and Bustin, 1975; Balkwill *et al.* 1975).

(b) The conglomerate unit at the top of the Tertiary section of Lake Hazen resembles, and possibly is correlative with, conglomerates of the north coast of Ellesmere Island (Wilson, 1976) and east-central Axel Heiberg Island (Balkwill and Bustin, 1975) that have been assigned to the Beaufort Formation. The Beaufort Formation, an uppermost Tertiary gravel and sand unit of the western Arctic Islands, was defined by Tozer (1956). Its age, based on the abundant contained floras, is probably middle to late Miocene (Hills, 1969; Hills *et al.*, 1974).

The possible Beaufort Formation at Lake Hazen has been sampled for palynological material, but useful forms have not been recovered so far. Thus, fossil evidence for the age of the upper conglomerate unit is lacking. The lower (Eureka Sound) sandstone and the upper (Beaufort?) conglomerate units are conformable and interbedded, so that the correlation with the Beaufort Formation suggested above remains uncertain. Among other possibilities, the Lake Hazen section may contain beds transitional between the two formations, or a regional unconformity or disconformity, not recognized, may be present.

The sequence of events in late Mesozoic and Tertiary times at Lake Hazen evidently was as follows.

(a) Folding in Late Cretaceous or early Tertiary time, perhaps accompanied by thrust faulting along the Lake Hazen Fault Zone to isolate a part of the Sverdrup Basin. Upper Paleozoic and Mesozoic beds were folded during this episode. Presumably, an early Grant Land Mountains system formed.

(b) Erosion of Paleozoic, Mesozoic, and possibly lower Tertiary beds resulted in detritus for the Eocene beds of Lake Hazen; this detritus was deposited in a local, continental basin overlying the nearly peneplained Hazen Plateau.

(c) Thrust faulting in Eocene or later time juxtaposed Eocene and upper Paleozoic-Mesozoic beds, with the older beds tectonically overlying the younger locally. The coarse, molassic (Beaufort?) debris of the upper part of the Tertiary section may have been derived from land to the north, tectonically uplifted during this phase of faulting.

References

Balkwill, H. R. and Bustin, R. M.
1975: Stratigraphic and structural studies, central Ellesmere Island, and eastern Axel Heiberg Island, District of Franklin; *in* Report of Activities, Part A, Geol. Surv. Can., Paper 75-1A, p. 513-517.

Balkwill, H. R., Bustin, R. M., and Hopkins, W. S., Jr.
1975: Eureka Sound Formation at Flat Sound, Axel Heiberg Island, and chronology of the Eurekan Orogeny; *in* Report of Activities, Part B, Geol. Surv. Can., Paper 75-1B, p. 205-207.

Blackadar, R. G.
1954: Geological reconnaissance, north coast of Ellesmere Island, Arctic Archipelago, Northwest Territories; Geol. Surv. Can., Paper 53-10.

Christie, R. L.
1976: Tertiary rocks at Lake Hazen, northern Ellesmere Island; *in* Report of Activities, Part B, Geol. Surv. Can., Paper 76-1B, p. 259-262.

Heer, O.
1878: Notes on fossil plants discovered in Grinnell Land by Captain H. W. Feilden; Quart. J. Geol. Soc., v. 34, p. 66-72.

Hills, L. V.
1969: Beaufort Formation, northwestern Banks Island, District of Franklin; *in* Report of Activities, Part A, Geol. Surv. Can., Paper 69-1A, p. 204-207.

Hills, L. V., Klovan, J. E., and Sweet, A. R.
1974: *Juglans eocinerea* n. sp., Beaufort Formation (Tertiary), southwestern Banks Island, Arctic Canada; Can. J. Botany, v. 52, p. 65-90.

Nassichuk, W. W.
1967: Studies of Permo-Carboniferous and Mesozoic strata on northern Ellesmere Island; *in* Report of Activities, Part A, Geol. Surv. Can., Paper 67-1A, p. 10-12.

Petryk, A. A.
1969: Mesozoic and Tertiary stratigraphy at Lake Hazen, northern Ellesmere Island, District of Franklin; Geol. Surv. Can., Paper 68-17.

Thorsteinsson, R. and Tozer, E. T.
1970: Geology of the Arctic Archipelago, Chap. X; *in* Geology and Economic Minerals of Canada, R. J. W. Douglas (ed.); Geol. Surv. Can., Econ. Geol. Rep. 1, 5th ed., p. 458-490.

Tozer, E. T.
1956: Geological reconnaissance, Prince Patrick, Eglinton, and western Melville Islands, Arctic Archipelago, Northwest Territories; Geol. Surv. Can., Paper 55-5.

Wilson, D. G.
1976: Eureka Sound and Beaufort Formations, Yelverton Bay, Ellesmere Island, District of Franklin; *in* Report of Activities, Part A, Geol. Surv. Can., Paper 76-1A, p. 453-456.

Project 740062

John L. Luternauer
Terrain Sciences Division, Vancouver

Purpose

The Fisheries and Marine Service and the Fisheries Research Board of Canada (Environment Canada) have identified the bank off Barkley Sound (Fig. 27.1) as one of the more important local codfish spawning areas and groundfish habitats (Westrheim *et al.*, 1975, 1976; Harling *et al.*, 1976). A cruise was planned in conjunction with Jergen Westrheim (Nanaimo Biological Station) and Don Tiffin and Ivan Frydecky (Marine Geology Group, REG) to define in detail the geologic character of the bank and environs. Cursory examinations of the area had already been carried out by Carter (1973) and Milliman (1976). Ultimately, it is hoped that enough can be learned about the local morphology, bathymetry, and substrate materials to determine what geologic conditions most favour the local ground fishery.

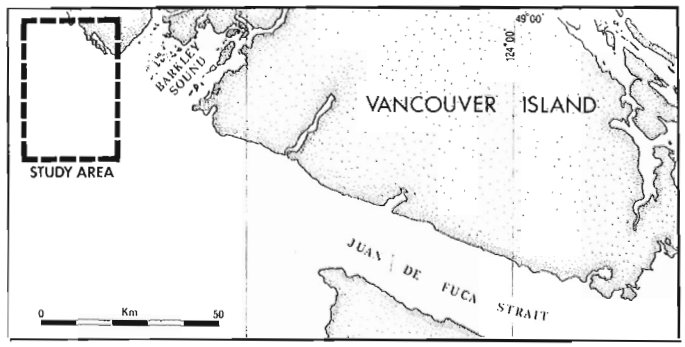

Figure 27.1. Location of study area.

Methods

Field work was performed from the research vessel G.B. Reed (July 6-20). The sea floor along a dense grid defined by Loran lines (Fig. 27.3A) was sampled with a Shipek device. Selected sample sites on the bank top were dredged (for approximately 0.5 km distances) to establish approximate maximum and mean sizes of the coarser material on the bank (58 cm x 88 cm dredge mouth). Although an effort was made to photograph the sea floor (with an EG&G camera) at numerous sites, only four successful exposures were obtained.

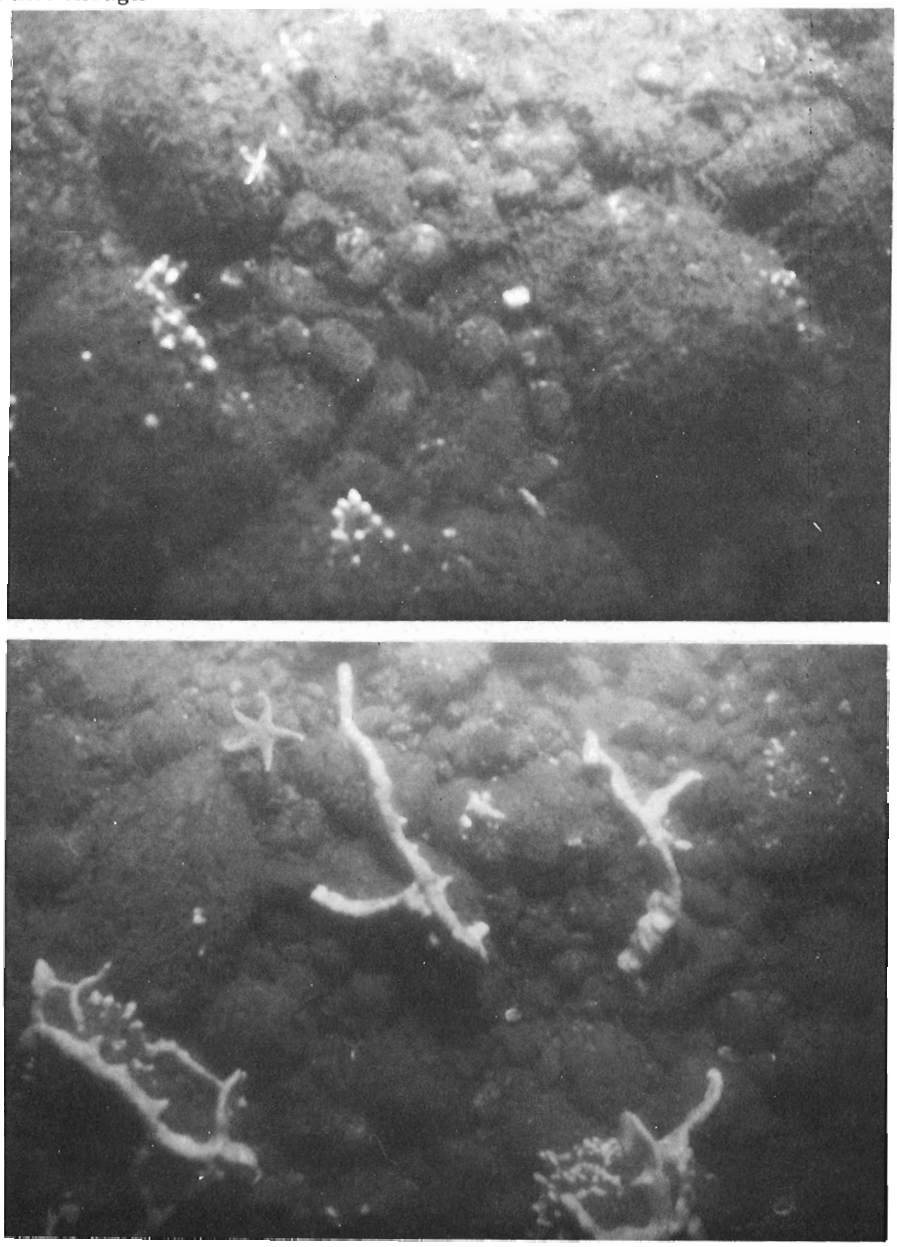

Figure 27.2.

Photographs of the sea floor near site no. 56 (in Fig. 27.3A). Largest boulder dredged in vicinity of the site where the photo was obtained was 35 cm. Surface of boulders and cobbles is covered with what probably is a mat of organisms and not finer sediments. White branch-like material may be bryozoan colony.

From: Report of Activities, Part C; Geol. Surv. Can., Paper 76-1C (1976).

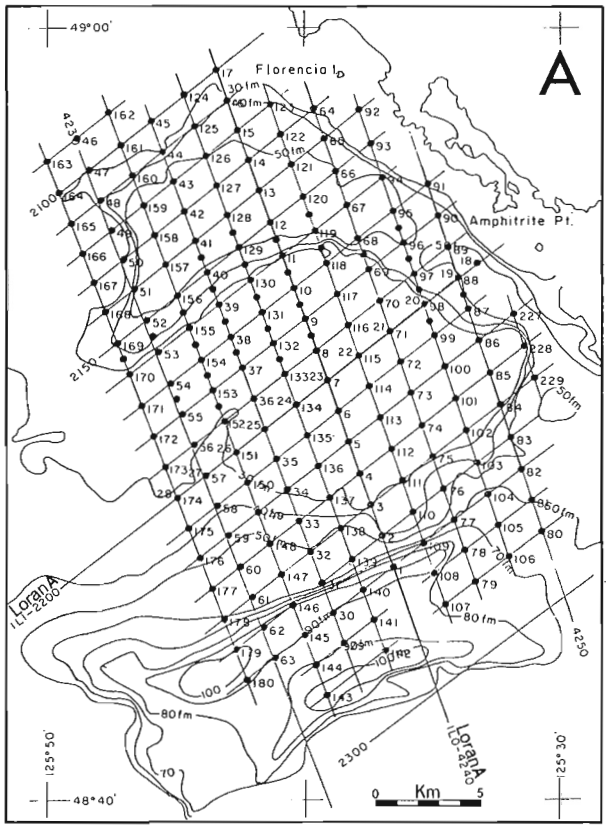

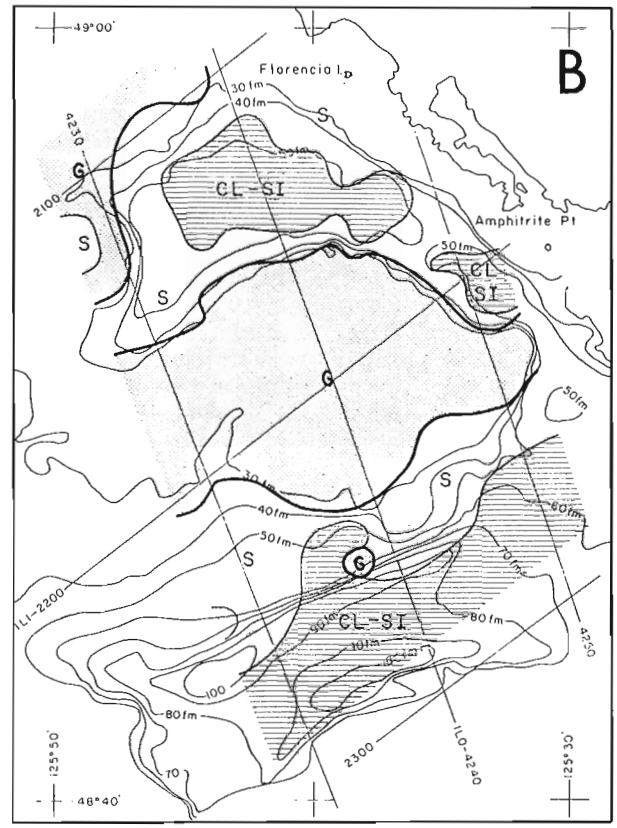

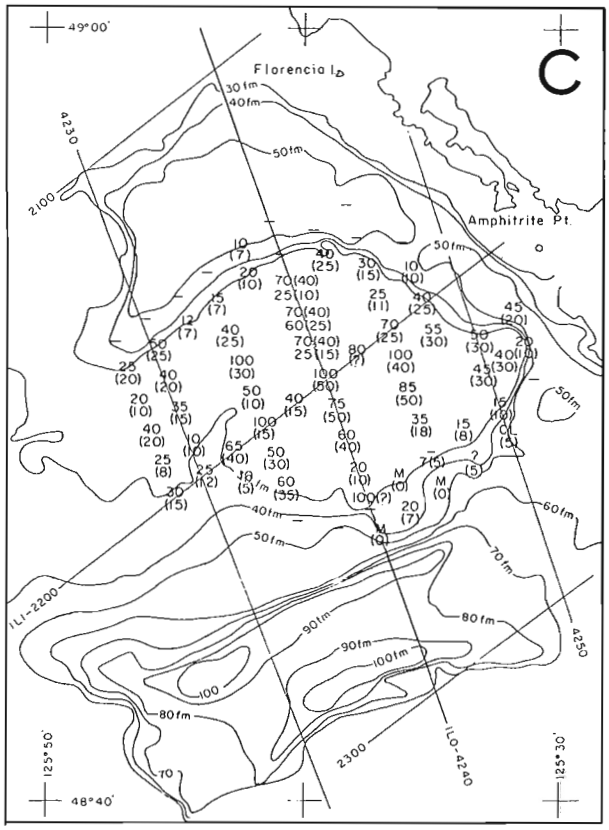

Figure 27.3.

A. Primary sampling grid. Shipek samples obtained at all sites noted. Locations having no numbers beside them have station numbers 0.5 higher than preceding number.

B. Distribution of sediment types suggested by field examination of obtained samples
G = gravel, S = sand, CL - SI = mud.

C. Measured maximum and estimated mean (in brackets) size (cm) of gravels in dredge haul.
M = compacted mud (possibly glacial flour).

N.B. Figures kindly supplied by J. Westrheim.

Results

It is apparent that the bank is mantled by a poorly sorted rubble heap (Figs. 27.3B, 3C, and 2) from which finer materials are being washed north and south onto the bank slopes and into adjacent troughs.

Further work

A cruise is planned by the Fisheries Service for March 1977 to define precisely the distribution of groundfish and to locate preferred spawning grounds. Further geological investigations may involve extensive colour photography, side scan sonar and precision echo-sounding surveys and detailed analysis of sediment grain size.

References

Carter, L.
1973: Surficial sediments of Barkley Sound and the adjacent continental shelf, west coast Vancouver Island; Can. J. Earth Sci., v. 10, p. 441-459.

Harling, W.R., Davenport, D., Wowchuk, R.M., and Wier, K.R.
1976: G.B. Reed groundfish cruises 75-3 (Oct. 7-24, 1975); Fish. Res. Brd. Can., Environ. Can., Ms. Rep. Ser. 1371, 31 p.

Milliman, J.D.
1976: Sand and gravel deposits off southwestern Vancouver Island, B.C.; *in* Report of Activities, Part A; Geol. Surv. Can., Paper 76-1A, p. 23-26.

Westrheim, S.J., Harling, W.R., Davenport, D., and Wowchuk, R.M.
1975: G.B. Reed groundfish cruises 75-1 (April 8-24) and 75-2 (July 8-24) (Data Record); Fish. Res. Brd. Can., Environ. Can., Ms. Rep. Ser. 1367, 56 p.

1976: G.B. Reed groundfish cruise 76-1 (Feb. 10-26, 1976); Fish. Mar. Serv., Environ. Can., Data Records No. 3, 25 p.

Project 740046

Pavel J. Kurfurst[1] and James A. Hunter[2]

A short drilling program and geophysics survey were carried out in March 1976 at the section of the Mackenzie Highway between Willowlake River (Mile 394.7) and River Between Two Mountains (Mile 411.6). The work was done by personnel from Terrain Sciences Division and Resource Geophysics and Geochemistry Division to confirm and supplement the detailed seismic and electrical surveys carried out by Terraquest Surveys Limited in this area in August and September 1974. This study was part of the Terrain Sciences Division's continuing program of assessment of terrain performance in the Mackenzie Valley and the Arctic Islands (Kurfurst, 1975, 1976).

Drilling Program

Six holes were drilled by the Department of Public Works in representative terrain units to confirm interpretation of geophysical surveys (seismic and electrical) already done. All drillholes were situated within 200 feet of the highway centre line on the Terraquest survey transects due to limited accessibility; the locations of drillholes are shown in Figure 28.1 with drillhole numbers corresponding to survey transect numbers.

The drill used was a Nodwell mounted, 4¼ inch open flight auger capable of coring through the hollow

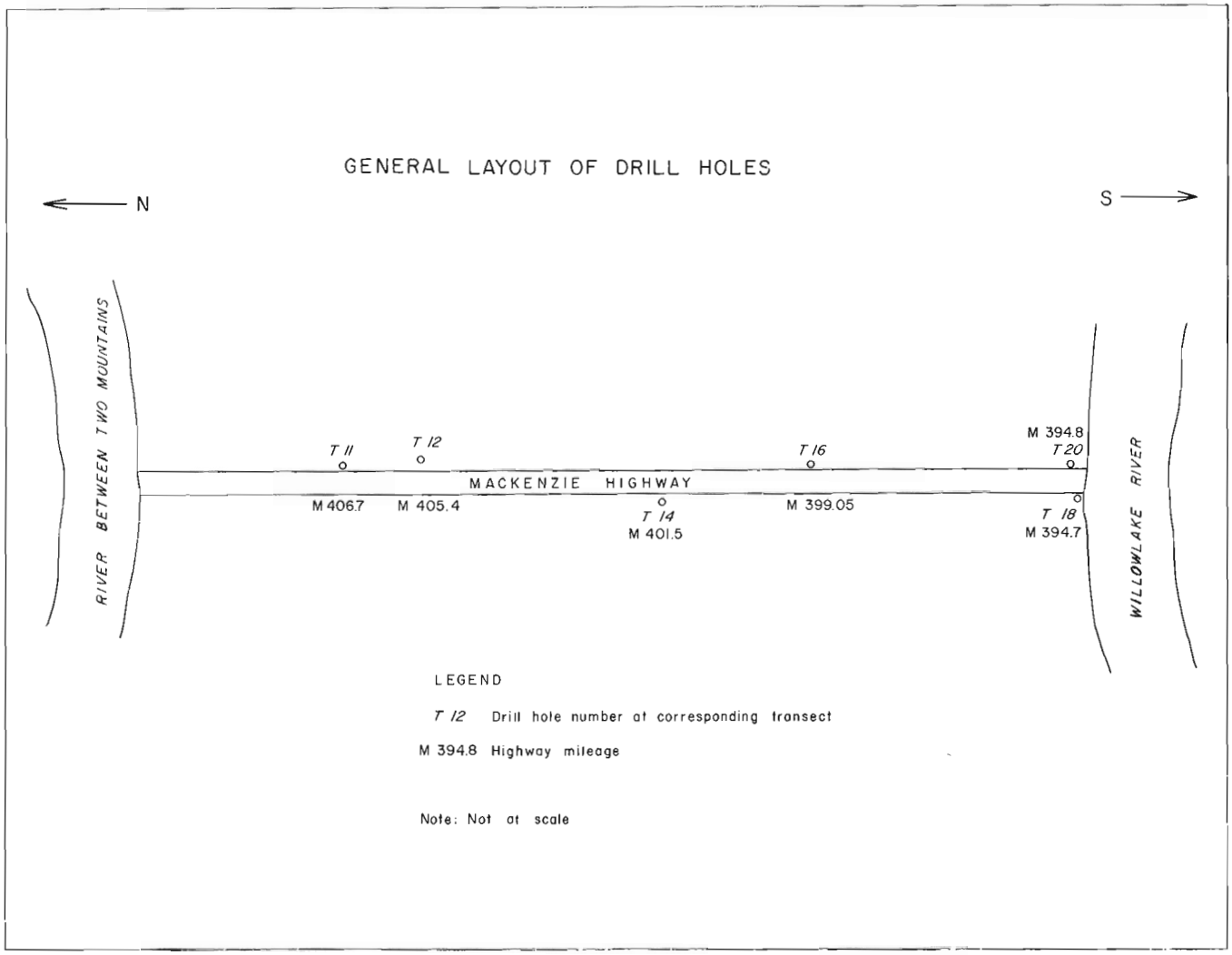

Figure 28.1.

[1]Terrain Sciences Division

[2]Resource Geophysics and Geochemistry Division

From; Report of Activities, Part C;
Geol. Surv. Can., Paper 76-1C (1976).

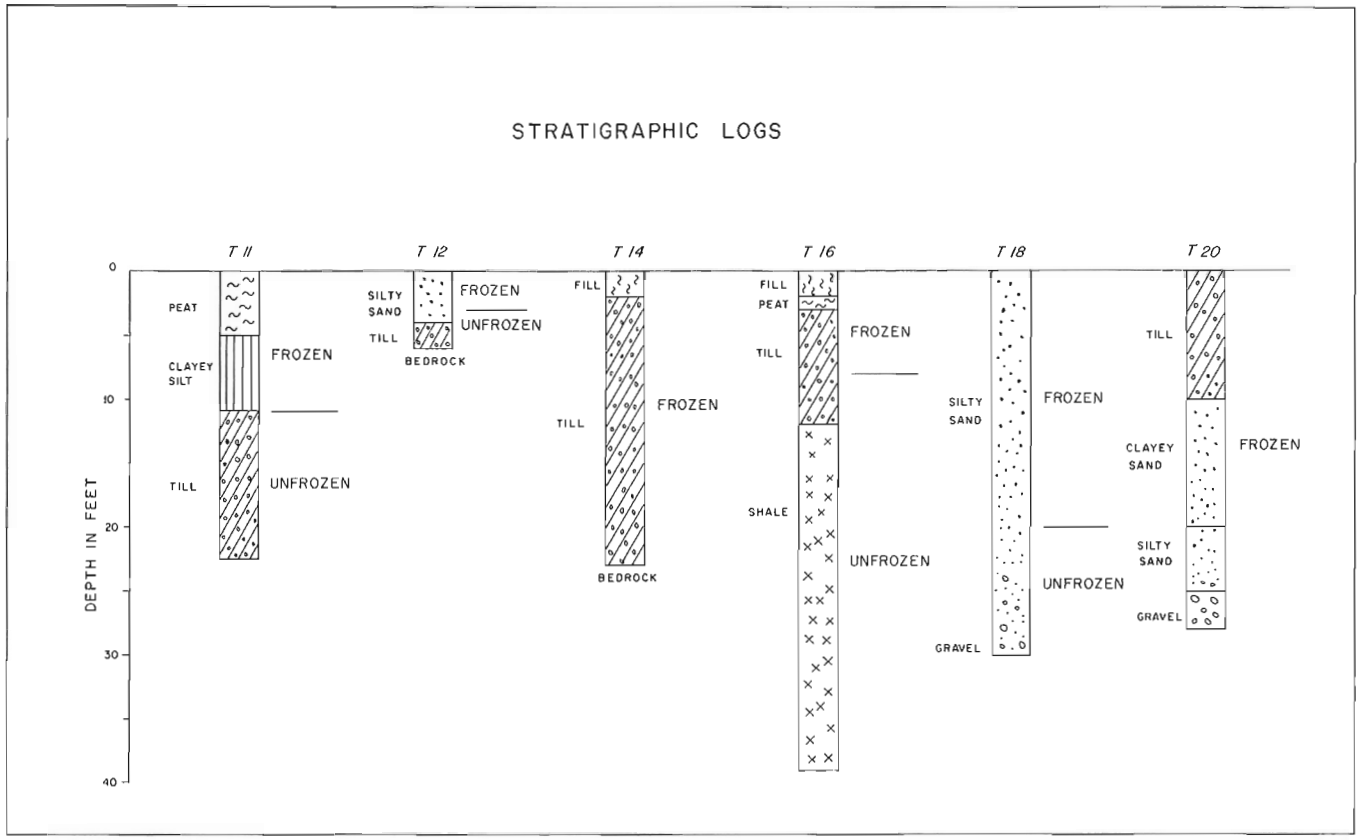

Figure 28. 2.

stem or with core barrel. The depth of drillholes varied from 6 to 39 feet depending on soil type, presence or absence of bedrock, and frozen or unfrozen state of sediments. A wide variety of soil types were encountered during drilling, ranging from sands and gravels to silts and tills to organics (peat). Frozen soils were present in each hole to various depths; however, in several drillholes (T-11, T-12 and T-16) it was presumably only seasonal frost.

Detailed stratigraphic logs with soils being shown as frozen or unfrozen are presented in Figure 28. 2.

Borehole Geophysics

Seismic and γ-γ density tools were run by the Geological Survey of Canada in five of the six boreholes mentioned above. Since hole T-12 was shallow, no logging was done.

The seismic borehole tool used was an OYO "borehole pick" consisting of a three component geophone which is clamped to the borehole wall by means of an expansible liquid-filler bladder. The seismic source was a 16 lb. hammer and plate fitted with a momentary contact switch for timing. Signal waveform was recorded on a single channel Bison enhancement seismograph and photographed from a monitor display on a Tektronix 465 oscilloscope. The vertical component of motion was recorded at 2. 5 foot intervals up each hole. All three components of motion were recorded in hole T-11 for future studies of later events. Onsets of first arrival times can be read to 0. 1 milliseconds, but because of the uncertainty in picking the break, an error no less than ±0. 2 milliseconds could be assigned. The first arrival transit times versus depth of receiver in the hole were plotted. Best fits of straight line velocity segments have been drawn through the results.

A Gerhart-Owens γ-γ density tool was run at one foot intervals up each hole. This unit has not been calibrated in this density range, and readings were taken in counts per second (cps). From previous logging work in permafrost, count rates exceeding 200 cps can be correlated with densities approaching 1. 0 g/cm^3 or lower and indicate the presence of frozen peat or material with excess ice.

Interpretation of Results

The combination of seismic, resistivity, and density surveys and the results from drilling provide a measure of control in the interpretation of permafrost conditions. Till, bedrock, and frozen gravel have a high velocity reading, but are not really distinguishable from seismic work alone; correlation with results of resistivity and density surveys is necessary. This has been corroborated during discussions with the Terraquest Surveys Ltd. personnel (R. Watson, pers. comm., 1976).

Compilation of drillhole and geophysical results for each borehole, including detailed interpretation, is presented below.

HOLE T-11

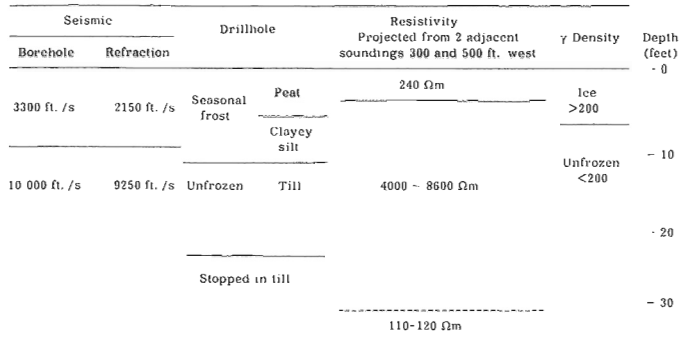

From the resistivity readings the frost appears to be 16 feet thicker than the drilling indicates; this is projected 300 and 500 feet from sides so poor correlation can be expected.

The seismic correlation is good and shows a frost velocity of 2150 to 3300 ft. /s.

Conclusion: Frost is shallow, till gives high velocity and resistivity bedrock is at about 30 feet or so and has low resistivity of 110 to 120 ohm-metres.

HOLE T-12

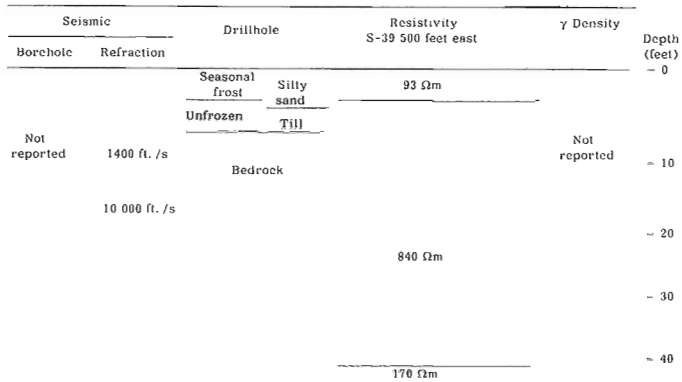

Resistivity sounding is 500 feet east so the position of the deep layer is uncertain. It appears that no permafrost is present and that there is a 30 foot layer of more resistive rock overlying the low resistivity shale at about 40 feet.

HOLE T-14

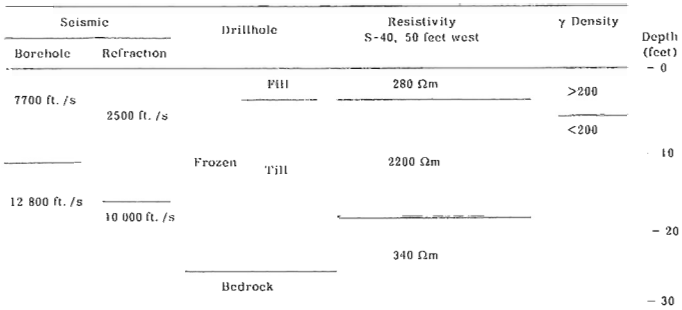

The 2200 ohm-metre resistivity layer represents the permafrost, although this seems to be a low value for frost. Bedrock is represented by the conductive shale of 340 ohm-metres resistivity.

The upper surface of permafrost is probably at a depth of three feet during August.

The velocity contrast at 10 to 13 feet represents a layering in the till.

HOLE T-16

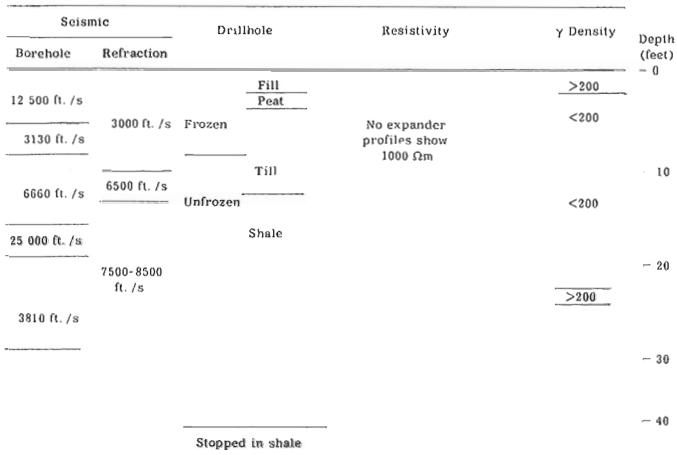

The nearest resistivity expanders are too far away to attempt any correlation.

The borehole seismic results accurately reflect the frost conditions at the time of drilling. The frost probably was not present in August, and the refraction velocities reflect the till (6500 ft. /s) and shale (7500 to 8500 ft. /s).

HOLE T-18

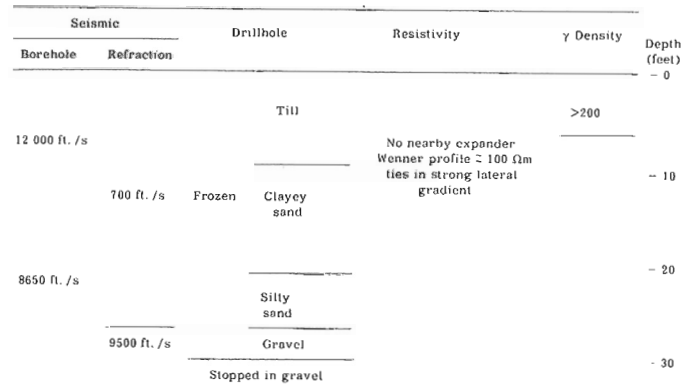

The borehole seismic results accurately reflect the frozen till and sand but are at odds with the refraction seismic result which shows 26 feet of low velocity material. Unfortunately there is no nearby expander to help clarify the picture. The picture is further complicated by a strong lateral resistivity gradient (Wenner) at this point indicating that the drillhole is at the edge of a permafrost layer.

HOLE T-20

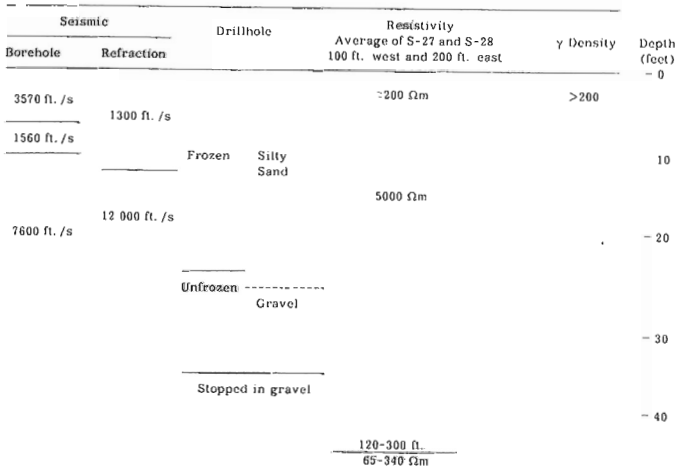

The resistivity was projected from 100 to 200 feet away and suggests that the upper surface of permafrost was at a depth of 4 feet. Evidently the resistivity of the gravel in the unfrozen part remains at 5000 ohm-metres which is slightly high but possible for dry, well drained material. The 12 000 ft. /s velocity layer could be the upper layer of frost.

The lowest resistivity layer is interpreted as the conductive shale at a depth of more than 100 feet. This depth is difficult to define because it is interpreted from only one or two final points on the expander.

References

Kurfurst, P.J.

1975: Assessment of terrain performance in the Mackenzie Valley and the Arctic Islands; *in* Report of Activities, Part B; Geol. Surv. Can., Paper 75-1B, p. 97-98.

Kurfurst, P.J. (cont.)

1976: Assessment of terrain performance in the Mackenzie Valley and the Arctic Islands; *in* Report of Activities, Part A; Geol. Surv. Can., Paper 76-1A, p. 277-279.

29. SEDIMENTARY PROCESSES AND SEDIMENTS, BABBAGE RIVER DELTA, YUKON COAST: A PROGRESS REPORT

Project 740086

D. L. Forbes[1]
Terrain Sciences Division

A study of sedimentation at the mouth of Babbage River (69°15'N, 138°25'W), near Kay Point on the Yukon sector of the Beaufort Sea coast, was initiated in 1974 and continued through 1976 (Forbes, 1975; *see* also Lewis, 1975). The study attempts to assess the hydrological and sedimentary response of the river-mouth zone to inputs of varying character, source, frequency, and magnitude. Special attention has been focused on vulnerability to storm flooding and potential oil invasion (Lewis and Forbes, 1976). Objectives of the project include: (1) documentation of Holocene sediments in the lower valley, delta, and estuary, with emphasis on facies distribution, surface morphology, and processes characterizing the sedimentary environment and (2) measurement of sediment inputs from river and coastal sources and estimation of net short- and long-term accumulation rates landward of the partial barrier extending southwestward from Kay Point (Fig. 29.1).

Sediment transfers are considered in the context of an arbitrarily defined system bounded laterally by the long-term limit of flooding, seaward by the spit and opening between Kay and Niakolik Points, and landward by gauging sections on Babbage River and Deep Creek upstream of tidal influence (*see* Fig. 29.1 for locations: B1 on Babbage, D1 on Deep Creek). The study seeks to assess sensitivity to varying sediment input at periods semidiurnal and greater; tidal effects, response to storms, seasonal trends, and long-term adjustments in climate and sediment supply are of particular interest. McDonald and Lewis (1973), Carson *et al.* (1975), Forbes (1975), and Lewis and Forbes (1976) have described the geographic and sedimentary environment of lower Babbage River. Borehole and seismic data indicate that the delta and lower valley are underlain by sands, silts, and clays, with one or more units of gravel up to 15 m thick within the upper 30 m. The gravel is overlain by fluvial, deltaic, and estuarine deposits of varying texture and ice content and by peat. The peat occurs in isolated units, 2 m or more in thickness, throughout the delta and lower valley. In a core near the delta front, it extended more than 1 m below mean sea level and was underlain by massive ground ice. A sample from the top of peat beneath 80 cm of alluvial silt at location 2 (Fig. 29.1) gave a radiocarbon date of 1270 ± 40 years B.P. (GSC-2157).

Flood Frequency and Extent

The system under study covers about 60 km^2, of which approximately 45 km^2 is subject to marine inundation during exceptional storm-surges. The limit of storm-surge flooding, determined from modern deposits of marine driftwood, is shown in Figure 29.1. Amplitudes and recurrence frequencies of major tidal excursions have been investigated by Henry (1975). Relatively long tidal records are available from Tuktoyaktuk, where one or more surges exceeding 1 m above mean sea level have occurred in most years. At Herschel Island, 35 km northwest of Kay Point, a surge of 1.3 m above mean was reported during the major storm of September 1970 (Canada Department of Public Works, unpublished report, 1971). The astronomical tide at Herschel Island is approximately equivalent to that at Kay Point, where the range is about 0.5 m.

Water levels have been recorded during parts of 1974 and 1975 behind Kay Point spit (point 1, Fig. 29.1) and on Babbage River above the delta (point 2, Fig. 29.1), in co-operation with Ocean and Aquatic Sciences, Environment Canada, Victoria. Tide data for 1975 (Fig. 29.2A) indicate a maximum range at the spit gauge of 1.1 m. Two minor surges occurred on August 10 and 27 (days 222 and 239) with a smaller extreme on August 17. The highest level in 1974 was some 13 cm lower than the 1975 peak, in part due to limited sea-ice withdrawal from the coast.

Flooding of the Babbage delta occurred during the August 10 and 27 surges of 1975, when approximately 65 per cent of the surge-susceptible area landward of Kay spit was inundated. Flooding of the delta plain occurred on three other occasions during 1974 and 1975, all in association with high spring river discharge preceding sea-ice breakup in Phillips Bay; such spring flooding is a common annual event (Lewis and Forbes, 1976, their Fig. 3).

Limits of tidal influence in Babbage River and Deep Creek lie close to the second connecting channel (C2 in Fig. 29.1). Extensive overbank flooding above the delta is rare and most commonly may be associated with ice-jamming during spring floods. Most flows are confined within banks and, in the Babbage, cover only portions of the unvegetated bar surfaces. Peak flows at about 500 m^3/s observed in 1975 and again in June 1976 occupied all active flood channels but failed to flood completely the bar at B1 (Fig. 29.1) and were confined below general bank level at all points above the delta. Ice-jam flooding has been observed during three spring seasons on the river and is partially responsible for the maintenance of active upper-bar surfaces. Ice also may cause anomalously high water levels if high flow occurs before breakup; the channel may remain substantially filled with winter ice which forms the temporary river bed.

[1]Department of Geography, University of British Columbia, Vancouver, B.C., V6T 1W5

From: Report of Activities, Part C;
Geol. Surv. Can., Paper 76-1C (1976).

Vulnerability to Oil

The Babbage estuary supports a large fish population, and adjacent surfaces below the highest storm flood line provide nesting sites for large numbers of waterfowl. Experience in analogous settings elsewhere indicates that effects of oil invasion could be substantial and prolonged. The confluence of longshore currents in Phillips Bay (Lewis, 1975) may tend to increase the probability of oil into the vicinity. Should such an occurrence coincide with a major storm, a typical combination of circumstances including high storm tide, northwesterly wind, and high suspended sediment concentration in the estuary would serve to encourage deposition of oil in the delta and estuary.

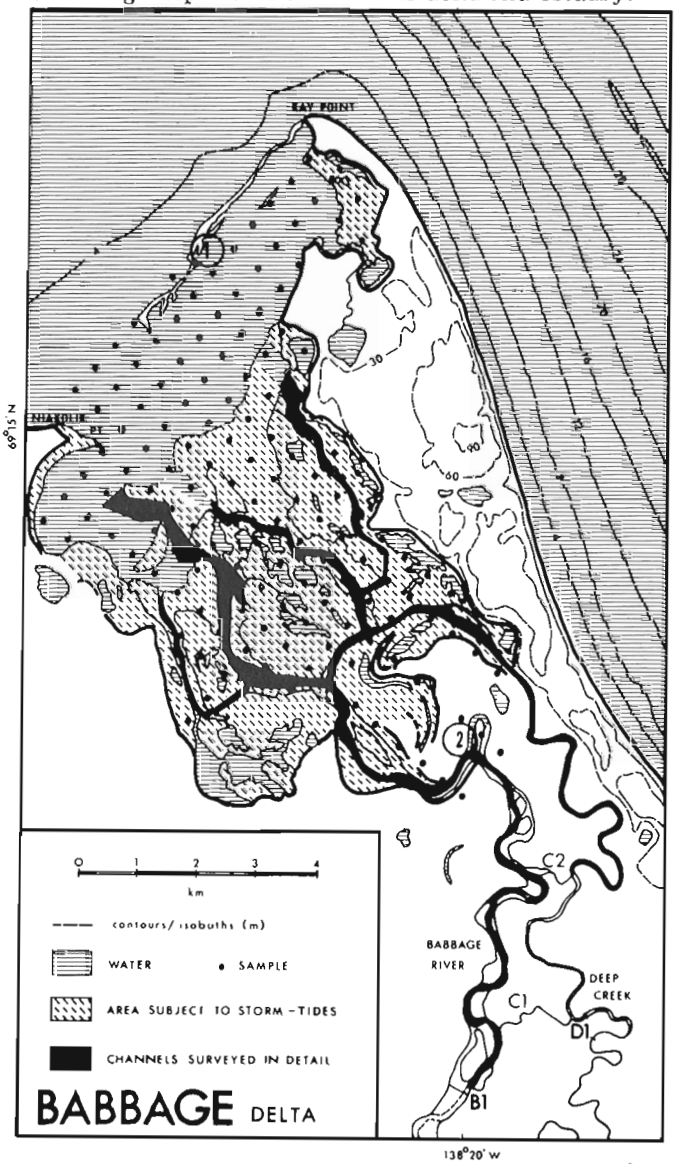

Figure 29.1. Babbage River delta, with locations of gauging sections (B1 and D1), tide gauges (1 and 2), and surface sediment samples. Channels surveyed in detail and zone vulnerable to storm-surge flooding also are indicated.

Near-surface sediments in the delta have segregated ice concentrations ranging from 0 to 90 per cent by volume; oil deposition on delta surfaces may pose a risk of thermal disturbance leading to thaw consolidation.

Water and Sediment Transfers

Detailed hydrometric observations were carried out at B1 and D1 during 1975 for the purposes of characterizing the relative importance of river inputs to the Babbage delta and estuary and of estimating total fluvial sediment supply to the system. The contribution from Deep Creek is relatively minor compared to input from the Babbage.

The 1975 hydrograph for the Babbage River at B1 (Fig. 29.2D) illustrates a seasonal pattern which is considered quasi-typical: characteristic dominance by spring snowmelt flooding in June; a long summer recession; subsequent late-summer resurgence associated with increasing storm frequency in August; recession following onset of cold temperatures in September. Differences in the mean position of the arctic front from year to year may cause variations in frequency and intensity of rain floods from June to September. Substantial storm flows have been observed in July 1972 (McDonald and Lewis, 1973) and in August 1974; it appears that such events may be poorly represented in the 1975 record.

The tidal and discharge data presented above allow a preliminary assessment of the relative impact of river discharge in the tidal portions of the system. Net water transfers into and out of the system were cumulated separately for flood and ebb tides; inputs from the Babbage were plotted as proportions of total net flood or ebb tide transfers (Fig. 29.2B; positive values correspond to flood, negative to ebb). It is apparent that river influence in the estuary varies considerably through the season. Tidal data for the snowmelt flood are not available, but river water clearly dominated during this event in June; water in the bay mouth off Niakolik Point was typically fresh at that time. On occasion, Babbage flow still accounted for more than the net flood-tide influx well into the recession from spring flood levels in early July (days 182-183). Discharge in the Babbage declined to near zero in late July 1975; river influence in the estuary diminished as a result and salinities off Niakolik Point reached 9‰ with higher concentrations observed further northeast in the bay toward Kay Point. Substantial though variable river contributions reappeared following the early August storm.

Preliminary current velocity measurements were obtained in the bay mouth off Kay Point spit during a two-week period in late August 1975. The record was obtained approximately 40 cm above bottom in more than 2 m of water, using an Aanderaa RCM4 meter. The data indicate common peak ebb flows exceeding 15 cm/s, with maximum flood speeds much lower. A peak flow of 29 cm/s was recorded during the storm surge of August 27.

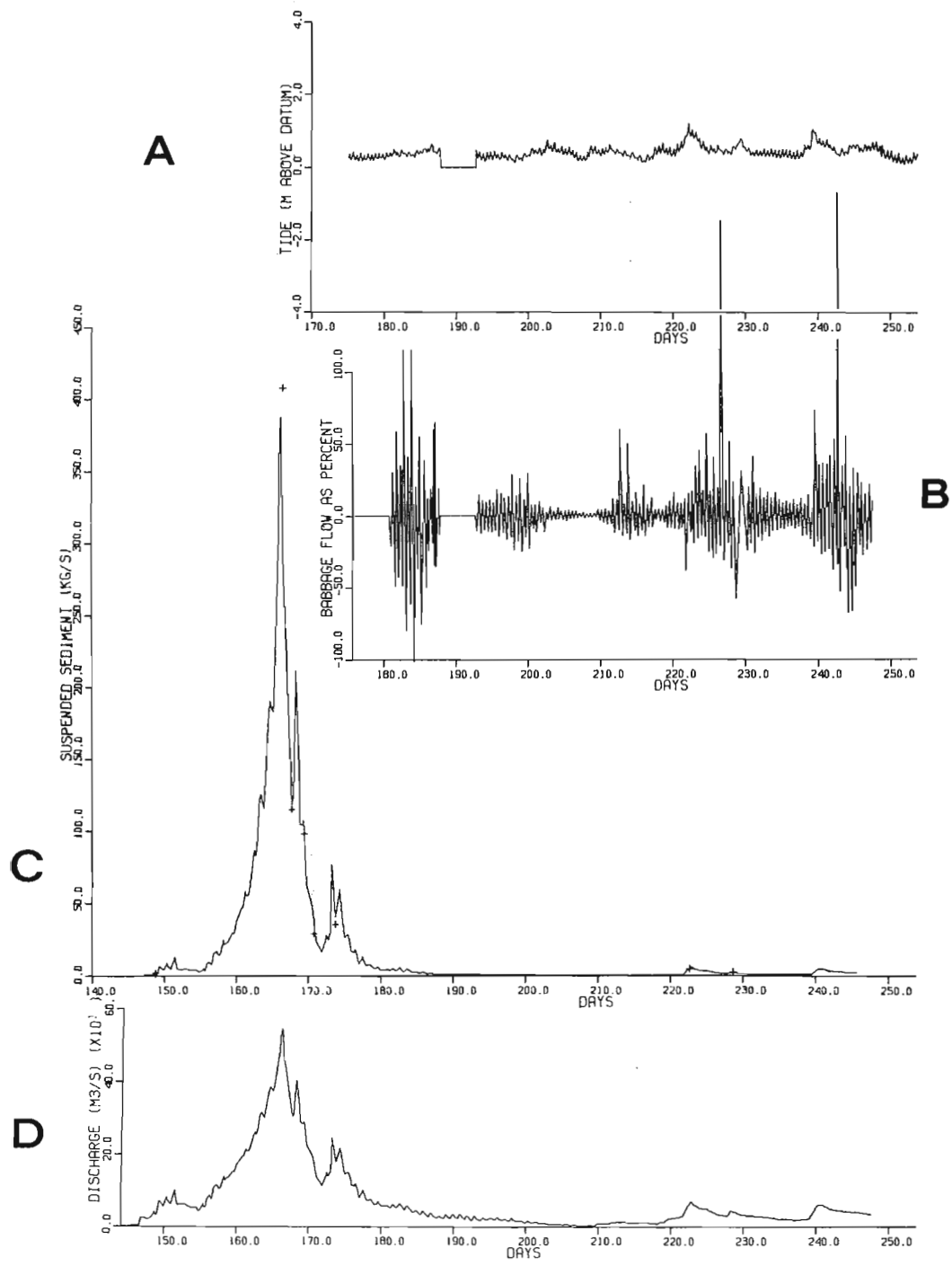

A. tide level at point 1 on inner side of Kay Point spit.

B. Babbage River inflow as percentage of net flood and ebb tide transfers.

C. preliminary estimate of suspended sediment discharge, Babbage River at B1.

D. discharge hydrograph (2-hour means) for Babbage River at B1.

Figure 29.2. Summary data for 1975 (days from January 1).

Instrument delivery problems forced postponement of plans to document suspended sediment and bedload transfers through the bay mouth. Water samples and Secchi disc observations in the estuary and delta provide some data on the time and spatial variations of suspended sediment concentration in the system.

Hydrometric data from the river sections provide the basis for estimation of total river sediment discharge. Acceptable bedload transport estimates are considered feasible and validation by direct measurement has been initiated in 1976. Suspended sediment discharge has been monitored using water samples obtained with a DH48 depth-integrating sampler. Results available from initial filtration through Whatman-40 paper (98% retention of particles coarser than 8×10^{-3} mm) provide a preliminary coarse suspended sediment series for the Babbage at B1 (Fig. 29.2C) and a tentative total of order 10^8 kg/year for 1975. Over 90 per cent of total suspended sediment discharge through B1 in 1975 occurred during June.

Sampling of surface sediments of the delta and estuary has been continued on a 500-m grid (*see* Fig. 29.1 for locations). Further evidence of erosion and degradation of the delta plain facies was noted in 1975. Deposition of fine sediment following spring flooding and the tidal surges of August was discontinuous and almost negligible. Little sediment was present on bottomfast ice in the estuary in June, indicating that most suspended sediment introduced with the spring freshet may be flushed through the system into Phillips Bay.

References

Carson, J.M., Hunter, J.A., and Lewis, C.P.
1975: Marine seismic refraction profiling, Kay Point, Yukon Territory; *in* Report of Activities, Part B; Geol. Surv. Can., Paper 75-1B, p. 9.

Forbes, D.L.
1975: Sedimentary processes and sediments, Babbage River delta, Yukon coast; *in* Report of Activities, Part B; Geol. Surv. Can., Paper 75-1B, p. 157.

Henry, R.F.
1975: Storm surges; Beaufort Sea Project, Tech. Rep. No. 19, Environ. Can., Victoria, 41 p.

Lewis, C.P.
1975: Sediments and sedimentary processes, Yukon Beaufort Sea coast; *in* Report of Activities, Part B; Geol. Surv. Can., Paper 75-1B, p. 165.

Lewis, C.P. and Forbes, D.L.
1976: Coastal sedimentary processes and sediments, southern Canadian Beaufort Sea; Beaufort Sea Project, Tech. Rep. No. 24, Environ. Can., Victoria, 68 p.

McDonald, B.C. and Lewis, C.P.
1973: Geomorphic and sedimentologic processes of rivers and coast, Yukon coastal plain; Environmental-Social Program, Northern Pipelines, Task Force on Northern Oil Development, Rep. 73-39, 245 p.

30. DATED ORGANIC MATERIAL BELOW MAZAMA(?) TEPHRA: ELK VALLEY, BRITISH COLUMBIA

Project 720083

J. E. Harrison
Terrain Sciences Division

A horizontal organic layer, 1 cm thick, was discovered in a 5 m-high silt cutbank on the east side of Elk River 14.5 km north of Elkford, British Columbia (Fig. 30.1). The horizon, containing burnt and/or decomposed wood, unidentifiable organic matter, and pollen, could be traced continuously for about 50 m upstream along the face of the exposure to where it was truncated by gravel channel fill. Figure 30.2 shows the site where samples were collected for ^{14}C dating; the stratigraphy of the site is sketched alongside the photograph. The sampled horizon overlies 3 m of massive silt and silty sand covered by colluvium. Above the horizon faintly bedded silts, 1 m thick, separate the organic material from a white tephra, 10 cm thick, believed to be Mazama. The metre of silt above the tephra shows faint bedding with the upper 30 cm oxidized and containing numerous small roots.

Two samples were collected by parting the silt along the organic horizon and scraping the black material from the surface of the blocks. Sample GSC-2142 collected in 1974 was dated at 11 900 ± 100 years B.P. The following summer a second sample, GSC-2275, was collected and submitted for analysis and produced a date of 12 200 ± 160 years B.P.

The sample site lies on a scarp of a terrace which is 5 to 7 m above river level. The terrace lies in a steep-walled, mile wide alluvial plain and is cut into till and outwash deposits. Across the valley from the collection site a 44 to 50 m-high scarp separates the flat upper surface of the till and outwash from the alluvial plain. The author believes the terrace was formed during downcutting of the river into the till and outwash. As the river channel migrated westwards across the valley, it left fine grained deposits in backwaters. The river migrated laterally as far west as the base of the present scarp before shifting eastwards again. During the lateral migration eastwards the channel was lowered 5 to 6 m by erosion, and thus it began to cut into former backwater deposits.

Organic material, possibly debris from a forest fire, was swept and later buried into these backwater deposits. The channel continued to collect sediment including Mazama tephra which fell on the area approximately 6600 years B.P. Continuing deposition of fine grained material buried the ash, and later forest cover developed.

Analysis of the 1974 sample for pollen (determined by R.J. Mott; unpublished Palynological Report 76-1) revealed an assemblage dominated by pine (*Pinus*), with only minor amounts of spruce (*Picea*), western hemlock (*Tsuga heterophylla*), birch (*Betula*), alder (*Alnus*), grasses (Gramineae), composit (Liguliflorae), and members of the evening-primrose family (Onagraceae). In addition a few grains of Douglas fir (*Pseudotsuga menziesii*), *Myrica*, and a clubmoss (*Lycopodium lucidulum*) were found. No mosses, diatoms, or plankton were found in the sample. The presence of evening-primrose pollen, one species of which is fireweed (*Epilobium angustifolium*), and the charred

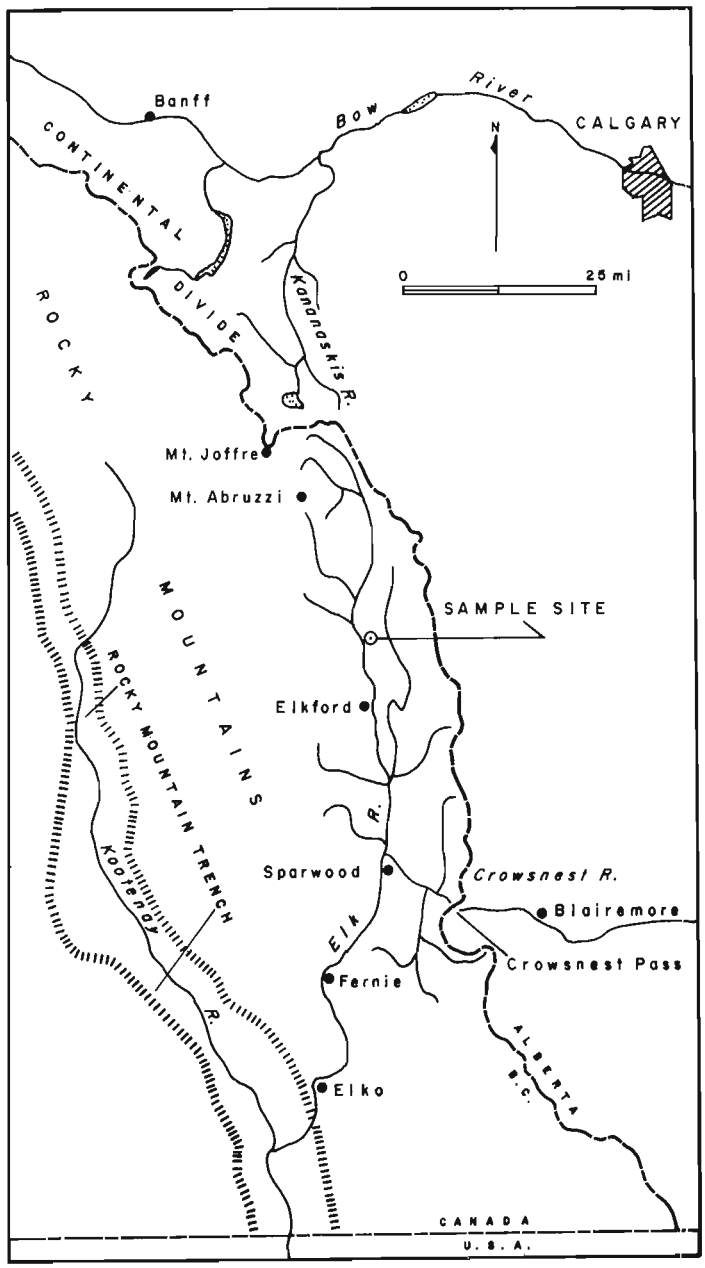

Figure 30.1. Location map showing sample site and features discussed in the text.

From: Report of Activities, Part C;
Geol. Surv. Can., Paper 76-1C (1976).

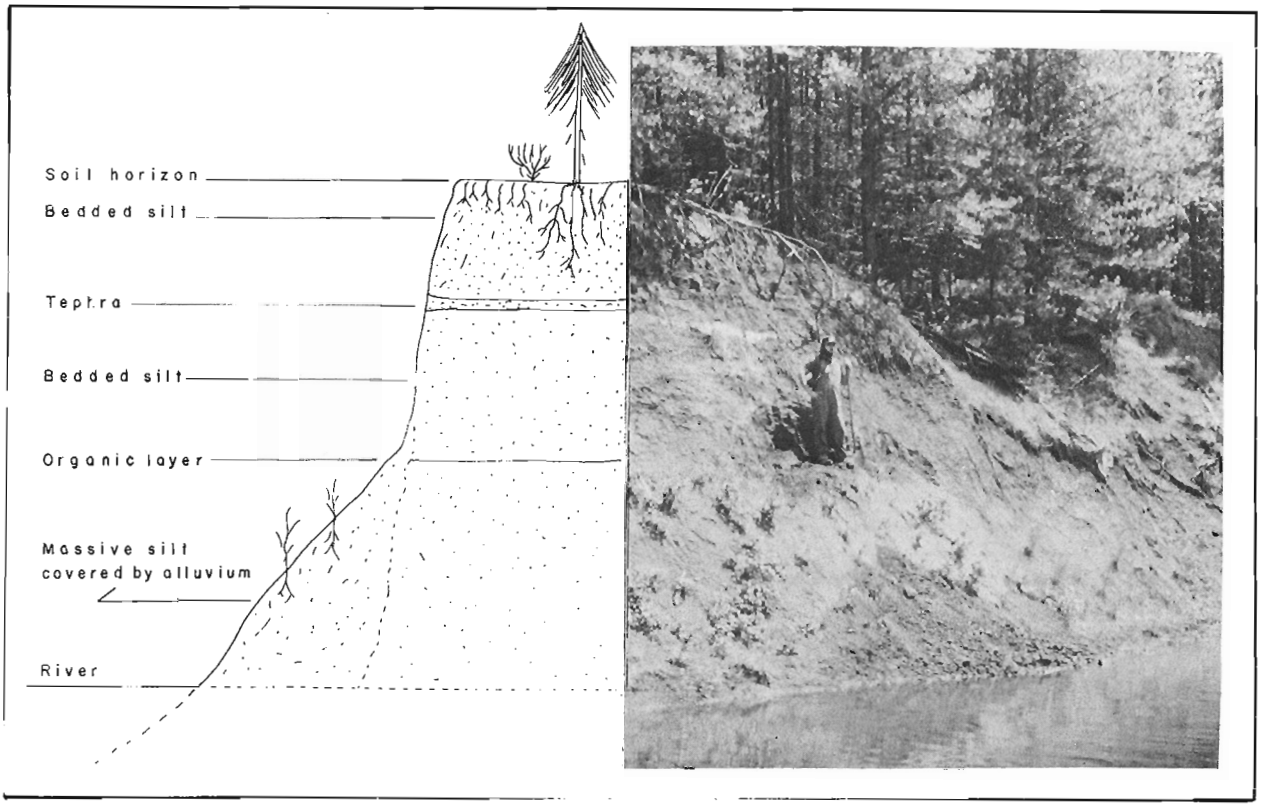

Figure 30. 2. Cutbank on east side of Elk River showing stratigraphic relationship of organic material, silts, and tephra.

nature of the woody material indicate the occurrence of a forest fire.

High percentages of pine pollen from the basal section of cores have been reported from southeastern British Columbia; this fact, together with the dates obtained, indicates that the pollen was derived from a recently deglaciated area.

The till and outwash valley fill into which the river has incised is graded to the 1375 m (4500 ft.) level of glacial Lake Elk. Glacial Lake Elk must have drained and Elk River eroded to the level of the sample site, 1356 ± 8 m a. s. l., before deposition of the dated material. Although glacial Lake Elk was created by damming of Elk Valley at Elko by ice in the Rocky Mountain Trench (Clague, 1973), deglaciation of that portion of the Trench also must predate deposition of the organic material dated.

Deglaciation of the sample site area occurred some time before 12 000 B. P. Today the site is only 24 km downstream from the ice field of Mount Abruzzi and 60 km downstream from the ice field of Mount Joffre. The Mount Joffre ice field lies on the divide between Kananaskis and Elk rivers. If the ice from this field had retreated up Elk Valley to above 1375 m elevation by 12 000 years B. P. and did not advance again below that level as indicated at the site, it is difficult to envision a major advance down Kananaskis Valley at a later date since these two valleys share a common ice source. This date, therefore might also serve as a minimum date for deglaciation of the lower and middle Kananaskis Valley. This does not rule out advances that did not reach 1375 m; in fact lakes in upper Elk Valley, which are dammed by glacial material at elevation 2100 m, may represent an equivalent to the Eisenhower Junction advance (Rutter, 1969) which flowed down Bow Valley to about the same elevation.

References

Rutter, N. W.
1969: A late-Pleistocene glacial advance, Bow River valley, Alberta, Canada; Quat. Geol. Clim. Publ. 1701, Natl. Acad. Sci., Proc., p. 104-109.

Clague, J. J.
1973: Late Cenozoic geology of the southern Rocky Mountain Trench, British Columbia; unpubl. Ph. D. thesis, Dept. Geological Sciences, University of British Columbia, Vancouver, B. C., 274 p.

31. POSTGLACIAL MARINE SUBMERGENCE AT LAC FORD, NORTHERN UNGAVA, QUEBEC

Project 750063

W. Blake, Jr.
Terrain Sciences Division

Introduction

During the last decade much new information has been gathered on the age and elevation of postglacial raised beaches and other features of marine origin in northern Quebec; *see* Haselton (1970), Walcott (1972), Plumet (1974), and Walcott and Craig (1975) for data on Richmond Gulf and nearby areas on the east coast of Hudson Bay, and Matthews (1967) for the northern coast of Ungava, fronting on Hudson Strait. One of the most neglected parts of the same region has been the coast of Ungava Bay itself, although work is being undertaken now along the western side of the Bay by staff members (C. Hillaire-Marcel and B. de Boutray) of the Département des Sciences de la Terre, Université du Québec à Montréal. The purpose of the present note is to report a recently obtained radiocarbon date on marine pelecypod shells from Lac Ford, just over 30 km southwest of the head of Hopes Advance Bay, and approximately 165 km northwest of Fort Chimo (Fig. 31.1).

Collection Site and Results

The collection on which this report is based was made in July 1975 by H. Ouellet, Assistant Curator of Ornithology, National Museum of Natural Sciences. The shells were extracted from clay some 2 m below the bog-covered ground surface, at the extreme west end of Lac Ford, where Rivière au Chien-Rouge debouches into the lake.

The sample consisted entirely of aragonitic shells of *Clinocardium ciliatum* (Fabr.); six valves (12.7 g), although apparently not pairs, were used for the age determination of 6270 ± 100 years B.P. (GSC-2311). This value is based on two 1-day counts in the 2-litre counter and is corrected for isotopic fractionation.

Discussion

Although the elevation of the collection site is estimated at 105 m a.s.l. by the collector on the basis of the 1:250 000 map-sheet (24 M, Peters Lake), unpublished data in the files of the Geodetic Survey, Surveys and Mapping Branch (pers. comm. to G. Mizerovsky), indicate that the correct elevation of Lac Ford is closer to 90 m, in which case the elevation of the sample is probably below 100 m. At the time the pelecypods were living, sea level was an unknown amount higher with respect to the land, so that 100 m is a minimum value for the contemporaneous sea level, and a value as high as 120 m may be correct. Thus the rate of emergence over the last 6000 years has averaged between 1.5 and 2 m per century. It is of interest to note that the shells at Lac Ford are somewhat higher in elevation than are mollusc shells in the 6000 to 6700 year-range along the northern coast of Ungava (Matthews, 1967; cf. also Rogerson *in* Andrews and Drapier, 1967). It seems reasonable to expect that the ice cover over this island site, which is bounded offshore by a relatively wide zone of shallow water in western Ungava Bay (Fig. 31.1, inset map), would have been thicker than the ice over the northern coast of Ungava, where much ice was drawn off to the southeast by the outlet glacier flowing through Hudson Strait.

The dated shells from Lac Ford not only provide information on the time of marine incursion and the rate of postglacial emergence on the west side of Ungava Bay, but they have a bearing on the age of the huge ice-dammed lakes which once existed in both northern Ungava and along the western side of the Labrador-Quebec boundary (cf. Fig. 31.1 and Prest *et al.*, 1968). By the time the northeastward-flowing ice (Fig. 31.2) on the west side of Ungava Bay had receded so that the sea could penetrate southward and westward as far as Lac Ford, the ice holding up the major lake in northern Ungava also must have thinned considerably and the lake drained.

In the same way it can be reasoned that, at a time when glacier ice still remained over the southeastern part of Ungava Bay (necessary to hold up the former lakes along the Quebec-Labrador border), it seems likely that the Lac Ford area was ice covered also. Ives *et al.* (1976, p. 51) stated, on the basis of two radiocarbon age determinations on lake sediment cores, that "these dates relate to the highest Naskaupi shoreline and indicate that the lake system began to form sometime after 8700 B.P. and that the major drainage had occurred prior to 6800 B.P.". It may well be that deglaciation of the Lac Ford area also had occurred by 6800 years ago. It is hoped that additional collections of marine mollusc shells and other datable materials will be made around the perimeter of Ungava Bay so that the chronology of deglaciation and the pattern of marine incursion can be worked out in detail.

Acknowledgments

Particular thanks are due to H. Ouellet of the National Museum of Natural Sciences, Ottawa for making the sample available for dating. Dr. A.H. Clarke, Jr., of the same organization, carried out the specific identification, and A. Roberts, of the Geological Survey's X-ray Diffraction Laboratory, determined the mineralogy of the shell material. Mrs. G. Mizerovsky kindly checked into the files with regard to the elevation of Lac Ford.

From: Report of Activities, Part C;
Geol. Surv. Can., Paper 76-1C (1976).

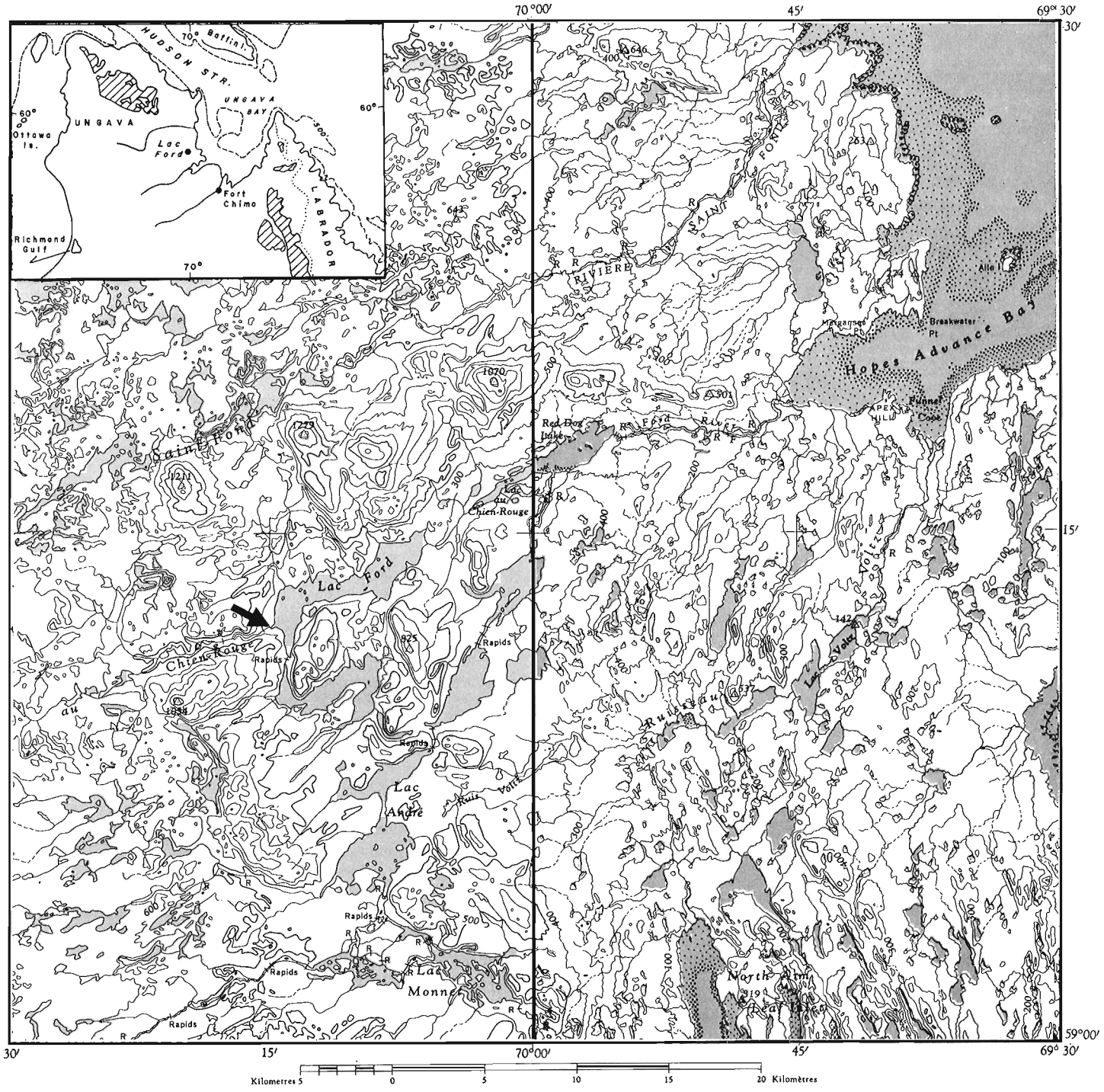

Figure 31.1. Location of Lac Ford, northern Ungava. Base map is a combination of the 1:250 000 map-sheets for 24 M, Peters Lake, and 24 N, Hopes Advance Bay, Surveys and Mapping Branch, Dep. EMR, 1965 and 1961, respectively; contour interval, 100 feet. The shell collection site at the western end of Lac Ford is indicated by the arrow. The inset map, adapted from the Atlas of Canada (4th edition, sheets 1-2 and 33-34), Surveys and Mapping Branch, shows the location of Lac Ford with respect to the former ice-dammed lakes (diagonal pattern) in northern Ungava and along the Quebec-Labrador boundary.

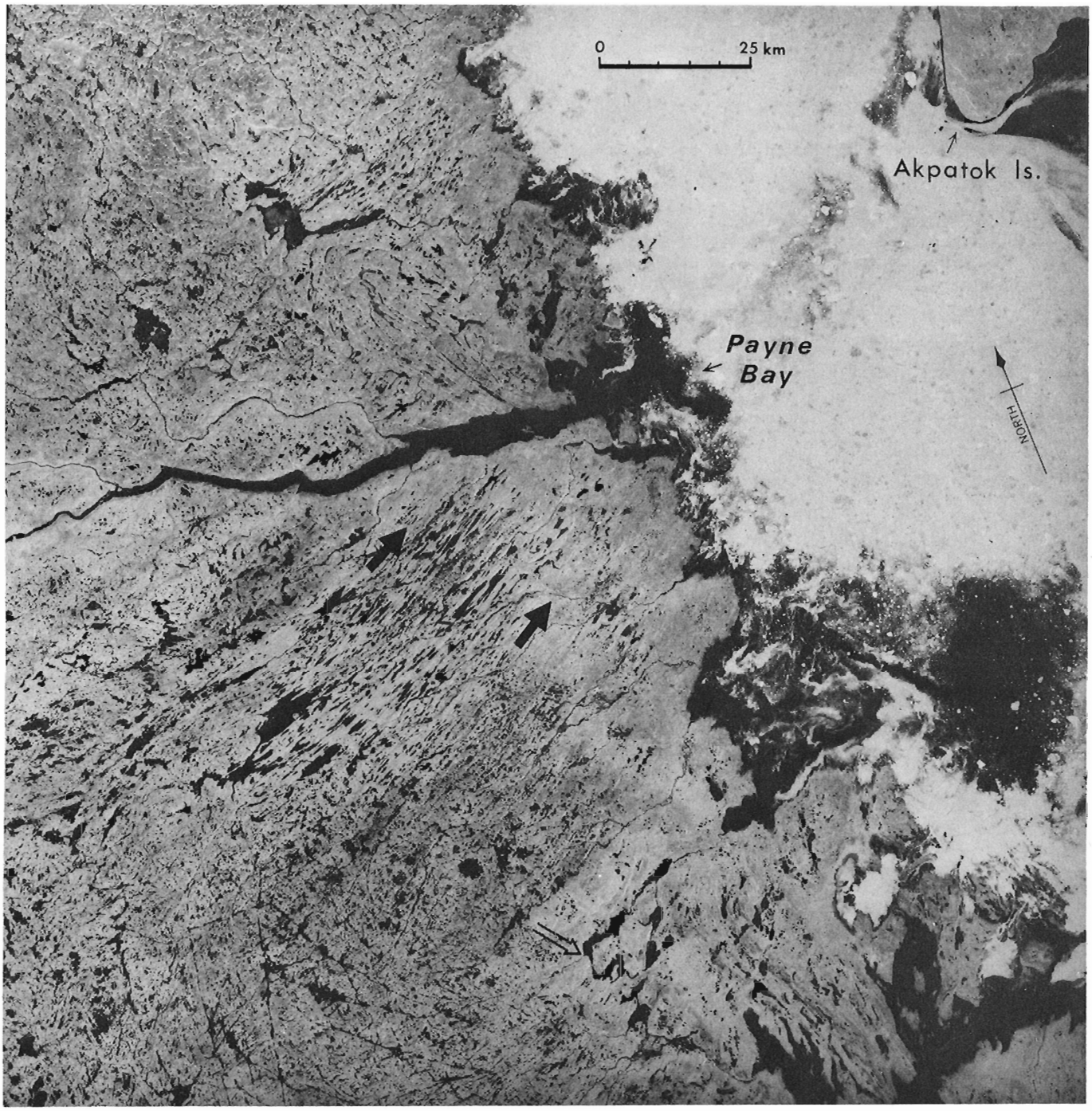

Figure 31.2. LANDSAT image showing the west side of Ungava Bay. The shell collection site at Lac Ford is shown by the open arrow. The direction of ice flow, southwest of Payne Bay, is indicated by the solid arrows. Image E-1712-15165 (spectral band 7) created July 8, 1974.

References

Andrews, J.T. and Drapier, L.
1967: Radiocarbon dates obtained through Geographical Branch field observations; Geogr. Bull., v. 9, p. 115-162.

Haselton, G.M.
1970: Marine beach investigations in the Richmond Gulf area, eastern Hudson Bay, Quebec (part of 34 C); *in* Report of Activities, Part A; Geol. Surv. Can., Paper 70-1A, p. 174-175.

Ives, J.D., Nichols, H., and Short, S.
1976: Glacial history and palaeoecology of north-eastern Nouveau-Québec and northern Labrador; Arctic, v. 29, p. 48-52.

Matthews, B.
1967: Late Quaternary land emergence in northern Ungava, Quebec; Arctic, v. 20, p. 176-202.

Plumet, P.
1974: L'archéologie et le relèvement glacio-isostatique de la région de Poste-de-la-Baleine, Nouveau-Québec; Rev. Géogr. Montréal, v. 28, p. 443-447.

Prest, V.K., Grant, D.R., and Rampton, V.N.
1968: Glacial map of Canada; Geol. Surv. Can., Map 1253A.

Walcott, R.I.
1972: Late Quaternary vertical movements in eastern North America: quantitative evidence of glacio-isostatic rebound; Rev. Geophys. Space Phys., v. 10, p. 849-884.

Walcott, R.I. and Craig, B.G.
1975: Uplift studies, southeastern Hudson Bay; *in* Report of Activities, Part A; Geol. Surv. Can., Paper 75-1A, p. 455-456.

32. THE DETERMINATION OF ATTITUDES OF PLANAR STRUCTURES BY STEREOGRAPHIC PROJECTION AND SPHERICAL TRIGONOMETRY

Project 740057

J. S. O. Lau and J. E. Gale
Terrain Sciences Division

Introduction

The strike and dip of a planar structure that intersects two or more drillholes can be determined from solutions obtained with graphs (Lyons, 1964), stereographic projection (Phillips, 1960; Ragan, 1968), solid analytical geometry (Mertie, 1943), or trigonometry (Stein, 1941). For the one drillhole problem, the attitude of any planar structure that intersects a single drillhole can be determined if the orientation of the core obtained from the drillhole is known.

As part of the subsurface containment of solid radioactive waste project (Gale *et al.*, 1976), procedures are being developed to measure and analyze the orientation, frequency, and hydraulic characteristics of planar features (primarily fractures) in drill cores and boreholes through the use of core orientators, core inscribers (Goodman, 1976), and borehole surveys. Central to such a program is the need to determine the true orientation of fractures, etc., from their angular relationships to some reference line or planar feature (reference plane which is used to orient the reference line if the orientation of the reference line is not known) that is present throughout the core and has a known orientation. Two angular measurements α and β can be used to relate the orientation of the planar structures to an oriented reference line on the core for the solution of problems by stereographic projection and spherical trigonometry relationships presented herein. Additional information required are the dip and the azimuth of dip of the drillhole at the point of intersection of the planar structure and the core.

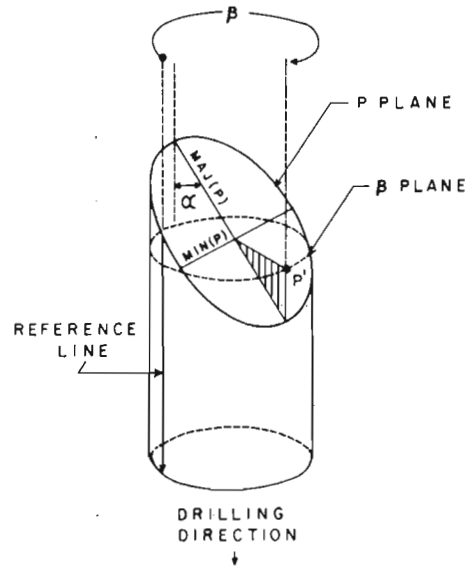

Figure 32. 1. Angles α and β and the reference line.

Angles α and β

Let β plane be the plane perpendicular to the axis of the core. Any planar structure that is not parallel or normal to the axis will intersect the core to form an ellipse. Goodman (1976) pointed out that for each planar structure, two angles can be measured: α the angle between the core axis and the major axis of the ellipse of intersection, and β, the angle at which the downward end of the major axis of the ellipse meets the core circumference measured in the β plane from a reference line and measured clockwise looking in the direction of drilling (Fig. 32. 1).

Solution by Stereographic Projection

The determination of the orientation of the reference line and subsequently the orientation of any planar structure by stereographic projection have been discussed by Goodman (1976), and therefore only a summary of the solution will be presented in this paper to facilitate the description of the solution by spherical trigonometric formulae.

The minor axis of the ellipse of intersection of the reference plane (R plane) and the core is the line of intersection of the R plane and the β plane. In Figure 32. 2 and β plane and the R plane are plotted stereographically. The R plane and the β plane intersect at MIN(R). The downward end of the major axis of the ellipse of

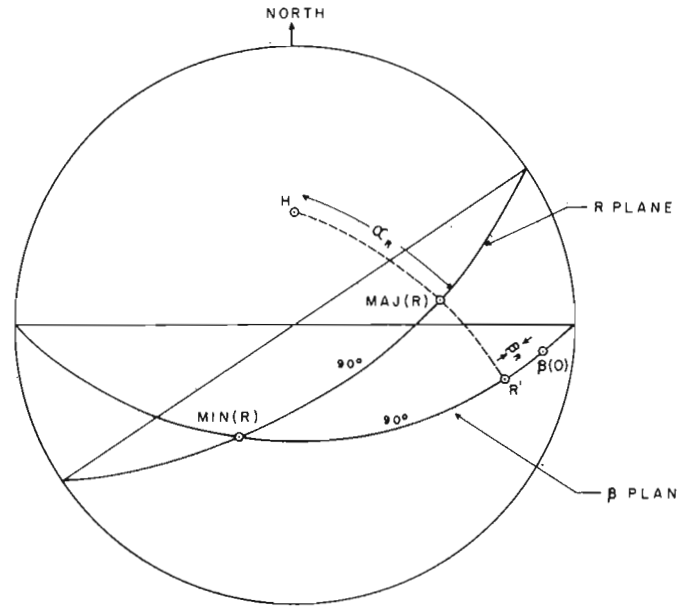

——— Great circle in the lower hemisphere

Figure 32. 2. Orientation of the reference line by stereographic projection.

From: Report of Activities, Part C; Geol. Surv. Can., Paper 76-1C (1976)

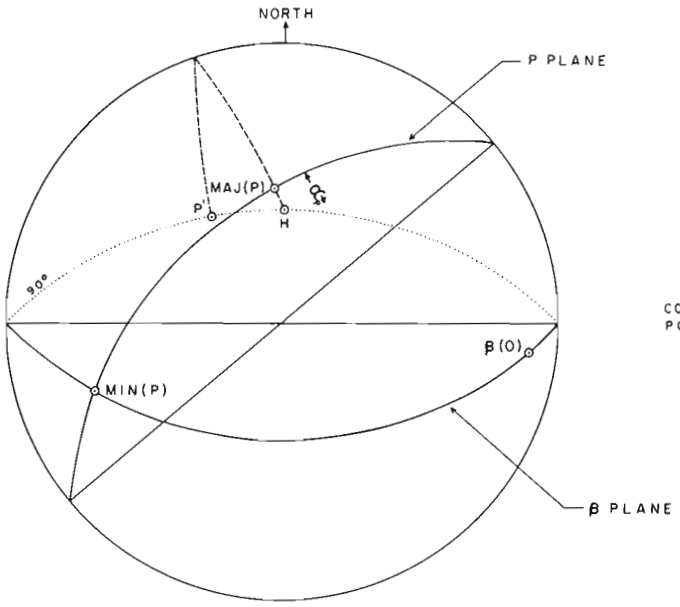

——— Great circle in the lower hemisphere

..... Great circle in the upper hemisphere

Figure 32. 3. Orientation of the P plane by stereographic projection.

intersection MAJ(R) projects into the β plane at 90° from MIN(R), meeting the β plane at R'. Since β_R, the β value for the R plane, is measured along the β plane from the reference line to MAJ(R), MIN(R) together with R' and the measured value of β_R determine the orientation of the reference line [β(o)].

To orient a planar structure, the P plane, first mark the point P' and β_p from the reference line along the P plane (Fig. 32. 3), where β_p is the β value for the P plane. Next determine the position of the downward end of the major axis, MAJ(P), of the ellipse of intersection of the P plane and the core MAJ(P) is located at α_p from H in the HP', where α_p is the α value for the P plane and H is the pole of the drillhole. Then plot the minor axis, MIN(P), of the ellipse at 90° from P' along the β plane. The P plane is constructed by the great circle common to MAJ(P) and MIN(P).

Solution by Spherical Trigonometry

From the stereograms in Figures 32. 2 and 32. 3, it is obvious that the values on the stereograms can be calculated by the use of the formulae in spherical trigonometry (Chauvenet, 1908). For the convenience of calculation, a control point and a sign convention are required. The sign convention is such that clockwise is positive and counterclockwise is negative. The control point is a point located at the primitive of the stereogram and measured clockwise 90° from the azimuth of the dip of the β plane. Since the orientation of the β plane is known, the orientation of the control point is known.

To determine the orientation of the reference line, i. e. to locate the position of β(0) with respect to the control point, the value of b has to be found (Fig. 32. 4).

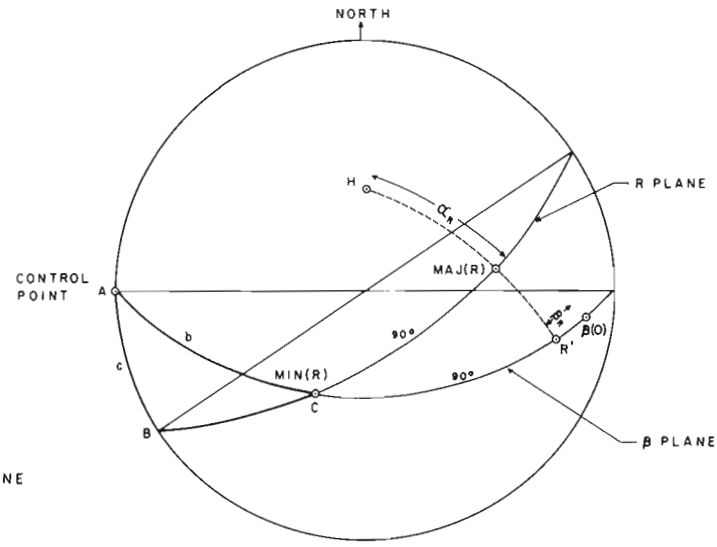

Figure 32. 4. Orientation of the reference line by spherical trigonometry.

In the spherical triangle ABC, two angles and the included side, or A, B and c are given (it should be noted that in a spherical triangle ABC, the angles of the triangle will be designated by A, B and C, and their opposite sides will be designated by a, b and c), where

A = dip of β plane

B = 180° minus dip of R plane

c = azimuth of dip of β plane minus azimuth of dip of R plane

The value of b can be found by solving the following formula, the derivation of which will not be presented because it is purely mathematical.

$$\cot b = \frac{\sin A \cos B + \cos A \sin B \cos c}{\sin B \sin c}$$

Respecting the sign convention given, β(0) will be located at $BO = -b - 90° - \beta_R$ from the control point along the β plane.

In the stereogram of the β plane and the P plane (Fig. 32. 5), MIN(P) is located at $x = BO + \beta_p - 90°$ from the control point. To determine the orientation of the P plane, X and e have to be found. In the spherical triangle, AXE, A and x are known and one more part of the spherical triangle is required to solve the triangle. The angle E can be computed from the spherical triangle DEF.

In the spherical triangle DEF, the three sides d, e' and f are given, where

$$d = 90°$$

$$e' = 90° + \alpha_p$$

$$f = 90°$$

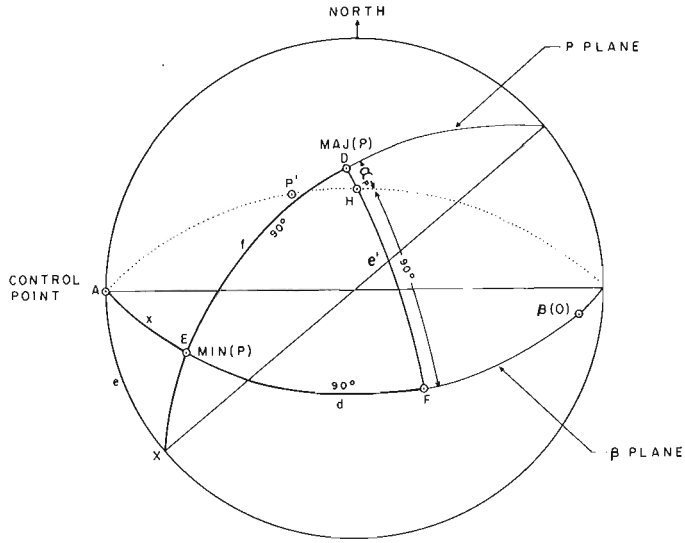

Figure 32.5. Orientation of the P plane by spherical trigonometry.

E is expressed by the formula

$$\tan \tfrac{1}{2}E = \frac{\sin (s - d) \sin (s - f)}{\sin s \sin (s - e')}$$

where $s = \frac{1}{2} (d + e' + f)$

Now that E is known, X and e can be calculated. In the spherical triangle AXE, two angles and the included side, or A, E and x are give, X and e can be computed from the formulae:

$$\cos X = - \cos E \cos A + \sin E \sin A \cos x$$

$$\cot e = \frac{\sin A \cos E + \cos A \sin E \cos x}{\sin E \sin x}$$

The orientation of the P plane then can be determined by the expression:

Dip of P plane = X

Azimuth of dip of P plane = azimuth of dip of β plane + 180° − e

Conclusions

The use of stereographic projection and formulae in spherical trigonometry to determine the attitude of a planar structure with the measured values of angles α_R, β_R, α_p, and β_p is demonstrated in this paper. It should be noted that although, for the problem discussed in this paper, the spherical triangles lie on the lower hemisphere, the spherical triangles could lie on the upper hemisphere, or partly on the lower hemisphere and partly on the upper hemisphere, depending on the location of points R' and P'. This method has an advantage over other methods for determining the attitudes of planar structures because the formulae presented in this paper can be programmed. A FORTRAN computer program is being developed using this method to determine the attitudes of planar structures intersecting vertical and inclined drillholes.

References

Chauvenet, W.
1908: Plane and Spherical Trigonometry; J. B. Lippincott Company, Philadelphia, 256 p.

Gale, J. E., Raven, K., Dugal, J., and Brown, P.
1976: Subsurface containment of solid radioactive wastes; *in* Report of Activities, Part B; Geol. Surv. Can., Paper 76-1B, p. 147-150.

Goodman, R. E.
1976: Methods of Geological Engineering in Discontinuous Rocks; West Publishing Company, New York.

Lyons, M. S.
1964: Interpretation of planar structure in drill-hole core; Geol. Soc. Am., Spec. Paper No. 78; New York, p. 65.

Mertie, J. B., Jr.
1943: Structural determinations from diamond drilling; Econ. Geol, v. 38, no. 4, p. 298-312.

Phillips, F. C.
1960: The Use of Stereographic Projection in Structural Geology; Edward Arnold (Publishers) Ltd., London, p. 85.

Ragan, D. M.
1968: Structural Geology; Wiley and Sons, New York, 166 p.

Stein, H. A.
1941: A trigonometry solution of two-drillhole problem; Econ. Geol., v. 36, no. 1, p. 84-94.

33. THE GOLDTHWAIT SEA AND ITS SEDIMENTS: GODBOUT — SEPT-ILES REGION, QUEBEC NORTH SHORE

Project 710083

L.A. Dredge
Terrain Sciences Division

Configuration of the Goldthwait Sea

The Goldthwait Sea refers to the area formerly submerged by postglacial marine inundation in the Gulf of St. Lawrence and in the estuary east of Saguenay River. The term was first proposed by Elson (1969) to distinguish this area from the Laflamme Sea which occupied Saguenay Valley and from the Champlain Sea in the St. Lawrence Lowlands. The development of the Goldthwait Sea in the region discussed here was time-transgressive. Deglaciation and inundation were earliest in the southeast, but the timing of the marine episode in that area has not been determined. Figure 33.1 shows the configuration of the sea about 9300 years B.P. when the ice front had retreated to a position now marked by a belt of end moraines (Dredge, 1976). Ice completely withdrew from the area in the succeeding 400 years, and the Goldthwait Sea developed to its maximum extent during that time (Fig. 33.2). At its maximum, the general configuration of the Goldthwait Sea was parallel to and about 15 km inland from the present coast, but fiords penetrated inland an additional 70 km.

The elevation of the marine limit increases from southwest to northeast across the area. The marine limit is 100 m a.s.l. at Godbout (west end), 105 m at Baie-Trinité, 120 m at Pentecôte, and 130 m at Sept-Iles (east end). This trend can be attributed to the time-transgressive nature of ice retreat and eustatic rise during the period of inundation if the southern area was deglaciated at about 13 000 years B.P. If deglaciation of the south coast occurred at a later date, however, the eustatic factor is not sufficient to account for the differences in elevation, and differential flexure, caused by differences in superincumbent ice loads over the area, must have been a factor as well. The elevation and geographic distribution of radiocarbon dates (Table 33.1) suggest that the latter may well be the case.

The lower limit of the Goldthwait Sea is taken to be the level at which present marine processes are operating.

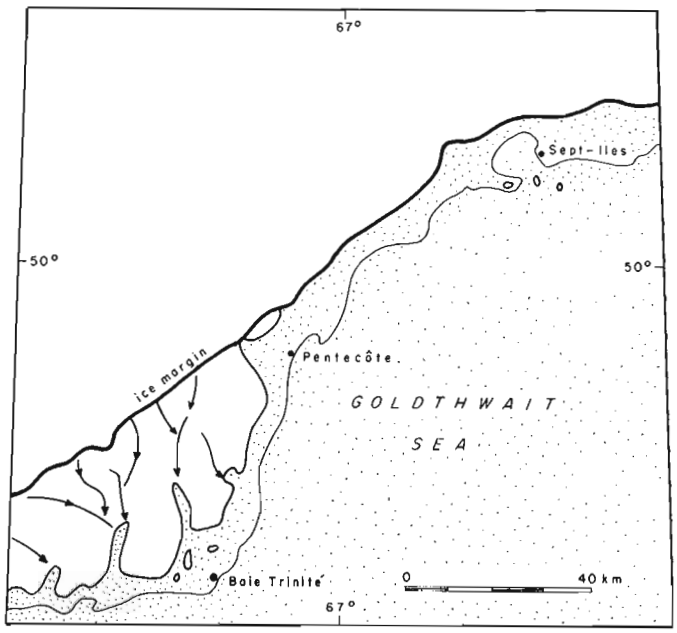

Figure 33.1. Location of ice margin, meltwater channels, and the Goldthwait Sea, about 9300 years B.P.

Sediments of the Goldthwait Sea

The coarsening upwards sequence of sediment types observed in this area indicates a continuous offlap sequence of sedimentation. Three types of deposits are present, and they represent three major environments of sedimentation:

1. Offshore silt and clay were deposited in deep water near the coast and in the estuary beyond the influence of river currents.
2. Nearshore deltaic sands were dumped where sediment-laden currents entered the main estuary.
3. A blanket of littoral sand was deposited over the entire area as the sea regressed.

Offshore Silt and Clay

The offshore clays are very poorly sorted and fine grained, the average textural composition being 15% sand, 56% silt, and 34% clay (< 2μ). The material is almost free of pebbles, which indicates that the deposits represent true marine, rather than glacio-marine, conditions. On the basis of texture, the clays can be subdivided into two main sediment types: a marine unit, homogeneous throughout, which is situated beyond the zone of river-generated currents, and a banded unit whose distribution is related to areas susceptible to fluctuations in river regimes.

The banded unit is stratified into cosets of clayey silt about 2 cm thick, separated by partings of sand. hese sediments were transported by turbidity currents which originated either in the delta foreset environment or as cold freshwater bottom currents. The cosets are akin to varves but both layers probably were deposited in summer. The coarser load may have been transported at the head and base of tractive bottom currents and deposited in deep water when the currents lost velocity. Because of the density of the saline environment (density ~ 1.03 g/cc), the fine tail of the turbidity

From: Report of Activities, Part C;
Geol. Surv. Can., Paper 76-1C (1976).

Table 33.1

Radiocarbon data relating to the Goldthwait Sea episode in the Godbout — Sept-Iles area, Quebec North Shore.

Site	Material dated	Enclosing material	Elevation	Date	Reference
1. Moisie R.	shells	offshore clay	76 m	9140 ± 200	GSC-1337[a]
2. Moisie R.	shells	offshore clay	8 m	7060 ± 190	GSC-1522[b]
	wood	foreset sand	27 m	6380 ± 150	GSC-1482[b]
3. R. Rapides	shells	nearshore sand	72 m	7580 ± 70	GSC-1809[c]
4. R. Pentecôte	shells	nearshore sand	40 m	8280 ± 80	GSC-1856

[a]Lowdon *et al.*, 1971

[b]Lowdon and Blake, 1973

[c]Lowdon and Blake, 1975

current (density ~1.01 g/cc) tended to rise to the surface, but as particles flocculated, they settled out into a fine grained but poorly sorted layer.

The massive unit is texturally similar to the finer part of the banded unit. It was deposited from a flocculated, uniform suspension in deep water beyond the influence of tractive currents.

The offshore deposits are composed primarily of rock flour and are similar in composition to their parent material, till. The principal minerals, as determined by X-ray diffraction (Dredge, in prep.) are quartz and feldspar, especially plagioclase. Illite is also a significant component of the -2μ fraction.

Natural water contents average 38 per cent of the dry weight and slightly exceed the liquid limit. The clays have a low plasticity ($I_p < 15$) and are classed as inactive.

Nearshore Deltaic Deposits

A coarsening upward layer of stratified sand overlies the clays. The thickest accumulations are deltaic wedges, situated where sediment-laden currents emptied into the sea. The lowermost bottomset beds are gradational with banded clays and consist of beds of fine sand alternating with laminae of steel-grey clay. The upper and most extensive unit is the delta foresets, consisting of tabular cross-beds of micaceous fine sand exhibiting internal ripple-drift laminations. The presence of turbidite lobes and irregular bedding structures and the relatively loose density of the sand suggest that sedimentation was rapid. The succession of dates at Moisie (Table 33.1) indicates that most of the sediment accumulated in a 1000-year period.

Littoral deposits

As the sea regressed, prograding beach ridges made up of medium to coarse, well sorted sand blanketed the other deposits. Granulometric changes along beach ridges and the development of recurved spits indicate

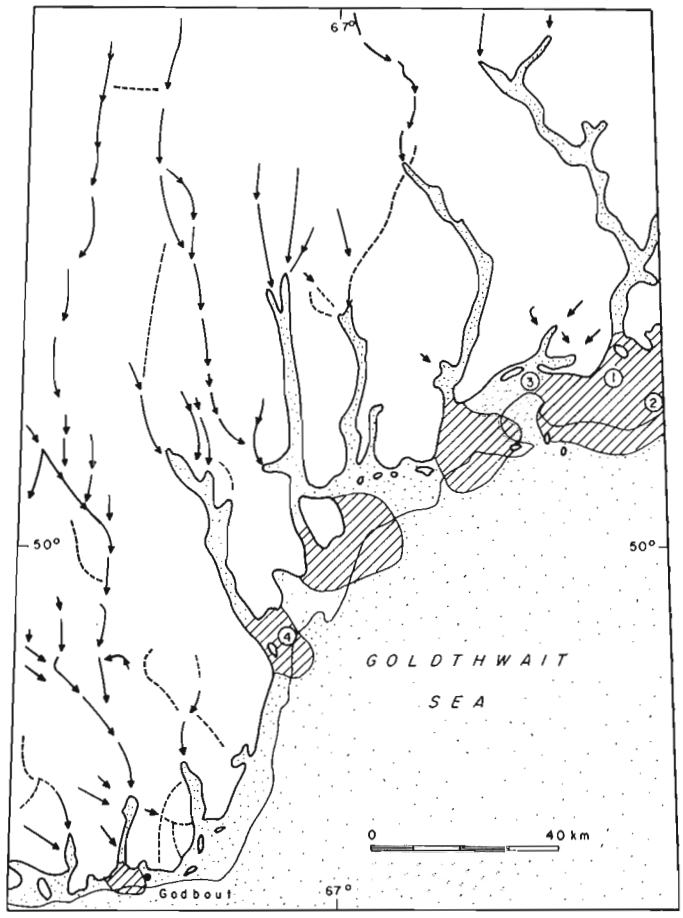

Figure 33.2. Maximum extent of the Goldthwait Sea, major outwash (arrows) and overflow channels (dashed lines), and principal deltas (stripes). Circled numbers refer to radiocarbon control points in Table 33.1.

that littoral currents originally moved along the coast from west to east. These currents reversed between 7000 and 8000 years ago and have since flowed from east to west. The directional change probably was related to shifts in the Labrador current, but changing wind systems could also have been a factor.

Tidal flats developed in backwater areas of the Goldthwait Sea but these were limited to the area around Sept-Iles. Tidal flat clays are distinguished from deepwater clays described above by the presence of black mottles, burrough casts, and ice-rafted boulders.

References

Dredge, L.A.
1976: Moraines in the Godbout — Sept-Iles area, Quebec North Shore; *in* Report of Activities, Part C; Geol. Surv. Can., Paper 76-1C.

Surficial geology and geomorphology of the Quebec North Shore; Ph.D. thesis, Univ. Waterloo, Waterloo, Ontario. (in prep.)

Elson, J.A.
1969: Late Quaternary marine submergence in Quebec; Rev. Géogr. Montréal, v. 23, p. 247-258.

Lowdon, J.A., Robertson, I.M., and Blake, W. Jr.
1971: Geological Survey of Canada Radiocarbon dates XI; Geol. Surv. Can., Paper 71-7, p. 268.

Lowdon, J.A. and Blake, W. Jr.
1973: Geological Survey of Canada Radiocarbon dates XIII; Geol. Surv. Can., Paper 73-7, p. 11.

1975: Geological Survey of Canada Radiocarbon dates XV; Geol. Surv. Can., Paper 75-7, p. 10.

Project 710083

L. A. Dredge
Terrain Sciences Division

The distribution of moraines along the central part of the Quebec North Shore is indicated in Figure 34. 1. Those shown are visible on 1: 60 000 scale aerial photographs, which were used as a mapping base.

The main band of morainic ridges stretches northeast-southwest across the area and consists of three main segments. The Daigle and Valley Front moraines lie just above the marine limit, at elevations between 120 and 140 m, and are oriented parallel to both the present coast and the shoreline of the Goldthwait Sea. The upland segment crosses rugged hills which extend to an elevation of 600 m.

East of Pentecôte the moraines are well defined and sharp-crested. The Daigle moraine, with a length of 12 km and a maximum width of 200 m, is the largest. In plan this moraine consists of two broadly arcuate subparallel ridges and a hummocky boulder-strewn area between the ridge crests. Its eastern limb appears to arc northwards along Moisie River valley. The Valley Front ridges are thinner and more discontinuous. They once continued straight across the river valleys in the central part of the area, but most have been breached after their formation.

Both ridge sets are composed of sandy till with minor amounts of subangular gravel and fines. The till is generally diamictic, although some poorly developed lenses and cross-beds are present and indicate that some sorting has occurred. Pebble fabrics are oriented parallel to the direction of ice flow and dip in an upglacier direction. Although these ridges are geographically associated with the marine limit, the textural data indicate that the till was neither sedimented in standing water nor reworked by marine processes. The till therefore is interpreted as being a melt-out deposit originating at the base of a grounded ice sheet.

Within this sector, isolated patches of hummocky till have been found below the marine limit. These hummocks commonly consist of boulder piles; the sandy matrix that generally characterizes the till is absent or is present in very small amounts. They are interpreted as segments of moraine which have been intensely reworked by wave or current activity during the Goldfield Sea episode.

West of Pentecôte the moraine becomes dissociated with the marine limit and crosses the Laurentian upland. This segment was not investigated in the field but appears on aerial photographs as a discontinuous, diffuse band of hummocky topography with multiple ridge crests. The ridges in this segment could not be traced into major river valleys.

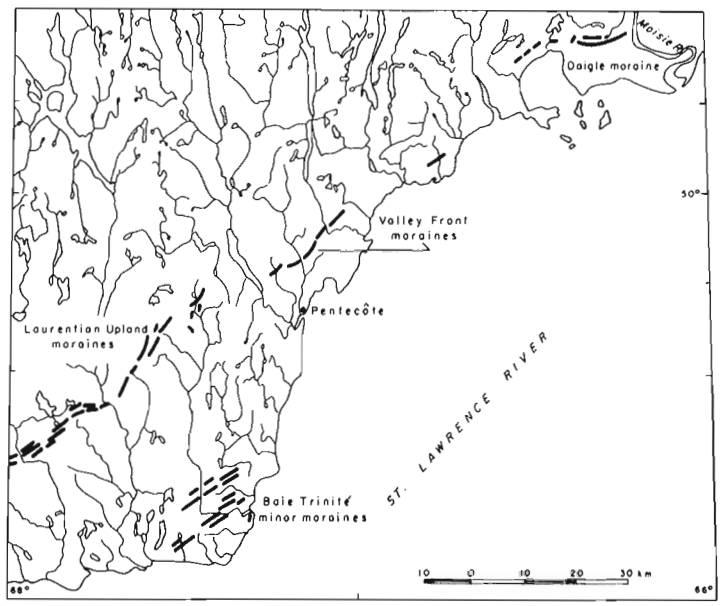

Figure 34. 1. Principal moraines along the Quebec North Shore, Godbout — Sept-Iles area.

Correlation

In the west, the moraine can be traced beyond the area mapped to join with those near Manic 2 reported by Sauvé and LaSalle (1968); on the east, the moraine joins the Moisie moraine which has been mapped by Dubois (1976). It thus appears that the moraines shown in Figure 34. 1 are part of a system which may extend all along the North Shore. The exact age of the moraines in this area has not been determined. Most likely, they were formed about 9300 years ago. A radiocarbon date of 9140 ± 200 years B. P. (GSC-1337; Lowdon *et al.*, 1971) on marine molluscs south of the Daigle moraine gives the approximate age of the marine limit in this area, and interfingerings of till, outwash, and beach sand in the south part of the Daigle moraine indicate that the moraine was approximately contemporaneous with the maximum level of the Goldthwait Sea.

Minor moraines

A set of subparallel ridges about 5 m high and 300 m apart is located near Baie-Trinité. They consist of till similar to that in the moraines described above, but portions below marine limit (about 105 m in that area) have been waterwashed, and the internal structure has been altered. These moraines may be deposits resulting from the movement of debris up shear planes

From: Report of Activities, Part C;
Geol. Surv. Can., Paper 76-1C (1976).

behind an ice front that was thin and possibly brittle. At the time of formation, the ice front may have been grounded at the edge of the Laurentian Trough (Dredge, in prep.). The orientation of these moraines and the major belt farther north suggest that the southeast coastal zone was deglaciated before the northeast and that the pattern of ice retreat therefore, was, not parallel to the present coast.

References

Dredge, L.A.
Surficial geology and geomorphology of the Quebec North Shore; Ph.D. thesis, University of Waterloo, Waterloo, Ontario. (in prep.)

Dubois, J.M.
1976: Levé préliminaire du complex moranique de Manitou-Matamek sur la côte nord de l'estuaire maritime du Saint Laurent; *in* Report of Activities, Part B; Geol. Surv. Can., Paper 76-1B, p. 89-93.

Lowdon, J.A., Robertson, I.M., and Blake, W. Jr.
1971: Geological Survey of Canada radiocarbon dates XI; Geol. Surv. Can., Paper 71-7, p. 268.

Sauvé, P. and LaSalle, P.
1968: Notes sur la géologie glaciaire de la région de Manic 2; Natur. Can., v. 95, p. 1293-1300.

35. MEGABLOCKS, OR THE ENORMOUS ERRATICS OF THE ALBERTAN PRAIRIES

Project 740089

A. MacS. Stalker
Terrain Sciences Division

Megablock is the term used here for certain large masses of material that have been moved to their present location by glaciers. The author prefers this term, rather than the word erratic used either singly or in combination, because some of these blocks may not have been moved far enough nor moved onto a different rock type, which is a criterion necessary for the designation of erratics. Also, for several reasons, but particularly because of their enormous size, they do not fit the normal concept of an erratic. Megablocks are probably common in Alberta, although few have been recognized so far. The known ones consist principally of bedrock, but may contain other material (*see* numbers 3 and 4, below). It is generally the white bentonitic sandstone and siltstone beds, coal seams, and ironstone bands that attract attention to them and cause them to be recognized; thus megablocks consisting solely of till or other surficial material, although they may be present or even common, would be difficult to distinguish from other drift and usually would not be noticed.

Most are found where exposed along the banks of modern rivers. In describing sections along Oldman Valley, Stalker (1963, p. 6) stated:

> They [the megablocks] are present... in practically every exposure along Oldman River between Section 3 [Kipp Section] and the junction with the Bow River, a distance of about 100 miles (about 60 miles in a straight line). In some places a continuous block of this intertill bedrock is more than a mile long, and in some instances may possibly extend continuously for several miles... The large bedrock masses are thought to be in equivalent stratigraphic positions in all exposures, and thus they form an extremely valuable and easily recognized marker horizon.

For a time the author assumed that the megablocks were confined to large, preglacial valleys, particularly the Oldman, and as suggested in the above quotation that they had been emplaced during a single episode. The discovery of additional blocks at the surface and away from the ancient valleys (for instance numbers 1 and 6 of Table 35. 1) has shown both assumptions to be false. It is now known that megablocks can occur almost anywhere on the Canadian Prairies and that they have been emplaced at various times and by different glaciers.

Six Albertan megablocks (Table 35. 1) are chosen for description here, and their locations are shown in Figure 35. 1. Of the six, number 1 is known only from boreholes, number 6 is an outcrop, and the others are well exposed along valley walls. Other megablocks are present, and drilling reports of considerable thicknesses of bedrock interposed in drift are fairly common, but knowledge of the subsurface is insufficient to estimate the extents of such bedrock masses. Even for those megablocks exposed along river valleys, only thickness and length can be determined. Further, due to overgrowth and slumping, the continuity of megablocks 2, 5, and 6 is not certain, but it would be unusual if they were present at every exposure but missing between.

Description of Individual Megablocks

Catchem (Number 1)

Information on the Catchem megablock was kindly supplied by Rene Barendregt of Picture Butte, Alberta, to whom the writer extends his grateful thanks. This megablock is named after a former post office that was a short distance to the west. It lies near the top of a divide about 19 km directly southeast of Manyberries in the N ½ sec. 35, tp. 3, rge. 5, and S ½ sec. 2, tp. 4, rge. 5, W 4th mer. Information comes from only two

Table 35. 1

Some Albertan megablocks

Reference Number	Name of megablock	Approximate altitude of top (m)	Estimated length (km)	Maximum known thickness (m)	Location of approximate centre of megablock						
					¼ or ½	section	township	range	meridian	Latitude (north)	Longitude (west)
1	Catchem	960	1.5		N	35	3	5	4	49°15'30"	110°35'00"
2	Laundry Hill	710	1.5+	13	NE	36	8	22	4	49°41'30"	112°51'20"
3	Kipp	875	1.5+	10	E	18	9	22	4	49°43'50"	112°57'50"
4	Wolf Island	735	1	10	S	20	11	14	4	49°55'30"	111°53'00"
5	Driftwood Bend	760	4	25	NW	25	11	16	4	49°56'40"	112°04'00"
6	Cooking Lake	735	4+	12	W	9	51	21	4	53°28'30"	113°02'00"

From: Report of Activities, Part C;
Geol. Surv. Can., Paper 76-1C (1976).

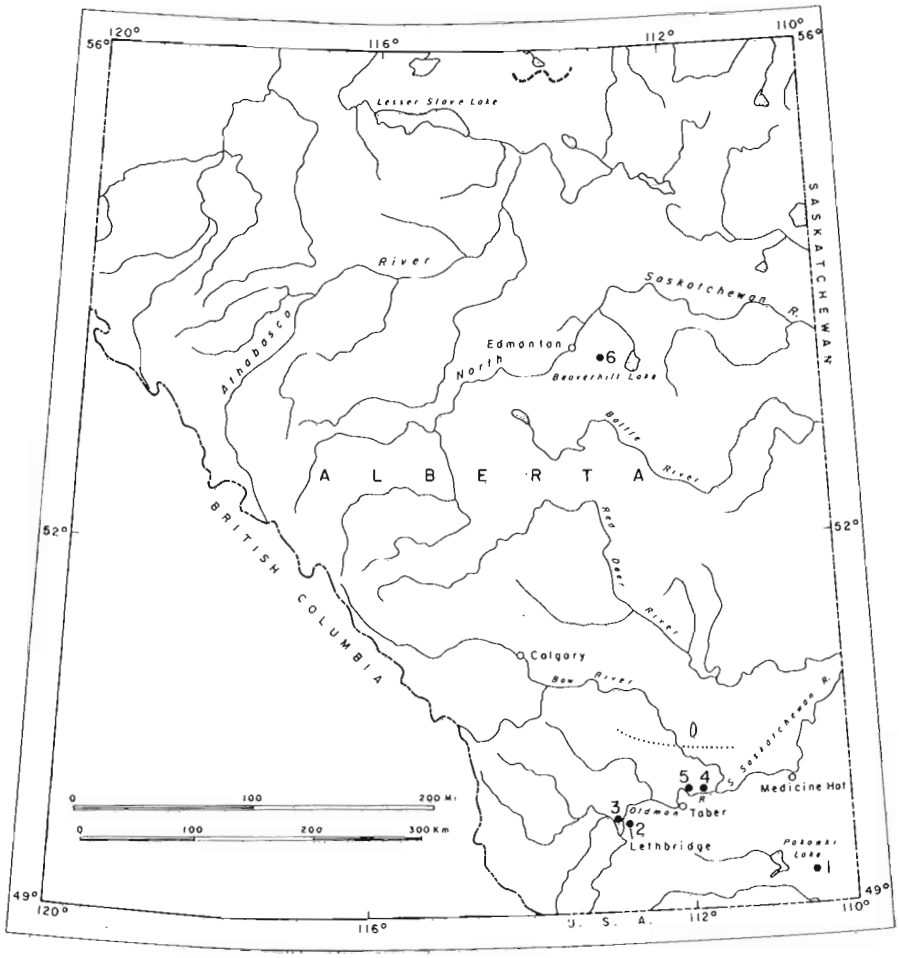

Figure 35. 1

Location of some Albertan megablocks:

1 – Catchem;
2 – Laundry Hill;
3 – Kipp;
4 – Wolf Island;
5 – Driftwood Bend;
6 – Cooking Lake.

Approximate southern limit of preglacial gravel of Bow Valley lithology.

southernmost outcrops of the Lower Cretaceous, Grand Rapids Formation.

boreholes, and so less is known about this megablock than about any of the others. Additional boreholes put down nearby did not penetrate it, and thus it probably does not extend over more than 1 km^2. Its source and distance of transport are unknown.

Laundry Hill (Number 2)

Laundry Hill megablock was described by Stalker (1975). It is entirely within the city limits of Lethbridge and is thickest and best displayed along a coulee near Laundry Hill, from which it gets its name. It outcrops along the east bank of Oldman River from NE ¼ lsd. 6, sec. 1, tp. 9, rge. 22 south to lsd. 1, sec. 36, tp. 8, rge. 22; south of there the bank becomes overgrown and cannot be traced farther. If small exposures of bedrock material at the same level on the far (west) wall of the valley are remnants of this block, it originally was more than 1 km wide. Stalker (1975, p. 422) states: "The investigation showed that the mass was nearly horizontal, that it was singularly thin considering its lateral extent, and that many parts of it displayed remarkably little disturbance for a block of comparatively weak rock that had been transported into place, whether by a glacier or by other means." This megablock originally had a weight of more than 3 000 000 tons. Its source and direction and distance of movement are unknown.

Kipp (Number 3)

This megablock is named after Kipp Bluff, about 8 km west-northwest of Lethbridge, which follows the outer side of a meander of Oldman River in the E ½ sec. 18, tp. 9, rge. 22, W 4th mer. Stalker (1963, p. 19-22; 1972, p. 70-72) described the stratigraphic section. The megablock extends the full length of the exposure, more than 1.5 km, at a height of about 25 m above the river and 60 m below the top of the bluff. Tills are present both below and above it. Slumping and overgrowth preclude its further tracing to the north and south, and the distance of its extension into the bank is unknown. The bedrock material in it consists of white consolidated sandstone, clay partings, coaly lenses, and an ironstone band.

This megablock is remarkable for its thinness, relative to its length, for the bedrock in it is rarely more than 5 m thick and in places is less than 1 m thick. Despite this, it seems continuous, its beds show remarkably little deformation, and it retains approximately the same altitude along the length of the cut. The bedrock slab, however, locally is overlain

by up to 6 m of alluvium, which likely forms part of the megablock. Before the realization that the alluvial beds also formed part of the megablock, their presence was considered a major problem (Stalker, 1963, p. 6); it was difficult to conceive how, with glacier deposition of the megablock, the beds could have been interposed between the bedrock slab and the till of the transporting glacier. If this alluvium is part of the megablock, which is still far from certain, the puzzling question of the relative thinness of the block is lessened a little. The source of this megablock and its direction and distance of transport, are unknown.

Wolf Island (Number 4)

This megablock is named after Wolf Island in Oldman River, which is just opposite the megablock. It is about 20 km east-northeast of Taber, Alberta and is exposed on the north side of the river in the Wolf Island North Bluff. The stratigraphic section was first described by Dawson (1885, p. 141C) and later by Stalker (1963, p. 12-15). The bluff follows the outer side of a river meander for 1.5 km, and the megablock extends most of that distance, although in places it is hidden by gullying, slumping, or overgrowth. The bluff is 75 m high, and the megablock is about one-third of the way up. It overlies gravel, silt, and a dark till, and it is overlain by two lighter coloured tills and other surficial materials.

The bedrock part of the block is primarily dark shale with some coal but includes white bentonitic sand near its centre. This bedrock slab is also thin relative to its length, reaching a maximum thickness of about 13 m; in places it is merely 1 or 2 m thick. It is fairly horizontal, but the beds are deformed in places, particularly near the base where they locally intermix with the underlying till.

This megablock includes as much as 3 m of "preglacial" gravel directly above its bedrock part. Evidently the bedrock and overlying gravel were picked up together and carried to their present location as a unit. This gravel is important not only because it confirms that megablocks can contain material other than bedrock, but also because it indicates that these megablocks could have come long distances. This gravel has a Bow Valley lithology, which is dissimilar to, and readily distinguished from, preglacial gravel of the Oldman River system, such as is found near the base of Wolf Island North Bluff. The closest sources for the Bow type gravel are more than 50 km to the north, northeast, or northwest, as indicated in Figure 35.1; therefore, a glacier carried this megablock at least that distance and probably crossed intervening ground 30 to 100 m higher than the present altitude of the megablock.

Driftwood Bend (Number 5)

The most detailed description of this megablock is found in Johnston and Wickenden (1931, p. 31-34) where it is described as an interglacial deposit, despite the presence of a coal seam in it, because its immense size and continuity seemed to preclude it being anything else. This megablock receives its name from Driftwood Bend, where Oldman River swings south 15 km north-northeast of Taber. It outcrops intermittently along the left (east) bank of Oldman River from NW ¼ sec. 36 to SW ¼ sec. 24, tp. 11, rge. 16, W 4th mer. Where it is not exposed, the bank is slumped or overgrown. The distance this megablock extends east, back from the riverbank, is unknown, but seismic shothole logs indicate that it is considerable. It reaches a maximum known thickness of about 25 m and averages about 10 m; as it probably extends over more than 10 km^2, it could weigh several hundred million tons and is one of the largest known. It is underlain by some 25 m of surficial material, including till, and is covered by 15 m of drift, also including till. The source of this megablock and its distance of travel are unknown.

Cooking Lake (Number 6)

Much of the information about this megablock, which is perhaps the most important and informative of them all, was supplied by the Alberta Research Council and by L. A. Bayrock, who was then with the Council. Bayrock carried out the chief study of this megablock, and the age of the bedrock was determined by C. Singh, Alberta Research Council, through microfloral studies. The writer extends his appreciation to all persons who supplied information on this megablock.

The Cooking Lake megablock lies about 25 km east-southeast of Edmonton and directly north of the centre of the lake that gives it its name. This block occurs at the surface, rather than being revealed by a river valley as are most of the others. Its surface extent is indicated by the areas in tp. 52, rge. 21, W 4th mer. that were mapped originally as bedrock outcrop by Bayrock and Hughes (1962). These bedrock outcrops later were recognized to be exposures of a large megablock.

The continuity of the Cooking Lake megablock between exposures is not established, but there is no reason to assume that it is not continuous. Apparently it covers all of section 9, all but the southeast of section 10, most of the west half of section 3, much of the north half of section 4, most of the south halves of sections 15 and 16, and the southeast quarter of section 17; its extent to the west and south is unknown. It appears to cover at least 10 km^2, and boreholes have indicated that it is up to 10 m thick. The block is underlain by surficial materials. It is an immense megablock, certainly comparable to the Driftwood Bend one in size.

The material composing this megablock is different from the soft, bentonitic Upper Cretaceous bedrock found over this general area; it is better indurated and cemented, harder, and more brittle. The studies by C. Singh showed that it is of Lower Cretaceous age and from the Grand Rapids Formation. The closest known outcrops of this formation, as shown in Figure 35.1, are about 250 km to the north. If this immense megablock came from those outcrops, not only was it

carried nearly directly south for that distance, but also was raised between 40 and 160 m, depending upon the outcrop source. This megablock, being at the surface, was apparently brought into place by the last glacier, unlike those lying under two or more tills (i.e. Wolf Island megablock) which were emplaced earlier.

References

Bayrock, L.A. and Hughes, G.M.
1962: Surficial geology of the Edmonton District, Alberta; Res. Coun. Alta., Prelim. Rept. 62-6, 40 p.

Dawson, G.M.
1885: Report on the region in the vicinity of the Bow and Belly rivers, Northwest Territory; Geol. Surv. Can., Rept. Prog., 1882-84, Pt. C.

Johnston, W.A. and Wickenden, R.T.D.
1931: Moraines and glacial lakes in southern Saskatchewan and southern Alberta, Canada; Roy. Soc. Can. Trans., 3rd ser., v. XXV, sec. IV, p. 29-44.

Stalker, A. MacS.
1963: Quaternary stratigraphy in southern Alberta; Geol. Surv. Can., Paper 62-34, 52 p.

1972: Southern Alberta; *in* Quaternary geology and geomorphology between Winnipeg and the Rocky Mountains; eds. N.W. Rutter and E.A. Christiansen; 24th Int. Geol. Cong., Montreal, Guideb. Field Excursion C-22, p. 62-79.

1975: The large interdrift bedrock blocks of the Canadian Prairies; *in* Report of Activities, Part A, Geol. Surv. Can., Paper 75-1A, p. 421-422.

36. DIFFERENTIATION OF TILLS IN THE PAKOWKI-PINHORN AREA OF SOUTHEASTERN ALBERTA ON THE BASIS OF THEIR MAGNETIC SUSCEPTIBILITY

Project 650027

R.W. Barendregt[1], A. MacS. Stalker[2], and J.H. Foster[3]

Measurement of magnetic susceptibility of tills in the Pakowki-Pinhorn area of southeastern Alberta has yielded two groups of sites with significantly different values. Measurements were carried out on 170 core samples from 25 different locations collected for paleomagnetic stratigraphy studies. The measurements were made on a toroid-transformer bridge (Christie and Symons, 1969). The tills from the Pakowki Lake internal drainage area have significantly higher values of magnetic susceptibility than those of the Sweetgrass-Comrey Upland area. The mean apparent magnetic susceptibility for each site was then determined and plotted on a base map (Fig. 36.1). The mean apparent magnetic susceptibility values fell into two groups which, in turn, were distributed over two topographic units, separated by the 3000-foot contour line (Table 36.1). The lower values occurred on the Sweetgrass-Comrey Uplands area, and the higher values occurred in the Pakowki Basin (Table 36.2).

As sampling was done at numerous levels along the till exposures, all tills probably have been sampled. These measurements show that in the basin all the tills, of which there may be anywhere from one to four (Westgate, 1968; Barendregt, 1976), have a mean value of apparent magnetic susceptibility ranging from 1.008×10^{-5} emu to 1.584×10^{-5} emu (volume susceptibility). The average of the mean apparent magnetic susceptibility values for all the sites located within the basin is 1.319×10^{-5} emu.

On the upland surface the magnetic susceptibility measurements are consistently lower than those of the basin. Here the tills, and again there may be anywhere from one to four tills present, have mean apparent values ranging from 0.072×10^{-5} emu to 0.936×10^{-5} emu. The average mean value for all sites in the uplands area is 0.612×10^{-5} emu, or only about half the value found in the basin.

The boundary determined by these magnetic susceptibility measurements corresponds closely with the boundary of the Pakowki drift (Westgate, 1968; Barendregt, 1976). Drift deposited by two separate glacial advances would be expected to have somewhat different magnetic susceptibility values. The ferromagnetic minerals in the tills of the Pakowki-Pinhorn area undoubtedly were derived from the Canadian Shield. However, assuming all the tills to be Laurentide, the average mean apparent magnetic susceptibility values should not differ greatly since the material in both groups of tills was carried over a vast distance and, in both cases, by ice moving in much the same direction.

The position of the magnetic susceptibility boundary was determined largely by the direction of ice movement and by topography. An earlier, stronger glacial advance passed over both areas and deposited drift over the entire area — a drift that probably contains more than one till, while a weaker, sluggish advance deposited tills in the Pakowki Basin. The southeastward advance of this weaker glacier was arrested at approximately the 3000-foot contour level. The moraine left during its recession yielded some of the samples.

The results of these measurements are too consistent and strongly grouped to be explained as coincidences. This study demonstrates that the magnetic susceptibility properties provide a distinctly unique signature for each drift sheet. They not only indicate a means for extending the boundary into adjacent areas but also provide a means for differentiating and correlating tills over broad areas.

Table 36.1

Site	Mean apparent magnetic susceptibility
SC	1.498×10^{-5} emu
VA	1.555×10^{-5} emu
LS	1.440×10^{-5} emu
MC	1.210×10^{-5} emu
PC	1.051×10^{-5} emu
ML	1.390×10^{-5} emu
PS	1.066×10^{-5} emu
EE	1.440×10^{-5} emu
RS	1.462×10^{-5} emu
PW	1.080×10^{-5} emu
SH	0.893×10^{-5} emu
KC	0.914×10^{-5} emu
RS	0.720×10^{-5} emu
PR	0.648×10^{-5} emu
SP	0.684×10^{-5} emu
EN	0.763×10^{-5} emu
DC	0.742×10^{-5} emu
BE	0.554×10^{-5} emu
MR	0.842×10^{-5} emu
OR	0.072×10^{-5} emu
PW	0.526×10^{-5} emu
RR	0.641×10^{-5} emu

[1]Department of Geography, Queen's University, Kingston

[2]Terrain Sciences Division

[3]Regional and Economic Geology Division

From: Report of Activities, Part C;
Geol. Surv. Can., Paper 76-1C (1976).

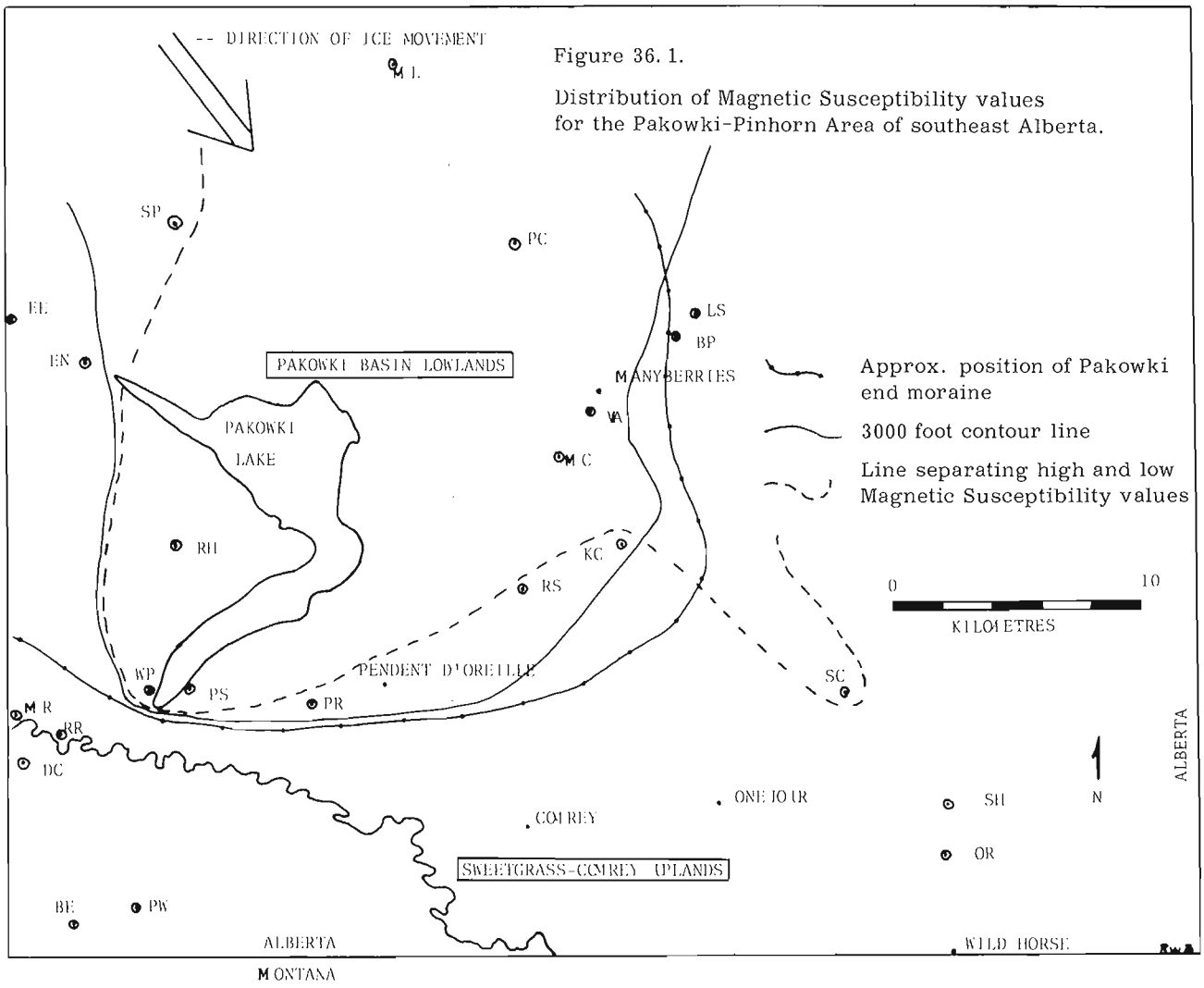

Figure 36. 1.

Distribution of Magnetic Susceptibility values for the Pakowki-Pinhorn Area of southeast Alberta.

Table 36. 2

	Pakowki Lowland	Sweetgrass-Comrey Upland
Range of mean apparent magnetic susceptibility	1.008×10^{-5} emu to 1.584×10^{-5} emu	0.072×10^{-5} emu to 0.914×10^{-5} emu
Average mean apparent magnetic susceptibility	1.319×10^{-5} emu	0.612×10^{-5} emu

References

Barendregt, R. W.
1976: A detailed geomorphological survey of the Pakowki-Pinhorn area, southeastern Alberta; unpubl. Ph. D. thesis.

Christie, K. W. and Symons, D. T. A.
1969: Apparatus for measuring magnetic susceptibility and its anisotrophy; Geol. Surv. Can., Paper 69-41.

Westgate, J. A.
1968: Surficial geology: Foremost-Cypress Hills area, Alberta; Alta. Res. Counc., Bull. 22.

37. PALEOMAGNETIC STRATIGRAPHY OF THE WELLSCH VALLEY SITE, SASKATCHEWAN

Project 650027

J.H. Foster[1] and A. MacS. Stalker[2]

The Wellsch Valley site near Swift Current, Saskatchewan has been a productive site for mammalian fossils for many years. Some collections and studies are described in Stalker and Churcher (1972) and Stalker (1971, 1972). Of the various exposures of fossiliferous sediments at this site, "Jaw Face" is best known. "Jaw Face" is in lsd. 8, sec. 4, tp. 20, rge. 14, w 3rd mer. (50°40'N, 107°52'25"W). This face is on the east side of Wellsch Valley which trends north to the South Saskatchewan River. Studies of mammalian fossils from "Jaw Face" have now been complemented by a study of fossil magnetism or paleomagnetic stratigraphy.

Lithostratigraphy

A 10 m-high section of "Jaw Face" is shown in Figure 37.1. Most bones come from the sand layer between 6.5 and 6.8 m of the section; fossils are rare below 7 m. Scattered fossils of small animals are found up to and within the volcanic ash bed at 2.5 m.

Biostratigraphy

Most fossils were collected by, and all were identified by, C.S. Churcher of the Department of Zoology, University of Toronto. The faunal list is given in Table 37.1.

Table 37.1

Faunal List

Order Xenarthra

Xenarthra, indet. – large ground sloth.

Order Lagomorpha

Hypolagus sp., ?*Hypolagus limnetus* – Gazin's marsh rabbit.

Order Rodentia

Citellus sp. – ground squirrel.
Cynomys sp. ?*Cynomys meadensis* – Meade prairie dog.
Thomomys bistylis n. sp. – extinct southern pocket gopher.
Thomomys cf. *talpoides* – northern pocket gopher.
Synaptomys (Myctomys) kansasensis – Kansan bog lemming.
Microtus deceitensis – extinct Cape Deceit vole.
Pliomys cf. *deeringensis* – extinct Deering vole.
?*Oryzomys* – rice rat.
Rodentia indet.

Order Carnivora

Borophagus diversidens – Cope's bone-eating dog.
Lynx sp., *Lynx* cf. *rufus* – lynx or bobcat.

Order Proboscidea

Mammuthus imperator haroldcooki – Cook's mammoth.

Order Perissodactyla

Equus pacificus – extinct Pacific horse.
Equus complicatus – extinct eastern horse.

Order Artiodactyla

Platygonus sp., ?*P. bicalcaratus* – extinct peccary.
Camelops sp. – extinct camel.
Antilocapridae indet. ?*Tetrameryx* sp. – extinct prongbuck.
Bovidae, Ovibovini indet., ?*Preptcoeras* sp. – extinct shrub-ox.

[1]Regional and Economic Geology Division

[2]Terrain Sciences Division

From: Report of Activities, Part C;
Geol. Surv. Can., Paper 76-1C (1976).

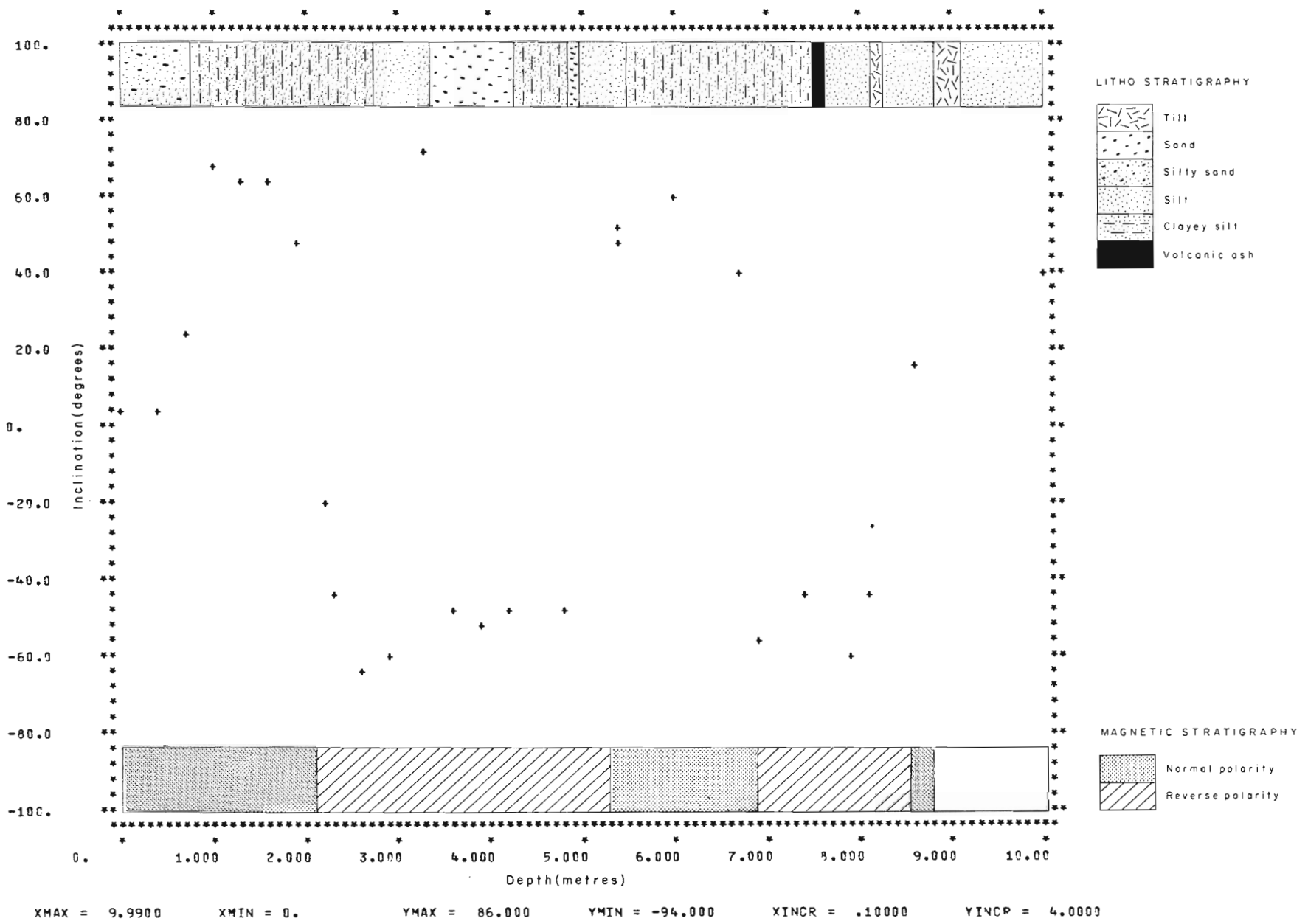

Figure 37.1. Plot of inclination of the remanent magnetism of Wellsch Valley sediments.

Magnetic Stratigraphy

Twenty-three levelled blocks were collected for Stalker from the 10 m-high section of "Jaw Face" (Fig. 37.1). One specimen cut from each block was subject to 12 steps of alternative current demagnetization at peak fields of 50 to 1000 Oersteds. The natural remanent magnetization, and the remanent magnetization after each step of demagnetization, was measured on a Schonstedt Digital Spinner Magnetometer. Analysis of the data was done with the aid of five plots per specimen on a computer line printer. The five plots were: (1) stability index, (2) normalized remanent intensity, (3) north-east plane Zijderveld, (4) north-vertical plane Zijderveld, and (5) equal area stereographic projection. Each of the 23 specimens showed a single component of remanent magnetization. For each specimen the remanent magnetization that best represented this single component is given in Table 37.2. Declination values are omitted from Table 37.2 as the original blocks were levelled, with tops noted, not collected as oriented blocks with a known azimuth on them. A plot of the inclination of the remanent magnetization of the "Jaw Face" section is shown in Figure 37.1.

Discussion

The faunal assemblage is consistent with the beginning of the Irvingtonian Land Mammal Age. If this faunal assignment of age is correct, the reversal pattern found on "Jaw Face" should be the Olduvai Event. The most significant point of this piece of research is that the sediments of "Jaw Face" will give excellent quality data for magnetic stratigraphy. There are no immediate plans to follow up this research; however, the authors would strongly encourage any additional work on the magnetic stratigraphy of the Wellsch Valley site. Such work would permit a correlation of the combined faunal and magnetic stratigraphies of the Wellsch Valley site with similar fossil localities presently under this type of investigation.

Table 37.2

Depth (m)	Demagnetization (Oersteds)	Inclination (Degrees)	Remanent Intensity (10^{-5} emu/cc)
0.4	500	2.3	1.5
0.7	300	24.8	1.6
1.0	200	67.6	1.1
1.3	200	65.4	3.4
1.6	300	62.1	0.9
1.9	400	47.6	1.2
2.2	400	-20.5	1.9
2.4	400	-43.6	1.3
2.7	400	-64.5	1.8
3.0	200	-59.0	1.8
3.3	200	72.1	0.8
3.6	200	-47.7	2.4
3.9	400	-51.9	1.0
4.2	300	-49.3	2.8
4.8	400	-48.3	2.6
5.4	400	50.0	1.4
6.0	200	58.6	0.6
6.7	100	38.2	0.4
7.0	800	-55.8	1.6
7.5	500	-44.6	2.6
7.9	600	-59.4	2.4
8.1	400	-44.8	1.7
8.6	100	14.5	6.7

References

Stalker, A. MacS.
1971: Quaternary studies in the southwestern Prairies; *in* Report of Activities, Part A; Geol. Surv. Can., Paper 71-1A, p. 180-181.

1972: Quaternary studies in the southwestern Prairies; *in* Report of Activities, Part A; Geol. Surv. Can., Paper 72-1A, p. 67.

Stalker, A. MacS. and Churcher, C.S.
1972: Glacial stratigraphy of the southwestern Canadian Prairies; the Laurentide record; 24th Int. Geol. Congr., Montreal, Sect. 12, p. 110-119.

38. SULPHUR ISOTOPE COMPOSITION AND STRONTIUM CONTENT OF BARITE FROM DEVONIAN ROCKS IN NORTHEASTERN BRITISH COLUMBIA

Project 750085

D. W. Morrow[1], G. C. Taylor[1], K. R. Dawson[1],
R. W. Krouse[2], and E. C. Ghent[3]

Introduction

Devonian rocks in northeastern British Columbia contain several large deposits of barite and barite-fluorite which were visited by the first three authors during the summer of 1974 (Fig. 38. 1). The lowermost stratigraphic occurrence of barite at the top of the Lower Devonian Wokkpash Formation is near Mile 472 on the Alaska Highway (Fig. 38. 1). Economically significant deposits of bedded barite occurs at the base of the Middle Devonian Stone Formation on nearby Sulphur Creek. Some bedded barite also occurs at the base of the Stone Formation near Mile 472. The 110 Creek deposit has a combined barite-fluorite mineralogy and occurs in the upper part of the Stone Formation (Fig. 38. 2) on 110 Creek. The Liard Fluorite deposit is mainly fluorite and occurs near the top of the Middle Devonian Dunedin Formation (Fig. 38. 2).

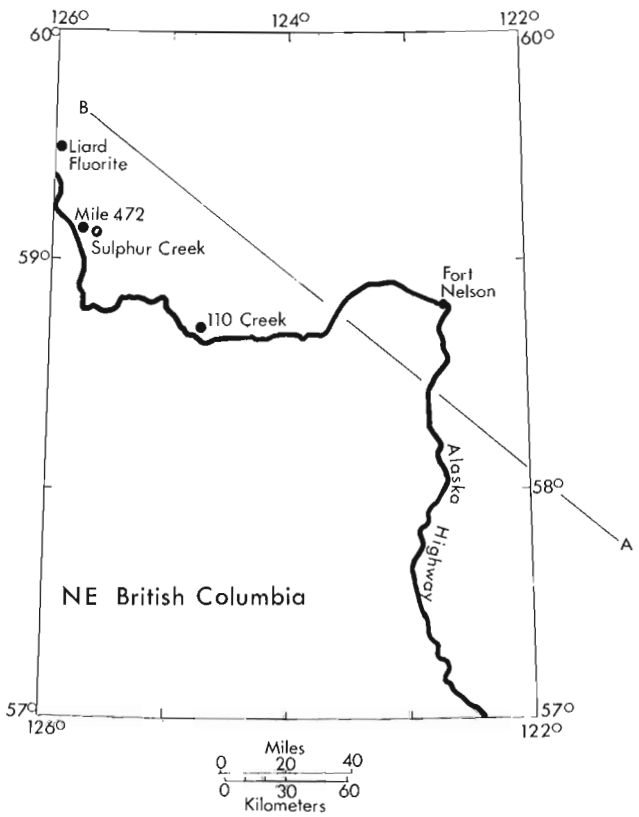

Figure 38. 1. Index map showing location of the Sulphur Creek, 110 Creek and Mile 472 barite deposits and the Liard Fluorite deposit.

Sulphur Creek and 110 Creek

Dawson (1974) classified the barite with minor amounts of fluorite at 110 Creek as a combined stratiform-replacement type of deposit and the bedded barite at Sulphur Creek as a purely stratiform type of deposit. Several units of bedded barite 1 to 2 m thick are interbedded with the host rock dolomite near the top of the Stone Formation at 110 Creek. This bedded barite is associated with solution-collapse (Fig. 38. 3). Sheet-like solution cavities that formed parallel to bedding were initially encrusted with purple fluorite (Fig. 38. 3). In thin section, this fluorite crust appears to be corroded. After deposition of a thin crust of fluorite, less than 1 cm thick, the remaining pore space was filled with very coarsely crystalline barite (Fig. 38. 3). Fan-like sheafs of barite blades with blades up to 5 cm long radiate from one side of a solution cavity to the other. White calcite and dolomite occur as a final cavity fill in many places. The dark grey host rock between cavity fillings is replaced almost entirely by finely crystalline fluorite. Randomly oriented blades of replacement barite up to 1. 5 cm long (Fig. 38. 3) are common in the dark wall rock.

The largest barite deposit in northeastern British Columbia occurs at Sulphur Creek. There barite and dolomite in beds from several centimetres to tens of centimetres thick are interbedded in a 15-m-thick unit at the base of the Stone Formation (Fig. 38. 2). This deposit rests directly on the Wokkpash Formation.

The bedded barite in this deposit also shows evidence of solution-collapse. The hand sample shown in Figure 38. 4 was taken from a point 3 m above the base of the Stone Formation at the Sulphur Creek locality. The centre of the sample displays some collapse breccia. Brecciation occurred after, and possibly during, barite precipitation and before a final infill of calcite cement. Barite of the Sulphur Creek deposit is more finely crystalline than the barite at 110 Creek by an order of magnitude and is formed of fibrous arrays of barite blades several millimetres long oriented perpendicular to bedding. The dolomite interbeds have been replaced largely by very finely crystalline barite with only a small proportion of the original dolomite remaining.

Mile 472 Creek

The contact of the Wokkpash Formation with the overlying Stone Formation is deeply weathered and oxidized in the region where barite occurs in the Stone Formation (Taylor and Mackenzie, 1970). In a few

[1]Geological Survey of Canada

[2]Department of Physics, University of Calgary

[3]Department of Geology, University of Calgary

From: Report of Activities, Part C;
Geol. Surv. Can., Paper 76-1C (1976)

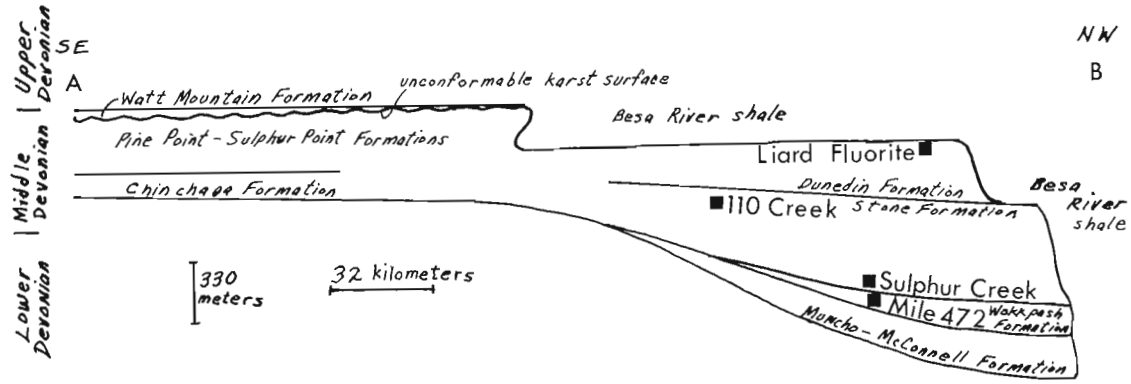

Figure 38. 2. Schematic cross-section showing stratigraphic setting of barite-fluorite deposits in northeast British Columbia. Line of section is on Figure 38. 1.

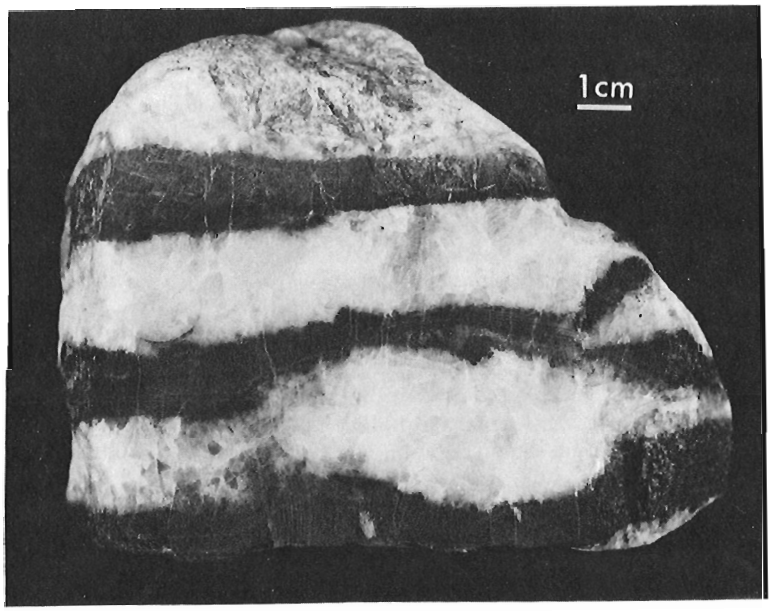

Figure 38. 3.

Barite-fluorite mineralization from 110 Creek. Coarse bladed barite appears to be an open space filling of irregular solution porosity. Dark layers of host dolomite have been largely replaced by fluorite and a few blades of barite. This barite has a $\sigma\ ^{34}S$ value of +28. 2 ‰ (sample 5 in Table 38. 1).

places, such as at Mile 472 Creek, a conglomerate composed of angular to subrounded dolomitic limestone and barite fragments occurs within the upper several feet of the yellow- to orange-weathered zone. Figure 38. 5 is a typical hand sample of this barite lag conglomerate.

Taylor and Mackenzie (1970) and Dawson (1974) regarded this barite as being a lag deposit presumably reworked from an older bedded or barite vein deposit. The white barite clasts are formed of finely to coarsely crystalline barite blades (Fig. 38. 5) that are similar in appearance to the nearby Sulphur Creek bedded barite deposit. The buff to dark grey matrix is dolomitic calcisiltite. This barite conglomerate has not been reported to occur anywhere other than in close proximity to bedded barite in the overlying Stone Formation at Sulphur Creek. Barite does not occur in any well sections of either the Stone or Wokkpash formations in northeastern British Columbia. This was confirmed by X-ray analyses of selected well cuttings.

Liard Fluorite

The Liard Fluorite deposit is several metres thick and occurs at the contact of the Dunedin Formation limestone with the overlying Besa River shale north of Liard Hot Springs (Fig. 38. 1). Fluorite, witherite and barytocalcite occurs in a chaotic breccia which is interpreted as a solution collapse breccia (Woodcock, 1973). This deposit contains barite in small amounts along with quartz, bitumen and H_2S.

Sulphur Isotope Data

Sulphur isotope analyses of barite samples are expressed as per mil deviation from a standard (sulphur in troilite from the Canyon Diablo Meteorite) as σ (del) ^{34}S ‰:

$$\sigma^{34}S‰ = \frac{{}^{34}S/{}_{32}S \text{ sample} - {}^{34}S/{}_{32}S \text{ standard}}{{}^{34}S/{}_{32}S \text{ standard}} \times 10^3$$

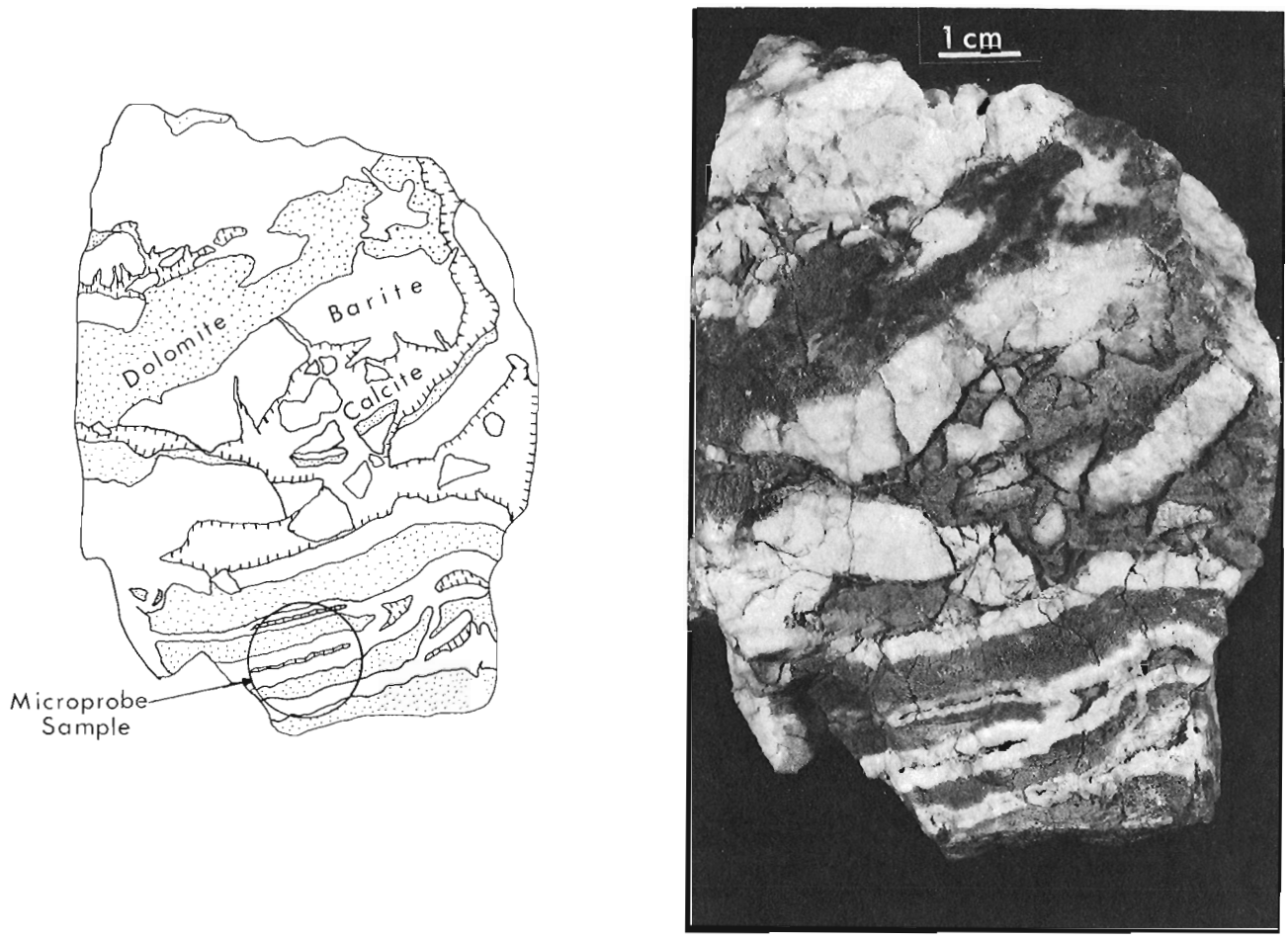

Figure 38. 4. Barite mineralization in a sample taken 3 m above the base of the Stone Formation at Sulphur Creek. Some collapse and brecciation of barite-encrusted laminae has occurred before a final infilling by calcite. This barite has a $\sigma\ ^{34}S$ value of +26. 0‰ (sample 2 in Table 38. 1).

All isotope analyses were performed by H. R. Krouse in the Stable Isotope Laboratory of the Department of Physics at the University of Calgary.

All samples except for sample 7 fall within a relatively narrow range of sulphur isotope ratios from +25. 1 to +28. 9‰ $\sigma\ ^{34}S$ (Table 38. 1). Samples 1 to 6 are from the Sulphur Creek, 110 Creek and Mile 472 deposits, whereas sample 7 with its anomalously high value of +38. 1 ‰ $\sigma\ ^{34}S$ comes from the Liard Fluorite deposit further north (Fig. 38. 1).

Dawson (1974) noted that the Sulphur Creek and 110 Creek deposits are not close to any known occurrences of igneous rocks. This also is true of the Mile 472 deposit. The enrichment in ^{34}S appears to rule out an igneous source for the SO_4^{2-} in these deposits. Holser and Kaplan (1966) note that springs and fumaroles of volcanic origin have $\sigma\ ^{34}S$ in the range -10 to +15 ‰. Jensen (1959) found that the primary sulphide minerals in igneous and metamorphic hydrothermal deposits displayed $\sigma\ ^{34}S$ values ranging from about +15 ‰ to -45 ‰ . Deposits that are entirely magmatic in origin display a range of $\sigma\ ^{34}S$ values of only 5 ‰ and are clustered about 0 ‰ $\sigma\ ^{34}S$. The wide range of $\sigma\ ^{34}S$ ‰ values in other hydrothermal deposits may reflect the participation of a variety of subsurface fluids, including connate and meteoric groundwaters, in the formation of many hydrothermal deposits. In marked contrast, the barite of northeastern British Columbia (Samples 1 to 6) displays very high positive values of $\sigma\ ^{34}S$ with a narrow spread. This suggests that the SO_4^{2-} for barite in northeastern British Columbia was derived from a single homogeneous source of SO_4^{2-} with a $\sigma\ ^{34}S$ ratio of about +25‰ to +29 ‰ .

One possible source for sulphate with the requisite attributes is ancient sea water. The isotopic composition of present day sea water is +20 ± 0. 5 ‰ $\sigma\ ^{34}S$ and strontian barite forming in equilibrium with sea water on the sea floor has a $\sigma\ ^{34}S$ value of +19. 5 ‰ (Holser and Kaplan, 1966). Ancient sea water has undergone considerable shifts in its sulphur isotope composition (Fig. 38. 6). The host formations (Table 38. 1) of the epigenetic barite deposits in northeastern British Columbia range in age from Early to Middle Devonian (Fig. 38. 2). During this time world ocean water had a $\sigma\ ^{34}S$ value of about +17‰ to +23 ‰. From Middle to Late Devonian time the $\sigma\ ^{34}S$ ratio of the ocean increased

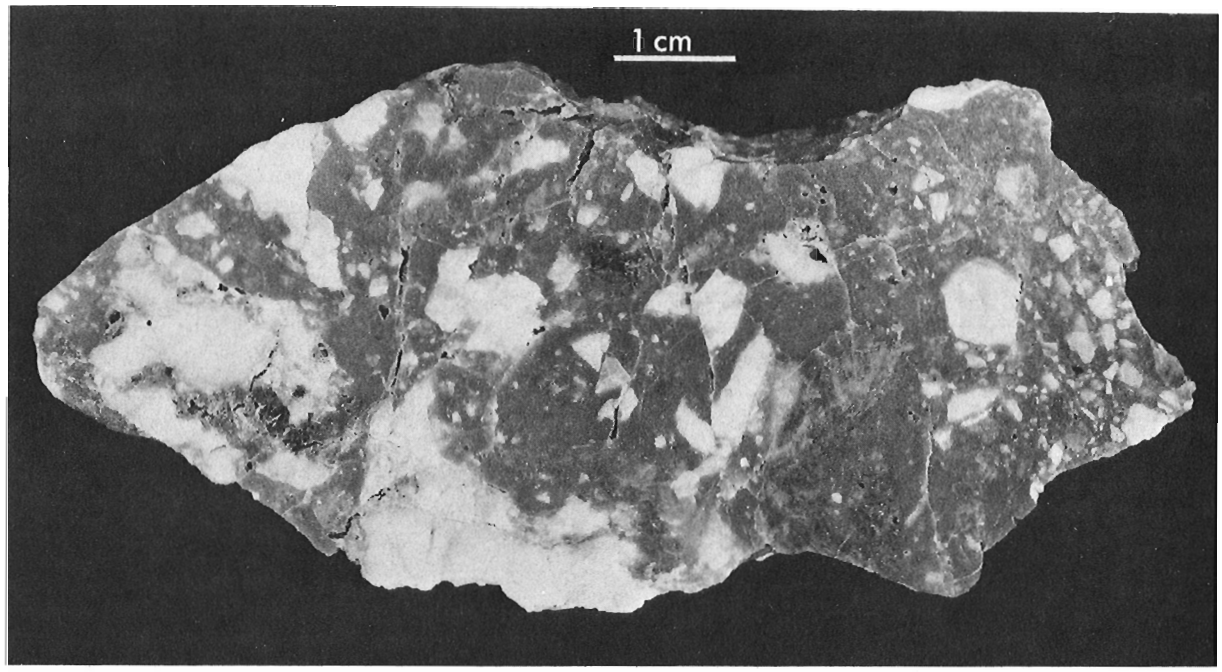

Figure 38. 5. Barite breccia and conglomerate from the top of the Wokkpash Formation at Mile 472. This barite has a $\sigma\ ^{34}S$ value of +26. 8‰.

TABLE 38. 1

Sulphur Isotope ratios in barite from northeastern British Columbia

Specimen	Locality	Host Formation	Major Mineralogy	$\sigma\ ^{34}S$ ‰
1	Sulphur Creek	Stone	barite	+ 25. 1
2	Sulphur Creek	Stone	barite	+ 26. 0
3	Mile 472	Wokkpash	barite	+ 26. 0
4	Mile 472	Wokkpash	barite	+ 26. 8
5	110 Creek	Stone	barite	+ 28. 2
6	Mile 472	Wokkpash	barite	+ 28. 9
7	Liard Fluorite	Dunedin	Witherite	+ 38. 1

dramatically to more than +30‰ in early Late Devonian time. This period of rapid shift of $\sigma\ ^{34}S$ ratio in the ocean coincides with the time of deposition of the Watt Mountain Formation (Figs. 38. 2 and 38. 6). Deposition of the shallow water Watt Mountain sandy shales may have been linked with the development of a coastal freshwater aquifer that extended seaward up to 100 km, and occupied the Stone and Dunedin formations (Morrow, 1975). Mixing of fresh groundwater and euxinic, barium-bearing sea water along the seaward edge of this aquifer has been suggested as a mechanism for the replacement of the Stone Formation carbonates by barite (Morrow, 1975). The $\sigma\ ^{34}S$ values of barite from the Sulphur Creek and 110 Creek deposits is consistent with this hypothesis.

Solution of older Paleozoic evaporites would also supply SO_4^{2-} enriched in ^{34}S to a mineralizing solution. However, bacteriogenic reduction should have affected the $\sigma\ ^{34}S$ values of any mineralizing groundwater

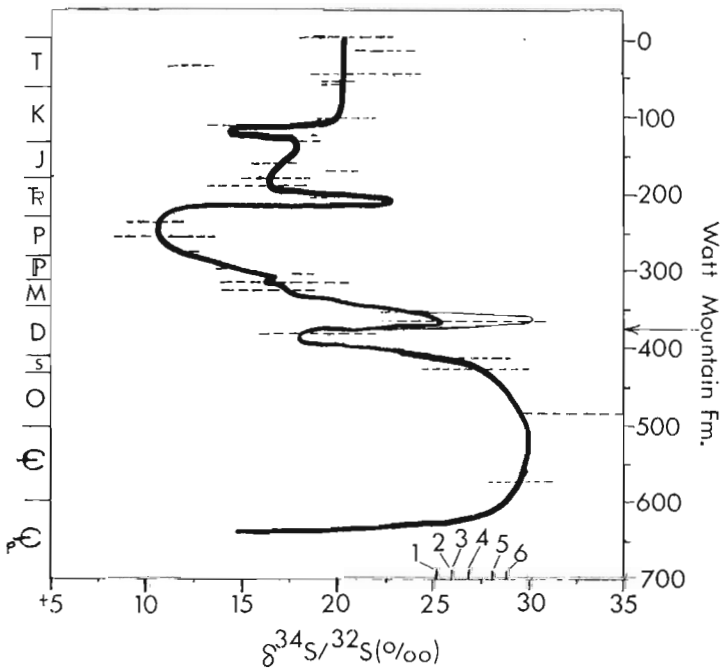

Figure 38. 6. Variation in sulphur isotope composition of sea water sulphate with time (Holser and Kaplan, 1966). $\sigma\ ^{34}S$ values of barite in samples 1 to 6 is given in Table 38. 1.

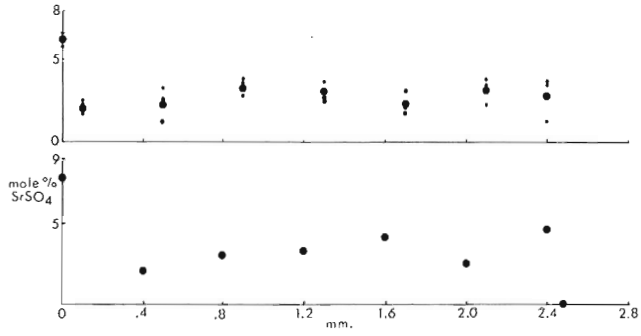

Figure 38. 7. Plots of strontium content along the growth direction of blades of space-filling barite from the sample shown in Figure 38. 4. The first $SrSO_4$ determination in each traverse is on the barite crust adjacent to the dolomite wall rock. The last $SrSO_4$ determination is from the central calcite fill.

solution that underwent long distance subsurface migration. Barite formed from sulphate that has undergone one or more stages of biogenic reduction to sulphide followed by re-oxidation to sulphate probably would display more negative $\sigma\ ^{34}S$ values than those observed in barites from northeastern British Columbia. The nearest sulphate-bearing units are the Chinchaga and Pine Point formations (Fig. 38. 2). There is no indication that there has been any solution of evaporites from these units. Neither of these formations contain large amounts of evaporites in British Columbia.

The similarity of $\sigma\ ^{34}S$ values of the detrital barite at the top of the Wokkpash Formation at Mile 472 with those of the barite in the immediately overlying bedded barite in the Stone Formation at Sulphur Creek suggests a common origin. One possibility is that this coarse fragmental barite (Fig. 38. 5) may be a detrital cave accumulation at the base of the zone of cavernous porosity developed during barite mineralization of the overlying Stone Formation. Barite fragments may have filtered downward on to the Wokkpash regolith and may have been reworked into the regolith. If the detrital barite at the top of the Wokkpash Formation is a regolith accumulation, the older source barite vein or bed should be very near, but no source has been identified. In modern settings, coarse barite fragments are not present in regolithic soils that have incorporated vein barite from underlying bedrock (Merefield, 1975). Instead barite is broken down to fine sand and silt sizes. If the detrital barite at Mile 472 is in fact a regolithic reworking of a bedded barite deposit near the top Wokkpash Formation then it is unlikely that it derived its sulphate from contemporaneous late Early Devonian sea water which had a low $\sigma\ ^{34}S$ ratio of +20‰.

The very high $\sigma\ ^{34}S$ value of the single sample from the Liard Fluorite deposit is anomalous. More analyses of samples from this deposit are required to verify whether this is a representative value. Local fractionation of sulphur isotopes during precipitation may explain this high value. Or, possibly the Liard Fluorite is genetically distinct from the other deposits.

Electron Microprobe Data[1]

Barite ($BaSO_4$) forms a continuous solid solution series with celestite ($SrSO_4$). The amount of $SrSO_4$ in barite is a function of the Ba/Sr ratio in the solution from which the barite precipitated (Hanor, 1968). Consequently, inter- and intra-crystal variations in mole $\%SrSO_4$ should give some insight into the precipitation history of barite. Figure 38. 7 shows the variation of mole $\%\ SrSO_4$ along individual blades of barite that precipitated in solution cavities and seams in the sample shown in Figure 38. 3 of a sample from the Sulphur Creek deposit. The two traverses are about 0. 1 mm apart and follow two individual blades of barite from the host dolomite wall rock to the centre of the cavity fill which is infilled with calcite. Figure 38. 4 shows the location of the microprobe sample. The probe traverse was run near the centre of the microprobe sample. Both traverses begin on equant blocky barite that forms a crust 40 to 50 microns thick on the dolomite wall rock. This is reflected in the high mole $\%SrSO_4$ of the first point of each traverse. All subsequent points follow along the length of individual blades of barite to the centre of the cavity filling.

The low mole $\%SrSO_4$ content (2% to 8%) is typical of many barite deposits (Hanor, 1968) and reflects a high Ba/Sr ratio in the mineralizing solution. The slight increase in mole $\%SrSO_4$ towards the distal ends of barite blades is a function of the speed of circulation of the mineralizing solution with respect to the rate of crystal growth. As barite precipitates from solution, the Ba/Sr ratio increases in the solution resulting in a progressive increase in the mole $\%SrSO_4$ of later formed barite. The extent of this increase depends on how much of the total Ba + Sr in solution is precipitated which is, in turn, dependent on the speed of circulation of the solution. The increase is from about 0. 02 to 0. 04 mole fraction $SrSO_4$. As may be seen in Figure 38. 8 this small degree of strontium enrichment of barite during precipitation probably indicates that only a small part of the total Ba + Sr in solution was precipitated.

If this bladed barite were deposited in equilibrium with a single pore volume of solution then Figure 38. 8 indicates that the initial mole fraction of Sr in the liquid with respect to total Ba + Sr was about 0. 5 and that precipitation continued until a maximum of about one quarter of the total Ba + Sr in solution had been precipitated. It seems unlikely, however, that the bladed barite could have been deposited from a single, stationary, pore volume of solution. Mineralizing solution with an assumed initial composition (0. 5 mole fraction Sr) may have been continuously circulating through the porosity and mixing with pockets of solution

[1]Electron Microprobe analyses were performed on the electron microprobe of the Dep. of Geology of the University of Calgary. D. W. Morrow, under the supervision of E. C. Ghent and B. Rutherford, carried out the analyses. Strontianite was used as a standard and a beam diameter of 10 μ was employed. Counting time per analysis was 100 seconds.

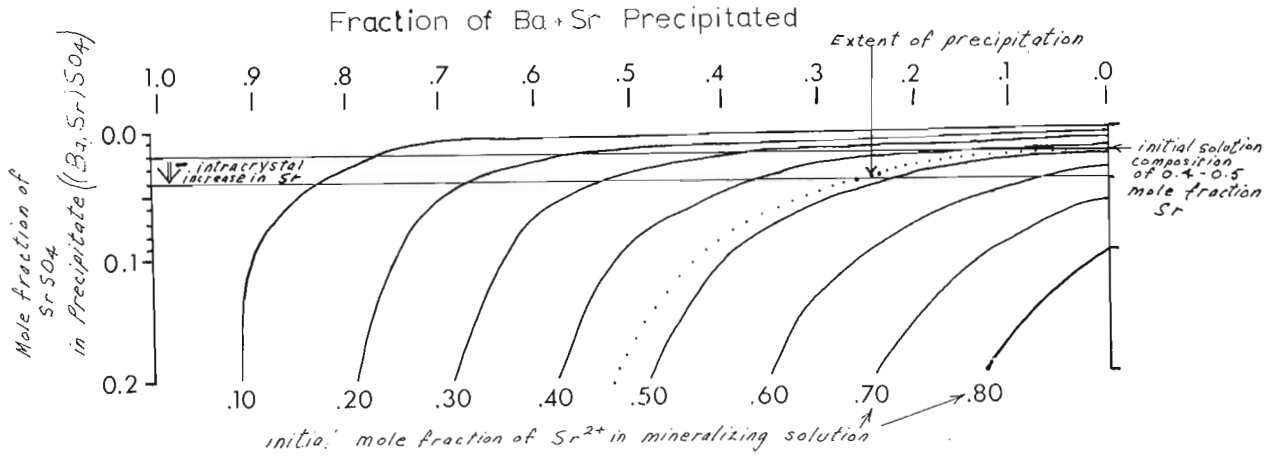

Figure 38. 8. Composition of the last-formed precipitate of (Ba, Sr) SO_4 as a function of the mole fraction of Ba plus Sr precipitated out of solution for a series of initial mineralizing solution compositions. Initial solution compositions are given as the mole fraction of Sr with respect to total Ba + Sr in solution. Two horizontal lines define the amount and variation of $SrSO_4$ within barite crystals from Sulphur Creek and the extent of precipitation of Ba + Sr from solution. Adapted from Hanor (1968, p. 1219).

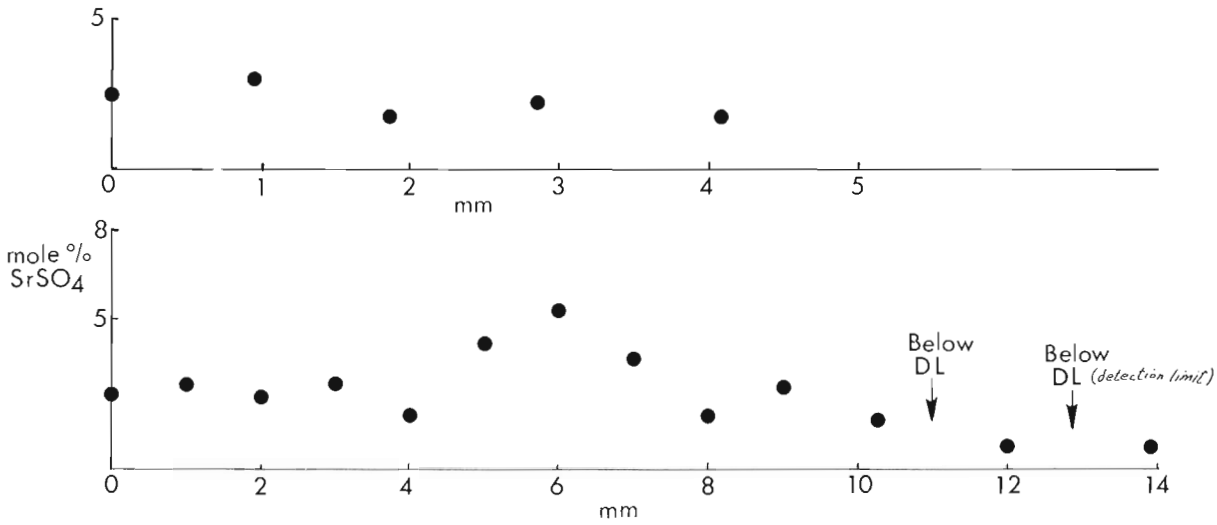

Figure 38. 9. Graphs of strontium content along the growth direction of blades of barite in the sample shown in Figure 38. 3 from 110 Creek.

that had previously precipitated barite and that had become enriched in strontium. The successive increases and decreases of the mole %$SrSO_4$ along barite blades (Fig. 38. 7) may reflect variations in the rate of introduction of fresh solution. One extreme occurs where the amount of fresh mineralizing solution that entered the porosity greatly exceeded the portion of pre-existing altered pore fluid that remained in the porosity. This may have caused the decrease in mole % $SrSO_4$ within the analyzed barite blades at about 1. 5 to 2. 0 mm along the crystals (Fig. 38. 7). The increase in mole %$SrSO_4$ from 2. 0 to 2. 4 mm in the lower plot of Figure 38. 7 implies that the pore fluid was relatively stationary during precipitation of this portion of barite allowing Sr to increase in solution during local barite precipitation. The overall increase in the mole %$SrSO_4$ along barite blades may indicate progressive stagnation of the mineralizing solution as the porosity was slowly infilled.

Microprobe traverses along barite blades in the open space filling barite from 110 Creek show a decline in mole %$SrSO_4$ along the growth direction of individual barite blades (Fig. 38. 9) and have a lower average mole %$SrSO_4$ content (Fig. 38. 10). The very low strontium content of less than 1 mole %$SrSO_4$ at some points (Fig. 38. 9) indicates that the mole fraction of strontium with respect to total Ba + Sr in the mineralizing solution was as low as 0. 2 (Fig. 38. 8). As before, individual increases and decreases in the mole %$SrSO_4$ content along barite blades are explicable in terms of variations in the rate of circulation of the mineralizing solution. However the overall decrease in the mole %$SrSO_4$ along

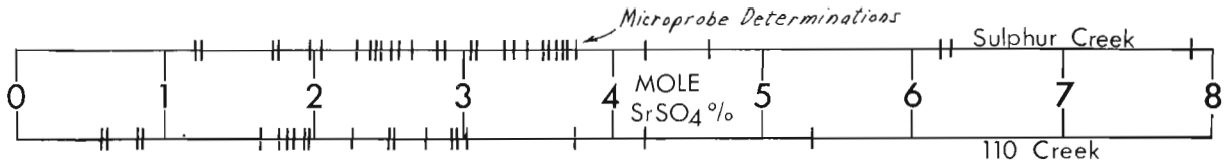

Figure 38. 10. Comparison of microprobe determinations of the $SrSO_4$ content in the sample shown in Figure 38. 4 from Sulphur Creek against the $SrSO_4$ content of the sample shown in Figure 38. 3 from 110 Creek.

barite blades is inconsistent with the concept that the mineralizing solution stagnates as the porosity is infilled. Perhaps the Ba/Sr ratio of the mineralizing solution entering the system increased during precipitation of 110 Creek barite. The evident difference in the inferred Ba/Sr ratio of the mineralizing solutions of the Sulphur Creek versus the 110 Creek deposits supports this hypothesis. The very coarse crystallinity of the 110 Creek deposit indicates that precipitation occurred over a much longer time period than did precipitation of the Sulphur Creek deposit. Therefore changes in the Ba/Sr ratio of the source solution are more likely to be reflected in barite of the 110 Creek deposit.

The small proportion of total $Ba^{+2}Sr^{+2}$ and SO_4^{2-} precipitated from the mineralizing solution in both the Sulphur Creek and 110 Creek deposits indicates that fractionation effects are not likely to affect their sulphur isotope ratios.

Conclusions

1. Barite in the Sulphur Creek and 110 Creek deposits appears to have undergone solution collapse after and possibly during barite precipitation and replacement.

2. Sulphur isotopes in barite from the Sulphur Creek and 110 Creek deposits ranges from +25. 1 to +28. 2 ‰ $\sigma\ ^{34}S$ appears to rule out a direct igneous source for these deposits. Sea water of early Late Devonian age had sulphur isotope ratios similar to those displayed by these barites. Consequently, it is possible that early Late Devonian sea water or sea water-derived solutions provided the SO_4^{2-} for these deposits.

3. The similarity of the sulphur isotope ratios in barite from the Mile 472 deposit with the ratios in barite from the Sulphur Creek and 110 Creek deposits may indicate that these deposits are cogenetic. One possible explanation is that the Mile 472 deposit was formed from collapsed fragments of barite that filtered downward from the Sulphur Creek deposit as it underwent solution-collapse during mineralization.

4. Variations in the mole % $SrSO_4$ along barite blades suggests that during precipitation there may have been changes in the rate of circulation of the mineralizing solution. Even during periods of relative stagnation however, only a small fraction of the total dissolved ions were precipitated out of solution. The lower strontium content of barite from 110 Creek indicates that the Ba/Sr ratio of the source solution was higher during precipitation of 110 Creek barite than during precipitation of Sulphur Creek barite.

References

Dawson, K. R.
1974: Barite, Fluorite, and celestite deposits and occurrences in Canada; *in* Report of Activities, Part A; Geol. Surv. Can., Paper 75-1A, p. 257-259.

Hanor, J. S.
1968: Frequency distribution of compositions in the Barite-Celestite series; Am. Mineral., v. 53, p. 1215-1222.

Holser, W. T. and Kaplan, I. R.
1966: Isotope geochemistry of sedimentary sulphates; Chem. Geol., v. 1, p. 93-135.

Jensen, M. L.
1959: Sulphur isotopes and hydrothermal mineral deposits; Econ. Geol., v. 54, p. 374-394.

Merefield, J. R.
1975: Incorporation in soil of barytes derived from mineral veins in southwest England; Sediment. Geol., v. 14, p. 135-148.

Morrow, D. W.
1975: The Florida Aquifer: a possible model for a Devonian paleoaquifer in northeastern British Columbia; *in* Report of Activities, Part B; Geol. Surv. Can., Paper 75-1B, p. 261-266.

Taylor, G. C. and MacKenzie, W. S.
1970: Devonian stratigraphy of northeastern British Columbia; Geol. Surv. Can., Bull. 186.

Woodcock, J. R.
1973: Liard Fluorspar Mineralization – northeastern British Columbia; *in* Sedimentary Geology and Mineral Deposits of the Canadian Cordillera, Cordilleran Section, Geol. Assoc. Can., p. 22-23.

39. LATE QUATERNARY PALEOMAGNETIC STRATIGRAPHY FROM EAST-CENTRAL LAKE ONTARIO

Project 680055

T. W. Anderson[1], R. J. Richardson[1], and J. H. Foster[2]

It is becoming apparent that the Great Lakes of North America provide a promising area in which to study the many environmental and physical aspects of the Late Quaternary (Fritz *et al.*, 1975; Creer *et al.*, 1976a, b). Unlike ocean sediments, the sediments of the Great Lakes are characterized by rapid deposition rates and, hence, greater resolution of the various events can be expected. This is especially the case with respect to known short-term events in the history of the earth's geomagnetic field which recently has been documented in cores from Lake Erie (Creer *et al.*, 1976a) and Lake Michigan (Creer *et al.*, 1976b; Dodson *et al.*, 1976).

This report discusses further exploratory studies into the paleomagnetism of Great Lakes sediments. Detailed magnetic measurements are carried out on a long piston core (PC 28) collected in 177 m water depth in east-central Lake Ontario, 40 km northeast of Rochester, New York (Anderson and Lewis, 1975). The study is compared with the records obtained from Lake Erie and will contribute a great deal to our understanding of the geomagnetic stratigraphy of the Late Quaternary.

J. H. Foster provided laboratory facilities and technical advice throughout the study; R. J. Richardson carried out the magnetic measurements and produced the magnetic plots; T. W. Anderson provided the stratigraphy and chronology and was largely responsible for the manuscript preparation.

Sediment Description, Chronology, and History

The piston core was obtained during a piston and gravity coring-echo sounding survey of Lake Ontario in 1974 aboard the M.V. Martin Karlsen (Anderson and Lewis, 1975). The core penetrated to a depth of almost 15 m and incorporates a good portion of late Wisconsinan and Holocene stratigraphy beginning in till and extending through the entire sequence of glaciolacustrine and postglacial sedimentation.

The lowermost 3 m is a silty, sandy till with many pebbles throughout. The till unit probably represents more than one late Wisconsinan-aged till. The upper part of the unit, however, may be correlative with the Lower Leaside Till, the principal till mapped on the northwest shore of Lake Ontario.

The till is overlain by about 1 m of interbedded, stony, fine to medium coarse sand and laminated clay which is interpreted as an ice-contact deposit in an early stage of glacial Lake Iroquois. The earliest accepted date for inception of Lake Iroquois is 12 660 ± 400 years B. P. (W-861; Rubin and Alexander, 1960). The sediments are distinctly varved from 10. 65 to 8. 70 m, but gradually become very finely laminated between 8. 70 and 5. 50 m. These glaciolacustrine varved and laminated clays are believed to have accumulated during the time interval of high-level Lake Iroquois through the post-Iroquois "falling" lakes phases, Frontenac to the Admiralty low-level stage (Sly and Lewis, 1972).

Preliminary pollen analyses were carried out on the upper half of the core in an effort to correlate the data with those from small lake and bog sediments nearby and to apply age estimates to the sediment column. Thus a date of 10 500 years B. P. is placed at 5. 70 m for the end of the spruce maximum and the rise in pine. By this time the ice front was well out of the Ontario Basin, and the waters of Lake Ontario were at or near their lowest level. Proto-Lake Ontario probably resembled a small-lake environment at this time as the pollen is well preserved from about 5. 75 to 5. 50 m. Pollen preservation, however, deteriorates noticeably around 5. 50 m and coincides with a sediment change to distinctly reddish-grey, laminated, compact clays. It is suggested that these clays accumulated in early Lake Ontario which was rising as a result of isostatic uplift of the eastern end of the basin. The exposed basin slopes would have been susceptible to widespread erosion and downcutting with older materials reworked and redeposited in the progressively deepening lake. This is supported by the fact that spruce pollen is still prominent up to the 3. 80 m level, which is dated at just over 10 300 years B. P., and the pollen, in general, is very poorly preserved.

Grey, finely laminated and/or mottled muds dominate from about 4. 70 m to the surface and represent an accumulation of over 10 000 years as the water level rose to that of present Lake Ontario. High pine pollen percentages give way to hemlock and maple at the 3. 10 m level, dated at approximately 7600 years B. P. The offshore muds probably accumulated rapidly, but uniformly, from this time onward to the present.

Paleomagnetic Results

Declination, inclination, and remanent intensity (moment) were measured at 2 cm intervals throughout the length of the core before cleaning (NRM) and after demagnetization in a field of 200 oersteds. Computer printouts of the analyses were produced, and the results after demagnetizing at 200 oersteds are shown in Figure 39. 1. Stability index plots also were produced which showed that the samples were well behaved magnetically.

Declination and inclination show much scatter as a result of widespread fluctuations throughout the till and overlying interbedded sands and clays, i. e. from the base of the core to about 10. 8 m. The fluctuations become strongly erratic, especially towards the top of the till and at the base and top of the overlying unit. The abrupt directional changes are not synchronous, however, and the strongly active interval is generally more compressed

[1]Terrain Sciences Division

[2]Regional and Economic Geology Division

From: Report of Activities, Part C;
Geol. Surv. Can., Paper 76-1C (1976).

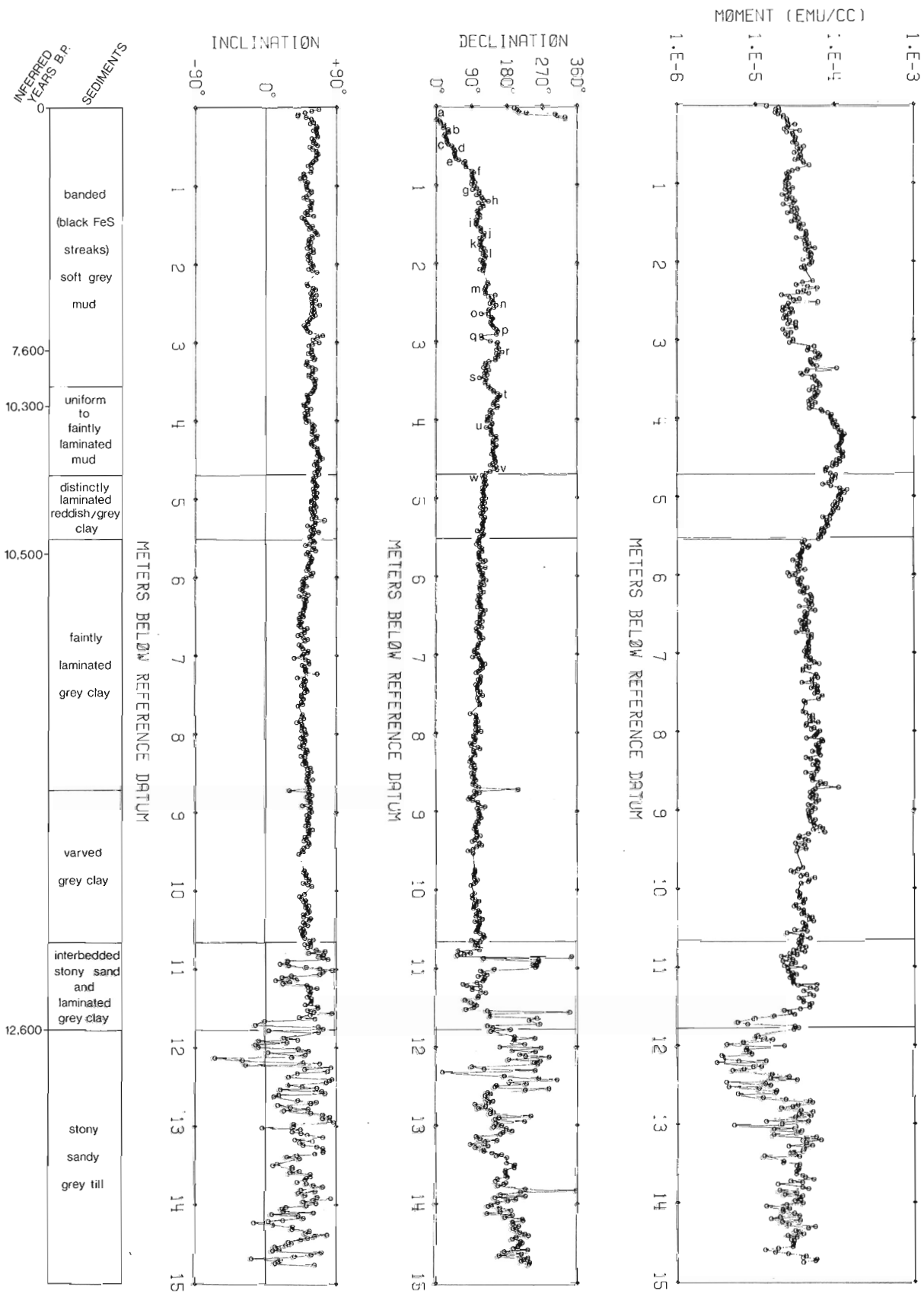

Figure 39. 1. Profiles of inclination, declination, and moment (remanent intensity) after cleaning in 200 oersteds, and depth of sediment below lake bottom at Piston Core 28, east-central Lake Ontario. The 12 600 year-date is inferred for the beginning of glacial Lake Iroquois; the younger dates are based on pollen analysis and correlation with pollen and radiocarbon-dated sites on land (Lowdon *et al.*, 1971; Terasmae, 1968; Dyck and Fyles, 1964).

in the inclination than in the declination profile. The sharp fluctuations in declination near the top of the till (below 12 m) precede those of inclination, and inclination becomes stable earlier than declination in the overlying unit.

Both profiles are characterized by a number of oscillations and amplitude changes typical of geomagnetic secular variation. Declination attains highest positive values within the top metre of the till and swings to its lowest values in the overlying unit. Inclination generally varies between 0 and 90 degrees positive in the lowermost part of the till, but negative inclinations are common in the upper 50 cm of the till and in the bottom 30 cm of the overlying lacustrine sediments. At 12.13 m, the inclinations approach 70 degrees negative, which is indicative of a short polar reversal at this time.

The NRM directions remain positive and display uniform trends from near the top of the interbedded sands and clays, i.e., from 10.8 m upward to the surface of the postglacial muds. Declination, in particular, becomes cyclic above the 5 m level, with possibly as many as eleven complete oscillations occurring during the last 10 500 years, with the swing peaks labelled a to v in Figure 39.1.

Remanent intensity (moment), like declination and inclination, is variable throughout the till and in the overlying interbedded sands and clays. Values are high at the base of the till but are considerably lower in the area of greatest fluctuation in inclination and declination, i.e., near the top of the till and at the base of the overlying unit. Intensity remains more or less constant in the glaciolacustrine sediments from about 11.5 to 5.60 m. The sudden increase at 5.60 to 5.50 m appears to correspond with the sharp break in the sediments at this level. Intensity reaches maximum strength between 4 and 5 m, fluctuates upward in somewhat cyclic fashion, and drops off again to low values in the surficial muds.

Interpretation of Results

A significant feature of the magnetic profiles is the presence of large-scale fluctuations in declination, inclination, and intensity throughout the early glacial sediments. The fluctuations are not totally restricted to the till but extend well into sediments believed to represent proglacial interbedded sands and clays of Lake Iroquois. This interval of widespread fluctuations is interpreted as unstable geomagnetic field conditions and represents a late Wisconsinan geomagnetic excursion which is correlative with part of the Erieau Excursion of Lake Erie (Creer *et al.*, 1976a). The core does not penetrate through to the onset of the excursion as shown in the Lake Erie profiles. The negative and/or reversed inclinations at the top of the till and the base of the overlying lacustrine sediments, however, correspond well with the shallow, upward directed (negative or reversed) inclinations near the surface of the glacio-lacustrine sediments in Lake Erie. The excursion, therefore, seems to have lasted at least until after 12 660 years B.P. and probably ended shortly after the inception of glacial Lake Iroquois, or around 12 500 years B.P. It, therefore, does not extend into the early post-glacial as is clearly documented in the Lake Erie records. There seems to be no satisfactory explanation for this anomaly at the present. It might be possible that this portion of the Lake Erie records is peculiar to Lake Erie sediments only, on account of the Early Lake Erie hiatus and succeeding shallow depositional environment of the early postglacial.

Remanent intensity declines to a minimum at the level of negative or reversed inclinations and at the steep changes in declination. Such a relationship is known in other magnetic profiles of freshwater lakes, i.e. in Lake Erie core 13194 (Creer *et al.*, 1976a), in Mono Lake, California (Denham and Cox, 1971), and in deep-sea sediments (Løvlie, 1976). It is suggested that this decay behaviour of intensity at the level of steep changes in declination and inclination is primarily due to the presence of opposing magnetic directions inherent in the sediment (Løvlie, 1976).

In contrast to the lower part of the record, the interval 10.8 m to the surface is characterized by uniform and compact profiles of declination and inclination, implying that the earth's geomagnetic field has been comparatively stable since about 12 500 years B.P. The profiles are especially tight between 10.8 and 5.0 m, the interval of high sedimentation rates associated with glacial Lake Iroquois and the post-Iroquois lake stages. The glacial-postglacial boundary, which is dated at roughly 10 500 years B.P., is tentatively placed at 5.7 m and closely corresponds with the sharp change in sediments and pollen stratigraphy at 5.6 to 5.5 m discussed earlier. A sudden increase in intensity at this depth reflects either an increase in the strength of the geomagnetic field, or more than likely, a significant change in the magnetic mineral constituents corresponding with the change in sediments brought about as a result of rising early Lake Ontario.

While the patterns of declination, inclination and intensity above the 5 m level indicate that the geomagnetic field has been relatively stable since about 10 500 years B.P., some polar wandering is indicated by the cyclic nature of the profiles. The cycles are more exaggerated than in the deeper sediments, probably because of the lower sedimentation rates during the postglacial. The declination swings are typical of postglacial secular variation as observed in other profiles, for example, Lakes Windermere (Creer *et al.*, 1972) Erie (Creer *et al.*, 1976a), and Michigan (Creer *et al.*, 1976b). There could be as many as eleven oscillations of declination in the Lake Ontario core since approximately 10 500 years B.P., giving an average period of just less than 1000 years for each oscillation. However, assuming that the declination record of the uppermost 80 cm, labelled a to f in Figure 39.1, corresponds to that labelled A to B in the upper 1.50 m of Lake Erie core 13194 (and the trends of the inclination profiles from each lake suggest that this is so), the eleven oscillations could be reduced by two and one-half, giving an average cycle period of just over 1200 years, which is still substantially lower than the 1920 year estimate for Lake Erie.

Thus it would seem that more profiles are needed in order to establish whether the cyclic pattern in declination is consistent for the Great Lakes region as is implied in Creer *et al.* (1976a). If it could be shown that this is indeed the case, then these cycles have great potential as regional time-stratigraphic marker horizons.

Taken as a whole, the magnetic profiles of the Lake Ontario core are similar to those from Lake Erie in that they feature two separate and distinct divisions of Late Quaternary geomagnetic stratigraphy. A lower division dominates from the base of the Lake Ontario core to 10.80 m, i.e., during deposition of the early glacial sediments, and is distinguished by widespread fluctuations in declination, inclination, and intensity (moment) correlative with the Erieau Excursion in Lake Erie. An upper division extends from 10.8 m to the surface and is characterized by tighter and more uniform profiles than in the early glacial sequence, especially throughout the later glacial sediments, and also by a cyclic pattern in declination in the postglacial. The record of the Lake Ontario profiles from approximately 11.0 m to about 5.5 m is missing in the Lake Erie cores because of the early Lake Erie hiatus. The Lake Ontario paleomagnetic stratigraphy is believed to be continuous and, hence, represents a more complete record of the Late Quaternary than that of Lake Erie.

The implications of this study concern its application as an additional means to correlate and to date Quaternary events in and outside the Great Lakes area, for example, the well known Champlain Sea incursion of the St. Lawrence Lowlands. Preliminary paleomagnetic studies are in progress on the oldest marine sediments in the Ottawa River valley. It is hoped that the Champlain Sea magnetic stratigraphy is correlative with the magnetic character of the Lake Ontario profiles and that more reliable estimates can be made for the age of the marine sediments.

References

Anderson, T.W. and Lewis, C.F.M.
1975: Acoustic profiling and sediment coring in Lake Ontario, Lake Erie and Georgian Bay; *in* Report of Activities, Part A; Geol. Surv. Can., Paper 75-1A, p. 373-376.

Creer, K.M., Anderson, T.W., and Lewis, C.F.M.
1976a: Late Quaternary geomagnetic stratigraphy recorded in Lake Erie sediments; Earth Planet. Sci. Lett., v. 31, p. 37-47.

Creer, K.M., Gross, D.L., and Lineback, J.A.
1976b: Origin of regional geomagnetic variations recorded by Wisconsin and Holocene sediments from Lake Michigan, U.S.A. and Lake Windermere, England; Geol. Soc. Am., Bull., v. 87, p. 531-540.

Creer, K.M., Thompson, R., and Molyneux, L.
1972: Geomagnetic secular variation recorded in the stable magnetic remanence of recent sediments; Earth Planet. Sci. Lett., v. 14, p. 115-127.

Denham, C.R. and Cox, A.
1971: Evidence that the Laschamp Polarity Event did not occur 13 300 – 30 400 years ago; Earth Planet. Sci. Lett., v. 13, p. 181-190.

Dodson, R., Dunn, J.R., Fuller, M., and Kean, W.
1976: Secular variation records from Lake Michigan sediments (Abst.); Am. Geophys. Union, Trans., v. 57, p. 237.

Dyck, W and Fyles, J.G.
1964: Geological Survey of Canada radiocarbon dates III; Geol. Surv. Can., Paper 64-40, p. 3.

Fritz, P., Anderson, T.W., and Lewis, C.F.M.
1975: Late-Quaternary climatic trends and history of Lake Erie from stable isotope studies; Science, v. 190, p. 267-269.

Løvlie, R.
1976: The intensity pattern of post-depositional remanence acquired in some marine sediments deposited during a reversal of the external magnetic field; Earth Planet. Sci. Lett., v. 30, p. 209-214.

Lowdon, J.A., Robertson, I.M., and Blake, W. Jr.
1971: Geological Survey of Canada radiocarbon dates XI; Geol. Surv. Can., Paper 71-7, p. 271-272.

Rubin, M. and Alexander, C.
1960: U.S. Geological Survey radiocarbon dates V; Am. J. Sci., Radiocarbon Supp. 2, p. 129-185.

Sly, P.G. and Lewis, C.F.M.
1972: The Great Lakes of Canada – Quaternary geology and limnology; 24th Int. Geol. Cong., Excursion A43, Montreal, Quebec. p. 92.

Terasmae, J.
1968: A discussion of deglaciation and the boreal forest history in the northern Great Lakes region. Proc. Entomological Soc. Ont. v. 99, p. 31-43.

Project 750077

T. J. Day and P. A. Egginton
Terrain Sciences Division

Introduction

Engineering and environmental concern for the integrity of bridge crossing sites along the proposed route of the Mackenzie Highway, Northwest Territories has prompted a long-term study (four to five years proposed) of river processes and form (Egginton, 1975). One aspect of this study is the determination of channel migration patterns and rates.

The study is focused on three rivers that are tributary to the east bank of Mackenzie River, Little Smith Creek, Saline River, and Steep Creek, which flow east-west from the Franklin Mountains of the McConnell Range (Fig. 40.1). A brief summary of stream properties is given in Table 40.1. The proposed highway route crosses these tributaries within 2 km of their junction with Mackenzie River, and intensive study has been restricted to these lower reaches. An outline of channel features is given in Table 40.2 and describes channel features under the three main headings of pattern, islands, and bars (Kellerhals *et. al.*, 1976).

The streams studied exhibit a typical subarctic nival runoff regime characterized by a snowmelt flood in spring and generally low levels of flow throughout the summer. Summer rain-storm events may interrupt flow recession and at times may exceed the spring snowmelt flood (Church, 1974).

Method

Lateral migration was investigated by matching aerial photographs taken over an approximate span of 25 years. The aerial photographs used for Little Smith Creek were taken in 1949 (A11974-307, scale 1:10 068) and in 1975 (A24030-224, scale 1:6831); for Saline River, 1945 (A11974-222, scale 1:10 068) and 1972 (A22887-42, scale 1:6780); for Steep Creek, 1949 (A11974-164, scale 1:10 068) and 1972 (A22887-21, scale 1:6780). The time span between photographs is 26 years for Little Smith Creek, 27 years for Saline River, and 23 years for Steep Creek.

River reaches first were identified on the older photographs, and enlargements and transparencies were made. The transparencies were matched with enlargements of the recent photographs, common geomorphic reference points assisted in scale matching.

Unfortunately, without extensive ground measurements, the accuracy of these comparisons cannot be determined. Errors are dependent upon: (1) the original scale and definition of the photographs; (2) the scale of enlargement; (3) the degree of distortion on the photographs; (4) the number and reliability of reference points; and (5) the precision of the matching procedures. In a similar study of river crossing sites along the Alaska Pipeline route, Brice (1971) estimated the matching precision error as 1 to 2 mm, which for an enlargement scale of 1:3000, for example, amounts to an error of ±4 m. The matching precision error, however, is only part of the total error. For the three streams in this study, ground measurements of lateral movements have not been possible, and consequently migration distances can only be considered gross estimates. Dendrochronologic studies, similar in purpose to those of Hickin and Nanson (1975), are being initiated. Even though migration

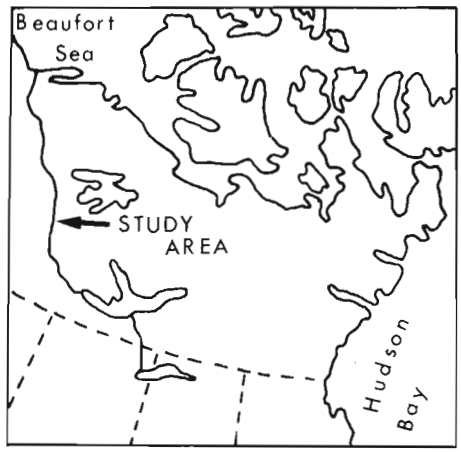

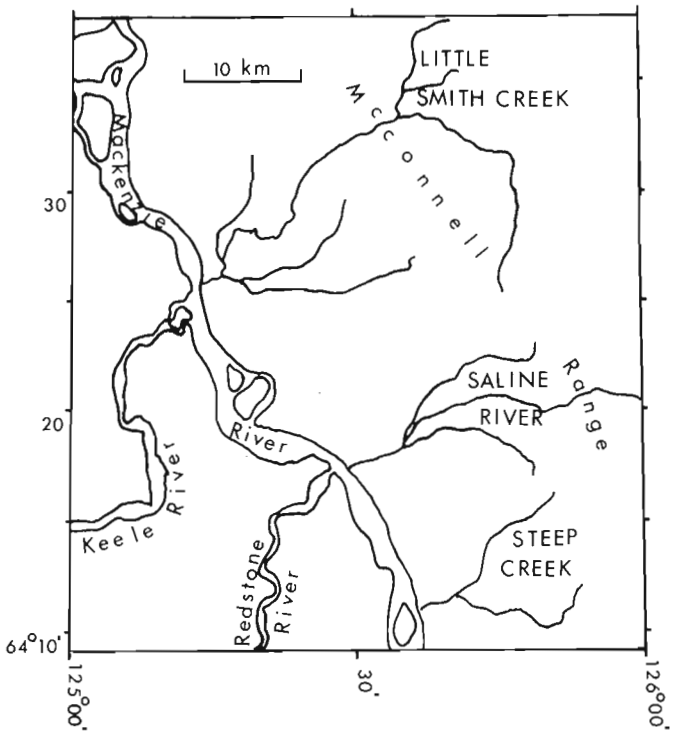

Figure 40.1. Location map of study reaches.

From: Report of Activities, Part C;
Geol. Surv. Can., Paper 76-1C (1976).

Table 40.1

Basic Stream Properties

Study Site	Highway Kilometre	Contributing Drainage Area (km^2)	Longitudinal Gradient
Steep Creek	823.8	148	0.0133
Saline River	838.6	303	0.0071
Little Smith Creek	859.1	477	0.0033

distances may only be estimates, these studies are important in their identification of sites which show a propensity to erosion. This identification is of particular importance where erosion is irregular.

Lateral Migration

Channel maps produced by the above procedure are shown in Figures 40.2, 40.3 and 40.4 for Steep Creek, Saline River, and Little Smith Creek, respectively. The amount of lateral movement varies not only among the streams but along any one stream as well. Maximum erosion is found on Little Smith Creek, where up to 39 m of movement occurs at the outside of meanders. Figure 40.5 shows bank erosion on the outside of a meander bend of Little Smith Creek. The erosion or migration pattern for this stream is relatively coherent and is an example of the downstream progression of a meander train. The erosion pattern of Saline River is similar, but as its meander train is more irregular, erosion distances are more variable, although the pattern is still closely associated with plan form geometry. Figure 40.6 shows an active bank erosion site on Saline River. On the other hand Steep Creek shows irregular erosion, characteristic

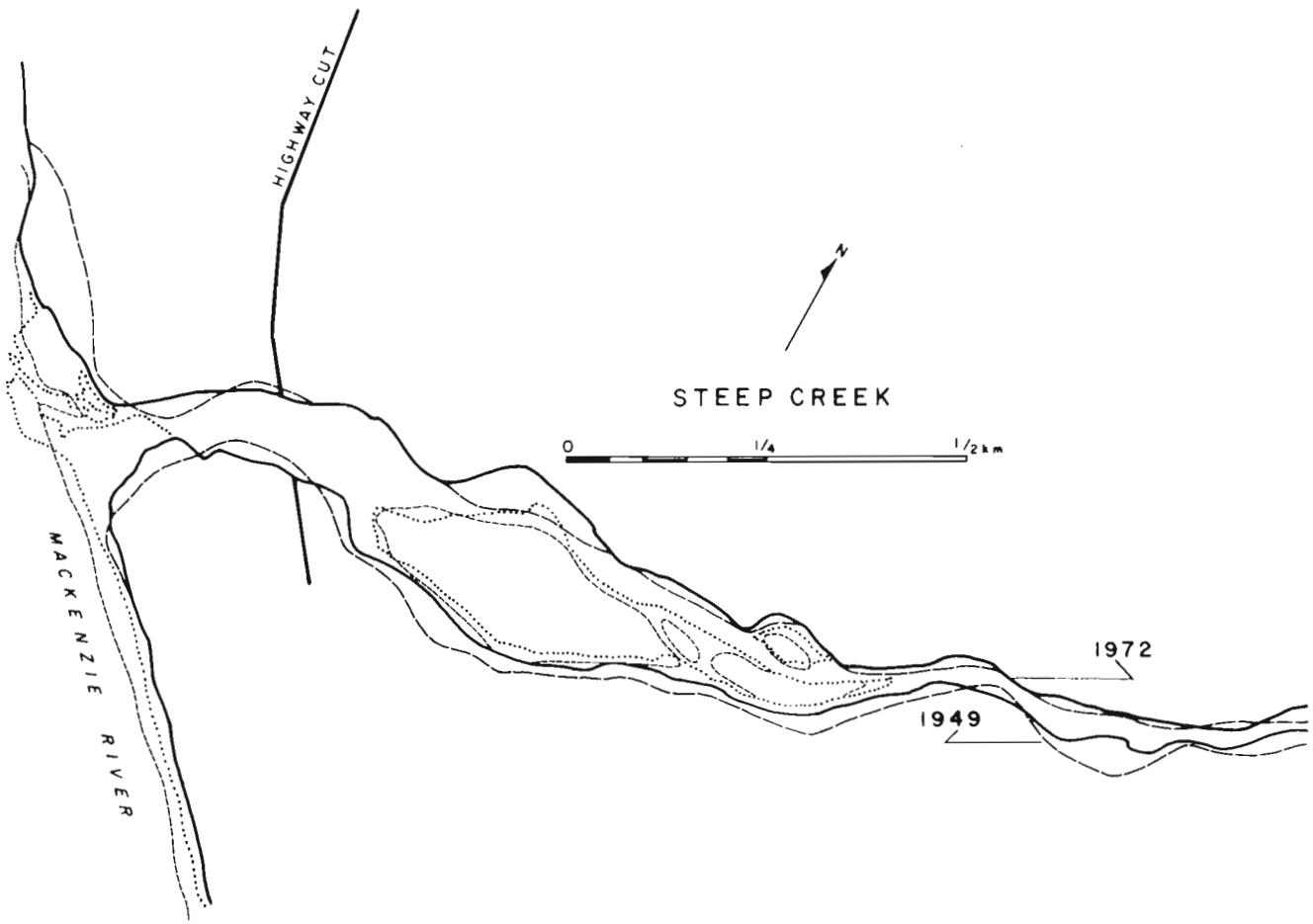

Figure 40.2. Channel migration map for Steep Creek, 1949 to 1972. The dashed lines within the flood plain outline channel bars shown in the 1949 photograph; the dotted lines show the 1972 channel bar positions.

Table 40. 2

Channel Descriptions

Channel Features	Steep Creek	Saline River	Little Smith Creek
Pattern	sinuous	irregular meanders	regular meanders
Islands	split	frequent	frequent
Bars	diamond diagonal	diamond diagonal	point bar side bars
Lateral Activity	irregular	irregular to slight downstream progression	downstream progression

of irregular channel patterns. Figures 40. 7 and 40. 8 show two actively eroding bank sites along Steep Creek.

These streams presently are downcutting through alluvial deposits. Portions of the banks of Steep and Little Smith Creeks, however, are composed of glaciofluvial gravels, and the banks of Saline River in the study reach are composed of glaciolacustrine material. Although erosion rates can be expected to differ with bank composition, any existing patterns remain obscured by the paucity of data. Investigations at the specific crossing sites indicate: (1) that the south bank of Little Smith Creek and Steep Creek have eroded 15 to 30 m

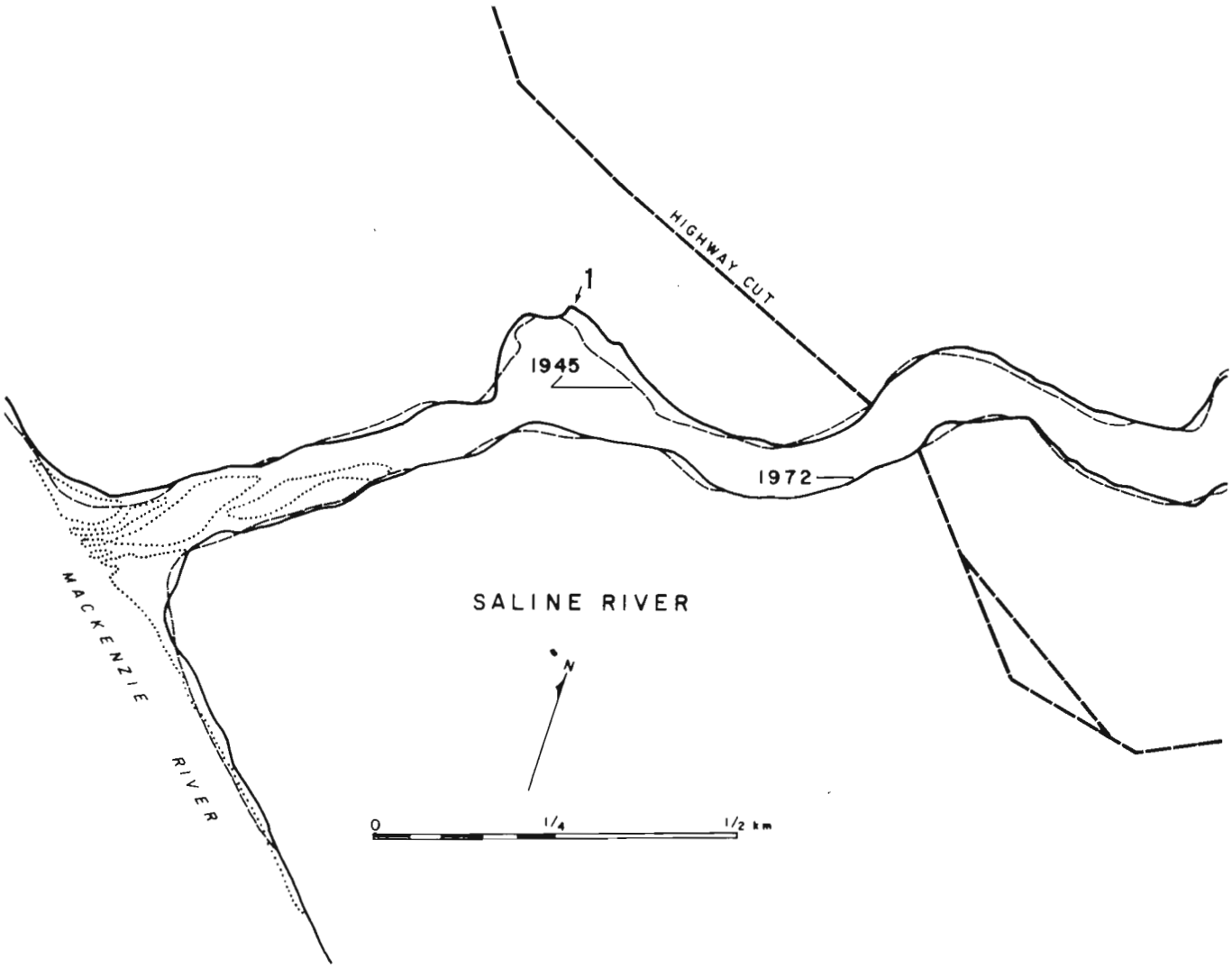

Figure 40. 3. Channel migration map for Saline River, 1945 to 1975. The dotted lines show channel bar positions.

since the mid to late 1940's and as such protective spur dykes may be necessary and (2) that the north bank of Saline River 100 m upstream from the crossing is rapidly eroding (estimated at 1 m per year) and river training should be considered.

Degradation

Between 1949 and 1972 Steep Creek has abandoned the southern channel marked in Figure 40.9. In the 1949 aerial photograph both the north and south channels are active; by 1972, however, the stream has shifted its flow into the northern channel only, and by 1976 the southern channel has been revegetated (Fig. 40.10). During this period of 27 years the northern channels appear to have degraded approximately 1.2 to 1.8 m below the bed of south channel (Fig. 40.11).

Discussion

The relationships between streamflow (hydrology and hydraulics) and channel instability are most complex. For meandering rivers, such as Little Smith Creek, Hickin and Nanson (1975) stated that the rate of lateral migration, M, can be expressed by

$$M = f\,(Q,\ s,\ c,\ h,\ v,\ r_m/w_m)$$

where Q, s, c, h, v and r_m/w_m are, respectively, a discharge factor, water-surface slope, character of the boundary material, height of the concave (outside) banks, bank vegetation, and the ratio of radius of channel curvature to channel width. To date, the flow structure variations and their relation to erosion in meanders have not been treated successfully nor is there sufficient field information on a wide range of stream scales, bank materials, etc. with which to predict, even tentatively, erosion rates.

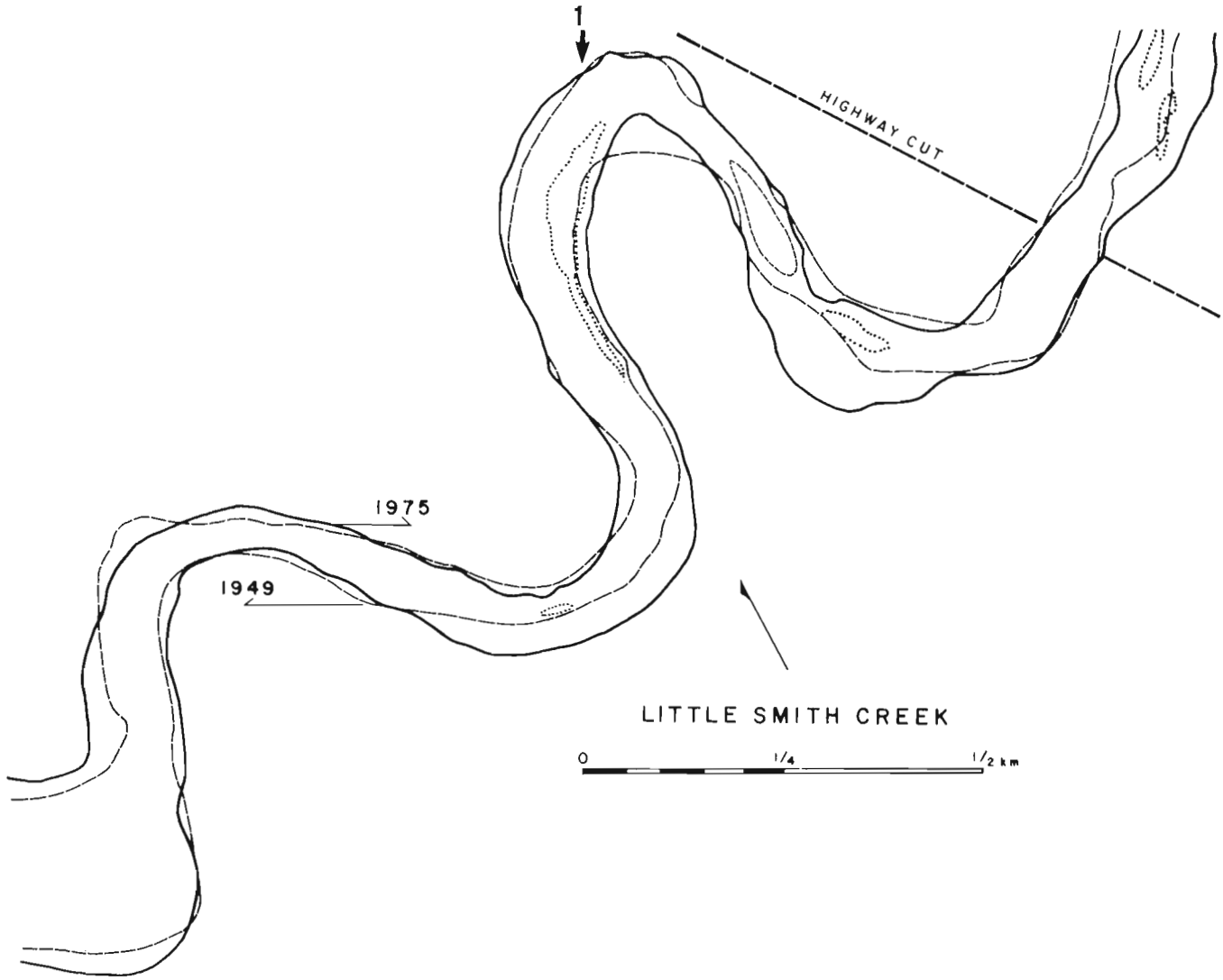

Figure 40.4. Channel migration map for Little Smith Creek, 1949 to 1975. The dotted lines show channel bar positions.

Figure 40. 5. Photograph of bank erosion on the outside of a meander bend, Little Smith Creek; view is towards north. Backwater deposit of sand and silt is in foreground. This site is located at 1 in Figure 40. 4. (GSC-203091-F)

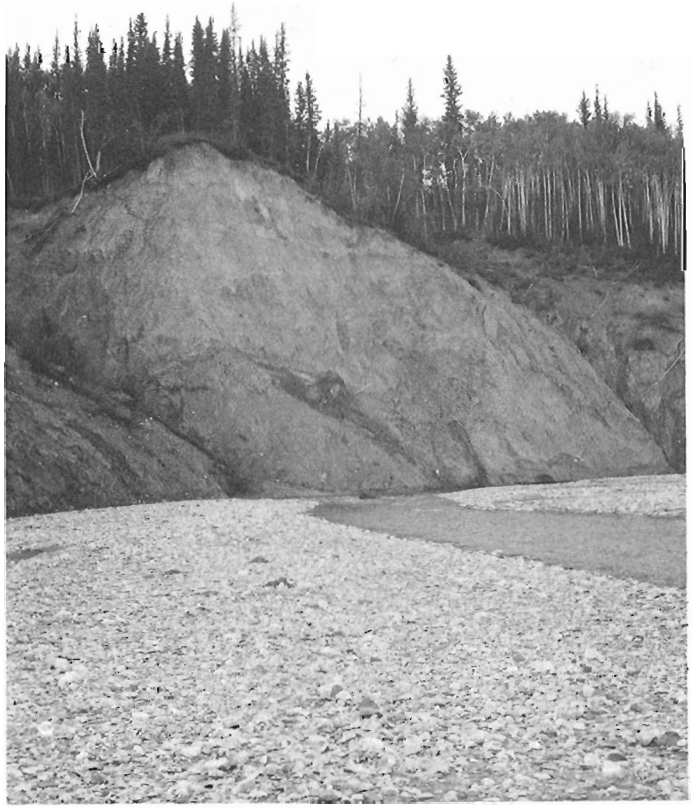

Figure 40. 6.

Photograph of bank erosion on the north bank of Saline River; view is towards north. This site is located at 1 in Figure 40. 3. (GSC-203091-G)

Presumably for streams possessing more irregular plan form geometries, relationships between the controlling parameters and erosion are much more complex. The irregular erosion pattern of Steep Creek is similar to those of streams studied by Brice (1971) which exhibited similar irregular channel patterns with beds composed of many islands and bars. Sites of bank erosion may be a result of avulsion within the active flood plain. Where channel shifting occurs in an apparent chaotic manner, such as on Steep Creek, prediction of erosion zones will be difficult, if at all possible.

It has not yet proved possible to determine erosion rates for the three Mackenzie River tributaries. Dendrochronologic studies, as used by Hickin and Nanson (1975), are complicated by ice destruction of vegetation. Also, long-term hydrologic records are lacking. Hickin and Nanson (1975) stated that Beatton River in northeastern British Columbia, appears to migrate gradually over a number of years, with the migration rate being some function of r_m/w_m. For irregular channels, however, the relationship between migration rate and time (hydrologic regime) cannot be expected to be as coherent as that for meandering channels. It is possible that the channel migration for Steep Creek shown in Figure 40. 2 occurred during a single catastrophic event.

A complicating factor common to the three streams is the backwater effect of Mackenzie River. According to MacKay and Mackay (1973) ice jamming can increase Mackenzie River stage as much as 10 to 15 m above summer stage in this area. The resulting backwater effects extend upstream to the proposed highway crossings in each tributary. The most marked effect of this backwater is the massive sedimentation which can occur in the tributary mouth (Fig. 40.12). On the basis of bedding structures these deposits appear to be constructed of sand and silt transported by the tributaries. Field observations further indicate that the deposits are restricted to the first several hundred metres upstream of the tributary mouths. The presence of these deposits, as well as the backwater, modifies both the hydraulics and the morphology of the tributary. Most of these modifications or adjustments appear to be confined to the active flood plain where the tributaries sequentially fill then scour their lower reaches as the backwater advances and recedes.

Figure 40.7. Photograph of eroding north bank of Steep Creek near the highway crossing. (GSC-203091)

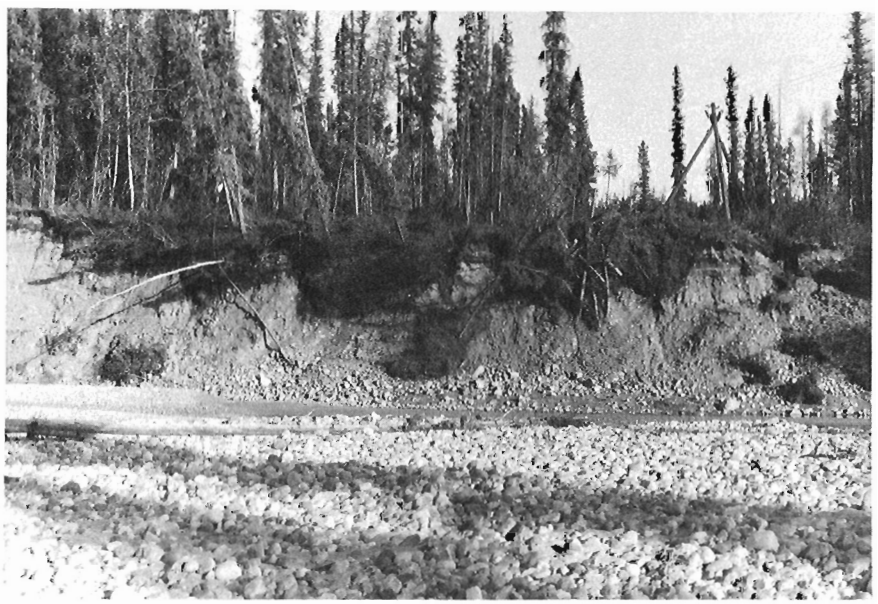

Figure 40.8. Photograph of eroding north bank of Steep Creek near its mouth. (GSC-203091-A)

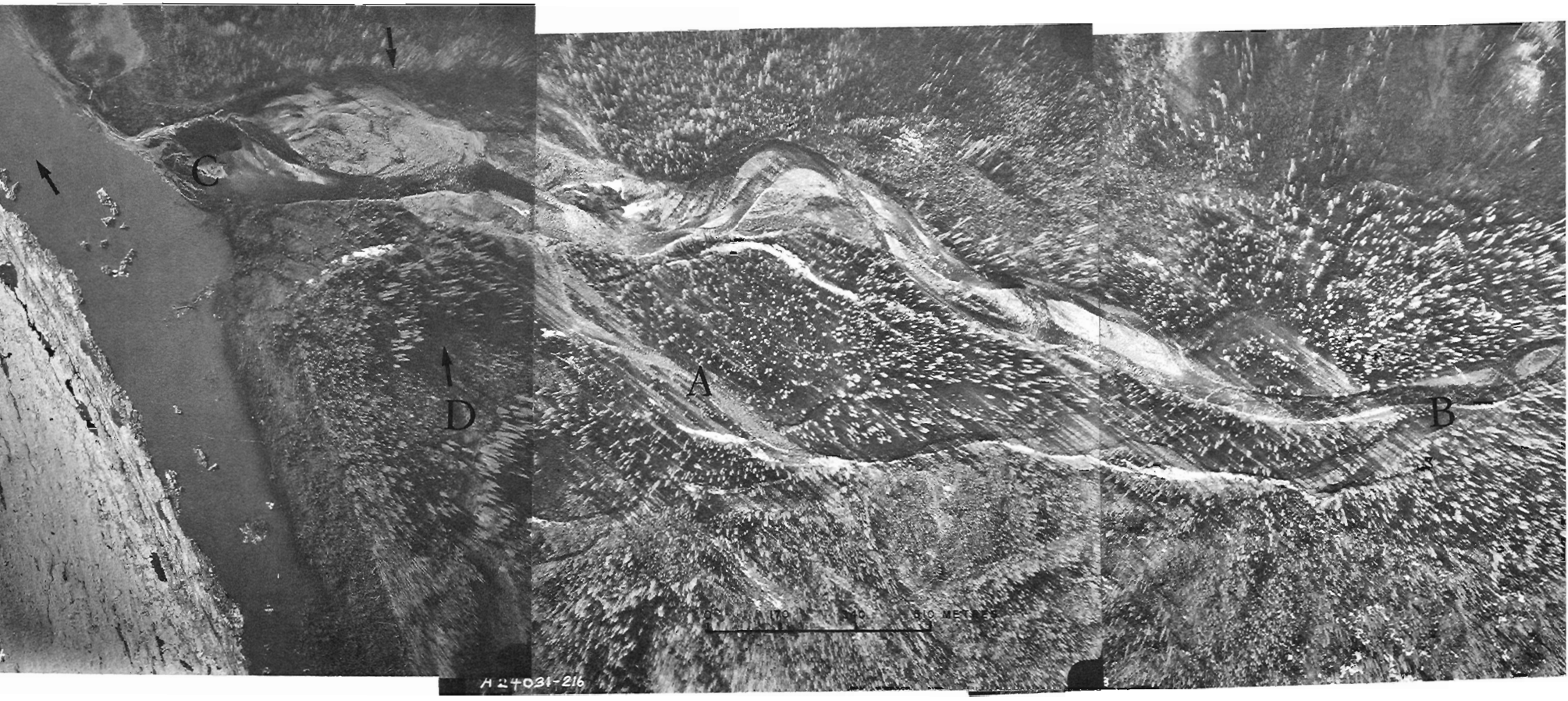

A. the abandoned southern channel (cf. Fig. 40.10);

B. the old junction site of the southern and northern channels (cf. Fig. 40.11);

C. minor backwater from Mackenzie River;

D. is the highway cut.

Figure 40.9. Aerial photographs (A24031-214, 216, 218) of Steep Creek (May 2, 1975).

Figure 40. 10. Downslope view (July 1976) of Steep Creek showing abandoned southern channel. (GSC-203079)

Figure 40. 11. Junction of abandoned southern (1) and northern (2) channels, Steep Creek (July 1976). (GSC-203025)

Figure 40. 12. Massive sand deposits formed in the mouth of Saline River during backwater conditions (July 1976). Note that the surface of the sand deposit has a lower slope than the present stream bed. (GSC-203079-A)

Acknowledgments

The authors are grateful to S. Miller and Mrs. G. Mizerovsky for their assistance in preparing the channel migration maps.

References

Brice, J.
1971: Measurement of lateral erosion at proposed river crossing sites of the Alaska Pipeline; U. S. Geol. Surv., Open File Rep., Water Res. Div., Alaska, 39 p.

Church, M.
1974: Hydrology and permafrost with reference to northern North America; *in* Permafrost Hydrology, Proc. Workshop Sem., Environ. Can., p. 7-20.

Egginton, P. A.
1975: Hydraulic, morphologic, and morphometric studies of selected rivers along the route of the Mackenzie Highway; *in* Report of Activities, Part A; Geol. Surv. Can., Paper 75-1A, p. 229-231.

Hickin, E. J. and Nanson, G. C.
1975: The character of channel migration on the Beatton River, northeast British Columbia, Canada, Geol. Soc. Am., Bull., v. 86, p. 487-494.

Kellerhals, R., Church, M., and Bray, D. I.
1976: Classification and analysis of river processes; Am. Soc. Civ. Eng., Proc., J. Hydraul. Div., HY 7, p. 813-829.

MacKay, D. K. and Mackay, J. R.
1973: Break-up and ice jamming of the Mackenzie River, Northwest Territories; *in* Hydrologic aspects of northern pipeline development; Rep. 73-3, Environ. Can., p. 227-232.

Convention de recherche 1135/D13-4-121/75

S. Occhietti[1]
Division de la science des terrains

L'exploration du territoire des cartes de Shawinigan (31 I/10), Mattawin (31 I/15), Montauban (31 I/16) et des relevés complémentaires sur la carte de Trois-Rivières (31 I/17), ont permis d'observer les dépôts suivants dans l'ordre chronologique de leur mise en place:

1) Le till de Bécancour (Gadd, 1960) est présent, sous les dépôts de St-Pierre, sur une coupe de la rive gauche du St-Maurice, en amont des Vieilles-Forges.

2) Aux Vieilles-Forges, les varves de Deschaillons sont surmontées par plusieurs mètres de sables massifs ou de sables silteux stratifiés qui indiquent un changement dans le type de sédimentation et le rapprochement du front glaciaire.

3) Le till de Gentilly montre trois subdivisions dans le secteur des Vieilles-Forges, sur les coupes naturelles du St-Maurice: a) la subdivision inférieure est très sableuse à sa base (till local) puis devient compacte et riche en pierres et blocs dans sa partie supérieure; b) la 2e subdivision est caractérisée par un ou deux niveaux de sable ou de gravier et galets séparés par un niveau de diamicton; c) la subdivision supérieure a une matrice compacte à sa base et ressemble à un till d'ablation au sommet.

4) Un petit bourrelet frontal à structure en écaille de chevauchement à St-Louis-de-France, à 5 km au sud du système morainique de St-Narcisse, indique un retrait progressif du front de l'inlandsis, dans cette partie de la vallé du St-Laurent, avant la phase de St-Narcisse.

5) Dans le Bas-St-Maurice, le système morainique de St-Narcisse (Osborne, 1951) est une forme construite

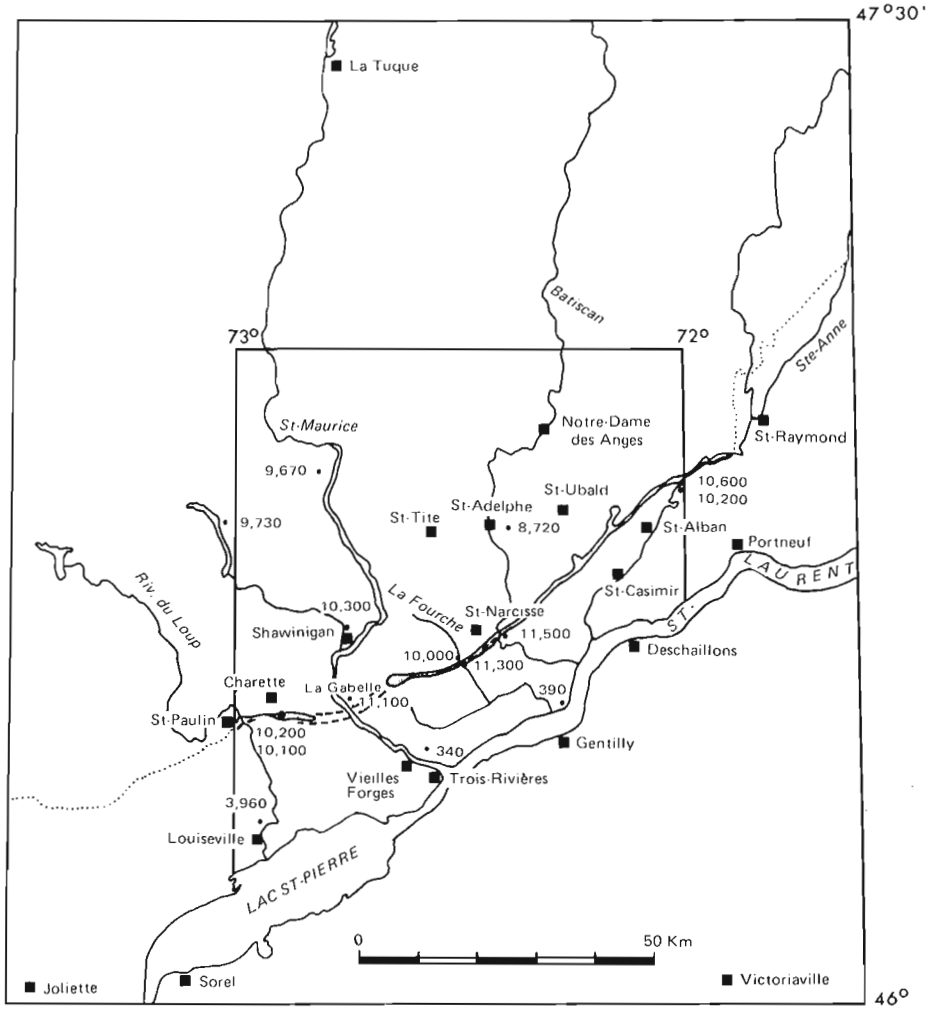

· Datations au ^{14}C

Dépôts glacio-marins

Figure 41. 1.

Carte de localisation de la Mauricie et du système morainique de St-Narcisse.

[1]Section géographie
Université du Québec à Trois-Rivières
Trois-Rivières, Québec

Tableau 41.1

Liste des radiodatations au ^{14}C du Wisconsinien récent de la Mauricie

Lab., n°	Age, erreur	Localité	Altitude	Matériel daté	Auteurs
GSC-1526	11 500 ± 630	Coupe sur la Batiscan		Foraminifères, dépôts glacio-marins	Gadd, N.R.
GSC-1729	11 300 ± 160	Rivière la Fourche, St-Narcisse	81 m	*Portlandia arctica*, dépôts glacio-marins	Occhietti, S.
GSC-2045	11 100 ± 90	Barrage de La Gabelle sur le St-Maurice	11 m	*Portlandia arctica*, dépôts glacio-marins	Occhietti, S.
GSC-2090	10 600 ± 160	St-Alban, 2 km au sud de la moraine de St-Narcisse	71 m	*Balanus hameri*, silts marins pierreux	Occhietti, S.
GSC-2101	10 300 ± 100	Shawinigan	129 m	*Mya arenaria*, dépôts littoraux	Occhietti, S.
GSC-2150	10 200 ± 90	St-Alban, (même site que GSC-2090)	78 m	*Macoma calcarea*, sommet des silts marins pierreux	Occhietti, S.
GSC-1700	10 200 ± 160	Charette	128 m	*Macoma balthica*, moraine de St-Narcisse remaniée	Occhietti, S.
GSC_1444	10 100 ± 150	Charette		*Hiatella arctica* et *Macoma balthica*	Gadd, N.R.
GSC-1739	10 000 ± 150	Rivière la Fourche	98 m	*Hiatella arctica*, silts marins	Occhietti, S.
GRO-1922	8480 ± 80	St-Adelphe	126 m	Base de la Tourbière	Terasmae, J.
I-8496	9730 ± 140	Lac Wapizagonke, parc de la Mauricie	230 m	Gyttja, profondeur: 570 - 560 cm	Richard, P.
I-8495	6080 ± 135	*idem*		Gyttja, profondeur: 400 - 390 cm	Richard, P.
I-8497	9760 ± 190	Sud du lac du Noyer, parc de la Mauricie	270 m	Gyttja sableuse, profondeur: 455 - 448 cm	Richard, P.
I-8842	9205 ± 385	*idem*		Gyttja sableuse, profondeur: 445 - 440 cm	Richard, P.
I-8825	8230 ± 270	*idem*		Gyttja, profondeur: 430 - 425 cm	Richard, P.
I-8824	5745 ± 235	*idem*		Gyttja, profondeur: 325 - 320 cm	Richard, P.
I-8823	5145 ± 155	*idem*		Gyttja, profondeur: 230 - 225 cm	Richard, P.
GSC-1022	3960 ± 130	Rivière Chacoura, Louiseville		Bois enfoui par un glissement de terrain	Karrow, P.F.
GSC-142	390 ± 140	Batiscan		Charbon de bois	Lévesque, R.
GSC-1855	340 ± 80	St-Louis-de-Champlain	53 m	Rostre d'un poisson: *Xiphias gladius*	Ribes, R.

complexe composée de deux parties; une racine de dépôts glacio-marins et des bourrelets de till et de dépôts proglaciaires (Occhietti, 1973). La racine discontinue de dépôts glacio-marins fossilifères, longue au moins de 70 km, de St-Paulin jusqu'au nord de St-Casimir, a été construite à l'emplacement du contrefort laurentidien enfoui sous les dépôts quaternaires. Les dépôts glacio-marins sont relativement épais (de 5 à 20 m) et larges (4 km à La Gabelle). Leur âge est compris entre 11 500 et 11 000 ans ^{14}C; plus précisément entre 11 300 et 11 100 B.P. (GSC-1526, 1729, 2045, *cf.* tableau 1). Ils sont interprétés comme le résultat d'une stabilisation locale du front de l'inlandsis au contact de la mer Champlain, stabilisation liée à la dynamique de la glace et à la topographie du substratum rocheux.

Le système morainique de St-Narcisse comprend, d'autre part, entre St-Paulin et St-Raymond-de-Portneuf, un alignement de bourrelets parfois dédoublés (St-Thuribe) et construits avec du till à structure de chevauchement en écailles, du till délavé et remanié, des dépôts juxtaglaciaires et proglaciaires, des deltas proglaciaires perchés (Charette, Mt-Carmel) et un sandur à kettles (St-Raymond). Ces bourrelets ont été construits au contact de la mer Champlain sur 120 km de long. Selon des auteurs, ces bourrelets se prolongeraient vers l'ouest sur 160 km (Elson, 1962, etc.) et vers l'est sur 200 km (LaSalle *et al.*, 1972, etc.); jusqu'à maintenant, l'isochronie de cet alignement sur 500 km n'est pas démontrée. En Mauricie, des coupes transversales montrent que les dépôts glacio-marins s'étendent surtout du côté distal du relief de St-Narcisse. Des structures plissées indiquent des fluctuations de la marge glaciaire. Le till à structure en écailles représente une ancienne moraine de cisaillement et témoigne de la présence d'une glace active qui s'écoulait vers le sud-est, comme le montrent la trame du till et les stries glaciaires. Ces éléments caractérisent le système de St-Narcisse qui correspond à une réactivation de la glace. La seule preuve, non stratigraphique, de réavancée, est décrite par Rondot (1974) dans la région de Baie-St-Paul où un petit lobe orienté nord-sud recouvre une région à stries glaciaires orientées vers l'est. L'âge du système morainique de St-Narcisse se situe à l'intérieur de l'écart 11 500 - 10 300 B.P., si l'on accepte de considérer la réactivation de la glace comme, 1) tardive par rapport à l'accumulation des dépôts glacio-marins, 2) nettement plus ancienne que 10 300 B.P. (GSC-2101), âge du niveau à *Mya Arenaria* reposant sur 6 m de silts marins fossilifères, à 12 km au nord du système de St-Narcisse. Une colonie de *Balanus hameri*, datée de 10 600 ± 160 B.P. (GSC-2090), située à 2 km au sud du bourrelet de St-Narcisse et incluse, après un léger transport, dans des silts pierreux à strates massives, semble être contemporaine soit du front glaciaire de St-Narcisse soit de sa phase ultime de déglaciation. La phase de St-Narcisse proprement dite se situe par conséquent entre 11 100 et 10 600 ans ^{14}C, vraisemblablement entre 11 000 et 10 700 B.P. En l'absence de données suffisantes sur l'écart entre les âges au ^{14}C des végétaux terrestres et des coquilles de mers froides, les corrélations avec la région des Grands Lacs sont délicates. Si l'on accepte les âges non corrigés et sa position actuellement publiée, on peut corréler provisoirement le système de St-Narcisse avec le début du stade Algonkin de Saarnisto (1974), nettement postérieur à l'épisode Valders.

6) Le retrait glaciaire post-St-Narcisse est marqué par une vingtaine de petits bourrelets (Cossetteville) et par des accumulations proglaciaires perchées disposées en travers du rentrant de St-Tite – Notre-Dame-des-Anges ou du débouché des vallées laurentidiennes.

7) En Mauricie, la transgression de la mer Champlain a commencé au sud du système de St-Narcisse avant 11 300 B.P. Elle est caractérisée par des dépôts marins rythmés à la base ou des silts pierreux fossilifères (*Portlandia arctica*) à strates massives à proximité des dépôts glacio-marins, puis par des silts massifs ou stratifiés selon la localité, fossilifères (*Portlandica arctica* à la base, *Macoma balthica* vers le sommet). Localement, un pavage non continu marque une lacune d'érosion surmontée par les sables et graviers du proto – St-Laurent ou par des sables deltaïques. Au nord du système de St-Narcisse, la transgression a commencé avant 10 300 B.P. (GSC-2101), probablement vers 10 600 B.P. Les argiles et silts marins sont massifs ou stratifiés et reposent, selon le cas, sur le roc, sur des formes fluvio-glaciaires ou sur des dépôts fluvio-glacio-marins. En dehors des zones littorales, on trouve *Portlandia arctica* vers la base et *Macoma balthica* vers le sommet. Les fossiles dans les dépôts littoraux traduisent plus clairement les fluctuations thermiques secondaires des eaux marines; en simplifiant, on assiste à un réchauffement des eaux culminant avec *Mya arenaria*, il y a 10 300 B.P. (GSC-2101) suivi d'un léger refroidissement. Des deltas perchés à 195 m d'altitude au-dessus du niveau marin actuel et des dépressions non comblées au fond de rentrants au-dessous de l'altitude 210 m, indiquent un relèvement isostatique régional de l'ordre de 200 m.

8) L'exondation est marquée, selon la localité, soit par des dépôts d'épandage sablo-graveleux, soit par des sables silteux prodeltaïques, soit par des deltas sableux.

9) Des formes éoliennes, des tourbières, des terrasses fluviatiles, des epandages deltaïques caracterisent l'Holocène de la région qui a continué de se relever par compensation isostatique. P. Richard (1975) date le début de la colonisation végétale du parc de la Mauricie vers 10 000 B.P.

Bibliographie

Elson, J.A.
1962: Pleistocene Geology of the St. Lawrence Lowlands; guidebook field trip no. 2, New England intercollegiate geological Conference, Univ. McGill, Montreal.

Evenson, E.B., Dreimanis, A.
1975: Late glacial (14 000 - 10 000 years B.P.) History of the Great Lakes Region and Possible Correlations; Paper presented at the Bellingham, Washington, meeting of the IGCP Project: Quaternary glaciations in the Northern Hemisphere – a preprint.

Gadd, N.R.
1960: Géologie de la région de Bécancour, Québec; (dépôts meubles) 31 I/8; Comm. géol. Can., Etude 59-8.

1971: Pleistocene geology of the Central St. Lawrence Lowland, with selected passages from an unpublished manuscript: The St Lawrence Lowland, by J.W. Goldthwait; Geol. Surv. Can., Mem. 359.

Hillaire-Marcel, C.
1972: Exemples de biocénoses dans la faune champlainienne de la région d'Oka; Annales ACFAS, vol. 29, p. 76.

Karrow, P.F.
1957: Pleistocene geology of the Grondines Map-Area, Quebec; Unpub. Ph.D. thesis, Univ. of Illinois.

LaSalle, P., Elson, J.A.
1975: Emplacement of the St. Narcisse Moraine as a Climatic Event in Eastern Canada; Quaternary Research, vol. 5, p. 621-625.

LaSalle, P., Hardy, L. et Poulin, P.
1972: Une position du front glaciaire au Nord et au Nord-Est de la ville de Québec; Min. Richesses Nat. Québec, Rap. S-135.

Occhietti, S.
1973: Eléments caractéristiques du système morainique de St Narcisse, en Mauricie et la région de Charlevoix; 2e colloque sur le Quaternaire du Québec, Montréal; Résumés des communications.

1974: Dépôts et faits quaternaires du Bas St Maurice, Québec; Comm. géol. Can.; Etude 74-1, partie B, p. 217.

Osborne, F.F.
1951: Parc des Laurentides Ice Cap and the Quebec Sea; Le Naturaliste canadien, v. 68, p. 221-251.

Parry, J.T., McPherson, J.C.
1964: The St. Faustin-St. Narcisse Moraine and the Champlain Sea; Rev. Géog. de Montréal, vol. 18, p. 235-248.

Richard, P.
1975: La vulgarisation des travaux de paléobiogéographie effectués dans le Parc national de la Mauricie; Service à la Recherche en analyse pollinique. Univ. du Québec à Chicoutimi.

Richard, S.H.
1975: Surficial geology Mapping: Ottawa Valley Lowlands (Parts of 31 G, B, F.); Geol. Surv. Can., Paper 71-Part B, p. 113-117.

Rondot, J.
1974: L'épisode glaciaire de St Narcisse dans Charlevoix, Québec; Rev. Géog. de Montréal, vol. 28, no. 4, p. 375-388, cart h.t.

Saarnisto, M.
1974: The deglaciation history of the Lake Superior Region and its climatic implications; Quaternary Research, v. 4, p. 316-339.

Terasmae, J.
1960: Contribution to Canadian palynology, No. 2; pt. 1, a palynological study of post-glacial deposits in the St Lawrence Lowlands; Geol. Surv. Can., Bull. 56.

INTERPRETATION OF TRIDEM AIRBORNE E.M. DATA

Project 730004

A.K. Sinha
Resource Geophysics and Geochemistry Division

Introduction

Airborne electromagnetic surveying, although still being used mostly in mineral exploration, in recent years has found increasing use in geological mapping (Collett, 1965; Dyck *et al.*, 1974). Various excitation sources have been used for this purpose, for example, in the airborne AFMAG, VLF and E-Phase surveys, the sources are plane waves generated naturally or artificially (last two cases). Finite sources have also been used as in the INPUT mapping surveys, where transient pulses are used (Dyck *et al.*, 1974). Collett (1969) has provided a good summary of these developments.

Oscillating magnetic dipoles may also be used for airborne mapping purposes. A theoretical study on the performance of different coil configurations for airborne mapping was published by Sinha (1973). Until recently, however, all airborne e.m. survey systems using harmonic current sources had either one frequency or measured the quadrature components at two frequencies. It is known, however, that for resolving layer parameters several frequencies are required, and preferably both in-phase and quadrature components. This was accomplished when Scintrex Ltd. introduced the Tridem System about three years ago. In the system, both in-phase and quadrature components of the induced secondary fields are measured simultaneously at three widely separated frequencies, namely, at 500, 2000 and 8000 Hz. Tridem is a wing-tipped system where there are two vertical coplanar coils fixed rigidly to the wings at a constant separation of 58.33 feet. The data at six channels as well as the altimeter trace are recorded digitally aboard the aircraft. Bosschart and Seigel (1974) has adequately described the system.

The Tridem System was flown under contract to Geological Survey of Canada in the Hawkesbury and Timmins areas of Ontario in 1974 in order to test its capability for resolving the underlying layer parameters in terms of conductivity and thickness values. The surveys were flown at a nominal flying height of 175 feet and the line separations were 0.25 miles in both areas. The Geological Survey received the survey data in the summer of 1975. This paper will summarize the work that has been done so far in interpreting the data from the Timmins area.

Data Characteristics

The survey area in Timmins is located approximately at latitude 48°30' and longitude 81°40' (*see* Fig. 42.1). There are several small copper, zinc, lead and silver mines in the area. Figure 42.2 shows the raw Tridem data over one line (line 103). The fiducial values have been plotted along the abscissa, 20 fiducials being approximately equal to 1 km. The six in-phase and quadrature-phase channels are designated by P5, P2, P8 and Q5, Q2 and Q8 to indicate that they have been measured at 500, 2000 and 8000 Hz respectively. The altimeter trace is indicated by ALT. Along the ordinate, two divisions indicate 500 parts per million of anomaly or 200 feet. From an initial examination of the data, it is clear that the data is noisy, the altitude varied between 120 and 230 feet and that the zeros in the anomaly scales indicated by horizontal dashes are wrong. It is known that for any homogeneous or layered model structures the anomalies are always positive for this coil configuration. Since there are many negative anomalies on almost all lines, corrections will have to be applied for the shifting of zero level before any interpretation is done.

Reduction of Data

There are mainly three steps in the reduction of the data. Firstly, the original data is filtered to reduce the noise in the altimeter trace and in the high frequency components. The noise reduction filter is based on a time-domain 65 coefficient low-pass filter which cuts off all signal whose frequency exceeds 0.1 cycles/data interval. The filter program was kindly provided by A. Becker of the Mineral Exploration Research Institute, Montreal. The program considers an 'infinite length' low-pass filter and the Parzen window factor to derive the filtered values. Figure 42.3 shows the filtered data for all channels after applying the filter. The data look much smoother and the high frequency

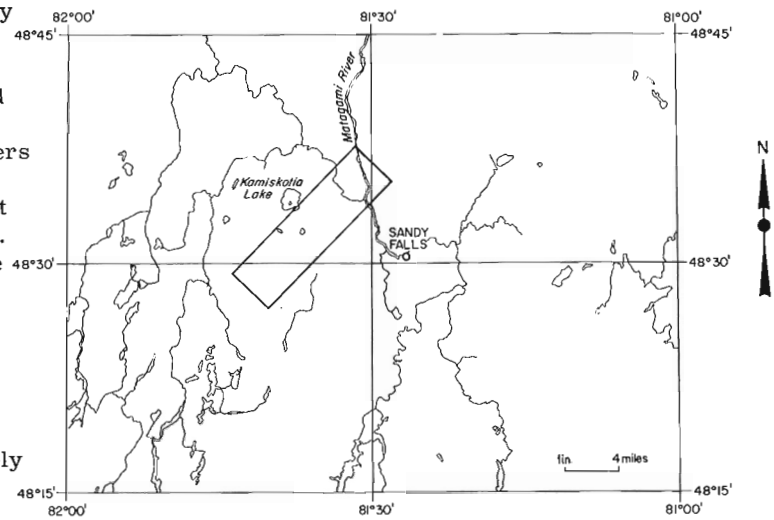

Figure 42.1. Location map for Tridem survey in the Timmins area.

From: Report of Activities, Part C;
Geol. Surv. Can., Paper 76-1C (1976).

variations have been elimated. It should be noted that in the process of filtering, the first and last 32 points are lost from the original data.

The filtered values exhibit several anomalies which are negative. Hence appropriate zero corrections are applied to the data to remove that error. Since the altimeter trace shows a large variation, an altitude correction will have to be applied to reduce the filtered and zero corrected data to the uniform altitude of 175 feet, the nominal flying height.

Theoretically, it is not possible to correct for the variation of the altitude since the correction program will need information about the layer characteristics below the surface, something the survey is supposed to find out. However, if rough models of the ground below are assumed, some sort of altitude correction is possible. The correction program, originally supplied by A. Becker, was subsequently modified to suit our purpose.

Interpretation of Data

In any interpretation of geophysical data, one has to assume some model. For mapping purposes, the models are generally taken to be layered earth sections. The final corrected data were examined to see what type of layered earth model would be most appropriate for the area. For that purpose, the field data were compared with theoretically generated data for several types of layered models. It was apparent that a two-layer model with highly resistive substratum will fit the data best. It also became apparent that at Timmins, the data at the lowest frequency (500 Hz) can hardly be used for interpretation since the magnitude of the anomalies at 500 Hz were, in many areas, below the noise level at that frequency. Thus, only 2 and 8 Khz data were used for subsequent interpretations. Figure 42.4 is a plot of the theoretical interpretation

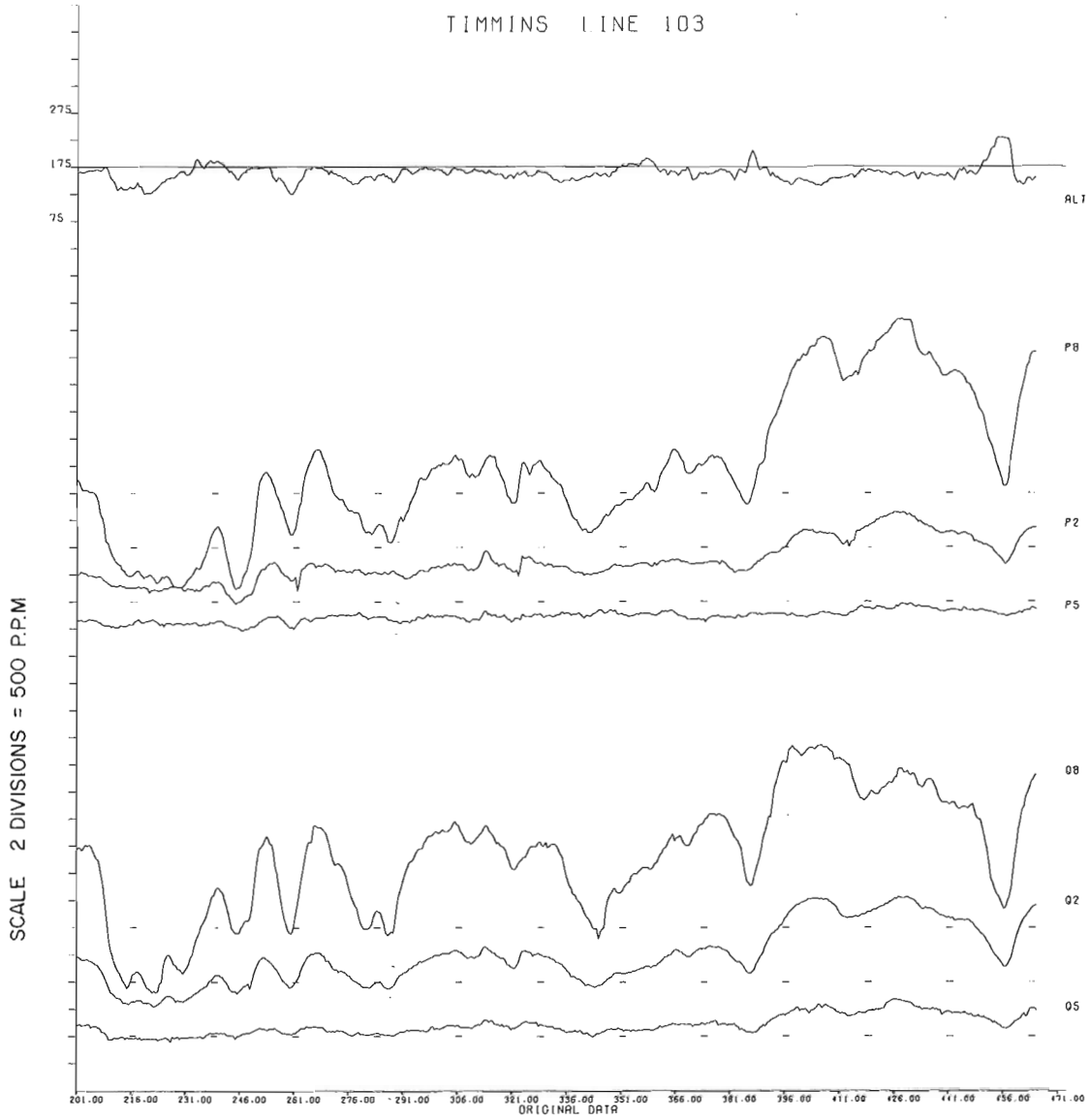

Figure 42.2. Plot of the raw Tridem data and altimeter trace over line 103 in Timmins area.

diagram. It is a plot of the amplitude of the response versus the phase in radians for a two-layer model with perfectly resistive substratum for several values of B and D/B given by

$$B = RH/\delta_1 = RH\left(\frac{\omega\mu\sigma_1}{2}\right)^{\frac{1}{2}} \quad \ldots\ldots\ldots (1)$$

$$D/B = 2d/RH,\ \delta_1 = \left(\frac{2}{\omega\mu\sigma_1}\right)^{\frac{1}{2}} \quad \ldots\ldots\ldots (2)$$

where

RH = Coil separation in metres

d = Thickness of the top layer in metres

ω = 2π x frequency (Hz)

μ = Magnetic permeability = $4\pi \times 10^{-7}$ H/m

σ_1 = Conductivity of the top layer in S/m

Using the corrected data and the interpretation diagram, values of B and D/B are obtained independently at 2 and 8 Khz. From equations 1 and 2, the conductivity σ_1 and the thickness d of the top layer may easily be determined. If there are no errors in the data and the chosen model is the correct one, the two sets of σ_1 and d should be identical. In practice, however, the two sets of values yield slightly different results; in that case their average values are taken. This process has been automated on the computer to yield d and σ_1 values for all points on a line.

However, if the subsurface geology is complex, as it is known to be in the Timmins area, the layered model assumption may not be valid at all positions. In such cases, it is either impossible to obtain the parameter values at the two frequencies, or the two sets of values at 2 and 8 Khz yield widely different parameters. For example, over a swarm of dykes, it will be impossible

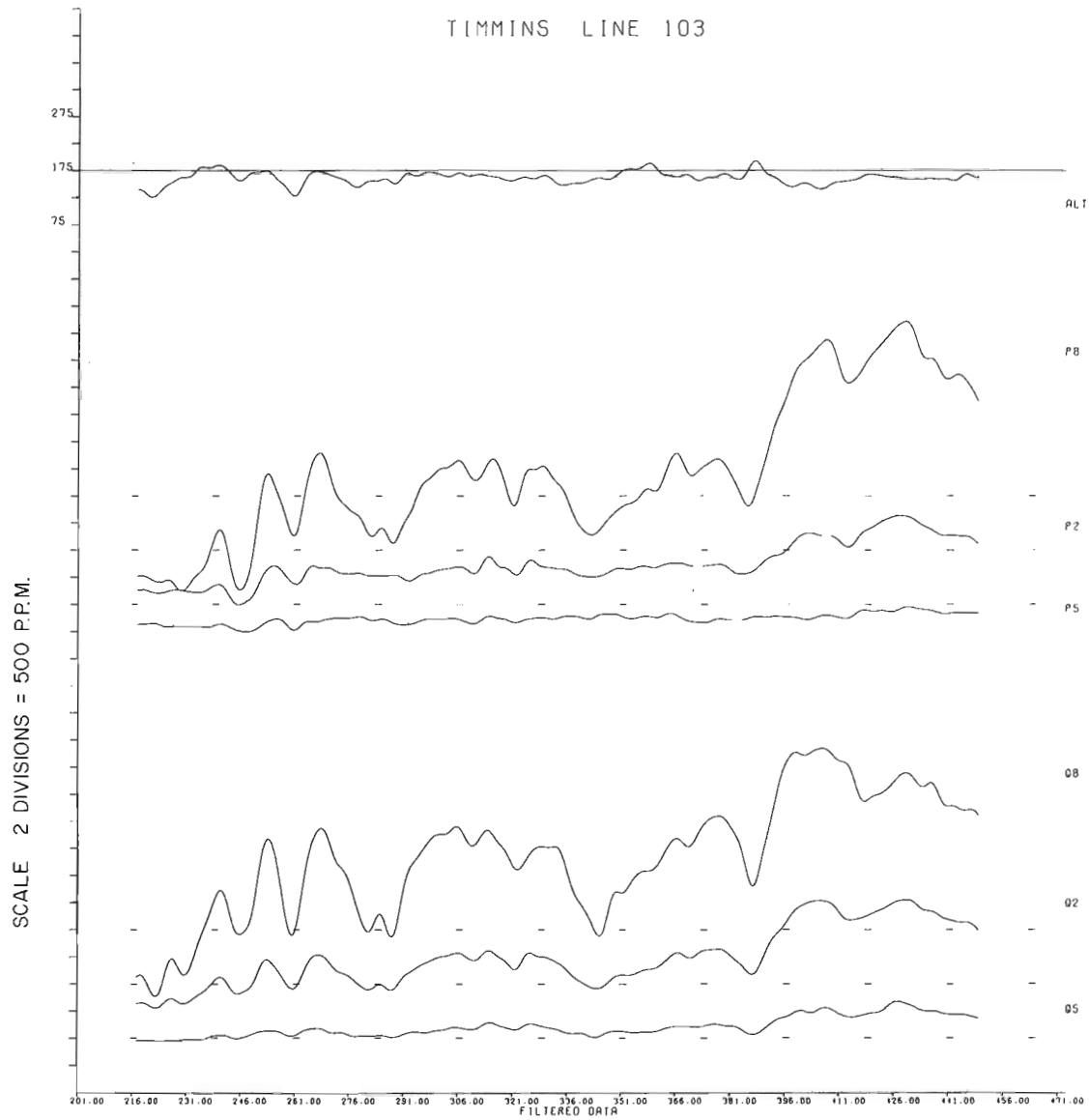

Figure 42.3. Tridem data over line 103 after filtering to reduce high frequency noise.

to obtain any value of σ_1 and d. In such cases, the points are not plotted on the final interpretation diagram. Figure 42.5 shows the interpretation for line 103 in terms of the resistivity ρ_1 ($1/\sigma_1$) in Ω-m of the top layer and its thickness in m. The points which are blank are the ones where our model is unsuitable. There are, in general, two possibilities in such cases. Firstly, the layers may not be horizontal (e.g. vertical intrusions) or the top layer may be less conducting. This is possible near hills where the top layer may be dry and resistive but the bottom layer may be conducting. This condition may be dealt with if at least three frequencies are available. Since in the Timmins area only two useful frequencies are available, it is not possible at present to explore this possibility more thoroughly.

Acknowledgments

The author thanks A. Becker of the Mineral Exploration Research Institute, Montreal, for supplying computer programs for filtering and altitude corrections and for many stimulating discussions about the work.

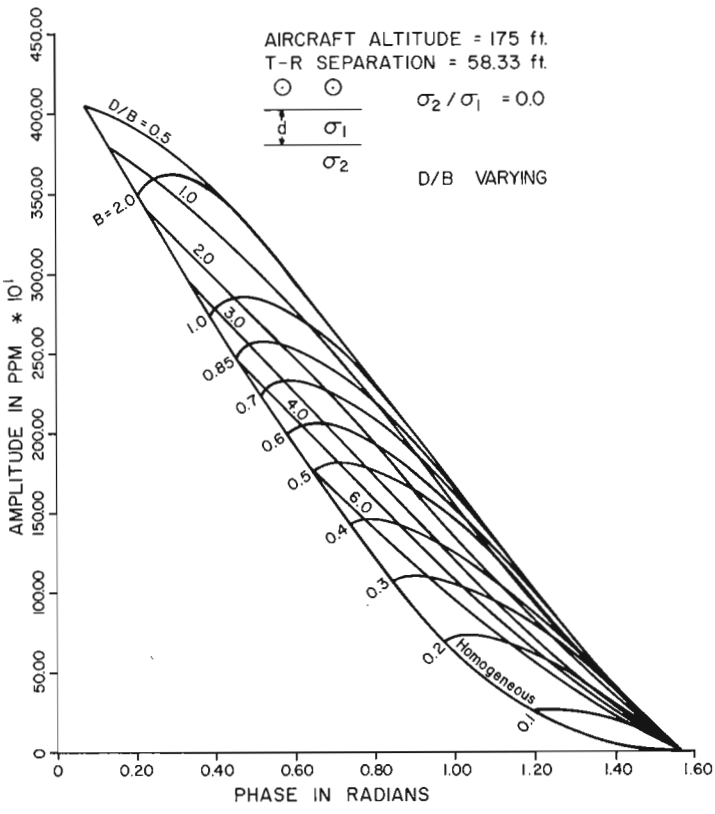

Figure 42.4. Theoretical diagram for the interpretation of Tridem data in the Timmins area.

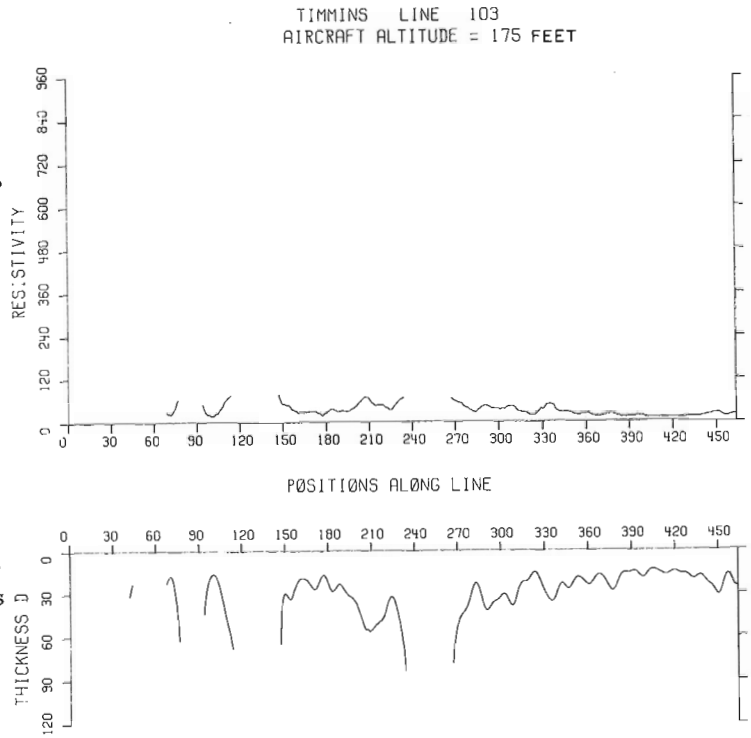

Figure 42.5. Plot of the resistivity in ohm-m and thickness in meters of the top layer for line 103 in the Timmins area.

References

Bosschart, R.A. and Seigel, H.
1974: The Tridem three frequency airborne electromagnetic system; Can. Min. J., v. 95, no. 4, p. 68-69.

Collett, L.S.
1965: The measurement of the resistivity of the surficial deposits by airborne pulsed electromagnetic equipment; 35th Annual SEG Meeting, Dallas, Texas.

1969: Resistivity mapping by electromagnetic Methods; Proc. Can. Centennial Conf. on Mining and Groundwater Geophysics, Ed. L.W.Morley, Niagara Falls, Canada, p. 615-625.

Dyck, A.V., Becker, A., and Collett, L.S.
1974: Surficial conductivity mapping with airborne INPUT system; Can. Min. Metall., Bull., v. 67, no. 744, p. 104-109.

Sinha, A.K.
1973: Comparison of airborne e.m. coil systems placed over a multilayer conducting earth; Geophysics, v. 38, no. 5, p. 894-919.

Beaufort Sea

Project 730004

A. K. Sinha
Resource Geophysics and Geochemistry Division

Introduction

In the last few years, several techniques have been tried for determining remotely the thickness of sea ice by geophysical means (Evans and Smith, 1969; Adey, 1970; Christoffersen, 1970; McNeill and Hoekstra, 1973; Campbell and Orange, 1974). With the discovery of oil, gas and other resources in the Canadian Arctic in recent years, it is expected that exploration and production activity will continue there in the near future. This has brought the importance of an inexpensive reconnaissance technique of sea-ice thickness determination into sharp focus since heavy equipment must be transported over the sea ice between arctic islands and, therefore, one must know the thickness and strength of the ice.

Radar depth sounding experiments have been carried out over sea ice in the last few years (Campbell and Orange, 1974) with fair success. However, the radar method although accurate is also expensive. Therefore, there is a need for an inexpensive and portable instrument for sea-ice thickness determination which may be operated by one or two men and would provide reasonably accurate results *in situ*. It was then realized that a portable double-dipole electromagnetic system may be tried for this purpose. Because two portable instruments, Geonics EM-15 and Apex Parametrics double-dipole systems were already available in the market, a theoretical study was conducted (Sinha, 1974) to see if these two could indeed be useful for sea-ice thickness determination. It was clear from that analysis that for typical sea-water and sea-ice resistivities, both instruments would be capable of measuring sea-ice thicknesses up to 6 or 7 m.

Field Studies and Results

It was decided therefore to undertake field testing of these two instruments in the Arctic to see their actual performance. The testing was carried out over the frozen Beaufort Sea off the coast of Tuktoyaktuk, Northwest Territories in the spring of 1975. The area was chosen because of its proximity to the Polar Continental Shelf Project base at Tuktoyaktuk which served as the base camp. The tests were conducted over two areas, one off the coast about 2 miles from the shore, the other area was about 30 miles out over the sea.

The original plan called for the measurement of the real and the imaginary parts of the mutual coupling ratio (Z/Z_0) for the two instruments at each station. Then estimates of the sea-ice thickness were to be obtained at each position from precalculated curves for the mutual coupling ratios versus thicknesses for assumed resistivity values of sea water and sea ice (in fact, the curves vary little from each other if the resistivity contrast is greater than 300, as it should be if the seawater is saline). Then, it was planned to drill holes through the ice at each position to measure the ice thickness directly for comparison with the calculated values.

It was soon realized, however, that absolute measurements of the mutual coupling ratios would be impossible with the instruments since they do not have preset zeros in the scales. It meant that the zero values in the instruments had to be set at each location which meant that only relative measurements are possible with them. This was understandable since the two instruments are designed mainly for mineral exploration, and prospecting people are interested in the relative anomalies only. One consequence of this was that we could not use the theoretical curves which considered the absolute anomalies (e. g. Sinha, 1974).

For relative measurements, a wooden table, 46 inches (1. 168 m) high was built in Tuktoyaktuk so that two

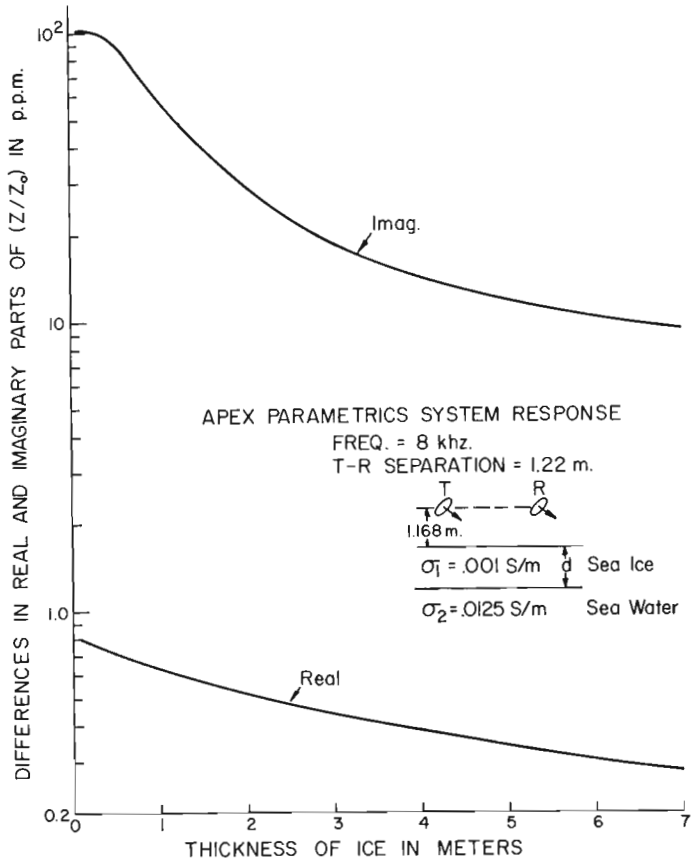

Figure 43. 1. Variation of the differences in real and imaginary parts of Z/Z_0 against the thickness of sea ice for the APEX instrument for fresh sea water.

From: Report of Activities, Part C;
Geol. Surv. Can., Paper 76-1C (1976)

TABLE 43.1

Results from 4 stations in an area 2 miles off the coast

Stn.	Diff. in Real Z/Z_o (ppm)	Diff. in Imaginary Z/Z_o (ppm)	'd' from Real (metres)	'd' from Imaginary (metres)	Measured 'd' (metres)
		APEX PARAMETRICS			
1	20	30	N.O.	1.95	2.58
2	86	20	N.O.	2.75	2.15
3	45	53	N.O.	1.16	1.89
4	40	38	N.O.	1.58	1.94
		GEONICS EM-15			
1	5	21	N.O.	2.1	2.58
2	13	30	N.O.	1.47	2.15
3	6	40	N.O.	1.15	1.89
4	7	34	N.O.	1.31	1.94

N.B. N.O. means Not Obtainable because the values fall outside the range of the theoretical plots.

observations could be taken for each instrument at each station with the instruments being on the surface and on the table, and considering the difference readings. Care was taken to exclude all metal objects in fabricating the table which could be taken apart and carried easily after each observation. Since the difference readings were often small, care was taken to make sure that there were no metal objects in the neighbourhood of the instrument and that the observer did not come too close to the instrument while taking the reading to reduce the static noise generated by his presence.

Figure 43.1 shows a theoretical plot of the differences in the real and imaginary parts of the coupling ratio Z/Z_o in parts per million (p.p.m.) for the Apex Parametrics instrument, where the coil axes are inclined at an angle of 54.7 degrees from the horizontal to achieve the minimum coupled configuration. The coil separation and the frequency of the instrument are 1.22 m and 8 Khz respectively. The conductivity values σ_1 and σ_2 for the ice and water in the diagram are obtained from observations made in the first area just off the coast. In both areas, samples of seawater were taken from each hole and the conductivity of the water samples were measured later in the laboratory. The ice resistivity values were taken from published values in the literature. In the first area, the average resistivity of the seawater was found to be 80 Ω.m which meant that the water was fresh. For sea ice, a resistivity value of 1000 Ω.m was chosen and these values were used in obtaining Figure 43.1.

Because the conductivity contrast is small ($\sigma_2/\sigma_1 = 12.5$) in this area, the real Z/Z_o values and their differences are small and hence only imaginary Z/Z_o values and their differences show recordable

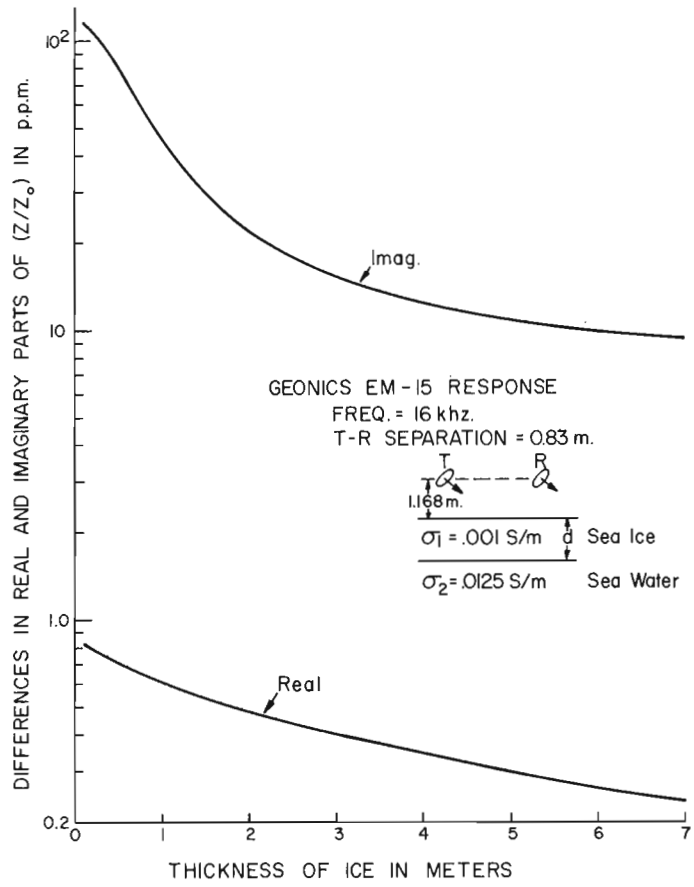

Figure 43.2. Variation of the differences in real and imaginary parts of Z/Z_o against the thickness of sea ice for the Geonics EM-15 instrument for fresh sea water.

TABLE 43.2

Results from 4 stations in an area about 30 miles off the coast

Stn.	Diff. in Real Z/Z_o (ppm)	Diff. in Imaginary Z/Z_o (ppm)	'd' from Real (metres)	'd' from Imaginary (metres)	Measured 'd' (metres)
		APEX PARAMETRICS			
A	2000	7100	0.26	0.72	0.25
B	1235	4070	0.80	1.15	0.72
C	1930	7050	0.30	0.73	0.27
D	1800	6900	0.40	0.75	0.24
		GEONICS EM-15			
A	1795	8000	0.28	0.36	0.25
B	1140	3700	0.75	0.90	0.72
C	1710	7900	0.32	0.37	0.27
D	1711	7640	0.32	0.40	0.24

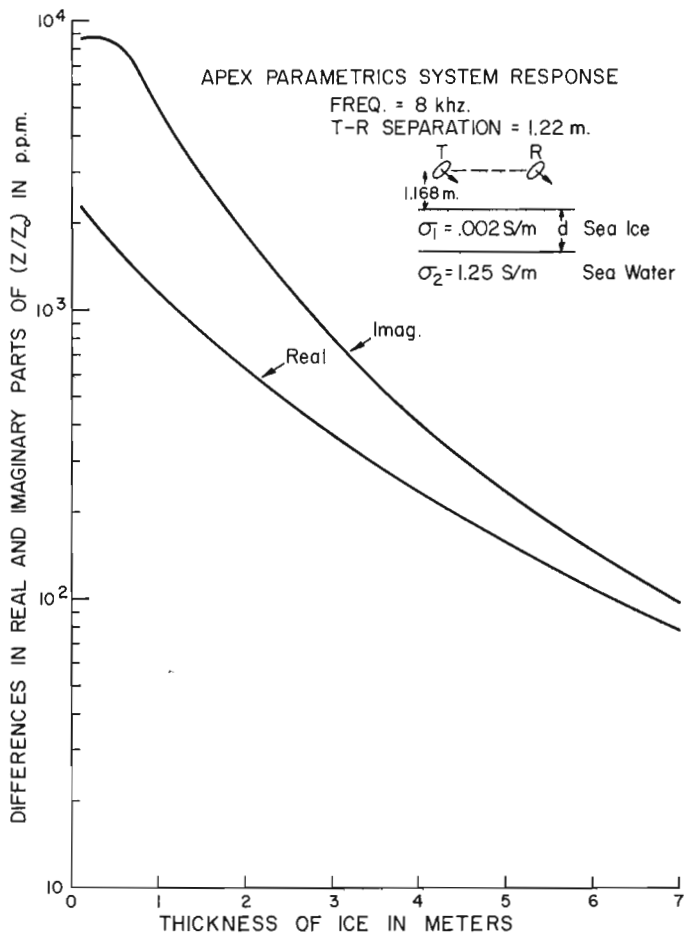

Figure 43.3. Plot of the real and the imaginary parts of $\Delta Z/Z_o$ versus sea-ice thickness for the APEX instrument for saline sea water.

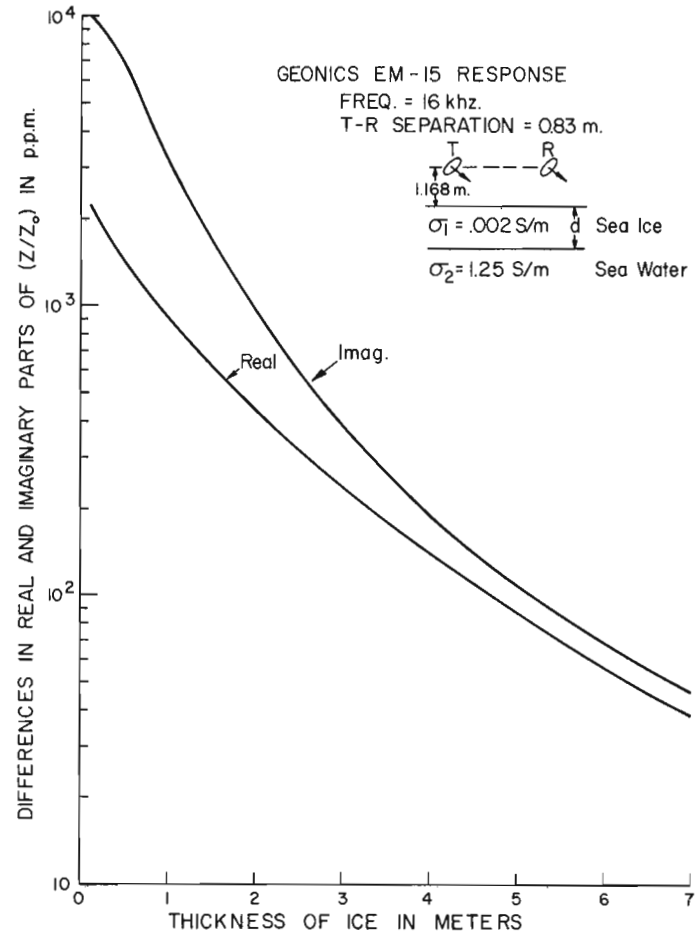

Figure 43.4. Plot of the real and the imaginary parts of $\Delta Z/Z_o$ versus sea-ice thickness for the Geonics EM-15 instrument for saline sea water.

variation with ice thickness. Figure 43.2 shows a similar theoretical plot for the Geonics EM-15 instrument assuming identical resistivity values for the sea ice and water. Geonics EM-15 has the same coil configuration as the Apex Parametrics, but its coil separation and frequency values are 0.83 m and 16 Khz respectively. This instrument normally measures only real Z/Z_o, but the instrument was modified for us by the manufacturer to record both real and imaginary parts of Z/Z_o in parts per million. Figures 43.1 and 43.2 look similar in general, but the rate of fall off of anomaly with thickness is sharper in the case of Geonics EM-15.

Table 43.1 shows some results of the difference values in real and imaginary parts of Z/Z_o, the computed thicknesses, and the actual thicknesses at four stations in the area just off the coast for both instruments. It is apparent that the difference values in real Z/Z_o are much higher than they should be, particularly for the Apex instrument. Since the accuracies of the instruments are in the order of 5 ppm, neither is capable of measuring the small difference (less than 1 ppm) values that are involved. It is believed the high values in real Z/Z_o are probably due to minor misorientation of the coils or due to electrostatic noise or crossfeeding in the internal circuitry.

Figures 43.3 and 43.4 indicate the theoretical plots for the two instruments with resistivity values suitable for the second area which was about 30 miles from the coast. The water was saline (σ_2 = 1.25 S/m) here and the resistivity of the sea ice was believed to be somewhat lower (σ_1 = 0.002 S/m). As the sea water was conducting in the area, the computed differences in both real and imaginary parts of Z/Z_o were much larger in magnitude. It is clear from the diagrams that the difference values for the imaginary parts of Z/Z_o will be larger than the corresponding real parts for all thickness values. Hence imaginary parts of Z/Z_o may be more useful than the real components because field and instrumental errors would likely have lesser influence on them.

Table 43.2 presents the results of the field survey at four stations where the ice thicknesses varied from 0.24 to 0.72 m. In this area, interpretations of ice thicknesses could be obtained independently from the difference values of both real and imaginary parts of Z/Z_o. However, the real part seems to yield more accurate estimates of the thickness values for both instruments. Another point worth noting is the interpreted thickness values from the imaginary parts of Z/Z_o although, in general, less accurate show better agreement with actual thickness values in the case of Geonics EM-15. From Figures 43.3 and 43.4 it appears that reliable results should be obtained with this technique for ice thicknesses up to 4 or 5 m provided the seawater was saline, as it should be a few miles off the coast.

Concluding Remarks

The results of the field tests showed that if the seawater is saline, these instruments could provide reasonably accurate estimates of the sea-ice thickness. However, if the seawater is fresh, as it was in the first area of the survey, the results are not very reliable. In fact, it then becomes impossible to use the real Z/Z_o variations.

Unfortunately, because of time limitations, the instruments could not be tested over thicker sections of sea ice. However, the principle of the method has been proven when the conductivity contrasts are high and it is hoped that more extensive testing will be carried out in the near future to test the full potentials of this technique of sea-ice thickness determination.

References

Adey, A.W.
1970: A survey of sea-ice thickness measuring techniques; Rep. 71-14, Communications Res. Center, Dep. of Communications, Ottawa, Canada, p. 1-28.

Campbell, K.J. and Orange, A.S.
1974: A continuous profile of sea ice and freshwater ice thickness by impulse radar; Polar Record, v. 17, no. 106, p. 31-41.

Christoffersen, P.D.
1970: Recent radar soundings of freshwater ice and sea ice; Proc. Intl. Conf. Radioglaciology, Lyngby, Denmark, p. 149-153.

Evans, S. and Smith, B.M.E.
1969: A radio echo equipment for depth sounding in polar ice sheets; J. of Sci. Instruments, Ser. 2, v. 2, p. 131-136.

McNeill, D. and Hoekstra, P.
1973: *In situ* measurements on the conductivity and surface impedance of sea ice at VLF; Radio Science, v. 8, no. 1, p. 23-30.

Sinha, A.K.
1974: Determination of sea-ice thickness by electromagnetic means; *in* Report of Activities, Part B, Geol. Surv. Can., Paper 74-1B, p. 111-112.

44.

GEOCHEMICAL RECONNAISSANCE FOR URANIUM IN CANADA: NOTES ON METHODOLOGY AND INTERPRETATION OF DATA

Project 750051: Uranium Reconnaissance Program

E. M. Cameron
Resource Geophysics and Geochemistry Division

Introduction

The Federal-Provincial Uranium Reconnaissance Program commenced in 1975; at the time of writing the second field season is closing. The program consists of complementary airborne radiometric and geochemical surveys. The former is a common method used for all environments, i.e., the only restrictions are that the terrain be suitable for low-level flying and that surface variations in radioactivity are measured. By contrast, a number of geochemical methods are being employed in the program, each of which is considered optimal for the specific geological and physiographic environment. This paper briefly discusses these geochemical methods, their implementation, and the apparent response they give to uranium mineralization. Although the discussion will be largely concerned with the search for uranium, the geochemical component of this program attempts to outline areas with a potential for a variety of mineral commodities.

During 1975, work was concentrated mainly on areas within the Canadian Shield using methods of lake sediment reconnaissance that had been developed in previous years by the Geological Survey and others in the Northwest Territories (e.g. Allan *et al.*, 1973; Cameron and Durham, 1974), Newfoundland (e.g., Davenport *et al.*, 1975; Hornbrook *et al.*, 1975), Saskatchewan (e.g. Arnold, 1970; Hornbrook and Garrett, 1976) and Ontario (e.g. Coker and Nichol, 1975). Also a trial well water survey of parts of the

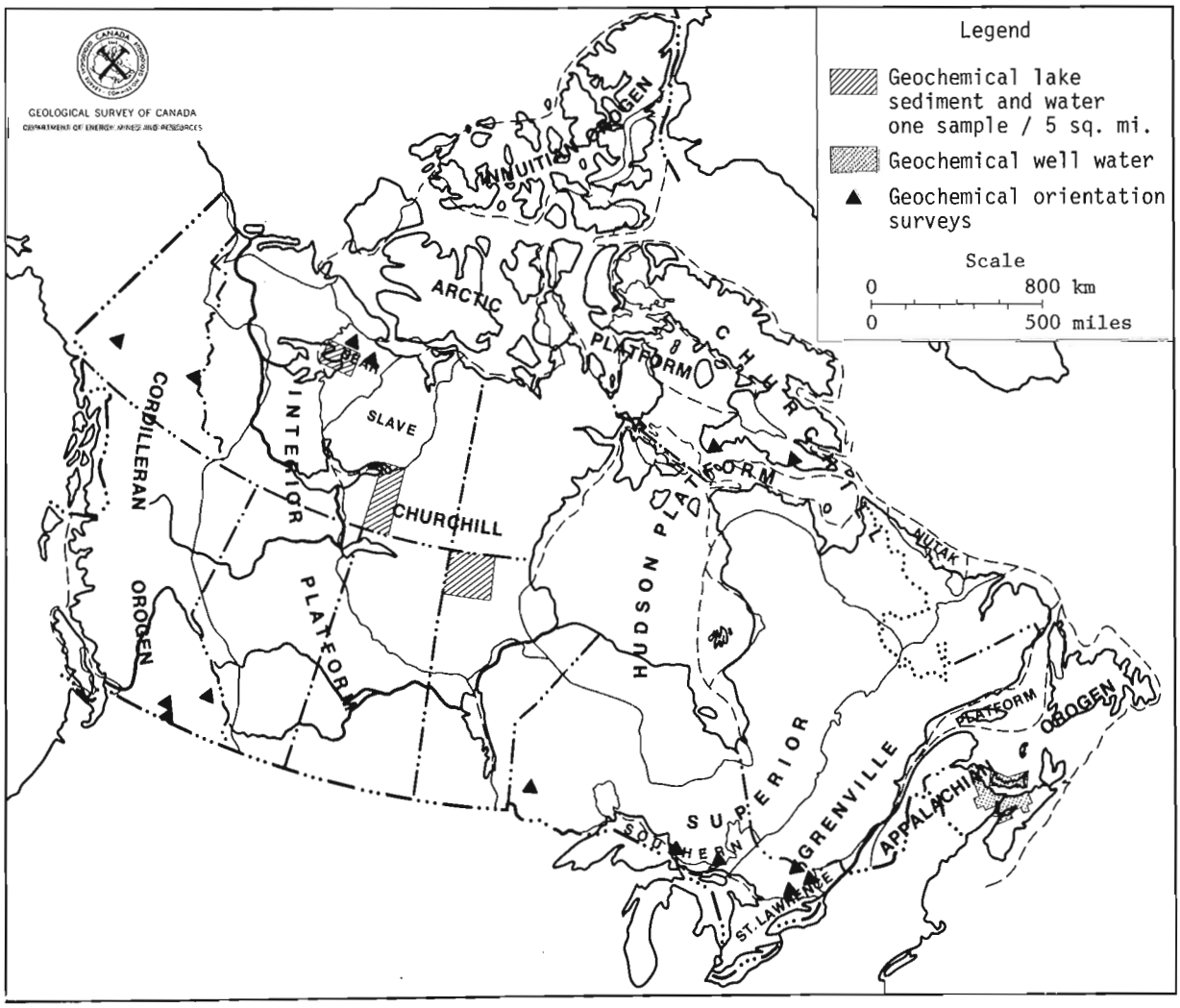

Figure 44.1. 1975 geochemical surveys, Federal-Provincial Uranium Reconnaissance Program.

From: Report of Activities, Part C;
Geol. Surv. Can., Paper 76-1C (1976).

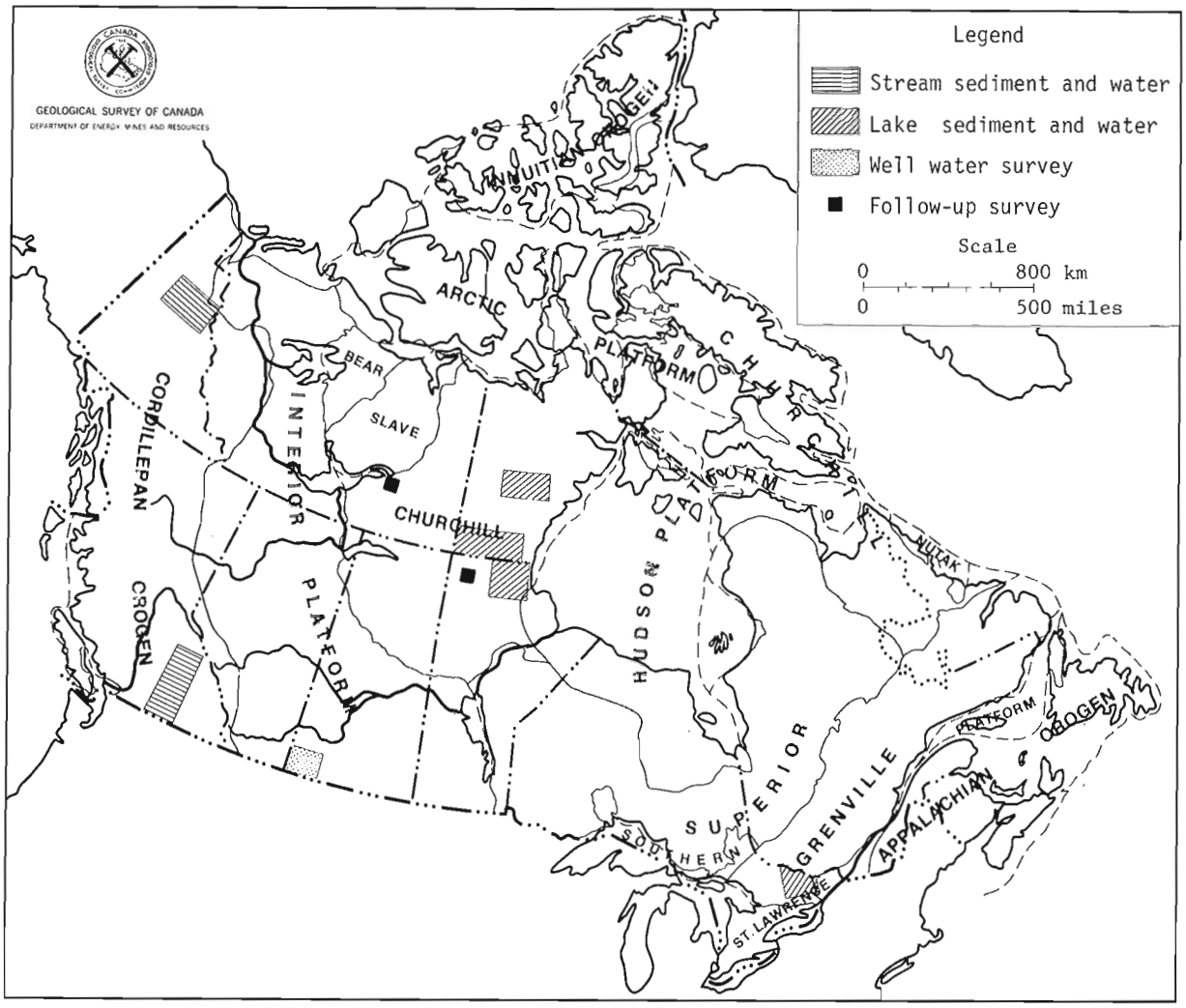

Figure 44. 2. 1976 geochemical surveys, Federal-Provincial Uranium Reconnaissance Program.

Carboniferous Basin of the Maritime Provinces was carried out (Dyck *et al.*, 1975, 1976). In a number of areas where full-scale reconnaissance surveys were anticipated for future years, orientation surveys were performed in 1976, including work in Ontario (Coker and Jonasson, 1976), Baffin Island (Maurice, in press), British Columbia (Ballantyne and Bottriell, 1975), the Yukon Territories (Gleeson and Jonasson, 1975) and the Great Bear Lake area (Durham and Cameron, 1975). These various 1975 activities are summarized in Figure 44. 1.

The 1976 geochemical reconnaissance program can be subdivided as follows: -

(a) Further lake sediment and lake water reconnaissance in the Canadian Shield, specifically in southeastern Ontario, northern Manitoba, southern Keewatin, and the Baker Lake area. The total area covered is 44 000 square miles.

(b) Follow-up investigations in areas where lake sediment reconnaissance was carried out in 1975.

(c) Large-scale stream sediment and water reconnaissance in southern British Columbia and the Yukon, totalling 29 000 square miles. The Yukon work included a substantial amount of further orientation surveys.

(d) The application of the well water techniques used in the Maritime Provinces in 1975 to a 6000 square mile area of southwestern Saskatchewan.

The locations of these various activities are shown in Figure 44. 2. Reports 45, 47, 48, 49, and 50 of this publication describe the 1976 work of the Uranium Reconnaissance Program. Report 46 presents results of the 1975 orientation studies in the Yukon.

National Geochemical Reconnaissance

In a national program of this type it is important that the data are comparable from year to year and between different areas of the country. To achieve this it is necessary to establish consistent sampling,

sample preparation, analysis, and data presentation methods and to monitor these with effective quality control procedures. The approach will be applied to a variety of federal and federal-provincial geochemical programs, not only the Uranium Reconnaissance Program. The term National Geochemical Reconnaissance (N.G.R.) is applied to data obtained by these consistent methods.

It should be recognized that these N.G.R. data, as well as serving the immediate purposes of mineral exploration and resource evaluation, provide an important national source of information that can be applied to environmental, agricultural, or geological investigations. For example, in 1976 the Inland Waters Branch of the Department of the Environment commenced studies of natural toxic metal anomalies based on N.G.R. data.

N.G.R. surveys are subdivided into five district phases: sample collection, sample preparation, analysis, data compilation and cartography, and quality control. In 1975, at the start of the program, the sampling of lake sediments and the analysis were carried out by Canadian contractors, with the Geological Survey responsible for the other three phases. In 1976, sample preparation was completed under contract also and by 1977 it is anticipated that, in addition, data compilation and cartography will be by contract. The Geological Survey of Canada will continue to be responsible for quality control, which is carried out at each phase of the work.

The primary form of N.G.R. data release is 1:250 000 scale element symbol maps and data listings, both printed and on magnetic tape. In response to requests from industry for a cheap and readily stored format for these data, the maps of the 1976 surveys will also be available on microfiche. The release of this primary information has been made in the spring of the year following field work, in order that the data may be used by mining companies for summer field programs. As the program expands, with further provinces joining, it will probably be necessary to spread the release of data over a longer period of the year. As well as 1:250 000 presentation, 1:1 000 000 element compilation maps will be published as data accumulate for large areas of the country.

The cost of geochemical surveys for the Uranium Reconnaissance Program was originally budgetted at $10-$15 square mile. This provided, for instance, a sampling density of 1 per 10 square miles in the Canadian Shield. Through increased efficiency, particularly in sampling, it has been possible to maintain this cost during the 1975 and 1976 operations, while, in the Shield, increasing the sampling density to 1 per 5 square miles. This includes the analysis of 13 components in sediment and water samples. Studies are presently being carried out to determine optimum sampling intervals for various indicator elements in different environments, using the 1975 and 1976 N.G.R. data. This may cause a change in the sampling density employed in 1977 and subsequent years and a more flexible approach to sampling density, based on the requirements of the particular terrain.

The methods used in the N.G.R. surveys have been devised and implemented by E.H.W. Hornbrook, R.G. Garrett, and J.J. Lynch. The work is carried out under their direction.

Follow-up Studies

An important part of the Uranium Reconnaissance Program is to monitor the effectiveness of the program and to gain a better understanding of the processes that lead to the development of geochemical and radiometric anomalies. With this information it will be possible to reach the most appropriate balance between radiometric and geochemical methods; to upgrade the reconnaissance methods; and to provide guidelines on the interpretation of the data.

Much of this knowledge hopefully will come from the mining companies that use the data in their exploration programs. In addition, there will be a limited amount of follow-up work by the Geological Survey and by the provincial departments particularly during the early years of the program. This will allow study of not only anomalies related to mineralization of possible economic interest but also anomalies related to variations in bedrock composition, or to features of the environment.

In 1976 the most comprehensive follow-up study was in northwestern Manitoba in areas surveyed by airborne radiometric and lake sediment reconnaissance in 1975. This involved complementary geochemical, geophysical, geological and surficial geological investigations directed by W.B. Coker, B.W. Charbonneau, and L. Dredge. A similar study, under the direction of Y.T. Maurice, was carried out in the Nonacho belt, Northwest Territories, to follow-up lake sediment reconnaissance also completed in 1975. Both these operations had field laboratory facilities, that are considered essential for geochemical follow-up.

Many of these detailed studies were carried out in areas that had been acquired by mining companies as claims or permits as a result of the release of the 1975 reconnaissance results and earlier work. By arrangement with these companies, publication of results from these areas will be delayed. Thus specific details of the field data are not contained in Reports 49 and 50 of this publication. However, both reports present preliminary findings of a general nature.

Geochemical Reconnaissance Methods for Uranium

The use of centre-lake sediments for geochemical reconnaissance in the Shield depends on two important factors: one logistical, the other geochemical. The first is that samples may be collected routinely, rapidly and economically by helicopter. The second is that uranium is dispersed widely in solution from a point source of mineralization, before being precipitated in the sediments of a lake. The Shield is an area of generally low relief where immobile elements, such as lead, can only travel short distances along the lake drainage systems (Cameron, 1975). If a geochemical exploration method was to rely on mechanical dispersion,

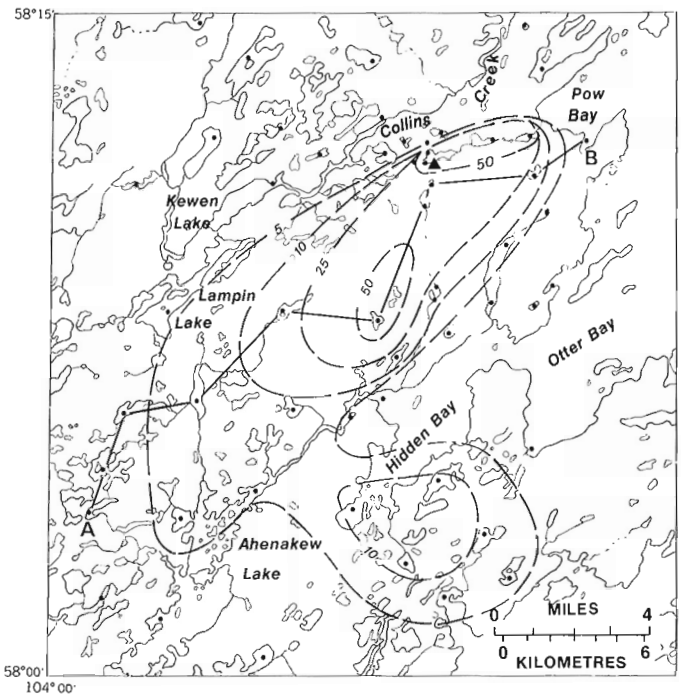

Figure 44.3. Uranium in lake sediments, as parts per million, Rabbit Lake area, Saskatchewan. Uranium deposit shown by solid triangle.

close sampling intervals would be required; intervals that would be prohibitively expensive for reconnaissance purposes. Fortunately, uranium is a highly mobile element in the secondary environment. It retains the mobility at the near-neutral pH values that are characteristics of most Shield lakes. This is in contrast to the behaviour of many heavy metals that become less mobile with increasing pH. Notwithstanding the above, samples are also analyzed for immobile elements in the Shield Uranium Reconnaissance Program. This is because such elements, derived from widespread sources, such as rock units of distinctive composition, or till sheets, rather than point sources, can provide useful information at reconnaissance-level sampling.

If the concept that anomalous levels of uranium in lake sediments have been transported in solution is correct, there should be a relatively close correlation between uranium in sediments and uranium in the waters of the same lakes. In many cases this is true. For instance, in the area of the Rabbit Lake uranium deposit, Saskatchewan, a close relationship exists between the anomaly patterns for uranium in the two media (Figs. 44.3 and 44.4; Table 44.1). A detailed description of these data are given by Cameron and Ballantyne (in prep.). In carbonate-rich alkaline environments, uranium forms highly soluble complexes. This may delay the precipitation of uranium in the bottom sediments and weaken or destroy the correlation between the uranium content of the two media (Dyck, 1974; Cameron and Hornbrook, in press; Maurice, in press).

In view of the above discussion it is reasonable to ask why waters are not the primary sampling media in the Shield because they can be collected more rapidly and economically than lake sediments. In part the answer is demonstrated by examining the anomaly patterns for the Rabbit Lake area (Figs. 44.3 and 44.4). The anomaly for uranium in water is more restricted in areal extent than the sediment anomaly. The water anomaly is apparently truncated by the detection limit of the fluorimetric method of analysis of 0.05 ppb U. Although this is of little importance in the case of the Rabbit Lake area because of the extent and intensity of both anomalies, it may be important in places where the signal given by mineralization is much weaker.

The uranium content of lake waters in the Shield is generally low as is shown by the two examples given in Figure 44.5; both are from areas that are reasonably prospective for uranium mineralization. The vast majority of waters must be measured at the parts per trillion level, rather than in parts per billion. While this is possible at the research level, proper procedures for the collection, preservation and analysis of thousands of samples have not yet reached the stage that we feel confidence in using waters as the primary sampling medium in the Shield. This may change with greater sophistication of the methods. For elements that are rather less mobile than uranium in the surface environment (e.g. Cu), the use of sediments is even more important.

Only a small part of the variation shown on geochemical reconnaissance maps for uranium is due to the influence of potentially economic uranium mineralization. The great majority of the variation is due to compositional differences in the rocks of an area

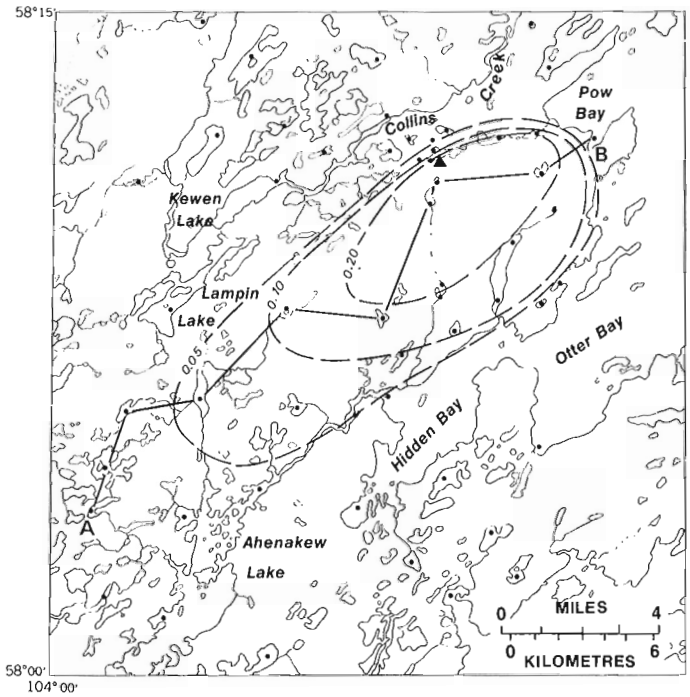

Figure 44.4. Uranium in lake waters, as parts per billion, Rabbit Lake area, Saskatchewan.

Table 44.1

Uranium in lake sediments and lake waters along the profile A-B, Rabbit Lake area, Saskatchewan (*see* Figs. 44.3 and 44.4)

	U, ppm in sediments	U ppb in waters
A	3	0.04
	3	0.04
	3	0.04
	8	0.08
	14	0.14
	83	0.16
	43	0.44
	32	0.24
	11	0.27
B	4	0.04

and the surficial cover. It is one of the purposes of the follow-up studies to classify the various types of anomaly. Some general conclusions may be drawn from the 1976 studies and from earlier work (e.g. Dyck and Cameron, 1975). A distinct lake sediment and water anomaly may be derived from a point source of uranium mineralization (Fig. 44.6a). Alternatively, an equally strong anomaly may be generated by a weaker, but more widely distributed source of labile uranium (Fig. 44.6b). Such a source may often be granitic or pegmatitic terrain enriched in uranium. Because uranium is highly mobile relative to most of the other components of the granitic rock (e.g. Si, Al, K, Th), there may be considerable enrichment of uranium in the lake sediment compared to the source. Apparently enrichments of an order of one magnitude are not uncommon. A similar phenomenon has been shown by Allan *et al.* (1973) for zinc and copper in areas of sulphide-veined rocks.

Much attention has been devoted recently to concepts of the genesis of uranium deposits by surface and near-surface leaching of uranium than transportation and concentration. The resulting deposits are located near unconformities (e.g. Knipping, 1974). The processes upon which geochemical reconnaissance for uranium in the Shield depends are the same as those required for the genesis of these deposits. The present-day process depicted in Figure 44.6b mimics the development of certain unconformity-related uranium deposits. Recent work in southern British Columbia shows that this analogy is not too far fetched (Smee and Ballantyne, 1976). Uranium occurs at the Fuki-Donen deposit and related prospects in conglomerates at the base of a Tertiary basalt sequence. The conglomerates rest on Cretaceous granites and granodiorites, samples of which contain readily leachable uranium. Measurements of stream waters derived from areas of these granitic rocks contain anomalously high contents of uranium. Because some of these streams drain through the permeable conglomerates they may have contributed in the recent geological past, or even at present, to the development of the uranium mineralization (Fig. 44.6c).

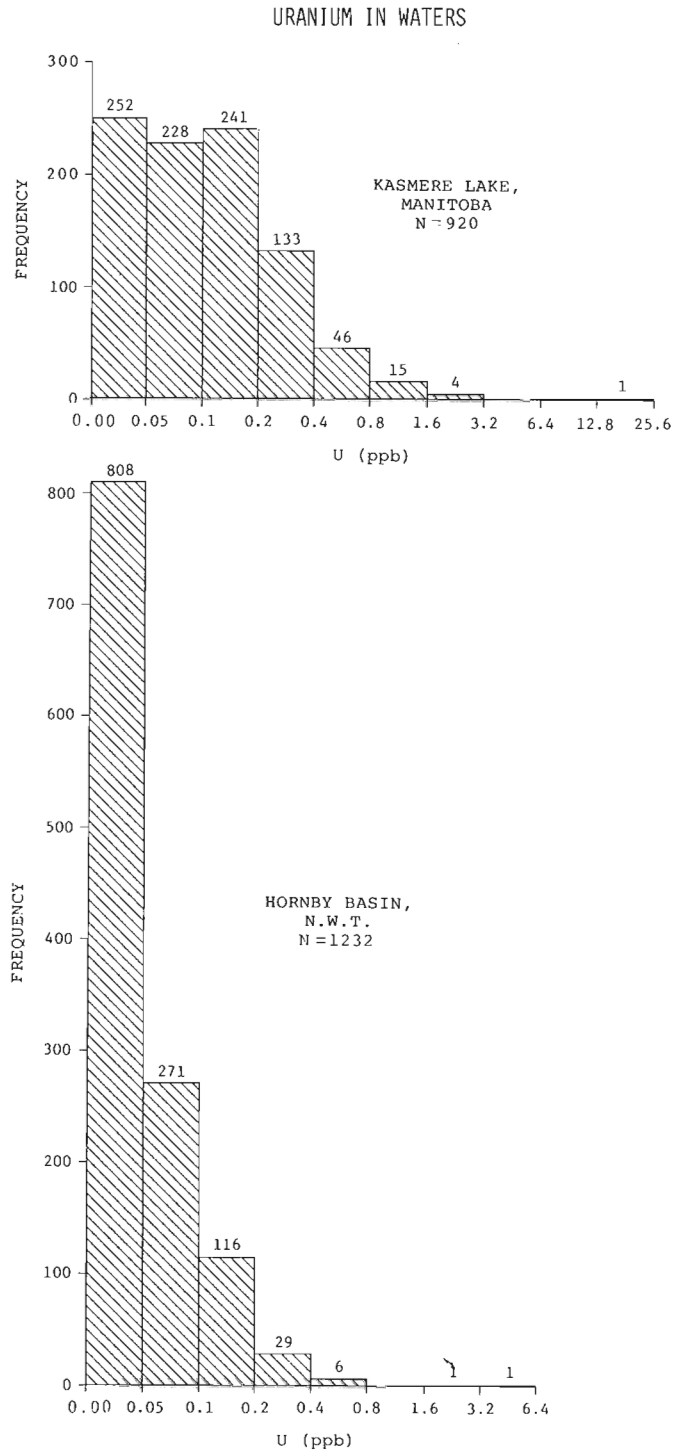

Figure 44.5. Histograms of the distribution of uranium in surface lake waters from the Hornby basin, Northwest Territories, and from the Kasmere Lake map-area, Manitoba.

Anomalies derived from widespread source areas of labile uranium require careful interpretation. A few of these enriched rock bodies may, of course, contain sufficient local concentrations to warrant

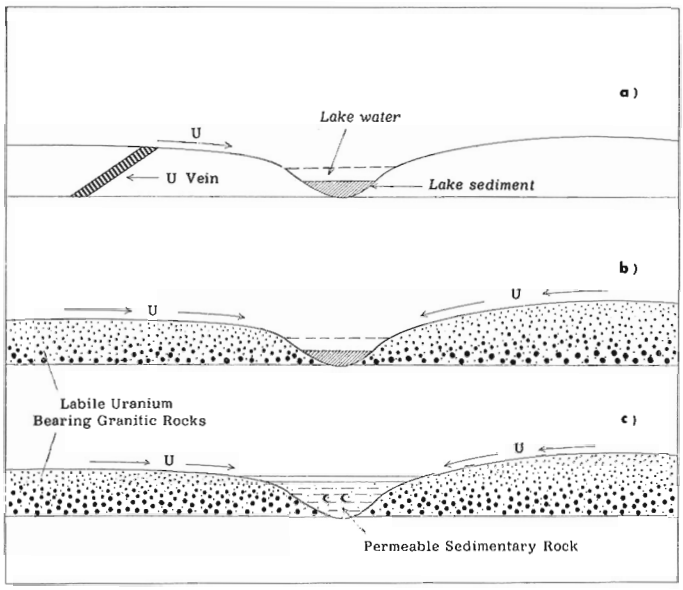

Figure 44.6. Derivation of uranium anomalies in lake sediments and waters from concentrated (a) and dispersed (b) sources. The same processes of weathering and dispersion can lead to the formation of ore deposits (c).

exploration. However, all such bodies are potential sources for the secondary leaching, dispersion and concentration of uranium. The information provided by the geochemical data must be integrated into the total appraisal of geological environments suitable for uranium ore genesis.

The concepts of geochemical reconnaissance for uranium discussed above is biassed to the Canadian Shield environment, where the Geological Survey recently has had its greatest amount of experience. However, these concepts can readily be extended into the other environments in which the Uranium Reconnaissance Program is active.

In the Cordillera both mechanical and hydromorphic dispersion in streams may be considered as bases for geochemical reconnaissance. The high relief allows extensive mechanical dispersion along streams, and also promotes active ground-water flow conducive to hydromorphic dispersion. Both the 1975 orientation work (e.g. Gleeson and Jonasson, 1975) and the 1976 reconnaissance and detailed studies have attempted to evaluate the relative importance of the two processes in terms of geochemical exploration. The preliminary indications are that water analysis may be an important complement to stream sediment analysis in parts of the Cordillera.

The work of Dyck and his colleagues on well water reconnaissance for uranium (Dyck *et al.*, 1975, 1976a, b) is a novel application of geochemical exploration to Canada. It is designed principally for areas of relatively flatlying sedimentary rocks that may be host to roll-type or similar uranium deposits. The identification of aquifers with anomalous concentrations of uranium or other indicator elements, such as radon, helium or copper, may be one or few possible methods of locating prospecting targets. However, the difficulties of interpreting such anomalies are greater than for most other environments.

In the western United States exploration for roll-type deposits has, in general, proceeded from known surface occurrences to concealed deposits. It is possible that in Canada these deposits may occur in areas where there are only minor or surface showings. In the Carboniferous Basin of the Maritimes, the humid environment will promote the removal of surface occurrences. Exploration for this type of mineralization may be more analagous to oil exploration with careful attention to stratigraphy, structure and hydrodynamics.

Elements other than Uranium

Costs of analysis are generally small in proportion to sampling costs and this allows a variety of elements to be determined on samples collected for this program. These data serve two purposes. Firstly, since uranium deposits contain a variety of elements, additional evidence of the presence of uranium mineralization is revealed. Secondly, information is provided on a wide range of other mineral commodities. A number of collaborating provinces consider that this information is at least as important as the data provided on uranium.

In the Cordillera much information has been gained since the Second World War on the use of geochemistry in the search for base metals. The Uranium Reconnaissance Program surveys will utilize this knowledge and, hopefully, add to it. In the 1976 reconnaissance surveys in the Cordillera U, Zn, Cu, Pb, Ni, Co, Mo, Ag, Ba, W, Mn and Fe are being determined in stream sediments and U and F in waters.

For the Canadian Shield samples U, Zn, Cu, Pb, Ni, Co, Mo, Ag, As, Hg, Mn, Fe, and Loss on Ignition are being determined on centre lake sediment samples and U in waters. Within the northern Shield, where the greatest number of Geological Survey studies have been carried out, the active oxidation of many base metal deposits and the wide dispersion of mobile elements, such as zinc and nickel, is favourable to reconnaissance geochemistry. Work in the southern part of the Shield has shown the environment to be more complex, which appears to give rise to less clearcut reconnaissance data. Features that contribute to this complexity are the more extensive surficial cover and the greater biological activity which produces a greater range of limnological environments and greater metal-organic complexing (Nichol *et al.*, 1976). Also the rate of oxidation of base metal deposits in the south relative to the north is not known. Greater attention by geochemists at the Geological Survey to these problems are planned for 1977 and, in addition, this department is currently supporting research at Queen's University and the University of New Brunswick on mechanisms of element dispersion from base metal deposits.

Acknowledgments

The work described here is the product of the efforts of many colleagues in the Geological Survey of Canada and the staff of contractor companies. Special thanks are due to the geologists and geochemists of a number of provincial governments, who have contributed their knowledge to the design of the geochemical program.

References

Allan, R.J., Cameron, E.M., and Durham, C.C.
1973: Lake geochemistry – a low sample density technique for reconnaissance geochemical exploration and mapping of the Canadian Shield; *in* Geochemical Exploration 1972, M.J. Jones, Ed., Inst. Min. Metall., London, p. 131-160.

Arnold, R.G.
1970: The concentrations of metals in lake waters and sediments of some Precambrian lakes in the Flin Flon and La Ronge areas; Circ. Geol. Div. Sask. Res. Council 4, 30 p.

Ballantyne, S.B. and Bottriell, K.
1975: Geochemical orientation surveys for uranium in southern British Columbia; *in* Report of Activities, Part C, Geol. Surv. Can., Paper 75-1C, p. 211-312.

Cameron, E.M.
1975: Geochemical methods of exploration for massive sulphide mineralization in the Canadian Shield; *in* Geochemical Exploration 1974, Assoc. Expl. Geochem., Spec. Publ. 2, Elliot, I.L. and Fletcher, W.K., Eds., Elsevier Scientific Publ. Company, Amsterdam (1975), p. 21-49.

Cameron, E.M. and Durham, C.C.
1974: Geochemical studies in the eastern part of the Slave Province, 1973; Geol. Surv. Can., Paper 74-27, 20 p.

Cameron, E.M. and Hornbrook, E.H.W.
Current approaches to geochemical reconnaissance for uranium in the Canadian Shield; *in* Exploration of Uranium Ore Deposits, I.A.E.A., Vienna (in press).

Coker, W.B. and Jonasson, I.R.
1976: Geochemical exploration for uranium in the Grenville Province of Ontario – abstract; Can. Min. Metall., Bull., v. 69, no. 767, p. 79.

Coker, W.B. and Nichol, I.
1975: The relation of lake sediment geochemistry to mineralization in the northwest Ontario region of the Canadian Shield; Econ. Geol., v. 70, p. 202-218.

Davenport, P.H., Hornbrook, E.H.W., and Butler, A.J.
1975: Regional lake sediment geochemical survey for zinc mineralization in western Newfoundland; *in* Geochemical Exploration 1974; Assoc. Expl. Geochem. Spec. Publ. 2, Elliot, I.L. and Fletcher, W.K., Eds., Elsevier Scientific Publishing Company, Amsterdam (1975), p. 555-578.

Durham, C.C. and Cameron, E.M.
1975: A hydrogeochemical study for uranium in the northern part of the Bear Province, Northwest Territories; *in* Report of Activities, Part C, Geol. Surv. Can., Paper 75-1C, p. 331-332.

Dyck, W.
1974: Geochemical studies in the surficial environment of the Beaverlodge area, Saskatchewan, Geol. Surv. Can., Paper 74-32, 30 p.

Dyck, W. and Cameron, E.M.
1975: Surface water uranium-radon survey of the Lineament Lake area, District of Mackenzie; *in* Report of Activities, Part A, Geol. Surv. Can., Paper 75-1A, p. 209-211.

Dyck, W., Garrison, E.W., Wells, G.S., and Godoi, H.O.
1975: Well water uranium reconnaissance in eastern Maritime Canada; *in* Report of Activities, Part C, Geol. Surv. Can., Paper 75-1C, p. 313-315.

Dyck, W., Garrison, E.W., Godoi, H.O., and Wells, G.S.
1976: Minor and trace element contents of well waters, Carboniferous basin, eastern Canada; Geol. Surv. Can., Open File 340, 35 p.

Dyck, W., Whitaker, S.H., and Campbell, R.A.
1976b: Well water uranium reconnaissance, southwestern Saskatchewan; *in* Report of Activities, Part C, Geol. Surv. Can., Paper 76-1C, Rep. 47.

Gleeson, C.F. and Jonasson, I.R.
1975: Geochemical pilot studies, Yukon, 1975; internal report, Geological Survey of Canada.

Hornbrook, E.H.W., Davenport, P.H., and Grant, D.R.
1975: Regional and detailed geochemical exploration studies in glaciated terrain in Newfoundland; Province of Newfoundland, Dept. Mines and Energy, Report 75-2, 116 p.

Hornbrook, E.H.W. and Garrett, R.G.
1976: Regional geochemical lake sediment survey, east-central Saskatchewan, Geol. Surv. Can., Paper 75-41.

Knipping, H. D.
1974: The concepts of supergene versus hypogene emplacement of uranium at Rabbit Lake, Saskatchewan, Canada; *in* Formation of Uranium Ore Deposits, I.A.E.A., Vienna, p. 531-549.

Maurice, Y. T.
Geochemical methods applied to uranium exploration in southwest Baffin Island; Can. Min. Met., Bull. (in press).

Nichol, I., Coker, W. B., Jackson, R. G., and Klassen, R. A.
1976: Relation of lake sediment composition to mineralization in different limnological environments in Canada; *in* Prospecting in Areas of Glaciated Terrain, 1975 (Editor, M. J. Jones) Inst. Min. Metall.: London, p. 112-125.

Smee, B. W. and Ballantyne, S. B.
1976: Examination of some Cordilleran uranium occurrences; *in* Report of Activities, Part C, Geol. Surv. Can., Paper 76-1C, Rep. 48.

45. GEOCHEMICAL ORIENTATION AND RECONNAISSANCE SURVEYS FOR URANIUM IN CENTRAL YUKON

Project 750051: Uranium Reconnaissance Program

W. D. Goodfellow, I. R. Jonasson, and N. G. Lund
Resource Geophysics and Geochemistry Division

Introduction

Reconnaissance and detailed surveys were carried out in central Yukon in the summer of 1976 in support of the Uranium Reconnaissance Program (Darnley *et. al.*, 1975). Since this was the first year of this long-term program, it was desirable to obtain experience in a variety of terrains. To obtain representative coverage of the different physiographical and geological regions, reconnaissance surveys were conducted in the Wernecke, Ogilvie, Tombstone and Richardson mountains as well as the Bonnet Plume and Eagle Plains basins (Fig. 45. 1). The reconnaissance survey involved helicopter-supported sampling of approximately 2200 stations for stream sediment and water over an area of 28 490 km^2. During the detailed survey, which included traversing streams, 1000 stations were sampled for stream sediments and waters in areas that were previously chosen on the basis of geology, physiography, and the presence or absence of particular mineral occurrences. The detailed survey of eight areas, comprising a total of 2072 km^2 within the reconnaissance survey area (Fig. 45. 2), was designed in conjunction with the reconnaissance survey to give as much information as possible of the processes affecting the dispersion elements in the secondary environment.

Water samples were shipped to Barringer Laboratories in Whitehorse in order to obtain a rapid turnabout of U, F and pH determinations. Upon completion of U, F and pH analyses, the samples were acidified and shipped to Geological Survey laboratories in Ottawa to be analyzed at a later date for Cu, Zn, Co, and Ni. The stream sediments were shipped directly to the Survey in Ottawa to await analyses for U, Zn, Cu, Pb, Ni, Co, Ag, Mn, Fe, Mo, W, and Ba.

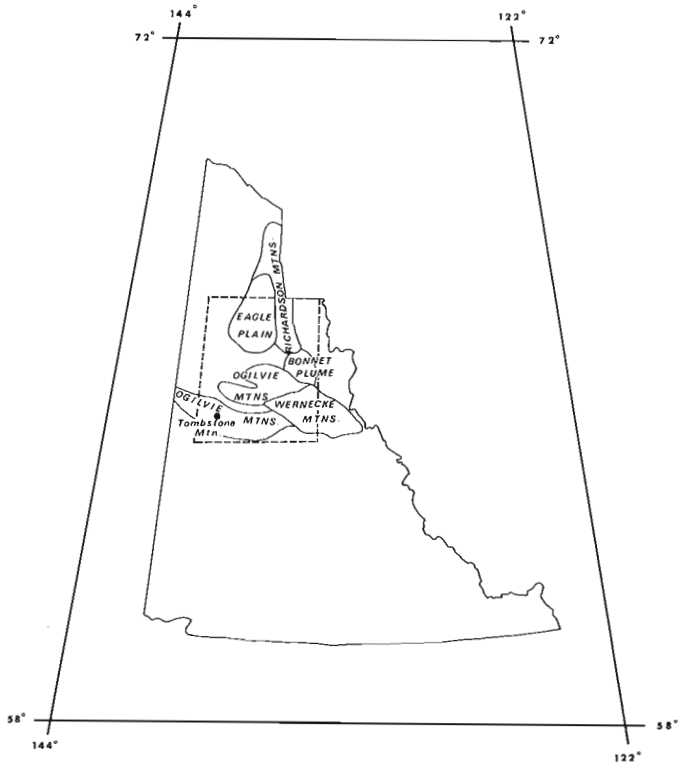

Figure 45. 1. Physiographic divisions of the central Yukon (adapted from Bostock, 1961). Dashed line outlines area in Figure 45. 2.

General Geology

The geology of the central Yukon most recently described by Green (1972) and by Norris (1975) is composed of rocks ranging in age from Proterozoic (Helikian) to Quaternary with rocks from almost every period represented. In the Helikian volcanic and sedimentary rocks, uranium mineralization occurs near unconformities with younger Precambrian and possibly Cambrian sedimentary rocks. The uranium mineralization in the areas investigated occurs either in quartz-pyrite or barite-magnetite-hematite veins filling fractures in the older rocks. Uranium mineralization has also been reported to occur in cherty breccias with a hematitic matrix. The older Precambrian rocks are commonly rich in brannerite which often occurs as knobs protruding from the iron formation matrix while the younger rocks are regarded as containing appreciably more pitchblende.

Formations in the Phanerozoic considered geologically favourable for uranium mineralization, but lacking known occurrences, include the following: -

(1) the Cambrian conglomerate-sandstone sequence as a host for secondary uranium mineralization

(2) the Ordovician Road River shales which were shown by Gleeson and Jonasson unpublished manuscript to have abnormally high concentrations of uranium

(3) the Cretaceous syenitic and quartz-monzonitic stocks of the Tombstone Mountains which have been shown by Garrett (1971) to have high concentrations of uranium. Sediments from streams draining syenitic stocks in the Tombstone Mountains are also concentrated in uranium (Gleeson and Jonasson, unpublished manuscript)

(4) the Cretaceous-Tertiary Eagle Plains and Bonnet Plume Basins composed of semi-consolidated gravels, sands and coal seams as hosts for secondary uranium mineralization.

From: Report of Activities, Part C;
Geol. Surv. Can., Paper 76-1C (1976)

Detailed Surveys

To date, exploration for uranium in the central Yukon by private companies included both geophysical and geochemical methods. Geochemical techniques included sampling at ¼ to ½ mile intervals and analyzing the minus 80-mesh fraction of stream sediments by fluorometric methods. Follow-up of stream sediment anomalies included sampling stream sediments in greater detail in addition to talus and soil. The exploration for uranium has had mixed success undoubtedly due to the absence of orientation surveys necessary to interpret the analytical data. For example no detailed investigations were conducted to determine what size fraction of stream sediment should be analyzed and the methods of analysis for the varied types of uranium occurrences of the central Yukon. Uranium occurring in resistate minerals such as brannerite will be mechanically dispersed and concentrated in the coarse fraction. Consequently, the fluorometric method of analysis after a nitric acid leach would account for a small percentage of the total uranium present in resistate minerals such as brannerite.

Because of the difficulty of interpreting analytical data in the past, detailed surveys of stream systems from eight areas within the reconnaissance survey area were conducted with the following objectives:

(1) to determine the processes whether they be mechanical, chemical or a combination of both affecting element migration from known uranium and base metal occurrences. An understanding of the mechanisms of element migration is necessary in selecting the optimum size fraction of stream sediment that will best reflect the uranium potential of an area, and also in determining the possible benefits of the use of water.

(2) to determine the length and intensity of uranium dispersion trains reflected in stream waters and the various size-fractions of stream sediments. This aspect of the detailed survey was necessary to determine the optimum sample density on a reconnaissance scale.

(3) to determine which accessory elements may be useful in a given geological environment as 'path-finders' to uranium mineralization.

(4) to determine background and threshold levels for uranium and associated elements in stream waters, stream sediments and rocks from representative geological formations. This aspect of the detailed survey was done in conjunction with the reconnaissance survey.

To achieve these objectives sediment and water from streams intersecting a variety of geological environments both with and without known uranium occurrences were sampled at ¼ mile intervals. Rock samples from the known occurrences of uranium as well as representative lithologies were collected to aid in interpreting the stream geochemistry. It is interesting to note that radioactive rocks of the central Yukon commonly contain barite and visible chalcopyrite which is significant considering the number of Cu showings in Helikian rocks of the Yukon. To determine further the possible association of copper and uranium of the central Yukon, one detailed survey was conducted

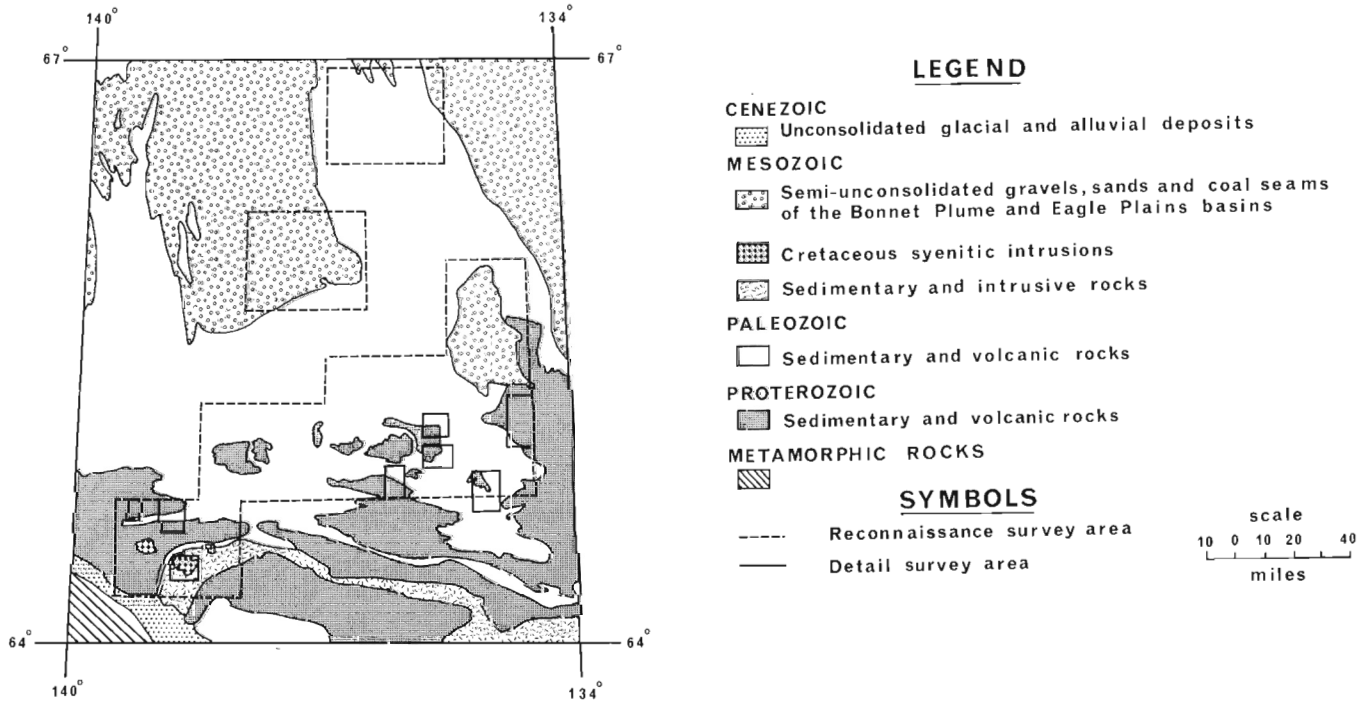

Figure 45. 2. General geology of central Yukon with the locations of reconnaissance and detailed survey areas (geology after Green (1972) and Norris (1975)).

in the Kiwi Lake area which included copper and uranium showings in chalcopyrite-hematite and barite-magnetite-hematite mineral assemblages respectively (Fig. 45. 3). Preliminary analytical results for uranium show a subtle anomaly in stream waters draining the uranium showing and extending at least three miles downstream. Past the confluence with the main stream, the high uranium is undoubtedly derived from streams draining the uranium showing and from streams draining the north slope of the stream valley. The source of

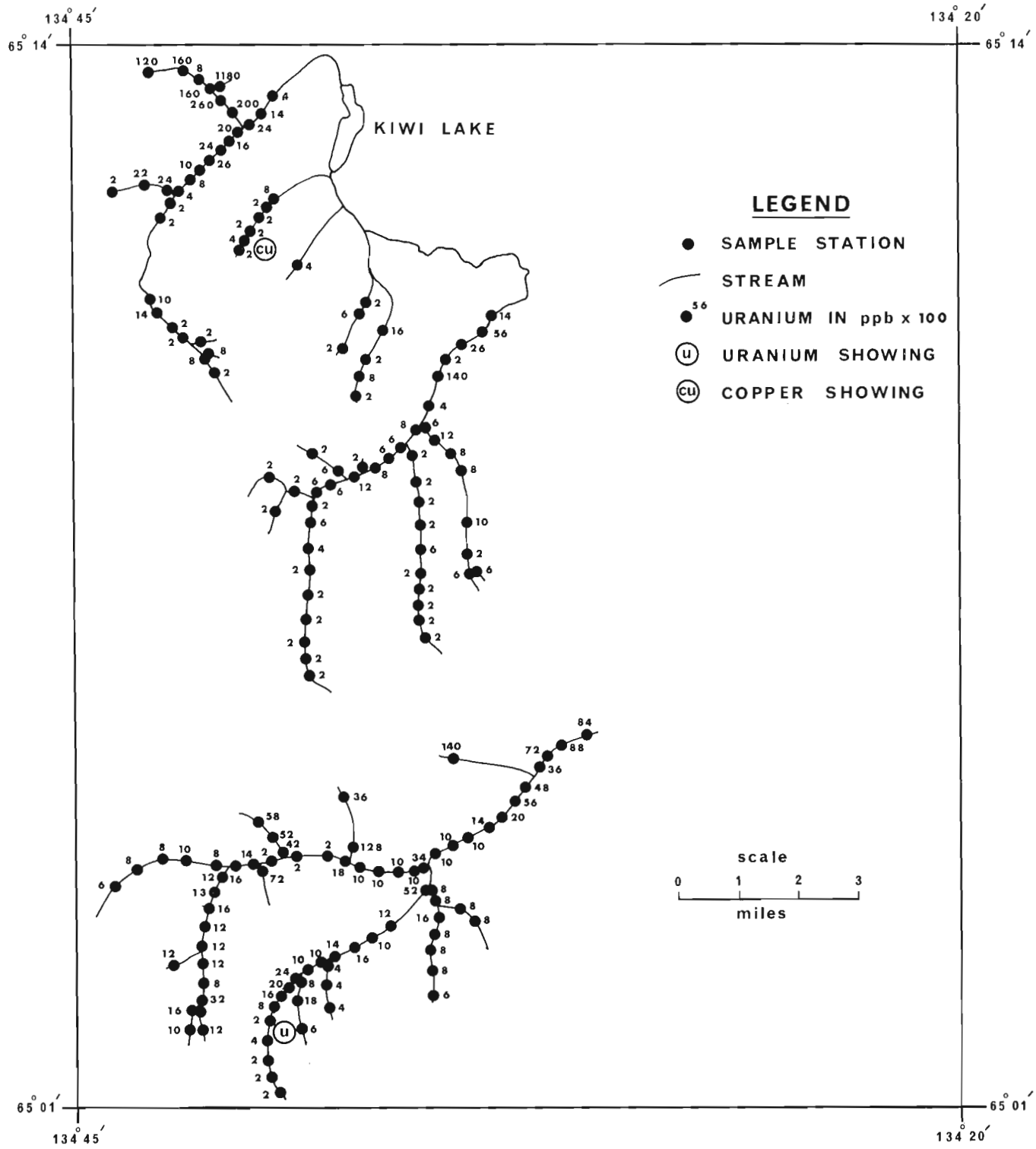

Figure 45. 3. Uranium concentration (ppb x 10^2) in stream waters from the Kiwi Lake detailed survey area of central Yukon.

uranium in streams draining the north slope of the stream valley is as yet unexplained. A second area of interest is the primary stream immediately west of Kiwi Lake where the uranium concentration is several orders of magnitude greater than streams draining the known uranium occurrence. In this stream the uranium concentration ranges up to 11. 8 ppb compared to a high of 0. 24 ppb from the stream draining the known uranium occurrence and an apparent background concentration of less than 0. 06 ppb. Although the source of uranium in this stream is unknown, it is interesting to note the rapid dilution of uranium upon intersecting the main tertiary stream. The stream draining the known copper showing immediately southwest of Kiwi Lake has a low concentration of uranium which is supported by the absence of significant radioactivity at this showing.

A more rigorous treatment of the Kiwi Lake detail area will result when all the analytical data is received for stream sediments, waters and rocks collected in the area.

Reconnaissance Surveys

Reconnaissance surveys of stream sediments and waters were carried out over an approximately 28 490 km^2 area of central Yukon. The objectives of the reconnaissance survey were: -

(1) to determine the feasibility and logistics of carrying out a helicopter-supported survey sampling stream sediments and waters at a density of one sample in five square miles. This becomes of paramount importance when determining contract specifications for any future geochemical surveys conducted in the Yukon.

(2) to determine, in conjunction with the detailed surveys, the various physical and chemical factors affecting the secondary dispersion of uranium and associated elements from known mineral occurrences.

(3) to establish background and threshold levels of concentration for the various elements in waters and sediment from streams intersecting different geological formations.

Objectives 2 and 3 can be evaluated only after analytical data for stream sediment and water are available. As far as objective 1 and the technical aspects of conducting a low density stream sediment and water survey, this is possible at an average sampling rate of 16 sites per hour in mountainous terrain and 12 sites per hour in flat-lying areas. In contrast to mountainous areas where the helicopter could land within feet of the stream, the relative abundance of trees in the Bonnet Plume and Eagle Plains basins made helicopter landing difficult. Consequently, the sample collection rate and sample density decreased in these areas. Also, the stream sediment and water were commonly organic-rich which may make interpreting the geochemical data difficult.

Samples were generally collected at a break in slope where fine sediment was deposited behind boulders and/or near the margins of streams. In situations where the streams were torrential and/or the underlying bedrock was such that it contributed minor fine sediment to the stream, the moss common along the stream bank, as noted by Gleeson and Jonasson (unpublished manuscript), proved invaluable in trapping fine sediment. Except for some streams drying up in late July and August water sampling posed no problem in the central Yukon.

References

Bostock, H. S.
1961: Physiography and resources of the northern Yukon; Can. Geogr. J., v. LXIII, no. 4, p. 112-119.

Darnley, A. G., Cameron, E. M., and Richardson, K. A.
1975: The Federal-Provincial uranium reconnaissance program; *in* Uranium Exploration 1975; Geol. Surv. Can., Paper 75-26, p. 49-68.

Garrett, R. G.
1971: Molybdenum, tungsten and uranium in acid plutonic rocks as a guide to regional exploration, S.E. Yukon; Can. Min. J., v. 92, p. 37-40.

Green, L. H.
1972: Geology of Nash Creek, Larsen Creek, and Dawson map-areas, Yukon Territory; Geol. Surv. Can., Mem. 364, 157 p.

Norris, D. K.
1975: Geology of Hart River (116 H), Wind River (106 E) and Snake River (106 F) 1: 250 000 sheets; Geol. Surv. Can., Open File 279.

46. ON THE USEFULNESS OF WATER SAMPLES IN RECONNAISSANCE SURVEYS FOR URANIUM IN THE YUKON TERRITORY

Project 740081: Uranium Reconnaissance Program

I.R. Jonasson and C.F. Gleeson[1]
Resource Geophysics and Geochemistry Division

Introduction

The search for uranium occurrences in the Yukon Territory is a recent development in the mineral exploration of that region. Until recently published reports gave very few indications of the possible presence of uranium in economic quantities.

In July 1975, the authors conducted a series of pilot geochemical studies in the southern part of the Yukon Territory with a view to investigating the feasibility of mounting low density reconnaissance, helicopter-supported surveys to define uraniferous areas.

One of the objectives of the project was to ascertain the usefulness of collecting stream and spring water samples to complement data derived from a conventional stream sediment survey.

Areas that were given priority included those underlain by Tertiary sedimentary rocks and acid intrusions, fluorite-bearing granitic rocks, Paleozoic black shale units and Precambrian sedimentary rocks, (Fig. 46.1).

Waters were collected unfiltered and shipped unacidified to the Geological Survey laboratories in Ottawa where they were subsequently analyzed for Zn, Cu, Pb, (M1BK - extraction of APDC complexes followed by AAS determination), Fe, Mn (direct aspiration AAS), U (fluorimetric), F, Cl, SiO_2 and $SO_4^=$.

Results and Discussion

Results for truck mounted reconnaissance traverses are presented in tabular form according to NTS map-sheet number. More detailed stream drainage basin studies are described in both tables and figures.

Table 46.1 summarizes results for stream and spring waters from a number of different locations in southern Yukon. Quick inspection of the data suggests that of the elements studied U, F and Zn would appear to be immediately useful in defining anomalous areas with Cu and S (as $SO_4^=$) proving useful under certain conditions of hydrogeochemistry. Tables 46.2 and 46.3, present data which further support this contention. Underlined values are considered anomalous.

Stream sediment data, which are used here merely to illustrate the coincidence of certain types of element anomalies within water samples, will be the subject of a later, more detailed discussion (Jonasson and Gleeson, in prep.).

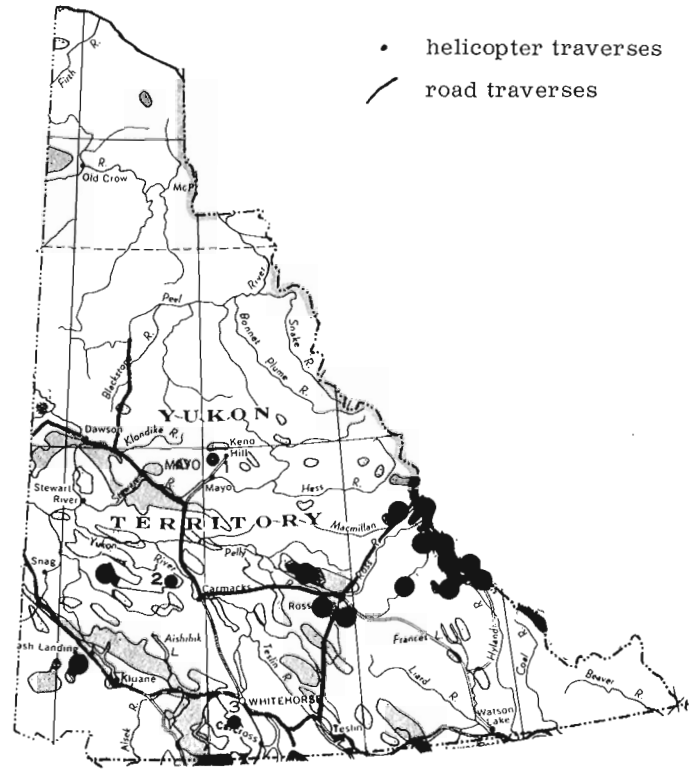

Figure 46.1. Sample location map.

Faro area (105 K)

Although one sample of a spring water at Mt. Mye revealed little of significance, the Cretaceous granites of this region remain of interest in prospecting for uranium.

Flat Lake area (105 I)

In this area pyritic Ordovician shales and baritic Devonian shales have been described by Blusson (1976). Zinc occurrences are also known. The single water sample collected in a narrow gorge which cuts through these rocks strongly indicated the presence of Zn, Fe and sulphides. U and F are low, a feature which proved to be uncharacteristic of waters draining similar rocks elsewhere. It is worth noting that pH is generally around 7.5 in such settings. The ubiquitous presence of carbonate in rocks of all types has a dominant influence on the water chemistry and therefore supports the dispersion of Zn and U at the expense of elements such as Cu, Pb or Ag. High values for Fe and Mn accompanying high Zn and U should be interpreted in

[1] C.F. Gleeson, Consultant, 764 Belfast Road, Ottawa.

From: Report of Activities, Part C;
Geol. Surv. Can., Paper 76-1C (1976).

Table 46.1

Spring and Stream waters from parts of the southern Yukon

NTS	Sample	Type	pH	F	SiO_2	Cl	Mn	Fe	Cu	Zn	Ag	Pb	U	$SO_4^=$	Comments
105 K	74.3057	SPWT	7.37	108	5.00	0.19	2.5	5.0	0.2	1.0	0.2	1.3	0.80	8.0	Faro area
105 I	74.3087	STWT	7.60	55	1.35	0.29	2.5	26.8	0.2	86.0	0.2	1.3	0.20	22.7	Creek into Flat Lake
105 O	75.3089	STWT	3.72	65	3.28	0.38	43.8	699	37.5	26.5	0.2	1.3	2.00	33.1	Tom Creek (Fig. 46.2)
105 O	75.3090	STWT	4.55	29	3.55	0.12	19.8	8.4	4.4	3.1	0.2	1.3	0.42	6.4	Tom Creek
105 O	75.3091	STWT	3.77	56	3.15	0.19	38.6	279	47.8	68.0	0.2	1.3	1.38	31.1	Tom Creek
105 O	75.3092	STWT	3.84	110	2.80	0.12	58.9	797	64.0	234	0.2	1.3	1.66	40.3	Tributary Tom Creek
105 O	75.3093	SPWT	5.18	315	3.51	0.11	882	867	1150	4250	0.2	16.7	12.20	164	Tom Adit flow
105 O	75.3094	STWT	5.07	28	1.91	0.12	19.3	5.0	6.5	20.5	0.2	22.5	0.22	5.3	Tributary Tom Creek
105 O	75.3096	STWT	5.89	115	2.50	0.10	31.9	63.2	2.0	101	0.2	1.3	0.64	34.0	South MacMillan River 8 miles downstream
115 P	75.3137	STWT	6.20	145	5.91	0.12	2.5	5.0	0.2	1.0	0.2	1.3	0.44	17.2	Henry Gulch
115 P	75.3138	STWT	6.35	120	3.82	0.05	26.2	1291	5.5	1.5	0.5	1.3	0.34	12.9	Clear Creek
115 P	75.3139	STWT	6.40	112	4.41	0.10	2.5	8.1	0.2	1.0	1.0	1.3	0.40	42.3	Barlow Creek
116 B	75.3149	STWT	7.21	115	2.05	0.05	2.5	5.0	0.2	18.5	0.2	1.3	0.24	65.2	East Blackstone River
116 B	75.3150	STWT	7.13	74	3.12	0.05	2.5	5.0	0.2	11.0	0.5	1.3	0.14	24.0	North Klondike River
116 G	75.3140	STWT	6.62	275	2.01	4.00	2.5	125	0.2	57.0	0.5	1.3	4.60	115	Big Creek at Ogilvie River
116 G	75.3141	STWT	6.77	375	2.40	3.25	65.2	818	0.2	206	0.2	1.3	6.40	141	Big (Engineer) Creek
116 G	75.3143	SPWT	6.86	1175	5.70	112	7.7	11.2	0.2	6.0	0.2	1.3	2.40	372	Sulphur spring, Big Creek
116 G	75.3144	SPWT	6.61	700	1.75	0.43	543	1753	0.2	684	0.2	1.3	0.70	308	Iron springs, Big Creek
116 G	75.3145	STWT	6.91	350	2.50	3.25	58.4	660	0.8	98.5	0.2	1.3	7.20	158	Big Creek
116 G	75.3146	STWT	6.98	460	2.92	3.63	119	2368	0.5	256	0.2	1.3	4.80	199	Red Creek at Big Creek
115 G	75.3182	STWT	6.93	165	2.85	0.05	2.5	51.2	0.2	0.5	0.2	1.3	1.80	15.5	Amphitheatre Mountain

Notes:
1. SiO_2, Cl^- and $SO_4^=$ are in ppm; others are in ppb.
2. STWT = stream water, SPWT = spring water
3. Underlined values are considered worthy of comment
4. Detection limits for certain elements in this and the other tables are as follows (ppb):

   Mn = 0.5 Fe = 10.0 Cu = 0.5 Zn = 1.0 Ag = 0.4 Pb = 2.5

terms of originating from a common source rather than as controlling the mechanical dispersion of each metal by some adsorptive process. Elevated sulphate values generally accompany the metals under these conditions.

MacMillan Pass area (105 O)

In this area seven water samples were collected from terrain underlain mostly by Upper Devonian black shales. The area is best known for the presence of a bedded Pb-Zn-barite deposit (TOM, Hudson Bay Mining and Smelting Co.) which reportedly contains 10 million tons of 15 per cent Pb-Zn.

Samples were taken from Tom Creek and its tributaries, all of which drain through the zone of known mineralization (Fig. 46.2). One sample was collected from the South MacMillan River about eight miles downstream from the confluence of Tom Creek.

The main feature of the data lies in the record of very acidic pH values, presumably a result of oxidizing pyrite within the sulphidic shale units and the ore body itself. Sampling of Tom Creek was restricted to tributaries and upstream from an adit and rubble piles. Below this point, fresh metal-rich iron oxide precipitates have contaminated the stream bed to such an extent that iron stains persist for several miles down the South MacMillan River.

Further descriptions of the mineralization at Tom Creek and of the effects of acid waters on geochemical sediment surveys can be found in Fletcher and Doyle (1974).

The effects of acidic stream waters are apparent. All waters contain high levels of Mn, Fe, Cu, Zn, $SO_4^=$, as well as some local highs of U and Pb. Iron oxide-charged waters (3093) gushing from an adit on the property are loaded with high quantities of all the elements noted above. It is interesting to observe that pH is actually lower above the adit than below it perhaps due to increased amounts of carbonate in the ores. It is also lower at stream sites which are updrainage from the strike of known mineralization. It is possible that the ore zone is more widely distributed than previously recognized. As might be expected, the acid waters have caused a marked depletion of some metal levels in the fine stream silts (-80 mesh). Zn ranges from 5 to 57 ppm, Pb from 51 to 358 ppm, U from 3.5 to 6.5 ppm, Cu from 16 to 77 ppm and Ag from 0.9 to 4.0 ppm.

Zn in stream silts from such an environment is clearly not a good indicator element — the more immobile Pb and Ag may offer a better contrast between mineralized zones and barren zones. It is clear however that water analyses provide a very useful clue to the presence of Pb-Zn black shale-hosted mineralization at Tom Creek. It is also clear that further work is required to characterize the chemical controls operating on the waters of this stream system.

The hydrogeochemistry of this system will be discussed in detail in a future publication. Uranium, as at Flat Lake, is present in both stream waters and sediments and its increased abundance is reflected in certain metaliferous pyritic black shales. It is possible that such rocks could host a large tonnage of low

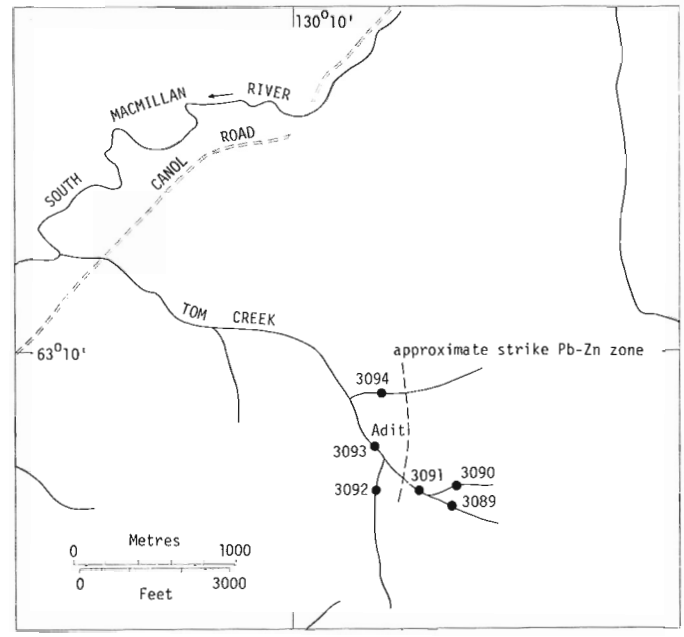

Figure 46.2. Tom Creek (105 O/1). Waters and sediments.

grade U minerals in similar rocks elsewhere in the Yukon, particularly where other metals such as P, V, Mo, Zn are also abundant.

The water sample (3096) taken from the south MacMillan River about eight miles downstream indicates than an acid pH is maintained (5.9). The presence of high Zn, Fe, U(?), Mn and $SO_4^=$ suggests two possibilities; that the dispersion of acid waters from TOM is indeed spread over eight miles, or that there are some metal-rich sources contributing within the intervening distance.

The "immobile" element Cu is depleted in the water (3096) suggesting that the source is not close by. On the other hand, the sediment contains significant quantities of Zn (610), Pb (60), Ag (1), U (10.7), Cu (77) and low Fe (3.69%). The last value suggests that iron precipitates have not been primarily responsible for transporting the other metals to this site; i.e., solution transport is the likely pathway. Under these circumstances, it is advisable to collect both sediments and waters in order to appreciate more fully the nature and extent of the metal dispersion patterns.

Clear Creek area (115 P)

Work centred on Henry Gulch because of a report that an airborne radiometric anomaly was related to uranium mineralization in a coarse grained granite (Barlow dome area). In 1975 some 200 claims (Ura) were staked by Beach-gold Mines (Northern Miner; July 24, 1975) to cover this anomaly.

Table 46.1 indicates that U was present in stream waters at background levels only. Waters showed pH at levels typical of granite terrain and metal levels were considered low except for a small Cu (Fe and Mn)

feature in Clear Creek. This may be a result of the fact that Clear Creek was very muddied from upstream gold placer operations.

Fluoride levels were elevated but are likely typical of streams within such terrain. Stream sediments confirmed the relative absence of U in the area (unless it is at depth in a deeply-leached profile). U ranged from 4.0 to 5.3 ppm.

South Dempster Highway (116 B)

Two stream waters, one from the East Blackstone River and another from the North Klondike River, were sampled. Aside from a small Zn anomaly there was little of interest in them. The fact that sulphate contents are also elevated to match Zn suggests that Ordovician black shales in the area may well be the source rocks. Zn also appears in the stream sediments (275 140 ppm).

Table 46.2

Stream waters from NTS 105 F: McConnell River and Bacon Creek areas (Pelly Mountains)

Sample	pH	F	SiO_2	Cl	Mn	Fe	Cu	Zn	Ag	Pb	U	$SO_4^=$	Comments
75.3051	7.01	155	4.58	0.10	2.5	9.4	0.2	0.5	0.2	1.3	34.0	340	Glacier Cr, Canol Road
75.3058	7.48	155	1.65	0.05	2.5	9.4	0.2	1.0	0.2	1.3	1.18	11.0	McConnell River (Fig. 46.3)
75.3059	7.44	212	2.30	0.05	2.5	6.3	0.2	0.5	0.2	1.3	1.28	10.0	McConnell River
75.3060	7.50	218	2.40	0.05	2.5	5.0	0.2	0.5	0.2	1.3	1.22	10.4	McConnell River
75.3061	7.50	370	3.25	0.05	2.5	5.0	0.2	1.2	0.2	1.2	0.78	63.5	McConnell River
75.3062	6.51	120	2.50	0.19	2.5	12.2	0.2	1.2	0.2	1.3	1.52	34.4	McConnell River
75.3063	7.66	94	2.20	0.05	2.5	5.0	0.5	0.5	0.2	1.3	1.02	21.2	White Creek
75.3064	7.75	142	2.60	0.10	2.5	5.0	0.2	1.2	0.2	1.3	1.32	32.5	McConnell River
75.3065	7.80	69	2.12	0.05	2.5	5.0	0.2	0.5	0.2	1.3	1.30	21.1	White Creek
75.3066	7.87	46	2.05	0.29	2.5	5.0	0.2	0.5	0.2	1.3	0.66	16.8	White Creek
75.3067	7.87	36	2.00	0.29	2.5	5.0	0.2	0.5	0.2	1.3	0.58	11.5	White Creek
75.3068	7.86	59	2.12	0.10	2.5	5.0	0.2	0.5	2.0	1.3	1.40	32.0	White Creek
75.3069	7.93	51	1.98	0.10	2.5	5.0	0.2	0.5	1.5	1.3	1.48	42.5	White Creek
75.3070	8.08	57	2.19	0.19	5.7	6.9	0.2	0.5	0.2	1.3	1.22	33.9	McConnell River
75.3071	8.08	115	2.70	0.19	2.5	5.0	0.2	0.5	0.2	1.3	1.20	43.5	McConnell River
75.3072	8.13	57	2.39	0.19	2.5	5.0	0.2	0.5	0.2	1.3	0.98	30.3	McConnell River
75.3073	8.02	205	2.26	0.19	2.5	5.0	0.2	0.5	0.5	1.3	1.34	98.0	McConnell River
75.3074	8.09	112	2.65	0.05	6.2	8.4	0.2	0.5	1.2	1.3	0.78	37.9	McConnell River
75.3075	8.08	200	2.80	0.10	6.9	5.0	0.2	0.5	0.2	1.3	0.44	58.7	McConnell River
75.3076	809	67	2.59	0.10	2.5	5.0	0.2	0.5	0.2	1.3	0.96	27.5	McConnell River
75.3077	8.27	82	2.12	0.10	2.5	5.0	0.2	0.5	0.2	1.3	0.62	15.0	McConnell River
75.3078	7.92	69	2.85	0.19	2.5	5.0	0.2	0.5	0.2	1.3	0.54	10.0	Bacon Creek (Fig. 46.4)
75.3079	7.89	70	3.25	0.19	2.5	5.0	0.2	0.5	0.2	1.3	0.28	7.1	Bacon Creek
75.3080	8.23	34	2.30	0.29	2.5	5.0	0.2	0.5	0.5	1.3	0.26	6.4	Bacon Creek
75.3081	8.15	42	2.00	0.29	2.5	5.0	0.2	0.5	0.2	1.3	0.30	6.1	Bacon Creek
75.3082	8.00	48	2.25	0.10	2.5	5.0	0.2	0.5	0.5	1.3	0.34	9.6	Bacon Creek
75.3083	7.93	53	2.55	0.29	2.5	6.9	0.5	0.5	0.2	1.3	0.64	9.2	Bacon Creek
75.3084	7.67	65	2.60	0.10	2.5	7.6	0.2	0.5	0.2	1.3	0.82	12.5	Bacon Creek
75.3085	7.83	64	2.71	0.05	2.5	11.1	10.7	0.5	0.2	1.3	0.58	10.2	Bacon Creek

Notes:
1. SiO_2, Cl^- and $SO_4^=$ are in ppm; others are in ppb.
2. Underlined values are considered worthy of comment.

The pH of the waters is considered normal and U levels are also regarded as normal. The latter are matched by values of U at 4.4 and 4.6 ppm from a shaley sediment. Water-borne Zn could be used in this terrain as a prospecting aid for bedded Pb-Zn ores.

Central Dempster Highway (116 G)

In this area sampling centred around an outstanding geochemical feature along Big (Engineer) Creek which drains to the Ogilvie River. Seven water samples from springs and streams were collected. The area is underlain predominantly by sediments (shales and carbonates) of the Ordovician Road River Formation.

Stream sediments in Big Creek from Red Creek to Ogilvie River, a distance of fifteen miles, are stained extensively with red iron oxides originating from the oxidation of pyritic black shales. Waters were slightly acidic in spite of the local presence of considerable amounts of carbonates interbedded with black shales. They contain above normal quantities of Zn, Fe, Mn, F, Cl, $SO_4^{=}$ and U in steadily decreasing levels from Red Creek to the Ogilvie River.

At Red Creek there are two springs perhaps 100 feet apart, one precipitating sulphur and relatively devoid of metal ions but rich in anionic species such as $SO_4^{=}$, Cl^-, F^- and silicate, the other precipitating iron oxides and which is relatively enriched in Zn, Fe, Mn but poor in Cl^-, F^- and silicate. U is richer in the sulphur spring; anionic complexes of fluoride or carbonate (not determined) may be responsible for this. Undoubtedly there is a source of heavy metals within the shales contributing these high levels and further study is clearly warranted.

However, the presence of these metals provides some opportunity to look into the processes of water-borne uranium dispersion.

The two springs are prime sources of the elements found farther down Big Creek. U remains roughly constant, as do Cl^-, F^- and $SO_4^{=}$ over the fifteen miles to the Ogilvie River. On the other hand, Zn and Fe fall off quite noticeably. These observations support the contention that anionic complexes, probably of UO_2^{++} are likely involved in the transportation of U. The same patterns are reflected in the sediments for Fe, Zn, but U also tends to decline from source area (18 ppm) to sink (9.5 ppm). Moreover U levels are higher in the precipitates of the iron spring (26 ppm) than in those from the sulphur spring (5.7 ppm). Thus, precipitating iron oxides have a definite scavenging effect on water-borne U but it certainly is not overwhelming as evidenced by the persistent U in water dispersion down river.

Amphitheatre Mountain (115 G)

One water sample was collected from an area underlain by Tertiary sandstones, conglomerates and coal measures. It contains above normal Fe, F and U. Matching stream sediments yielded U in the range 2.5-3.6 ppm; similar values to those found in the rocks and coal themselves. There appears to be little U present in these formations.

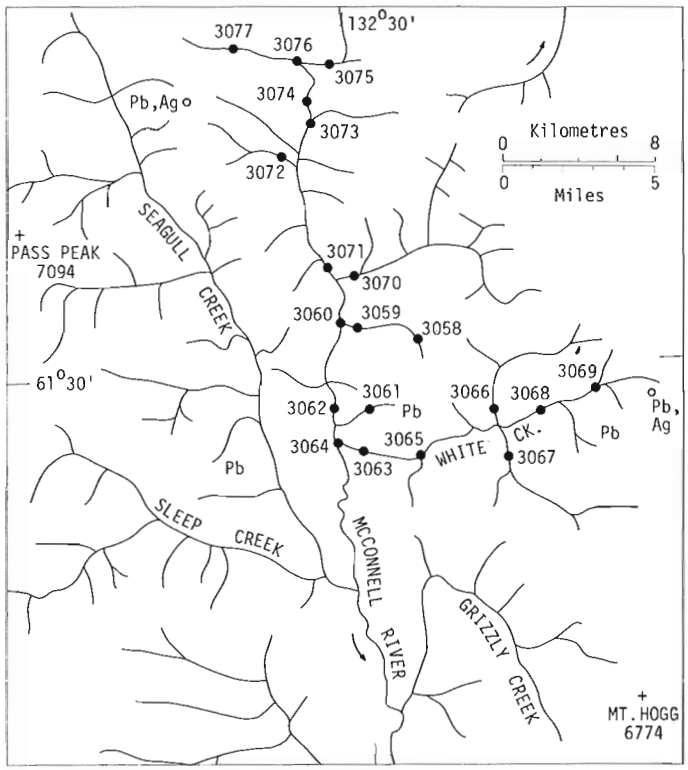

Figure 46.3. McConnell River-White Creek (105 F/7-10). Waters and sediments.

McConnell River area (105 F)

Table 46.2 presents a summary of the water chemistry of the McConnell River drainage basin, (Fig. 46.3). The area was systematically sampled using a Hughes 500C helicopter and landing in the stream beds where possible. It was selected because of the presence in the region of fluorite-bearing syenitic rocks of Mississippian age. There are also a number of small occurrences of galena which commonly are found in quartz-fluorite veins within the syenite.

The pH of the water samples is generally in the range 7.44 to 8.27, except in the upper McConnell River where it is 6.51. This value is supported by an elevated Fe level (12.2 ppm) and suggests an Fe sulphide source nearby. However, in general, pH would seem to be controlled by carbonate which is present in veins everywhere. Alkaline pH would be expected to restrict dispersion of Fe, Pb, Ag and Cu, and this does appear to be so. Occasional appearances of Ag in White Creek are worth a second look as they seem to reflect known showings of galena in the area.

Strong relationships between F(?), $SO_4^{=}$ and U are recognizable especially in upper tributaries where Pb veins and fluorite can be found. The mineralogical relationship of U to these elements is at present uncertain. Analyses of stream sediments confirm the validity of the water-borne anomalies. Pb, Zn, Fe, Mn and U show coincident anomalies in the upper reaches of the McConnell River whilst the Ag anomaly on White Creek is reinforced by above normal Cu and Pb in sediments.

Table 46.3

Stream water samples from NTS 115 J: Nisling River and Klotassin River areas (Dawson Ranges)

Sample	pH	F	SiO_2	Cl	Mn	Fe	Cu	Zn	Ag	Pb	U	$SO_4^=$	Comments
75.3161	7.50	210	3.62	0.05	2.5	5.0	0.2	3.9	0.5	7.5	0.14	1.6	All samples are from two stream systems which drain to the Klotassin River and Nisling River respectively (Fig. 46.5).
75.3162	7.40	235	5.39	0.25	2.5	10.3	0.2	1.0	0.2	1.3	1.26	1.6	
75.3163	7.40	315	5.00	0.19	2.5	12.8	0.2	3.5	0.2	1.3	0.94	3.1	
75.3164	7.27	225	5.39	0.10	2.5	28.1	0.2	0.5	0.2	1.3	0.48	4.6	
75.3165	6.98	365	5.55	0.10	2.5	14.3	0.2	0.5	0.2	1.3	1.18	2.7	
75.3166	6.96	640	5.60	0.19	2.5	10.3	0.2	0.5	0.5	1.3	0.86	2.7	
75.3167	6.96	460	5.91	0.10	2.5	16.5	0.2	0.5	0.2	1.3	1.24	3.5	
75.3168	6.96	975	6.50	0.05	2.5	25.6	0.2	0.5	0.2	1.3	0.98	7.1	
75.3169	6.88	580	5.81	0.10	2.5	13.4	0.2	0.5	0.2	1.3	1.60	3.5	
75.3170	6.98	385	5.55	0.19	2.5	9.7	0.2	0.5	0.2	1.3	0.10	5.5	
75.3171	7.00	650	6.03	0.05	2.5	17.1	0.2	0.5	0.2	1.3	0.54	3.5	
75.3172	7.04	450	5.75	0.10	2.5	11.9	0.2	0.5	0.2	1.3	0.34	2.5	
75.3173	7.00	740	6.35	0.12	2.5	14.7	0.2	1.0	0.2	1.3	0.46	3.4	
75.3174	7.06	640	6.71	0.10	2.5	19.1	0.2	2.5	0.2	1.3	0.24	1.8	
75.3175	7.05	670	4.50	0.10	2.5	6.7	0.2	3.2	0.2	1.3	0.18	2.5	
75.3176	7.00	750	4.91	0.10	2.5	5.0	0.2	2.0	0.2	1.3	0.26	2.0	
75.3177	6.95	910	4.75	0.05	2.5	5.0	0.2	3.1	0.2	1.3	0.40	1.5	
75.3178	6.80	940	3.31	0.05	2.5	6.4	0.2	5.0	0.2	1.3	5.80	2.3	
75.3179	6.93	1000	4.70	0.10	2.5	5.0	0.2	3.5	0.2	1.3	1.12	2.3	
75.3180	6.97	860	4.95	0.05	2.5	10.7	0.2	0.5	0.2	1.3	0.78	2.5	
75.3181	6.96	780	4.39	0.05	2.5	13.9	0.2	0.5	0.2	1.3	1.24	5.2	

Notes: 1. SiO_2, Cl^- and $SO_4^=$ are in ppm; others are in ppb.
2. Underlined values are considered worthy of comment.

U ranges from 6.0 to 12.3 ppm over a background of about 3 ppm. Within the McConnell River system, some samples of syenites, in places fluoritic, contained U between 13.9 and 25.7 ppm. The same samples were also anomalous in Pb and Zn. Quartz veins with visible galena contained much less U at about 5 ppm.

Bacon Creek area (105 F)

The Bacon Creek drainage is underlain by late Precambrian (Windemere) phyllitic rocks and quartzites. Eight waters were sampled (Fig. 46.4). The pH of waters is generally alkaline in the range commonly buffered by carbonate equilibria. Uranium content is quite low averaging about 0.5 ppb. Fluoride is also low as is sulphate. Except for one sample in the lower reaches of Bacon Creek which contains a little Fe (11.1 ppb) and an unusual quantity of Cu (10.7 ppb), the data of Table 46.2 are relatively featureless. It is suggested that because of the alkaline pH (7.83) of this sample, the Cu source is likely nearby. This section of the Windemere does not appear to be promising for the discovery of U occurrences by hydrogeochemistry. The absence of indicator elements is also discouraging although some rocks samples were found to contain up to 22.5 ppm U.

Nisling River — Klotassin River area (115 J)

Twenty-one water samples were collected (Fig. 46.5). The sample area is underlain by a Tertiary miarolitic granite in which fluorite and molybdenite occur. The area forms part of the Dawson Ranges and is unglaciated, a fact of some geochemical significance. The first point of interest is the virtually invariable pH value which is always close to 7.00. Carbonate is apparently not present in the rocks and this is reflected in the near neutral pH levels of drainage waters. Thus low values for U are to be expected. Normal levels would seem to be around 0.5 ppb with anomalous levels reaching 5.80 ppb. Fe levels are surprisingly high, perhaps an indicator of the presence of considerable amounts of nontronite, a ferrous montmorillonite, in the exposed granites. In places, extensive iron staining is visible. Fluoride is abnormally high everywhere and reaches 1000 ppb. These are matched by high silicate concentrations. Thus, although carbonate is probably insignificant as a transporter of U and $SO_4^{=}$ is very low, F^- is possibly the prime mobilizing agent for U (as UO_2^{++}). The only other feature in the water data is one pair of above normal Pb and Zn analyses. By contrast, the stream sediments contained between 13.8 and 33.8 ppm U in anomalous zones. The water-borne anomalies observed are matched by sediment U, but perhaps the best indication of U presence is with F. Analysis of granitic chips in these areas reveals little or no U. There seems to be no other elemental associations of possible significance.

The fact that the sample area is unglaciated may well be an important reason for the absence of surface indications of radioactivity. Deep leaching or weathering

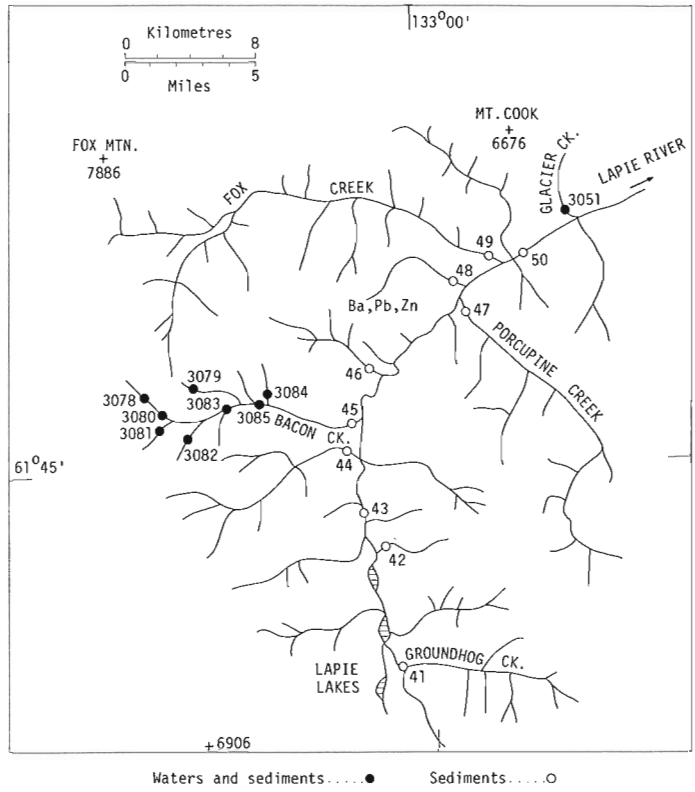

Figure 46.4. Bacon Creek-Lapie River (105 F/14).

of surface rocks has probably removed much of the radioactivity which might be expected from granites which yield U in such significant quantities in stream sediments. U is clearly present but is in complete disequilibrium with its radioactive daughters. A search for and sampling of fissure waters, seeps or springs for U and F in combination with stream sediment surveys seems to be the best approach to prospecting in such terrain. Targets would include zones of secondary enrichment as well as radioactive fluorite granites, syenites and alaskites.

Conclusions

Areas of potential interest can be outlined by water surveys using U, F, Zn and $SO_4^{=}$ in any combination. U itself is obviously the best indicator of U mineralization but the apparent close association between U and F strongly promotes the use of F as well. Measurements of pH and Fe are valuable for interpretative purposes; clues to the presence of oxidizing sulphides and knowledge of adsorption controls on dispersion processes for U would be the main benefits. Background levels for U in waters from all regions studied are generally in excess of 0.5 ppb, a convenient level for rapid routine analysis. Levels of F under normal conditions usually are greater than 50 ppb which puts them into the most useful range of a fluoride electrode. Anomalous levels for Zn are often in excess of 5 ppb over a background of 0.5-1.5 ppb depending on local geology.

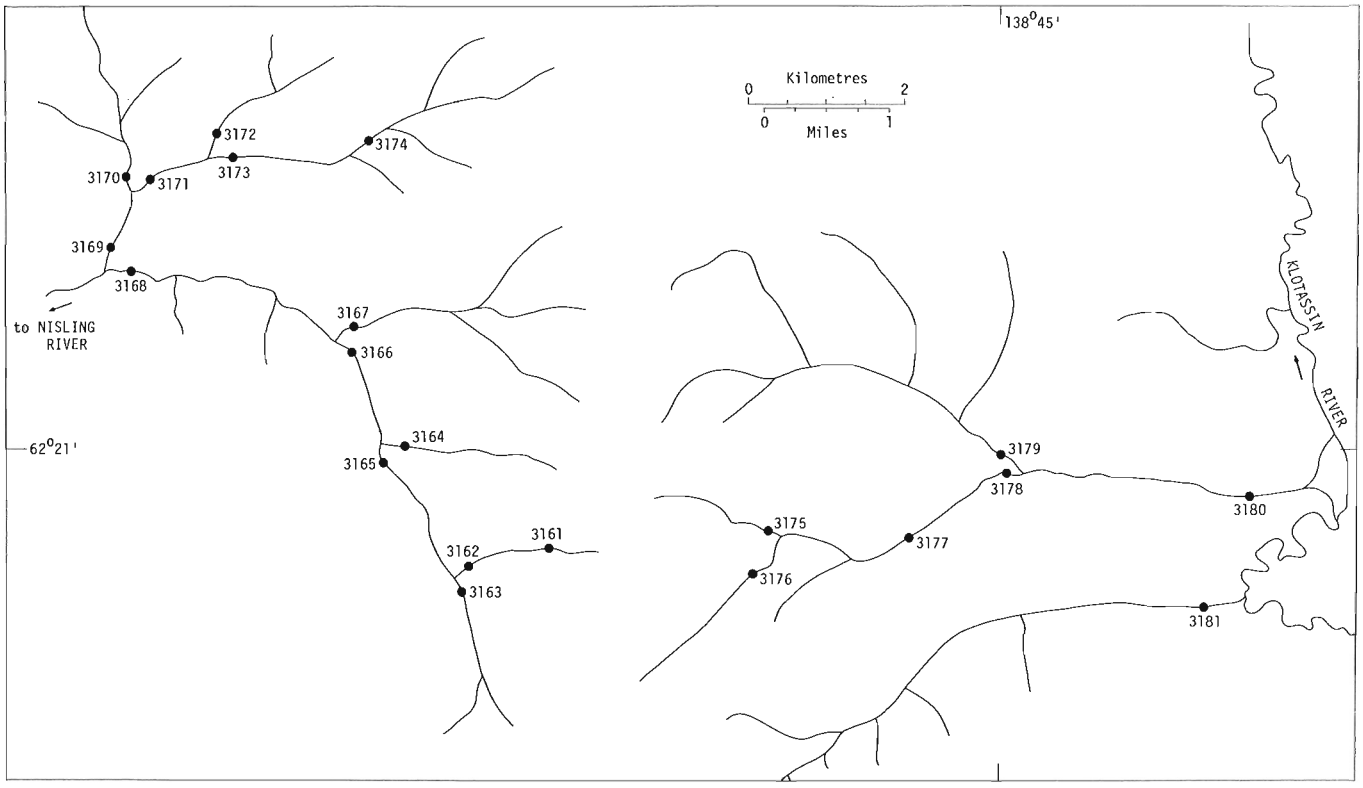

Figure 46.5. Nisling River-Klotassin River (115 J/7). Waters and sediments.

Analysis for $SO_4^{=}$ at the prospecting level, especially in areas underlain by black shales, may become a useful adjunct to data from Zn and U analyses.

Cu dispersion, normally severely limited by alkaline pH, can become useful when pH falls below 6. Analysis for Cu is not recommended under other conditions except in very local work when its presence may indicate proximity of source mineralization. Similar comments apply to Pb in waters.

References

Blusson, S.L.
1976: Selwyn Basin, Yukon and District of Mackenzie; *in* Report of Activities, Part A., Geol. Surv. Can., Paper 76-1A, p. 131-132.

Fletcher, K. and Doyle, P.
1974: Factors influencing trace element distribution in the Eastern Yukon. Can. Min. Metall., Bull., v. 67(741): p. 61-65.

47. WELL WATER URANIUM RECONNAISSANCE, SOUTHWESTERN SASKATCHEWAN

Project 720067

W. Dyck,[1] S.H. Whitaker,[2] and R.A. Campbell[1]

Introduction

The geological similarities of the Cypress Hills, Saskatchewan and the Gas Hills, Wyoming areas have long been used to postulate the existence of uranium deposits in the first area similar to those in the Gas Hills. Uranium-enriched coal and lignite seams (Cameron and Birmingham, 1970), not unlike those in the Dakotas (Denson and Gill, 1965; Deuson, *et al.*, 1959), and radioactive fossil bones (Bell, *et al.*, 1976) in the Cypress Hills lend further support to this hypothesis. However, extensive overburden has made it difficult or impossible to detect uranium mineralization in bedrock by the conventional scintillometer tests of outcrops. Wells penetrate the overburden in many places and therefore can serve as windows to see deeper. The well water orientation survey carried out in the Carboniferous basin of Eastern Canada (Dyck, *et al.*, 1976) has proven to be useful in detecting U and other mineralization.

The orientation survey described in this report, a joint venture of the Geological Survey of Canada, the Saskatchewan Geological Survey, and the Saskatchewan Research Council, is funded by the newly established Federal-Provincial Uranium Reconnaissance Program (Darnley, *et al.*, 1975). The purpose of the survey is to determine regional trends in the U content of groundwater, and by relating these trends to known mineral occurrences, to determine whether such surveys are useful for prospecting.

This report presents some field and field laboratory results obtained mainly from the northeast quarter of map-area 72F and draws tentative conclusions from these results. Complete synthesis of all data including the dissolved gases He and CH_4, other trace elements, and minor constituents will be presented at a later date.

Sampling and Analytical Procedures

Approximately 940 well and 60 spring water samples were collected from a 17 900 km^2 (6900-square miles) area bounded by boundaries of maps 72F, 72K/1, and 72K/2. On the average, one site per 13 km^2 was sampled where possible. Depth of well and type of pressure system and material were recorded where available.

In the field laboratory, set up in the skating rink in the town of Eastend, the samples were analyzed for U, Rn, F, O_2, Eh, pH, alkalinity, and conductivity. U was analyzed by the fluorimetric method without removal of U quenching components. Rn was determined by degassing an 120-ml aliquote into a ZnS (silver activated) cell and measuring the alpha particel emanation rate with a Rn counter. Alkalinity was determined by titrating a 25-ml aliquote to a pH of 4.65 with 0.01N H_2SO_4. F, O_2, Eh, pH, and conductivity were measured with appropriate electrodes. To check on the sampling and analytical precision of the results there was inserted in every group of 17 samples one blank (distilled water), one reference (home-made trace element standard mixture) and one unknown duplicate sample.

Results and Discussion

The ranges of the variables and estimates of backgrounds are listed in Table 47.1. While the U values are appreciably higher and the Rn values lower than those encountered in the Carboniferous basin of Eastern Canada (Dyck, *et al.*, 1976), they are still much lower than the 18 000 ppb U observed in the U ore-bearing Morrison Formation of the Colorado Plateau (Phenix, 1960), or the 200 000 pc/1 Rn observed by Harshman in the U-bearing district of Wyoming (Harshman, 1968). Admittedly such highs reflect ore grade environments, hence none of the samples collected in this survey likely came from ore grade environments.

The U and Rn distribution in wells of the northwest quarter of map-area 72F is shown in Figures 47.1 and 47.2 respectively. The geological information for these figures was taken from Whitaker (1966). Contour levels were estimated from the values in Table 47.1. This map-area was sampled earlier in the season. It is the most interesting section geologically and also turned out to be the most populated area of map-area 72F, thus a fairly uniform sample density of 1 per 13 km^2 could be achieved over most of it. As was discovered during the rest of the season, the remainder of map-area 72F

TABLE 47.1

Ranges and estimated background modes of variables determined in the field

Variable	Dimensions	Range	Background
U	ppb	0.00 – 240.00	0.5
Rn	pc/1	0.00 – 4135.00	250.0
Depth	m	2.00 – 457.00	15.0
F	ppm	0.00 – 4.10	0.2
O_2	ppm	0.40 – 14.00	3.0
Eh	mv (H_2el.)	-127.00 – 906.00	400.0
pH	–	4.86 – 8.82	7.6
Total Alkalinity	ppm ($CaCO_3$)	8.00 – 1867.00	300.0
Conductivity	μ mhos/cm	110.00 – 8300.00	900.0

[1]Geological Survey of Canada, Ottawa, Ontario.

[2]Saskatchewan Research Council, Saskatoon, Saskatchewan.

From: Report of Activities, Part C;
Geol. Surv. Can., Paper 76-1C (1976)

Figure 47. 1.

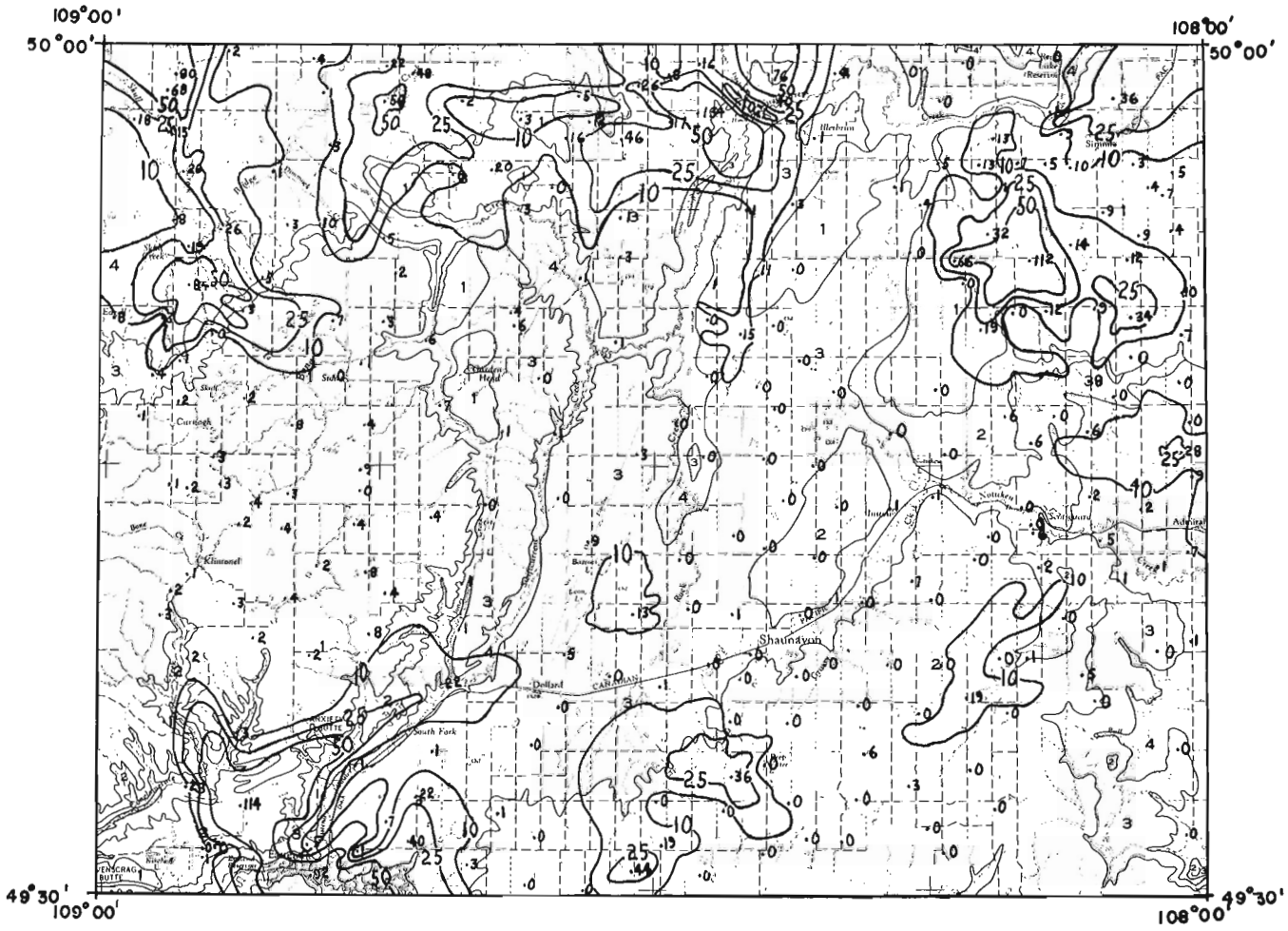

FORMATIONS

1	CYPRESS HILLS
2	RAVENSCRAG
3	FRENCHMEN,BATTLE,WHITEMUD,EASTEND
4	BEARPAW,JUDITH RIVER

Geology by S. Whitaker

0 Kilometers 15

0 Miles 8

URANIUM .X ppb ~5~

Figure 47. 2.

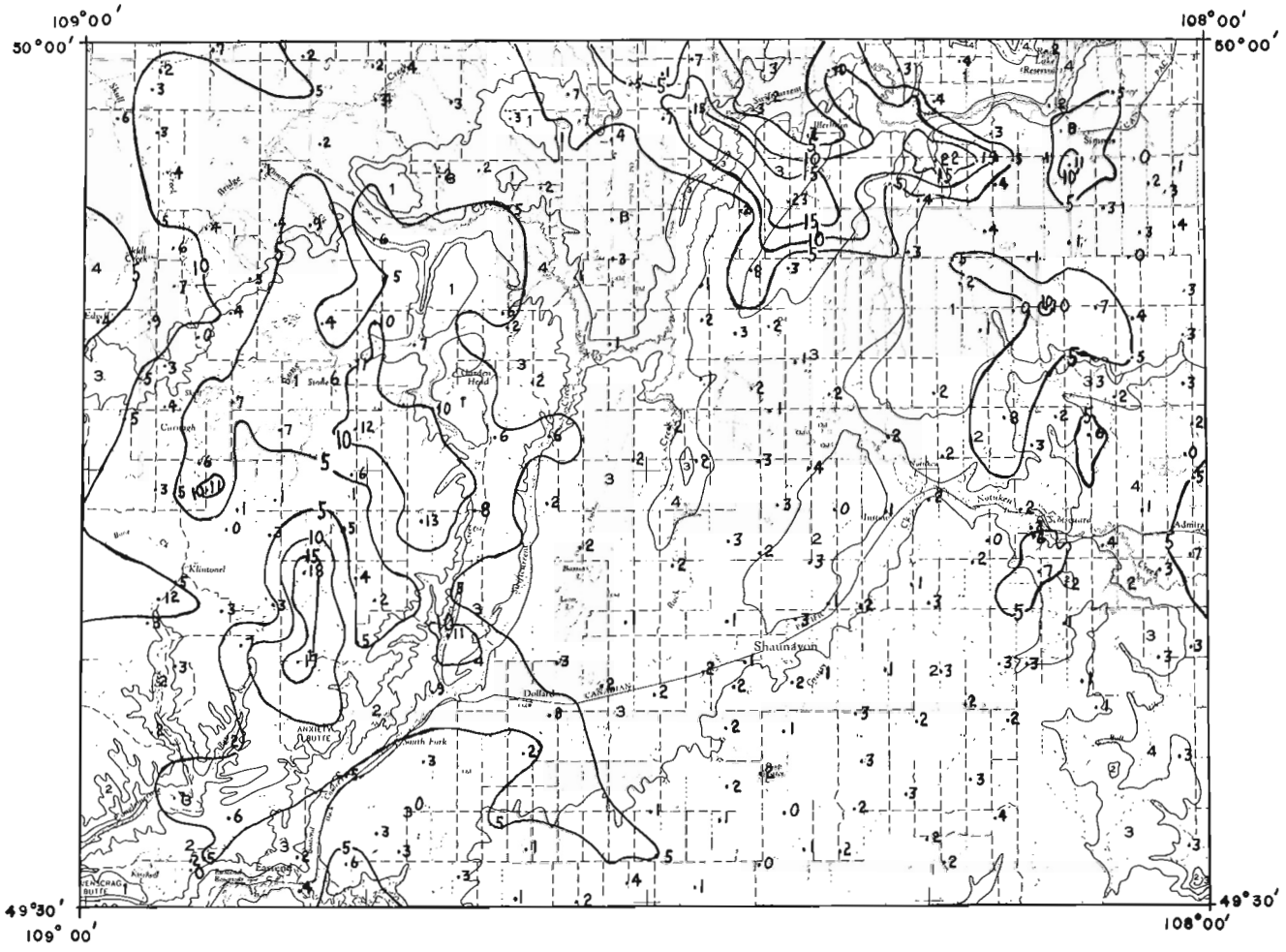

FORMATIONS

1	CYPRESS HILLS
2	RAVENSCRAG
3	FRENCHMEN,BATTLE,WHITEMUD,EASTEND
4	BEARPAW,JUDITH RIVER

Geology by S. Whitaker

0 Kilometers 15

0 Miles 8

RADON .X pc/l/100

TABLE 47. 2

Comparison of Uranium, Radon and Depth By Rock Formation

A – 12 Deepest Wells compared to 12 Shallowest Wells

Rock Formation	DEEPEST						SHALLOWEST						"t"[1]			PROBABILITY[2]		
	Depth		Uranium		Radon		Depth		Uranium		Radon							
	$\bar{X}$	S	$\bar{X}$	S	$\bar{X}$	S	$\bar{X}$	S	$\bar{X}$	S	$\bar{X}$	S	Depth	U	Rn	Depth	U	Rn
Cypress Hills	62.8	11.3	3.8	4.8	493	562	11.7	6.7	20.9	30.9	405	363	13.5	-1.89	0.46	0.00	0.07	0.75
Ravenscrag	92.2	29.3	1.1	2.9	310	229	14.3	5.3	11.0	15.0	564	1135	9.06	-2.23	-0.76	0.00	0.03	0.45
Eastend,Whitemud Frenchman	53.6	10.5	0.6	0.9	261	199	6.1	1.8	7.13	7.18	451	315	15.5	-3.12	-1.77	0.00	0.00	0.09
Bearpaw	54.5	26.7	7.1	11.3	285	123	5.3	1.6	22.2	26.9	521	259	6.38	-1.80	-2.76	0.00	0.08	0.01

B – 12 Highest U Sites compared to 12 Lowest U Sites

	HIGHEST						LOWEST											
Cypress Hills	28.2	15.1	30.1	30.9	578	420	53.8	23.5	0.4	0.9	255	159	- 3.17	3.33	2.50	0.00	0.00	0.02
Ravenscrag	24.4	19.0	31.4	31.4	650	1230	96.9	45.3	0.0	0.0	164	104	- 4.71	3.48	1.37	0.00	0.00	0.17
Eastend, Whitemud & Frenchman	24.3	23.0	50.7	33.8	429	419	48.2	28.5	0.5	0.9	326	209	- 2.27	5.14	0.76	0.03	0.00	0.45
Bearpaw	16.0	18.5	45.3	30.0	401	195	65.1	89.8	1.6	1.2	205	92	- 1.86	5.05	3.07	0.08	0.00	0.00

[1]"t" – Test of significance between means

[2]Probability – Of having "t" this large or larger by chance.

was much more sparsely populated with the result that fairly large holes in the sample site pattern are present. To make up for these, at least partially, certain areas were sampled in somewhat greater detail. No distinction has been made between wells and springs in these areas. Most of the springs were located near the edge of the Cypress Hills in the western part of map-area 72F. In general the chemical composition of such waters suggest that a spring can be equated with a shallow well.

Regionally the Rn highs are more closely associated with the Cypress Hills Formation than are the U highs. In the northeast corner of the sample area there is good agreement between the U and Rn highs; in the western part of Figures 47. 1 and 47. 2 the U is displaced to the north and south with respect to the Rn. The short range of Rn in the natural environment relative to U and the high relief in this area suggest that the Cypress Hills Formation is the source of much of this U, but it is migrating in the ground to lower elevations. In the northeast corner where relief is weak, Rn and U highs coincide. Leaching of radioactive lignite seams in the Ravenscrag and older formations by the highly alkaline waters must also contribute to high U values but the extent and location of these, other than at exposed river bank cuts, is not known. The two U anomalies in the southeastern part of Figure 47. 1 seem to be due to such leaching and concentration without an undue rise in the Rn level. A careful analysis and comparison of the results with depth, alkalinity, and location of lignite is required to confirm the above interpretation.

The importance of depth, or rather, the changes in the chemical character of the groundwater with depth, is evident in the results listed in Table 47. 2. Most of the results used in calculating the means listed in Table 47. 2 come from sites within the area portrayed in Figures 47. 1 and 47. 2. Only in the case where there were fewer than 24 sites available from a rock formation, were sites outside that area included. Both the depth-ranked and the U-ranked results show clearly for all four formations that the deeper wells are lower in U and Rn. The following mechanism could explain this observation: leaching of near-surface material by oxygenated alkaline waters and gradual downward movement of water and dissolved constituents. Since Ra is less mobile than U, less is dissolved and transported. Hence the difference in the Rn values is less pronounced. As the sinking waters enter reducing environments U^{6+} is reduced to U^{4+} and precipitated, resulting in the low U values in the waters from the deepest wells. Lateral transport from the sampled area via intermediate or shallow aquifers could also account for the lack of U at greater depth.

The results in Table 47. 2 also shows that the waters of the two youngest formations, i. e., the Cypress Hills and the Ravenscrag, contain more Rn than the older ones but for U the reverse is evident. One is tempted to conclude from this that the younger formations contain a greater proportion of the U minerals. But there are a number of factors, such as grain size, porosity, Rn emanation efficiency, oxidation potential, alkalinity, U content of the rock, type of U mineral in the rock, etc., that can influence the Rn and U content in the water.

Looking in somewhat more detail at the U and Rn maps one can see U and Rn correspondence at individual sites, but more often there is a lateral shift, with the higher U sites downslope from the high Rn sites. Such drifts can be explained by the different physio-chemical properties of these two elements resulting in different mobilities and ranges.

Conclusions

Regional well water U and Rn surveys in populated areas such as the Cypress Hills, Saskatchewan region are practical in delineating U highs.

Leaching of U from near-surface materials by groundwater and reprecipitation in deeper formations or lateral transport over long distances appear to be active mechanisms of redistribution of U in the area surveyed.

In view of the relatively low Rn levels, the arid climatic conditions of the area, the highly alkaline waters, and the existence of weakly radioactive coals and lignites, none of the U anomalies are strong enough to postulate a significant ore body in the study area. This opinion should be tempered by the preliminary nature of well water geochemistry in the area.

References

Bell, R. T., Steacy, H. R., and Zimmerman, J. B.
1976: Uranium-bearing bone occurrance; *in* Report of Activities, Part A, Geol. Surv. Can., Paper 76-1A, p. 339-340.

Cameron, A. R. and Birmingham, T. F.
1970: Radioactivity in western Canadian Coals; Geol. Surv. Can., Paper 70-52, 35 p.

Darnley, A. G., Cameron, E. M., and Richardson, K. A.
1975: The Federal-Provincial Uranium Reconnaissance Program – *in* Uranium exploration 75; Geol. Surv. Can., Paper 75-26, p. 49-68.

Denson, N. M. *et al.*
1959: Uranium in coal in the western United States; U. S. Geol. Surv., Bull. 1055.

Denson, N. M. and Gill, J. R.
1965: Uranium bearing lignite and carbonaceous shale in the southwestern part of the Williston Basin – A regional study; U. S. Geol. Surv. Prof. Paper 463.

Dyck, W., Garrison, E. W., Godoi, H. O., and Wells, G. S.
1976: Minor and trace element contents of well waters, Carboniferous basin, eastern Canada; Geol. Surv. Can., Open File 340, 35 p., 23 maps.

Harshman, E. N.
1968: Uranium deposits of the Shirley Basin, Wyoming; In Ore deposits of the U. S. 1933-1969; Vol. 1, p. 852, Ed. J. O. Ridge; Am. Min. Met. Pet. Eng., New York.

Phenix, D. A.
1960: Occurrence and chemical character of ground water in the Morrison Formation; in part 4 of Geochemistry and mineralogy of the Colorado Plateau uranium ores; U. S. Geol. Surv. Prof. Paper 320, p. 55-64.

EXAMINATION OF SOME CORDILLERAN URANIUM OCCURRENCES

Project 750051: Uranium Reconnaissance Program

B.W. Smee and S.B. Ballantyne
Resource Geophysics and Geochemistry Division

Introduction

An examination of some uranium occurrences in Washington and south-central Idaho was undertaken in early August, 1976. Three types of geological environments were chosen for study, based on their similarity to the British Columbia environments encountered during the Federal-Provincial Uranium Reconnaissance Program surveys in south-central British Columbia.

The geochemical survey in British Columbia undertaken under this program during the 1976 field season covered 82 E, L and M, 1:250 000 map-sheets (Fig. 48.1), and was done by a contract crew under the supervision of S.B. Ballantyne. An attempt to sample this 46 800 km^2 area at a mean density of one sample per 13 km^2 necessitated the use of ground sampling teams in four-wheel drive vehicles, teams in boats on the large lake systems, and a team in helicopter-supported sampling operations. Samples of stream waters and stream sediments were collected; the water samples being analyzed immediately for uranium, fluorine and pH. Sediment samples were dried and sent to Ottawa for preparation and analysis. Results for the water analysis have shown anomalous results in uranium and fluorine near known uranium mineralization, plus numerous heretofore unknown situations.

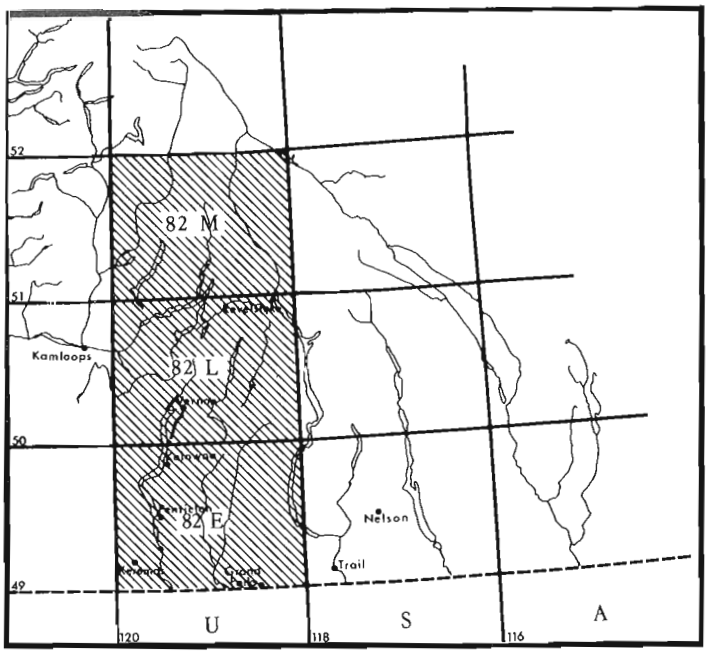

Figure 48.1. British Columbia Uranium Geochemical Reconnaissance Program, 1976.

Midnite Mine, Washington

The Midnite uranium mine, owned by the Dawn Mining Co., is on the south flank of Spokane Mountain, about 65 km northwest of Spokane. The mine office and concentrator is in Ford, Washington. Mineralization at the Midnite mine occurs primarily in a Precambrian roof pendant of argillites, phyllites, quartzites and dolomites which lies within a Cretaceous granitic intrusive.

An area of known uranium mineralization in Custer County, Idaho was chosen for study because of a number of similarities to the Fuki-Donen and Tyee Lake Resources uranium occurrences in south-central British Columbia. Bedded sedimentary deposits at the base of a volcanic series as well as vein deposits in batholithic rocks occur within the same drainage basin. The Idaho mineralization has been well documented (Kern, 1959; Choate, 1962) and a number of showings have been exposed by localized stripping and surface mining. A geochemical orientation survey, completed by the U.S. Atomic Energy Commission (Illsley, 1961), indicated that the sampling of stream waters was a successful method for detecting uranium mineralization in mountainous topography. This earlier study provided a useful comparison to the refined analytical methods used in the present British Columbia program and aided the interpretation of the 1975 orientation survey near the Fuki-Donen prospect area (Ballantyne and Bottriell, 1975).

Intrusive rocks, within which the roof pendant lies, consist of a coarsely crystalline porphyritic quartz monzonite containing large potassium feldspar phenocrysts. Locally, the intrusive has been intensely weathered, leaving grains of quartz and feldspar crystal remnants at surface. The contact between the intrusive and the roof pendant is undulatory, creating numerous pendant-filled hollows which may have been channels for uranium-bearing solutions. The major uranium host has been pelitic rocks which have been metamorphosed to phyllite, schist and hornfels. Calc-silicate hornfels and amphibolite are also hosts. Uranium occurs as pitchblende and coffinite in shears and as disseminations along foliation (Nash, 1975). In the oxidized zones uranium occurs primarily as meta-autinite, both at the base of the intrusives and the upper portions of the metasediments.

The majority of the economic concentrations occur in depressions in the intrusive (Fig. 48.2). Mineralization is usually tabular and crosses lithologic boundaries. The most likely mode of origin of the deposits is the migration of uranium-bearing groundwaters through permeable sections of pyrite-rich metasediments (Sheldon, 1959; Nash, 1975).

From: Report of Activities, Part C;
Geol. Surv. Can., Paper 76-1C (1976).

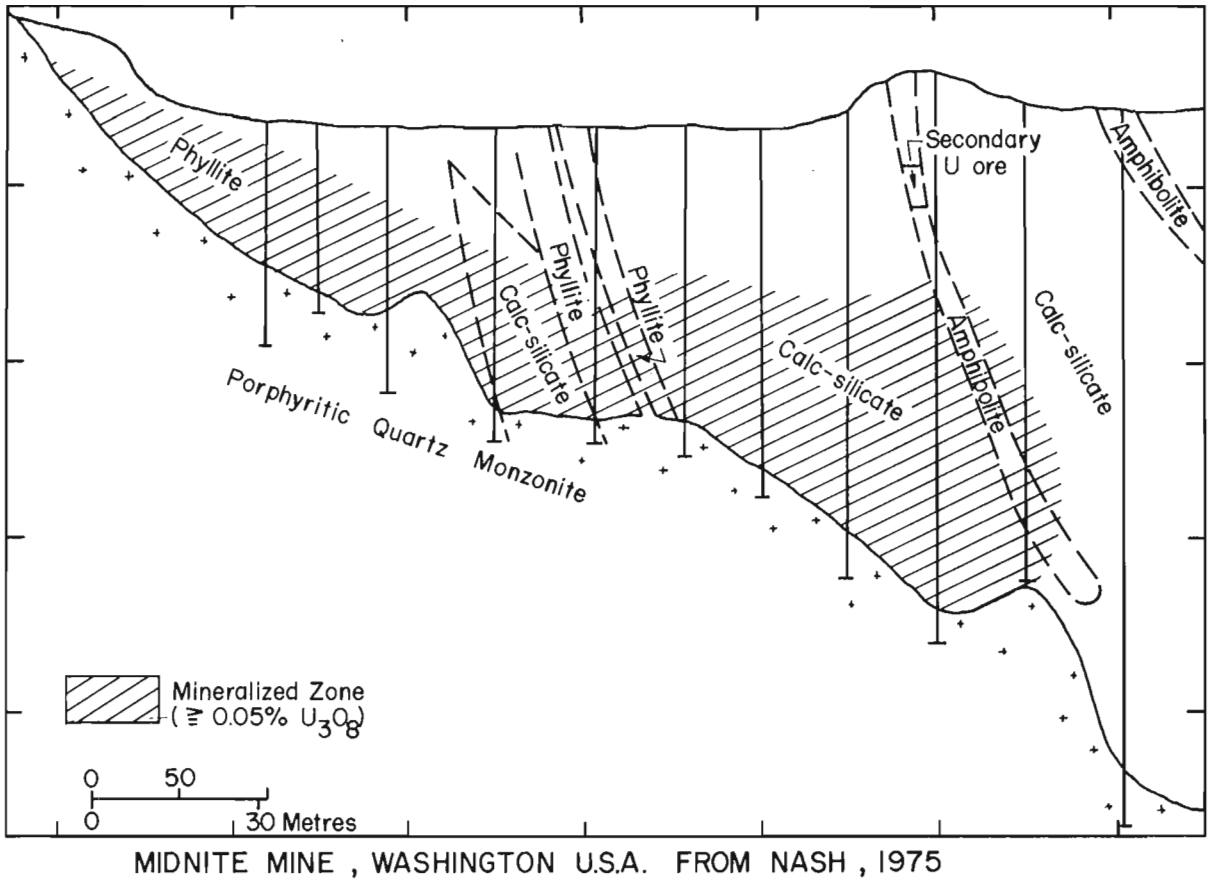

Figure 48.2. Cross section through an ore zone. Mineralization crosses lithologic boundaries and occupies depressions in the monzonite.

Other uranium deposits are known in the area, the most promising being the Sherwood Prospect about 8 km south of the Midnite Mine. The Sherwood Prospect lies in an unconsolidated sedimentary horizon within a Tertiary volcanic series and is estimated to contain 15 million pounds of U_3O_8 (Mr. E. Craig, pers. comm.).

Idaho Deposits

The uranium deposits studied lie in Township 11N, Ranges 13 and 14E, Boise Principal Meridian, Custer County, Idaho (lat. 44°17', long. 114°50'). Access to the area is by U.S. Highway 93, a paved road leading from Stanley to Sunbeam, about 125 km northeast of Boise. Most of the mineral occurrences have access to roads which are passable to 4 wheel-drive vehicles.

The Stanley uranium area lies in the Salmon River mountain belt, with elevations ranging from 1800 to 2660 m. The hills have steep sides but exhibit rounded tops. North-facing slopes support conifers while south-facing slopes have a cover of sage brush and isolated trees. Precipitation is about 40 cm annually, falling mostly as winter snow. In general, the area is similar in appearance to the Kamloops and Okanogan regions of British Columbia.

Two rock units predominate (Fig. 48.3). The most widespread comprises intrusive rocks belonging to the Idaho Batholith of Cretaceous age (Choate, 1962). The composition and texture of these intrusive rocks are not uniform throughout but grade from quartz monzonite to granodiorite and from coarse grained porphyritic near the contact to fine- to medium-grained granitic near the western boundary. In the immediate area of the uranium deposits the intrusive is notably porphyritic with phenocrysts of microcline predominating. The intrusive is heavily fractured and deeply weathered. The Nelson batholithic rocks near Beaverdell, British Columbia show similar features.

The intrusive is unconformably overlain by the Challis volcanic series. Paleontological evidence indicates an Oligocene age (Ross, 1962) which is similar to the Kamloops Group of south-central British Columbia (Jones, 1959). The volcanics grade from andesite to rhyolite in composition; thick sequences of porphyritic tuff have been exposed and overlie a number of uranium occurrences.

The basal portion of the Challis series is an irregular band of sedimentary rocks derived by erosion from the batholith prior to volcanism. The lowest portion of this sedimentary sequence consists of arkosic sandstone, arkose, and conglomerate, all of which are

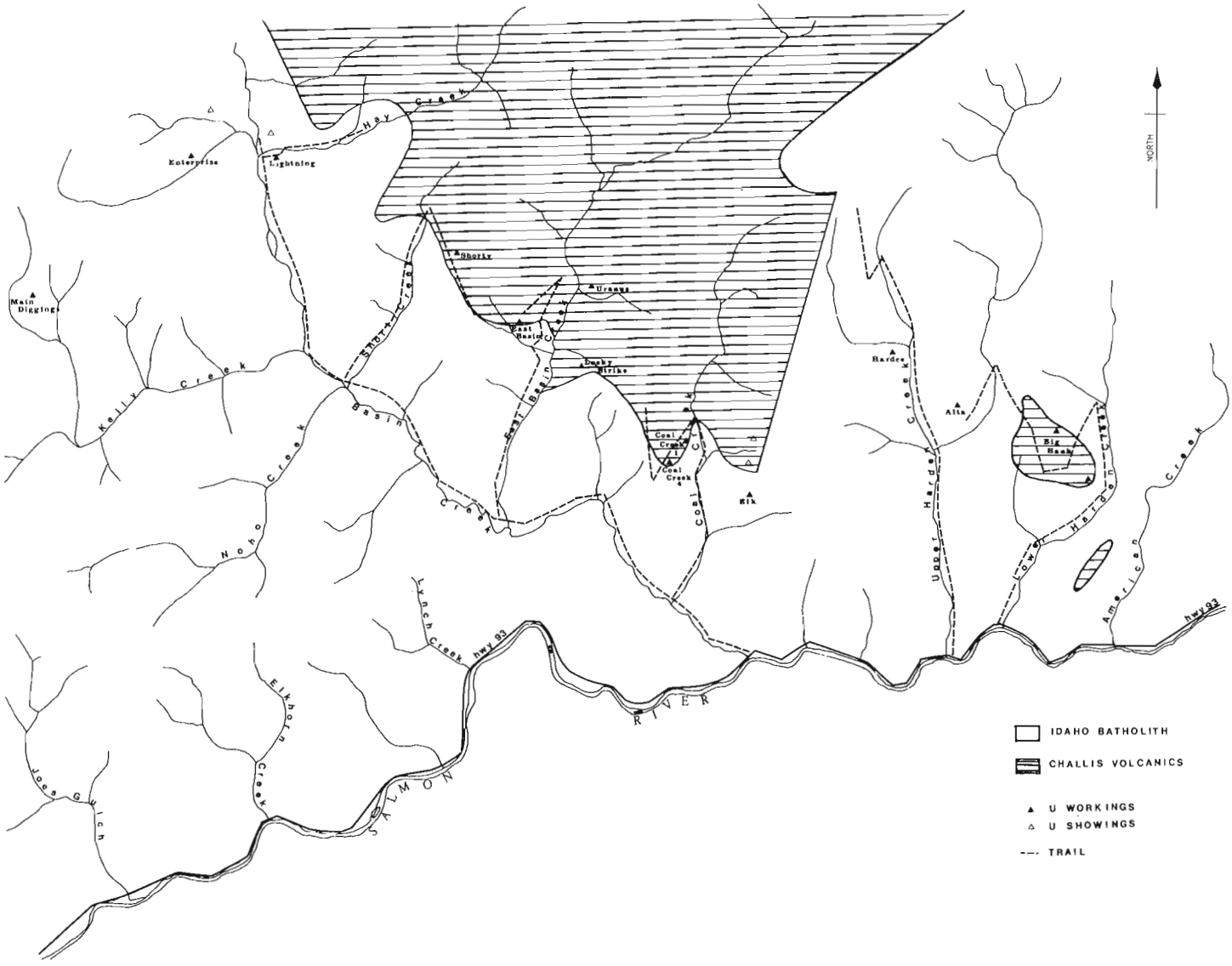

Figure 48.3. Distribution of Idaho Batholith and Challis Volcanic rocks in Stanley area, Idaho.

highly carbonaceous. In places the sediments are less than one metre thick but elsewhere more than 30 m have been measured. The carbon-rich sedimentary rocks at the base of this sequence are the main hosts for uranium mineralization in the Stanley area.

Vein Type Uranium - Lightning Occurrence

Mineralization consists of sooty pitchblende stringers within a vein-filled fault zone in the batholith at the Lightning occurrence on Hay Creek. These stringers range in thickness from less than 1 to more than 20 mm and often occur with chalcedony. Fluorite is known in the area and stibnite, molybdenum, pyrite and gold have been observed near the uranium mineralization (Kern, 1959). In the rock-suite collected near the surface at the Lightning occurrence, secondary uranium minerals tentatively identified as uranophane and autinite were noted on fracture surfaces. Up to 1960, a total of 691 tons of ore grading 0.17 per cent U_3O_8 was shipped from the Lightning zone.

Sedimentary Type Uranium - Coal Creek Occurrence

The Coal Creek No. 1 pit on the west bank of Coal Creek is a well exposed example of the sedimentary type of uranium occurrence referred to previously. Mineralization occurs in the matrix of a poorly consolidated cobble conglomerate which fills an ancient stream channel. The channel, cut in quartz monzonite, parallels a fracture set and probably followed pre-existing fractures in the intrusive. Ore-grade mineralization occurs over 2 m above the quartz monzonite, with the highest grade ore occurring in a greyish black layer 20 to 40 cm thick at the base of the main channel. Carbonaceous material was observed

throughout the conglomerate matrix; a 3-cm stringer of highly radioactive lignite coal occurred at the channel base at one locality. Autinite staining on surface boulders and within the surface layers of the quartz monzonite suggests that the remobilization of uranium minerals is occurring at present. This type of occurrence strongly resembles the Fuki-Donen type of sedimentary uranium mineralization presently under investigation near Beaverdell, British Columbia.

Exploration Geochemistry

Previous work in the Cordillera suggested that sampling of stream waters may be a valid exploration technique in the search for uranium (Illsley, 1961; Nash, 1975). In addition to the analysis for uranium, fluorine may act as a useful pathfinder. Background values for uranium in stream waters typically are below 0.1 ppb. Values of 1.0 ppb may indicate proximity to mineralization and values exceeding 10 ppb are not uncommon near mineralization of the Fuki-Donen type. It must be stressed however, that high values of uranium in stream waters may not be directly indicative of weathering mineralization. Values approaching 10 ppb have been obtained in the United States and in central British Columbia from creeks draining deeply weathered potassium-rich porphyritic intrusive rocks which contain no known ore-grade uranium mineralization. The geological environment within each anomalous drainage basin must be studied closely when placing priorities on geochemical anomalies.

Basin areas which the Kamloops volcanic series has infilled, such as those around Hydraulic Lakes and their more northerly occurrences should be examined. Areas of Cretaceous and more recent intrusives which exhibit distinct surface weathering should be studied closely to ascertain groundwater movement and direction. Structures associated with these intrusives may yield responses.

Other basin areas in the Okanogan may yield anomalous uranium results. The stratigraphy of these small basins should be mapped and thicknesses of sediments correlated. Some areas in the southern part of the area surveyed contain pegmatite veins which have yielded uranium responses. The extent of these vein systems is unknown.

Dispersion of uranium in water from known mineralization of the Fuki-Donen type can be up to 8 km, providing the dilution of the major drainage by background creeks is not excessive. Sampling of secondary drainages where stream length is less than 3 km from a suspected target will increase anomaly contrast and definition.

Examination of the Midnite Mine, the Stanley Basin mineralization and the Fuki-Donen area has shown a number of similarities. A porphyritic, potassium-rich intrusive of probable Cretaceous age lies near all deposits. The intrusive is characteristically deeply weathered leaving a surface rubble of quartz grains and feldspar phenocrysts. An aquifer unconformably overlying the intrusive and in turn overlain by a competent cap rock occurs at each site. Within each aquifer a means for precipitating uranium from solution has been noted, either carbonaceous material or an abundance of iron-bearing minerals. The collection basins for ore-grade mineralization in each of the deposits is areally small, usually between 0.8 and 0.4 km in length, and about 100 m wide.

The authors would like to thank Mr. Earl Craig of the Dawn Mining Company, Ford, Washington, and Mr. Carl Savage, Associate Chief, Idaho Bureau of Mines and Geology, Moscow, Idaho for their assistance and information during the property examinations.

References

Ballantyne, S.B. and Bottriell, K.
1975: Geochemical orientation surveys for uranium in southern British Columbia; *in* Report of Activities, Part C, Geol. Surv. Can., Paper 75-1C, p. 311-312.

Choate, Raoul
1962: Geology and ore deposits of the Stanley area; Idaho Bur. Mines Geol; Pamphlet 126.

Illsley, C.T.
1961: Hydrogeochemical reconnaissance for uranium in the Stanley area, south-central Idaho; Grand Junction Colorado, U.S. Atomic Energy Commission.

Jones, A.G.
1959: Vernon map-area, British Columbia; Geol. Surv. Can., Mem. 296.

Kern, B.F.
1959: Geology of uranium deposits near Stanley, Custer County, Idaho; Idaho Bur. Mines Geol.; Pamphlet No. 117.

Nash, J.T.
1975: Geology of the Midnite uranium mine, Stevens County, Washington; U.S. Geol. Surv. Open File Rept. 75-402.

Ross, C.P.
1962: Stratified rocks in south-central Idaho; Idaho Bur. Mines Geol.; Pamphlet 125.

Sheldon, R.F.
1959: Midnite Mine Geology and Development; Min. Eng., May 1959, p. 531-534.

49. DETAILED GEOCHEMICAL INVESTIGATIONS FOR URANIUM AND BASE METAL EXPLORATION IN THE NONACHO LAKE AREA, DISTRICT OF MACKENZIE

Project 760043: Uranium Reconnaissance Program

Y. T. Maurice
Resource Geophysics and Geochemistry Division

Introduction

The work described in this report was carried out in the summer of 1976 under the auspices of the Federal-Provincial Uranium Reconnaissance Program and consists in the follow-up of anomalous geochemical results obtained from a reconnaissance lake sediment survey undertaken in the Nonacho Lake area in 1975. During this survey, close to 2700 samples were collected at a density of one in five square miles thus covering all of 1: 250 000 NTS map sheets 75C, F and K. The analytical data for twelve elements (U, Zn, Cu, Pb, Ni, Co, Ag, Mn, As, Mo, Fe, Hg) and loss on ignition to estimate the organic carbon content, were released as Geological Survey Open Files 324, 325 and 326 earlier this year.

The objectives of the 1976 work were: 1) to determine the usefulness of reconnaissance geochemical surveying as a guide to mineral exploration in the Nonacho Lake area, 2) to establish a useful follow-up procedure that may be employed in future exploration programs in the area, and 3) to collect data that may help assess the mineral (particularly the uranium) potential of the area surveyed.

Uranium mineralization occurs at several localities south of the East Arm of Great Slave Lake and is particularly abundant within and around the Nonacho sedimentary basin. It is most interesting to note the wide variety of geological settings in which the radioactive minerals occur; host rocks include arkosic conglomerates, arkoses, greywackes and other clastic sediments, dolomites, basic intrusives, granites and granitic pegmatites, granodiorites and a variety of gneisses and schists. The radioactive minerals are often found in structurally controlled veins and lenses emplaced in fractures or shear zones, but in many cases, they are disseminated in the host rocks. In several of the showings, small quantities of sulphides, most frequently chalcopyrite and molybdenite, are associated with the radioactive minerals.

A few base metal showings (mainly copper) are known in the area and these occur mainly along the shores of the East Arm of Great Slave Lake.

During the first two weeks of field work, several showings were visited and sampled by the writer for mineralogical and chemical determinations. This work will, it is hoped, permit the identification of potential pathfinders that may later assist in the interpretation of the regional reconnaissance as well as the follow-up data. In addition, visiting the showings allowed the field crew to become familiar with the different types of mineral occurrences that may be encountered during the field operations.

Field Procedures

The 1975 reconnaissance lake sediment survey outlined several areas of anomalous metal concentrations. Several of these were found to be related to existing showings, but most do not appear to be associated with any known mineralization. The strongest anomalies were found in undifferentiated basement rocks, generally within ten miles of the unconformity that underlies the Nonacho sediments. Although the Nonacho basin itself is characterized by lower background concentrations and weaker anomalies than the surrounding Archean basement, anomalies that occur within the sedimentary basin were considered particularly interesting because of the presence of radioactive minerals in this geological unit.

Several uranium and base metal anomalies were outlined north of the McDonald Fault within the Slave Province. A moderately strong uranium anomaly was also outlined within the Great Slave Supergroup and appears to be related to a granodiorite laccolith (Hoffman, 1968), the same type of rock which hosts uranium mineralization at the Ridley Mines, about 20 miles to the southwest.

Seventeen anomalous areas, ten in NTS map-area 75K and seven in NTS map-area 75F, representing a total surface area of approximately 550 square miles were selected for follow-up work (*see* Figs. 49. 1 and 49. 2). Three of these are strictly base metal anomalies and the rest are uranium anomalies that, except for two that occur in the Nonacho basin, are combined with one or more base metals.

In each of these areas, detailed sampling of centre-lake sediments and waters was carried out with the support of a Hughes 500-C turbo-helicopter. An attempt was made to sample every lake shown on the 1: 50 000 topographical maps resulting in a density averaging 2. 1 sites per square mile. Water samples were collected by hand in 500 ml polyethylene bottles from the lake surface. An improved version of the Hornbrook sediment sampler allowed a sampling rate averaging 21 per hour.

The water samples were selectively analyzed in the field for uranium and total heavy metals, depending on whether uranium and/or base metals were initially enriched in the reconnaissance samples. A Jarrell-Ash fluorimeter using AC power supplied by a Honda, 1000 watts generator, was used for uranium determinations. These analyses were performed using the method described by Smith and Lynch (1969). Heavy metal concentrations were determined using a colorimetric technique. Specific conductivity and pH measurements on all water samples and alkalinity (HCO_3^-) determinations on uranium-rich waters were also performed in

From: Report of Activities, Part C;
Geol. Surv. Can., Paper 76-1C (1976).

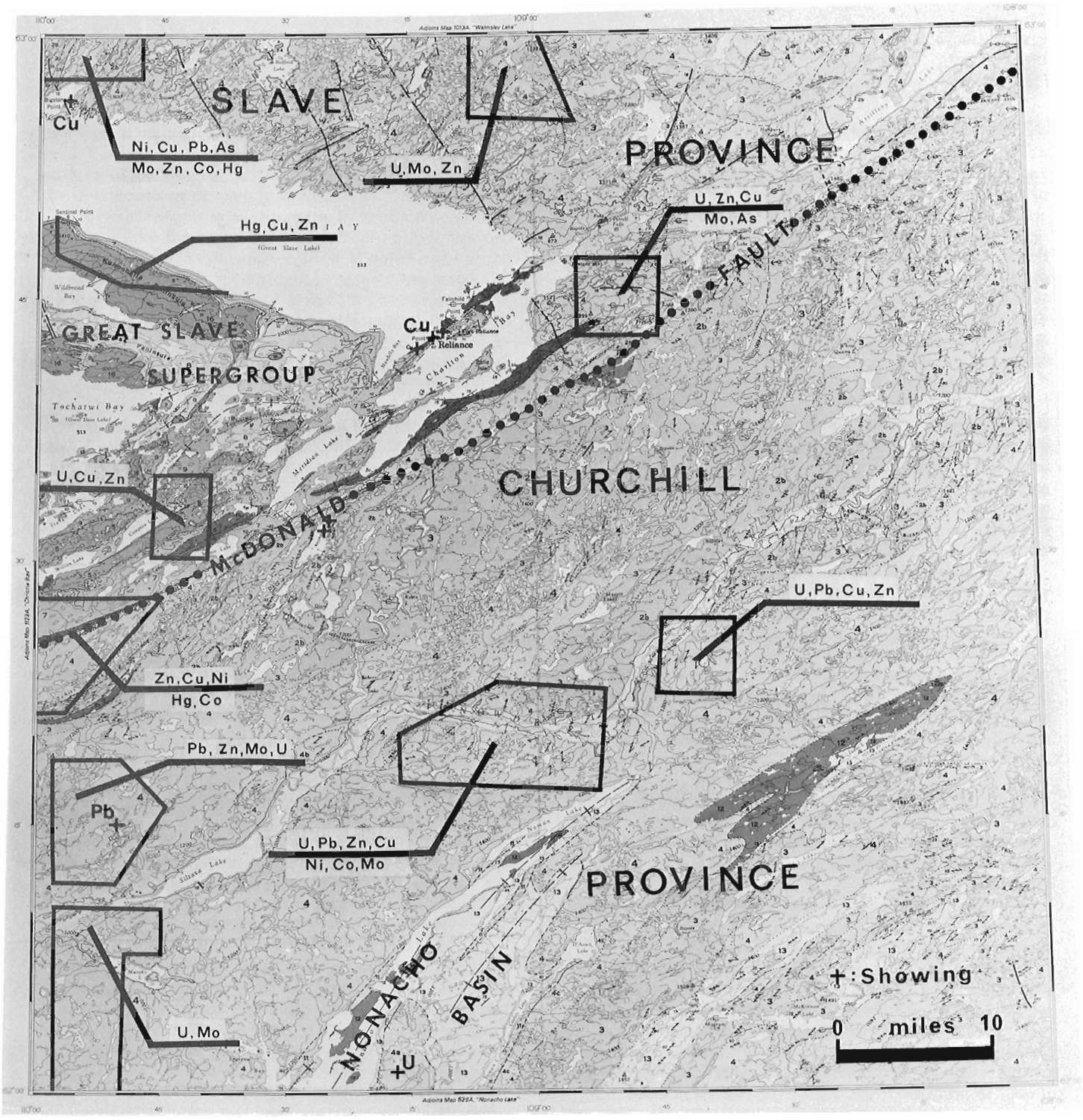

Figure 49. 1. Location of study areas and elements enriched in lake sediments in NTS map 75K. (Geol. Surv. Can. Map 1123A, 1968)

the field laboratory. The sediments were dried in the field and sent to Ottawa to be analyzed at a later date.

From the water results, a limited number of ground traverses were carried out to examine the drainage basins of anomalous lakes. The purpose of this work was primarily to gather geological and secondary environmental information that will help in the interpretation of the lake geochemical data. Portable radiometric equipment was carried at all times during these traverses, to record radioactivity directly from exposed bedrock and boulders.

Results and Discussion

The uranium results obtained by analyzing lake waters in the field were generally satisfactory, and with the exception of those areas that occur within the Nonacho sedimentary basins, the uranium anomalies, as outlined by the reconnaissance lake sediment survey, are confirmed anomalous by the water data. With respect to the total heavy metals, the water data indicates less contrast between background and anomalous concentrations than for uranium. Nevertheless, a few

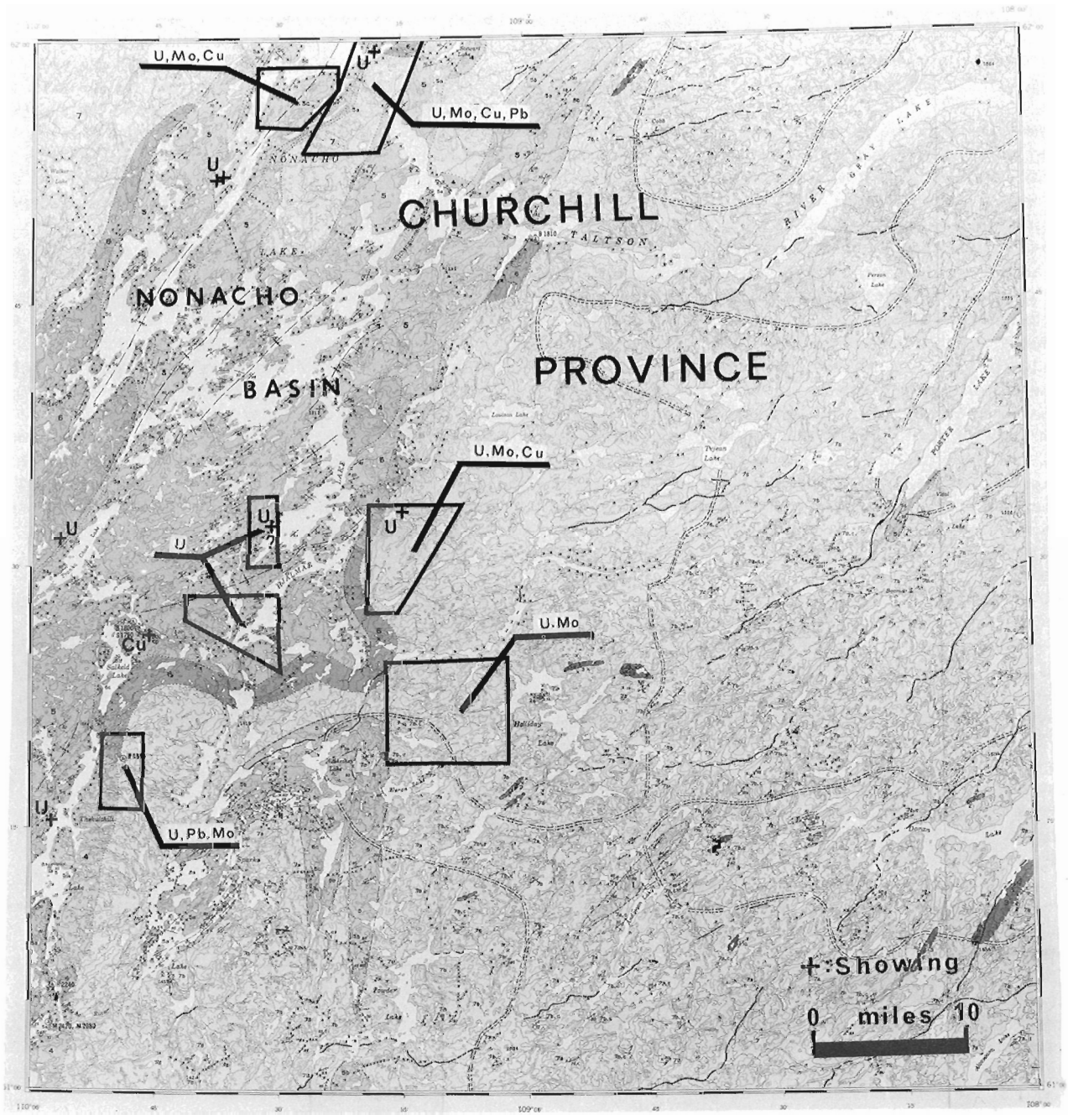

Figure 49. 2. Location of study areas and elements enriched in lake sediments in NTS map 75F. (Geol. Surv. Can. Map 1281A, 1971).

ground traverses were carried out in anomalous drainage basins, but more useful information concerning base metal distribution in the area is expected from the sediment data.

The uranium in lake water results generated a large numbers of individual anomalies that preliminary ground observations show to be related to one or a combination of three factors:

1. Concentrated uranium mineralization that occurs in relatively small areas,
2. Large areas of certain rock types that contain above average uranium concentrations, and,
3. Secondary environmental conditions that cause appreciable enhancement of uranium in lake waters.

In order to conduct the most efficient follow-up work on as many lake water anomalies as possible, it is important to identify the nature of these anomalies and exercise some form of discrimination. No doubt that multielement analysis of sediment and bedrock samples (including data from representative mineral occurrences in the area) will provide valuable information to that effect, but on the basis of water results only, the problem is somewhat more difficult.

Anomalies that are caused by more or less concentrated uranium mineralization (factor 1 above) are small, generally involving no more than a single basin and sometimes, a single lake. Their intensities seem to depend on the size and location of the radioactive rocks in relation to the drainage pattern on the size of the lakes within the basin. This last point is particularly important as showings located near the shores of large bodies of water, such as Nonacho Lake, failed to generate lake water anomalies. On the other hand, uranium mineralization located in proximity to smaller lakes generally showed intense water anomalies (from 2 to 5 ppb U). It is hoped that sediments collected in small inlets of large lakes will be more revealing than the waters as they may not be diluted to the same extent.

Anomalies related to factor 2 are generally of low intensity, often extending into several drainage basins. This results in a high background effect with no distinct peaks and concentrations rarely exceeding 1.5 ppb U (the regional background is of the order of 0.1 ppb U). Rock units that have been found to generate this type of anomaly include granites in the Archean basement of the Churchill Province to the east of the Nonacho basin and in southern Slave Province, and porphyries in the Churchill Province, just north of the Nonacho basin. The porphyries are particularly interesting in that they also generated a few sharp and intense uranium-in-lake-water peaks that protrude over a generally uniform and high background generated by the porphyries. These peaks were found to be related to localized zones of previously unreported concentrations of uranium minerals within the porphyries. Their presence at the surface is revealed by large patches of yellow stains and moderately high radiation (from 700 to 1200 total counts/second (cps) over a background of less than 500 cps for unmineralized porphyry and less than 100 cps in country rock). At the time of writing, (September 1976) samples of biotite-rich material that occurs as narrow bands within the porphyritic bodies. They are moderately to strongly radioactive (up to 3200 cps) and may represent undigested inclusions of metasedimentary country rock that have been impregnated with mineralization fluids. Fluorite was found to be a common joint filling material in the porphyries and sulphide mineralization (pyrite and pyrrhotite) was observed in thick lenses within the metasediments, generally in close proximity to the contacts with the porphyries.

Anomalies that are related to secondary environmental conditions (factor 3) are those that are found in waters containing heavy organic suspensions or high levels of dissolved bicarbonate. Both these conditions are known to enhance the uranium content of lake waters (Meyer, 1969; Maurice, in press), and further studies are presently underway to estimate the best corrections to apply.

In addition to the geochemical surveying described so far, limited airborne gamma-ray spectrometry, using a McPhar, Spectra 1, 4 channel spectrometer, equipped with a 9 x 4 in. crystal, was also carried out in areas of geochemical anomalies. The instrument was installed in the same helicopter that had been used for geochemical surveying and a total of 260 line miles were flown at 100-foot ground clearance along several grids having 1500-foot line spacing. In general, the results obtained are in agreement with the geochemical pattern, particularly in areas of flat relief and good rock exposure. These radiometric data proved particularly helpful in assessing lake water anomalies of doubtful origin.

References

Hoffman, P. F.
1968: Stratigraphy of the Lower Proterozoic (Aphebian), Great Slave Supergroup, East Arm of Great Slave Lake, District of Mackenzie; Geol. Surv. Can., Paper 68-42.

Maurice, Y. T.
Geochemical methods applied to uranium exploration in southwest Baffin Island; Can. Inst. Min. Metall. Bull. (in press)

Meyer, W. T.
1969: Uranium in lake waters from the Kaipokok region, Labrador; Colo. Sch. Mines, Q., v. 64, no. 1, p. 377-394.

Smith, A. Y. and Lynch, J. J.
1969: Field and laboratory methods used by the Geological Survey of Canada in geochemical surveys, No. 11. Uranium in soil, stream sediment and water; Geol. Surv. Can., Paper 69-40.

50. GEOCHEMICAL FOLLOW-UP STUDIES, NORTHWESTERN MANITOBA

Project 760044: Uranium Reconnaissance Program

William B. Coker
Resource Geophysics and Geochemistry Division

Introduction

As part of the Federal-Provincial Uranium Reconnaissance Program (Darnley *et al.*, 1975) regional geochemical and airborne radiometric surveys were carried out in northwestern Manitoba during the summer of 1975.

The geochemical surveys covered map-sheets 64J, K, N and O and consisted of the collection of lake sediments at a density of one sample per five square miles. The lake sediment samples were analyzed for Zn, Cu, Pb, Ni, Co, Ag, Mn, As, Mo, Fe, Hg, U and L.O.I. (loss on ignition) and these data released as Open Files 320, 321, and 323 in the spring of 1976 (Hornbrook *et al.*, 1976a, b, c, d).

The airborne gamma-ray spectrometry, flown at five kilometer line spacings, covered map-sheets 64F, J, K, N and O. These data were presented as (1) contour maps of the integral count, the potassium, equivalent uranium and equivalent thorium concentrations, and the eU/eTh, eU/K and eTh/K ratios; and (2) stacked profiles of the seven radiometric parameters plotted for each flight line from each of the five map-sheets. These data were released as Open Files 315, 316, 317, 318 and 319 in the spring of 1976 (Resource Geophysics and Geochemistry Division, 1976a, b, c, d, e).

Thirteen areas, anomalous in uranium or having a known uranium occurrence, were selected for a geochemically oriented follow-up study on the basis of the regional geochemical and geophysical data (Fig. 50.1, areas 1 to 13; Table 50.1). The areas were chosen to cover as many of the different geological environments present in the area as possible. The geochemical data were also used to give an indication of any anomalous concentrations of other elements, associated with anomalous uranium values, in the selected areas. A complementary geophysically oriented follow-up program was carried out from the same base camp under the supervision of B.W. Charbonneau, Radiation Methods Section.

A further six areas anomalous in one or more of Cu, Ni, Zn, Ag and/or Mo were selected for follow-up investigations on the basis of the regional geochemical data (Fig. 50.1, areas 14 to 19; Table 50.2).

Objectives of Follow-up Program

The overall objective of the follow-up studies is to provide information which will maximize the usefulness of the regional reconnaissance surveys produced by the Uranium Reconnaissance Program by:

1. investigating the causes of anomaly patterns and selected individual anomalies in order to assemble examples and hence guidelines for the general interpretation of reconnaissance data.
2. by establishing effective follow-up procedures that can be employed by the mineral exploration industry.
3. identifying features in the reconnaissance data which in themselves or in conjunction with other geoscience data are most diagnostic of mineralization.

Northwestern Manitoba (64J, K, N, O)

General Geology

The earliest mapping in the area was carried out by the Geological Survey (Currie, 1961; Davison, 1962, 1963; Fraser, 1962).

Recently the government of Manitoba has carried out further geological mapping in the area, 64N and the north half of 64K (Weber *et al.*, 1975). The Manitoba Department of Mines, Resources and Environmental Management is currently continuing the mapping of the area in sheets 64J, 64O, and the south half of 64K.

Bedrock exposures in the area average one to two per cent and seldom exceed five per cent. The bedrock is Precambrian and forms part of the Churchill structural province. Weber *et al.* (1975) divided the bedrock into three main groups; Archean rocks, Aphebian rocks of mainly sedimentary origin, and Hudsonian igneous and metamorphic rocks.

The Archean rocks consist of foliated granitoid bodies, ranging in composition from quartz diorite to alaskite granite (Weber *et al.*, 1975). The Aphebian rocks in the northern part of the area are felt to be continuous with the Hurwitz Group sediments in the southern part of the District of Keewatin. The remainder of the Aphebian rocks lie in the extension of the Wollaston fold belt, as defined by Money (1968), in Saskatchewan. The igneous and metamorphic rocks produced during the Hudsonian orogeny include migmatite, plugs and stocks of anatexite, and syn- and late-orogenic batholiths. Most are massive and many truncate Hudsonian trends.

Although no mineral occurrences of economic significance have yet been found in the area there are a number of showings, base metal, uranium and radiometric, present in the area. These are described in detail by Weber *et al.* (1975).

One inch to four mile aeromagnetic maps 7146G, 7147G, 7150G and 7175G cover the project area.

Surficial Geology

As no surficial geology maps were available for the area R.W. Klassen, Terrain Sciences Division, prepared such maps from airphoto interpretation for 64N.

From: Report of Activities, Part C;
Geol. Surv. Can., Paper 76-1C (1976).

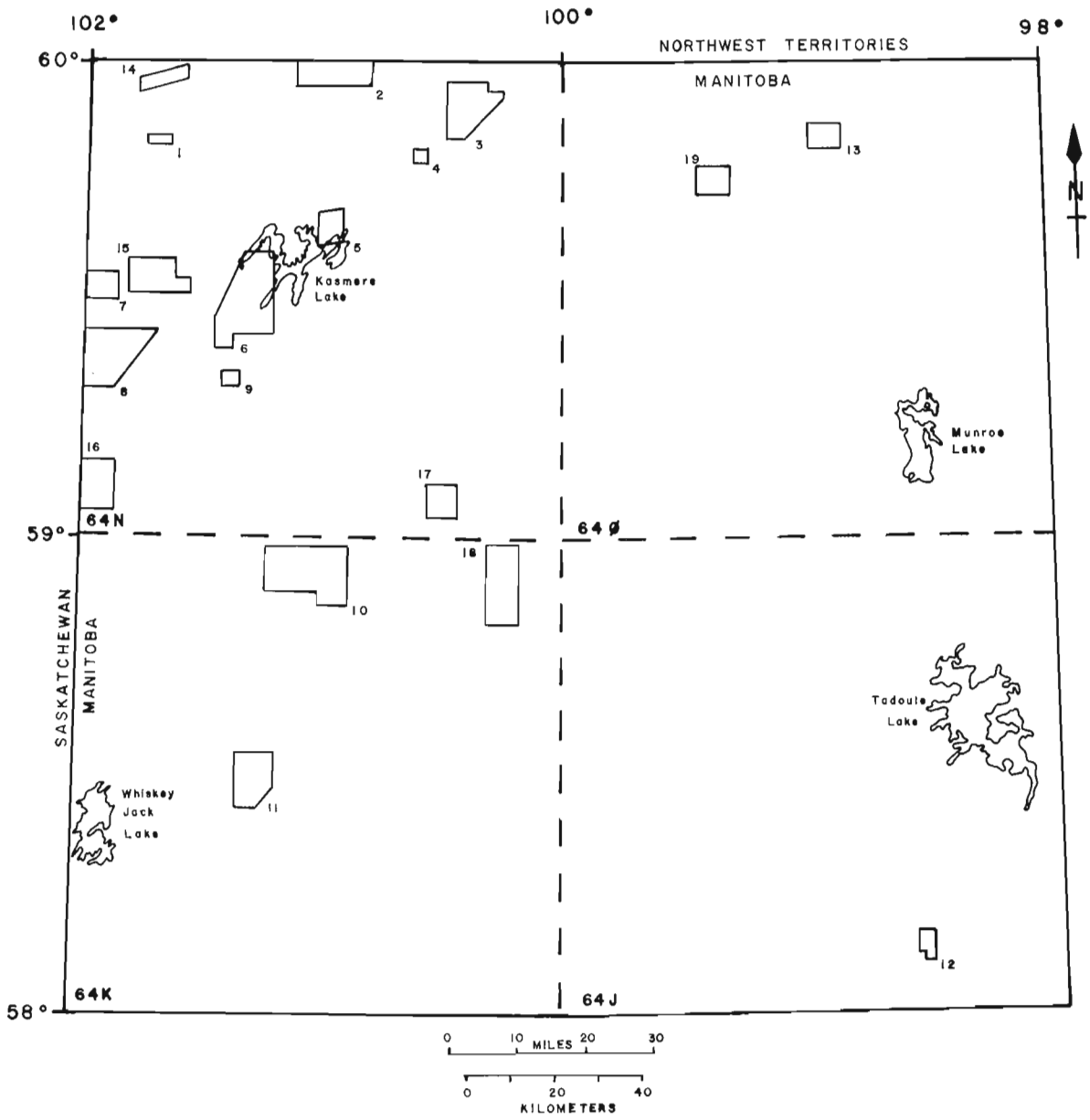

Figure 50.1. Areas of follow-up work, northwestern Manitoba.

Five main types of moraine units, two main types of glaciofluvial units and a till veneered bedrock unit were identified. Glacial features and landscapes in the form of drumlins, moraine ridges, hummocky moraine and esker complexes were noted over most of the map area (64N) and were felt to indicate an almost continuous blanket of drift (mostly till).

Follow-up Program

1. Detailed Regional Surveys

Detailed Lake Sampling

The first facet of the follow-up program involved the detailed sampling of lakes in the areas selected as anomalous in U and/or Cu, Ni, Zn, Ag and/or Mo (Fig. 50.1). The purpose of this work was to:

1. Verify the anomalous dispersion patterns outlined by the reconnaissance surveys, and;
2. Define more precisely the dimension and amplitude of the local anomalies thereby focusing on the cores of the reconnaissance anomalies and narrowing down the area requiring ground work.

Surface water and bottom sediments were collected from lakes at a density of approximately one sample site per km^2. Surface water pH, conductivity, temperature and dissolved oxygen levels were measured using a Martek Mark V Water Quality Analyzer. A Hughes 500-C helicopter was employed for this work.

Table 50. 1

Follow-up Surveys - Uranium, northwestern Manitoba

Area No. (Fig. 50. 1)	Name	N. T. S.	Anomaly type	Type of work performed*
1	Parsons L.	64 N 13	Known mineralization (U)	1, 2b, 3, 5
2	Schell – Lamontague L.	64 N 14/15	U, Cu	1
3	Leathwood L.	64 N 16	U, Mo	1, 2a, 3, 4, 5, 6
4	Saar L.	64 N 15	Known mineralization (U)	1, 2a, 3, 5
5	Northeast Arm Kasmere L.	64 N 10/11	U	1, 2a
6	Kasmere Falls	64 N 6/11	U	1, 2a, 2b, 3, 4, 5
7	Sharman L.	64 N 12	U	1, 3, 6
8	Grevstad L.	64 N 5	U, Cu	1, 2a, 3, 4, 5
9	Thanout L.	64 N 11	Known mineralization (U)	1, 2a, 2b, 3, 5
10	McGill L.	64 K 15/16	Radiometric	1, 3, 6
11	Sandy Hill L.	64 K 6/11	U, Mo	1, 3, 6
12	Gimby L.	64 J 2	U (?)	1
13	Blevins L.	64 O 15	U	1, 3, 4, 5

*1. Detailed lake sampling
2a. Airborne gamma-ray spectrometry, Skyvan
b. Airborne gamma-ray spectrometry, helicopter
3. Ground scintillometer and/or gamma-ray spectrometer measurements
4. Overburden sampling
5. Bedrock sampling, routine
6. Bedrock sampling, bedrock study

Lake sediments were collected, using a modified Hornbrook sampler, placed in waterproof kraft paper bags, field dried and shipped to Ottawa for later preparation and analyses.

Lake waters were collected in 500-ml polyethylene bottles. On the day of collection half of each sample was transferred to a second, 250-ml, bottle acidified and subsequently shipped to Ottawa for later check and additional element analyses. The remainder of the water samples were utilized, depending on the anomaly type, to determine the U content (by fluorimetry), the F content (by selective ion electrode), and the Cu, Zn and Ni contents (by colorimetry). The lake water analyses were performed in the field by G. E. M. Aslin and A. I. MacLaurin.

Detailed Airborne Gamma-Ray Spectrometry Surveys

Employing the G. S. C. Skyvan, airborne measurements were made using a four window spectrometer (U, Th, K and total counts), with twelve 22. 86 cm x 10. 16 cm NaI (T1) detectors, flown at a mean terrain clearance of 122 m and 190 km/hr. North-south flight lines were at 1-km line spacings and map-sheets 64N-5, 6, 10, 11, 15 and 16 were covered.

In addition, a helicopter-mounted McPhar airborne gamma-ray spectrometer was used for the detailed work on selected areas. The McPhar spectrometer utilizes a single 22. 86 cm x 10. 16 cm NaI crystal, contains a 1024 channel analog to digital converter, and a read only memory decodes 4 spectral windows corresponding to U, Th, K and total counts. North-south flight lines were at 0. 5 km line spacings flown at a mean terrain clearance of 45 m and 60 km/hr. This work was supervised by J. Parker.

The purpose of this work was essentially similar, while being confirmative, to the detailed lake sampling.

2. Ground Investigations

Utilizing the data from the detailed lake water and gamma-ray spectrometer surveys the core areas of the regional uranium anomalies were identified and ground work carried out over these areas to:

1. Verify on the ground and define more concisely the dimensions and amplitude of the local anomalies and relate these to the detailed and reconnaissance regional anomaly patterns.
2. Relate the results, obtained from the reconnaissance and detailed lake sediment and water surveys, to:
   (a) mineralization, unknown or known (if known and mineralization did not give an anomalous response, establish why).
   (b) surficial and/or bedrock composition.
   (c) known geology.

To establish the extent to which the anomaly patterns, both geochemical and radiometric, reflect

Table 50. 2

Follow-up Surveys - Cu, Zn, Ni, Ag and/or Mo, northwestern Manitoba

Area No. (Fig. 50. 1)	Name	N. T. S.	Anomaly type	Type of work performed*
14	Buckels L.	64 N 13	Cu, Ni	1
15	Brophy L.	64 N 12	Cu	1, 5
16	Quasso-Wolfe L.	64 N 4	Known mineralization (Zn)	1, 5
17	Barthelette L.	64 N 1/2	Mo	1, 5, 6
18	Magas L.	64 K 16	Ag	1, 4, 5
19	Macksimchuk L.	64 O 11/14	Zn, Ag	1

*1. Detailed lake sampling
4. Overburden sampling, dispersion study
5. Bedrock sampling, routine
6. Bedrock sampling, bedrock study

either surficial overburden, bedrock and/or mineralization systematic ground traversing was carried out over the core areas of the anomalies. This involved the taking of *in situ* radiometric measurements and the collection of overburden, bedrock and mineralized material for later analyses and laboratory identification and confirmation of the source of radioactivity. This phase of the work was carried out jointly with B. W. Charbonneau, who as well investigated some sharp spot radiometric anomalies in both Manitoba and Saskatchewan.

Within northwestern Manitoba several of the large granitoid bodies exhibit anomalous radiometric and/or geochemical characteristics. To establish to what extent these characteristics are a reflection of bedrock composition, paired bedrock samples were collected from a number of sites within these bodies. *In situ* radiometric measurements were also taken at the sample sites. The granitoid bodies sampled include (Fig. 50. 1):

3. Leathwood Lake; biotite-quartz monzonite
7. Sharman Lake; fluorite-quartz monzonite
10. McGill Lake; alaskite
11. Sandy Hill Lake; granite to quartz monzonite
17. Barthelette Lake; and surrounding bedrock unit of same composition; biotite-quartz monzonite (little radiometric or geochemical response for uranium-chosen as a background unit).

A study of the bedrock samples from these granitoid bodies will be undertaken, to examine their mineralogy, petrology, and geochemistry in order to determine the nature and form of the uranium present. This will involve chemical analyses, including leaching studies, and electron microprobe examination.

Only a minor amount of ground traversing, primarily involving the collection of bedrock samples, was carried out over the areas anomalous in one or more of Cu, Zn, Ni and/or Mo (Table 50. 2). The colorimetric tests for Cu, Zn and Ni in waters proved of little use in the field, the detection limits being generally higher than the levels encountered in most waters in the area. Solvent extraction – atomic absorption techniques are currently being applied to determine the Cu, Zn and Ni contents of the acidified surface lake water samples that were returned to Ottawa.

The Magas Lake Ag anomaly (Table 50. 2) was examined in detail, with L. Dredge, and both bedrock and surficial overburden samples were collected systematically from the area. Both geochemical and glacial dispersion studies will be carried out on this area, employing chemical and microscopic examination of the overburden samples, in order to assess the significance of the Ag anomaly.

Discussion

The results of the follow-up work are not yet available. However, some general comments regarding the findings in northwestern Manitoba can be made.

The field fluorimetric analysis of uranium in surface lake waters confirmed the uranium anomalies as outlined by the 1975 reconnaissance lake sediment survey. Within the anomalous areas patterns and trends of uranium concentrations were depicted and the core areas within the anomalies were clearly discernible by grouped anomalous samples.

Similarly, the detailed airborne gamma-ray spectrometer surveys verified the 1975 reconnaissance results, defining the anomalous areas in considerably more detail.

The detailed geochemistry and radiometrics produced analogous results enabling the areas requiring ground examination to be considerably lessened with regard to the original anomalous areas as outlined by the regional reconnaissance lake sediment and radiometric surveys.

The general lack of response of the field colorimetric tests for Cu, Zn and Ni in the lake waters of northwestern Manitoba illustrates the need to collect lake sediments as well as waters. The collection and analysis of lake sediments is necessary not only for outlining anomalous

concentrations of Cu, Zn, Ni, etc. but also to show the association of other elements with uranium. It is the association of other elements with uranium which may possibly be used to identify different types of uranium anomalies, a necessary step in assessing the economic potential of each anomaly.

The only analyzed element, other than uranium, detectable in the surface lake waters was fluorine. A close association was found to exist between uranium and fluorine in the surface waters of lakes located within most of the large granitoid bodies sampled. The uranium and fluorine results in the surface lake waters defined quite precisely the extent of these granitoid bodies even illustrating zoning within them. Further work will be done on this feature to examine how the associations and patterns for these elements in the surface lake waters and sediments relate to the bedrock itself.

It is the association of the other elements with uranium in the surface lake waters and, more significantly, in the lake sediments that can possibly be used to discriminate between large regional uranium anomalies related to elevated uranium levels in bedrock and point concentrations of possible economic significance. However, the possibility of a large-tonnage low-grade deposit must not be overlooked. But, perhaps in choosing an exploration target lake sediment anomalies that can be identified as related to elevated uranium levels in bedrock, on the basis of the other elements (F, Cu, Mo ?) associated with uranium, should be assigned a lower exploration priority.

References

Currie, K. L.
1961: Whiskey Jack Lake, Manitoba; Geol. Surv. Can., Map 52-1960.

Darnley, A. G., Cameron, E. M., and Richardson, K. A.
1975: The Federal-Provincial uranium reconnaissance programs; *in* Uranium Exploration 1975; Geol. Surv. Can., Paper 75-26, p. 49-68.

Davison, W. L.
1962: Tadoule Lake, Manitoba; Geol. Surv. Can., Map 30-1962.

1963: Munroe Lake, Manitoba; Geol. Surv. Can., Map 35-1963.

Fraser, J. A.
1962: Kasmere Lake, Manitoba; Geol. Surv. Can., Map 31-1962.

Hornbrook, E. H. W., Garrett, R. G., and Lynch, J. J.
1976a: Regional lake sediment geochemical reconnaissance data, north-central Manitoba, NTS 64J; Geol. Surv. Can. Open File No. 320, March 24, 1976.

1976b: Regional lake sediment geochemical reconnaissance data, northwestern Manitoba, NTS 64K; Geol. Surv. Can. Open File No. 321, March 24, 1976.

1976c: Regional lake sediment geochemical reconnaissance data, northwestern Manitoba, NTS 64N; Geol. Surv. Can. Open File No. 322, March 24, 1976.

1976d: Regional lake sediment geochemical reconnaissance data, north-central Manitoba, NTS 64O; Geol. Surv. Can. Open File No. 323, March 24, 1976.

Money, P. L.
1968: The Wollaston Lake fold-belt system, Saskatchewan-Manitoba; Can. J. Earth Sci., v. 5; p. 1489-1504.

Resource Geophysics and Geochemistry Division
1976a: Airborne gamma-ray spectrometry data, Brochet, Manitoba, NTS 64F; Geol. Surv. Can. Open File No. 315, March 24, 1976.

1976b: Airborne gamma-ray spectrometry data, Tadoule Lake, Manitoba, NTS 64J; Geol. Surv. Can. Open File No. 316, March 24, 1976.

1976c: Airborne gamma-ray spectrometry data, Whiskey Jack Lake, Manitoba, NTS 64K; Geol. Surv. Can. Open File No. 317, March 24, 1976.

1976d: Airborne gamma-ray spectrometry data, Kasmere Lake, Manitoba, NTS 64N; Geol. Surv. Can. Open File No. 318, March 24, 1976.

1976e: Airborne gamma-ray spectrometry data, Munroe Lake, Manitoba, NTS 64O; Geol. Surv. Can. Open File No. 319, March 24, 1976.

Weber, W., Schedewitz, D. C. P., Lamb, C. F., and Thomas, K. A.
1975: Geology of the Kasmere Lake-Whiskey Jack Lake (North Half) Area; Man. Min. Resourc. Div., Publ. 74-2.

51. CARBORNE GAMMA-RAY SURVEY, PRINCE EDWARD ISLAND

Project 760045

P. G. Killeen, G. R. Bernius, and N. Hall[1]
Resource Geophysics and Geochemistry Division

Introduction

A carborne gamma-ray spectrometer survey has been carried out over much of central Prince Edward Island, primarily recording the output of the total count channel. Virtually all of the roads shown (approximately 1350 line km) on the 1: 50 000 scale National Topographic System map-sheets covering the central part of Prince Edward Island have been traversed. The survey area was selected as the most favourable on the Island on the basis of a reconnaissance airborne gamma-ray spectrometer survey (Richardson and Holman, 1975) flown with the Geological Survey Skyvan in 1974 to Uranium Reconnaissance Program specifications. The road network covered by the carborne survey, along with the uranium map from the airborne gamma-ray spectrometer survey is shown in Figure 51. 1. Anomalous areas were retraversed three times in order to record the gamma-ray spectrometer output from the thorium, uranium and potassium channels' respectively, with the single pen chart recorder. Finally, some *in situ* analyses were made using the portable spectrometer and a 7. 6 x 7. 6 cm detector, and some samples were collected for lab analysis. The survey was carried out jointly by the Prince Edward Island Department of Industry and Commerce and the Geological Survey of Canada. Compilation and interpretation of the data are continuing.

Instrumentation

The four main components of the carborne system consisted of:

1. the detector package,
2. the high voltage supplies and amplifiers,
3. the four-channel portable gamma-ray spectrometer,
4. a single pen strip chart recorder with event marker.

The system was powered by two 12-volt car batteries connected in series completely independent of the vehicle battery supply.

1. The Detector

A 22. 9 x 10. 2 cm (9 x 4 inch) NaI(T1) detector inside a fibreglass container (with dimensions 40 x 40 x 45 cm) which was insulated with foam was shock mounted on a sheet of plywood in the rear of the vehicle as shown in Figure 51. 2. The shock mounting was particularly effective in cushioning the jolts from holes and rocks hidden in the grass along the roadside. The detector package which included four photomultiplier tubes was located as high as was practical inside the vehicle, on the right hand side. The vehicle was a four-wheel drive GMC Blazer with a fibreglass cap. The large detector volume of 4250 cm^3 (250 in^3) was particularly useful in providing good counting statistics in the relatively low count rate areas expected on the basis of the airborne reconnaissance survey results.

2. High Voltage Supply and Amplifiers

The high voltage power supply for the photomultiplier tubes and the preamplifiers were contained in a package designed by McPhar Instrument Corp. The package was relatively compact (10 x 15 x 35 cm) and operated from the 24-volt car battery arrangement.

3. The Four-Channel Portable Gamma-Ray Spectrometer

The four-channel portable gamma-ray spectrometer used in the carborne system was a McPhar Instrument Corp. Spectra 44. This instrument with dimensions 27. 9 x 17 x 9 cm was powered independently from its own set of 12 D cells. The total count channel recorded gamma-rays above 0. 4 MeV. The differential channels for K, U, and Th were centred at energies of 1. 46 MeV, 1. 76 MeV, and 2. 62 MeV with window widths of 200 keV, 200 keV, and 400 keV respectively.

The instrument energy calibration was carried out by centring the 0. 662 MeV peak from a Cs-137 source in a special calibration window.

Any one of the four channels could be selected for analog chart recording. A time constant (integrator) of 1 or 2 seconds was used. In digital mode the output from each of the four channels was displayed in sequence after a preset counting time.

The Spectra 44 was easily removed from the carborne system and connected to a 7. 6 x 7. 6 cm NaI(T1) detector for *in situ* analyses. This hand-portable system with the small detector had been previously calibrated in Ottawa at the Geological Survey calibration pads at Uplands Airport (Grasty and Charbonneau, 1974).

4. The Strip Chart Recorder

The recorder was a Hewlett Packard model 7155B single pen recorder with a fixed event marker pen. Pens were disposable cartridge felt-tip type. A wide selection of chart speeds and ranges was available, but the most commonly used settings were 0. 2 V/cm with a 30 s/cm chart speed. At 20 km per hour vehicle speed (5. 6 m/s) each centimetre of chart paper represented

[1]Prince Edward Island Department of Industry and Commerce

From: Report of Activities, Part C;
Geol. Surv. Can., Paper 76-1C (1976)

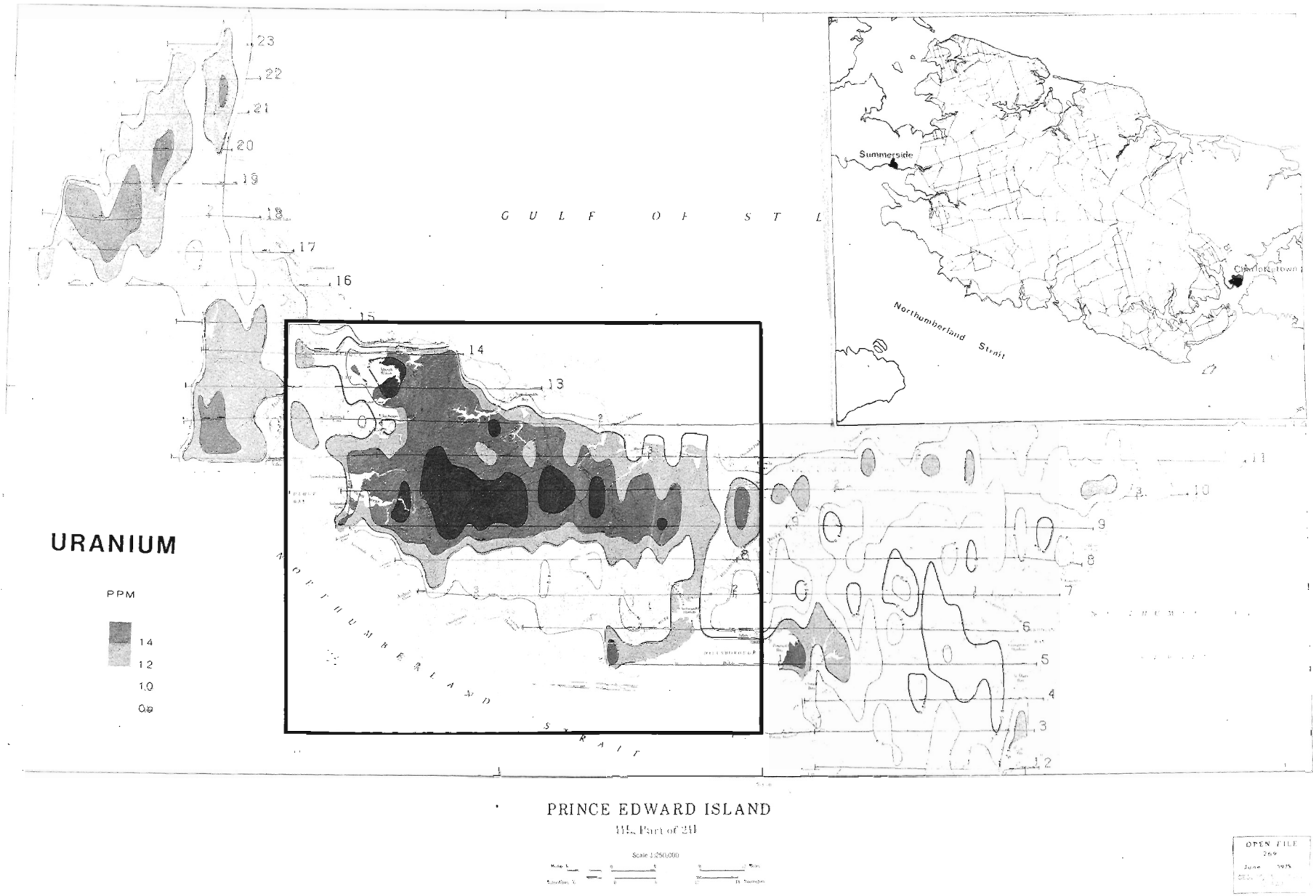

Figure 51.1. The road network traversed by the carborne gamma-ray survey, and the contoured uranium map from the airborne gamma-ray spectrometer survey of Prince Edward Island.

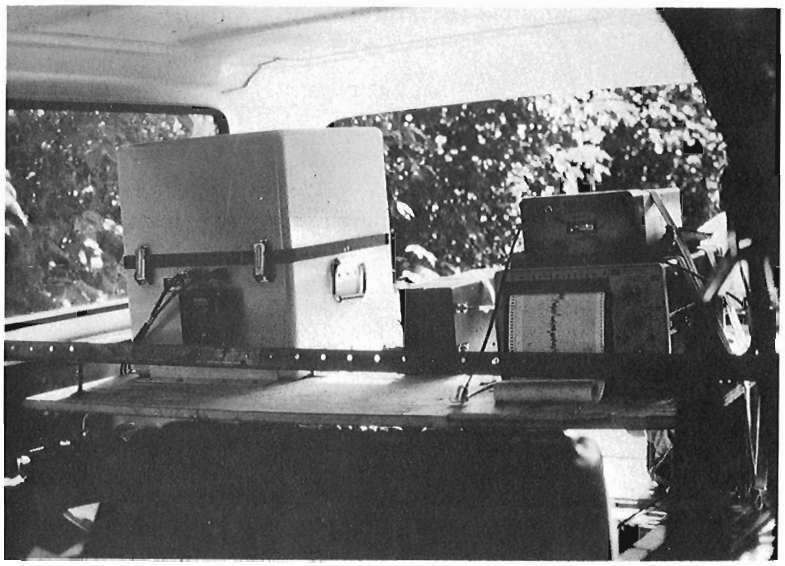

Figure 51.2.

The carborne gamma-ray survey instrumentation showing the detector package (left), high voltage and pre-amplifier (centre) and the chart recorder and portable gamma-ray spectrometer (right).

about 167 m (i.e. 6 cm of chart paper per kilometre). The chart recorder was capable of operating from external DC, AC, or internal rechargeable Nickel Cadmium batteries. It was normally powered by the 24 V external car battery supply. The count rate scale was adjusted to provide about 100 counts per second per centimetre of chart for total count recording and 10 cps/cm for K, U, and Th recording.

Survey Procedure

The survey was conducted over a ten-week period by two persons; a driver and an instrument operator. At the beginning and end of each day the energy calibration with the cesium source was carried out at a base station and data from several digital mode count periods were recorded as an aid in calibrating the chart paper. A base line was then traversed in order to establish that the carborne system was performing satisfactorily and that results were reproducible.

At the start of each road traverse a digital mode count was recorded to ensure that the pen excursions across the chart paper agreed with the digital count rate.

Traverses were made driving at 20 km/h along the shoulder of the road. A fiducial marker switch located on the dashboard of the truck was pressed to mark events on the strip chart such as beginning and end of traverse, road crossings, rivers or changes in road surface material. It was found that the best technique was to pre-mark event numbers on the 1:50 000 base map. The operator made appropriate notes in a log book about the event.

Discussion of Preliminary Results

At the time of writing, compilation of the survey results is incomplete, and the retraversing of anomalous zones while recording the output from the K, U, and Th channels of the spectrometer is still in progress.

Typical background count rates recorded with the system were 400 cps along paved roads and 500 cps along unpaved roads. Anomalous count rates were of the order of 700 cps. Several of the anomalies which were investigated were found to be primarily due to increases in potassium concentrations. Others were determined to be related to geometric effects such as embankments which had not been noted during the original traverse. Areas of outcrop also generally gave higher values than areas of overburden (Charbonneau *et al.*, in press).

It was also found that the carborne survey was able to locate accurately areas of increased radioelement concentration which had been indicated on the maps produced by the airborne reconnaissance survey. Some records which indicate an increase in potassium content along the traverse have been tentatively interpreted as due to a subtle change between two sub-units of a Permian sandstone.

The compilation of the data, correlation with geology, and interpretation must be completed before the direction of further work can be indicated.

References

Charbonneau, B.W., Killeen, P.G., Carson, J.M., Cameron, G.W., and Richardson K.A.
"The significance of radioelement concentration measurements made by airborne gamma-ray spectrometry over the Canadian Shield"; *in* Proceedings of International Symposium on Exploration of Uranium Deposits, IAEA Vienna 29 March – 2 April 1976, p. 20. (in press)

Grasty, R.L. and Charbonneau, B.W.
1974: "Gamma-ray spectrometer calibration facilities"; *in* Report of Activities, Part B, Geol. Surv. Can., Paper 74-1B, p. 69-71.

Richardson, K.A. and Holman, P.B.
1975: "Airborne radioactivity maps and profiles, Prince Edward Island"; Geol. Surv. Can., Open File 269.

SOME PROBLEMS IN THE USE OF GRAIN SIZE STATISTICS

Projects 740062, 740063

D. Swan, J.J. Clague, and J.L. Luternauer
Terrain Sciences Division, Vancouver

In recent years many attempts have been made to differentiate sedimentary environments using statistical parameters derived from grain size distributions. The potential of such an approach has been demonstrated by Pelletier (1975) in a study that isolates different energy regimes in the Beaufort Sea. It is evident, however, that techniques developed for specific areas cannot always be applied universally with equal success (Soluhub and Klovan, 1970).

In order to make optimum use of the large amount of grain size data available for marine sediments obtained off the west coast of Canada, the present authors are attempting: (1) to examine carefully the formulation of the various grain size statistical parameters presently in use and (2) to evaluate the effectiveness of the many techniques available for discriminating and classifying sedimentary environments.

Early in these investigations it became apparent that statistical parameters calculated by the two most widely used techniques, the graphic (Folk and Ward, 1957) and moment (for example, Friedman, 1962a), were not always comparable. Koldijk (1968), Davis and Ehrlich (1970), and Isphording (1972) found that graphic measures are less sensitive than moment measures. It is clear, however, that moment parameters should not have unqualified endorsement either. As was pointed out by Folk (1966) and later in more detail by Jones (1970) and Jaquet and Vernet (1976), the moment measures can be significantly in error, even for normally distributed samples, because of inaccuracies introduced by truncating and grouping data. Studies made by the present authors on theoretical distributions composed of 1000 digitally generated "grains" indicate that no simple factor (such as Sheppard's correction: Kendall and Stuart, 1958) can bring the ungrouped and grouped statistical parameters into exact agreement. Moreover, it was found that neither resieving at a smaller class interval nor artificially subdividing the grouped data (using either linear or probability type interpolations) can guarantee an improvement in the accuracy of values derived from grouped data.

At that stage of the study the authors became interested in the differences between data derived from sieving and data from thin section point counts. Although the fundamental difference between number frequency and weight frequency has been recognized by many authors (Pye, 1943; Grassy, 1943; Rosenfeld *et al.*, 1953; Van der Plas, 1962; Kellerhals *et al.*, 1975), most interest has been focused on converting thin section data into a form comparable to sieving data (Friedman, 1958, 1962b). Little effort has been made to discover what changes are produced when weight frequency, rather than number frequency, is used as the basis for calculating statistical parameters, despite an excellent discussion of the problem by Krumbein and Pettijohn (1938, p. 225-227) nearly forty years ago. It is generally assumed that the "mean" size calculated using the formula presented in Friedman (1962a) represents the average size of all the particles in a sample. A simple example demonstrates that this is not, in fact, the case.

If we consider four spherical particles having Φ sizes 0.5Φ through 3.5Φ and density $\rho = 2.65$ g/cm^3, it is simple to calculate the mass of the particles and hence the weight per cent represented by each "fraction" in this highly unusual "sample" (Table 52.1).

The phi mean size of the particles is 2.0, and their mean weight is 0.14013 mg. It can be shown that a particle of this weight would have a diameter equivalent to 1.1028Φ units. However, the phi "mean" size as calculated using a formula involving weight per cent frequencies is 0.6419, which is neither the true mean size nor the size of the particle having the mean weight of the grains in the sample. It may be that this number (0.6419Φ units) is as statistically useful a discriminator of environments as is the true mean. It is difficult, however, to establish what, exactly, a number thus generated represents. This problem becomes even greater for the higher moments. One can estimate the true moments by using a number frequency calculated by assuming that all the particles in a given size class (1) are spherical, (2) are the size of the midpoint of the class, and (3) have uniform density ρ

$$\text{i.e., } m = \rho v = \frac{4}{3} n\pi\rho r^3$$

Thus the number of particles in the ith size fraction, and the corresponding frequency (f) are, respectively

$$n_i = \frac{6m_i}{\pi\rho 2^{-3\Phi \text{mid}_i}}$$

$$f_i = \frac{n_i}{\Sigma n_i}$$

where the summation is taken over all the size fractions in a sample. Using this estimated frequency, rather than the weight per cent, should produce a better estimate of the true moments for the particles in a sample.

Apart from the above rather philosophical problems involved in the use of grain size statistics, several practical or operational difficulties have surfaced in the literature. The present writers have found it impossible to duplicate exactly the values given for statistical parameters published by several authors. One source of error may be the method used for calculation of graphic parameters. The originators of

From: Report of Activities, Part C;
Geol. Surv. Can., Paper 76-1C (1976).

Table 52.1

Calculation of diameter (d), radius (r), volume (v), mass (m), and weight per cent (w) for each of four particles

size	d(mm)	r(mm)	v(mm^3)	m(mg)	w
0.5	0.7071	0.3536	0.185120	0.490568	87.52
1.5	0.3536	0.1768	0.023140	0.061321	10.94
2.5	0.1768	0.0884	0.002893	0.007665	1.37
3.5	0.0884	0.0442	0.000362	0.000958	0.17

these measures required that percentiles be read from graphs plotted on probability paper. This means that machine calculations of these parameters must make use of probability or gaussian interpolations between known points, requiring the use of an inverse gaussian function:

$$\text{gauss}^{-1}(x) \quad \text{where}$$

$$x = \text{gauss}(z) = \frac{1}{\sqrt{2\pi}} \int_{-\infty}^{z} e^{-z^2/2} dz$$

The present writers are aware of at least two computer programs discussed in the literature (Koldijk, 1968; Isphording, 1970) which do not use this type of interpolation technique, even though the differences between the two methods can be substantial. The latter program also incorporates an apparently extraneous factor of two in the denominator of the skewness formula, a factor which, until recently, was in a program used by the present writers. The writers wish to caution any researchers using computer programs for the calculation of grain size statistical parameters and suggest that all values derived by such programs be checked thoroughly against results in publications which include both raw grain size data and derived values (Inman, 1952).

Further research is being undertaken in an effort to quantify the differences between ungrouped and grouped number frequency measures, grouped weight frequency measures, and percentile measures based upon frequency by weight distributions. It is hoped that these differences can be related to some independent characteristic of sediment samples, such as an χ^2 value.

References

Davis, M.W. and Ehrlich, R.
1970: Relationship between measures of sediment-size-frequency distributions and the nature of sediments; Geol. Soc. Am., Bull., v. 81, p. 3537-3548.

Folk, R.L.
1966: A review of grain-size parameters; Sedimentology, v. 6, p. 73-93.

Folk, R.L. and Ward, W.C.
1957: Brazos River bar: a study in the significance of grainsize parameters; J. Sediment. Petrol., v. 27, p. 3-26.

Friedman, G.M.
1958: Determination of sieve-size distribution from thin-section data for sedimentary petrological studies; J. Geol., v. 66, p. 394-416.

1962a: On sorting, sorting coefficients, and the lognormality of the grainsize distribution of sandstones; J. Geol., v. 70, p. 737-753.

1962b: Comparison of moment measures for sieving and thin-section data in sedimentary petrological studies; J. Sediment. Petrol., v. 32, p. 15-25.

Grassy, R.G.
1943: Use of the microprojector in the mechanical analysis of small samples of river sand; J. Sediment. Petrol., v. 13, p. 44-57.

Inman, D.L.
1952: Measures for describing the size distribution of sediments; J. Sediment. Petrol., v. 22, p. 125-145.

Isphording, W.C.
1970: Fortran IV program for the calculation of measures of central tendency and dispersion on I.B.M. 360 computer; J. Geol., v. 78, p. 626-628.

1972: Analysis of variance applied to measures of central tendency and dispersion in sediments; J. Sediment. Petrol., v. 42, p. 107-121.

Jaquet, J.M. and Vernet, J.P.
1976: Moment and graphic size parameters in the sediments of Lake Geneva (Switzerland); J. Sediment. Petrol., v. 46, p. 305-312.

Jones, T.A.
1970: Comparison of the descriptors of sediment grainsize distributions; J. Sediment. Petrol., v. 40, p. 1204-1215.

Kellerhals, R., Shaw, J., and Arora, V.K.
1975: On grain size from thin sections; J. Geol., v. 83, p. 79-96.

Kendall, M.G. and Stuart, A.
1958: The Advanced Theory of Statistics; Hafner, New York, N.Y., v. 1, 433 p.; v. 2, 676 p.; v. 3, 552 p.

Koldijk, W.S.
1968: On environment-sensitive grain-size parameters; Sedimentology, v. 10, p. 57-69.

Krumbein, W. C. and Pettijohn, F. J.
1938: Manual of Sedimentary Petrography; Appleton-Century-Crofts, Inc., New York, 549 p.

Pelletier, B. R.
1975: Sediment dispersal in the southern Beaufort Sea; Beaufort Sea Tech. Rept. 25a, Environ. Can.

Pye, W. D.
1943: Rapid methods of making sedimentological analyses of arenaceous sediments; J. Sediment. Petrol., v. 13, p. 85-104.

Rosenfeld, M. A., Jacobson, L., and Ferm, J. C.
1953: A comparison of sieve and thin-section techniques for size analysis; J. Geol., v. 61, p. 114-132.

Soluhub, J. T. and Klovan, J. E.
1970: Evaluation of grain-size parameters in lacustrine environments; J. Sediment. Petrol., v. 40, p. 81-101.

Van der Plas, L.
1962: Preliminary note on the granulometric analysis of sedimentary rocks; Sedimentology, v. 1, p. 145-157.

53. PRELIMINARY RESULTS OF FLUME STUDIES INTO THE ARMOURING OF A COARSE SEDIMENT MIXTURE

Project 750080

T.J. Day
Terrain Sciences Divison

Introduction

This paper presents some early results from an experimental study into the development and hydraulic performance of an armoured stream bed formed through degradation of a known sediment mixture. The armouring of a nonuniform sediment can occur through selective transport of the finer size fractions. In this study, a gravel bed is exposed to shear stress less than that required to induce general transport of all particles. Under the influence of these shear stresses the finer size fractions are removed until the bed is stabilized by a layer of coarse particles. This surface pavement or armour effectively prevents any further degradation. The size distribution of the armour layer and its roughness are then a function of the size distribution of the parent bed material and the imposed shear stress.

It is of economic consequence in stable channel design to know whether or not it is possible to use this self-stabilizing tendency of alluvial channels flowing in coarse, nonuniform sediments. More specifically this experimental project was initiated in support of reconnaissance studies of northern rivers (GSC projects 750077 and 750079). Knowledge of the formation of bed armour and its effect on channel hydraulics is of importance for: (1) channel stabilization for design effects — it is important to predict how much material will be eroded and the nature of the final stable channel surface; (2) prediction of the stage-discharge function, which is dependent upon both channel geometry and bed roughness; and (3) understanding the effect of bed disturbances resulting from construction.

Previous studies into armouring have been concerned with bed degradation over relatively gentle slopes and small particle sizes. Little (1972) studied the effect of size gradation on the resultant armour coat. Maintaining a constant geometric mean diameter, Little used five gradations (geometric standard deviation) ranging from 1.12 to 3.0. The flume slope was set at 0.002. Little found that the relations between the sediment properties of the original and armoured distributions and the flow properties could be defined empirically as

$$\frac{D_a}{D_o \sigma_o} = 0.908 \left[\frac{u_{*c}^3}{\gamma (s-1) g} \right]^{0.353} \qquad (1)$$

where D_a and D_o are the geometric mean diameters of the armoured and original sediment mixtures, σ is the geometric standard deviation of the original sediment mixture, u_{*c} is the critical bed shear velocity defined as gRS where g is the acceleration due to gravity, R is the hydraulic radius, S is the slope of the energy grade line, γ is the kinematic velocity of water, and s is the specific gravity of the sediment. For given flow conditions and original sediment properties, the geometric mean diameter of the armoured layer can be determined.

Davies (1974) developed another empirical equation for predicting D_a

$$\frac{D_a}{\log (D_o \sigma_o^2)} = 1.839 \left[\frac{u_*^3}{\gamma (s-1) g} \right]^{0.389} \qquad (2)$$

Davies also advanced a similar equation for the prediction of the geometric standard deviation of the armoured distribution. For these experiments the mean particle size ranged from 1.0 to 18.2 mm, the standard deviation from 1.89 to 15.44 mm, and the flume slope from 0.0026 to 0.0045. Davies (1974, p. 84) stated that Little's equation could not be accurately applied to sediments with a mean grain size other than 1 mm.

The objectives of this project are: (1) to investigate the armouring process over steeper slopes and coarser size fractions, as might be encountered in mountainous terrain and (2) to investigate the armouring processes under various sediment transport rates. The results presented herein refer to experiments in which a coarse sediment mixture is subjected to selected shear stresses. In particular, this report explains the experimental procedure and discusses the behaviour of the resistance law and changes in bed roughness.

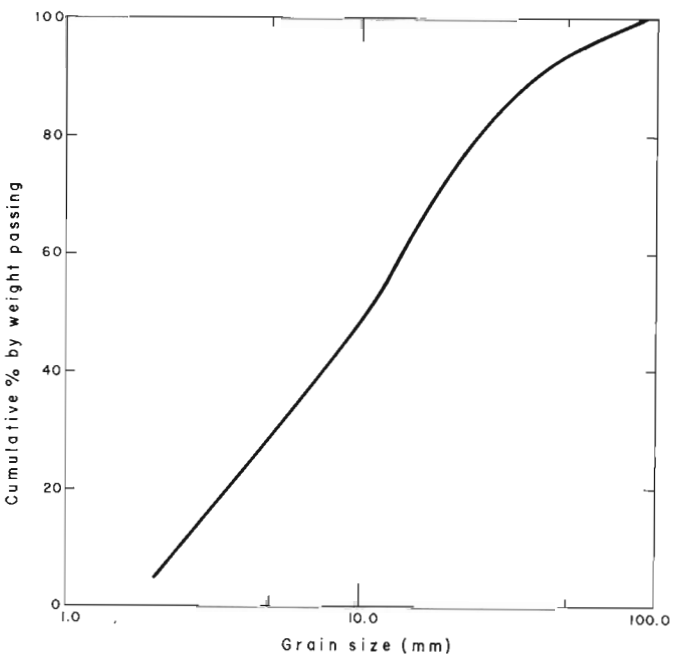

Figure 53.1. Mean grain size distribution for original bed material.

From: Report of Activities, Part C;
Geol. Surv. Can., Paper 76-1C (1976).

Table 53.1

Summary of Hydraulic Parameters

Test No.	No. of Flows	Flume Slope	Range of Hydraulic Variables: Discharge, Q (ℓ/s)	Mean Velocity, ū (cm/s)	Mean Depth, d (cm)	Shear Velocity, u (cm/s)	D_{90} (mm)	h_{90} (mm)
1	10	0.0069	32 - 105	44.4 - 93.2	8.6 - 15.6	6.8 - 8.6	43	22.5
2	4	0.0104	19 - 77	34.4 - 79.7	7.2 - 12.6	7.9 - 9.8	45	20.0
3	1-6	0.0053	24 - 94	26.6 - 62.8	11.8 - 19.5	6.8 - 8.2	63	22.5
	2-6	0.0075	17 - 94	19.6 - 67.6	11.3 - 18.1	8.0 - 9.5	63	22.5
	3-6	0.0100	20 - 97	29.1 - 80.3	8.9 - 15.8	8.5 - 10.5	63	22.5
	4-6	0.0126	20 - 96	30.3 - 81.5	8.6 - 15.4	9.3 - 11.7	63	22.5
	5-5	0.0157	18 - 93	35.3 - 92.2	6.7 - 13.2	9.4 - 12.3	63	22.5
	6-5	0.0179	20 - 90	34.8 - 98.5	7.5 - 11.9	10.5 - 12.6	63	22.5
	7-6	0.0205	18 - 90	30.3 - 103.9	7.6 - 11.3	11.4 - 13.2	63	22.5
4	1-6	0.0250	26 - 92	53.2 - 102.6	6.4 - 11.7	11.6 - 14.8	*	30.0

* unavailable at time of writing

Experimental Method

Flume

The study is being carried out in the sedimentation flume located at the Geological Survey of Canada, Ottawa. The flume is a recirculating model with a main channel 18.3 m long, 0.76 m wide, and 0.6 m deep. The maximum possible slope is 0.050. A detailed description of the flume can be found in McDonald (1972).

Bed Preparation

The flume was filled to a depth of 15 cm along 14 m of the channel (from 2 to 16 m). The upstream flow approached the sediment bed first over an angled mesh screen to lift the flow above the sediment bed and then over a block (1 x 0.76 x 0.10 m) of gravel with a resin matrix. This block was set to ensure a hydrodynamically rough surface.

To obtain the essential uniform flow, an underflow gate was installed at the downstream end of the flume. Adjustment of this gate prevents any drawdown effects. At the downstream end of the sediment bed a 1 x 0.76 m sloping aluminum plate was installed to minimize scouring. This hinged plate can be raised and lowered along metal threads connected to a transverse bar set across the flume top. The plate also assists sediment transported off the bed, out of the flume, and into a mesh collection basket.

Figure 53.2. Upstream view of the flume working section. The bed shown is that formed in test 3. (GSC-203091-E)

Figure 53. 3.

Photographic sequence of the sediment sampling procedure:

A - the predetermined surface area is spray-painted;

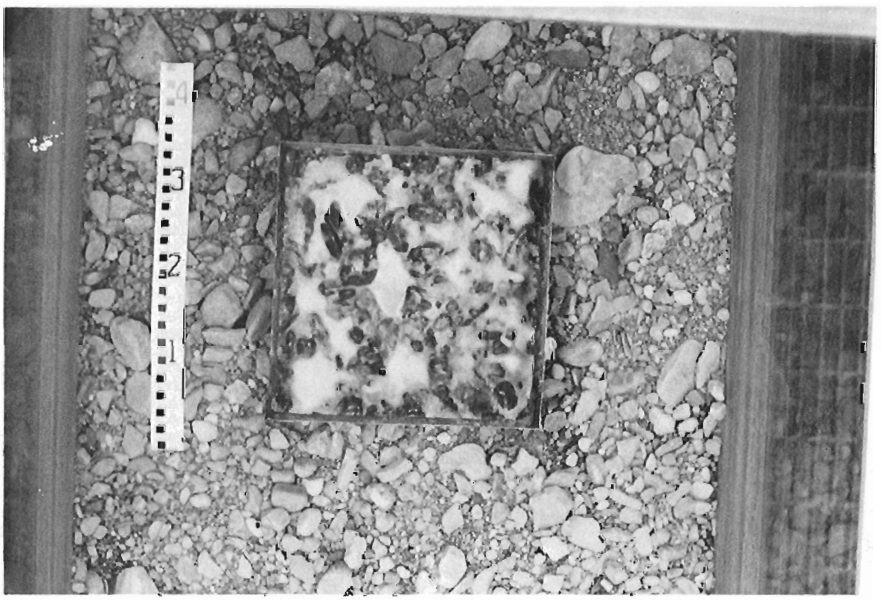

B - a wax cast is made of this surface area;

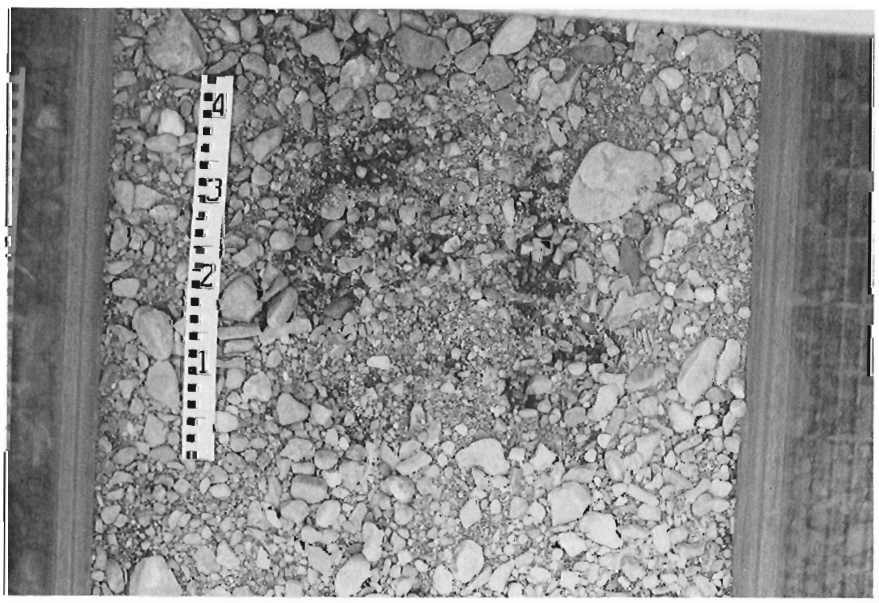

C - the flume bed after removal of the wax cast. (GSC-203091-B, C, D).

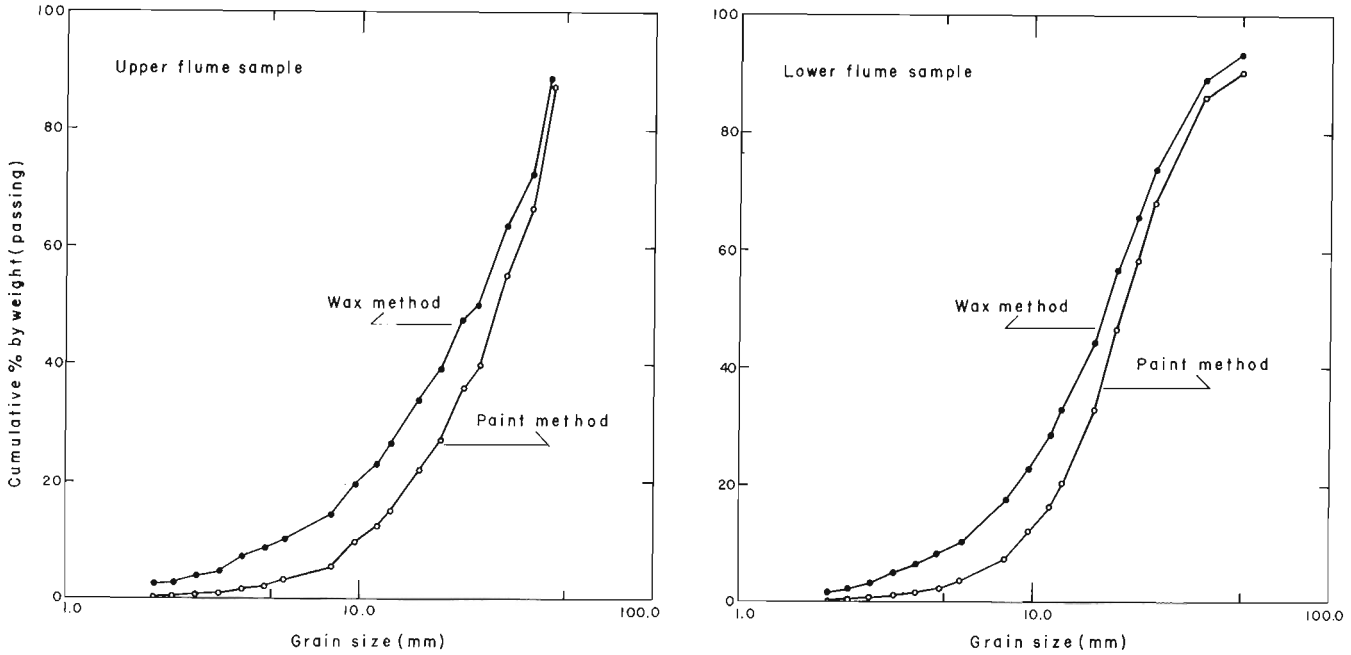

Figure 53.4. Two comparisons of grain size distributions using the paint and wax-casting methods.

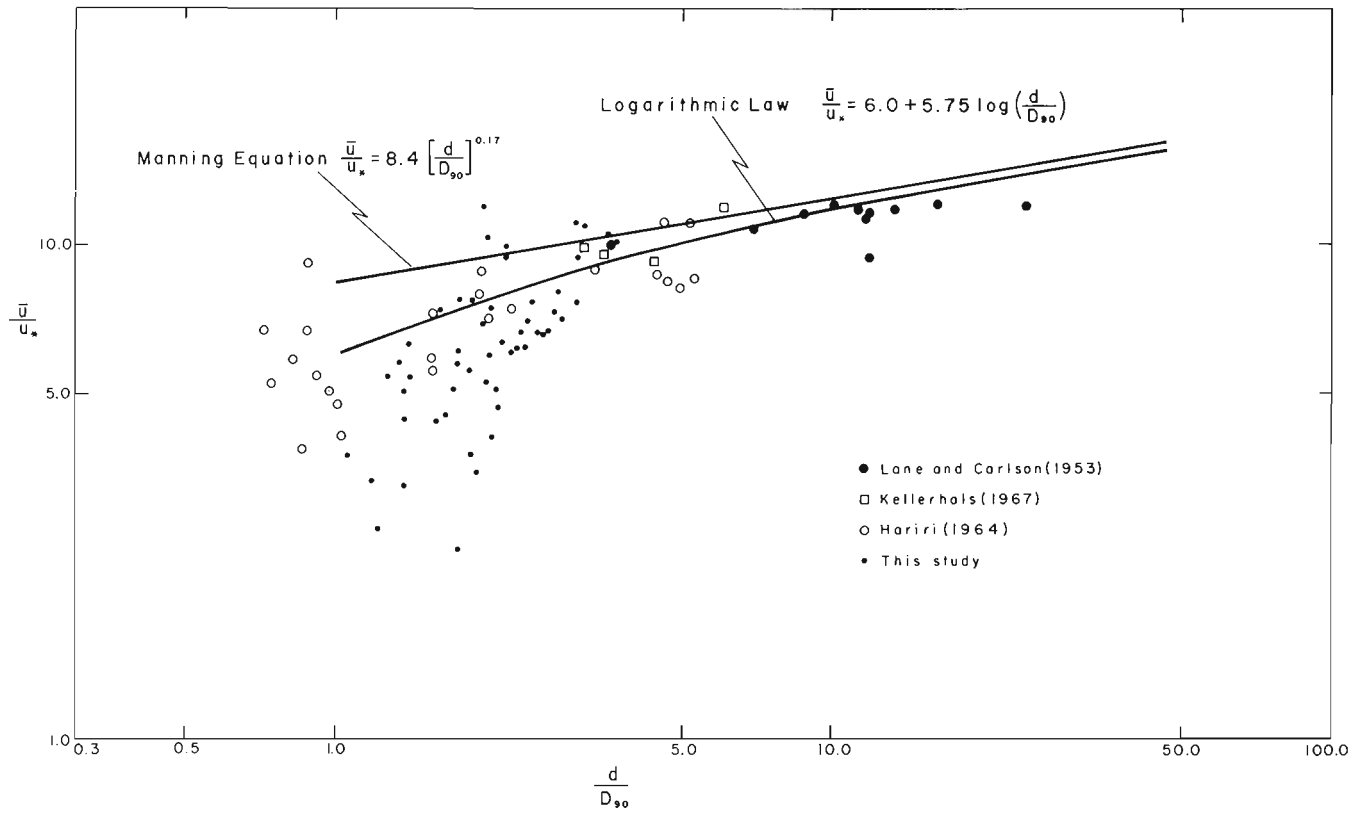

Figure 53.5. Flow resistance data for tests 1, 2, and 3 plotted with two resistance equations and selected data from other sources.

Bed Material

The initial sediment mixture was acquired from a local gravel pit and was sieved to produce a particle-size distribution with a range of 2 to 90 mm. This lower limit was set arbitrarily but is near the maximum competence of the flume. Once the sediment bed was prepared in the flume, a series of samples were taken to determine the grain size distribution and any variation along the flume. The mean distribution results from these samples are shown in Figure 53.1. The sediment bed was smoothed in preparation for the first experiment.

Due to expected scour problems at both upstream and downstream ends of the sediment bed, no measurements were made over the first and last 2 m. A 5 m-long working section was established midway along the flume, between the 6 and 11 m sections. This section is used for all hydraulic and bed roughness measurements. No sediment samples were taken in this section.

Test Sequence

A test series begins with the establishment of a flume slope, then a predetermined uniform flow is maintained until sediment movement becomes minimal and sporadic. Bed stabilization can require more than 24 hours. The hydraulic properties of the stabilized bed then are evaluated by running a sequence of lower discharges at the same flume slope. In text 3 the fixed bed was evaluated over both a range of discharges and a range of slopes. The flume is then drained and photographed, samples are taken, and a roughness profile is taken at 1 cm intervals through the working section. Figure 53.2 is an upstream view of the flume over the working section.

Data Summary

To date three test series (tests 1, 2, 3), and the initial flows of the fourth series (test 4) have been completed. A hydraulic summary of these 60 flows is presented in Table 53.1. The bed for test 1 was stabilized with a discharge of 105 ℓ/s (shear velocity of 8.9 cm/s) over a slope of 0.0069. Sediment transport was minor, and the bed more truly represented the original surface. In test 2 sediment transport was more general, as was the case in test 3. Only the stabilizing flow for test 4 is available at this time. The upper limit of flow is approximately the present capacity of the flume. The mean hydraulics are determined from rigorous measurements made at 0.1 m intervals longitudinally through the centre of the working section.

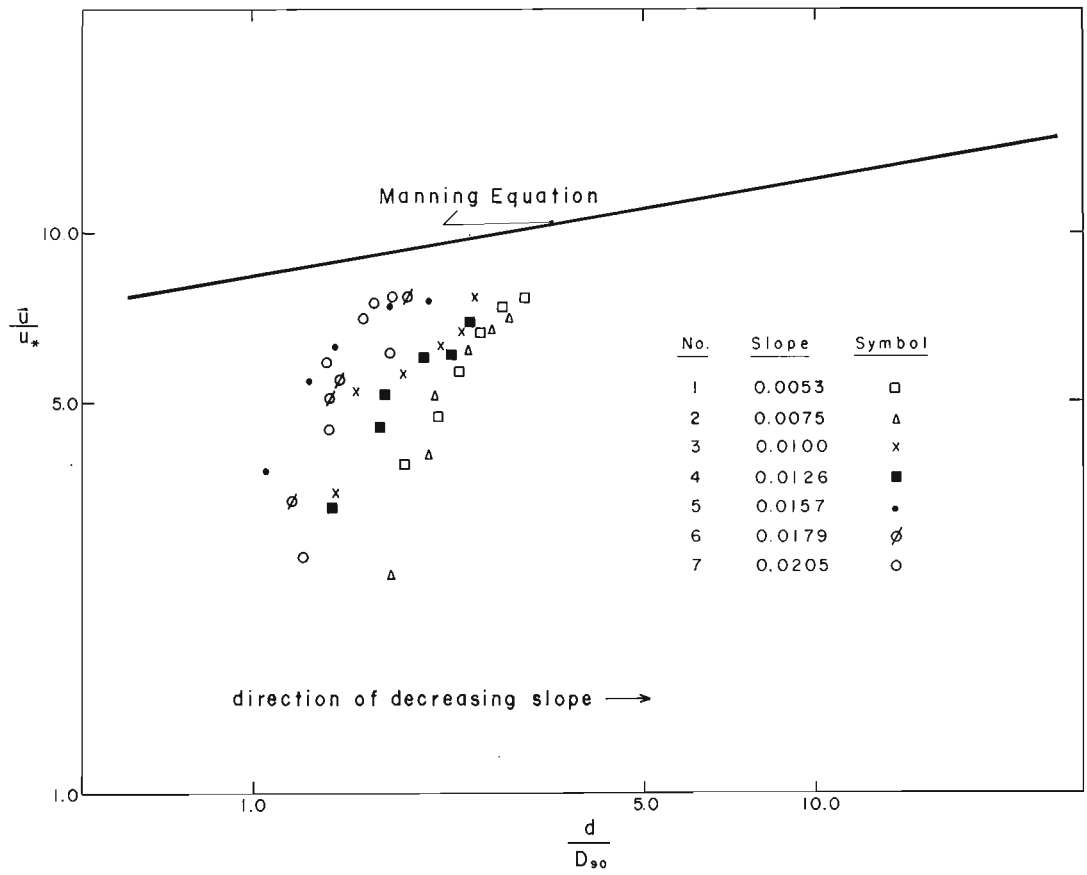

Figure 53.6. Flow resistance data for test 3 only, separated on the basis of original flume slope

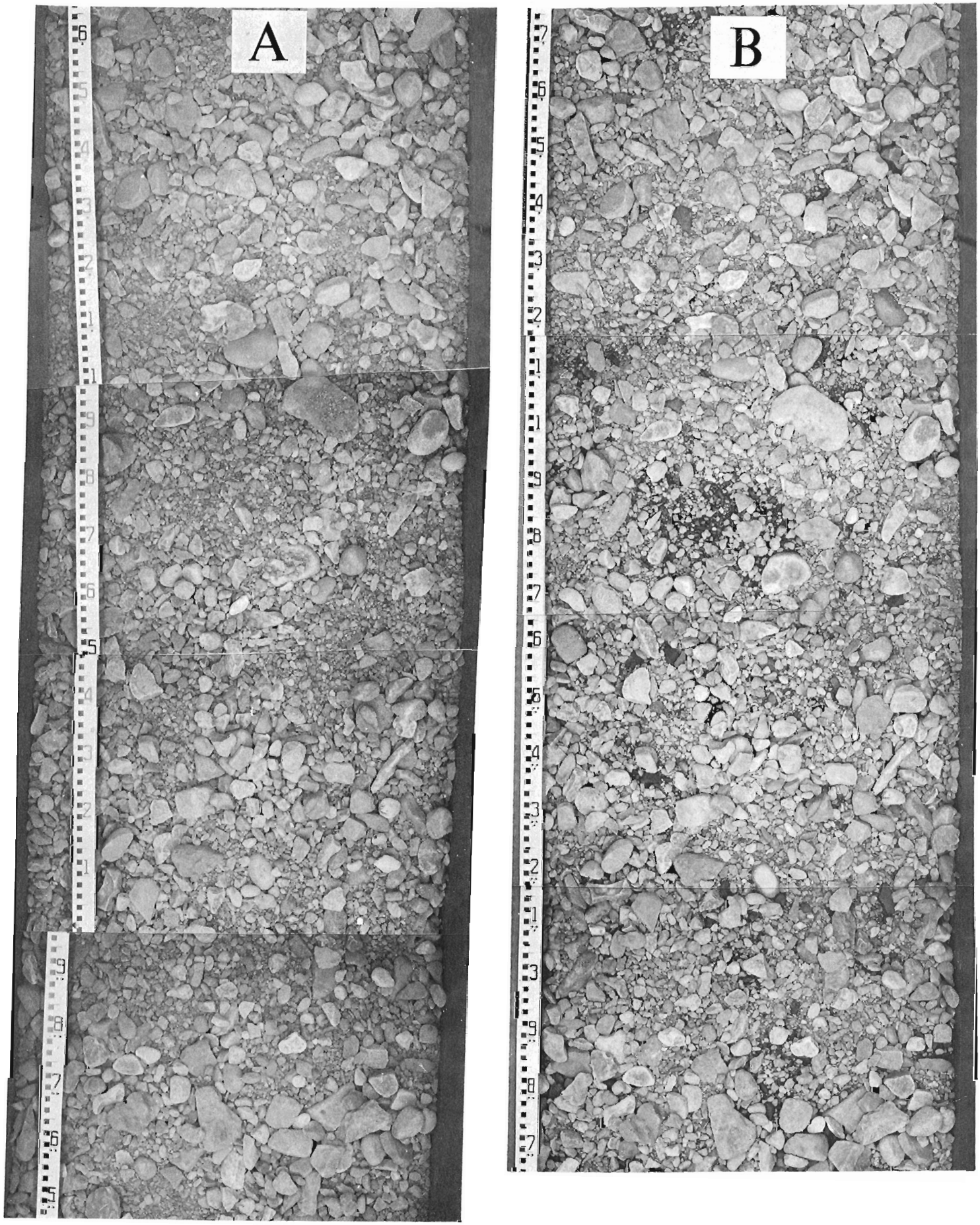
A
B

Figure 53. 7.

Vertical photographs of working section.

A - the original bed before experimentaion (GSC-203088-B, C, D, E);

B - flume bed after test 1 (GSC-203089-A, B, C, D);

C - flume bed after test 3 (GSC-203090-B, C, D, E)

Sediment Sampling

Two areal sampling variants are being used to sample the armour distribution. Previous studies have used the wax cast method where a predetermined surface area is coated with molten wax. After the wax has solidified, the cast is removed and the sediment is separated and sieved. Wax casting is being used in the present study as well as a second method which involves painting a predetermined area. The sampling sequence is shown in Figure 53.3 as both methods are used on the same sample (i.e. the wax cast is made over the painted surface), their results should be similar — that is, the methods are equivalent. Comparisons such as those shown in Figure 53.4, however, indicate that these techniques do not produce the same results. Using the wax method consistently results in an overrepresentation of the finer size fractions which apparently results from wax penetration below the armour layer. For the commercial wax used in these experiments, a temperature of approximately 50°C results in the molten wax solidifying upon contact with the bed. Further experimentation is required to determine the nature of the differences between the the two methods and how they vary with the size distribution of the armour layer, if at all.

Flow Resistance

Flow resistance over hydrodynamically rough boundaries commonly is described either by the logarithmic flow law (Keulegan, 1938)

$$\frac{\bar{u}}{u_*} = 6.0 + 5.75 \log \left[\frac{R}{k_s}\right] \qquad (3)$$

or by the Manning equation for particle resistance

$$\frac{\bar{u}}{u_*} = 8.4 \left[\frac{d}{D_{90}}\right]^{0.17} \qquad (4)$$

where $\bar{u}$ is the mean cross-sectional velocity, k_s is a length describing the boundary roughness, d is the mean flow depth, and D_{90} is that size fraction below which 90 per cent of the size distribution falls. The roughness parameter k_s represents the integrated effect of roughness height, spacing, and particle shape, and must be derived from equation (3). For convenience the grain size parameter D_{90} is used as a measure of the total resistance described by k_s, and the mean flow depth d can replace R for wide, shallow flows.

In their discussion of the hydraulics of shallow, gravel-bed streams, Church and Gilbert (1975) suggested that the resistance law should have a more generalized form

$$\frac{\bar{u}}{u_*} = c_1 \left[\frac{d}{D_{90}}\right]^{c_2} \qquad (5)$$

Their suggestion for this general power law relationship was based on evidence of the wide range in values for c_1 and c_2 found in natural channels. Kellerhals (1967), for example, found values of $c_1 = 6.5$ and $c_2 = 0.25$ (for $1.5 < d/D_{90} < 20.0$) for stable gravel-paved channels. Church (1972) found a mean c_2 value of 0.67 for shallow gravel-bed streams. These high exponents indicate a much more rapid decrease in resistance than either the logarithmic or Manning equation. Church suggested that changes in form resistance (e.g. pool and riffle sequence) and live bed conditions (sand transport smoothing the gravel bed) could produce such a rapid decrease in resistance.

The two parameters of the resistance equation have been calculated for the 54 flows of tests 1, 2, and 3, and these values are plotted in Figure 53.5. Both equations (3) and (4) are plotted in this diagram. Additional data from stable gravel-paved canals (Lane and Carlson, 1953), from flume experiments in gravel (Kellerhals, 1967), and from flume studies by Hariri (1964) also are shown in Figure 53.5.

As can be seen in Figure 53.5, the resistance data from the present study plot well below the standard particle resistance equations. The data show a general trend of initially high resistances which rapidly decrease as flow scale increases, similar to Church's observations. The scatter in these data is not surprising as a wide range in c_1 values is known to exist.

Some insight into the nature of the variables affecting the resistance law is offered in Figure 53.6, where the 40 flows of test 3 are separated according to the original flume slope. For this test the flume originally was set at 0.0205, and the bed was stabilized under a flow of 90 ℓ/s (shear velocity of 13.2 cm/s). Five lower flows were run over this bed at the original slope. Six additional runs of 5 or 6 discharges were tested over different slopes. From these data (Fig. 53.6 and Table 53.2) it is evident that the resistance law is sensitive to slope, with steeper slopes exhibiting higher initial resistances. These results mean that c_1 parameter is a function of slope. The c_2 exponent of the resistance law appears to be independent of channel slope. These observations support Hariri's (1964) results which indicated that the rate of increase of the mean velocity (the effect of decreasing resistance) is a function of the bed material only (bed roughness was fixed for the present test, and the c_2 values do not show any trend), and the initial resistance is a function of slope only.

Figure 53.6 also shows that the resistance law becomes nonlinear for values of u/u_* greater than 6 and that this nonlinearity tends to become more pronounced for larger slopes. A possible, although purely speculative explanation for this behaviour could be the drowning out of the larger size bed particles. At lower flows these particles may offer form resistance in that they cause major flow distortions. As flow increases, the effect of this form resistance law may approach the particle resistance equations as flow increases.

Bed Roughness

As bed degradation continues with increasing bed shear, the material of the armour layer becomes larger

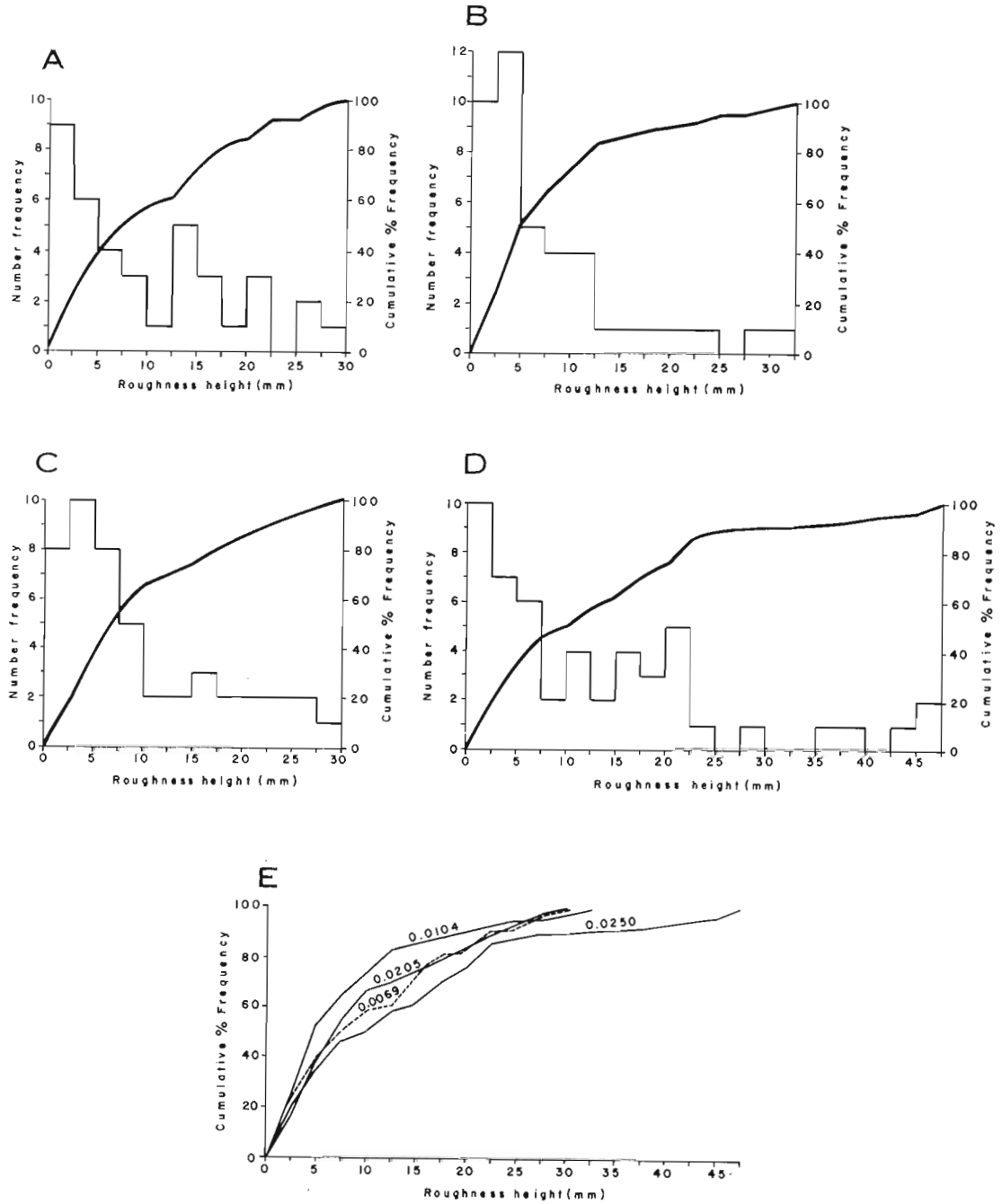

A - bed surface after test 1.

B - bed surface after test 2.

C - bed surface after test 3.

D - bed surface after test 4.

E - comparison of cumulative frequencies.

Figure 53. 8. Distribution of positive bed roughness heights for a 1 m length in the working section.

Table 53.2

Power Curve Fits for Resistance Equations

Test No.	Slope	No. of Data Points	Power Equation	r^2
1	0.00526	6	$\frac{\bar{u}}{u_*} = 1.63 \left[\frac{d}{D_{90}}\right]^{1.43}$	0.97
2	0.00745	6	$\frac{\bar{u}}{u_*} = 0.83 \left[\frac{d}{D_{90}}\right]^{2.18}$	0.87
3	0.0100	6	$\frac{\bar{u}}{u_*} = 2.73 \left[\frac{d}{D_{90}}\right]^{1.11}$	0.85
4	0.0126	6	$\frac{\bar{u}}{u_*} = 2.39 \left[\frac{d}{D_{90}}\right]^{1.23}$	0.93
5	0.0157	5	$\frac{\bar{u}}{u_*} = 4.05 \left[\frac{d}{D_{90}}\right]^{0.98}$	0.85
6	0.0179	5	$\frac{\bar{u}}{u_*} = 2.83 \left[\frac{d}{D_{90}}\right]^{1.56}$	0.89
7	0.0205	6	$\frac{\bar{u}}{u_*} = 1.97 \left[\frac{d}{D_{90}}\right]^{2.63}$	0.79

and the bed roughness should increase (this latter effect will not be true if concentration of the bed particles increases to the point where the bed, in effect, becomes smoother). The increase in particle size is shown in column 8 of Table 53.1. It must be remembered that the bed over which test 1 was made is really an inherited one and does not reflect a bed formed in response to a specific shear stress. Figure 53.7 shows a portion of the original working section and the changes in the bed after tests 1 and 3.

Bed roughness changes through the working section are being evaluated from a longitudinal profile measured at 1 cm intervals along the centre line. These results are being analyzed for height and spacing properties. An example of the changes in bed roughness in response to varying shear stresses is given in Figure 53.8. The data shown here are those positive heights above the mean bed for a 1 m section of the roughness profile. This diagram clearly shows that the armour layer is becoming rougher, and the packing or concentration of particles is irregular. The main effect of increasing shear stress is to produce more frequent mid and upper range roughnesses. A roughness height, h_{90}, for the tests is listed in Table 53.1.

In the first three tests the increased shear caused only rearrangement of bed particles. During the first few hours of test 4, however, gravel antidunes formed in the flume. As flow continued these features gradually degraded (cf. Fig. 53.9) until only the coarser particles remained. The surficial expression of these washed out antidunes is similar to that of transverse ribs (McDonald and Banerjee, 1971). The flume observations support Boothroyd's (1970) observation that transverse ribs may be relict antidunes.

Further Study

Experimentation will continue with larger shear stresses. If the data from these experiments are compatible with the results from other investigations, then the investigation will progress to its second stage of studying the effect of sediment transport rates on armour properties. If the present results are not compatible, further studies using different grain sizes will be required.

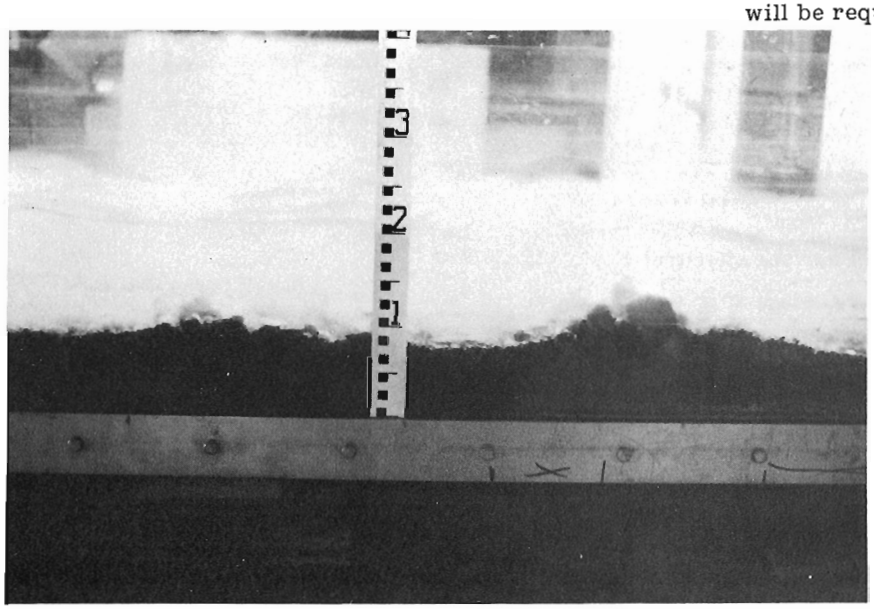

Figure 53.9.

Example of a degrading antidune during test 4 (photograph courtesy of R.J. Gale).

Acknowledgments

The author gratefully acknowledges the assistance of R.J. Gale and J.R. Luscombe.

References

Boothroyd, J.C.
1970: Recent braided-stream sedimentation, south-central Alaska; Am. Assoc. Pet. Geol., Bull., v. 54, p. 836, (Abstr.).

Church, M.
1972: Baffin Island sandurs: a study of arctic fluvial processes; Geol. Surv. Can., Bull. 216, 208 p.

Church, M. and Gilbert, R.
1975: Proglacial fluvial and lacustrine environments; *in* Glaciofluvial and Glaciolacustrine Sedimentation, eds. A.V. Jopling and B.C. McDonald, Soc. Econ. Paleontol. Mineral., Spec. Pub. no. 23, p. 22-100.

Davies, B.E.
1974: The armouring of alluvial channel beds; unpubl. M.Sc. thesis, University of Canterbury, Christchurch, 118 p.

Hariri, D.
1964: The relation between the bed pavement and the hydraulic characteristics of high gradient channels in noncohesive sediments; unpubl. Ph.D. thesis, Utah State University, Logan, 109 p.

Kellerhals, R.
1967: Stable channels with gravel-paved beds; Am. Soc. Civ. Eng., J. Water. Harb. Div., WW1, p. 63-84.

Keulegan, G.H.
1938: Laws of turbulent flows in open channels; J. Res. U.S. Geol. Surv., v. 21, Res. Paper 1151, p. 707-741.

Lane, E.W. and Carlson, E.J.
1953: Some factors affecting the stability of canals constructed in coarse granular materials; Int. Assoc. Hydraul. Res., Minneapolis, p. 37-43.

Little, W.
1972: The role of sediment gradation on channel armouring ; unpubl. Ph.D. thesis, Georgia Institute of Technology, 105 p.

McDonald, B.C.
1972: The Geological Survey of Canada sedimentation flume; Geol. Surv. Can., Paper 71-46, 12 p.

McDonald, B.C. and Banerjee, I.
1971: Sediments and bed forms on a braided outwash plain; Can. J. Earth Sci., v. 8, p. 1282-1301.

54. LATE WISCONSINAN ICE LIMITS IN THE ATLANTIC PROVINCES OF CANADA WITH PARTICULAR REFERENCE TO CAPE BRETON ISLAND, NOVA SCOTIA

Project 700056

D. R. Grant
Terrain Sciences Division

Field work on this project was concluded with the mapping of Quaternary features in the most inaccessible parts of the plateau surface and coastline of the Cape Breton Highlands and Mabou Hills (Fig. 54.1). Access was by foot along the western scarps of Mabou Hills and along the Aspy fault-line scarp to Cape North, by fishing boat along the west coast of the highlands, by forest access road in the southern highlands courtesy Nova Scotia Forest Industries Ltd., by helicopter in the vicinity of the Wreck Cove Hydroelectric project courtesy the Nova Scotia Power Corp., and throughout the interior of Cape Breton Highlands National Park, courtesy Eastern Ecological Research Ltd. which is conducting a biophysical mapping program.

Attempts were made to clarify the juxtaposition of thick drumlinized till areas on the southeastern plateau with extensive felsenmeer, sandy colluvium and grus in the central and northern plateaus. On the marginal lowlands, efforts were made to resolve more precisely the complex sequence of striations which indicates that ice flow initially was from the Gulf of St. Lawrence onto the west coast, then from the south through intermontane valleys to the west coast, and finally radially outward from the highlands.

Along the west coast, though rock types are like those on the east, slopes have a noticeably more mature and well graded catenary profile, and a peculiar bright-red pebbly silt of problematical origin thinly veneers most other sediments, including glaciofluvial gravels with which it is commonly graditional. The occurrences of a wave-cut platform a few metres above present high tide were carefully mapped for two reasons: because the platform probably is of interglacial age, as it is overlain by peats dating more than 40 ka, it serves as a datum for subsequent crustal movements both isostatic and tectonic and helps to define the limits of later glacial pulses as evidenced by the presence or absence of superimposed tills or striations.

By this means it was discovered that the effects of glacial scour and deposition are absent over the bench within a short distance along the coast laterally from the mouths of valleys that are clearly U-shaped and carry till and outwash. For the intervening stretches, the bench, as clearly recognized by its smoothed potholed surface and mantle of clean beach boulders, is buried by a gently slopping apron of substratified sandy rubbly diamicton interpreted as solifluction debris or "head" and/or by poorly sorted subrounded gravels obviously deposited in alluvial fans. Locally where the bench is backed by cliffs rising to the plateau, talus cones presently are accumulating over both head and gravel. No compact sediment, containing straited transported stones, that could be called till is found in such sequences of sorted materials. Thus the limits of glaciations since the formation of the bench can be defined, as well as the limit of the most recent (late Wisconsinan) ice to cover the area.

Using the relations at Cape North as the control or type area, data from previous reports on Cape Breton, specifically the three phase sequence of glacial expansions (Grant, 1971), tentatively are placed within the chronologic framework of the Wisconsinan Stage as summarized by Dreimanis (pers. comm., 1976) for example. Supported by essentially equivalent relations in the Yarmouth area of Nova Scotia (Grant, 1976), the deployment of ice can be inferred over the rest of the province where features are more ambiguous. Ice dispersal in New Brunswick and Prince Edward Island is consistent with the model of glaciation being developed for Nova Scotia, but for Gaspé Peninsula a separate and not very extensive ice field is indicated. In Newfoundland a parallel development took place: ice grew mainly from all interior uplands and from the largest highland plateaus, but in moving seaward it was insufficiently thick or extensive to overtop many high coastal tablelands so that numerous nunataks existed.

In retrospect, an understanding of the style and progress of Wisconsinan glaciation in the Atlantic Provinces would have been reached sooner had the mapping commenced in northern Cape Breton. Nevertheless, it has only just become clear what rank or duration of nonglacial interval is represented by the various ice-free areas that have been proposed for some time. Until recently for example, the significance of areas of weathered broken bedrock standing above till-covered or ice-scoured terrain was not appreciated; they were assumed to have developed since the last glaciation as a consequence of elevation. There are now compelling arguments about the antiquity of such discontinuities in northern Labrador, Baffin Island, the southern Queen Elizabeth Islands, Mackenzie Valley, Yukon, and even the Prairies where a much reduced late Wisconsinan glaciation is indicated. The revision of the limits set forth below is in good agreement with the new appreciation of late Wisconsinan Laurentide glacial limits for the country as a whole.

Cape Breton Island

On the northern plateau a small ice cap was centred more or less along the axis, such that the higher western tablelands produced reentrants in the ice margin which account for the fact that tills and ice-marginal features related to this ice cap are found only in the vicinity of major valleys reaching well into the highlands. Local glaciers apparently occupied a few smaller valleys along the west coast at the mouths of which hummocky end moraines were built. On the plateau and along the

From: Report of Activities, Part C;
Geol. Surv. Can., Paper 76-1C (1976).

coast between glaciated valleys, the supposed interglacial marine bench is unmodified and no tills are seen except for a red drift of Carboniferous lithology derived from the Gulf of St. Lawrence during an earlier flow of ice against Cape Breton. The northern and eastern sectors of the ice cap were drained by two vigorous outlet glaciers occupying Aspy Valley and the troughs at Ingonish. Along Aspy scarp the former ice tongue may have been joined by tributary cirque glaciers from the sidewall, but it did not extend more than a few kilometres beyond the present coast because the interglacial bench is untouched as far as Cape North. On its western side, it is uncertain whether the plateau ice cap flowed onto the coastal lowland at the latest stage, or if it only sent a tongue into the upper reaches of Margaree River. The southern margin of the ice cap is more uncertain. Along the eastern highlands coast the youthful glacial topography, a few striations, and the interlayering of reddish lowland tills with greyish crystalline highlands tills is taken to signify confluence with a larger ice dome that covered much of the southern lowland over Bras d'Or Lake and flowed northeastward onto the shelf off Sydney. This larger ice mass spread seaward across southern Cape Breton, with an ice divide trending eastward across Bras d'Or Lake. Its northwestward flowing quadrant, however, abutted against and deployed around uplands and plateaus (e. g. Mabou Hills) with tongues extending northward through three intermontane passes to the west coast. In George Bay its western flank was contiguous to the upland ice sheet on mainland Nova Scotia and extended northward perhaps as far as Port Hood. The northward

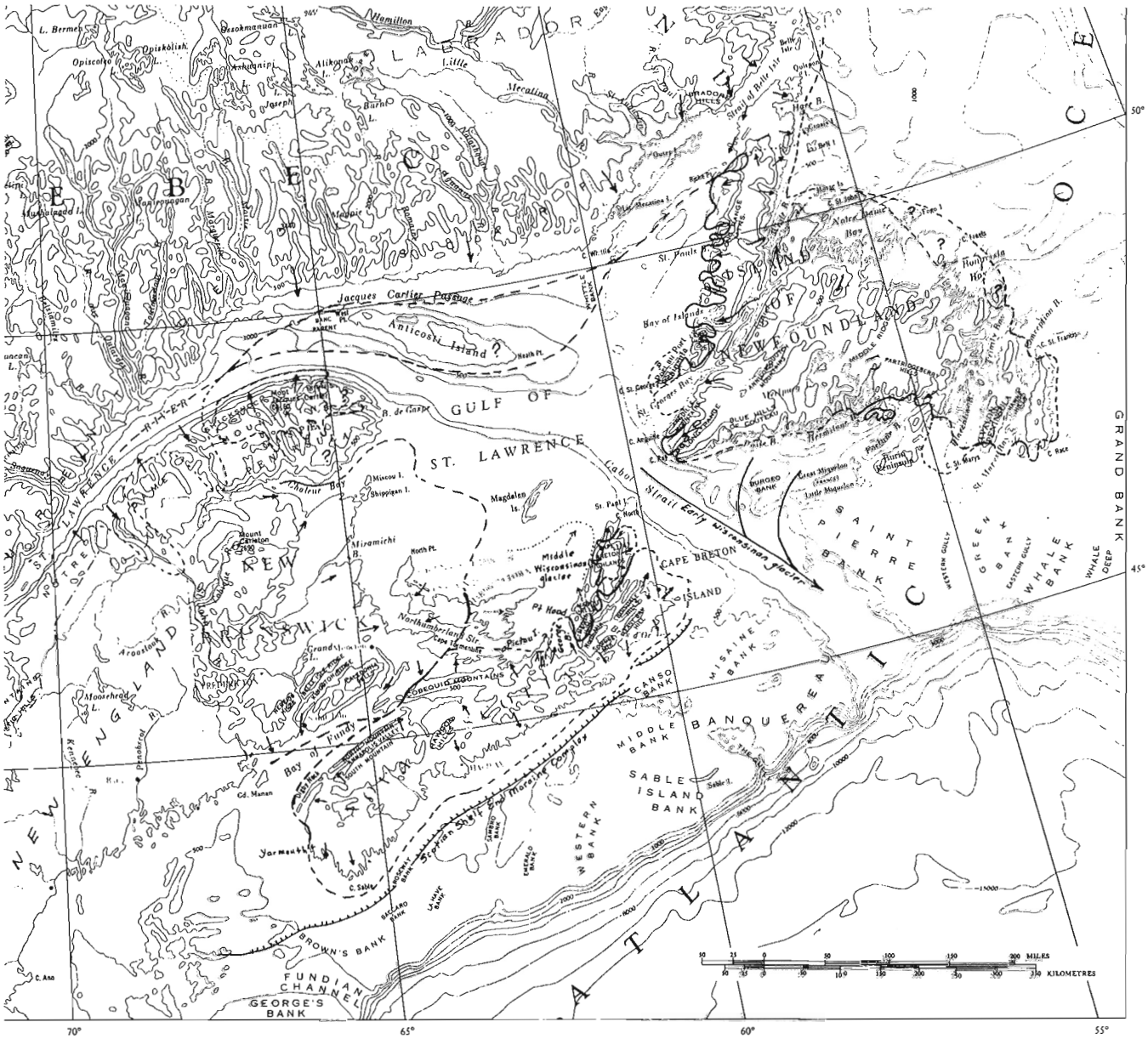

Figure 54. 1. Late Wisconsinan ice limits in the Atlantic Provinces.

limit is uncertain because during a preceding Wisconsinan Stadial, an earlier lowland ice dome also moved along a similar course into the Gulf of St. Lawrence along the west coast past Mabou Hills.

Mainland Nova Scotia

For the rest of the province a more regular outline is inferred because the central uplands, on which several local ice caps grew, are extensive and uniform and have few marginal prominences, except possibly the Antigonish Highlands and Cobequid Mountains to interrupt the gradient. The southern ice limit is almost certainly offshore on the Scotian Shelf, perhaps along the end moraine mapped by King (1969). Along the outer Bay of Fundy coast ice flow was northward radially offshore, with a discontinuity against southward directed features in the Yarmouth area where there is evidence that middle and early Wisconsinan deposits lie beyond the late Wisconsinan boundary (Grant, 1976). New Brunswick ice seems to have crossed upper Bay of Fundy and abutted southward against Cobequid Mountains where it was in contact with ice farther west in northern Nova Scotia which flowed northward into Northumberland Strait as far offshore as Pictou Island.

Prince Edward Island

Eastern Prince Edward Island has no Nova Scotian erratics and bears only a west-to-east glacial lineation, possibly resulting from an earlier glacial phase. In contrast, ice flow over western Prince Edward Island was varied and complex, with the latest movement being south and west as if from a separate source on the shelf. Such a centre is reasonable as the broad shelf around Magdalen Islands would have been completely emergent during the late Wisconsinan eustatically lowered sea level and could explain the curious deflection of eastward-flowing New Brunswick ice to the southwest down Bay of Fundy.

New Brunswick and Gaspé Peninsula

In northern New Brunswick the highlands sustained an ice cap that flowed eastward down Chaleur Bay where ice from Gaspé Peninsula was confluent, at least at an earlier stage. The Appalachian Mountains to the west were the source of ice that flowed southward across New England and was abutted on the north and locally was penetrated by Laurentide ice. On Gaspé Peninsula proper there is evidence that the high tablelands had a separate ice cap which thinned towards the coast into separate valley glaciers in some valleys. Many valleys, particularly those on the southern slopes, are glacially unmodified, and the terrain appears to have a distinct maturity of fluvial dissection as if it lay beyond at least the late Wisconsinan ice border.

Newfoundland

Glacial features throughout the island consistently indicate the presence of a single ice sheet or a complex of ice caps which spread radially to the sea, except for the northernmost part of the Long Range Mountains where striations and Labradorean erratics show a minor invasion by Laurentide ice across the shallow Strait of Belle Isle (Grant, 1969a). There, the line of confluence trended southwestward to Riche Point, west of which the two ice domains calved into a deep submarine channel. Laurentide ice thus is inferred to have been confined to the north side of the Gulf until it merged with Appalachian ice in the upper St. Lawrence estuary; Newfoundland ice deployed from a subordinate centre in the northern Long Range Mountains through fiords between nunataks (Grant, 1969b) to modest piedmont lobes a short distance offshore from the western lowlands.

Farther south it was interior ice located over Grand Lake and Annieopsquotch Mountains that squeezed through passes in the Long Range Mountains to terminate in fiords at Bay of Islands and St. Georges Bay, whereas extensive tablelands, such as the Lewis Hills, above 300 to 500 m remained as nunataks. Ice may have deployed around the high terminal portion of Port au Port Peninsula. Along the southern Long Range Mountains ice on the interior plateau flowed southwestward to Cape Ray, skirting extensive felsenmeer-covered nunataks on the Long Range summits. Independent valley glaciers headed in cirques along the west wall of Codroy Valley and coalesced as a separate trunk glacier heading towards Cabot Strait. Most of the Anguille Mountains were thus circumvented.

No ice-free enclaves are yet recognized along the more regularly sloping south coast, except possibly coastal summits above 200 m. Inland ice appears to have been drawn down into Hermitage Bay and Fortune Bay, thereby skirting inland of the rugged summits of Hermitage Peninsula where separate small valley glaciers built moraines into higher sea levels. Similar end moraines at tidewater mark the limit of inland ice across upper Burin Peninsula (which was subjected earlier to ice moving northward from a centre on the continental shelf (Grant, 1975b). At Avalon Isthmus, inland ice merged with a separate small ice cap complex on Avalon Peninsula (Henderson, 1972). There, because of the relief of bays and peninsulas, the ice cap was thin and digitate and extended down bays because of lower sea levels and skirted the termini of some peninsulas judging by prairie-like fields of felsenmeer delimited by small moraines and meltwater channels.

Little can be said of the northern Atlantic side of the island except that there is no evidence that the ice margin did not lie everywhere offshore, though Coleman (1926) speculated that Fogo Island and Bonavista Peninsula might lie beyond the ice border. The juncture with the northern Long Range Mountains ice cap is clearly along White Bay. Neither ice from the interior nor from the Long Range Mountains engulfed Groais and Bell islands, again judging by the felsenmeer fields as well as drowned but unmodified cirques which presumably were cut during lowered sea level (Grant, 1969a).

In summary, the recognition of glacial limits, inferred to be late Wisconsinan, in three areas – western Newfoundland, Cape Breton, and Gaspé Peninsula –

together with conclusive evidence of seaward spreading ice caps on uplands peripheral to the Gulf of St. Lawrence, and only localized Laurentide incursions, are regarded as sufficient grounds to conclude that ice flow in the region was centripetal to the Gulf and that grounded glaciers did not fill it (Grant, 1975a). The Magdalen Islands and parts of the adjacent shelf, therefore, could have escaped glaciation, and the Laurentian and tributary channels may have held only ice shelves. Glacial expansions of the preceding Wisconsinan Stadials appear to have had the same style but greater magnitude; initially, a glacier occupied Cabot Strait implying grounded (Laurentide?) ice in the Gulf.

References

Coleman, A.P.
1926: The Pleistocene of Newfoundland; J. Geol., v. 34, p. 193-223.

Grant, D.R.
1969a: Surficial deposits, geomorphic features, and Late Quaternary history of the terminus of the Northern Peninsula of Newfoundland and adjacent Quebec-Labrador; Mar. Sed., v. 5, p. 123-125.

1969b: Late Pleistocene readvance of piedmont glaciers in western Newfoundland; Mar. Sed., v. 5, p. 126-128.

Grant, D.R. (cont.)
1971: Glaciation of Cape Breton Island; *in* Report of Activities, Part B; Geol. Surv. Can., Paper 71-1B, p. 115-120.

1975a: Glacial style and the Quaternary stratigraphic record in the Atlantic Provinces; *in* Report of Activities, Part B; Geol. Surv. Can., Paper 75-1B, p. 109-110.

1975b: Glacial features of the Hermitage – Burin Peninsula areas of Newfoundland; *in* Report of Activities, Part C; Geol. Surv. Can., Paper 75-1C, p. 333-334.

1976: Reconnaissance of early and middle Wisconsinan deposits along the Yarmouth-Digby coast of Nova Scotia; *in* Report of Activities, Part B; Geol. Surv. Can., Paper 76-1B, p. 363-369.

Henderson, E.P.
1972: Surficial geology of Avalon Peninsula, Newfoundland; Geol. Surv. Can., Mem. 368, p. 121.

King, L.H.
1969: Submarine end moraines and associated deposits on the Scotian Shelf; Geol. Soc. Am., Bull., v. 80, p. 83-96.

55. USE OF AERIAL PHOTOGRAPHS TO MAP SEDIMENT DISTRIBUTION AND TO IDENTIFY HISTORICAL CHANGES ON A TIDAL FLAT

Project 740062

Edmund Medley and John L. Luternauer
Terrain Sciences Division, Vancouver

Introduction

During summer 1976, studies were undertaken to establish the feasibility of using available aerial photographs to:

(a) map Fraser River Delta (Fig. 55.1) tidal flat surficial sediment distribution on the basis of tonal variations in natural colour aerial photographs and
(b) identify the most significant historical changes in intertidal morphology. The examined photographs were exposed over a period spanning the last 25 years during which time a number of major engineering structures were erected across the delta front.

Study Methods

Sediment Distribution

Recent, low water, colour aerial photographs were used which varied in scale, emulsion, and clarity of detail (Table 55.1). The low level, large-scale photographs (IRP 142, *see* Table 55.1) offered the greatest detail and best tonal discrimination.

Green, grey, and brown tones dominated the photography. As greens were considered to represent vegetation, grey and brown tones were isolated (Table 55.2), classified into three (sediment) domains, and mapped. Samples collected over a broad grid (approximately 2 km) in 1974 (Luternauer, 1975, 1976) were used to determine the sediment types represented by the major tonal categories. The trends of apparent major hydrodynamic structures also were noted.

Infrared imagery from 1975 was used to establish the presence or absence of vegetation where natural colour tones appeared greenish-grey or to help define the contact between vegetated areas and sediment domains.

Historical Study

Aerial photographs of the Fraser River Delta tidal flats, obtained during the last 25 years, were carefully examined for evidence of morphologic variations. An effort was made to determine whether or not these were a response to the erection of causeways across the flats.

Specifically, the objective was to establish whether changes occurred in:

(a) areal extent and character of the leading edge of marshes,
(b) densities of creeks within the upper tidal flat marshes,
(c) areal extent and character of the major primary hydrodynamic structures, and
(d) orientation of lower tidal flat drainage channels.

The study was conducted at the British Columbia Institute of Technology using a Jena Interpretoskop (a differential zoom stereoscope). This instrument offers several advantages over the conventional apparatus available for photo comparison because it permits:

(a) stereo examination of aerial photographs of different scales,
(b) rapid scanning of magnified stereo imagery,

Table 55.1

Colour Imagery Used to Study Sediment Distribution

Film Roll No.		Emulsion	Scale	Flight Altitude (m)	Date
*RSA	30518	natural colour	1:110 000	9600	August 1971
RSA	37169	infrared colour	1: 62 000	9450	June 1975
RSA	37170	natural colour	1: 62 000	9450	June 1975
**IRP	142	natural colour	1: 50 000	3810	July 1974

*Film rolls prefixed RSA are federal government photographs, available through the National Air Photo Library, Ottawa.

**The roll prefixed IRP is available through Integrated Resources Photography Ltd., Vancouver.

From: Report of Activities, Part C;
Geol. Surv. Can., Paper 76-1C (1976).

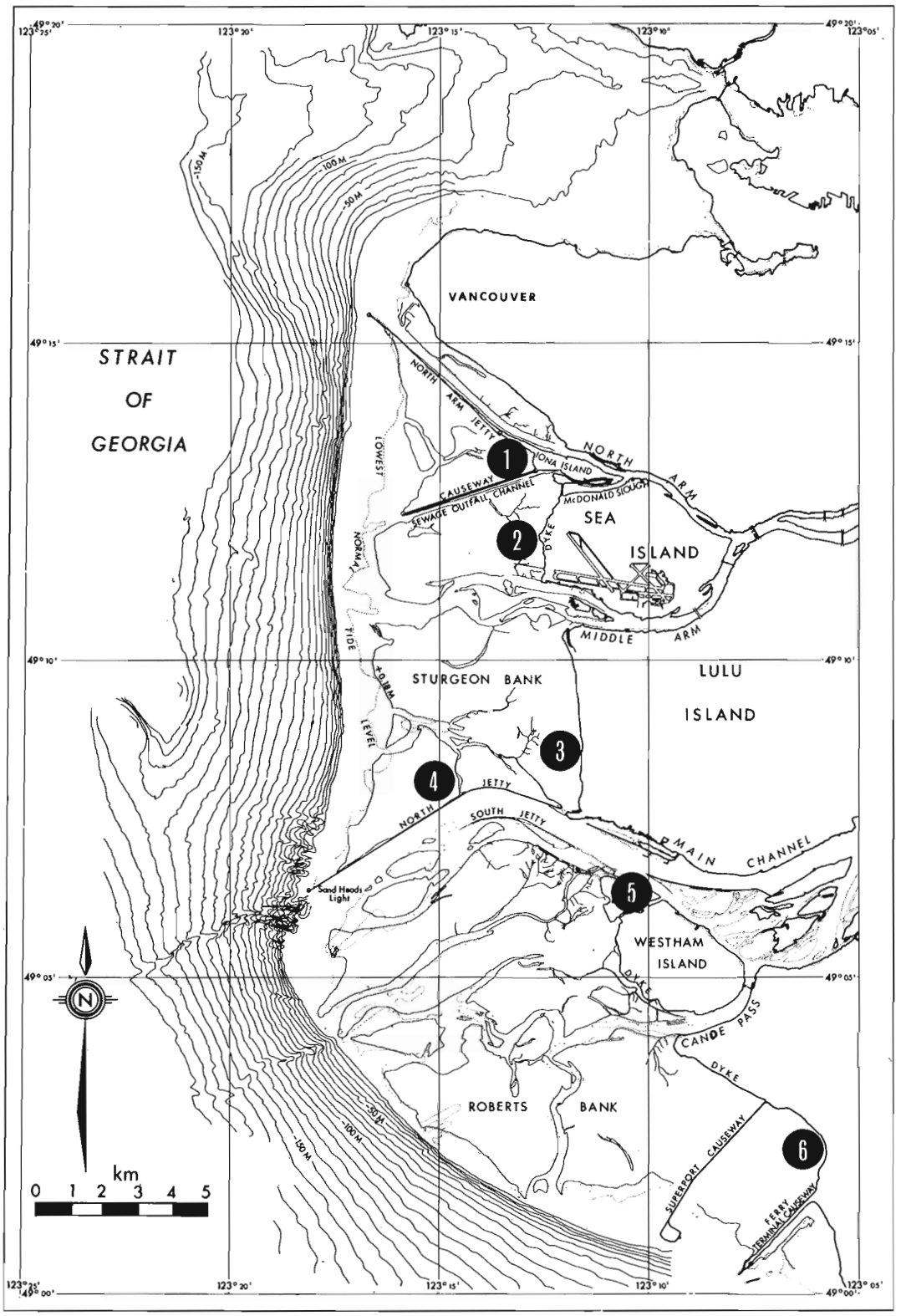

Figure 55. 1. Index map of geographic names referred to in text. Numbered black dots represent areas of particular interest discussed in Selected Locales section of text.

Table 55. 2

Sediment Tone Equivalence for Three Sets of Natural Colour Imagery Over the Tidal Flats

Domain	Film Roll No.	GSA Munsell Colour Code	Description
			(Darkest tones)
1	IRP 142	*5GY 3/2 (dark)	greyish-olive-green
1	A 37170	N3	dark grey
		5G 2/1	greenish-black
1	RSA 30518	N3	dark grey
		5Y 3/2	olive grey
			(Lightest tones)
2	IRP 142	10YR 6/4 (dark)	grey-orange to mod. yellow-brown
		5Y 7/4 (light)	grey-yellow to dusky yellow
2	A 37170	10Y 6/2	pale olive
		5Y 6/2	yellowish – light olive-grey
2	RSA 30518	10YR 8/6	pale yellowish-orange
		5Y 6/2	yellowish-grey
			(Intermediate tones)
3	IRP 142	10Y 4/2 (dark)	greyish-olive
		5Y 7/4 (light)	grey-yellow to dusky yellow
3	A 37170	5GY 2/1	greenish-black
3	RSA 30518	5Y 5/2	light olive-grey

*Since most photos have at least 60 per cent in-line overlap, colours for identical areas in adjacent frames may differ due to changed light conditions.

(c) recognition of lateral changes of reference lines (for example, a marsh edge) which are apparent as *height* displacements. By correcting the parallax, a measurement of horizontal displacement accurate to ±5 microns is possible. Measurements commonly were made against a standard reference photo. The measured displacement is then multiplied by the scale of the reference airphoto to calculate the true horizontal displacement.

(d) comparison of monochromatic photographs which have poor tonal discrimination with natural or infrared colour photographs. An indistinct feature where the stereo effect is poor, such as the fairly diffuse leading edge of a marsh, is easily identifiable by binocular comparison of the two images. This capability is of particular value in examining some of the earlier monochromatic photographs in which the leading edge of a marsh, commonly sparsely vegetated, can readily be confused with the sediment abutting against the marsh.

Results

Sediment Distribution

The sediment distribution indicated by tonal variations in natural colour photography (Table 55. 3, Figs. 55. 2 and 55. 3) clearly reveals the complex patterns of sedimentation on the inner half of the tidal flats. These are brought to light here for the first time. As variations in grain size within the sands on the outer flats are not recognizable on the natural colour photographs, it is evident that changes in sand regimes can only be identified by detailed field work.

Morphologic-Sedimentary Relationships Evident Within Sediment Domains

A number of close relationships between tidal drainage, relief, hydrodynamic structures, and sediment types were noted.

(1) Domain 1 (sands) commonly displayed some form of hydrodynamic structure. Megaripples having

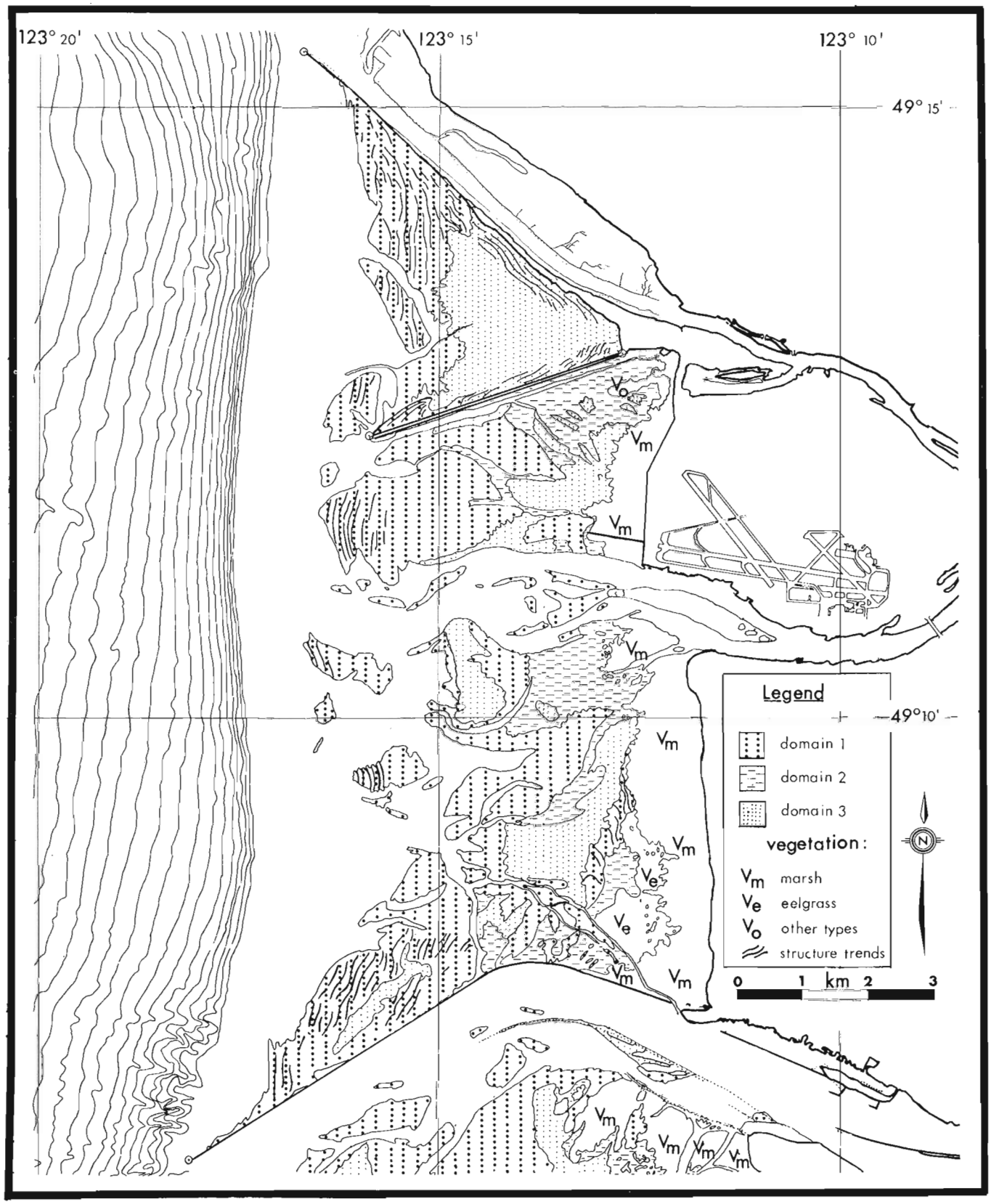

Figure 55. 2. Distribution of surficial sediments and vegetation on the Sturgeon Bank tidal flats in 1974. Sediment domains were defined by tonal variations in colour aerial photographs. Grain size data acquired in 1974 suggest that domain 1 represents sand, domain 2 muds, and domain 3 sandy silts.

wave lengths ranging between 50 m to 100 m and amplitudes below 1 m were identified readily on the smaller scale photos. The low level photographs (IRP 142) in addition revealed apparent linguoid and chaotic structures in places.

(2) Domain 1 sands generally are found on the outer tidal flats and adjacent to river distributaries. Domain 2 muds generally are located on the upper tidal flats, in troughs between major megaripples and sand banks or are found adjacent to major tidal channels. Domain 3 sandy silts are transitional sediments which generally lie between environments represented by domains 1 and 2.

(3) Water-free channels are common in domain 3 sandy silts. These are elongate, narrow features either oriented towards the waterline or issuing from some form of permanent tidal or marsh creek. The water-free channels are darker in tone because sediment flooring them is wetter than adjacent sediments. The lack of water in the channel indicates that sand is probably a component of the sediment.

(4) Dendritic patterns of permanently water-filled drainage channels are common in the relatively impermeable domain 3 sediments.

(5) Isolated patches of coarser sand along the upper flats commonly are associated with subdued sand mounds which may only be evident in photographs taken when water level is relatively high. These smaller scale features are not represented on available topographic maps of the flats.

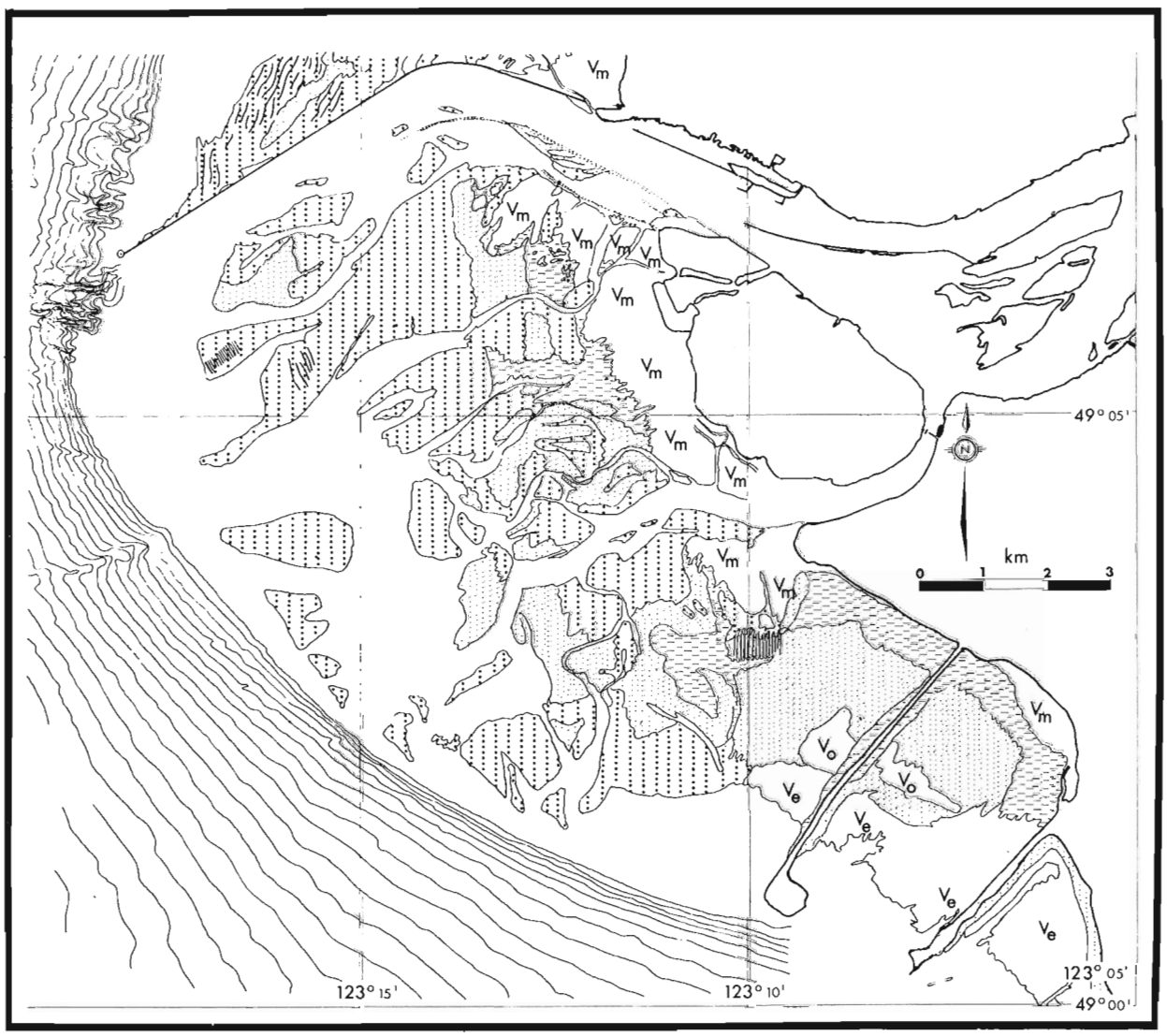

Figure 55.3. Distribution of surficial sediments and vegetation on Roberts Bank tidal flats. Refer to Figure 55.2 for legend and grain size equivalence of patterns represented on map.

Table 55.3

Sediment Domains

Domain	Qualitative Description	Φ Mean grain	Φ Sorting
1	Darkest tones; water-free channels commonly displaying hydrodynamic structures	2.5	0.5
2	Generally lightest tones; water-filled channels and structureless	>4.0	>1.5
3	Tones intermediate to those in above domains; generally water-free channels and sparse structures	2.5 to 4.0	0.5 to 2.7

Some Limitations Inherent in Aerial Photograph Identification of Tidal Flat Features

Some irksome problems hampered interpretation of tones:

(1) The identification of the waterline was often extremely difficult. Recently exposed domain 1 sediments (sands) bear a remarkable similarity to water in the photographs.

(2) Sand becomes lighter in colour as it dries, and thus it can be confused with wet muds. Sparse vegetation communities scattered over the mid tidal flats may be confused with sandy silts. This was recognized during a helicopter reconnaissance over an area off southern Lulu Island. Deposits that had been interpreted as sandy silts were found to be organic-rich muds vegetated with fine eelgrass. The vegetation was recognizable only on 1:50 000 scale infrared photographs which were only available after completion of this exercise; it could not be discerned clearly on the smaller scale imagery used during the course of the project (Table 55.1).

Tidal Flat Vegetation

Marsh vegetation extends about 1000 to 1500 m from the dykes into the tidal flats. The wide variety of flora can be broadly classified into three distinct communities (Figs. 55.2 and 55.3). The trizonal, parallel pattern of the three communities has been noted by Hoos and Packman (1974). This pattern is best developed on the Lulu Island marsh (Fig. 55.1).

Bullrush vegetation (*Scirpus* sp.) is the dominant colonizing community. Advance of the marsh appears to be by colonization upon features of locally higher relief, such as hummocks and sand banks. Apparently a mud fringe does not seem to be a prerequisite for an advancing or stable marsh edge upon the Fraser River Delta tidal flats. This is unlike what has been established for at least one other area (Pestrong, 1969).

Eelgrass development is restricted largely to southern Roberts Bank – principally between the Superport and Tsawwassen Ferry causeways. Presumably eelgrass has flourished here because the causeways have tended to divert turbid, fresh water away from the area (Levings, Fisheries Service, pers. comm., 1976).

The Relation of Topography to Sediment Distribution and Vegetation

The most detailed topographic map of the tidal flats available to the writers was one prepared in April 1967 by Lockwood Survey Corporation (now Pacific Survey Corporation). The contour interval of this map is 0.8 m. The leading edge of the marsh coincides approximately with the 3.8 m contour (above lowest normal water level). Except for the tendency for the sand (domain 1) to lie in the topographically lower outer margin of the tidal flats, there is generally *poor* correlation between mapped sediments and larger scale relief. Field investigation, however, demonstrates that smaller scale (1 m) local relief can have a marked effect on local sediment patterns. For example, mud commonly mantles the troughs of megaripples whereas rippled sands form their crests.

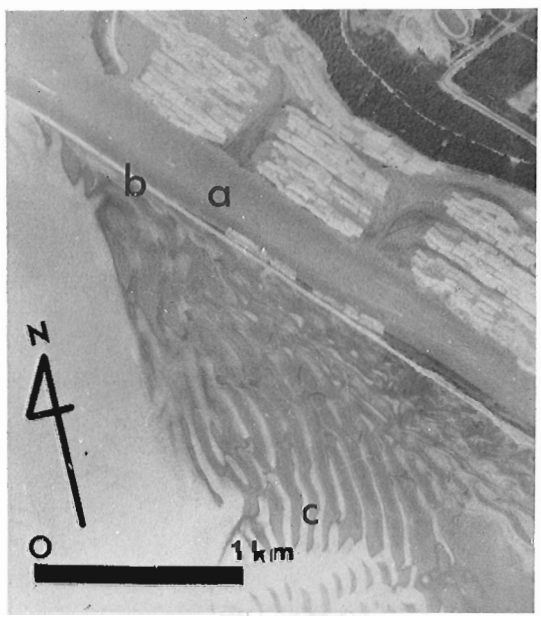

Figure 55.4. Outer tidal flats between North Arm Jetty and Iona Causeway. (IRP 142-65)

(a) North Arm of Fraser River
(b) North Arm Jetty
(c) megaripples in domain 1 sediments.

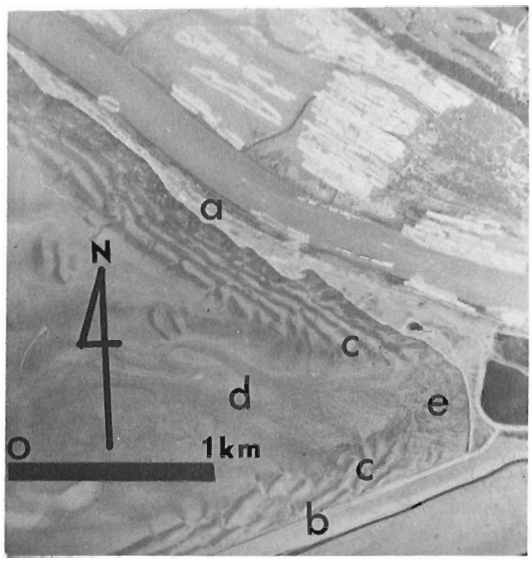

Figure 55.5. Upper tidal flats at junction of North Arm Jetty and Iona Causeway. (IRP 142-74)

(a) North Arm Jetty
(b) Iona Causeway
(c) megaripples in domain 3 sediments
(d) central basin in structureless domain 3 sediments
(e) chaotic zone.

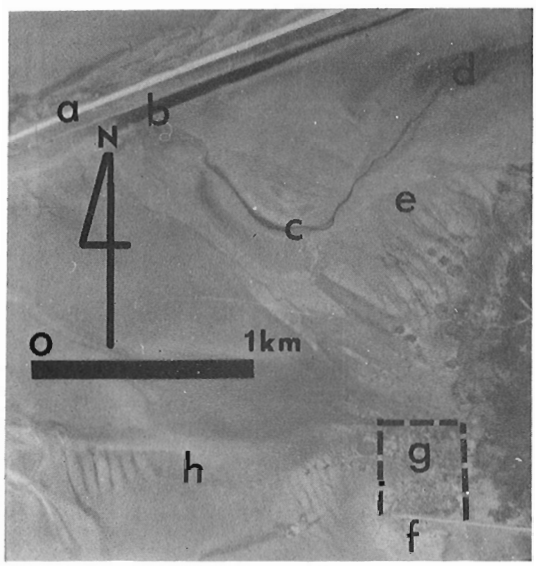

Figure 55.6. Upper tidal flats to northwest of airport Approach Lights Causeway. (IRP 142-76)

(a) Iona Causeway
(b) Iona sewage outfall
(c) relict Fraser River channel within domain 2 sediments
(d) patch of organic-rich, sparsely vegetated mud
(e) trellis pattern of water-free channels in domain 3 sediments
(f) airport Approach Lights Causeway
(g) area colonized by marsh since 1967
(h) structures in domain 1 sediments.

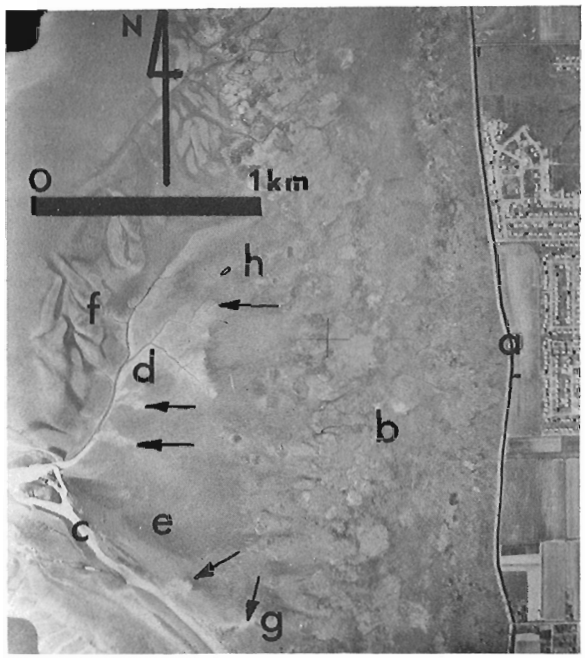

Figure 55.7. 1962 aerial photograph (Government of Canada A17729-75) showing relation of dendritic drainage to the marsh and dyke. Advance of dendritic drainage at the points indicated by the arrows is illustrated by comparison with Figure 55.8. Features labelled e, g and h are illustrated in Figures 55.8, 55.9, and 55.10.

(a) dyke
(b) marsh
(c) distributary of Fraser River
(d) dendritic drainage in domain 2 sediments
(e) eelgrass
(f) megaripples in domain 1 sediments
(g) small dendritic drainage (*see* Fig. 55.9 for ground detail)
(h) reference clump of marsh vegetation; note position with respect to northwest limit of dendritic drainage (arrow), and compare with location of limit in Figure 55.8.

Historical Study - General Observations

In view of the on-going concern over the use of Fraser River marsh lands, particular effort was made to determine whether the marshes have advanced, retreated, or remained stable over the 25 year period studied. It was concluded that the marsh edge generally is everywhere *stable*, except very locally (Luternauer, 1976). Marsh and tidal flat drainage patterns have remained largely unchanged. Research into the stability of individual sediment deposits is still in progress.

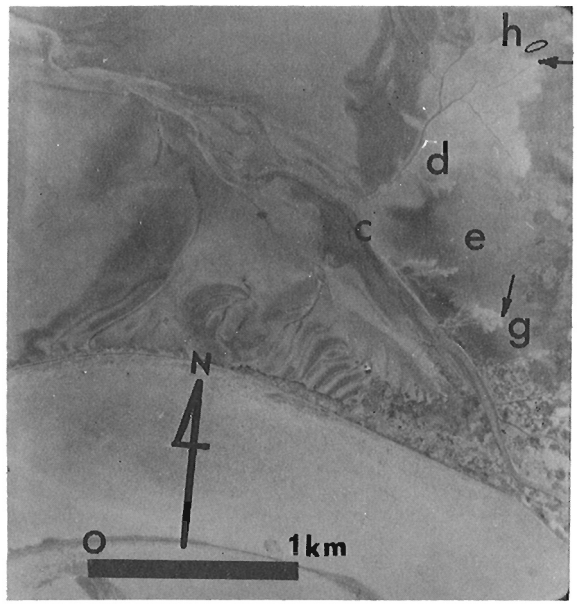

Figure 55.8. 1974 aerial photograph (IRP 142-82) showing advance of dendritic drainage since 1962 (cf. Fig. 55.7). Note, in particular, expansion of the lighter toned mud basins in the vicinity of the vegetation clump (h) and in the area denoted by g. Other letters represent the same features as listed in Figure 55.7.

Discussion of Selected Locales

A careful scrutiny of available aerial photographs and several field observations have aided the writers to identify a number of local areas with distinctive and possibly anomalous character; these local areas are shown in Figure 55.1 and are discussed below.

Area 1 - North Arm Jetty and Iona Causeway area

The tidal flats exposed between the two jetties can be subdivided into:

(a) an approximately 1500 m-wide sand zone where north trending megaripples with 100 m wave lengths are widespread (Fig. 55.4);

(b) two strips of sandy silt deposits adjacent to the jetties (Fig. 55.5). Megaripples with 50 m wave lengths parallel these structures. The strip neighbouring the Iona Jetty terminates in a distinct 'curl' at its western end;

(c) a central shallow basin of structure-free sandy silts (Fig. 55.5);

(d) a structurally and sedimentologically chaotic zone at the junction of the two structures (Fig. 55.5).

The Iona Causeway was constructed in 1961, and the areal extent of megaripples along the North Arm has not changed significantly since then. The megaripple zone just north of the Iona Causeway increased by 50 m northward between 1967 and 1974, and the 'curl' at the west end of the causeway advanced eastward by about the same amount.

Figure 55.9

Sharply incised drainage due to rapid backcutting into upper tidal flats. Channel walls are 50 cm high. View is towards the northwest from the head of the small dendritic drainage system (indicated as g in Figs. 55.7 and 55.8).

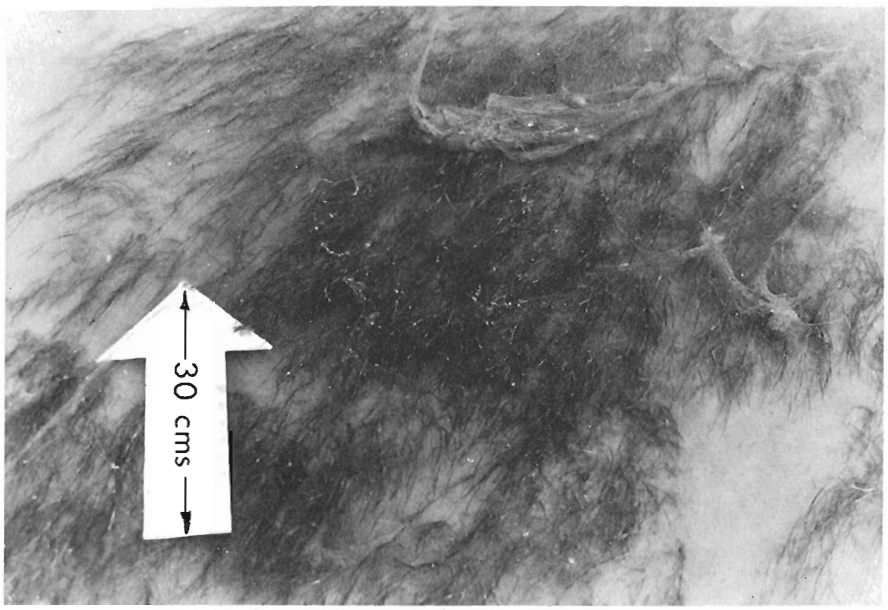

Figure 55.10

'Dwarf' eelgrass growing at the margin of the smaller dendritic drainage system (g in Figs. 55.7 and 55.8). This vegetation is typical of that found within that portion of the tidal flats being encroached upon by the networks of creeks.

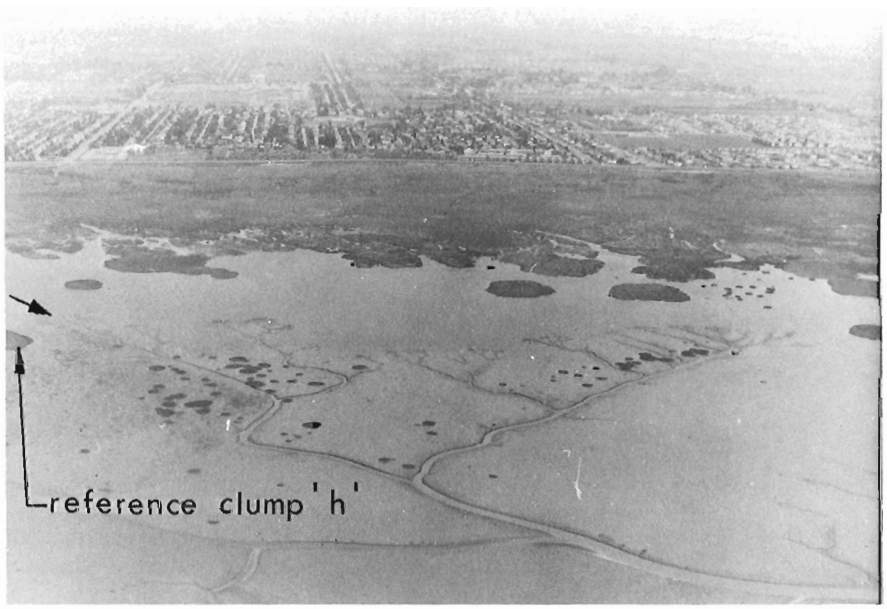

Figure 55.11

An oblique airphoto looking due east taken from an altitude of 350 m. A marsh and the municipality of Richmond are in the background, and dendritic drainage is in the foreground. The unlabelled arrow indicates the limit of the headwaters of the creek network (cf. Figs. 55.7 and 55.8) as of August 1976. The leading edge of the marsh is about 250 m from this point.

Two questions can be posed with respect to sediment dispersal within this area: is the sand being redistributed from within the shallow basin and/or is it being driven into the basin from the upper foreslope?

Area 2 - Tidal Flats West of Sea Island

The northern portion of Sea Island was joined to Iona Island by a short causeway at the time the Iona sewage outfall was constructed (1961). This cut off river flow around the south of Iona Island and may have led to the loss of much of the marsh land off northern Sea Island. The relict river distributary channel appears to be gradually silting up with organic-rich mud (Fig. 55.6).

Since the construction of the airport runway Approach Lights Causeway in the early 1960's, *marsh vegetation has colonized an additional 700 m^2 of tidal flats directly to the north of the causeway* (Fig. 55.6).

Area 3 - Southern Lulu Island Tidal Flats

A number of sharply incised dendritic tidal creeks are the most striking features in this area (Figs. 55.7 to 55.12). These drainage systems are tributary to a larger river distributary which branches off Main Channel at the head of Steveston North Jetty. The network of creeks lies within an 0.5 km^2 muddy area and is bounded to the west by a zone of megarippled sand and to the east by a field of apparently "dwarf" eelgrass (Fig. 55.10).

Figure 55. 12

Photo taken at the limit of dendritic drainage pattern south of reference clump h (Fig. 55.11). The turbulent water is flowing in sparse eelgrass-covered organic-rich mud.

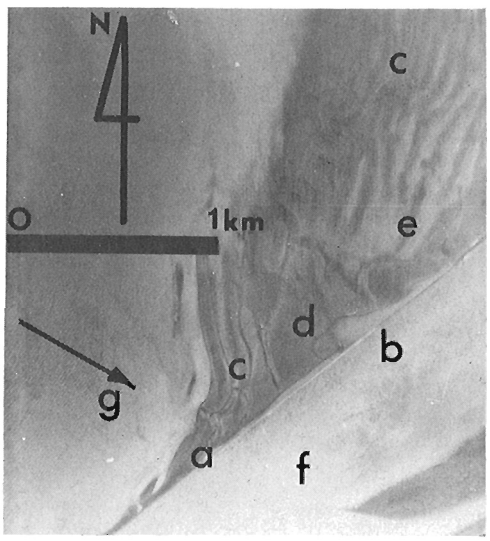

Figure 55. 13. Vertical airphoto (IRP 142-120) of the southwestern end of Steveston North Jetty showing megaripples in domain 1 sediments. A break in the jetty has led to the development of a structureless zone immediately to the north and a patch of domain 3 sediments. Wave orthogonal, paralleling prevailing wind direction, is indicated.

(a) Steveston North Jetty
(b) break in jetty
(c) megaripples, with wave lengths of about 100 m, in domain 1 sediments
(d) structureless domain 1 sediments adjacent to break
(e) smear of domain 3 sediments
(f) Main Arm of Fraser River
(g) wave orthogonal.

The tributaries of these tidal creeks have advanced into the eelgrass beds *by 250 m since 1954 and by about 150 m in the last ten years alone.*

Since the leading edge of the marsh is as close as 100 m from the perimeter of this basin (Fig. 55. 9) *it may take less than 10 years before this drainage system encroaches upon the marsh.* Mechanisms responsible for this apparent rapid backcutting should be investigated.

Area 4 - Steveston North Jetty

Northeast-trending megaripples are the most distinctive feature on the tidal flats immediately to the north of Steveston North Jetty (Figs. 55. 13 and 55. 14). Wave lengths vary between 50 to 100 m, and amplitudes are generally less than 1 m.

The jetty has a pronounced bend midway along its length. Megaripples to the east and northeast of the bend are mantled with muds during the freshet (Fig. 55. 14). The sands to the west and northwest of the bend, however, remain relatively well sorted. At a short break towards the west end of the jetty a 'small' zone of structureless sands and a patch of sandy silts have developed.

Since the present jetty was completed in 1932, few, if any, photos are available which show pre-jetty conditions. It was determined, however, that the megaripples appear to be stable — no change in character or displacement of individual megaripples was recognized.

These features, which have formed adjacent to the jetty, are similar to those which have formed along other such structures on the flats (Figs. 55. 4 and 55. 5).

Area 5 - Northern Westham Island

The construction of the southernmost jetty extending west from northern Westham Island was constructed in

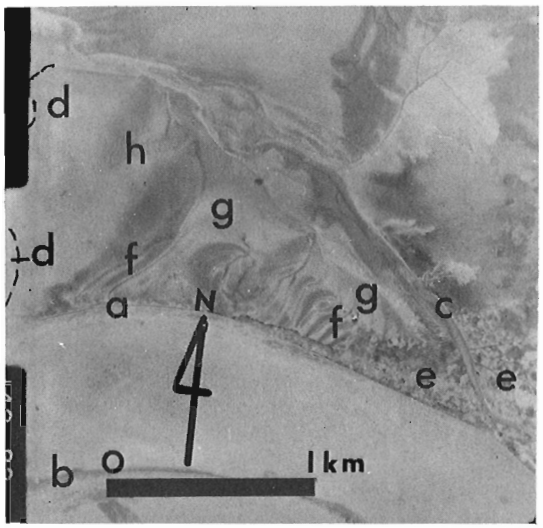

Figure 55.14. Vertical airphoto (IRP 142-82) showing area of megarippled domain 1 sediments mantled with a veneer of finer sediment. This is limited by the jetty, a distributary of Fraser River, and a north-south trending tidal channel (indistinct in photo).

(a) Steveston North Jetty
(b) Steveston South Jetty
(c) Fraser River distributary
(d) north-south trending tidal channel
(e) marsh
(f) megaripples, with wave lengths of 50 m to 75 m and amplitudes less than 1 m, in domain 1 sediments
(g) domain 2 sediments mantling megaripples
(h) domain 3 sediments

Figure 55.15. Oblique airphoto looking approximately northwest from an altitude of 70 m. Marsh has colonized sand banks developed to the south of the nearest jetty. Locally typical 'clumpy' development of marsh in the foreground with a fringe of domain 2 sediments.

the 1930's. Until recently, part of the dredge spoils from Main Arm at Fraser River were dumped to the north of this jetty (O. Isfeld, Dep. Public Works, pers. comm., 1976). Both the 20 year dumping history and the jetty itself appear to have contributed to the formation of sand banks immediately to the south and to the subsequent colonization by marsh vegetation (Fig. 55.15).

Between 1967 and 1974 there was minor development of isolated patches ('clumps') of marsh at the extreme northwest margin of this area.

Area 6 - Tidal Flats Between the Superport and Tsawwassen Ferry Causeways

The principal zone of interest identified here is the marsh to the west of the Tsawwassen Indian Reserve (Fig. 55.16).

Interest in the development of this portion of the Roberts Bank tidal flats has prompted studies of the conditions which have influenced the evolution of the marsh. The writers have attempted, in particular, to establish whether engineering structures have altered the stability of the marsh leading edge by studying aerial photographs spanning 20 years.

Three sites were located where apparent retreat of the order of 20 m had occurred. *This retreat occurred at two sites prior to the construction of the Tsawwassen Ferry Causeway (1960) and at a third site before the construction of the Superport Causeway (1970).*

Luternauer (1976) noted that field evidence indicated truncation and collapse of the leading edge of the marsh near local promontories. It should be emphasized that this marsh is of a different character than other marshes on the Fraser River Delta tidal flats. The marsh occupies an embayment in the upland shoreline which could have filled as sediment was transported north from the glacial deposits at Point Roberts (a short distance south of the Tsawwassen Causeway) by longshore drift. The north-trending

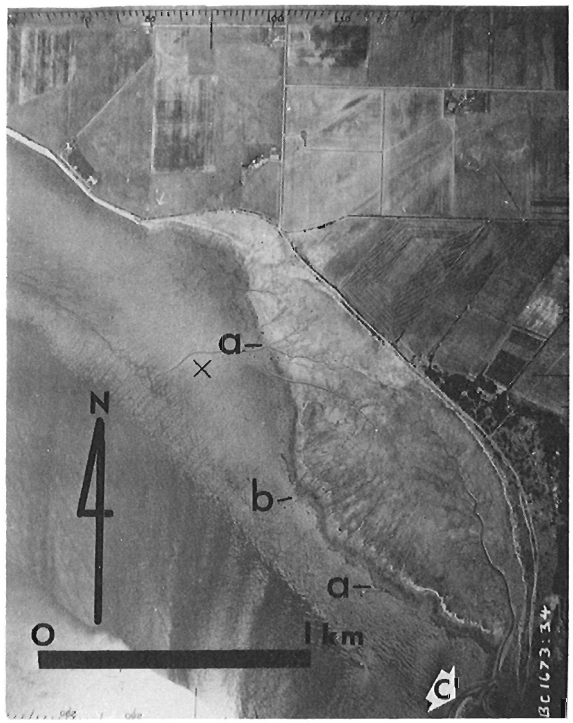

Figure 55.16. 1954 vertical airphoto (B.C. Government photo BC 1673-34) showing the Tsawwassen Indian Reserve marsh. The white line near the leading edge is storm debris. The dashes indicate identified sites of marsh leading-edge retreat.

(a) about 20 m retreat prior to construction of the Tsawwassen Ferry Causeway in 1960
(b) about 20 m retreat prior to construction of Superport Causeway in 1970
(c) accretion spit

spit at the southern limit of the embayment (A. Tamburi, Western Canada Hydraulics, pers. comm., 1976) clearly evolved in response to such a mechanism.

In view of this, the writers consider that geologic processes within this area may be different from those which prevail to the north.

Concluding Remarks

Low-level colour photography can be a valuable tool for discriminating sedimentary environments and establishing temporal changes in morphology within the intertidal zone. The methods described should be considered in the reconnaissance examination of similarily extensive deltas.

Acknowledgments

The writers are grateful to Bill Tupper and Larry Coghlan of the Survey Department, British Columbia Institute of Technology, Burnaby, British Columbia for access to their library of photographic material and for expert advice. The authors also would like to thank Mr. Tupper for suggesting the use of the Jena Interpretoskop for the historical study and for his instructions in its use.

Lesley Simpson of the Terrain Sciences Laboratory, Vancouver, gave much needed assistance during a hectic helicopter field trip in the study area.

References

Hoos, L.M. and Packman, G.A.
1974: The Fraser River estuary: status of environmental knowledge to 1974; Environ. Can., Spec. Estuary Ser. No. 1.

Luternauer, J.L.
1975: Fraser Delta sedimentation, Vancouver, B.C.; *in* Report of Activities, Part B, Geol. Surv. Can., Paper 75-1B, p. 171-172.

1976: Fraser Delta sedimentation, Vancouver, B.C.; *in* Report of Activities, Part A, Geol. Surv. Can., Paper 76-1A, p. 213-219.

Pestrong, R.
1972: Tidal-flat sedimentation at Cooley Landing, Southwest San Francisco Bay; *in* Sed. Geol., v. 8, p. 251-288.

56. SIMILARITY ANALYSIS OF A TRACER MASS DISPERSING ALONG A MEANDERING CHANNEL: LESSER SLAVE RIVER, ALBERTA

Project 750081

T.J. Day and S. Beltaos[1]
Terrain Sciences Division

Introduction

The continually increasing demand for knowledge of pollutant mixing in natural waterways and canals has prompted, in recent years, extensive studies into many aspects of the dispersion of fluid mass. Such studies are necessary to determine both the acceptable levels of effluent input and the concentration pattern of accidental inputs of toxic materials. Ideally, the velocity, density, and concentration of a pollutant should be known at all times and for all distances.

A common approach in evaluating the dispersive properties of a stream is to inject a slug or pulse of tagged particles into the flow. Injections are made as instantaneously as possible, and the tracers are passive (they are miscible and do not alter the density or velocity of the stream). For centre or main flow injection, the initially concentrated mass of tagged particles is advected rapidly downstream by the high midflow velocities. Turbulent velocity fluctuations (diffusion) transport tagged material across streamlines owing to nonuniformities of cross-sectional velocity distributions; this gives rise to differential advection which distorts the tracer cloud and enhances its longitudinal spread. Differential advection tends to enhance lateral and vertical concentration gradients, an effect which, in turn, enhances the intensity of turbulent diffusion.

The combined action of differential advection and diffusion, which results in a large magnification of longitudinal spread, commonly is termed dispersion so as to distinguish it from purely diffusive effects. A mathematical formulation of the movement and spreading of a dissolved substance in such a turbulent shear flow is inherently complex, and recourse to various simplified models has been necessary. In cases where the tagged particles do not alter the density of the flow medium, Taylor's (1954) analysis for turbulent diffusion in pipes has been applied.

Taylor's Analysis

It is beyond the scope of this report to present a detailed discussion of Taylor's analysis. It is necessary, however, to mention briefly the assumptions of this analysis and its success when applied to natural streams.

If the velocity of a particle (in a uniform pipe flow) is a stationary random function of time, and if the dispersion of particles is measured in a frame of reference moving with the mean cross-sectional velocity, Taylor (1954) noted that solutions to the ordinary diffusion equation were applicable. For one-dimensional flow the basic diffusion equation is:

$$\frac{\partial C}{\partial t} + \frac{u\partial D}{\partial x} = \frac{D\partial^2 C}{\partial x^2} \qquad (1)$$

where C is the concentration, t is time, u is the mean cross-sectional velocity, x is the distance, and D is a diffusion coefficient. The term $u\frac{\partial C}{\partial x}$ expresses the movement of the entire tracer cloud, and $D\frac{\partial^2 C}{\partial x^2}$ reflects the time-dependent change in concentration through dispersion. The solution to equation (1) for the initial conditions of a slug injected as a plane, instantaneous source at x=0, is

$$C = Bt^{-\frac{1}{2}} \exp \frac{-(x-ut)^2}{4K_x t} \qquad (2)$$

where B is a constant proportional to the amount of dispersing material and K_x is the longitudinal dispersion coefficient. For a fixed time equation (2) describes a Gaussian concentration distribution along the channel, and provided the evolution of the concentration distribution is relatively slow in comparison to its convection, the concentration as a function of time for a fixed x is also approximately Gaussian.

Further, Taylor showed that the dimensionless dispersion coefficient K_x/ru_* (where r is the pipe radius and u_* is the shear velocity) had the value $K_x/ru_* = 10.1$. For two dimensional flow with vertical variations and using a logarithmic velocity profile, Elder (1959) found $K_x/du_* = 5.9$. Further studies of two-dimensional flows by Fischer (1966a), Thackston and Krenkel (1967), and Sayre and Chang (1968) have produced values of K_x/du_* as large as 13 (where d is the flow depth).

Fischer (1966a, 1966b, 1967, 1968, 1973) extended the theory to prismatic channels of large width-to-depth ratio as a first approximation to natural stream flow. He noted that the dominant dispersive mechanism is, in this case, the transverse variation of velocity and calculated the dispersion coefficient as:

$$K_x = \frac{-1}{A}\int_0^w u'd \left[\int_0^z \left[\frac{1}{\varepsilon_z d}\left(\int_0^z \int_0^d u'dydz\right) dz\right] dz \qquad (3)$$

where A is the cross-sectional area, w is the water surface width, u' is the deviation of (time-averaged)

[1]Research Officer, Transportation and Surface Water Engineering Division, Alberta Research, Edmonton, Alberta.

From: Report of Activities, Part C;
Geol. Surv. Can., Paper 76-1C (1976).

velocity from the mean flow velocity, y, z are depth- and width-wise co-ordinates, d is the depth at the position z, and ε_z is the transverse mixing coefficient.

The concept of characterizing the dispersive properties of stream channels by a single coefficient and being able to relate the coefficient to bulk flow and channel geometry parameters (d and u_*) was very attractive to researchers. The application of Taylor's analysis to flows in natural channels, however, has met with mixed success. Studies have produced a wide range of values for K_x/du_* (1.95 to 7500). Although this variation could be explained partly by the tendency of K_x/du_* to increase roughly as the square of the aspect ratio, w/d, careful examination of the various data shows that K_x usually varies with x, but commonly an average value is reported. This is borne out by a recent compilation of empirical data (Nordin and Sabol, 1974) and by Day (1974, 1975). A variable K_x obviously contradicts the theory. The precise mechanism responsible for the discrepancy is not known at present. It must be pointed out, however, that natural streams are not prismatic, some less so than others. Meanders, dead zones, or pool-riffle sequences could influence the dispersive process in a way that suppresses fulfilment of the conditions underlying Taylor's theory.

The inadequacies of Taylor's analysis, when applied to natural channels, have long been recognized; however, in the absence of viable alternatives it has been customary to interpret results using this theory.

Similarity Analysis

Another approach to the study and prediction of dispersion in natural channels recently has been developed by Day and Wood (1976). Although this approach is based empirically on extensive field evidence of longitudinal dispersion in rugged mountain streams, there is limited supporting data to suggest that the general method may be applicable to a wide range of stream characteristics.

Day (1975) had shown that the longitudinal spreading in mountain streams (flow widths ranging from 1 to 20 m and channel lengths up to 2250 m) is a linear function of distance. A linear spreading rate means that the standard deviation of the particles increases as x^1 (variance therefore increases as x^2). Taylor's analysis is inapplicable to such flows.

A summary of Day's (1975) results is given in Table 56.1. The mean value for the slopes of the regression lines fitted to the variance data is 2.0, and therefore the spreading is linear. Supporting data from Godfrey and Frederick (1970) and Yotsukura *et al.* (1970) also are shown in Table 56.1. The latter's data are of particular interest as the experiment was undertaken in a meandering reach of a sand bed river. The width of this Missouri River test reach is approximately two orders of magnitude larger than the lowest flow in Day's study. These data, representing nearly 60 tracer tests (735 time-concentration curves) in a wide range of natural channels, offer convincing evidence that the spreading of fluid particles in natural channels proceeds faster than $x^{\frac{1}{2}}$. In mountain streams spreading is approximately linear. Similar rates are observed for some other streams; however, because the longitudinal spreading was not defined as rigorously as in Day's work, it is not yet known if all channels disperse fluid masses at this rate.

The mechanisms responsible for this near linear spreading in natural channels have not yet been isolated. If velocity variations are the sole producers of dispersion, the spreading would be approximately $x^{\frac{1}{2}}$ (there are,

Table 56.1

Analysis of Variance Trends

Data Source	Test Reach	No. of Observations	Regression Slope	Correlation Coefficient	95% Confidence Interval
Day (1975)					
	Bealy River	70	1.96	0.96	1.81-2.11
	Bruce Stream	161	2.30	0.95	2.18-2.42
	Craigieburn Stream	168	1.84	0.96	1.76-1.94
	Porter Stream	187	2.05	0.94	1.94-2.15
	Thomas Stream	93	2.13	0.96	2.08-2.29
Godfrey and Frederick (1970)					
	Cooper Creek	18	2.49	0.96	2.1 -2.89
	Clich River	18	1.34	0.69	0.59-2.09
	Cooper Creek	6	2.99	0.80	0.0 -6.07
	Powell River	5	2.87	0.95	1.21-4.53
	Clinch River	6	2.36	0.98	1.62-3.10
	Coachella Canal	5	1.45	0.99	1.27-1.63
Yotsukura *et al.* (1970)					
	Missouri River	4	2.17	0.97	0.60-3.74

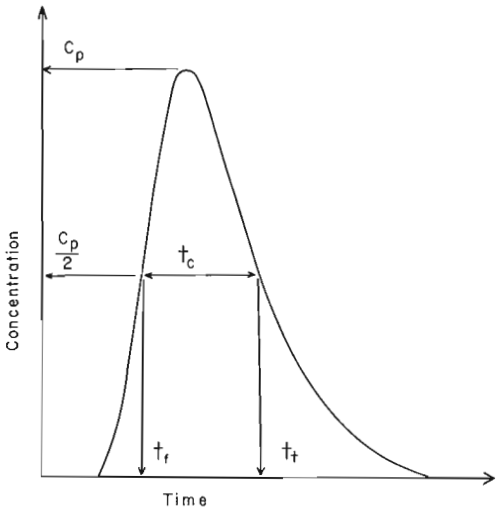

Figure 56.1

Definition sketch for similarity scaling parameters used to produce dimensionless time-concentration curves.

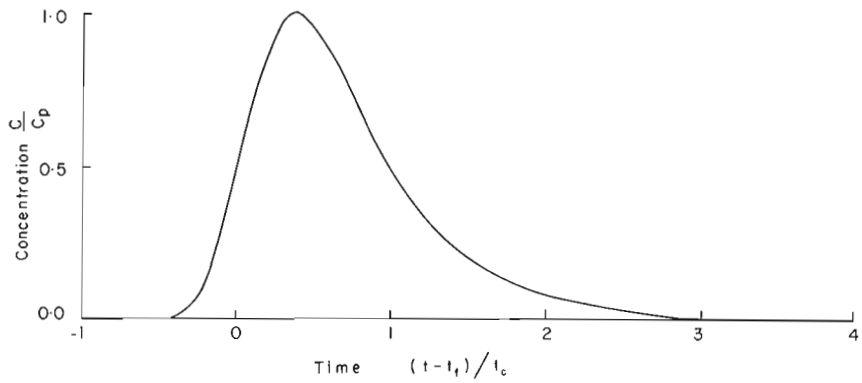

Figure 56.2. An example of a dimensionless time-concentration curve.

however, some stringent conditions for this spreading rate). Day suggested that the entrapment and subsequent slow release of tagged particles from dead or slowly moving zones along the flow boundary could lead to increased dispersion. It is possible to visualize that these retained tagged particles could never catch up to the main body of the tracer being convected along by the main flow. In mountain streams these traps may occur behind protruding bank and bed particles, whereas in larger streams, slowly moving zones caused by variations in plan form geometry may dominate the dispersion pattern.

The concept of entrapment is not new (Aris, 1959; Hays, 1966; Okubo, 1973). A common approach has been to divide the stream into two zones, the main channel and a boundary zone. Only turbulent exchange across the boundary of the two zones is possible, and the boundary zone has no component of longitudinal velocity. The one-dimensional model requires two differential equations (Hays, 1966):

$$\frac{\partial C}{\partial t} = \frac{-u\partial C}{\partial t} + D\,\frac{\partial^2 C}{\partial x^2} + k_1 (C-C_r) \qquad (4)$$

$$\frac{\partial C_r}{\partial t} = k_2 (C-C_r) \qquad (5)$$

where the index r refers to the boundary zone, and k_1 and k_2 are coefficients which reflect the exchange process and the relative size of the zones. This approach, however, does not produce the observed spreading characteristics. Aris (1959) applied his method of moments to dispersion in a pipe with dead zones distributed randomly on the flow boundary and showed that although such zones enhance the dispersion coefficient, the spreading still increases as $x^{\frac{1}{2}}$.

In addition to the linear spreading, Day (1975) found that the concentration distributions decayed as x^{-1}. These two features, coupled with the fact that the mean motion of the concentration distribution is also a linear function of distance, are the basic criteria for the similarity approach.

For Day's study of mountain streams it was possible to show that the concentration distributions maintain a persistent asymmetric shape, with a long tail of concentration extending upstream. These asymmetrical shapes have long been recognized, and many explanations have been advanced. Both Elder (1959) and Sullivan (1971) considered the laminar sublayer to play a role in producing skewness. Hays (1966) and Thackston and Schnelle (1970) showed how trapping can affect the shape of the concentration distributions. Fischer (1966a) believed that skewness develops during the convective period (before the tracer has evenly and completely sampled the flow cross-section) when the tagged particles adopt the form of the velocity profile.

Day's contribution was in recognizing that this asymmetry was both persistent and apparently constant. It was this constant shape and the linear dispersal characteristics that led Day and Wood (1976) to develop the similarity approach, for they recognized that the dispersion process exhibits the characteristics of self-similarity with constant velocity ratios and forms. It was shown that with the appropriate choice of concentration, length, and time scales, the concentration distributions could be made coincident. The most appropriate scaling parameter for the concentration axis is the peak concentration, C_p. Time co-ordinates must be scaled by a parameter which reflects both the spread of the concentration distribution and its position relative to initiation. The spread is characterized by the time parameter t_c, which corresponds to the time spread between the co-ordinates (t_f, $C_p/2$) and (t_t, $C_p/2$) where t_f is the time co-ordinate for $C = C_p/2$ on the leading edge and t_t is that for the trailing limb. A definition sketch of these parameters is shown in Figure 56.1. The position of the concentration distribution relative to its source can be scaled by choosing any time co-ordinate as the origin of the dimensionless form. The parameter t_f is one which is

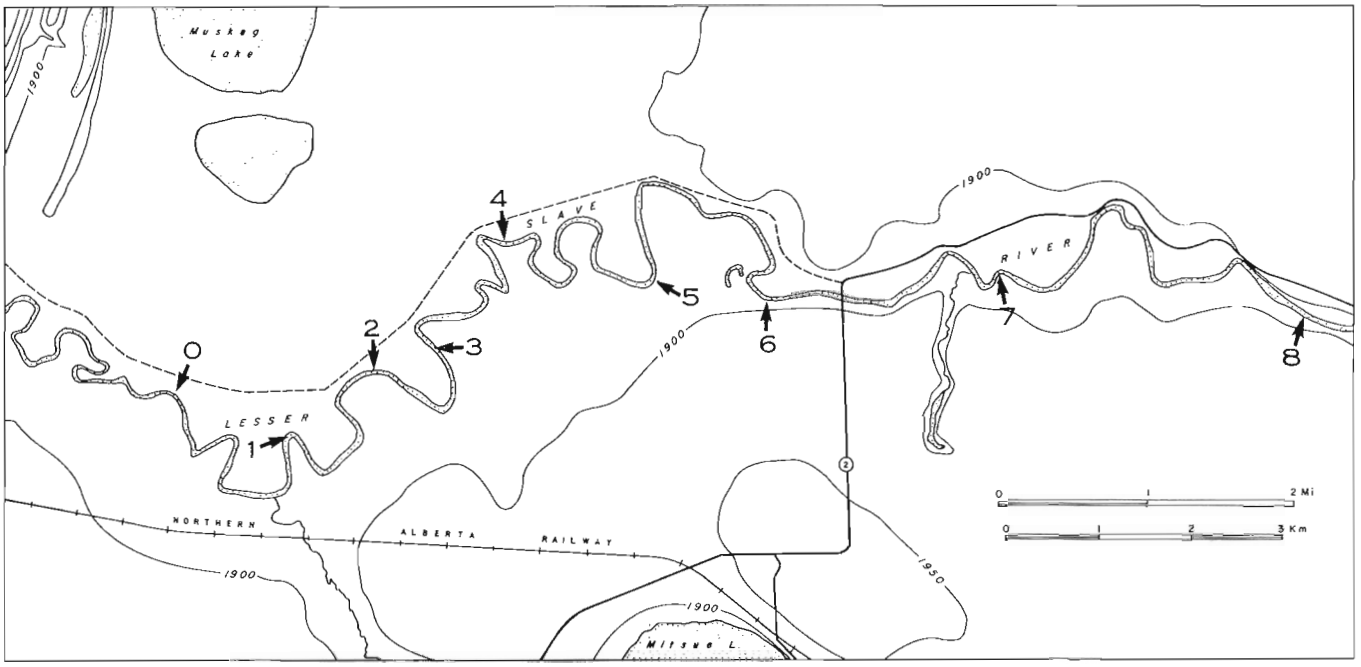

Figure 56.3. Plan view of test reach showing injection site (0) and the eight sampling sites (1 to 8).

both readily and clearly defined. The dimensionless time axis is $(t-t_f)/t_c$. By definition, the dimensionless concentration distributions are coincident where $(t-t_f)/t_c$ equals zero and 1.0, that is, when $t = t_f$ and $t = t_t$, respectively. A dimensionless time-concentration curve is shown in Figure 56.2.

Day and Wood (1976) showed that the dimensionless or similarity curves of fluid particles dispersing in mountain streams are remarkably constant. Variations among the curves across sixteen steep, gravel and boulder bed streams are small and apparently random. The authors suggest that a common dimensionless time-concentration curve may exist. It also was shown that the Missouri River data possessed a constant dimensionless form although it was slightly less asymmetrical than that established for mountain streams.

Prediction of dispersion pattern is relatively simple using the similarity approach. As the shape of the concentration distribution remains constant, its spread, peak concentration, and position in the channel relative to initiation alone need to be determined. The method developed by Day and Wood is based upon the equation implying conservation of tracer and empirical equations for determining t_f and t_c, the two time-scaling parameters.

The position of the concentration distribution for distances greater than the mixing length is determined from

$$\frac{t_f v}{w} = a + b\frac{x}{w} \qquad (6)$$

where v is the mean longitudinal velocity in the stream. A similar model for describing the spread of the concentration distribution is

$$\frac{t_c v}{w} = a + b\frac{x}{w} \qquad (7)$$

If the position of the wave and its spread are known, only the peak concentration remains unknown. Once t_c has been determined then C_p can be calculated from the equation for the conservation of tracer

$$M = \int_{t=0}^{t=\infty} QC\,dt \qquad (8)$$

Writing $C/C_p = C'$ and $t/t_c = t'$, then

$$M = QC_p t_c \int_{t'=0}^{t'=\infty} C'\,dt = QC_p t_c I' \qquad (9)$$

where I' is the area under the dimensionless time-concentration curve. Now M, the mass of tracer injected, equals VC_I, where V is the volume of tracer injected and C_I is its initial concentration. Hence

$$C_p = C_I V/t_c I'Q \qquad (10)$$

This equation states that for distances greater than the mixing length, the peak concentration can be determined from $V_I C_I$, Q, and t_c.

Comparisons of observed and predicted dispersion patterns showed that this method produced no bias towards mean velocity stream length or stream width. Errors in predicting C_p ranged from 1 to 25% with a mean of about 10%. The larger errors are associated with measurements near the mixing length.

The main advantage of this method is its simplicity and the fact that it is based on a large number of field

Table 56.2

Site Locations and Sampling Positions

Site No.	Distance Downstream (km)	Total Flow Width (m)	Cross-Sectional[1] Sampling Position (m)			Plan Form Description of Sampling Site
			a	b	c	
0	0.0	38.4		16.2		mild bend
1	3.0	35.5	11.0	19.8	26.2	sharp bend
2	5.1	44.5	9.8	21.3*	32.6	mild bend
3	6.7	58.0	16.5	29.3	38.4	straight
4	9.3	57.0	14.5	25.3	43.0	very mild bend
5	13.3	37.5	9.8	20.1	27.7	sharp bend
6	16.2	44.8	12.2	22.9	31.1	straight/mild bend
7	19.0	61.6	18.3*	30.5*	42.7*	sharp bend
8	23.6	57.6	14.0	27.4	42.7	very mild bend or straight

[1]Distances measured from the north bank
*Approximate

data. The most time consuming and complicated step in the procedure is a dilution gauging which is necessary to determine both the discharge and the mean flow velocity. Current metering also can be used to determine Q and u; however, the irregular cross-sections characteristic of mountain streams require several velocity determinations.

Although the general method may be transferable to various stream types, it is unlikely that the specific regression parameters in equations (6) and (7) are directly transferable. Day (1974) showed that for any fixed distance, x/w, both the position of a tracer cloud (mean motion) and its spread are considerably different between mountain streams and the Missouri River. As the regression constants reflect both the mean motion and the dimension of the tracer distribution, they can be expected to vary among streams.

Study Objectives

Searches of the available literature indicate that little comprehensive data are available for tracer tests in large rivers, and the span of river types is even more dismal. Part of the problem with obtaining such data is the rather massive logistics required. In view of the limited data, it is the general aim of this project to undertake a comprehensive series of large-scale tests representing a range of flow scales and stream characteristics. Within this general objective the Lesser Slave River test was undertaken as an example of longitudinal dispersion in a meandering sand bed river.

Description of Test Reach

The study reach is located along a 23.6 km stretch of the Lesser Slave River beginning about 6 km downstream of the outlet to Lesser Slave Lake in north central Alberta. The mid reach co-ordinates are 55°17'30"N and 114°37'W. This river reach was chosen for its accessibility and because its transverse mixing characteristics had been the subject of a previous study (Engmann and Kellerhals, 1974) involving both open-water and ice-covered conditions.

According to the hydraulic and geomorphic summary presented by Kellerhals *et al.* (1972), the long-term mean discharge of Lesser Slave River is 44 m^3/s with a minimum recorded flow of 5.4 m^3/s and a recorded maximum of 243 m^3/s (based on 20 years of record). The river slope surveyed near the Water Survey of Canada water level recorder (W.S.C. index No. 7BK-6) is 0.00011 (map slope of 0.00022). Estimated bankful discharge, based on the level of the valley flat, is 108 m^3/s.

The river is flowing through an old lake bottom, and the channel is a single thread with no bars or islands. The channel pattern is irregular, and some meanders are almost contorted. The meander pattern exhibits progression and cutoffs. Sinuosity is approximately 2.0 (channel length divided by distance along valley axis). The wave length is 0.60, and is the average length of a complete meander cycle measured along the valley axis.

The channel bed is probably composed of deep sand or silt. The relevant grain size parameters are D_{90} = 0.29 mm, D_{65} = 0.22 mm, and D_{50} = 0.20 mm. The channel banks are composed of silt and sand.

Experimental Design

The specific experimental objectives were: (1) to determine the longitudinal dispersion pattern for one flow level along a meandering sand bed channel; (2) to investigate the effect of cross-sectional channel shape on the dispersion characteristics; and (3) to investigate

Figure 56.4

Current metering at site 1. View is to the north, and flow is from left to right (GSC-203025-T).

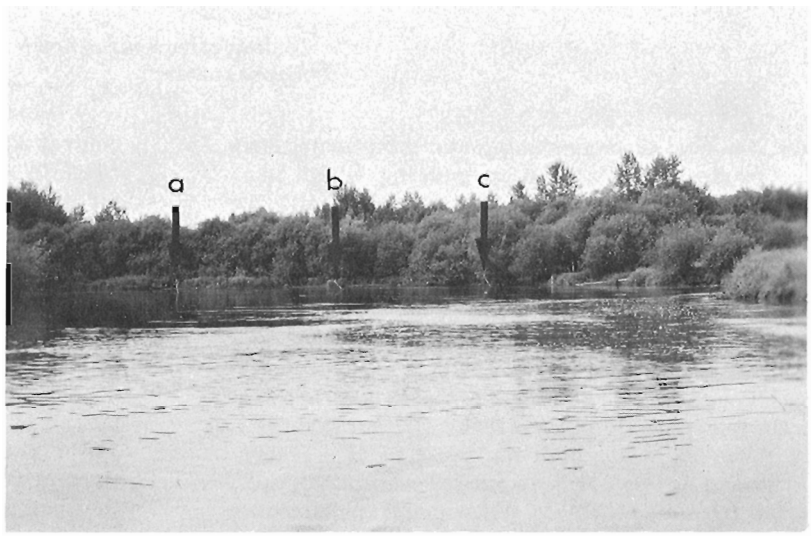

Figure 56.5

Upstream view of Lesser Slave River looking towards site 7. Lateral sampling positions are indicated (GSC-203025-S).

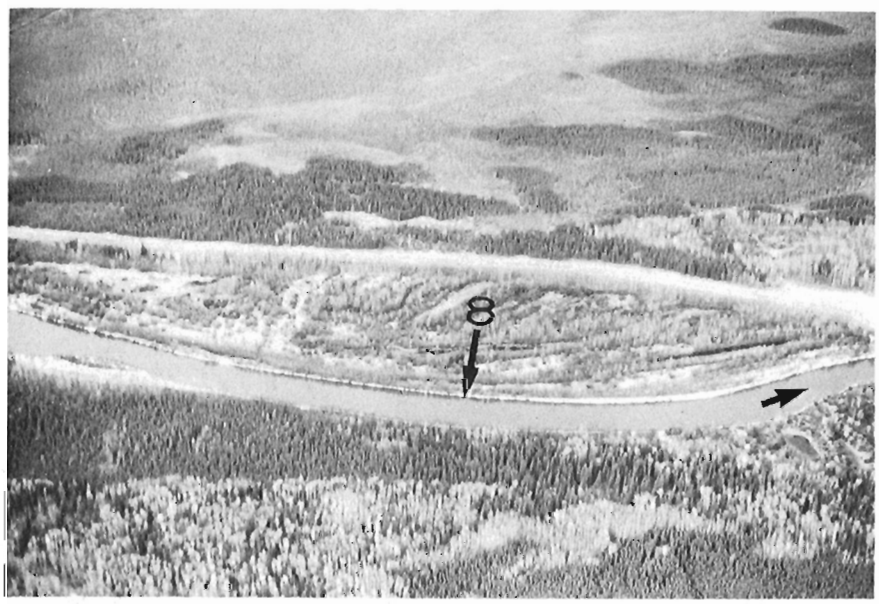

Figure 56.6

Aerial view of site 8; flow is from left to right (courtesy S. Beltaos).

Table 56.3

Hydraulic Data Summary

Site No.	Discharge (m^3/s)	Cross-Sectional Mean Velocity (m/s)	Cross-Sectional Flow Area (m^2)	Mean Flow Depth (m)	Surface Width (m)	Hydraulic Radius (m)	Shear Velocity (m/s)	Friction Factor
0	79.6	0.75	106.6	2.77	39.0	2.39	0.051	0.037
1	72.0	0.71	101.4	3.06	33.1	2.58	0.053	0.037
2*	-	0.61	121.1	2.72	44.5	2.42	0.051	0.057
3*	-	0.54	136.9	2.63	52.1	2.39	0.051	0.071
4	73.7	0.54	134.7	2.37	56.7	2.19	0.049	0.065
5	74.1	0.72	103.0	2.72	37.8	2.38	0.051	0.040
6*	-	0.57	129.7	2.90	44.8	2.56	0.053	0.071
7*	-	0.27	273.7	4.44	61.6	3.88	0.065	0.506
8	70.0	0.63	111.0	2.07	57.9	1.79	0.044	0.039
Mean	73.9	0.59	134.6	2.8	47.5	2.47	0.051	-
Standard Deviation	3.58	0.14	57.	0.71	10.0	0.60	0.006	-

*Sites not current metered. Discharge assumed equal to mean of metered section, 73.9 m^3/s, and all derived hydraulics based on this value of Q, the measured top width, and the channel area determined from echo soundings.

the lateral variations in dispersion characteristics. In the sampling program eight measurement sites were distributed along the channel, the first at 3 km from the injection site (designated site 0), and the last site located at 23.6 km downstream (Fig. 56.3). At each measurement site three sampling positions were determined roughly to divide the flow width into equal portions (Table 56.2).

The reach can be subdivided into two subreaches: a well defined meandering pattern from the injection site (0) to between sites 5 and 6, and a sinuous pattern extending downstream of this point. Within each subreach, sites were located to obtain samples at different types of plan form geometries (Table 56.2), i.e., at a bend or on a straight reach. Sites 1, 7, and 8 are shown in Figures 56.4, 56.5 and 56.6, respectively.

The injection was made at 16.2 m from the south bank of site 0 (all lateral positions are related to this bank). This position was chosen as it is the lateral point that bisects the discharge, i.e., 50% of the flow is on either side (Yotsukura and Cobb, 1972). The injection slug was 3.2 l of 20% Rhodamine WT diluted 2 or 3 times (sample retained). The slug was injected as instantaneously as possible at 0720 hours on August 21, 1975.

The day prior to injection cross-sections at sites 0, 1, 3, 4, 5, and 8 were current metered to permit mapping of velocity distributions. These cross-sections are shown in Figure 56.7. The mean cross-sectional velocities determined from these meterings were used to estimate the mean travel time of the tracer and the sampling times.

The procedure at each site was to collect discrete samples at all three sites for predetermined time intervals. At site 1 the sampling interval was one minute and at site 8 was about 20 minutes. These samples then were analyzed by a Turner III Flurometer.

Hydraulic Data

Cross-sections were determined from either current meterings (sites 0, 1, 3, 4, 5, and 8) or echo soundings. Two echo sounding traverses were made at each cross-section. Comparisons between the two methods, however, indicated that echo soundings resulted in a 10 to 20% larger flow section. As current metering is the more accurate method, cross-sectional parameters were determined from these depth measurements. Only sites 2, 6, and 7 have data based on echo soundings. A comparison of the depth soundings produced by the two methods is shown in Figure 56.7 for site 0.

The flow discharge, Q, and flow area, A, were determined graphically, and the mean cross-sectional velocity, v, was computed as Q/A. For the unmetered sites the discharge was taken as the mean of the other sites, 73.9 m^3/s. Flow area for these sites was determined from the echo soundings. All flow widths were surveyed.

Specific cross-sectional hydraulics and mean hydraulics and their precision (expressed in terms of the sample standard deviation) are listed in Table 56.3.

Mixing Length Estimates

The mean longitudinal motion of a tracer mass represents the mean characteristics of the stream only after an initial, transient period. Once the tracer has been injected into the stream, its rapid downstream and lateral motion eventually leads to its dispersal throughout the flow cross-section. At some point after some time interval, the tracer has sampled the flow sufficiently so that the cross-sectional concentration distribution is almost uniform and independent of injection. The time required for the attainment of this

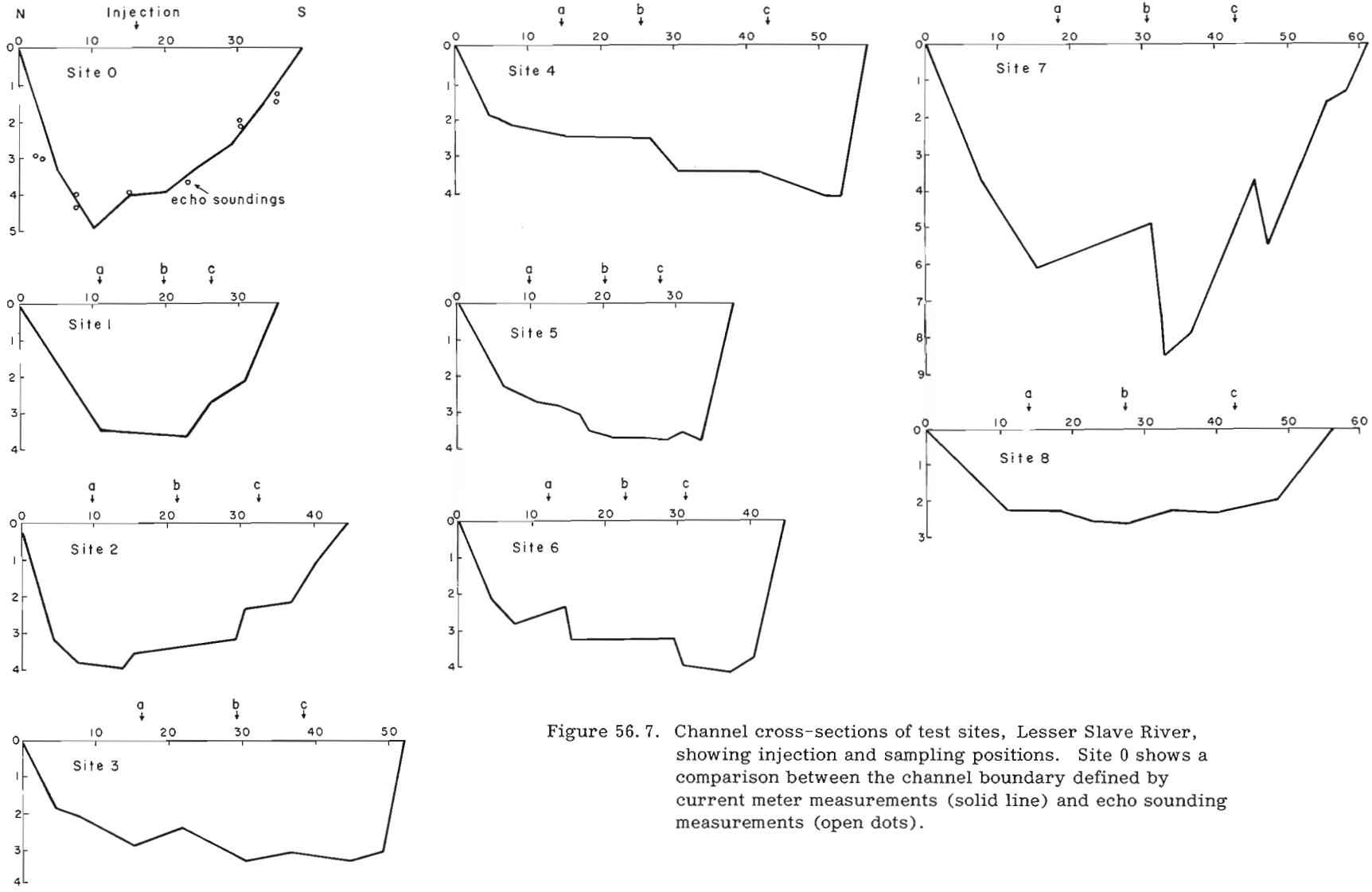

Figure 56.7. Channel cross-sections of test sites, Lesser Slave River, showing injection and sampling positions. Site 0 shows a comparison between the channel boundary defined by current meter measurements (solid line) and echo sounding measurements (open dots).

Table 56.4

Mixing Length Estimates

Source	Formula	Estimated Mixing Length for Centre Injections (km)
1. Fischer (1966a)	$x_m = 1.8\ell^2 u/Ru_*$	4.76
2. Barsby (1968)	$x_m = (w^2/d)\ (u/u_*)$	10.83
3. Glover (1964)	$I_s = w/4\ \varepsilon_y t$	11.24
4. Yotsukura and Cobb (1972)	$x_m = 0.25\ uw^2/u_* d$	10.83
5. Ward (1973)	$x_m = (T/C_y)\ (8/ff)\ (w^2/d)$*	6.30

Notation: w is the flow width; d is the mean cross-sectional depth; u is the mean cross-sections velocity; u_* is the shear velocity; ε_y is the lateral mixing coefficient; ℓ is a characteristic length taken as the distance between the farthest bank and the maximum velocity thread; R is the hydraulic radius; I_s is an index of lateral solution concentration which approaches unity as x_m, the mixing length, is approached; T is equal to $(\varepsilon_y t)/w^2$; C_y is equal to (ε_y/du_*).

*Ward's estimate is for 99% mixing.

condition is called the mixing time, and the channel length required is called the mixing length.

Various formulae are available for determining the mixing length, x_m; five formulae and their estimates are shown in Table 56.4. The hydraulic parameters used in the calculations are mean values for the test reach. This table shows a range from approximately 4.8 to 11.2 km for the estimated x_m; thus the transverse mixing could be complete between sites 1 and 5.

The averaged transverse mixing capacity of a river can be characterized conveniently (Sayre and Chang, 1968) by an exchange or mixing coefficient of the form

$$\varepsilon_z = ku_*R \qquad (11)$$

where k is a dimensionless constant. No reliable method is available, however, for predicting ε_z in rivers on the basis of channel geometry or bulk flow parameters. Okoye (1970) recently established an apparent dependence of k on the aspect ratio, w/d, for laboratory channels. Engmann and Kellerhals (1974) supported this conclusion with data from a number of natural rivers.

Engmann and Kellerhals presented data from a lateral mixing text on the Lesser Slave River. For $u_* = 0.049$ m/s, R = 2.5 m, and $\varepsilon_z = 0.40\ m^2/s$ (derived numerically), the authors determined a k of 0.33. For the present test the mean values of u_* and R are similar, 0.051 and 2.47, respectively. Consequently, the lateral mixing coefficient, determined from (11) should be $0.042\ m^2/s$. Engmann and Kellerhals' data are based on constant rate dye injection 5 m from the south bank of the river, approximately 0.26 km downstream of site 1 (*see* Fig. 56.3). The data were collected only over 1.9 km (approximate location of site 2) where 63% mixing had occurred. For the same degree of mixing, Ward's formulae (Table 56.4) produced a value of 3.8 km (based on assumptions of two-dimensional flow at shallow depth and fairly straight channels).

The similarity of the mean hydraulics of Engmann and Kellerhals' test and the test discussed here is sufficient justification for expecting a similar value for ε_z. The considerably shorter mixing length suggested by Engmann and Kellerhals' data as compared to, for example, Ward's estimate, indicated that either Ward's value of 6.3 km or Fischer's estimate of 4.8 km (Table 56.4) is acceptable as an approximate value of x_m. The centre injection employed in the present test also would lead to a shorter mixing length.

Concentration Data

The time-concentration curves for the 24 sampling positions are shown in Figure 56.8. Table 56.5 lists various time and concentration parameters for sites 1 to 8. Calculation of the basic integral, I, of these curves was based on

$$I = \int_{t_s}^{t_e} C(t)\,dt \qquad (12)$$

where t_s is the starting time of the concentration distribution, t_e is the final time of passage, and C(t) is the time-concentration curve. The mean travel time, t_m, is calculated as

$$t_m = \int_{t_s}^{t_e} C(t)\,dt \Big/ \int_{t_s}^{t_e} (C(t)/t)\,dt \qquad (13)$$

and t_m is identical to the mean travel time of the stream only if instantaneous mixing occurs. The mean velocity, v, of a concentration distribution is

$$v = x/t_m \qquad (14)$$

which represents the mean streamflow velocity only for instantaneous mixing, otherwise v always will be greater due to the rapid convection of the tracer within the mixing length.

The variance of the concentration distribution measured over time for a fixed x is

$$\sigma_t^2 = \left(\int_{t_s}^{t_e} t^2 \cdot C(t)\,dt \Big/ \int_{t_s}^{t_e} C(t)\,dt\right) - (t)^2 \qquad (15)$$

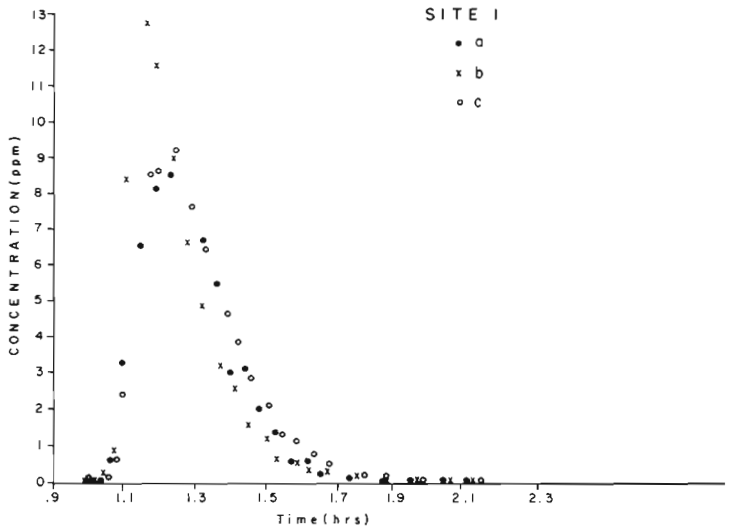
SITE 1
a
b
c
CONCENTRATION(ppm)
Time(hrs)

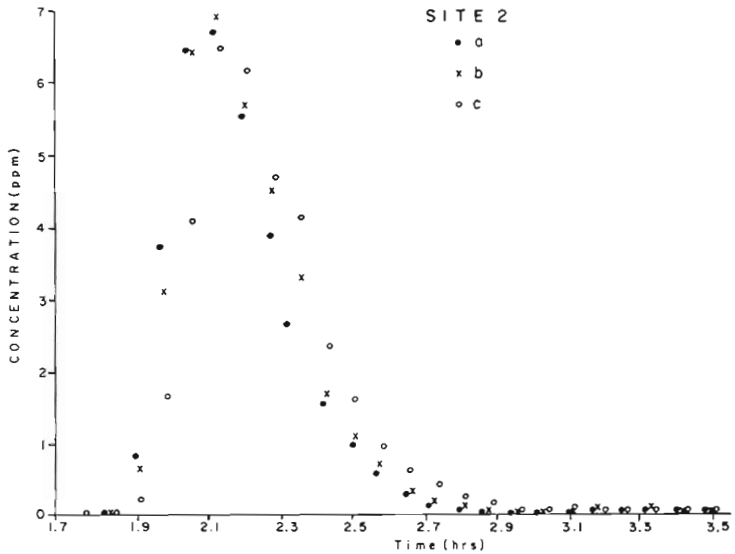
SITE 2
a
b
c
CONCENTRATION(ppm)
Time(hrs)

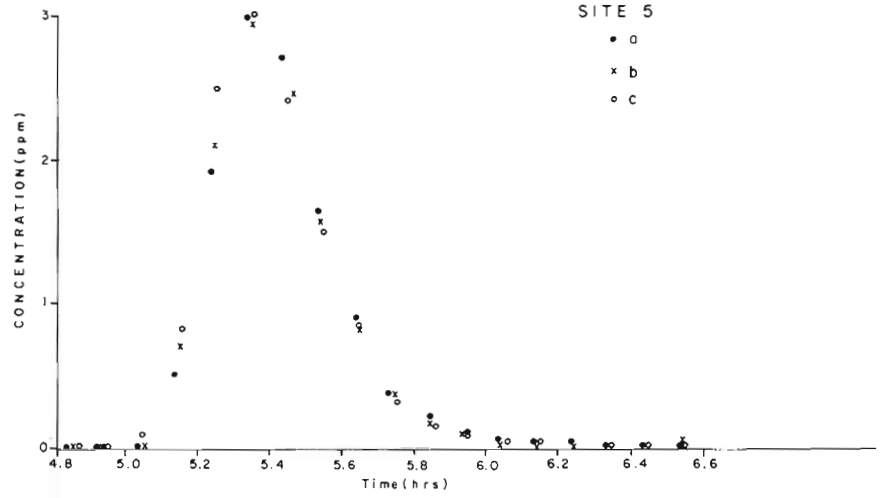
SITE 5
a
b
c
CONCENTRATION(ppm)
Time(hrs)

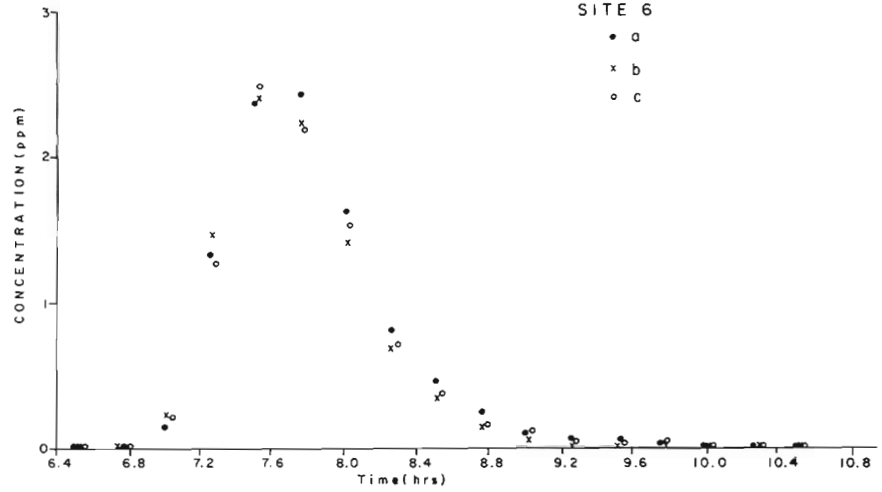
SITE 6
a
b
c
CONCENTRATION(ppm)
Time(hrs)

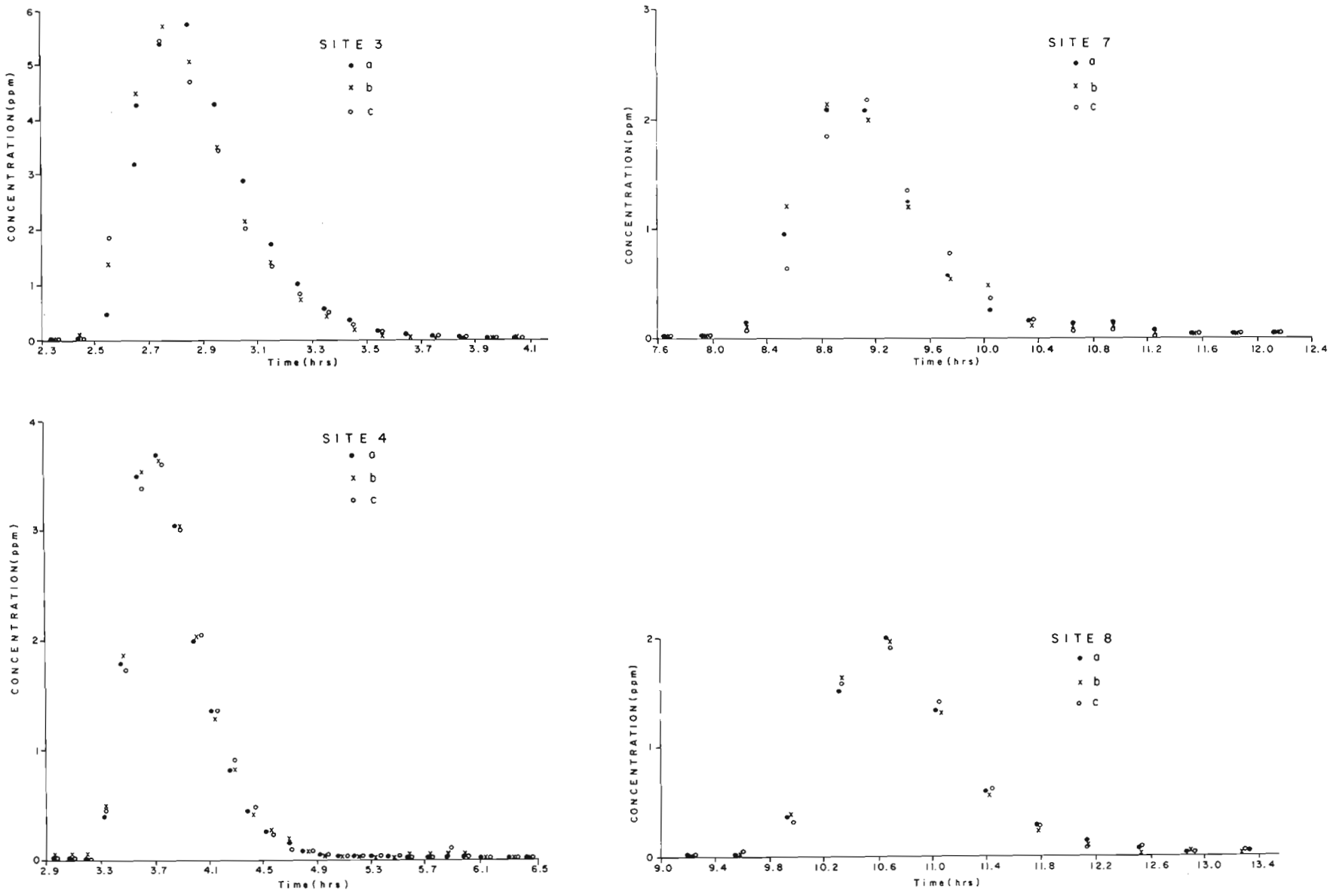

Figure 56.8. Time-concentration curves for the eight sampling sites. Note that the concentration and time axes are variable.

Editor's note: Line drawings used in Paper 76-1, Part C are reproduced from author's copy prepared according to general specifications. Figure 56.8 did not meet these specifications and as a result some of the finer detail present on the original may be lost in reproduction. However the senior author has indicated that the form of the curves is more important than specific data points and the figures have been reproduced with that proviso.

Table 56.5

Summary of Time and Concentration Parameters

Site No.	Distance Downstream (km)	Lateral Sampling Position	Tracer Integral		Tracer Variance (min^2)	Tracer Standard Deviation (min)	Peak Concentration (ppb)	Starting Time (min)	Peak Time (min)	Mean Residence Time (min)	Mean Travel Time (min)	Mean Tracer Velocity (m/s)
			ppb•s	variability (max I-min I) /average I								
1	3.0	a	10024		112.6	10.6	8.61	60.0	75.0	80.6	79.3	0.63
		b	8948	0.11	61.3	7.8	12.79	63.0	71.0	75.9	75.2	0.67
		c	9887		78.5	8.9	9.21	61.5	76.0	79.3	78.4	0.64
2	5.1	a	9131		109.3	10.5	6.68	108.5	126.5	130.0	129.2	0.66
		b	9488	.038	108.4	10.4	6.94	109.0	127.0	131.3	130.6	0.65
		c	9314		140.1	11.8	6.48	105.0	127.0	135.2	134.3	0.63
3	6.7	a	9494		176.4	13.3	5.77	146.0	170.0	173.7	172.7	0.65
		b	9289	.037	172.5	13.1	5.74	146.5	164.5	171.3	170.3	0.66
		c	9149		189.2	13.8	5.54	147.0	165.0	171.6	170.6	0.66
4	9.3	a	8489		343.8	18.5	3.66	216.5	248.0	254.2	252.9	0.61
		b	8756	.031	348.8	18.7	3.65	216.5	249.0	254.7	253.4	0.61
		c	8586		377.6	19.5	3.60	217.0	250.0	256.0	254.7	0.61
5	13.3	a	8337		484.2	22.0	3.00	312.0	348.0	358.7	357.4	0.62
		b	8233	.024	403.5	20.0	3.97	314.0	349.0	357.3	356.3	0.62
		c	8433		456.0	21.4	3.00	313.0	349.5	356.8	355.6	0.62
6	16.2	a	8837		813.6	28.5	2.44	405.0	465.0	468.5	466.9	0.58
		b	8365	.055	806.8	26.9	2.43	390.5	450.5	465.1	463.6	0.58
		c	8471		926.9	30.5	2.49	406.0	451.0	468.7	466.9	0.58
7	19.0	a	8255		933.7	30.6	2.15	476.0	530.0	549.0	547.4	0.58
		b	8688	.051	1038.8	32.2	2.16	494.3	530.3	549.2	547.4	0.58
		c	8293		1049.8	32.4	2.15	459.0	548.5	555.7	553.9	0.57
8	23.6	a	8410		1516.8	39.0	1.98	540.0	672.0	680.7	678.9	0.58
		b	8379	.011	1294.7	36.0	1.95	518.0	673.0	679.5	677.7	0.58
		c	8318		1544.7	39.3	1.91	563.0	673.0	683.7	681.6	0.58

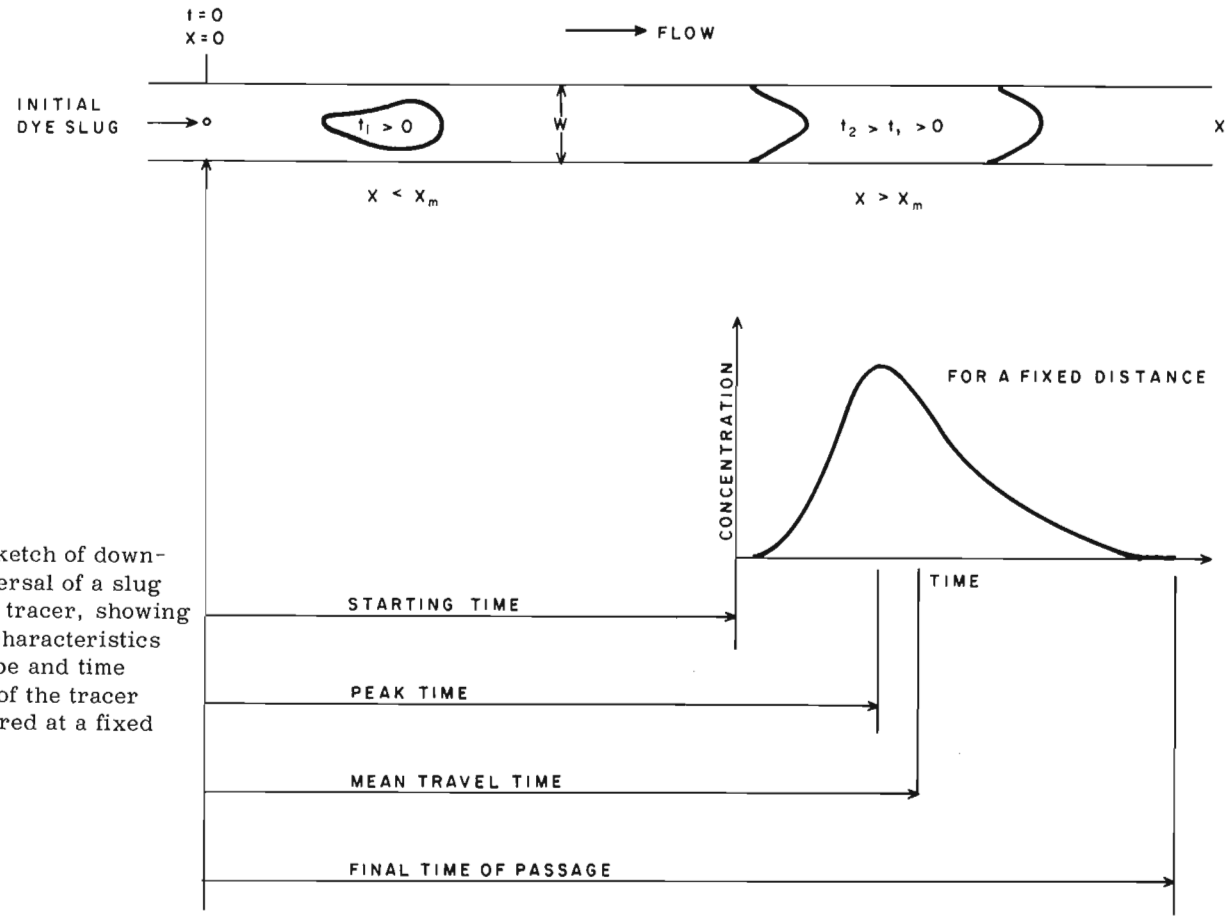

Figure 56.9

Definition sketch of downstream dispersal of a slug injected dye tracer, showing plan view characteristics and the shape and time parameters of the tracer when measured at a fixed distance.

where $\bar{t}$ is the mean residence time of the tracer determined as

$$\bar{t} = \left[\int_{t_s}^{t_e} t \cdot C(t)\, dt \Big/ \int_{t_s}^{t_e} C(t)\, dt \right] \qquad (16)$$

A diagram of tracer motion, spatial shape, and time parameters of a concentration distribution measured at a fixed distance is shown in Figure 56.9. Within the mixing length the tracer is confined (for centre injection) to the main flow. Cross-sectional variations in concentration are marked, and measurements of I, the tracer integral, across the tracer cloud can result in vastly different values (Day, 1974). As mentioned previously, these lateral variations diminish as the tracer continues to be dispersed. Beyond the mixing length the dilution of the tracer mass is constant (i.e., I = constant); however, at any fixed point, lateral variations in concentration and time distribution can occur. These lateral variations in tracer dimensions (but not the integrals) result from transverse velocity variations, as the tracer in the main flow is moved more rapidly. Tracer material near the banks arrives later, for a given distance, and its time of passage is longer as its mean motion is slowed by the lower velocities near the bank and entrapment of tracer material. The resultant spatial shape is arrow-like (Fig. 56.9), and intuitively one would expect the spatial concentration pattern to exhibit some asymmetry (contrary to Taylor's theory) due to the effects of slower moving tracer near the flow boundary. Whatever the specific nature of the dispersive mechanisms involved, lateral variations in concentration can be expected, and their characteristics also must be expected to vary among channel types and for various degrees of mixing.

The concentration data for site 1 (3 km) illustrate these points. Although the starting time for the mid-channel sampling position is in fact later than for the other position, the concentration distribution peaks earlier and passes by faster ($v = 0.67$ m/s and $t_m = 75.2$ min). Even though the peak concentration is greatest at the centre site, little variation is present among the integrals ((max I − min I) / average I = 0.11) indicating that mixing, at least within the sampling zone, is nearly complete. Day (1976) has shown that the precision of tracer integrals downstream of the mixing length (in mountain streams) can range from about 1 to 20% with median value of about 8%. The very small lateral variation of I at site 1, therefore, safely can be interpreted as nearly complete mixing.

At site 2 (5.1 km) the tracer has been sufficiently dispersed resulting in nearly constant peak concentration across the measurement zone. The peak times are all

virtually the same, with about 5 minute variations in the starting and mean travel times. Starting times (and final times) are never very precise because concentrations are low and background variations can mask initial values. The mean characteristics of the tracer mass are, in turn, sensitive to errors in the extremes of the distribution. The integrals have decreased by this site indicating that further dilution through the flow section has occurred. Within the measurement zone the dilution is almost constant (tracer integral, Table 56.5). There is little difference among the mean velocities, certainly within the units of experimental precision. Similar values for Cp, v, and I are shown for site 3 (6.7 km); the consistency in the latter parameter indicates that complete mixing across the entire flow section has occurred.

The tracer integrals at site 4 (9.3 km) are slightly lower than at sites 2 and 3. Since the variation of I does not seem to change with distance, these decreases in I are probably tracer losses rather than increased dilution. The integrals listed in Table 56.5 for site 4 to site 8 are similar, with a mean value of 8456.7 ppb•s and a coefficient of variation of 4.2%. These data can be interpreted to mean mixing was complete by site 4 (9.3 km), e.g. $x_m \leqslant 9.3$ km. The similarity in the integrals at sites 2 and 3 and the difference between these sites and those downstream are difficult to interpret. As tracer losses do not seem to occur between sites 4 and 8 (constance of I values), it is difficult to advance this argument for integral differences between sites 3 and 4.

Downstream of site 3 the mean wave velocities (mean residence time, Table 56.5) appear to be constant across each measurement zone. By site 6 (v = 0.58 m/s) the tracer has adopted the longitudinal properties of the channel and is nearly identical to the average cross-sectional velocity for the channel (u = 0.59 m/s). Upstream of site 6 the effect of the higher premixing length velocities is still noticeable, even though for sites 4 and 5 (at least) mixing is complete and the tracer is moving at the stream velocity.

The small differences among values of C_p across the measurement zone for sites 2 to 8, coupled with the close similarities between peak and mean travel times, indicate that the tracer arrives and passes the sampling sites without a distinctly arrow shape. The leading edge arrives as a broad front, at least within the measurement zone.

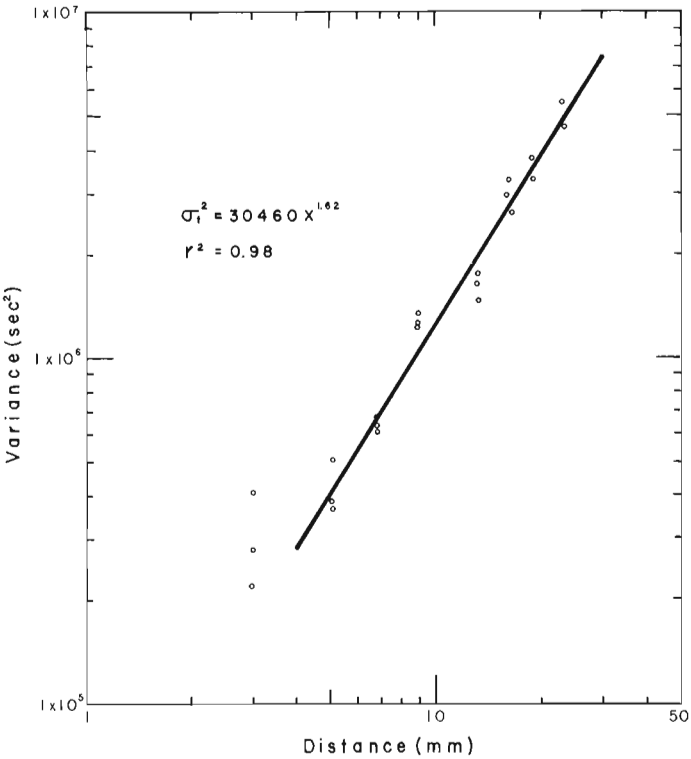

Figure 56.10. Longitudinal variance trend (s^2) of Lesser Slave River data.

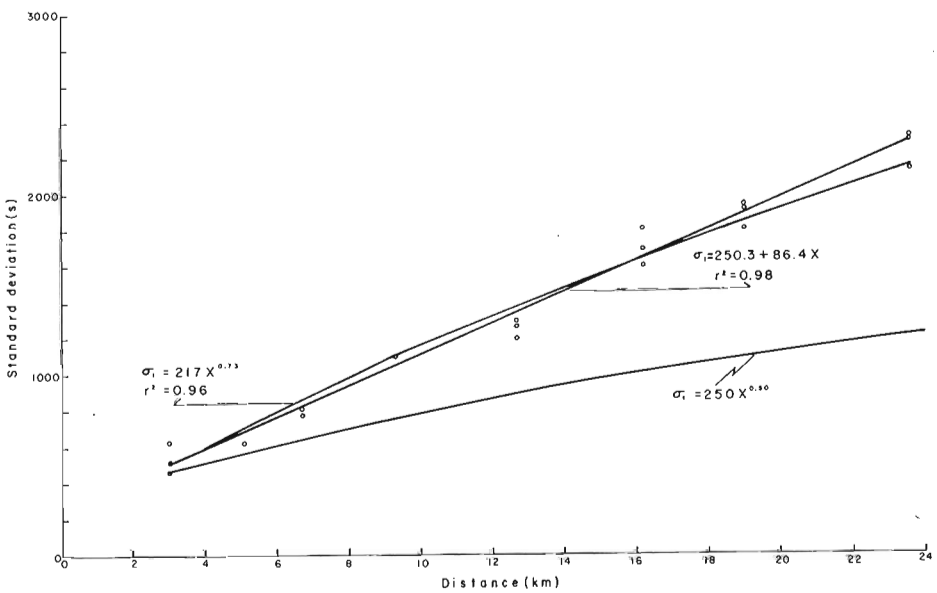

Figure 56.11.

Longitudinal trend of the standard deviation (s) of the tracer wave (open dots). The linear and power equations (equations (18) and (19)) are given for these data. The power equation $\sigma_t = 250 \times 0.50$ is the theoretical rate of spreading based on Taylor's analysis.

The effects of channel plan form variations on tracer characteristics appear to be minor; from the preceding discussion it is obvious that plan form variations do not cause noticeable changes in either v or C_p. For sites 2c (mild bend), 6a (straight-mild), and 7c (sharp bend), however, there are indications that the peak lags behind on the inside position in the bend (cf. starting time, Table 56.5; Fig. 56.3).

Similarity Analysis

Tracer variances (σ_t^2) were determined from equation (15) and are listed in column 5 of Table 56.5. As this moment characteristic is sensitive to the extremes of the distribution, particularly in the tails where definition is most difficult, some variations are to be expected. Table 56.5 shows that the most pronounced lateral variation in σ_t^2 (and the standard deviation, σ_t) occurs at sites 1 and 2.

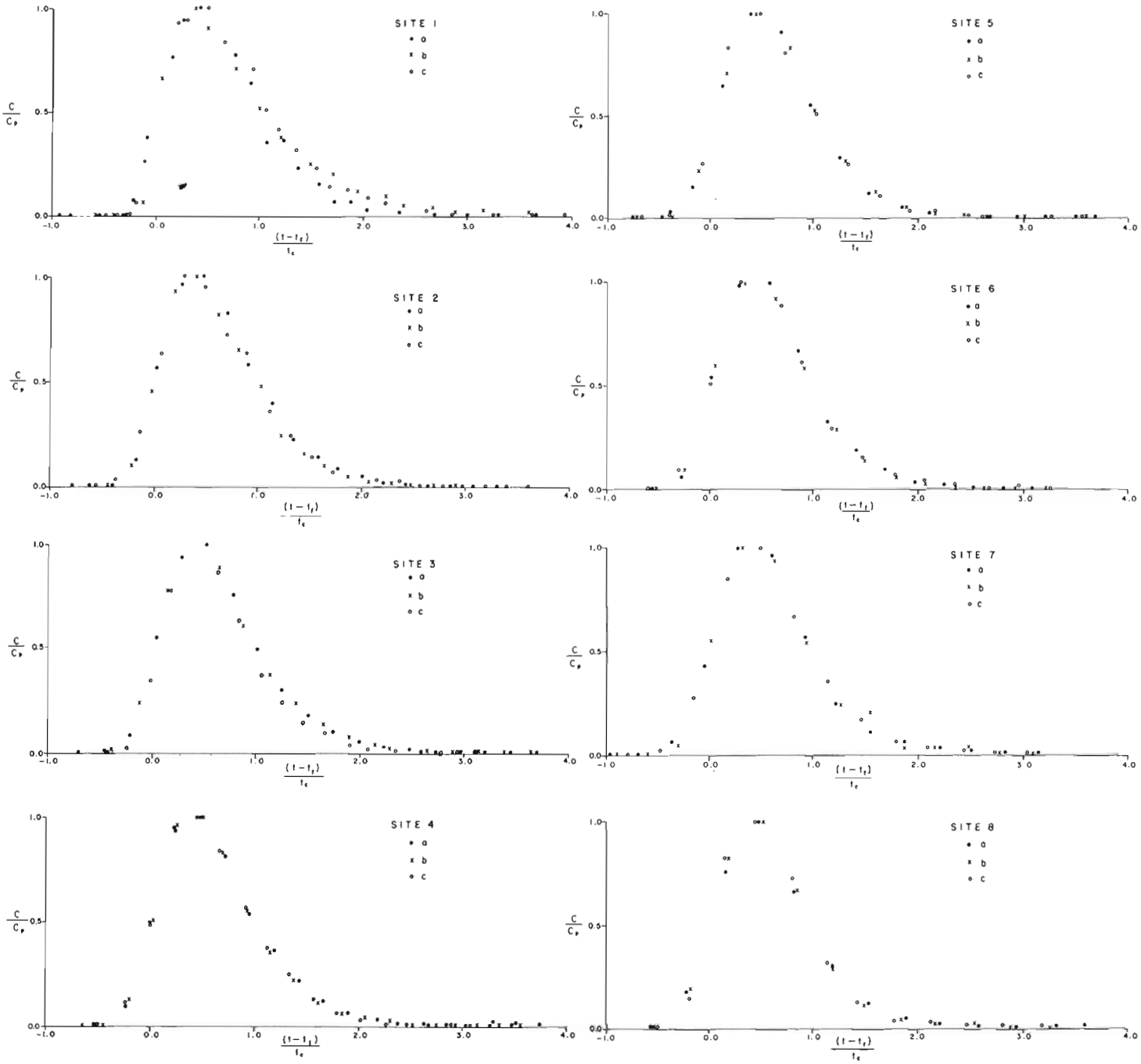

Figure 56.12. Dimensionless time-concentration curves for the eight sampling sites of Lesser Slave River.

Table 56.6

Time Parameters for Dimensionless Concentration Distributions

Site No.	Distance Downstream (km)	Lateral Sampling Position	t_s (min)	t_f (min)	t_c (min)	$(t_p-t_f)/t_c$	$(t_m-t_f)/t_c$
1	3.0	a	68.4	84.0	15.6	0.423	0.699
		b	67.2	78.0	10.8	0.352	0.741
		c	69.0	83.4	15.0	0.457	0.627
2	5.1	a	117.0	138.0	21.0	0.452	0.581
		b	118.8	140.4	21.6	0.380	0.546
		c	121.8	143.4	21.6	0.241	0.579
3	6.7	a	157.8	182.4	24.6	0.496	0.606
		b	156.0	180.0	24.0	0.354	0.596
		c	154.2	182.4	28.2	0.383	0.582
4	9.3	a	232.2	265.8	33.6	0.446	0.585
		b	232.2	267.6	35.4	0.467	0.599
		c	233.4	269.4	36.0	0.461	0.592
5	13.3	a	332.4	375.0	42.6	0.366	0.587
		b	331.8	373.8	42.0	0.410	0.583
		c	331.2	373.8	42.6	0.430	0.573
6	16.2	a	433.8	487.8	54.0	0.578	0.613
		b	432.6	484.8	52.2	0.343	0.594
		c	435.6	486.6	51.0	0.302	0.614
7	19.0	a	514.2	570.6	56.4	0.280	0.589
		b	510.6	569.4	58.8	0.335	0.626
		c	520.2	576.6	56.4	0.502	0.598
8	23.6	a	640.8	704.4	63.6	0.491	0.599
		b	640.2	705	64.8	0.506	0.579
		c	640.8	708	66.6	0.483	0.613
					Mean*	0.415	0.592
					Standard Deviation*	0.086	0.017

*Data from site 1 not included in calculation of mean or standard deviation.

The longitudinal variance trend is shown in Figure 56.10. A regression equation fitted to these data results in

$$\sigma_t^2 = 30460 \times^{1.62} \text{ or } \sigma_t = 174.5 \times^{0.81} \quad (17)$$

and explains 98% of the variance ($r^2 = 0.98$). Data from site 1 are not included because of the large variation, mainly resulting from σ_t^2 at lateral position a. Day (1975) has shown that the linear spreading in mountain streams begins within the mixing length, which suggests that site 1 data should be included in equation (17). It was decided, however, to omit site 1 data from equation (17) on the basis of the effect of this scatter on the equation.

The exponent in equation (17) is only 1.62, less than that shown for the mountain streams data of Day (1975) and the Missouri data (Yotsukura *et al.*, 1970), but is still greater than the value required for Taylor's analysis. This exponent reflects the structure of the dispersion process, and the intercept (30460) reflects its magnitude and hence flow scale and channel geometry.

The standard deviations of the concentration distributions at each site are shown in Figure 56.11. The proper defining equation is a power curve of the form

$$\sigma_t = 217 \times^{0.73} \quad (18)$$

with an r^2 of 0.96 (note that site 1 data are included). For comparative purposes another power curve of the form $\sigma_t = 250\ 0.50x$ also is shown. The intercept of this power curve is somewhat arbitrary but its exponent is that required for the application of Taylor's analysis. The discrepancy between the two rates of spreading is marked, particularly for large distances.

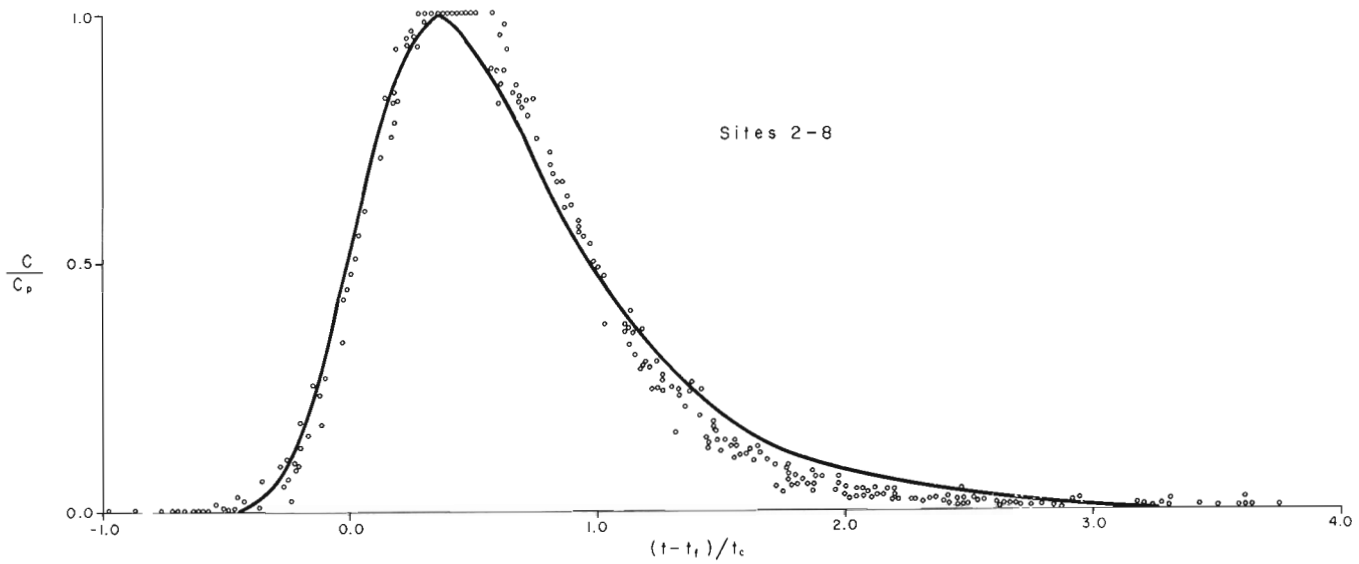

Figure 56.13. Comparison of a composite plot of the dimensionless time-concentration for sites 2 to 8, Lesser Slave River data (open dots) and a mean dimensionless shape (solid line) developed for mountain streams (Day and Wood, 1976).

The line expressed by equation (18) is near linear, at least for the 24 km of this study. A linear regression equation can be fitted to these data with the form

$$\sigma_t = 250.3 + 86.4x \qquad (19)$$

This equation explains 98% of the variance, which is slightly higher than for equation (18) but not significantly so. Although it is improper to apply a linear analysis to nonlinear data, equation (19) is an adequate approximation within the measured distances.

On the basis of Day and Wood's (1976) work, this near linearity in the spreading should result in similar dimensionless concentration distributions. These shapes, developed according to Figure 56.1, are shown in Figure 56.12; the largest variations occur at site 1, which indicates that the shape has yet not stabilized (Day and Wood show that the dimensionless shape developed within the mixing length for measurements in mountain streams). By site 2, variations among sampling positions have decreased, and these low values are maintained for all subsequent sites. When viewing these forms it must be remembered that the shapes, by definition, are forced through the co-ordinates (0.0, 0.5) and (1.0, 0.5), and hence any variations in shape will occur away from the midpoints of the rising and trailing limb. The accuracy of the method also depends upon the accuracy in defining C_p and the concentration distribution near the limb midpoints.

A summary of time parameters is listed in Table 56.6. Visual inspection of the dimensionless data for sites 2 to 8 (Fig. 56.12) indicates no systematic variations (at least within measurement precision) with either lateral position or plan form geometry of the sampling site. In Table 56.6 comparisons of the dimensionless positions of the peak time, t_p, and the mean travel time, t_m, show that variations do exist, but in no systematic form. The higher values of $(t_m-t_f)/t_c$ for site 1 presumably result from higher convective velocities and incomplete shape formation for this premixing length site. The similarity in these values for sites 2 to 8 (mean of 0.592, coefficient of variation of only 2.9%) is striking and indicates a constant or near constant shape for these sites. More variation is found in the values of $(t_p-t_f)/t_c$ (mean of 0.415, coefficient of variation of 20.8%), probably resulting from difficulty in accurately determining C_p. As t_m is a calculation based upon the spread of the concentration distribution, it is the stronger of the two comparisons. The longitudinal and lateral similarity in the dimensionless shapes implies that the specific structure of the cross-sectional velocity is not critical in determining the shape of the dimensionless concentration distributions. This is an important observation in terms of predicting the concentration pattern from cross-sectional data.

A more dramatic method of illustrating the longitudinal stability of the dimensionless shape is given in Figure 56.13, which shows a composite diagram for sites 2 to 8. The variations of the position t_p are evident, as is the general similarity of the shapes. Day and Wood (1976) have shown larger variations for the mountain streams data, without being able to determine the cause, except to demonstrate the apparent random behaviour of the data. Figure 56.13 also shows a comparison between the Lesser Slave River data and a mean dimensionless shape developed for mountain streams (Day and Wood, 1976). The rising or forward limbs are virtually identical. The mountain stream shape peaks early $(t_p-t_m)/t_c = 0.375$, compared to a mean position of 0.415 for the Lesser Slave River data. The descending or trailing limbs are different; the Lesser Slave River data shows a more symmetrical shape. Day and Wood have drawn a similar comparison

between the Missouri River data and the mountain streams data mean shape.

Another dispersion characteristic required for Taylor's analysis is a concentration decay rate of $x^{-0.50}$. Day (1974) has shown that decay rates in natural streams can vary from -0.67 (Missouri River) to -1.4 (mountain streams). The Missouri River decay rate can be expected to be low because significant tracer losses occurred. Day's data from mountain streams indicated a range of -0.9 to -1.4, with a mean of -1.17, and a standard deviation of -0.21. The decay rate for the Lesser Slave River data was determined from a regression analysis of the logarithmically transformed data. The resulting equation is

$$C_p = 25.3x^{-0.83} \qquad (20)$$

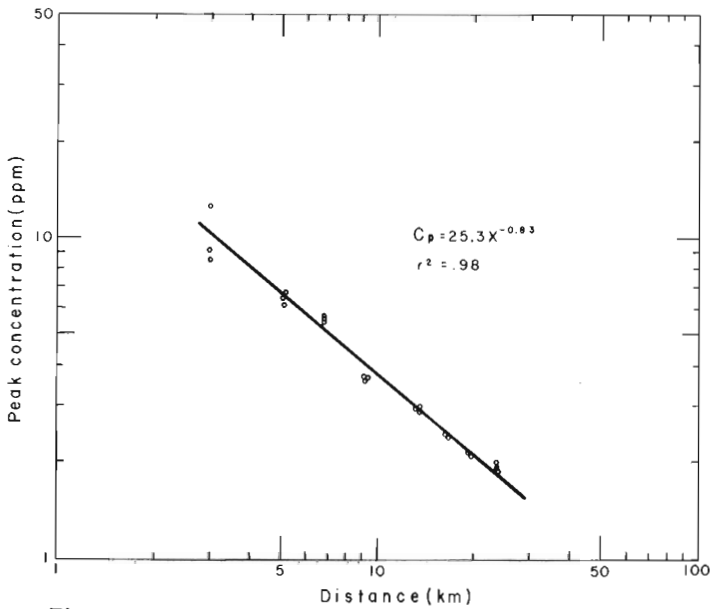

Figure 56.14. Exponential decay of peak concentration for Lesser Slave River data.

and has an r^2 of 0.98. Figure 56.14 shows the decay of the peak concentration and the best fitting regression line.

As mentioned in a previous section the linear spreading, the constant shape, and, for this experiment, the insensitivity of the dispersion process to the specific nature of cross-sectional velocity variations, greatly simplify problems with predictions. For this single experiment, however, it is not possible to test prediction, and therefore the following discussion is confined to both description and comparison between the Lesser Slave River data and data from more extensive tests in mountain streams.

For a given distance, two time parameters, t_f and t_c, must be determined. Studies in mountain streams have shown that the longitudinal characteristics of these two parameters, one representing the position of the concentration distribution in the channel and the other representing its spread or dimensions, can be described by simple linear equations such as (8) and (9). Similar equations can be developed for the Lesser Slave River data leading to

$$(t_f v)/w = -0.43 + 0.017(x/w) \qquad (21)$$

and

$$(t_c v)/w = 0.004 + 0.004(x/w) \qquad (22)$$

These equations explain 99.7% and 97.7% of the variance, respectively (the standard errors are 0.117 and 0.033). These regression equations are shown in Figure 56.15, where (21) is fitted to sites 3 to 8, and (22) is fitted to all data. Day and Wood (1976) have shown that two equations, similar to (21), are required to describe the downstream behaviour of t_f, with an equation for data measured before and after the mixing length ($x_m = 24x/w$ for mountain streams). The equation describing $(t_f v)/w$ downstream of x_m for mountain streams is

$$(t_f v)/w = -0.065 + 0.014(x/w) \qquad (23)$$

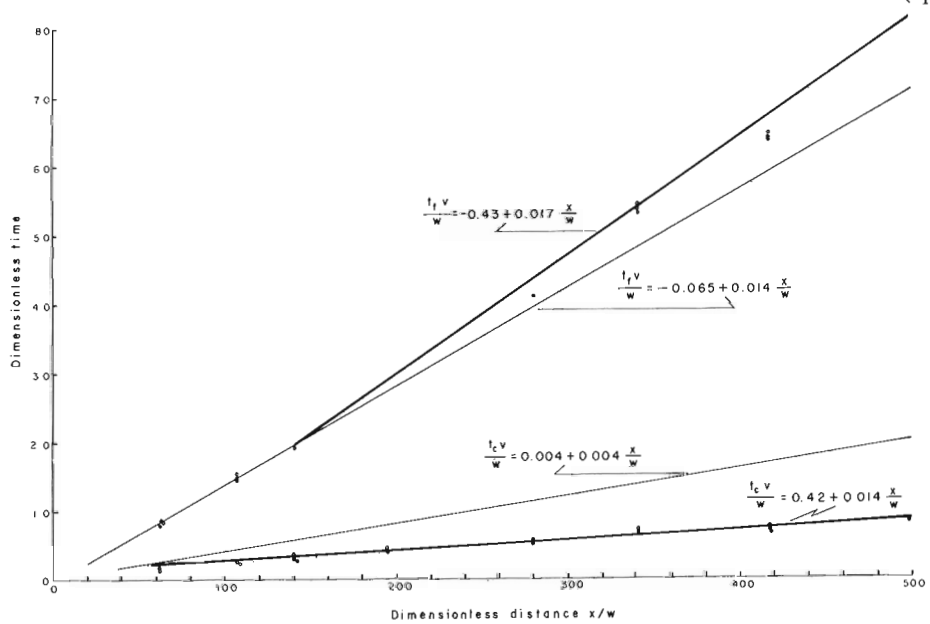

Figure 56.15.

Comparison of dimensionless time parameters. Lesser Slave River data (open dots) and best fitting linear equations (dark lines through open dots) compared to similar equations developed for mountain streams (Day and Wood, 1976).

and for $(t_c\ v)/w$ is, for all distances,

$$(t_c\ v)/w = 0.004 + 0.004(x/w) \qquad (24)$$

The choice of site 3 as a limit of equation (21) is somewhat arbitrary and somewhat contradictory as the dimensionless shape appears to stabilize by site 2. The highest value of r^2, however, occurred when sites 1 and 2 were excluded from equation (21), indicating that lateral mixing is not complete until site 3 (6.7 km). This site is located near the mixing length based on Ward's method (x_m = 6.3 km). The intercepts in equations (22) and (24) indicate that the concentration distributions have a virtual origin upstream of the injection point.

Comparisons between the two sets of defining equations, (21) and (22), and (23) and (24), illustrate differences in the magnitude of dispersion in the two channel types. Differences between equations (21) and (23) indicate that the passage of a tracer mass is slower in the Lesser Slave River, and differences in equations (22) and (24) show that the amount of dispersion (for a fixed distance) is less than half that shown for mountain streams. Variations in channel characteristics (shape, plan form, slope, roughness) and possibly in the nature of fluid traps (distribution, size, location) cause the differences in the intercept and slope values of the particular sets of equations. The specific nature of the interrelationships cannot be evaluated on the basis of these limited data, but it may be of interest to note that the results confirm the somewhat intuitive expectation that the highly non-uniform mountain streams are much more "dispersive" than more uniform, single-thread channels.

Conclusions

The analysis of this rather comprehensive tracer test in a meandering channel has lead to several significant observations. The rate of longitudinal spreading for this single test is $x^{0.73}$, considerably more than the $x^{0.50}$ value required for the application of Taylor's analysis, and less than the x^1 value suggested by Day (1975). Although the longitudinal spreading is not exactly linear, it is sufficiently close to permit its description by linear functions. This approximation does not lead to any significant inaccuracies and considerably eases the future problem of prediction, which is the ultimate goal of this project.

An important observation is the (measureable) insensitivity of the longitudinal spreading pattern to changes in channel plan form. This insensitivity means that the specific nature of the channel cross-section and its velocity distribution do not dominate, and therefore it is possible to characterize the longitudinal motion by readily attainable mean hydraulic parameters such as flow width and velocity. Should this be the case for other streams as well, predictions will be available more readily.

The main problem with the similarity approach is its lack (as yet) of theoretical basis and its consequent dependence upon empirical functions. Analysis of the Lesser Slave River data leads to the conclusion that the longitudinal motion of the tracer is less rapid, as is its dispersion, than in rugged mountain streams. Although these differences are isolated in the numerical value of the coefficients in the defining linear functions, no correlation as yet exists between these and readily available bulk flow and channel geometry parameters.

The near linear spreading and the high concentration decay rate results in close similarity of the dimensionless concentration distributions. This similarity has stabilized by site 2 (5.1 km downstream of injection) and is maintained throughout the lateral measurement zone and along the length of the test channel (23.6 km). Dimensionless concentration distributions derived from the Lesser Slave River data are shown to be more symmetrical than those shown for mountain streams.

Finally, one problem common to these experiments is the determination of the mixing length (e.g. Table 56.4). Interpretation of the data presented here (behaviour of $(t_f\ v)/w$, tracer integrals, stabilization of dimensionless shapes) indicates that the mixing length is located between (or including) sites 2 and 3, e.g. between 5.1 to 6.7 km, roughly at the position of Ward's (1973) estimate.

References

Aris, R.
1959: The longitudinal diffusion coefficient in flow through a tube with stagnant pockets; Chem. Eng. Sci., v. 11, p. 194-198.

Barsby, A.
1968: Determination of mixing lengths in dilution gauging; Int. Assoc. Sci. Hydrol., Gen. Assem. Bern, 1967, Publ. no. 78, p. 395-407.

Day, T.J.
1974: Dispersion in natural channels; unpubl. Ph.D. dissert., Univ. Canterbury, New Zealand, 130 p.

1975: Longitudinal dispersion in natural channels; Water Resour. Res., v. 11, no. 6, p. 909-918.

1976: On the precision of salt dilution gauging; J. Hydrol. (in press).

Day, T.J. and Wood, I.R.
1976: Similarity of the mean motion of fluid particles in a natural channel; Water Resour. Res. (in press).

Elder, J.W.
1959: The dispersion of marked fluid in turbulent shear flow; J. Fluid Mech., v. 5, pt. 4, p. 544-560.

Engmann, J.E.O. and Kellerhals, R.
1974: Transverse mixing in an ice-covered river; Water Resour. Res., v. 10, no. 4, p. 775-784.

Fischer, H. B.
1966a: Longitudinal dispersion in laboratory and natural channels; unpubl. Ph. D. dissert., California Inst. Technol., Berkeley, 250 p.

1966b: A note on the one-dimensional dispersion model; Air Water Pollut. Int. J., Pergamon Press, v. 10, p. 443-452.

1967: The mechanics of dispersion in natural streams; Am. Soc. Civ. Eng., Proc., J. Hydraul. Div., v. 93 (HY6), p. 187-216.

1968: Dispersion predictions in natural streams; Am. Soc. Civ. Eng., Proc., J. San. Eng. Div., v. 94 (SA5), p. 927-943.

1973: Longitudinal dispersion and turbulent mixing in open-channel flow; Rev. Fluid Mech., p. 59-77.

Glover, R. E.
1964: Dispersion of dissolved or suspended materials in flowing streams; U. S. Geol. Surv., Prof. Paper 433-B, 32 p.

Godfrey, R. G. and Frederick, B. J.
1970: Dispersion in natural streams; U. S. Geol. Surv., Prof. Paper 433-K, 70 p.

Hays, J. R.
1966: Mass transport phenomena in open channel flow; unpubl. Ph. D. dissert., Vanderbilt Univ., Tennessee, p. 138.

Kellerhals, R., Neill, C. R., and Bray, D. I.
1972: Hydraulic and geomorphic characteristics of rivers in Alberta; River Eng. Surf. Hydrol. Rept. 72-1, Res. Coun. Alberta, Edmonton, p. 52.

Nordin, C. F. and Sabol. G. V.
1974: Empirical data on longitudinal dispersion in rivers; U. S. Geol. Surv., Water Resour.-Invest. 20-74.

Okoye, J. K.
1970: Characteristics of transverse mixing in open channel flows; Rept. KH-R-23, W. M. Keck Lab. Hydraul. Water Resour., California Inst. Technol., Pasadena, 269 p.

Okubo, A.
1973: Effect of shoreline irregularities on streamwise dispersion in estuaries and other embayments; Neth. J. Sea Res., v. 6, no. 1-2, p. 213-224.

Sayre, W. W. and Chang, F. M.
1968: A laboratory investigation of open channel dispersion processes for dissolved, suspended and floating contaminants; U. S. Geol. Surv., Prof. Paper, 433-E, 71 p.

Sullivan, P. J.
1971: Longitudinal dispersion within a two-dimensional turbulent shear flow; J. Fluid Mech., v. 149, pt. 3, p. 551-576.

Taylor, G. I.
1954: The dispersion of matter in turbulent flow through a pipe; R. Soc. Lon., Proc., Ser. A, v. 233, p. 446-468.

Thackston, E. L. and Krenkel, P. A.
1967: Longitudinal mixing in natural streams; Am. Soc. Civ. Eng., Proc., J. San. Eng. Div., v. 93(SA5), p. 67-90.

Thackston, E. L. and Schnelle, K. B.
1970: Predicting effects of dead zones on stream mixing; Am. Soc. Civ. Eng., Proc., J. San. Eng. Div., v. 96(SA2), p. 319-331.

Ward, P. R. B.
1973: Prediction mixing lengths for river flow gauging; Am. Soc. Civ. Eng., Proc., J. Hydraul. Div., v. 99(HY7), p. 1069-1081.

Yotsukura, N. and Cobb, E. D.
1972: Transverse diffusion of solutes in natural streams; U. S. Geol. Surv., Prof. Paper 582-C, 19 p.

Yotsukura, N., Fischer, H. B., and Sayre, W. W.
1970: Mixing characteristics of the Missouri River between Sioux City, Iowa, and Plattsmouth, Nebraska; U. S. Geol. Surv., Water-Supply Pap. 1899, 29 p.

OUTLINE FOR A MARINE SCIENCE ATLAS OF THE BEAUFORT SEA

Project 720102

B. R. Pelletier
Terrain Sciences Division

Introduction

An abundance of geological, geophysical, biological, and oceanographic data became available upon completion of the HUDSON 70 cruise into the Beaufort Sea. From this data base, an outline of a Marine Science Atlas for the region was drawn. Additional workers were asked to contribute, and with the inception of the Beaufort Sea Environmental Project, sponsored jointly by a segment of the oil industry and government, the prospects of increasing the scope of the Atlas emerged. Now about 45 authors are preparing material for submission in the winter of 1976-77 with a view towards publishing in 1977.

The Atlas is designed to interest educators, engineers, petroleum geologists, and those interested in that part of Canada's North. Libraries, schools, the general public, government workers, and certain industries interested in environmental concerns and the development of our resources will be the main users of the Atlas.

Format

The Atlas is designed to cover many scientific disciplines and to represent the factual material in the form of maps, photographs, and graphs. A brief written account of about 50 words accompany each submission, although introductory statements may be somewhat longer.

Because of the dimensions of the Atlas (17 x 23 inches), the most suitable scale for presentation of the data base is 1: 1 000 000. Other scales, however, will be used according to the extent of the data base and the area of coverage. In all, about 120 maps will be prepared and will be accompanied with suitable legends, sketches, photographs, and text captions. Technical editing and layout is being provided by D. Monahan of the Canadian Hydrographic Service under an arrangement with the Dominion Hydrographer. The Atlas will be a joint DOE-EMR publication.

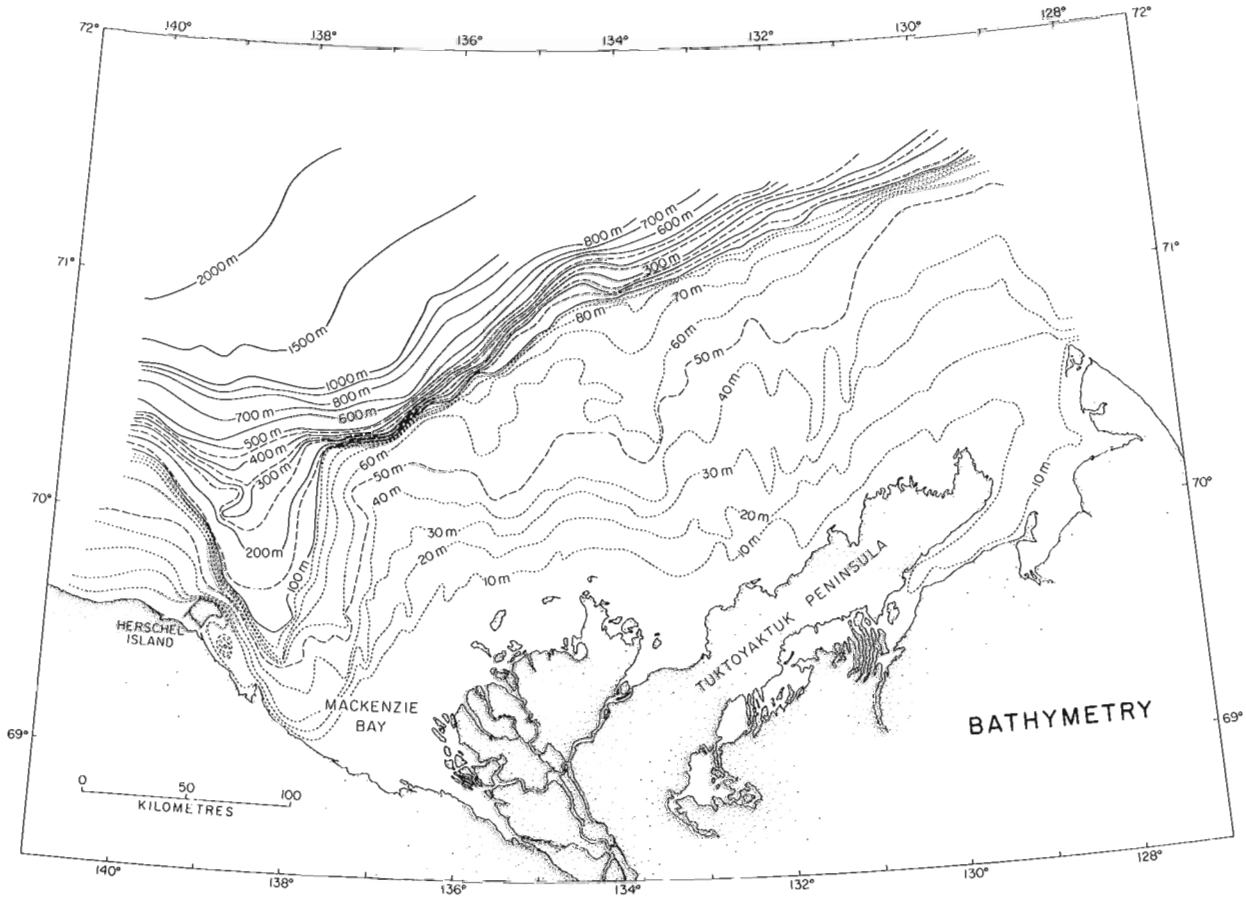

Figure 57.1. Bathymetric map showing continental shelf, slope, and the Mackenzie Canyon (Pelletier, Technical Report No. 25a).

From: Report of Activities, Part C;
Geol. Surv. Can., Paper 76-1C (1976).

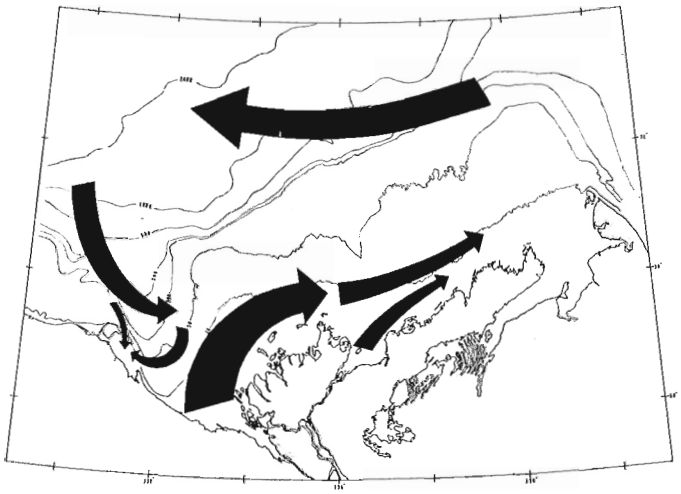

Figure 57.2. Circulation in the southern Beaufort Sea based on previous observations and on inferences from distribution of suspended matter (Bornhold, Technical Report No. 25b).

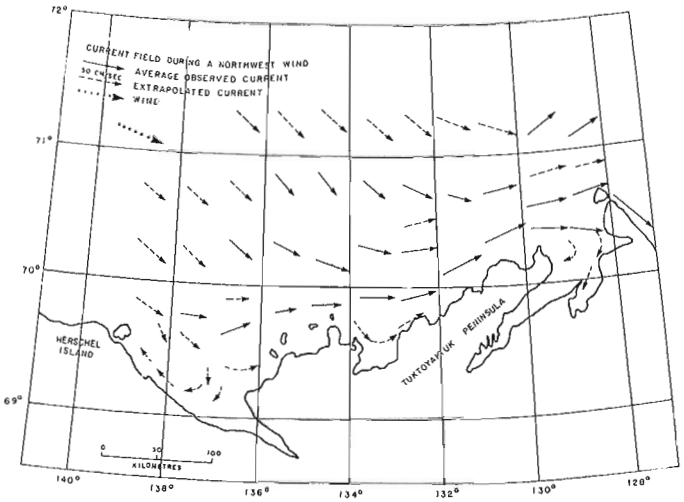

Figure 57.3. Surface currents and related effects of northeast wind (MacNeill and Garrett, Technical Report No. 17).

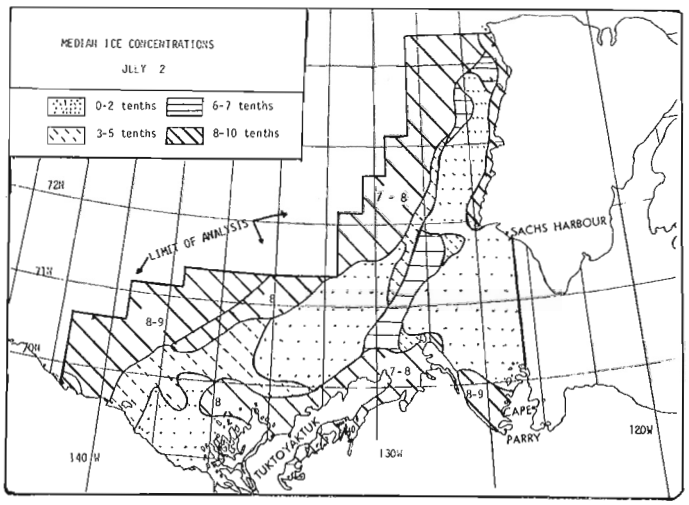

Figure 57.4. An analysis of ice concentration in the Beaufort Sea obtained from NOAA satellite imagery (Markham, Technical Report No. 26).

Content

The following major disciplines are included:

Meteorology - atmospheric conditions such as precipitation, temperature, air pressure, winds.

Oceanography - currents, tides, circulation, ice, structure, chemistry.

Hydrography - bathymetric charts, delineation of geomorphological features such as the continental shelf, continental slope, Mackenzie Canyon, pingos.

Biology - planktonic and benthonic micro-organisms, larger marine vertebrates (seals, whales, fish) and invertebrates (molluscs).

Geosciences
- geothermometry
- magnetics
- gravity
- seismology
- shallow seismic refraction
- shallow seismic reflection
- frozen ground studies
- bedrock maps and cross-sections
- dispersal of bottom and suspended sediments including mineralogical and textural analyses
- geomorphology (pingos, ice-scour features, major bathymetric features, ancient river channels, and mass wastage)
- coastal processes (erosion,
- sedimentation, geomorphology, and classification)
- micropaleontology (planktonic and benthonic organisms in bottom sediments and cores (forams and diatoms)).

Wildlife - birds, polar bear, fox

Exploration - voyages of discovery, commercial enterprise, scientific endeavours.

Demography and Culture - the people, occupations, access routes.

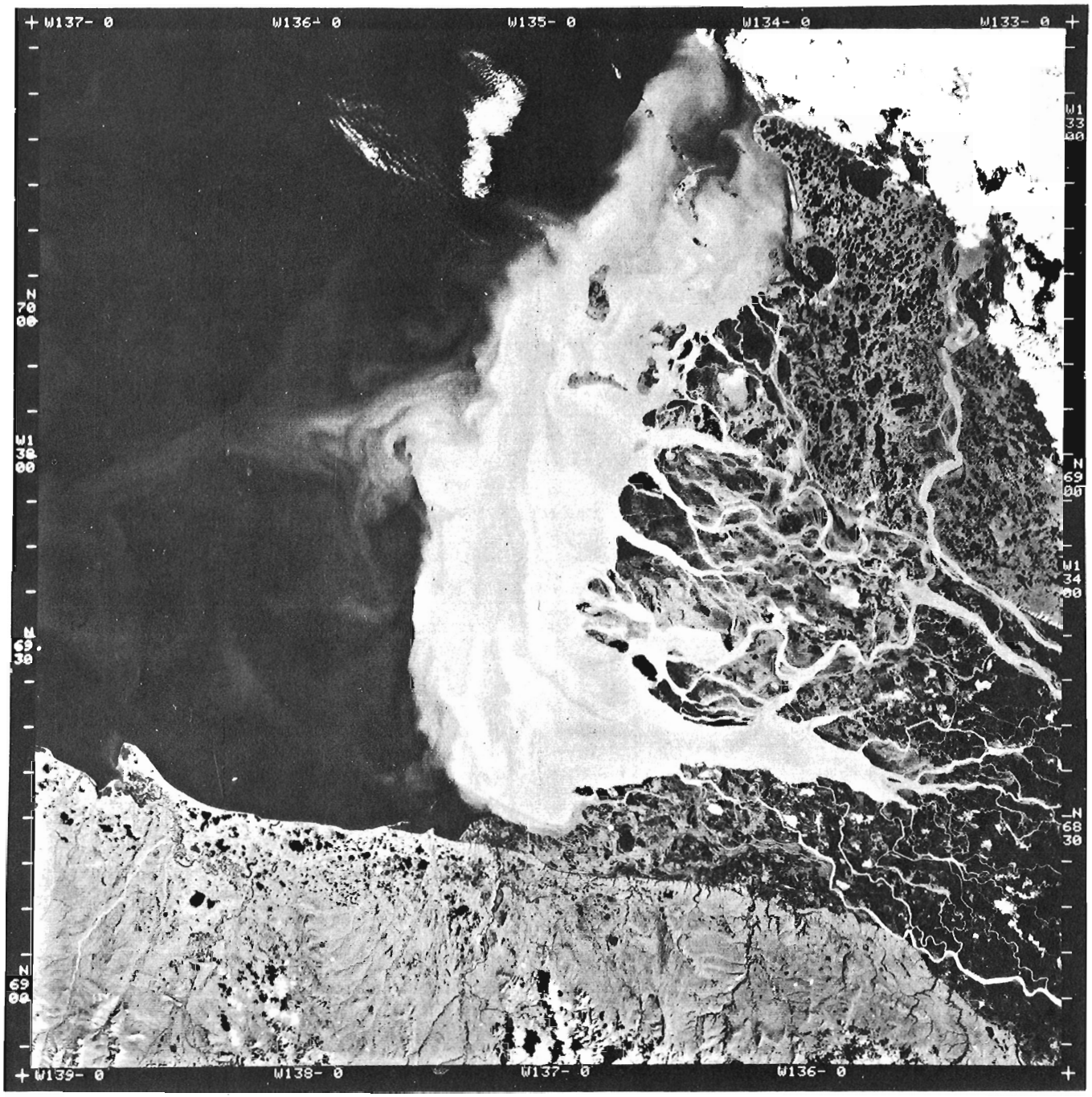

Figure 57.5. Satellite photograph of the sediment plume from the Mackenzie Delta, taken September 1, 1973 (Pelletier, Technical Report No. 25a).

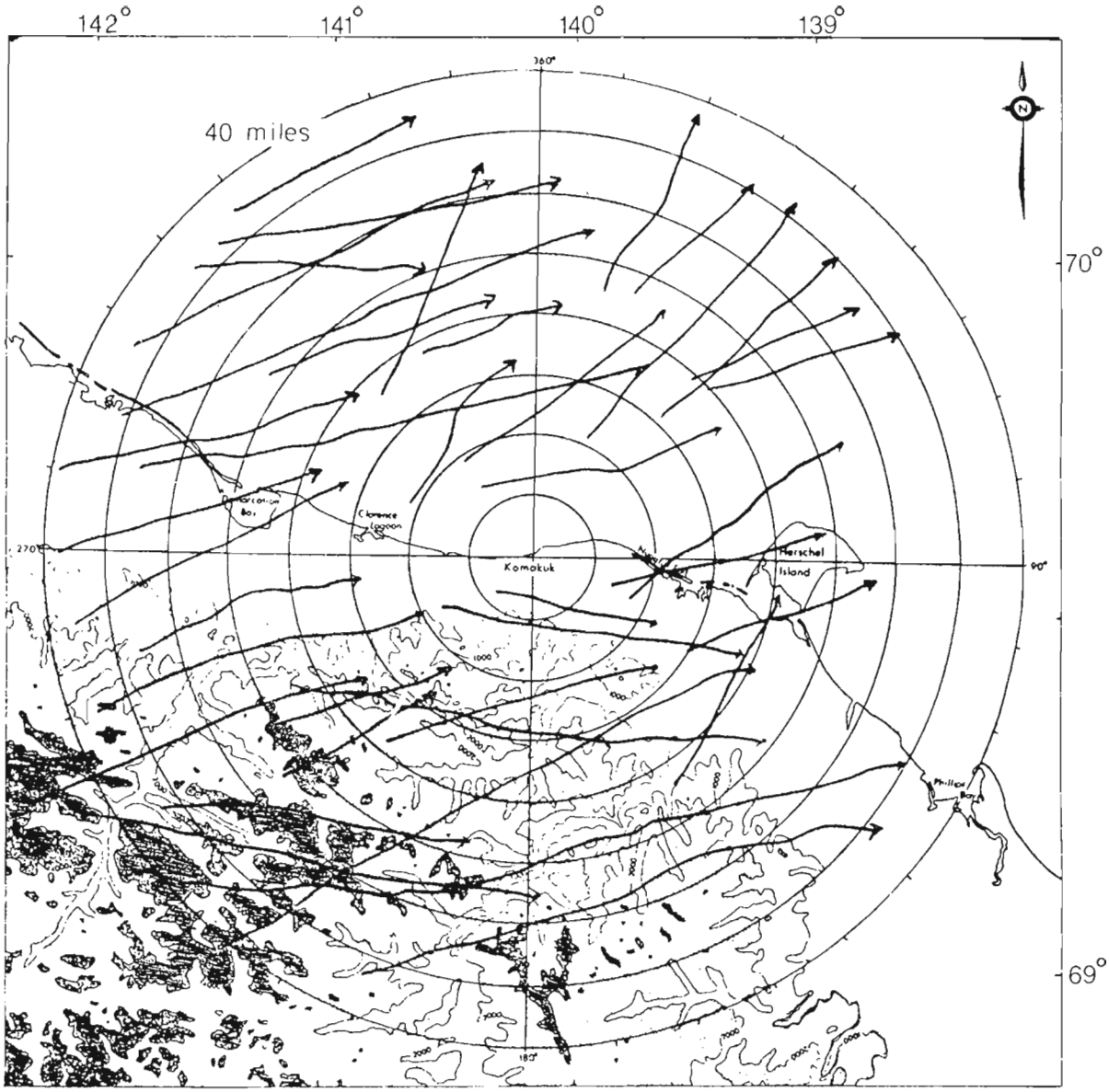

Figure 57.6. Radar tracing of paths of flocks moving north-northeast to east on May 27, 1975, 04:00-09:00 YST. The distinction between northeast and east movement is unclear on this date. Shore birds and Glaucous Gulls were the species most commonly detected moving east along the coast at this time but Brant were noted later in the day. The mean ground speed of flocks shown here was 77 km/h; their air speeds would be higher, since the wind was easterly (Richardson, Morrell and Johnson, Technical Report No. 3c).

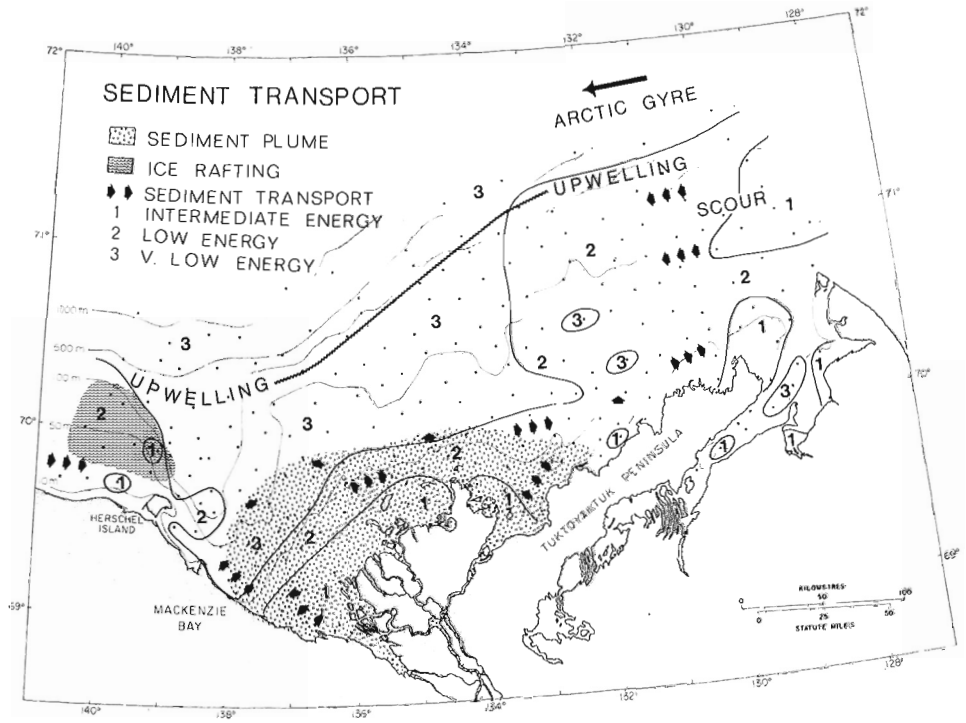

Figure 57.7. Model of sediment transport in the southern Beaufort Sea (Pelletier, Technical Report No. 25a).

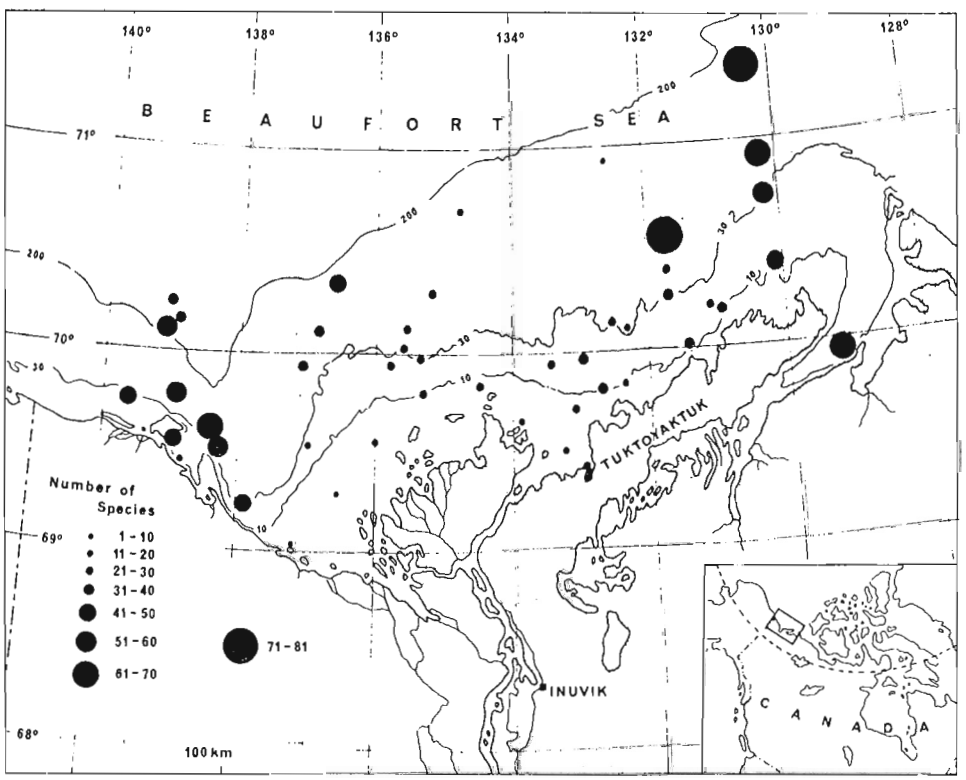

Figure 57.8. Diversity of zoobenthos of the southern Beaufort Sea (Wacasey, Technical Report No. 12b).

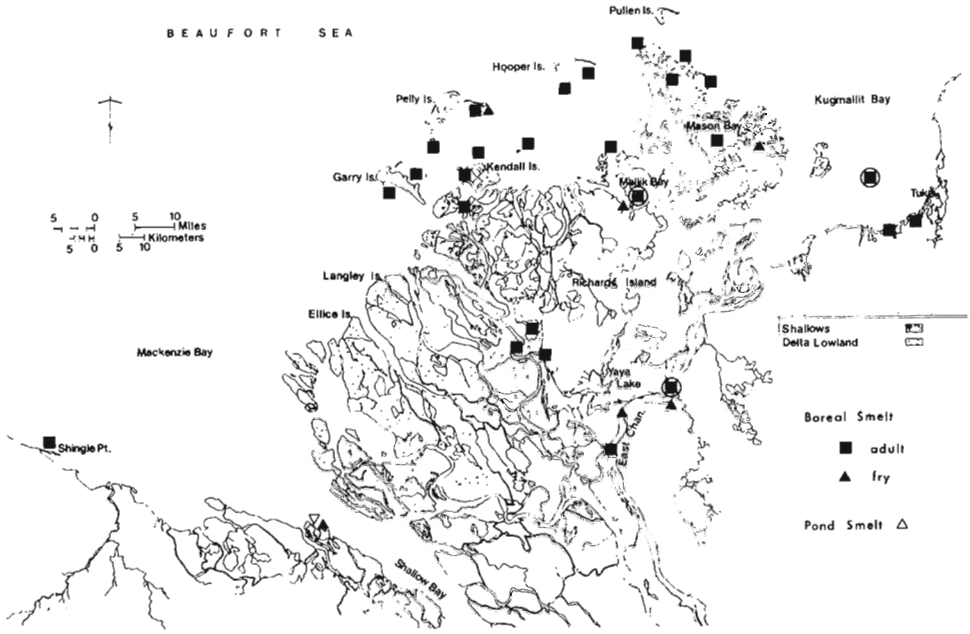

Figure 57.9. Distribution of boreal smelt and pond smelt in the outer Mackenzie Delta. Encircled symbols represent both summer and winter distributions (Percy, Technical Report No. 8).

Some of the aspects of this work are shown in Figures 57.1 to 57.9 and are extracts from technical reports by investigators in the Beaufort Sea Environmental Project. These reports may be obtained from:

Department of the Environment
512 Federal Building
1230 Government Street
Victoria, British Columbia
V8W 7W4

They include the following:

Bornhold, B.D.
Suspended matter in the southern Beaufort Sea; Technical Report No. 25b.

MacNeill, M.R. and Garrett, J.F.
Open water surface currents; Technical Report No. 17.

Markham, W.E.
Ice climatology of the Beaufort Sea; Technical Report No. 26.

Milne, A.R. and Smiley, B.D.
Offshore drilling for oil in the Beaufort Sea: A preliminary environmental assessment; Technical Report No. 39.

Pelletier, B.R.
Sediment dispersal in the southern Beaufort Sea; Technical Report No. 25a.

Percy, R.
Fishes of the outer Mackenzie Delta; Technical Report No. 8.

Richardson, W. John, Morrell, M.R., and Johnson, S.R.
Bird migration along the Beaufort Sea coast. Radar and visual observations in 1975; Technical Report No. 3c.

Stirling, I., Andriashek, D., Latour, P., and Calert, S.W.
Distribution and abundance of polar bears in the eastern Beaufort Sea; Technical Report No. 2.

Wacasey, J.W.
Bilogical productivity of the southern Beaufort Sea: zoobenthic studies; Technical Report No. 12b.

ERRATA

Report of Activities, Part A
Geol. Surv. Can., Paper 76-1A

Paper 76-1A, report 83, p. 397: contribution by W. F. Fyson, para. 4, line 8, should read "if the plutons were intruded before D_1 and D_2", not between D_1 and D_2.

Report of Activities, Part B
Geol. Surv. Can., Paper 76-1B

Paper 76-1B, p. 78, eq. 6 was omitted:

$$P = 100 \times \frac{[E_2(\mu h) - \cos\theta_1 E_2(\frac{\mu h}{\cos\theta_1}) + aE_3(\mu h) - a\cos^2\theta_1 E_3(\frac{\mu h}{\cos\theta_1})]}{E_2(\mu h) + aE_3(\mu h)} \quad \ldots (6)$$

Paper 76-1B, p. 143, Tables 29.1 and 29.2 were omitted. They follow on pages 332 and 333.

Paper 76-1B, p. 143: Soils: This should read: "The permafrost table is encountered within 1 metre of the surface...."

Paper 76-1B, p. 144: Sensitive Environments: 2) Should read: "The disturbance of vegetation and active layer...."

Table 29.1

Characteristics of Ecological Districts on Somerset Island

Ecological Region	Ecological District	Soils (% area)		Vegetation Type (% area)		% Ground Cover
High Arctic	A-1 (1.0, 1.1, 1.2) Northwest Plateau	Rego. T. Cryosol	80	Polar desert	80	1
		Brun. T. Cryosol	10	Arctic dwarf shrubs	10	10
		Glei. T. Cryosol	10	Moss-grass	10	50
High Arctic	A-2 West Somerset Upland	Rego. T. Cryosol	30	Polar desert	20	10
		Lith. R. T. Cryo.	30	Lichens	30	70
		Brun. T. Cryosol	30	Arctic dwarf shrubs	30	25
		Glei. T. Cryosol	10	Meadow	20	90
High Arctic	A-3 Cunningham Inlet	Rego. T. Cryosol	50	Polar desert	30	10
		Brun. T. Cryosol	20	Arctic dwarf shrubs	40	30
		Glei. T. Cryosol	30	Meadow	30	100
Mid-Arctic	M-1 Cape Garry Plateau	Brun. T. Cryosol	50	Arctic dwarf shrubs	50	30
		Rego. T. Cryosol	40	Polar desert	40	10
		Glei. T. Cryosol	10	Meadow	10	100
Mid-Arctic	M 2 South Somerset Till Plain	Brun. T. Cryosol	30	Arctic dwarf shrubs	40	50
		Lith. R. T. Cryo.	20	Lichen	20	75
		Rego. T. Cryosol	30	Polar desert	20	50
		Glei. T. Cryosol	20	Moss-grass	20	60
Mid-Arctic	M-3 (3.0, 3.1) South Somerset Ranges	Brun. T. Cryosol	40	Arctic dwarf shrubs	40	40
		Rego. T. Cryosol	40	Polar desert	40	10
		Glei. T. Cryosol	20	Meadow	20	100
Mid-Arctic	M-4 Central Creswell Valley	Brun. T. Cryosol	50	Arctic dwarf shrubs	80	50
		Rego. T. Cryosol	30			
		Lith. R. T. Cryo.	10	Lichen	10	30
		Glei. T. Cryosol	10	Meadow	10	100
Mid-Arctic	M-5 Creswell Lowland	Glei. T. Cryosol	60	Meadow	60	100
		Brun. T. Cryosol	30	Arctic dwarf shrubs	40	45
		Rego. T. Cryosol	10			
Mid-Arctic	M-6 (6, 6.1) Stanwell-Fletcher Basin	Brun. T. Cryosol	60	Arctic dwarf shrubs	70	70
		Glei. T. Cryosol	30	Meadow	30	100
		Rego. T. Cryosol	10			

Table 29.2

Characteristics of Ecological Districts on Prince of Wales Island

Ecological Region	Ecological District	Soils (% area)		Vegetation Type (% area)		% Ground Cover
High Arctic	A-1	Rego. T. Cryosol	70	Polar desert	70	10
	Cape Hardy	Brun. T. Cryosol	20	Arctic dwarf shrubs	20	30
	Highlands	Glei. T. Cryosol	10	Moss-grass	10	75
High Arctic	A-2	Rego. T. Cryosol	60	Polar desert	60	10
	North-Central	Brun. T. Cryosol	20	Arctic dwarf shrubs	10	30
	Uplands	Glei. T. Cryosol	20	Moss-grass	30	80
High Arctic	A 3	Rego. T. Cryosol	80	Polar desert	80	1
	Drake Bay Uplands	Brun. T. Cryosol	10	Arctic dwarf shrubs	10	30
		Glei. T. Cryosol	10	Moss-grass	10	80
High Arctic	A 4	Rego. T. Cryosol	60	Polar desert	60	1
	Mount Clarendon	Brun. T. Cryosol	20	Arctic dwarf shrubs	20	30
	Lowlands	Glei. T. Cryosol	20	Meadow	20	100
High Arctic	A 5	Glei. T. Cryosol	60	Meadow	60	100
	Back Bay Lowlands	Brun. T. Cryosol	40	Arctic dwarf shrubs	40	30
Mid-Arctic	M-1	Brun. T. Cryosol	60	Arctic dwarf shrubs	60	50
	East Prince of	Rego. T. Cryosol	20	Polar desert	20	15
	Wales Highlands	Glei. T. Cryosol	20	Meadow	20	100
Mid-Arctic	M-2	Brun. T. Cryosol	70	Arctic dwarf shrubs	80	60
	Cape Henry Kellett	Glei. T. Cryosol	30	Meadow	20	100
	Uplands					
Mid-Arctic	M-3	Rego. T. Cryosol	60	Arctic dwarf shrubs	60	5
	Central Prince of	Brun. T. Cryosol	20	Arctic dwarf shrubs	20	30
	Wales Lowlands	Glei. T. Cryosol	20	Moss-grass	20	50
Mid-Arctic	M 4	Rego. T. Cryosol	40	Arctic dwarf shrubs	40	15
	Mount Cowie	Brun. T. Cryosol	40	Arctic dwarf shrubs	40	30
	Lowlands	Glei. T. Cryosol	20	Meadow	20	100
Mid-Arctic	M-5	Brun. T. Cryosol	60	Arctic dwarf shrubs	60	40
	Marine Lowlands	Glei. T. Cryosol	40	Meadow	40	100
Mid Arctic	M 6	Brun. T. Cryosol	40	Arctic dwarf shrubs	40	60
	Prescott Island	Lith. R. T. Cryo.	40	Lichen	40	50
	Uplands	Glei. T. Cryosol	20	Meadow	20	100

AUTHOR INDEX

Bracketed numbers refer to individual reports within this publication